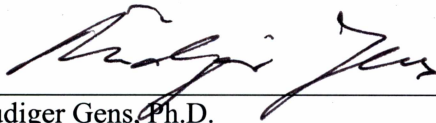


RETROGRESSIVE THAW SLUMPS AND ACTIVE LAYER DETACHMENT SLIDES
IN THE BROOKS RANGE AND FOOTHILLS OF NORTHERN ALASKA:
TERRAIN AND TIMING

By

Andrew W. Balsler

RECOMMENDED:



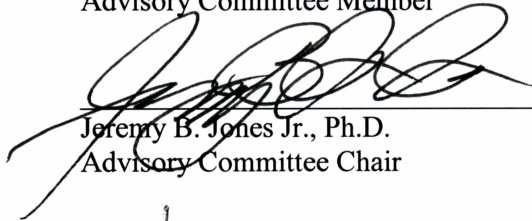
Rudiger Gens, Ph.D.
Advisory Committee Member



Michelle C. Mack, Ph.D.
Advisory Committee Member



Donald A. Walker, Ph.D.
Advisory Committee Member

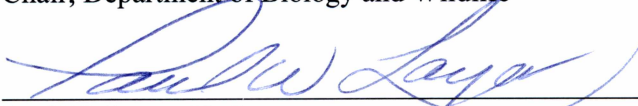


Jeremy B. Jones Jr., Ph.D.
Advisory Committee Chair

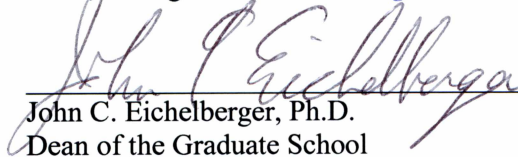


Diane Wagner, Ph.D.
Chair, Department of Biology and Wildlife

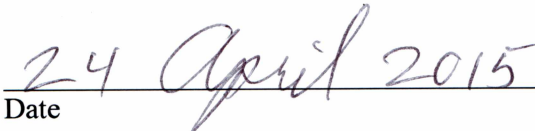
APPROVED:



Paul W. Layer, Ph.D.
Dean, College of Natural Science and Mathematics



John C. Eichelberger, Ph.D.
Dean of the Graduate School



Date

RETROGRESSIVE THAW SLUMPS AND ACTIVE LAYER DETACHMENT SLIDES
IN THE BROOKS RANGE AND FOOTHILLS OF NORTHERN ALASKA:
TERRAIN AND TIMING

A
DISSERTATION

Presented to the Faculty
of the University of Alaska Fairbanks

in Partial Fulfillment of the Requirements
for the Degree of

DOCTOR OF PHILOSOPHY

By

Andrew W. Balser, M.S., B.A.

Fairbanks, Alaska

May 2015

© 2015 Andrew Wentworth Balser

Abstract

Permafrost degradation is widespread throughout the circumpolar north, occurring by multiple modes and mechanisms on many types of landscapes. The pan-arctic rate of permafrost degradation is reportedly increasing, and permafrost carbon and nitrogen release are likely to be major contributors to global atmospheric greenhouse gas concentrations in coming decades. Locally, liberation of previously frozen substrates, organic materials, and nutrients alters the ecology of receiving streams, causes ecological and hydrobiogeochemical impacts in lake ecosystems, and impacts vegetation through disturbance, nutrient release, and succession on altered surfaces.

Understanding the diverse modes of permafrost landscape response to climate, within time and space, is critical to questions of future impacts and feedbacks to climate change. Active layer detachment sliding and retrogressive thaw slumping are important modes of upland permafrost degradation and disturbance throughout the low arctic, and have been linked with climate warming trends, ecosystem impacts, and permafrost carbon release. In the Brooks Range and foothills study region of northwest Alaska, active layer detachment slides and retrogressive thaw slumps are widespread and prominent modes of permafrost degradation. Their distribution has been partially correlated with landscape properties, especially upper permafrost characteristics. However, drivers of active layer detachment slide and retrogressive thaw slump distribution and initiation triggering mechanisms, are poorly understood in this region, and detailed spatial distribution of permafrost characteristics is particularly lacking for the entire area.

To better understand retrogressive thaw slump initiation triggers, this research used archived ERS-1 synthetic aperture RADAR data (1997-2010) to determine the year of first detection for 21 active retrogressive thaw slumps in the Noatak Basin, and examined weather records from remote and regional weather stations (1992-2011), along with satellite image-derived seasonal snowpack distribution (2000-2012) for correlations among weather, snowpack duration, and the timing of retrogressive thaw slump initiation. Most slumps first appeared within a 13 month span beginning June of 2004. Early summer 2004 was distinct in the weather records for anomalously warm early thaw-season temperatures, intense rainfall events in May, and unusually early dissipation of the annual snowpack. Results suggest that, regionally, retrogressive thaw slump initiation may be clustered in time, in response to seasonal shifts or anomalous weather events, and that future landscape response to climate change may depend on the nature and timing of climate change as much as overall magnitude.

The project examined inter-related and co-varying terrain properties at specific sites to identify relationships among terrain properties and permafrost characteristics. Consistent relationships among

vegetation, surficial geology and permafrost characteristics were found using multiple factor analysis ordination of empirical data from diverse field sites throughout the region. Ordination results suggest relevant relationships among these factors to support regional-scale spatial analysis of terrain and permafrost properties. Field sites were also found to form consistent groupings from hierarchical clustering of ordination results, suggesting that relationships among these factors remain relevant across diverse gradients of landscape conditions in the region.

Several thousand observed feature locations of active layer detachment slides and retrogressive thaw slumps were then used to examine region-wide terrain suitability based on terrain properties including: surficial geology, topography, geomorphology, vegetation and hydrology. Structural equation modeling and integrated terrain unit analyses confirmed and identified the nature and relative strength of relationships among terrain factors explaining observed feature distribution. These results may partially correspond with permafrost ground ice conditions as well, which is further supported by our ordination results. Analysis results drove mapped estimates of terrain suitability for active layer detachment slides and retrogressive thaw slumps across the region, enabling better estimates of permafrost carbon vulnerable to release, and ecosystems potentially impacted by these modes of permafrost degradation. Up to 57% of the study region may contain 'suitable' terrain for one or both of these features. Results support a 'state factor' approach as a useful organizing framework for assessing and describing terrain suitability, and for examining drivers of permafrost characteristics.

Table of Contents

	Page
Signature Page	i
Title Page	iii
Abstract	v
Table of Contents	vii
List of Figures	xiii
List of Tables	xix
List of Appendices	xxiii
Acknowledgements	xxvii
Dedication	xxix
Chapter 1. Introduction	1
1.0 Permafrost Landscapes	1
1.1 Active Layer Detachment Slides and Retrogressive Thaw Slumps	2
1.2 Degradation Modes and Terrain Properties	4
1.3 Terrain Properties as State Factors	5
1.4 Study Region	5
1.5 Goals of this Research	9
Chapter 2	10
Chapter 3	11
Chapter 4	12
1.6 Authorship	13

	Page
Chapter 2. Timing of Retrogressive Thaw Slump Initiation in the Noatak Basin, Northwest Alaska....	15
2.0 Abstract	15
2.1 Introduction.....	15
2.2 Methods.....	17
2.2.1 Study Area	17
2.2.2 Field Surveys of Retrogressive Thaw Slump Features in the Noatak Basin.....	18
2.2.3 Year of First Detection.....	19
2.2.4 Inter-annual Weather.....	20
2.2.5 Inter-annual Snow Cover	22
2.3 Results.....	22
2.3.1 Initiation Timing of Retrogressive Thaw Slumps	22
2.3.2 Inter-annual Weather Patterns.....	22
2.3.3 Inter-annual Snow Cover	23
2.4 Discussion	24
2.4.1 Timing of Weather Events	24
2.4.2 Weather & Initiation Mechanisms	25
2.5 Conclusions.....	26
2.6 Acknowledgements.....	26
2.7 References.....	27
Appendix 2. Retrogressive thaw slump features in the Noatak National Preserve from Chapter 2.....	45

	Page
Chapter 3. Relationship of Cryofacies, Surface and Subsurface Terrain Conditions in the Brooks Range and Foothills of Northern Alaska	53
3.0 Abstract.....	53
3.1 Introduction.....	53
3.1.1 Responses and Feedbacks to Climate	54
3.1.2 Landscape Variability	55
3.1.3 Integrating Terrain Properties	55
3.2 Methods.....	56
3.2.1 Study Region.....	56
3.2.2 Field Surveys	57
3.2.3 Data Analysis	58
3.2.3.1 Data Reduction.....	58
3.2.3.2 Multiple Factor Analysis Ordination	59
3.3 Results.....	60
3.3.1 Hierarchically Clustered Groupings.....	61
Group E1	61
Group E2	62
Group E3	62
Group E4	63
3.3.2 Relationships Among Sites and Groups.....	64
3.4 Discussion	64
3.5 Conclusions.....	67

	Page
3.6 Acknowledgements.....	67
3.7 References.....	67
Appendix 3. Field Codes for Site Survey in Chapter 3.....	91
Chapter 4. Drivers and Estimates of Terrain Suitability for Active Layer Detachment Slides and Retrogressive Thaw Slumps in the Brooks Range and Foothills of Northwest Alaska	95
4.0 Abstract.....	95
4.1 Introduction.....	95
4.2 Methods.....	98
4.2.1 Study Region.....	98
4.2.2 Analysis Overview.....	100
4.2.3 Steps for Terrain Suitability Analysis and Estimation.....	101
4.2.3.1 Collection and Preparation of Input Data.....	101
Feature Locations.....	101
Landscape Properties and Metrics	102
4.2.3.2 Integrated Terrain Unit Analysis.....	102
4.2.3.3 Structural Equation Modeling	103
4.2.3.4 Final Terrain Suitability Estimates (combined ITU and SEM results)	104
4.3 Results.....	105
4.3.1 Final Terrain Suitability Estimates	105
4.3.2 Active Layer Detachment Slide & Retrogressive Thaw Slump Terrain Descriptions.....	105
4.3.3 Integrated Terrain Unit Analysis Results.....	106
4.3.4 Structural Equation Modeling Results	107

	Page
4.3.5 Terrain Suitability Values and Thresholds.....	107
4.3.6 Landscape Properties by Final Terrain Suitability.....	108
4.4 Discussion.....	109
4.5 Conclusions.....	112
4.6 Acknowledgements.....	112
4.7 References.....	113
Appendix 4. Extended Methods and Results for Chapter 4.....	145
Chapter 5. Conclusions.....	191
5.1 Summary.....	191
5.2 Synthesis.....	191
5.3 References.....	194
Appendices.....	203

List of Figures

	Page
Figure 1.1. Active layer detachment slide.....	3
Figure 1.2. Retrogressive thaw slump	4
Figure 1.3. The central and western Brooks Range and foothills, northern Alaska.....	6
Figure 1.4. Western Baird Mountains, Brooks Range, northwest Alaska	12
Figure 2.1. Retrogressive thaw slump No. 14.....	32
Figure 2.2. Study area in the Noatak Basin in northwest Alaska	33
Figure 2.3. Imagery for RTS 9 and RTS 10 in the Cutler River drainage, Noatak Basin, Alaska	34
Figure 2.4. Locations of NOAA National Weather Service climate stations in northwest Alaska, active during 2003 and 2004.....	35
Figure 2.5. Year of first detection for 21 retrogressive thaw slumps in the Noatak Basin	36
Figure 2.6. Average daily summer temperature, thawing index, number of days averaging above 0°C, and seasonal thawing temperature distribution (as center of mass, C_T) from two remote automated weather (RAW) stations in the Noatak basin, 1992-2011	37
Figure 2.7. Monthly temperature and precipitation estimates as a departure from average, winter of 2003 through 2004	38
Figure 2.8. Snow cover metrics spatially clipped for the combined Noatak River and Wulik River watersheds (Figure 2.9), from the MODIS Snow Climatology (2001-2012) dataset.....	39
Figure 2.9. Spatial distribution of 2004 continuous snow season end date, as a difference from the mean end date for 2001 through 2012, calculated from the MODIS Snow Climatology (2001-2012) NASA dataset.....	40
Figure 3.1. Study region in northern Alaska.....	75
Figure 3.2. Generalized landscape characteristics of the study region	76
Figure 3.3. Permafrost degradation features providing access to permafrost profile exposures.....	77

	Page
Figure 3.4. Upper permafrost profile exposure.....	78
Figure 3.5. Field sites displayed by grouping and with active categorical variables overlain on graphed MFA results	79
Figure 3.6. Influence of quantitative variables, shown by block, on the 3-dimensional MFA ordination driving clustered site groupings	80
Figure 3.7. Dendrogram from hierarchic clustering of MFA results, showing groupings E1-E4.....	81
Figure 3.8. Distribution of field sites by grouping.....	82
Figure 3.9. Photos of sites from groups E1, E2, E3 and E4.....	83
Figure 4.1. Active layer detachment, Noatak Basin, northwest Alaska.....	121
Figure 4.2. Retrogressive thaw slump, Noatak Basin, northwest Alaska	122
Figure 4.3. Map of the study region.....	123
Figure 4.4. Initial conceptual model diagram of hypothesized landscape drivers of terrain suitability for active layer detachment slide (ALD) and retrogressive thaw slump (RTS) features	124
Figure 4.5. Overview of analysis approach for estimating active layer detachment slide (ALD) and retrogressive thaw slump (RTS) terrain suitability in the central and western Brooks Range, Alaska	125
Figure 4.6. Map of observed active layer detachment slides and retrogressive thaw slumps within the study region in the western Brooks Range and foothills of northern Alaska.....	126
Figure 4.7. Map of estimated terrain suitability for active layer detachment slides (green) and retrogressive thaw slumps (red) for the study region in the western Brooks Range of northern Alaska	127
Figure 4.8. Areal estimates of suitability for active layer detachment (ALD) and retrogressive thaw slump (RTS) terrain	128

	Page
Figure 4.9. Areas estimated as highly suitable terrain for A) active layer detachment slides (green) and B) retrogressive thaw slumps (red)	129
Figure 4.10. Active layer detachment slide and retrogressive thaw slump terrain in an upland setting .	130
Figure 4.11. Active layer detachment slide and retrogressive thaw slump terrain in a lowland setting .	131
Figure 4.12. Final, fitted structural equation model (SEM) diagram for active layer detachment slide (ALD) terrain suitability	132
Figure 4.13. Final, fitted structural equation model (SEM) diagram for retrogressive thaw slump (RTS) terrain suitability	133
Figure 4.14. Frequency distributions of estimated terrain suitability for active layer detachment slide features, retrogressive thaw slump features, and randomly generated landscape control points within the study region in the central and western Brooks Range, Alaska	134
Figure 4.15. Areal extent of categorical landscape properties by active layer detachment slide (ALD) and retrogressive thaw slump (RTS) terrain suitability, and for the study region in the central and western Brooks Range, Alaska.....	135
Figure A4.1.1. Map of the study region.....	162
Figure A4.1.2. Conceptual Model.....	163
Figure A4.1.3. Overview of analysis approach.....	164
Figure A4.1.4. Observed active layer detachment slides and retrogressive thaw slumps within the study region in the western Brooks Range and foothills of northern Alaska.....	165
Figure A4.2.5. Estimated terrain suitability for active layer detachment slides (green) and retrogressive thaw slumps (red) for the study region in the western Brooks Range of northern Alaska.....	166
Figure A4.2.6. Areal estimates of suitability for active layer detachment (ALD) and retrogressive thaw slump (RTS) terrain.....	167

	Page
Figure A4.2.7. Areas estimated as highly suitable terrain for A) active layer detachment slides (green) and B) retrogressive thaw slumps (red) for the study region in the western Brooks Range of northern Alaska	168
Figure A4.2.8. Active layer detachment slide (ALD) and retrogressive thaw slump (RTS) terrain suitability in an upland setting	169
Figure A4.2.9. Active layer detachment slide (ALD) and retrogressive thaw slump (RTS) terrain suitability in a lowland setting	170
Figure A4.2.10. Final, fitted structural equation model (SEM) diagram for active layer detachment slide (ALD) terrain suitability	171
Figure A4.2.11. Final, fitted structural equation model (SEM) diagram for retrogressive thaw slump (RTS) terrain suitability	172
Figure A4.2.12. Frequency distributions of estimated terrain suitability for active layer detachment slide features, retrogressive thaw slump features, and randomly generated landscape control points within the study region in the central and western Brooks Range, Alaska	173
Figure A4.2.13. Areal extent of categorical landscape properties by active layer detachment slide (ALD) and retrogressive thaw slump (RTS) terrain suitability, and for the study region in the central and western Brooks Range, Alaska	174
Figure AB.1 Map of study area.....	330
Figure AB.2 DOC loss in water from collapsing permafrost and reference water tracks after 40 days of lab incubation at room temperature and initial DOC concentration.....	331
Figure AB.3 Fitted vs. actual DOC loss.....	332
Figure AB.4 DOC loss after 40 day incubation at room temperature.....	333
Figure AB.5 Response of fast BDOC (DOC loss from $t_0 - t_{10}$) to nutrient addition.....	334
Figure AB.6 Comparison of BDOC between thaw slump and gully thermokarst features while controlling for activity level.....	335

	Page
Figure AB.7 Comparison of BDOC and SUVA ₂₅₄ between moist acidic tundra (MAT), moist non-acidic tundra (MNAT), and shrub tundra (Shrub), controlling for activity level.....	336
Figure AB.8 Seasonal patterns of DOC biodegradability for two gullies and two water tracks.....	337
Supplementary Figure AB.1 Photos of the three most common upland thermokarst morphologies in the foothills of the Brooks Range on the North Slope of Alaska.	338
Supplementary Figure AC.1 Map: Terrain Suitability for Active Layer Detachments and Retrogressive Thaw Slumps in the Brooks Range and Foothills of Northern Alaska.(24" x 48" GeoPDF)	Map Sheet

List of Tables

	Page
Table 2.1. Retrogressive thaw slump features in the Noatak Basin chosen for this study.....	41
Table 2.2. Maximum temperature and number of days with temperature above freezing for NOAA and RAWS stations proximal to the study area.....	42
Table 2.3. May 2004 precipitation at the NOAA and RAWS stations in the study area.....	43
Table 2.4. Full snow season (FSS) and continuous snow season (CSS) end date metrics for 2004 in the combined Noatak and Wulik River basin study area, and in the smaller subset of the Noatak River basin from the headwaters through the Mission Lowlands.....	44
Table A2.1. Retrogressive thaw slump feature locations in the Noatak National Preserve.....	45
Table 3.1. Variables characterizing conditions in the vicinity of each permafrost profile exposure.....	84
Table 3.2. Variables characterizing soil and permafrost properties in the vicinity of each permafrost profile exposure.....	85
Table 3.3. Active (response) and supplemental (explanatory) variables used for statistical analysis and subsequent grouping by hierarchical clustering.....	86
Table 3.4. Summary values for field-estimates characterizing soil and permafrost properties in the vicinity of each permafrost profile exposure, presented by grouping from hierarchical clustering of MFA ordination results.....	87
Table 3.5. Site groupings compared by permafrost degradation mode.....	88
Table 3.6. Field sites by group with ground coordinates (Geographic decimal degrees, NAD83).....	89
Table 4.1. Input data sets used for terrain suitability analyses for active layer detachment slides (ALD) and retrogressive thaw slumps (RTS) within the study region in the central and western Brooks Range of northern Alaska.....	136
Table 4.2. Derived variables used in structural equation model (SEM) analyses.....	137
Table 4.3. Pearson correlation coefficients for variables tested with structural equation modeling, calculated for the entire study region.....	138

Table 4.4. Areal estimates of active layer detachment slide (ALD) and retrogressive thaw slump (RTS) terrain suitability for integrated terrain unit (ITU) and structural equation model (SEM) analyses, and for the final model which combines ITU and SEM results	138
Table 4.5. Categorical landscape properties as a percentage study region, by percentage retrogressive thaw slump (RTS) and active layer detachment slide (ALD) distribution, and differential .	139
Table 4.6. Structural equation model fit metrics (Hooper et al., 2008) from ten bootstrapped model runs for active layer detachment slide (ALD) and ten bootstrapped model runs for retrogressive thaw slump (RTS) terrain suitability in the central and western Brooks Range, Alaska	140
Table 4.7. Structural equation model R2 values from ten bootstrapped model runs for active layer detachment slide (ALD) and ten bootstrapped model runs for retrogressive thaw slump (RTS) terrain suitability in the central and western Brooks Range, Alaska.....	141
Table 4.8. Numeric landscape properties within the study region, and by terrain suitability for active layer detachment slides and retrogressive thaw slumps.....	142
Table 4.9. Numeric landscape properties for randomly-assigned control locations, and for observed active layer detachment slide and retrogressive thaw slump features.....	143
Table A4.1.1. Input data sets used for terrain suitability analyses for active layer detachment slides (ALD) and retrogressive thaw slumps (RTS) within the study region in the central and western Brooks Range of northern Alaska	175
Table A4.1.2. Derived variables used in structural equation model (SEM) analyses.....	176
Table A4.1.3. Variables and values used for categorical analysis of terrain suitability for the study region in the central and western Brooks Range, Alaska.....	177
Table A4.1.4. Pearson correlation coefficients for variables tested with structural equation modeling, calculated for the entire study region.....	179
Table A4.2.5. Areal estimates of active layer detachment slide (ALD) and retrogressive thaw slump (RTS) terrain suitability for integrated terrain unit (ITU) and structural equation model (SEM) analyses, and for the final model which combines ITU and SEM results.....	179

Table A4.2.6. Pearson correlations for active layer detachment slide (ALD) and retrogressive thaw slump (RTS) terrain suitability estimates from integrated terrain unit (ITU) and structural equation model (SEM) analyses.....	180
Table A4.2.7. Categorical landscape properties as a percentage study region, by percentage retrogressive thaw slump (RTS) and active layer detachment slide (ALD) distribution, and differential.....	181
Table A4.2.8. Structural equation model fit metrics from ten bootstrapped model runs for active layer detachment slide (ALD) and ten bootstrapped model runs for retrogressive thaw slump (RTS) terrain suitability in the central and western Brooks Range, Alaska	182
Table A4.2.9. Structural equation model R^2 values from ten bootstrapped model runs for active layer detachment slide (ALD) and ten bootstrapped model runs for retrogressive thaw slump (RTS) terrain suitability in the central and western Brooks Range, Alaska	183
Table A4.2.10. Areal extent of glacial geology units and noncarbonate lithologies within the study region, and by terrain suitability for active layer detachment slides (ALD) and retrogressive thaw slumps (RTS) in the central and western Brooks Range, Alaska	184
Table A4.2.11. Areal extent of ecotypes within the study region, and by terrain suitability for active layer detachment slides and retrogressive thaw slumps	185
Table A4.2.12. Numeric landscape properties within the study region, and by terrain suitability for active layer detachment slides and retrogressive thaw slumps.....	186
Table A4.2.13. Numeric landscape properties for randomly-assigned control locations, and for observed active layer detachment slide and retrogressive thaw slump features	187
Table A4.2.14. Area of suitable climate conditions for active layer detachment slides and retrogressive thaw slumps for the 1910-1919 and 1990-1999 timeframes	188
Table A4.2.15. Climate metrics for randomly-assigned control locations, and for observed active layer detachment slide and retrogressive thaw slump features	189

	Page
Table A4.2.16. Climate metrics within the study region, and by terrain suitability for active layer detachment slides and retrogressive thaw slumps.....	190
Table AA.1. Active layer detachment slides and retrogressive thaw slump locations within the study region; central and western Brooks Range, Alaska.....	204
Table AB.1 Summary of site characteristics including DOC concentration and biodegradability, feature type, vegetation, and ecotype	339
Table AB.2 Carbon, nitrogen and water chemistry parameters by thermokarst activity level	340
Table AB.3 Correlations between water chemistry parameters, site activity, and DOC biodegradability	341
Table AB.4 Multiple linear regression models for four metrics of DOC biodegradability	342

List of Appendices

	Page
Appendix 2. Retrogressive thaw slump features in the Noatak National Preserve from Chapter 2	45
Appendix 3. Field Codes for Site Survey in Chapter 3	91
A3.1. Field Code Data Sheets used for Field Surveys in Chapter 3	92
Appendix 4. Extended Methods and Results for Chapter 4	145
A4.1 Extended Methods.....	145
A4.1.1 Study Region	145
A4.1.2 Overview of terrain suitability analysis	148
A4.1.3. Steps for terrain suitability analysis and estimation.....	149
A4.1.3.1 Collection and preparation of input data	149
A4.1.3.2 Integrated terrain unit analysis	150
A4.1.3.3 Structural equation modelling	151
A4.1.3.4 Final terrain suitability estimates (combined ITU and SEM results).....	152
A4.1.3.5 Terrain suitability thresholds.....	152
A4.1.4 Landscape properties by terrain suitability	153
A4.2. Extended results	153
A4.2.1 Final terrain suitability estimates	153
A4.2.2 Active layer detachment slide and retrogressive thaw slump terrain descriptions.....	153
A4.2.3 Integrated terrain unit (ITU) analysis results	155
A4.2.4 Structural equation modeling (SEM) analysis results	155
A4.2.5 Terrain suitability values and thresholds.....	156

	Page
A4.2.6 Landscape properties by final terrain suitability	156
A4.3 References for extended methods and results	158
Appendix A. Active layer detachment slide and retrogressive thaw slump locations within the study region for Chapter 4	203
Appendix B. Elevated dissolved organic carbon biodegradability from thawing and collapsing permafrost	309
AB.1 Key Points	309
AB.2 Abstract	309
AB.3 Key words.....	309
AB.4 Introduction	310
AB.5 Methods.....	311
AB.5.1 Study sites.....	311
AB.5.2 Sample collection and analysis.....	312
AB.5.3 BDOC assays.....	312
AB.5.4 Nutrients and DOC chemical composition.....	314
AB.5.5 Thermokarst activity, type, and vegetation	314
AB.5.6 Seasonal changes in BDOC.....	315
AB.5.7 Additional statistics	315
AB.6 Results	315
AB.6.1 Site activity.....	315
AB.6.2 Nutrients and DOC chemical composition.....	316
AB.6.3 Feature and vegetation type.....	317

	Page
AB.6.4 Seasonal patterns of BDOC.....	318
AB.7 Discussion	318
AB.7.1 Permafrost DOC pools and biodegradability.....	318
AB.7.2 DOC composition.....	318
AB.7.3 Nutrients	319
AB.7.4 Acidic and nonacidic tundra DOM biodegradability.....	320
AB.7.5 BDOC and thermokarst morphology.....	321
AB.7.6 Why is permafrost DOC so biodegradable?	321
AB.8 Conclusions	322
AB.9 Acknowledgments	323
AB.10 References	323
Appendix C. Terrain Suitability for Active Layer Detachments and Retrogressive Thaw Slumps in the Brooks Range and Foothills of Northern Alaska.(24" x 48" GeoPDF)	Map Sheet
Appendix D. Active Layer Detachment and Retrogressive Thaw Slump Terrain Suitability in the Brooks Range and Foothills of Northern Alaska.(Multiband GeoTIFF)	Digital Data

Acknowledgements

Among Dr. Jeremy B. (Jay) Jones' multiple titles is 'advisor', and I can think of no one who fits the description better. His willingness to translate his experience and perspective into efficient, effective, actionable advice has been invaluable, and is something for which I will always be very grateful. His dedication to the integrity of the process and the resulting science created a rewarding atmosphere that made many of the difficult questions within the research much easier to tackle. I also extend great thanks to my graduate committee of Dr. Rudiger Gens, Dr. Michelle C. Mack, and Dr. Donald A. (Skip) Walker. Through conversations with each of them, I had the enjoyment of feeling my ideas and thinking evolve in real-time (though some of their questions may have made me think a little more than was comfortable at that moment). Their thoughts about the science, and about topics well beyond, stick with me in all the best of ways.

M. Torre Jorgenson was very generous in sharing his deep and extensive experience with landscapes, permafrost, cryostructures, and vegetation; I am still amazed by how much he taught me. Equally appreciated was his sense of humor while standing knee-deep in mud, in a sideways downpour, trying to keep a thawing permafrost exposure prepped and clear for sampling. The friendly encouragement and generous support of Dr. Daniel J. Hayes were helpful beyond measure during the final stages of this dissertation, and served as strong inspiration to pay it forward and pay it back.

My years in Alaska, much less this degree, would likely have never happened without the serendipitous intervention of Dr. William G. Howland, and Dr. Steven B. Young in Vermont. Both of them were pivotal in transforming a youthful fascination with the natural world and with the north into a career and a life path. Hikes up Mt. Mansfield, and my first remote sensing project with Bill are still vivid, great memories. Steve's forbearance with a van full of un-showered, eccentrically-humored college kids rumbling along endless kilometers of Canadian washboard roads for weeks on end is still the stuff of legend, and that last trip to Feniak Lake was simply incredible.

Dr. John G. (Jock) Irons was here at the other end, helping me get my first job in Fairbanks in 1993, and helping to form the Frosty Bottom Boys (and Girl), which really helped get me through this dissertation research. Picking tunes with all of you has been a real privilege and a great pleasure. Fellow students, lab mates and friends are equally treasured, through field work, winter trips, the White Mountains 100, and many other things. Archana Bali's smile stands out especially, and her kindness, especially during my comps, is still humbling.

My parents may not fully understand the attraction to places regularly bathed in frigid temperatures and total darkness, but they never hesitated to encourage me to pursue ideas, dreams and

challenges, in spite of the real sacrifices required on their part. That encouragement made all else possible. I like to think they get to live the best parts of it vicariously, and have enjoyed the occasional smoked salmon, moose dinners and outhouse visits.

Finally, the steady encouragement, genuine support, quiet patience, and sane, grounded perspective of Teri C. Balsler are appreciated beyond measure. All of it makes the biggest difference, and for no better partner could I wish.

The aviation skill and safety of pilots Tom George, Stan Hermens, Tommy Levanger, Terry Day, Jim Kincaid, Christian Cabanilla and Buck Mackson were indispensable to this work. Coming back from amazing places with the data in-hand is a great thing; coming back safely and in one piece is even better.

The National Park Service Arctic Network has been a key partner in many aspects of this research, beginning in 2005. Many of these results would not have been possible without their initiative and support, and their dedicated stewardship of some of our greatest public-trust resources provides us a legacy well beyond the bounds of ecological research. This work was supported by a University of Alaska Fairbanks Center for Global Change (CGC) Student Research Grant, and by National Science Foundation (NSF) ARCSS Program (ARC-0806465).

Dedication

To my daughter, Madeleine
in hopes that you remain elemental,
and fondly remember where you were born.

*"There is an ecstasy that marks the summit of life, and beyond which life cannot rise.
And such is the paradox of living, this ecstasy comes when one is most alive, and it
comes as a complete forgetfulness that one is alive."*

- J. London

Chapter 1. Introduction

1.0 Permafrost Landscapes

Permafrost degradation is widespread throughout the circumpolar north, occurring by multiple modes and mechanisms across diverse landscapes (Serreze et al. 2000, Hinzman et al. 2005, Anisimov and Reneva 2006, Jorgenson et al. 2008a). Pan-arctic rates of permafrost degradation are increasing, and permafrost soils are estimated to store roughly 1,700 Pg of soil carbon, which is more than half of the global soil carbon stock and twice the current atmospheric load (Zimov et al. 2006, Tarnocai et al. 2009, Zimov et al. 2009). Permafrost carbon and nitrogen release will likely be major contributors to atmospheric greenhouse gas concentrations in coming decades (Schuur et al. 2008, Grosse et al. 2011, Schaefer et al. 2011), though estimated amounts and pathways are still under much debate (Slater and Lawrence 2013, Schaefer et al. 2014). Carbon and nitrogen released from frozen substrates may substantially contribute to atmospheric concentrations of CH₄, CO₂, and N₂O, and strongly affect global biogeochemistry and climate (Walter et al. 2006, Walter et al. 2007, Schuur et al. 2008, Desyatkin et al. 2009, Gooseff et al. 2009, Tarnocai et al. 2009, Grosse et al. 2011). Locally, liberation of previously frozen substrates, organic materials, and nutrients alters the ecology of receiving streams (Bowden et al. 2007, Bowden et al. 2008, Frey and McClelland 2009, Gooseff et al. 2009, Rozell 2009), impacts sediment loads of streams and rivers (Walker et al. 1987, Walker and Hudson 2003, Gooseff et al. 2009), and causes ecological and hydrobiogeochemical impacts in lake ecosystems (Kokelj et al. 2005, Thompson et al. 2008, Kokelj et al. 2009b, Mesquita et al. 2010). Vegetation within and adjacent to permafrost degradation is also directly impacted through disturbance, nutrient release, and succession on altered surfaces (Lantz and Kokelj 2008, Lantz et al. 2009).

Diverse permafrost landscapes are critical components of global climate change, but responses and feedbacks depend on ecosystem properties which vary markedly among landscapes throughout the low arctic. Permafrost landscape structure develops through a complex interplay among climate, substrate and surficial processes operating at multiple spatial and temporal scales (Shur and Jorgenson 2007). At the interface between the atmosphere above and the deep permafrost below, vegetation, soil, and upper-permafrost cryostructures respond to climate shifts and disturbance (Viereck 1973, ACIA 2005, Jorgenson et al. 2010a, Jorgenson et al. 2013), and mediate the influence of climate on deeper permafrost (Shur and Jorgenson 2007, French and Shur 2010). Vegetation and upper permafrost horizon development have been linked with terrain property and climate drivers (Kreig and Reger 1982, Shur 1988, Shur and Jorgenson 2007, Pastick et al. 2014a), and are mutually influential at local and circumarctic scales, though the nature and extent of relationships among vegetation and permafrost is only partially understood (Raynolds and Walker 2008, Walker et al. 2008, French and Shur 2010, Lantz et

al. 2010, Kokelj and Jorgenson 2013). Terrain properties and permafrost characteristics co-vary, and consistency of associations among permafrost, terrain and vegetation may enable landscape-scale analysis on that basis (Jorgenson and Kreig 1988, Reynolds and Walker 2008, Jorgenson et al. 2010a, Jorgenson et al. 2013, Pastick et al. 2014a).

Local to global impacts of permafrost degradation may be highly dependent on the particular mode of degradation (Abbott 2014, Lamoureux and Lafreniere 2014), and mode of degradation is highly dependent upon permafrost landscape terrain characteristics (Lewkowicz 1992, Jorgenson et al. 2008a, Kokelj and Jorgenson 2013). Distinct modes of permafrost degradation correlate with specific combinations of surficial landscape properties, each with a different influence on ecological, hydrological, and biogeochemical shifts, and characterized by distinct morphologies and processes (Hinzman et al. 2005, Jorgenson et al. 2008b, Schuur et al. 2009, Lafreniere and Lamoureux 2013). Modes of permafrost degradation include active-layer deepening, as well as an array of subsidence features broadly termed ‘thermokarst’ (Hinzman et al. 2005, Jorgenson et al. 2008b). These different modes affect ecosystems at different depths, rates, and scales, in turn driving the nature and magnitude of impacts and feedbacks (Jorgenson et al. 2013). Modes of permafrost degradation in response to climate perturbation or disturbance are driven by local surficial conditions, including thermal properties, thaw stability, slope, hydrology and ground ice characteristics (Leibman et al. 2003, Lewkowicz and Harris 2005, Jorgenson et al. 2008b, Kokelj et al. 2009a, Jorgenson et al. 2010a, Lantuit et al. 2012). Thermal properties, thaw stability, and hydrology are influenced by cryostructure distribution and ground ice content, vegetation, soil composition and organic layer development (Shur and Jorgenson 2007).

1.1 Active Layer Detachment Slides and Retrogressive Thaw Slumps

Active layer detachment sliding (ALD) and retrogressive thaw slumping (RTS) are widespread and are the most prevalent of nineteen identified modes of permafrost degradation in the Brooks Range and foothills of northwest Alaska. Active layer detachment sliding and retrogressive thaw slumping include thaw of ice-rich permafrost on hill slopes or bluffs, causing soil structural instability and mass-wasting subsidence (Burn and Lewkowicz 1990, Leibman 1995, Leibman et al. 2003, Lewkowicz and Harris 2005, Jorgenson et al. 2008a). Active layer detachment sliding occurs on hill slopes where shear strength of active layer soils is exceeded by pore water pressures, and the destabilized active layer slides down slope, exposing the permafrost table below (Figure 1.1; Jorgenson and Osterkamp 2005, Lewkowicz and Harris 2005, Lewkowicz 2007).

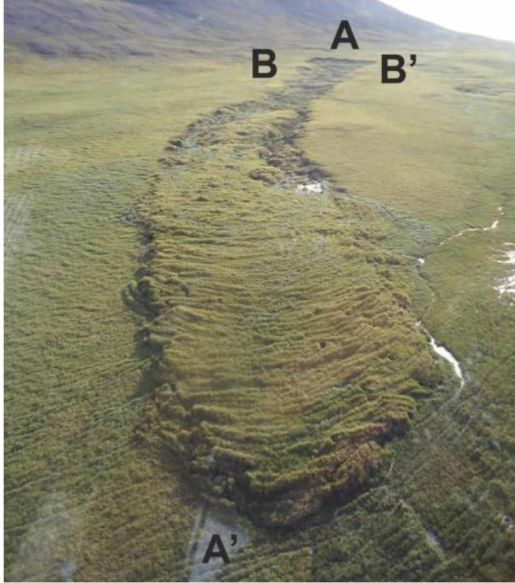


Figure 1.1. Active layer detachment slide.

Active layer detachment slide on a northeast facing 6° slope, on a deposit of colluvium and loess in the upper Fauna Creek drainage Noatak Basin, northwest Alaska. Length from headwall (A) to end of overburden debris flow (A') is 483 m; width at widest point (B to B') is 58 m, as of July 2011. Deepest point was 3.5 m in the upper portion near the headwall (A). Photo: A. W. Balser, 2011

Warm weather and intense precipitation events have both been observed as ALD triggers (Leibman et al. 2003, Lamoureux and Lafreniere 2009), particularly where warm pulses or rainfall accelerate thaw front advance through syngenetic cryofacies containing an ice-rich intermediate layer beneath the active layer (Shur 1988, French and Shur 2010). Active layer detachment sliding is episodic, with features often appearing clustered together in space and time, and with active degradation confined to one or two consecutive thawing seasons (Leibman 1995, Lamoureux and Lafreniere 2009, Lamoureux and Lafreniere 2014). In some settings, conditions at prior active layer detachment sites redevelop over decades or centuries, with repeat initiation in response to triggering events (Leibman 1995, Khomutov 2012).

Retrogressive thaw slump formation can stem from at least several distinct mechanisms leading to exposure of ice-rich permafrost deposits (including pore, segregation, and massive ice). In coastal and riparian settings, lateral thermal erosion of protective overburden from adjacent bluffs can expose permafrost deposits typically rich with massive ice (Burn and Lewkowicz 1990, Lantuit et al. 2012, Kokelj and Jorgenson 2013). Wildfire which removes protective vegetation and organic layers, promoting thaw front advance through the active layer, may cause instability and disturbance (Lacelle et al. 2010). Channelized flow of surface water over networks of ice wedge polygons can melt ice wedges, creating thermo-erosion gullies with progressive downward and lateral thaw into the permafrost (Jorgenson and Osterkamp 2005). Intense precipitation may be a particular trigger for thermo-erosion gullies leading to retrogressive thaw slump initiation (Bowden et al. 2008, Balser et al. 2014). Retrogressive thaw slumps may develop from any of these exposures where conditions promote continued instability with downward

subsidence of thawed material (Burn and Lewkowicz 1990, Jorgenson and Osterkamp 2005, Lacelle et al. 2010, Godin and Fortier 2012, Kokelj and Jorgenson 2013). Once initiated, retrogressive thaw slumps continue to deepen and expand, typically forming a steep headwall up to 20 m deep, an arcing headwall scarp, a floor of thawed and flowing debris, and a run out of re-stabilizing deposits (Figure 1.2; Burn and Lewkowicz 1990, Lacelle et al. 2010, Lantuit et al. 2012, Kokelj and Jorgenson 2013).

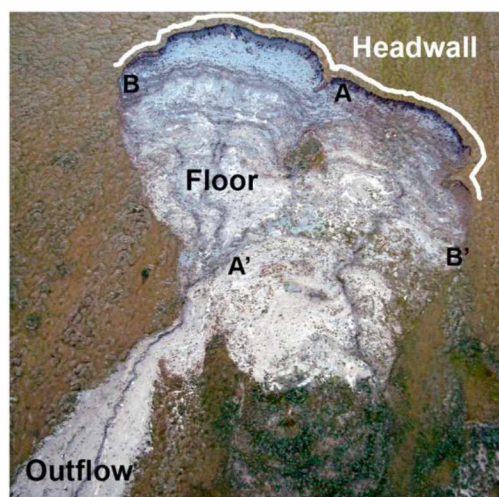


Figure 1.2. Retrogressive thaw slump. Retrogressive thaw slump on a west facing 6° slope on a late Pleistocene glaciolacustrine deposit in the upstream portion of the Aniuk Lowlands, Noatak Basin, Alaska. This slump is polycyclic, having initiated in 2004 from a previously re-stabilized and inactive retrogressive thaw slump. Length from headwall to beginning of outflow (A to A') is 181 m; width at widest point (B to B') is 287 m, as of July 2011. Deepest point was 14m at the base of the headwall near (A). Photo: A. W. Balsler, 2011

Headwall retreat rate ranges from several to tens of meters annually and is correlated with headwall height, ice content, and local climate (Kokelj and Jorgenson 2013). Expansion may continue for decades if thawed debris continues to subside and expose the headwall, and if newly exposed deposits are ice rich and receive sufficient energy for thaw (Lacelle et al. 2010). Retrogressive thaw slumps are frequently polycyclic, alternating between extended periods of stabilized, revegetated dormancy, and active degradation when slumps reinitiate within, or adjacent to, older slump scars. Re-initiation may be caused by mechanisms described above (Lantuit et al. 2012, Kokelj and Jorgenson 2013), with sublimic talik expansion as an additional significant driver in kettle lake basin settings (Kokelj et al. 2009a). Increased retrogressive thaw slump frequency and expansion rates have been generally linked with decadal-scale climate warming trends, but the relative importance of a general warming trend compared with specific weather events is not well-quantified (Lacelle et al. 2010).

1.2 Degradation Modes and Terrain Properties

Permafrost degradation modes have been linked with characteristic terrain properties, and these properties in turn may drive: 1) development of permafrost cryofacies assemblages associated with these modes, and 2) vulnerability to thaw (Jorgenson and Osterkamp 2005, Shur and Jorgenson 2007,

Jorgenson et al. 2008a, Balsler et al. 2009, Gooseff et al. 2009, Jorgenson et al. 2010a). Terrain properties including parent material/surficial geology, topography, geomorphology, vegetation, hydrology, climate and time have been presented as co-varying factors controlling permafrost distribution and active layer thickness (Pastick et al. 2014b), permafrost evolution, permafrost ecosystem response to climate and fire disturbance (Shur and Jorgenson 2007, Jorgenson et al. 2013), active layer depth (Pastick et al. 2014b) and active layer detachment and retrogressive thaw slump occurrence (Jorgenson et al. 2008a, Kokelj and Jorgenson 2013). Positive and negative feedbacks among multiple terrain properties have been identified as key determinants and mediators of landscape response to climate warming and disturbance, and to the distribution of ALD and RTS features (Jorgenson et al. 2008a, Kokelj and Jorgenson 2013) with particular influence on thermal properties of substrate profiles (Shur and Jorgenson 2007, Xie and Gough 2013).

1.3 Terrain Properties as State Factors

Terrain properties have been usefully grouped within a 'state factor' framework and applied to models of soil, permafrost, and vegetation development and distribution (Jenny 1941, van Cleve et al. 1991, Jorgenson et al. 2013). The five state factors: 1) parent material, 2) topography, 3) biota, 4) climate and 5) time (van Cleve et al. 1991) provide an organizational structure to help ensure inclusion of all generally relevant factors, and for testing the nature and strength of relationships among various terrain properties by grouping them in general, functional categories. While these principles are generally accepted, the importance of and relationships among individual terrain properties and state factors as drivers of permafrost conditions and of overall terrain suitability for active layer detachment slide (ALD) and retrogressive thaw slump (RTS) processes are not fully understood, particularly in the Brooks Range and foothills of northwest Alaska.

1.4 Study Region

The study region spanned a gradient of arctic tundra and shrub landscapes abutting the forested, arctic-boreal ecotone, from the east-central portion of Alaska's North Slope (centered on Toolik Field Station) west through the central portion of Alaska's Brooks Range mountains, continuing westward through the Noatak Basin to the Mission Lowlands, near the Noatak River delta (Figure 1.3). These periglacial landscapes are within the continuous permafrost zone (Jorgenson et al. 2008b) and are part of Arctic Bioclimate Subzone E (CAVM-Team 2003). The study region covers approximately 75,000 km², which is slightly larger than the state of West Virginia.

Toolik Field Station sits in the northern Brooks Range foothills on Alaska's North Slope within a matrix of landscapes of varying glacial age, and ecotypes. Physiography ranges from low mountains at

the edge of the Brooks Range to subtle foothills stretching more than 75 km from the mountains to the edge of the arctic coastal plain. Data since most recent glaciation ranges from early Pleistocene to Holocene for field sites surrounding Toolik Field Station, with acidic and nonacidic, graminoid and shrub tundra vegetation reflecting duration of ecosystem development and local site conditions (Walker et al. 1994, Walker et al. 1995, Hamilton 2003, Walker and Maier 2008). Lake and stream density is variable by landscape age-class and related with glacial and periglacial landforms (Hobbie et al. 1991, Kling 1995, Hamilton 2003).

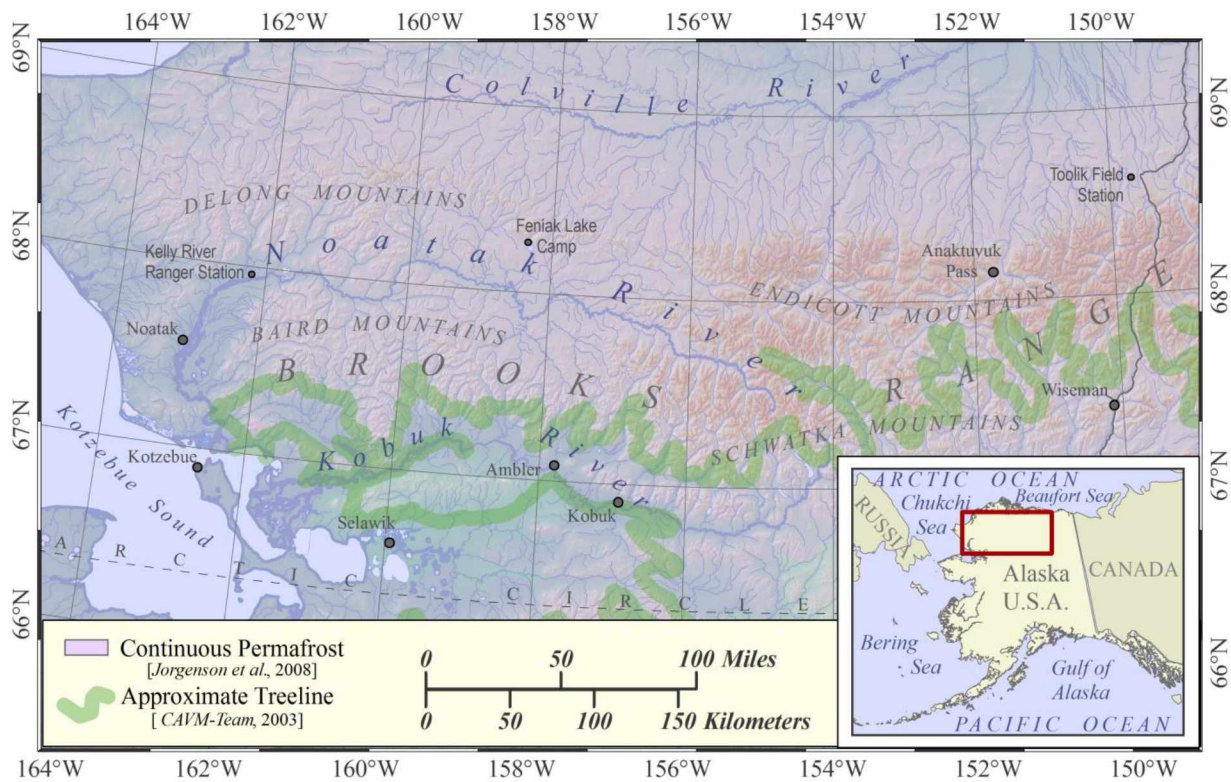


Figure 1.3. The central and western Brooks Range and foothills, northern Alaska. Map by A.W. Balsler.

The central Brooks Range is primarily mountainous terrain within Gates of the Arctic National Park and Preserve (U.S. National Park Service). From the highest elevation on the horn of Mt. Igikpak (2523 m), landscapes grade through foothills to glacially-sculpted valley bottoms containing major rivers flowing radially outward to the north, south, and west. The Noatak River Basin begins in the central Brooks Range and flows 730 km along a westward course at approximately 68° N latitude within the western sub-ranges of the Brooks Range Mountains (Figure 1.3). Most of the basin falls within the Noatak National Preserve (U.S. National Park Service) and is recognized as a UNESCO Biosphere Reserve. Physiographic provinces include high mountains of the Central Brooks Range, through

foothills, valley bottoms and the Aniak Lowland westward, entering the broad, Mission Lowland at the arctic/boreal ecotone near the Noatak mouth (Wahrhaftig 1965, Young 1974).

The study region was periodically glaciated throughout the Pleistocene and contains a patchwork of glacial and periglacial landscapes dating from early Pleistocene to present times (Hamilton 2010, Hamilton and Labay 2011). Mountain physiographic provinces contain significant expanses of exposed bedrock at high elevations, with upper toe slopes covered by thin, often colluvially mixed and re-deposited soils derived from loess, weathered bedrock, and drift, with local pockets of active solifluction (Young 1974, Jorgenson et al. 2010b, Hamilton and Labay 2011). Mountain valley bottoms are primarily underlain by late Pleistocene glacial drift deposits with adjacent ice-contact features, terraces, glacial inwash and outwash. Areas of solifluction become larger and more common with decreasing elevation, and modern alluvium prevails along narrow, contemporary river corridors at lower elevations where mountains grade to foothills (Hamilton 2010, Hamilton and Labay 2011). Rounded foothills interspersed with upland valleys, most of which were overtopped by Pleistocene glaciers, contain a mixture of thin soil deposits over near-surface bedrock on hilltops, below which are loess and middle and late Pleistocene glacial drift, with glacial outwash common at drift deposit margins (Young 1974, Hamilton 2010, Jorgenson et al. 2010b, Hamilton and Labay 2011). Lowland physiographic provinces (Wahrhaftig 1965) are characterized by extensive lateral, recessional, and terminal ice-cored moraines, as well as kettle topography, all associated with middle and late Pleistocene glacial drift surfaces. Lowland bottoms are commonly over-draped with expansive, deep, ice-rich glaciolacustrine deposits from extensive and long-lived Pleistocene proglacial lakes (Hamilton 2009, 2010, Balser et al. 2015). Glaciolacustrine deposits become thinner along a gradient from lowland bottoms rising toward glacially rounded foothills, and large outwash deposits may abut terminal and recessional moraines. Modern alluvium covers broad, meandering river corridors, frequently bounded by bluffs of glacial drift and glaciolacustrine deposits exposed through millennia of erosional down-cutting (Hamilton 2009, 2010). A loess cap of variable thickness is common throughout landscapes in the study region (Jorgenson et al. 2010b, Balser et al. 2015).

The study region is within the zone of climate-driven, ecosystem-modified permafrost (Shur and Jorgenson 2007), with ground ice conditions suitable for active layer detachment slide and retrogressive thaw slump processes distributed among landscapes throughout the region. Upper permafrost in thin soils over near-surface bedrock in mountainous terrain is primarily syngenetic (French and Shur 2010). Segregated ground ice exceeding 30% by volume, comprised mainly of ataxitic and reticulate cryostructures, has been observed in the top meter of permafrost in these locations (Balser et al. 2015). An ice-rich intermediate layer (Shur 1988, Shur et al. 2005), with an ice layer of several centimeters at the

interface of the active layer and permafrost table may also be present across hill slopes (Balser et al. 2015). Episodes of solifluction and colluvial re-deposition contribute to successive syngenetic permafrost development above buried soil surfaces, thickening both overall soil and permafrost through time (Balser et al. 2015). Regional-scale ground ice estimates for these areas range from low (<10%) to moderate (10%-40%) (Jorgenson et al. 2008b).

At low elevations, permafrost of glacial and glaciolacustrine origin includes extensive deposits of deep, ice-rich, syngenetic and epigenetic permafrost, with massive ice deposits (Balser et al. 2015). In the Mission and Aniuk Lowland, regional ground ice estimates range from moderate (10%-40%) to high (>40%) and include broad areas of active Holocene and inactive Pleistocene ice wedges (Young 1974, Jorgenson et al. 2008b, Balser et al. 2015) with deposits of relict glacial ice scattered throughout (Hamilton 2009, 2010). Late-Pleistocene glaciolacustrine deposits can be especially ice-rich (Balser et al. 2015), as is common across the low arctic (Shur and Zhestkova 2003). Syngenetic cryofacies at the top of the permafrost table have been observed in these lowlands, often within a loess cap up to several decimeters thick (Balser et al. 2015). Conditions may be highly variable, corresponding with surficial geology, landforms, and vegetation (Balser et al. 2015).

Permafrost in the foothills comprises an intermingling of conditions characteristic of alpine and lowland landscapes. Upper hill slopes include predominantly syngenetic permafrost cryofacies, periodically overtopped by solifluction and colluviation resulting in progressive permafrost aggradation, while lower slope positions may also include some ice wedges, relict glacial ice within Pleistocene drift, and older syngenetic permafrost associated with Pleistocene glaciolacustrine deposits (Young 1974, Balser et al. 2015). There is no permafrost borehole monitoring within the study region, but adjacent boreholes to the north and south report average annual temperatures of -5°C and 1°C respectively, while mean annual air temperature estimates for the study region are -7°C to -12°C (Jorgenson et al. 2008b).

Land cover comprises a broad suite of vegetation in various landscape settings including arctic and alpine tundra, shrublands and lowland boreal forest along the arctic-boreal ecotone (Young 1974, Viereck et al. 1992, Parker 2006, Jorgenson et al. 2010b). Thirty-six ecotypes have been identified and mapped within our study region (Jorgenson et al. 2010b), with more than 50% of the land surface covered by various shrub-graminoid ecotypes. Alpine and arctic dwarf shrub tundras are most prevalent in the highest elevations, and within north-draining watersheds, while low shrub, tall shrub, and tussock tundras are common in mid-elevation valleys and throughout the Noatak Basin. Lowland valleys within the southwest portion and along the southern boundary of the study region are part of the arctic-boreal

ecotone, and include open and closed stands of conifer and broadleaf species along floodplains (Young 1974, Viereck et al. 1992, Parker 2006, Jorgenson et al. 2010b).

Differing lithologies have been strongly linked with soil properties within the study region. Carbonate, non-carbonate, mafic and ultramafic lithologies are correlated with differences in soil development, soil chemistry, and grain size proportions (Jorgenson et al. 2010b). These are in turn linked with vegetation, and with surface organic depth (Jorgenson et al. 2010b). These factors are known to influence permafrost characteristics (Davis 2001, Shur and Jorgenson 2007), though the full extent of these influences has not been reported for the study region. Lithology may exert more influence in upland settings where a larger proportion of surfaces derive from the adjacent and underlying bedrock, compared with lowlands containing deep and extensive deposits of mixed origin transported from elsewhere through glacial and periglacial processes.

Generally, upland hill slopes with an ice-rich intermediate layer may be more favorable for active layer detachment sliding, while lowlands of glacial and glaciolacustrine origin offer prime settings for retrogressive thaw slump development, but these relationships are not obligate. Retrogressive thaw slumps are widespread along lowland lake margins, river banks, and bluffs. However, they also occur in upland settings, often where an active layer detachment slide has exposed the upper permafrost, and prior, episodic colluviation has accumulated a layer of ice-rich, syngenetic, upper permafrost which is more than 2 m deep and vulnerable to sustained, retrogressive thaw slumping (Hamilton 2009, Swanson 2010, Swanson and Hill 2010, Balser et al. 2014). Active layer detachments are most frequently found on broad, upland hill slopes, but have also been observed in lowlands, typically adjacent to river bluffs on mild slopes where an ice-rich intermediate layer has developed (Balser et al. 2009, Gooseff et al. 2009, Swanson 2010, Balser et al. 2014).

Overall, conditions throughout the region represent a broad range of typical low-arctic landscapes. Alpine, foothill, and valley bottom settings include many characteristic ecotypes of the North American low arctic, a suite of periglacial landforms, diverse lithologies, and a broad continuum of permafrost characteristics and cryofacies. Our study deliberately included this breadth of conditions over a large geographic area to represent a diversity of low-arctic landscapes.

1.5 Goals of this Research

There is yet much uncertainty regarding factors and processes driving the timing and distribution of active layer detachment slides and retrogressive thaw slumps across circumarctic landscapes. Whereas terrain properties influence permafrost and ground ice characteristics, and in turn drive conditions determining terrain suitability for active layer detachment slide and retrogressive thaw slump processes,

the nature and strength of these relationships are poorly understood, particularly within the Brooks Range and foothills of northern Alaska. Prior research suggests that a state factor approach may be useful for striking the best balance between inclusion of all relevant factors, while emphasizing parsimony as much as possible. While regional-scale triggering events for active layer detachment slides have been documented from multiple locations in the arctic, it is still unclear whether retrogressive thaw slump initiation is dispersed through time, with very localized responses to general warming and meteorological events, or whether slumps initiate within narrow time windows regionally, responding to shifts in seasonal climate patterns and anomalous weather events.

Better estimates of permafrost carbon vulnerability and ecosystem impacts and feedback to climate change within this region depend upon answers to questions about ALD and RTS terrain suitability and initiation timing. Do surficial characteristics correlate consistently with permafrost properties across the region? Can these correlations be exploited for models estimating ALD and RTS terrain suitability synoptically across landscapes? Where may these modes of permafrost degradation be most prevalent? How much landscape may be suitable for these modes, and which sorts of triggers are most likely to initiate them? Answers to these questions may help us better identify which ecosystems are most likely to be impacted under different climate change scenarios, how they may be impacted, and how much permafrost carbon may be vulnerable to release by these modes of permafrost degradation.

The following overviews introduce our questions and approach for each chapter.

Chapter 2. Timing of Retrogressive Thaw Slump Initiation in the Noatak Basin, Northwest Alaska

Retrogressive thaw slump frequency and expansion rates have been generally linked with decadal-scale climate warming trends, but the relative importance of a general warming trend compared with specific weather events is not well-quantified (Lacelle et al. 2010). While long-term climate warming may act as a preconditioning agent, shorter-term weather patterns or specific meteorological events are likely required to trigger thaw slump formation (Lewkowicz 1991, Lacelle et al. 2010). Repeat aerial photography has revealed increased retrogressive thaw slump activity during the climate warming trend dating back to the 1930s (Lantuit and Pollard 2008, Kokelj et al. 2009a, Lacelle et al. 2010, Lantuit et al. 2012), but the decadal repeat increment of historic aerial photography does not clearly distinguish whether regional-scale feature initiation occurs one by one, dispersed through the years, or rather is concentrated in narrow time windows, responding to specific meteorological conditions at a regional scale.

In this chapter, we used archived time-series of synthetic aperture RADAR (SAR) imagery to examine timing of retrogressive thaw slump initiation in the Noatak Basin. Thawing season imagery acquired on a bi-weekly basis from 1997 to 2010, and long-term weather station records and satellite-derived, interannual snow metrics were examined to 1) determine whether slump initiation occurs evenly across years, or is concentrated in specific years, 2) identify possible weather and meteorological triggers for slump initiation, and 3) identify correlations among weather patterns, snow cover, and possible mechanisms of permafrost degradation associated with retrogressive thaw slump formation. Our results provide new information on the role of weather events and their timing on retrogressive thaw slump initiation.

Chapter 3. Relationship of Cryofacies, Surface and Subsurface Terrain Conditions in the Brooks Range and foothills of Northern Alaska

A general approach describing relationships among terrain properties and permafrost, congruent with the state factor framework (Shur and Jorgenson 2007), has been developed to better estimate permafrost vulnerability among different landscapes. While the importance of surficial deposits (Kreig and Reger 1982, Jorgenson et al. 2008b) and vegetation (Viereck 1973) to ground ice content and permafrost development have long been recognized, landscape-scale methods for integrating terrain factors are not fully developed. Toward improved terrain factor integration, we hypothesized that: 1) vegetation and permafrost properties consistently correlate with specific terrain conditions across landscapes due to these relationships, 2) that diverse landscapes may fall into general groupings from statistical analysis of empirical field data for these combined properties, 3) that these relationships can be used to help identify which terrain factors, in combination, facilitate spatial characterization of surficial landscape properties in the Brooks Range and foothills of northern Alaska, and 4) that a state factor framework is useful for organizing relevant terrain properties.

Our research tested these ideas statistically using ordination of empirical field survey data collected from sites representing diverse landscapes in the Brooks Range and foothills of northern Alaska. Identifying statistically-supported linkages between permafrost properties including ground ice content and cryostructures, and terrain properties including vegetation and surficial geology, may justify and facilitate regional scale estimation of permafrost vulnerability and estimation of ground ice conditions, and better inform models examining regional resilience, response and feedbacks to climate.

Chapter 4. Drivers and Estimates of Terrain Suitability for Active Layer Detachment Slides and Retrogressive Thaw Slumps in the Brooks Range and Foothills of Northwest Alaska

Inter-relationships among key terrain properties driving permafrost distribution, characteristics and degradation have been analyzed and modeled using both integrated terrain unit approaches, and statistical analyses of complex, causal linkages. Both of these approaches have advanced our understanding of terrain property relationships and ecological processes, and have contributed to predictive, spatial estimates of permafrost characteristics, distribution, and degradation at scales ranging from field sites of several square meters, to locales of several dozen square kilometers, up through regional and pan-arctic domains (Jorgenson et al. 2008b, Walker et al. 2008, Harris et al. 2009, Daanen et al. 2011, Gruber 2012, Khomutov 2012, Pastick et al. 2014a).

This chapter describes: 1) the first analysis testing hypothetical inter-relationships of specific terrain factor drivers of active layer detachment slide and retrogressive thaw slump distribution at a regional scale in the Brooks Range and foothills of northwest Alaska, 2) the first spatial estimates of terrain suitability for ALD and RTS features focused on this region, 3) general landscape characteristics of ALD and RTS terrain, and 4) the results in context of the state factor framework.

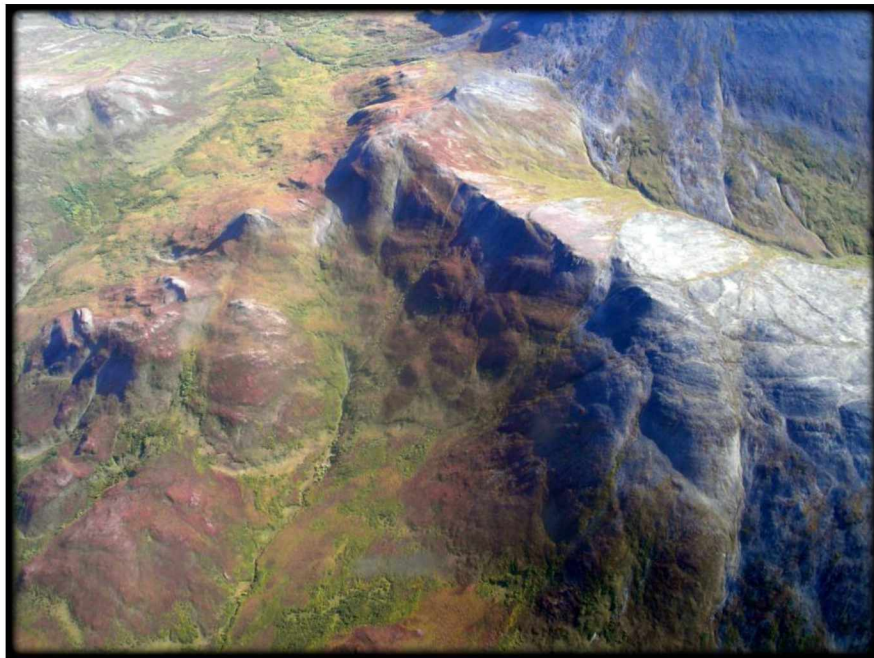


Figure 1.4. Western Baird Mountains, Brooks Range, northwest Alaska. A complex landscape of manifold components and properties, driven by processes interacting across gradients of spatial and temporal scale. It is an expanse of complex beauty, resisting reductionist quantification, and retaining much unseen in the shadows. Photo: A. W. Balsler, 2008.

1.6 Authorship

The work contained in this dissertation was not a sole effort. I was lead investigator and lead author of chapters 1 - 5, with the following contributions and participation by the individuals listed below.

Chapter 2.

Rudiger Gens¹ was instrumental in the evolving conversation on use of synthetic aperture RADAR for detecting and monitoring active layer detachment slides and retrogressive thaw slumps, and Jeremy B. Jones² contributed to development of analytical approaches for weather and snowpack data. Sarah E. Godsey³ suggested adapting the Stewart, Cayan and Dettinger center of mass calculation (Stewart et al. 2005) for representing median Julian date of annual thawing temperatures.

Chapter 3.

M. Torre Jorgenson⁴ provided expertise and training for sampling and interpreting permafrost profile exposure characteristics, for identifying cryostructures and cryofacies, and for general approach to permafrost site survey, as well as discussion on relationships among terrain properties and permafrost. Erin Trochim⁵ suggested use of multiple factor analysis as a choice for ordination, and provided advice and instruction on use of software. Teresa Hollingsworth² and Rebecca Hewitt² contributed discussions of ordination approaches. Donald A. (Skip) Walker² and Steven B. Young⁵ provided discussion and perspective on landscape interactions and scaling.

Chapter 4.

M. Torre Jorgenson⁴ and Steven B. Young⁵ provided perspective and discussion of landscape development and interactions among terrain properties, vegetation and permafrost. Thomas D. Hamilton⁶ added interpretation and perspective to surficial geologic map units in the region. Michelle C. Mack⁷ and Amanda V. Bakian⁸ provided feedback and suggestions on structural equation modeling.

¹ Geophysical Institute, University of Alaska Fairbanks, Fairbanks, AK, 99775 USA. ² Department of Biology & Wildlife and Institute of Arctic Biology, University of Alaska Fairbanks, Fairbanks, AK, 99775 USA. ³ Department of Geosciences, Idaho State University, Pocatello, ID 83209 USA. ⁴ Alaska EcoScience, Fairbanks, AK, 99709 USA. ⁵ Center for Circumpolar Studies, Wolcott, VT 05680 USA. ⁶ U.S. Geological Survey, Anchorage, AK 99508 USA. ⁷ Center for Ecosystem Science and Society, Northern Arizona University, Flagstaff, AZ 86011 USA. ⁸ School of Medicine, University of Utah, Salt Lake City, UT 84132 USA.

Chapter 2. Timing of Retrogressive Thaw Slump Initiation in the Noatak Basin, Northwest Alaska¹

2.0 Abstract

In the North American low arctic, increased retrogressive thaw slump frequency and headwall retreat rates have been linked with climate warming trends since the mid-20th century, but specific weather drivers of slump initiation timing are less clear. We examined relationships among retrogressive thaw slump initiation and annual air temperature, precipitation and snow cover using time series of satellite imagery and weather station data in northwest Alaska. Synthetic aperture RADAR and optical imagery were used to examine retrogressive thaw slump initiation between 1997 and 2010. Over 80% of the slump features examined in this study first appear within a 13 month span from late June 2004 to July 2005. Remote weather station data show that 2004 and 2005 are among several years exhibiting above average thawing indices and average summer temperatures between 1992 and 2011. However, 2004 is distinct from the rest of the record, with unusually warm temperatures primarily occurring early in the thaw season between April and early June, and including two intense precipitation events in May. Regional weather reported by the NOAA National Weather Service also reflects these local findings. Snowmelt timing in 2004 corresponded with warmer air temperatures and precipitation between April and May, exposing the ground surface more than two weeks earlier than average for 2001-2012 within the Noatak Basin. Future rates of thaw slump initiation may be linked with changing trends in the timing of weather, in addition to general climate warming.

2.1 Introduction

Permafrost degradation is widespread throughout the circumpolar north, occurring by multiple modes and mechanisms on many types of landscapes (Serreze et al. 2000, Hinzman et al. 2005, Anisimov and Reneva 2006). The pan-arctic rate of permafrost degradation appears to be increasing, and permafrost carbon release is likely to be a major contributor to atmospheric greenhouse gas concentrations in coming decades (Schuur et al. 2008, Grosse et al. 2011, Schaefer et al. 2011). At regional to global scales, carbon and nitrogen released from frozen substrates may substantially contribute to atmospheric concentrations of CH₄, CO₂, and N₂O, with impacts to global biogeochemistry and climate (Walter 2006, Walter et al. 2007, Schuur et al. 2008, Desyatkin et al. 2009, Gooseff et al. 2009, Tarnocai et al. 2009, Grosse et al. 2011). Locally, liberation of previously frozen substrates, organic materials, and nutrients alters the ecology of receiving streams (Bowden et al. 2007, Bowden et al. 2008, Frey and McClelland 2009, Gooseff et al. 2009, Rozell 2009), impacts sediment loads of streams and rivers

¹ Published as Balsler, A. W., J. B. Jones, and R. Gens (2014), Timing of Retrogressive Thaw Slump Initiation in the Noatak Basin, Northwest Alaska, USA, *Journal of Geophysical Research: Earth Surface*, 2013JF002889, doi:10.1002/2013JF002889.

(Walker et al. 1987, Walker and Hudson 2003, Gooseff et al. 2009), and causes ecological and hydrobiogeochemical impacts in lake ecosystems (Kokelj et al. 2005, Thompson et al. 2008, Kokelj et al. 2009b, Mesquita et al. 2010). Vegetation within and adjacent to retrogressive thaw slump scars are also directly impacted through disturbance and succession on altered surfaces (Lantz and Kokelj 2008, Lantz et al. 2009).

Retrogressive thaw slumping is an important process of permafrost degradation in which thaw of ice-rich permafrost on bluffs or hill slopes causes soil structural instability and mass-wasting subsidence (Burn and Lewkowicz 1990). Retrogressive thaw slump frequency and expansion rates have been generally linked with decadal-scale climate warming trends, but the relative importance of a general warming trend compared with specific weather events is not well-quantified (Lacelle et al. 2010). Repeat aerial photography has revealed increased retrogressive thaw slump activity during the climate warming trend dating back to the 1930s (Lantuit and Pollard 2008, Kokelj et al. 2009a, Lacelle et al. 2010, Lantuit et al. 2012). While long-term climate warming may act as a preconditioning agent, shorter-term weather patterns or specific meteorological events are likely required to trigger thaw slump formation (Lewkowicz 1991, Lacelle et al. 2010).

Several distinct mechanisms can lead to retrogressive thaw slump formation by exposing deposits of ice-rich permafrost, including pore, segregation, and massive ice. In coastal and riparian settings, lateral thermal erosion of protective overburden from adjacent bluffs can expose permafrost deposits (Burn and Lewkowicz 1990, Lantuit et al. 2012, Kokelj and Jorgenson 2013). Wildfire which removes protective vegetation and organic layers, promoting thaw front advance through the active layer may cause instability and disturbance (Lacelle et al. 2010). Channelized flow of surface water over networks of ice wedge polygons can melt ice wedges and create thermo-erosion gullies (Jorgenson and Osterkamp 2005), with progressive downward and lateral thaw into the permafrost. Intense precipitation may be a particular trigger for thermo-erosion gullies (Bowden et al. 2008). Active layer detachment sliding occurs on hill slopes where shear strength of active layer soils is exceeded by pore water pressures (Lewkowicz 2007), and the destabilized active layer slides down slope, exposing the permafrost table below (Jorgenson and Osterkamp 2005). Warm weather and precipitation events have both been observed as slide triggers (Leibman et al. 2003, Lamoureux and Lafreniere 2009), particularly where warm pulses or rainfall accelerate thaw front advance through an ice-rich transient layer (Shur et al. 2005) at the bottom of the active layer. Retrogressive thaw slumps may develop from any of these exposures where combined slope and ground ice content in the permafrost promote continued instability with downward subsidence of thawed material (Burn and Lewkowicz 1990, Jorgenson and Osterkamp 2005, Lacelle et al. 2010, Godin and Fortier 2012, Kokelj and Jorgenson 2013).

Once initiated, retrogressive thaw slumps continue to deepen and expand, (Fig. 2.1) forming a steep headwall up to 20 m deep, an arcing headwall scarp, a floor of thawed and flowing debris, and a run out of re-stabilizing deposits (Burn and Lewkowicz 1990, Lacelle et al. 2010, Lantuit et al. 2012, Kokelj and Jorgenson 2013). Headwall retreat rates range from several to tens of meters annually and are correlated with headwall height, ice content and local climate (Kokelj and Jorgenson 2013). Expansion may continue for decades if thawed debris continues to subside and expose the headwall, and if newly exposed deposits are ice-rich and receive sufficient energy to thaw (Lacelle et al. 2010).

Retrogressive thaw slumps are frequently polycyclic, alternating between extended periods of stabilized dormancy, and active degradation when slumps re-initiate within or adjacent to older slump scars. Re-initiation may be caused by mechanisms described above (Lantuit et al. 2012, Kokelj and Jorgenson 2013), with sublimic talik expansion as a significant driver in kettle lake basin settings (Kokelj et al. 2009a).

Herein, we use archived time-series of synthetic aperture RADAR (SAR) imagery to examine timing of retrogressive thaw slump initiation in the Noatak Basin. Thawing season imagery acquired on a roughly bi-weekly basis from 1997 to 2010 and long-term weather station records and satellite-derived, interannual snow metrics were examined to 1) determine whether slump initiation occurs evenly across years, or is concentrated in specific years, 2) identify possible weather and meteorological triggers for slump initiation, and 3) identify correlations among weather patterns, snow cover, and possible mechanisms of permafrost degradation associated with retrogressive thaw slump formation. Our results provide new information on the role of weather events and their timing on retrogressive thaw slump initiation.

2.2 Methods

2.2.1 Study Area

Our research was conducted within the Noatak River Basin in northwest Alaska. The Noatak River flows 730 kilometers along a predominantly westward course at approximately 67.5° N latitude (Fig. 2.2). Most of the 33,100 km² basin falls within the Noatak National Preserve (U.S. National Park Service) and is recognized as a UNESCO Biosphere Reserve. This low-arctic region falls within Arctic Bioclimate Subzone E (CAVM-Team 2003) abutting the boreal-arctic ecotone, and is underlain by continuous permafrost near the boundary between the continuous and discontinuous permafrost zones (Jorgenson et al. 2008). The Noatak Basin generally contains climate-driven, ecosystem-modified permafrost (Shur and Jorgenson 2007). Land cover includes a suite of arctic and alpine ecotypes, and

ranges from high mountain to lowland physiographic provinces (Wahrhaftig 1965, Young 1974, Viereck et al. 1992, Parker 2006, Jorgenson et al. 2010).

The Noatak Basin was periodically glaciated throughout the Pleistocene and contains a patchwork of periglacial landforms within numerous surficial geologic units (Hamilton 2010, Hamilton and Labay 2011). The Aniuk Lowland and Mission Lowland physiographic provinces (Wahrhaftig 1965) are characterized by extensive lateral, recessional and terminal ice-cored moraines on mid-late Pleistocene glacial drift surfaces. Lowland bottoms are commonly over-draped with deep, ice-rich glaciolacustrine deposits from extensive and long-lived, proglacial lakes (Hamilton 2010). Glaciolacustrine deposits become thinner along a gradient from lowlands rising into the glacially rounded foothills. Extensive deposits of deep, ice-rich permafrost of glacial and glaciolacustrine origin in the Mission and Aniuk Lowlands offer a favorable setting for retrogressive thaw slump development along lake margins, river banks, and bluffs (Hamilton 2009, Swanson and Hill 2010). Retrogressive thaw slumps occur on at least six different ecotypes which have active layer depths ranging from 30 to 200 cm, organic layer thickness of 1 to 30 cm, on slopes ranging from 6° to 14° (Balser et al. 2009, Jorgenson et al. 2010). Ground ice estimates are moderate (10-40%) to high (>40%) and include extensive active Holocene and inactive Pleistocene ice wedges (Young 1974, Jorgenson et al. 2008) and widespread deposits of relict glacial ice (Hamilton 2009, 2010) throughout the lowlands. There is no permafrost borehole monitoring within the Noatak National Preserve, but adjacent boreholes to the north and south report temperatures of -5°C and 1°C respectively, while mean annual air temperatures estimates for the Noatak lowlands are -7°C to -9°C (Jorgenson et al. 2008).

2.2.2 Field Surveys of Retrogressive Thaw Slump Features in the Noatak Basin

Aircraft-supported field campaigns and airphoto surveys in 2006, 2007, 2010, and 2011 were used to identify and map active retrogressive thaw slumps in the Noatak Basin. The initial survey of 2006 (Aniuk Lowland) and 2007 (Mission Lowland) was estimated to have covered > 85% of each lowland region. Initial fixed-wing surveys were used to identify the general distribution of retrogressive thaw slumps, active layer detachment slides and thermo-erosional gullies within the study area. Subsequent helicopter-supported surveys were used to mark the location of features in the field with a Garmin eTrex GPS, and each feature was noted as active (exposed ground ice melting from headwall) or dormant (no exposed ground ice, re-stabilized or re-vegetated slump scar). Vertical aerial photography was acquired using a Nikon D2X digital camera mounted within a small, fixed-wing aircraft. The surveys were repeated in 2010 (Mission Lowland) and in 2011 (Aniuk Lowland) to ascertain the active/dormant status of known features, and to search for newly formed features. Our geodatabase of retrogressive thaw

slumps in the Noatak Basin was expanded and augmented through a subsequent National Park Service survey of the Noatak National Preserve using high-resolution satellite imagery (Swanson and Hill 2010).

A subset of 21 retrogressive thaw slumps from the 326 identified were chosen for inclusion in this study (Table 2.1; Fig. 2.2). Minimum criteria for inclusion of each slump were: 1) confirmed present and actively degrading within the survey period of 2006-2011, 2) large enough to be reliably identifiable on ERS SAR imagery (>8 ha and > 100 m in at least one horizontal dimension, not including the feature outflow), and 3) within areas of low to moderate topographic relief (< 15° slope) to minimize confounding effects of topography on SAR image geometry and backscatter return. Prior ground surveys of 47 retrogressive thaw slumps distributed from headwater areas to the Noatak valley bottom revealed most slumps occurred on slopes between 6° and 14° (mean 9.45°, sd 3.44°), so this criterion also helped exclude outliers occurring on steeper slopes. Of the 326 features initially mapped, 298 were excluded by size (many were also inactive, and/or abutted flowing water), four by inactivity alone, two by the slope criterion alone, and one by proximity to a river with significant lateral erosion (outside the context of this study).

2.2.3 Year of First Detection

Archived ERS-1 and ERS-2 SAR data, available for each slump feature as multiple summer scenes in each year throughout the study period, were used to determine year of first detection. SAR backscatter should respond to several key characteristics of large retrogressive thaw slumps, including feature morphology, surface texture (in contrast with the adjacent vegetated landscape), exposed headwall ice, and wet headwall and floor surfaces. SAR data were deemed preferable for this application for their particular sensitivity to surface geometry, texture, and by dielectric constant, which is strongly influenced by the presence and state of water within surface materials (Ulaby et al. 1982, Cloude and Pottier 1997, Lee and Pottier 2009), which are directly influenced by retrogressive thaw slump characteristics. Over 300 ERS images covering 1997-2010 summer months were preprocessed and analyzed. Images were geocoded to average scene elevation as determined using the ASTER DEM (USGS 2009) within ASF MapReady 2.3 software, resampled to 25 m pixels using nearest neighbor interpolation with no filtering algorithm.

Landsat TM/ETM/ETM+ optical imagery is the only other alternative for continuous satellite data during this time period, but lacks consistent annual, cloud-free coverage and cannot readily distinguish active from inactive features. However, optical Landsat, airphoto, and high resolution satellite imagery were used extensively as corroborative tools for SAR image analysis.

Visual interpretation (Fig. 2.3) was used to determine the presence or absence of slumps in SAR imagery. Each feature was examined for detection on each available ERS-1 and ERS-2 SAR image from 1997 through 2010 using snow-free image dates. Because the size of features (100 m - 300 m) is small relative to the ground resolution of the imagery (~25 m, depending on ground range), misregistration errors and mixed pixel effects render automated detection routines unreliable. Slump features had to be visually distinct from the immediate surroundings, and consistent in size, location and shape with field and airphoto data to be counted as 'detected' in SAR imagery. If a feature was confirmed detected in at least one image in a given year, the feature was counted as 'detected' for that year.

2.2.4 Inter-annual Weather

Daily temperature and precipitation data from two remote weather stations were used to characterize overall temperature and seasonal temperature distribution for 1992-2011 (the period of record). Thawing season weather was then compared with timing of retrogressive thaw slump initiation to identify correlations between slump initiation and weather at seasonal to inter-annual time scales. Weather data were collected through the Remote Automated Weather System (RAWS) program of the Western Regional Climate Center (<http://www.raws.dri.edu/>; Fig. 2.2). For the period of April 1 - September 30 of each year, we examined average daily air temperature, thawing index (Van Everdingen 2005), and total number of days with average temperature above 0°C. A center-of-mass timing C_T calculation, adapted from hydrological discharge analysis, was used to characterize the seasonal distribution of thawing degree days for each year (Stewart et al. 2005). This calculation provides the median day of a given year around which total thawing degree days are evenly distributed. (C_T) is calculated as:

$$C_T = \frac{\sum(t_i q_i)}{\sum q_i} \quad (2.1)$$

where t_i is day of year (Julian date) and q_i is thawing degree days on day t_i .

One period (April 23 - June 8, 2004 for the Noatak RAWS Station) had to be gap-filled using empirical data from the Kelly and Kavet RAWS stations. Gap-filling was done by regressing all existing inter-annual Noatak RAWS daily temperature data for the April 23 - June 8 time period against corresponding Kelly and Kavet RAWS data for the period of record (1992-2011). Regression results (Equations 2.2 & 2.3) for average and maximum daily temperatures were statistically significant and were used to calculate gap-fill values for missing period in the Noatak RAWS data.

$$\text{No}T_{\text{Ave}} = 0.22(\text{Ke}T_{\text{Ave}}) + 0.88 (\text{Ka}T_{\text{Ave}}) - 11.49 \quad (2.2)$$

$$n = 487, R^2 = 0.87, p\text{-value} < 0.05$$

$$\text{No}T_{\text{Max}} = 0.36(\text{Ke}T_{\text{Max}}) + 0.65(\text{Ka}T_{\text{Max}}) - 6.60 \quad (2.3)$$

$$n = 487, R^2 = 0.81, p\text{-value} < 0.05$$

where T_{Ave} is average daily temperature ($^{\circ}\text{C}$), T_{Max} is maximum daily temperature ($^{\circ}\text{C}$), and Ka, Ke and No are the Kavet, Kelly River and Noatak RAW stations.

Frequent data gaps in the precipitation portion of the RAWS datasets precluded statistical analysis of precipitation at inter-annual time scales, though individual precipitation events were examined. Gap filling of precipitation data was attempted for critical periods for the Kelly River and Noatak RAW stations. Regression results for precipitation data among the Kavet, Kelly and Noatak RAW stations for those periods throughout the 1992-2011 record were not sufficient to support gap-filling of precipitation data for the RAWS stations (best result: $R^2 = 0.34$, $p\text{-value} > 0.05$).

Annual values for average thawing season temperature, total thawing degrees, thaw degree days, and seasonal thawing degree distribution were plotted against averages for the 1992 to 2011 period to detect warmer than average periods driving retrogressive thaw slump initiation could have occurred. Results from the Noatak RAW station were used for primary interpretation because that station is proximal to 19 of 21 slump features examined (Fig. 2.2).

Regional weather data from the National Oceanic and Atmospheric Administration (NOAA) National Weather Service climate stations were used to compare weather within the Noatak Basin with the surrounding region and to provide broader context for our results (Fig. 2.4). Temperature and precipitation data for NOAA climate stations are available through monthly and annual statewide reports distributed through the NOAA National Environmental Satellite, Data and Information Service (NESDIS, <http://www.ncdc.noaa.gov/IPS/cd/cd.html>). Monthly temperature and precipitation for the Kotzebue and Bettles climate stations, active since 1941 and 1944, respectively, and regional estimates for the Arctic Drainage division as a whole, which have been calculated since 1950, were examined to ascertain if relevant weather events captured at local RAW stations were also reflected in regional data. Our analysis also included data from the NOAA climate station at Noatak Village, which only reports precipitation from December 1996 through November 2009.

2.2.5 Inter-annual Snow Cover

The MODIS-derived Snow Metrics (2001-2012) dataset (Zhu and Lindsay 2013) was used to examine inter-annual variation in snow cover for the combined Noatak and Wulik River basins. Data were clipped to basin spatial boundaries as defined using the ASTER DEM (USGS 2009) within an ArcGIS 9.3 watershed delineation analysis. MODIS-derived snow metrics describe the full snow season (FSS), which includes dates in the autumn and spring with temporally discontinuous snow cover, and the continuous snow season (CSS), representing unbroken consecutive dates of snow cover. The data do not include snowpack properties such as depth or snow water equivalence. Snow metrics depicting the start and end dates and total number of days for both FSS and CSS were spatially examined and then statistically summarized for each year for the combined Noatak and Wulik basins, with average values calculated for each year from all pixels within the basin boundaries.

2.3 Results

2.3.1 Initiation Timing of Retrogressive Thaw Slumps

Of the 21 retrogressive thaw slumps examined, eight were confirmed polycyclic retrogressive thaw slumps, associated with visible, adjacent, re-stabilized scars. No new slump features were observed during the 2010 and 2011 resurveys of the same area. Sixteen of the twenty-one retrogressive thaw slump features first appear in ERS imagery in either 2004 or 2005, three features predate the study period (pre-1997), and one slump appeared in 1998 (Fig. 2.5). In every case, a slump detected in a given year was detected in all subsequent years. Some SAR images were excluded from analysis due to the confounding, combined influence of ground range (for particular ascending and descending satellite passes) and local topography on SAR backscatter.

2.3.2 Inter-annual Weather Patterns

Overall summer temperature in 2004 was warmer than average within the Noatak Basin, but the early seasonal distribution of thawing degrees in 2004 sets it apart from all other years (Fig. 2.6). 2004 was among the warmest years from 1992 to 2011, but it was only slightly above average in thawing index, with a comparatively short thawing season at the Noatak RAW Station (Fig. 2.6). Several measures of inter-annual temperature showed years containing significant departures from average values from 1992 through 2011, but only C_T was markedly different in 2004, with the earliest thawing temperature distribution of any year. The total distribution of thawing degree days throughout the season was significantly earlier than average in 2004 at both Kelly River and Noatak RAW stations, while only one other year was significantly earlier than average for C_T within the entire data record (Fig. 2.6g & 2.6h).

The early season warming anomaly was regional but most concentrated from Kotzebue, near the mouth of the Noatak River, through the Noatak Basin attenuating in the central Brooks Range near the Noatak headwaters (Fig. 2.4). Temperatures remained well above average for April, May and June of 2004 at Kotzebue, Bettles and both RAW stations (Fig. 2.7). For the Arctic Drainage as a whole, which is weighted toward the Arctic Coastal Plain north of the Brooks Range (Fig. 2.4), temperatures for this period are close to average. Temperature at Bettles, while above average, showed less warming anomaly than at Kotzebue or the RAW stations.

Maximum temperatures rose above freezing almost every day from April through June at the RAW stations, Kotzebue, and Bettles, and include maximum values well above freezing beginning in April at all stations (Table 2.2). By 10 April 2004, daily maximum temperature had exceeded 5°C at all stations and had exceeded 10°C at all but the Kotzebue station by April 30. Maximum temperatures exceeded 20°C in May, and 30°C by June 8 for all stations except Kotzebue (which is a coastal location). NOAA reported that temperatures included multiple record highs during both May and June at Kotzebue and Bettles.

May 2004 had unusually high precipitation in the region, including two intense precipitation events. NOAA stations reported above average precipitation at the Kotzebue, Noatak Village, and Bettles stations, while the Arctic Drainage division overall reported average precipitation (Fig. 2.7). RAW stations did not provide a consistent enough data record to calculate monthly averages. Two intense precipitation events occurred across much of the region between May 6 and 11, and May 22 and 24 (Table 2.3) accounting for 5.9 cm of the May total of 6.9 cm at Noatak Village, and 6.7 cm of May total of 8.1 cm at Kelly River. The May precipitation anomaly and the intensity of the two events increases from Kotzebue, up the Noatak drainage through Noatak village and the Kelly River RAW station, and attenuates somewhere between the Kelly River RAW station and Bettles, though missing data for the Noatak RAW station leave it less clear where this occurred. Only Bettles and Kotzebue have long enough continuous data for NOAA to acknowledge record values for precipitation events, with the Kotzebue station reporting record rainfall in May 2004.

2.3.3 Inter-annual Snow Cover

Snow cover in the study area showed a corresponding, anomalous seasonal shift in 2004 (Fig. 2.8). Both the full and continuous snow seasons ended earlier than any other year within the 2001-2012 data record, with both ending 15 days earlier in the spring than the average (Fig. 2.8b & 2.8d). At the start of the 2004 snow season (autumn 2003), the first detected snow cover also came anomalously early in the autumn (Fig. 2.8a), with the continuous snow season beginning 12 days later (Fig. 2.8c & 2.8e). Both the

full and continuous snow seasons were shorter than average in 2004 (Fig. 2.8e & 2.8f), with the entirety of the shortening at the end of the season in the spring. Spatially, the anomaly in snow season end dates for 2004 was greatest toward the westward portion of the study area (Fig. 2.9). Snow cover analyses were duplicated for just the Noatak watershed from the headwaters through the Mission Lowland, to evaluate the influence of the westward portion on the overall results. Resulting statistical patterns from both analysis boundaries were similar, though systematically offset by calendar date (Table 2.4).

2.4 Discussion

In the Noatak Basin, general warming likely serves as a preconditioning agent, while specific weather events are linked with particular triggering mechanisms. While weather events comparable to those in 2004 occur periodically in the data record, their timing early in the thaw season is unusual. The combination of warm periods and heavy precipitation provide the basis for slump initiation by multiple mechanisms. The timing of the events, all in the early thaw season, increased the likelihood of slump initiation in 2004. Five of the eight polycyclic slumps and 11 of 13 non-polycyclic slumps, occurring among six ecotypes, were first detected in 2004 and 2005. Together, these findings suggest weather events and their timing in 2004 were significant enough to drive retrogressive thaw slump initiation among diverse conditions and by multiple mechanisms throughout the Noatak region.

2.4.1 Timing of Weather Events

Early thawing season temperature and precipitation events in 2004 drove early snowmelt, advanced the timing and likely increased the intensity of energy transfer to the ground surface, and extended the thawing season. Initial warm temperature coincided with the first intense precipitation event from May 6 to 11 which closely correlates with the end of the continuous snow season in the Noatak watershed (Table 2.4, Fig. 2.9). This was likely the signature event ending the continuous snow season in 2004. Continued warm temperature likely initiated seasonal thaw front advance through the active layer, allowing rainfall between May 22 and 24 to penetrate upper soil layers. Rainwater was potentially an important vector of energy transfer to the upper permafrost. As channelized runoff, rainwater contributed to thermal erosion, while rainwater penetrating the soil transferred heat initially by advection, then by conducting energy from solar radiation and ambient air masses as daily maximum temperatures continued to rise in the following weeks.

Early snowmelt may be especially important for potential solar energy flux to the upper permafrost. Early snowpack removal exposes the ground surface during the period approaching summer solstice, when the sun angle is highest and daily potential solar exposure is longest. In addition, cloud cover is typically minimized during this part of the thawing season due to remaining sea ice cover on the adjacent

Beaufort and Chukchi Seas (Fig. 2.4). Maps provided by the National Snow and Ice Data Center (<http://nsidc.org>) show May 2004 sea ice still completely covering the Beaufort and Chukchi Seas and extending south into the Bering Sea, even though overall arctic sea ice extent in 2004 was at a then record low for the month of May. Coupled with the high daily maximum temperature before, between, and after the two precipitation events, this suggests that cloud cover was minimal for much of that period. Also, plant activity is not fully active during this period, with reduced deciduous leaf area and correspondingly minimized interception of incident solar radiation by leaf structures. Together, these factors could significantly increase the amount of energy from solar radiation reaching the ground surface and accelerating thaw front advance.

Conditions during the preceding autumn and winter are also likely relevant to these interpretations, but the nature of their role is less clear. Average weather conditions prevailed throughout most of the winter in the study region, but anomalously high temperature (October) and precipitation (November) were recorded at the NOAA and RAW stations throughout the study region (Fig. 2.7). We suspect these early winter conditions are also an important explanatory component, but gauging the nature and magnitude of their impact is speculative, especially given that both anomalies occurred after onset of the continuous snow season (Fig. 2.8).

2.4.2 Weather & Initiation Mechanisms

Weather events in 2004 were sufficient to trigger retrogressive thaw slumping through both active layer detachment slides and thermo-erosional gullies. Warm temperature and precipitation both accelerated thaw front advance through the active layer, promoting high pore pressures and active layer detachment. Though the proportional contributions of temperature and precipitation are unknown, their co-occurrence likely increased thaw front, especially through drier, less thermally conductive active layers which may have better resisted thaw from either warm weather or rainfall occurring in isolation. Active layer detachment slides are extensively reported in the Noatak Basin (Balser et al. 2009, Gooseff et al. 2009, Swanson and Hill 2010), with ice-rich transient layers (Shur et al. 2005) evident in active features. Active layer detachment slides in this area are primarily associated with non-acidic graminoid vegetation, over colluvial deposits (Balser et al. 2009, Gooseff et al. 2009). Lowland sites of retrogressive thaw slumps in this study also include a high proportion of acidic tussock and low shrub tundra, glaciolacustrine and glacial drift deposits, extensive networks of active ice wedge polygons (Young 1974, Jorgenson et al. 2008, Balser et al. 2009, Hamilton 2010), which are more likely settings for thermo-erosional gullies. Intense precipitation events in May 2004 likely drove thermal erosion and new gully formation within ice wedge polygon networks. This is especially likely since the continuous snow season ended with the first precipitation event, exposing the ground surface for the second event.

Warm temperatures and precipitation support both active layer detachment sliding and thermo-erosional gullies as mechanisms, their co-occurrence may have enhanced thaw front penetration for a broader range of active layer conditions, and early timing likely increased their impact within the 2004 thawing season.

Wildfires are not considered a trigger for retrogressive thaw slumping in the Noatak in 2004 and 2005. Throughout interior Alaska, 2004 was the warmest and driest year on record, and consequently the most extreme Alaskan wildfire year on record (Shulski et al. 2005). However, within the Noatak Basin overall 2004 temperature was not as extreme as in the rest of the interior, and only one wildfire is recorded in the Alaska Fire Service database within 15 km of any of our study features for any year between 1990 and 2010 (1999; 4 km from RTS 2).

Considered in the broader context of climate change, early thawing-season warmth and snowmelt may be a critical factor in landscape to regional scale change trajectories, impacts, and feedbacks from retrogressive thaw slumps. Active layer deepening, which occurs with general climate warming (Osterkamp and Romanovsky 1999, Frauenfeld et al. 2004), is at least partially reversible with subsequent cooling. Deeper degradation and mobilization of upper permafrost layers, as with retrogressive thaw slumping, may be a more permanent phenomenon with differing and stronger impacts locally and globally. The temporal pattern of climate change may therefore be critical in determining rate of retrogressive thaw slump initiation and associated impacts and feedbacks, with potentially very different outcomes depending upon future changes in temporal weather patterns.

2.5 Conclusions

Retrogressive thaw slump initiation in the Noatak Basin was heavily influenced by early thawing-season warming, snowmelt and precipitation in 2004. The early season timing of these weather events likely increased their capacity to advance the thaw front through the active layer, as well as lengthening the thaw season. The timing of weather events, as well as their magnitude, may critically influence retrogressive thaw slump initiation. Future rates of thaw slump initiation will likely be linked with changing trends in the timing of weather, in addition to general climate warming.

2.6 Acknowledgments

This work was supported by a University of Alaska Fairbanks Center for Global Change (CGC) Student Research Grant, and by NSF grant ARC-0806465. We gratefully acknowledge Sarah Godsey, M. Torre Jorgenson, Steven B. Young, Michael N. Gooseff, W. Breck Bowden, Benjamin W. Abbott, and Thomas D. Hamilton for invaluable discussion and assistance in the field, and Michelle Harbin of the Alaska Satellite Facility for assistance using the ASF DAAC. We also thank several anonymous reviewers for

their very constructive comments on a prior version of this manuscript. The Polar Geospatial Center of the University of Minnesota provided high-resolution, optical satellite imagery for corroborative analysis. The aviation skill and safety of pilots Tom George, Stan Hermens, Tommy Levanger, Terry Day, Jim Kincaid, and Buck Mackson were indispensable to the success of this research.

2.7 References

- Anisimov, O., and S. Reneva (2006), Permafrost and changing climate: The Russian perspective, *Ambio*, 35(4), 169-175.
- Balser, A., M. N. Gooseff, J. Jones, and W. B. Bowden (2009), Thermokarst distribution and relationships to landscape characteristics in the Feniak Lake region, Noatak National Preserve, Alaska; Final Report to the National Park Service, Arctic Network (ARCN)Rep., Fairbanks, AK.
- Bowden, W. B., M. N. Gooseff, A. Balser, A. Green, B. J. Peterson, and J. Bradford (2008), Sediment and nutrient delivery from thermokarst features in the foothills of the North Slope, Alaska: Potential impacts on headwater stream ecosystems, *Journal of Geophysical Research*, 113. G02026. doi:10.1029/2007JG000470.
- Bowden, W. B., A. W. Balser, A. D. Huryn, C. Luecke, D. M. Sanzone, B. Peterson, G. Burkart, J. Larouche, and S. M. Parker (2007), Aquatic biodiversity, community composition and ecosystem processes in the Noatak River WatershedRep. NPS/AKRARC/NRTR-2006/01, 1 - 86 pp, US National Park Service, DOI.
- Burn, C. R., and A. G. Lewkowicz (1990), Retrogressive Thaw Slumps *The Canadian Geographer*, 34(3), 273-276.
- CAVM-Team (2003), Circumpolar Arctic Vegetation Map, Scale 1:7,500,000, Conservation of Arctic Flora and Fauna (CAFF) Map No. 1. U.S. Fish and Wildlife Service, Anchorage, Alaska.
- Cloude, S. R., and E. Pottier (1997), An Entropy Based Classification Scheme for Land Applications of Polarimetric SAR, *IEEE Transactions on Geoscience and Remote Sensing*, January 1997, 35(1).
- Desyatkin, A. R., F. Takakai, P. P. Fedorov, M. C. Nikolaeva, R. V. Desyatkin, and R. Hatano (2009), CH₄ emission from different stages of thermokarst formation in Central Yakutia, East Siberia, *Soil Science and Plant Nutrition*, 55(4), 558-570.
- Frauenfeld, O. W., T. J. Zhang, R. G. Barry, and D. Gilichinsky (2004), Interdecadal changes in seasonal freeze and thaw depths in Russia, *Journal of Geophysical Research-Atmospheres*, 109(D5).
- Frey, K. E., and J. W. McClelland (2009), Impacts of permafrost degradation on arctic river biogeochemistry, *Hydrological Processes*, 23(1), 169-182.
- Godin, E., and D. Fortier (2012), Geomorphology of a thermo-erosion gully, Bylot Island, Nunavut, Canada, *Can J Earth Sci*, 49(8), 979-986.

- Gooseff, M., A. Balsler, W. Bowden, and J. Jones (2009), Effects of hillslope thermokarst in northern Alaska. , 90: 29-31., *Eos, Transactions of the American Geophysical Union*, 90(4), 29-31.
- Grosse, G., et al. (2011), Vulnerability of high-latitude soil organic carbon in North America to disturbance, *J. Geophys. Res.*, 116, G00K06.
- Hamilton, T. D. (2009), Guide to surficial geology and river-bluff exposures, Noatak National Preserve, northwestern Alaska: U.S. Geological Survey Scientific Investigations Report 2008-5125Rep., 116 pp.
- Hamilton, T. D. (2010), Surficial Geologic Map of the Noatak National Preserve, Alaska, *U.S. Geological Survey (in cooperation with U.S. National Park Service), Scientific Investigations Map 3036, 1 : 250,000 scale, and accompanying report*, 21p.
- Hamilton, T. D., and K. A. Labay (2011), Surficial Geologic Map of the Gates of the Arctic National Park and Preserve, Alaska, *U.S. Geological Survey (in cooperation with U.S. National Park Service), Scientific Investigations Map 3125, 1 : 300,000 scale, and accompanying report*, 19p.
- Hinzman, L., et al. (2005), Evidence and Implications of Recent Climate Change in Northern Alaska and Other Arctic Regions, *Climatic Change*, 72(3), 251-298.
- Jorgenson, M. T., and T. E. Osterkamp (2005), Response of boreal ecosystems to varying modes of permafrost degradation, *Canadian Journal of Forest Research*, 35, 2100-2111.
- Jorgenson, M. T., J. E. Roth, P. F. Miller, M. J. Macander, M. S. Duffy, A. F. Wells, G. V. Frost, and E. R. Pullman (2010), An ecological land survey and landcover map of the Arctic Network. Natural Resource Technical Report NPS/ARC/NRTR—2009/270., edited, National Park Service, Fort Collins, Colorado.
- Jorgenson, T., K. Yoshikawa, V. Romanovsky, M. Kanevskiy, J. Brown, Y. Shur, S. Marchenko, G. Grosse, and B. Jones (2008), Map of Permafrost Characteristics in Alaska, edited, Proceedings of the Ninth International Conference on Permafrost (NICOP), Fairbanks, AK June 30 - July 4, 2008.
- Kokelj, S. V., and M. T. Jorgenson (2013), Advances in Thermokarst Research, *Permafrost and Periglacial Processes*, 24(2), 108-119.
- Kokelj, S. V., B. Zajdlik, and M. S. Thompson (2009a), The Impacts of Thawing Permafrost on the Chemistry of Lakes across the Subarctic Boreal-Tundra Transition, Mackenzie Delta Region, Canada, *Permafrost and Periglacial Processes*, 20, 1-15.
- Kokelj, S. V., R. E. Jenkins, D. Milburn, C. R. Burn, and N. Snow (2005), The influence of thermokarst disturbance on the water quality of small upland lakes, Mackenzie Delta Region, Northwest Territories, Canada, *Permafrost and Periglacial Processes*, 16(4), 343-353.

- Kokelj, S. V., T. C. Lantz, J. Kanigan, S. L. Smith, and R. Coutts (2009b), Origin and Polycyclic Behaviour of Tundra Thaw Slumps, Mackenzie Delta Region, Northwest Territories, Canada, *Permafrost and Periglacial Processes*, 20, 1-12.
- Lacelle, D., J. Bjornson, and B. Lauriol (2010), Climatic and Geomorphic Factors Affecting Contemporary (1950–2004) Activity of Retrogressive Thaw Slumps on the Aklavik Plateau, Richardson Mountains, NWT, Canada, *Permafrost and Periglacial Processes*, 21(1-15).
- Lamoureux, S. F., and M. J. Lafreniere (2009), Fluvial Impact of Extensive Active Layer Detachments, Cape Bounty, Melville Island, Canada, *Arct. Antarct. Alp. Res.*, 41(1), 59-68.
- Lantuit, H., and W. H. Pollard (2008), Fifty years of coastal erosion and retrogressive thaw slump activity on Herschel Island, southern Beaufort Sea, Yukon Territory, Canada, *Geomorphology [Geomorphology]*. Vol. 95, no. 1-2.
- Lantuit, H., W. H. Pollard, N. Couture, M. Fritz, L. Schirmer, H. Meyer, and H. W. Hubberten (2012), Modern and Late Holocene Retrogressive Thaw Slump Activity on the Yukon Coastal Plain and Herschel Island, Yukon Territory, Canada, *Permafrost and Periglacial Processes*, 23(1), 39-51.
- Lantz, T. C., and S. V. Kokelj (2008), Increasing rates of retrogressive thaw slump activity in the Mackenzie Delta region, NWT, Canada, *Geophysical Research Letters*, 35(6).
- Lantz, T. C., S. V. Kokelj, S. E. Gergel, and G. H. R. Henry (2009), Relative impacts of disturbance and temperature: persistent changes in microenvironment and vegetation in retrogressive thaw slumps, *Global Change Biology*, 15(7), 1664-1675.
- Lee, J., and E. Pottier (2009), *Polarimetric RADAR Imaging: From Basics to Applications*, CRC Press, Boca Raton, FL USA.
- Leibman, M. O., A. I. Kizyakov, L. D. Sulerzhitsky, and N. E. Zaretskaya (2003), Dynamics of the landslide slopes and mechanism of their development on Yamal peninsula, Russia. , paper presented at Proceedings of the Eight International Conference on Permafrost, A.A.Balkema Publishers, Rotterdam, Netherlands Zurich 21-25 July 2003.
- Lewkowicz, A. G. (1991), Climate Change and the Permafrost Landscape, paper presented at Arctic Environment: Past, Present and Future, McMaster University, Hamilton, ON.
- Lewkowicz, A. G. (2007), Dynamics of Active-layer Detachment Failures, Fosheim Peninsula, Ellesmere Island, Nunavut, Canada, *Permafrost and Periglacial Processes*, 18, 89 - 103.
- Mesquita, P. S., F. J. Wrona, and T. D. Prowse (2010), Effects of retrogressive permafrost thaw slumping on sediment chemistry and submerged macrophytes in Arctic tundra lakes, *Freshwat. Biol.*, 55(11), 2347-2358.

- Osterkamp, T. E., and V. E. Romanovsky (1999), Evidence for warming and thawing of discontinuous permafrost in Alaska, *Permafrost and Periglacial Processes*, 10(1), 17-37.
- Parker, C. L. (2006), Vascular plant inventory of Alaska's Arctic National Parklands: Bering Land Bridge National Preserve, Cape Krusenstern National Monument, Gates of the Arctic National Park & Preserve, Kobuk Valley National Preserve, and Noatak National Preserve., *ARCNI&M, National Park Service, Alaska Region, Final Report*(NPS/AKRARC/NRTR-2006/01), 142p.
- Rozell, N. (2009), Selawik Slump grows unabated, threatens fishery, in *Anchorage Daily News*, edited, Anchorage, AK.
- Schaefer, K., T. Zhang, L. Bruhwiler, and A. P. Barrett (2011), Amount and timing of permafrost carbon release in response to climate warming, *Tellus B*, no-no.
- Schuur, E. A. G., et al. (2008), Vulnerability of Permafrost Carbon to Climate Change: Implications for the Global Carbon Cycle, *Bioscience*, 58(8), 701-714.
- Serreze, M. C., J. E. Walsh, F. S. Chapin, T. Osterkamp, M. Dyurgerov, V. Romanovsky, W. C. Oechel, J. Morison, T. Zhang, and R. G. Barry (2000), Observational Evidence of Recent Change in the Northern High-Latitude Environment, *Climatic Change*, 46(1 - 2), 159-207.
- Shulski, M., G. Wendler, S. Alden, and N. Larkin (2005), An extraordinary summer in the interior of Alaska. , paper presented at Proceedings of the 85th AMS Annual Meeting, P3.24, San Diego, CA, 9- 13 January 2005.
- Shur, Y., K. M. Hinkel, and F. E. Nelson (2005), The transient layer: implications for geocryology and climate-change science, *Permafrost and Periglacial Processes*, 16(1), 5-17.
- Shur, Y. L., and M. T. Jorgenson (2007), Patterns of Permafrost Formation and Degradation in Relation to Climate and Ecosystems, *Permafrost and Periglacial Processes*, 18, 7 - 19.
- Stewart, I. T., D. R. Cayan, and M. D. Dettinger (2005), Changes toward earlier streamflow timing across western North America, *Journal of Climate*, 18(8), 1136-1155.
- Swanson, D. K., and K. Hill (2010), Monitoring of Retrogressive Thaw Slumps in the Arctic Network, 2010 Baseline Data: Three-dimensional Modeling with Small-format Aerial Photographs, edited, p. 58, U.S. Department of the Interior, National Park Service, Natural Resource Data Series NPS/ARC/NRDS—2010/123, Natural Resource Program Center, Fort Collins, CO.
- Tarnocai, C., J. G. Canadell, E. A. G. Schuur, P. Kuhry, G. Mazhitova, and S. Zimov (2009), Soil organic carbon pools in the northern circumpolar permafrost region, *Global Biogeochemical Cycles*, 23(GB2023), 1-11.
- Thompson, M. S., S. V. Kokelj, T. D. Prowse, and F. J. W. . (2008), The impact of sediments derived from thawing permafrost on tundra lake water chemistry: An experimental approach, paper presented at Proceedings of the 9th Permafrost International Conference, Fairbanks, AK.

- Ulaby, F. T., R. K. Moore, and A.K. Fung. (1982), *Microwave Remote Sensing: Active and Passive, Vol. II -- Radar Remote Sensing and Surface Scattering and Emission Theory*, 609 pp., Addison-Wesley, Advanced Book Program, Reading, MA.
- USGS, E. D. C. (2009), ASTER Global Digital Elevation Model V001 Sioux Falls, SD.
- Van Everdingen, R. (2005), Multi-Language Glossary of Permafrost and Related Ground-Ice Terms, in *World Data Center for Glaciology*, edited by R. V. Everdingen, National Snow and Ice Data Center, <http://nsidc.org/fgdc/glossary/>, Boulder, CO.
- Viereck, L. A., C. T. Dyrness, A. R. Batten, and K. J. Wenzlick (1992), The Alaska Vegetation Classification, edited by U. S. D. o. A. F. Service, p. 278, Gen. Tech. Rep. PNW-GTR-286, Portland, OR.
- Wahrhaftig, C. (1965), Physiographic Divisions of Alaska *Rep.*, U.S.G.S. Professional Paper 482. 52 pp.
- Walker, H. J., and P. F. Hudson (2003), Hydrologic and geomorphic processes in the Colville River delta, Alaska, *Geomorphology*, 56(3-4), 291-303.
- Walker, J., L. Amborg, and J. Peippo (1987), Riverbank Erosion in the Colville Delta, Alaska, *Geografiska Annaler Series a-Physical Geography*, 69(1), 61-70.
- Walter, K. M. (2006), Methane emissions from lakes in northeast Siberia and Alaska, PhD thesis, 143 pp, University of Alaska Fairbanks, Fairbanks.
- Walter, K. M., M. E. Edwards, G. Grosse, S. A. Zimov, and F. S. Chapin (2007), Thermokarst lakes as a source of atmospheric CH₄ during the last deglaciation, *Science*, 318(5850), 633-636.
- Young, S. B. (1974), The environment of the Noatak River basin, Alaska. *Rep.*, Contributions of the Center for Northern Studies, Wolcott, VT.
- Zhu, J., and C. Lindsay (2013), MODIS-derived snow cover metrics for Alaska v1.0 (1 August 2000 to 31 July 2012). Fairbanks, Alaska USA: Geographic Information Network of Alaska. Digital media (Available from <http://www.gina.alaska.edu/projects/modis-derived-snow-metrics>). *Rep.*

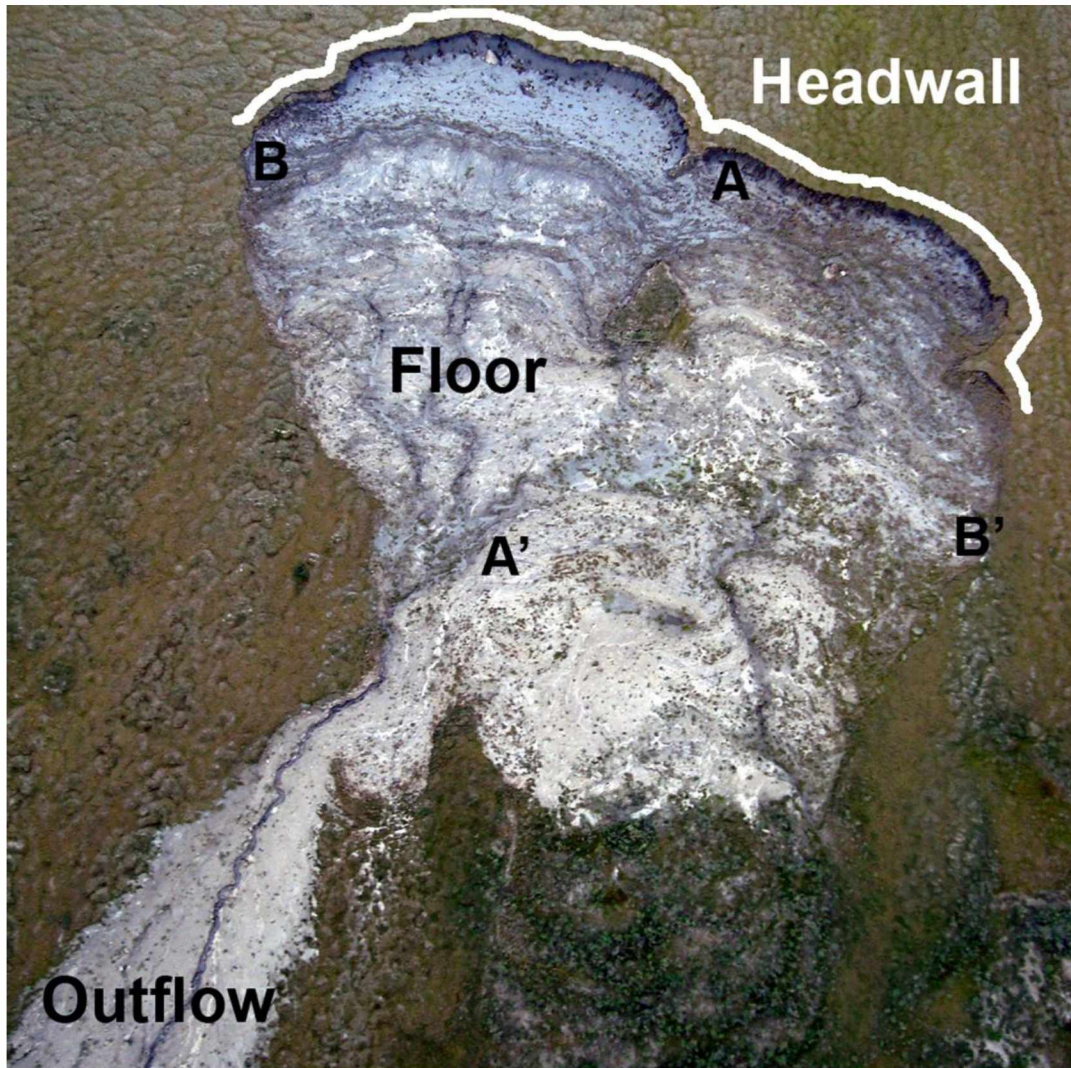


Figure 2.1. Retrogressive thaw slump No. 14 (Fig. 2.2, Table 2.1). This retrogressive thaw slump sits on a west-facing 6° slope on a late Pleistocene glaciolacustrine deposit in the upstream portion of the Aniuk Lowlands, Noatak Basin, Alaska. This slump is polycyclic, having initiated in 2004 from a previously re-stabilized and inactive retrogressive thaw slump. Length from headwall to beginning of outflow (A to A') is 181 m; width at widest point (B to B') is 287 m, as of July 2011. Deepest point was 14 m at the base of the headwall near A. Photo: A.W. Balsler, 2011

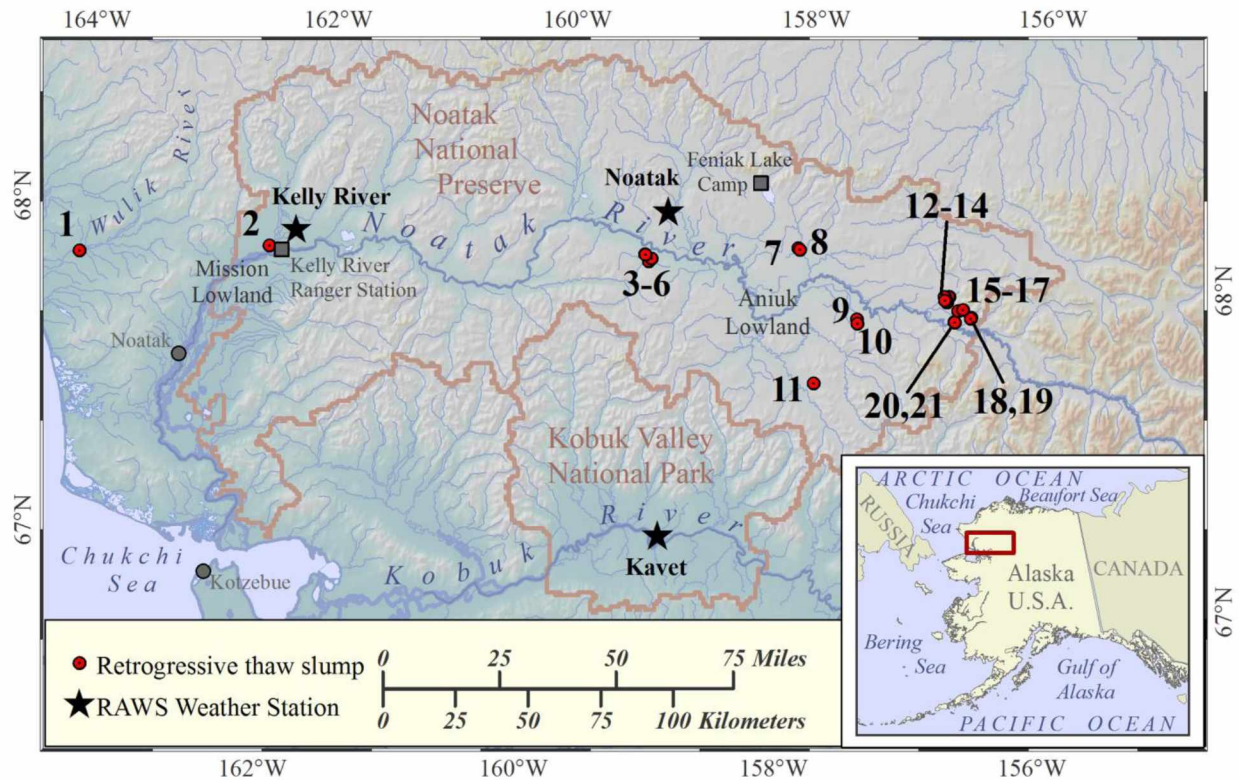


Figure 2.2. Study area in the Noatak Basin in northwest Alaska. RTS 1 is set back from the north bank of the Wulik River on land administered by the State of Alaska. All other RTS features are within the Noatak National Preserve, US National Park Service. RTSs are predominantly but not exclusively within lowland physiographic provinces (Tables 2.1 & Appendix 1), with some occupying polycyclic thaw slump basins surrounding kettle lakes, and others are situated on hill slopes flanking floodplains. Features directly adjacent to flowing water were excluded from analysis to eliminate hydrothermal erosion as a possible mechanism of initiation.

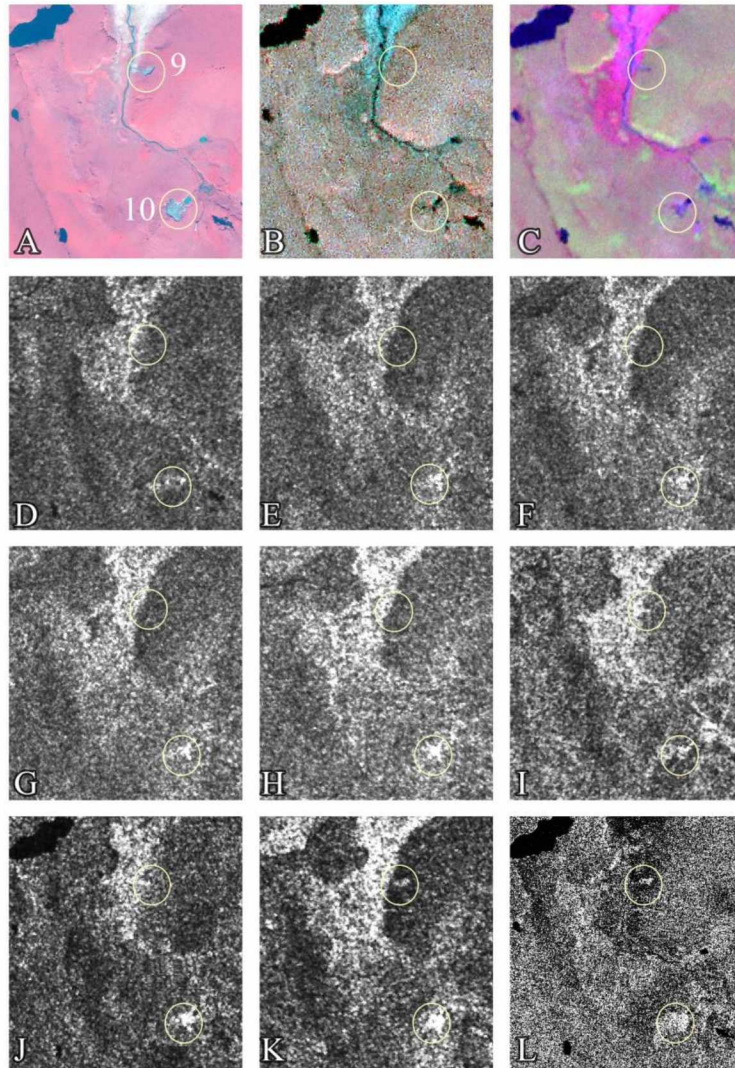


Figure 2.3. Imagery for RTS 9 and RTS 10 in the Cutler River drainage, Noatak Basin, Alaska.

A. IKONOS image, CIR composite, (8/9/2008); B. Landsat ETM image, CIR composite, (7/29/2002); C. Landsat ETM+ image, bands 543 composite (7/21/2005); D. ERS2 image (8/6/1997); E. ERS2 image (7/31/1998); F. ERS2 image (8/20/1999); G. ERS2 image (6/26/2002); H. ERS2 image (7/8/2002); I. ERS2 image (9/27/2004); J. ERS2 image (7/23/2005); K. ERS2 image (9/25/2006); L. ALOS PALSAR image, HV polarization (9/18/2006). RTS 10 re-initiated in 1998 from the scar of a pre-existing, stabilized, polycyclic slump, and is apparent as a growing feature in imagery from 1998 - 2007. RTS 9 is not detectable in any imagery through 2003, appearing first in July 2004 and in all subsequent years of analysis. RTS 9 initiated ~220 m from the river, at ~40 m higher elevation than the river bank based on ground reconnaissance and image analysis, eliminating hydrothermal erosion as a plausible triggering mechanism.

Ground resolution for each image type is: IKONOS = 3.3 m; Landsat = 28.5 m, ERS, ~25 m (varies with ground range), ALOS PALSAR ~10 m (varies with ground range).

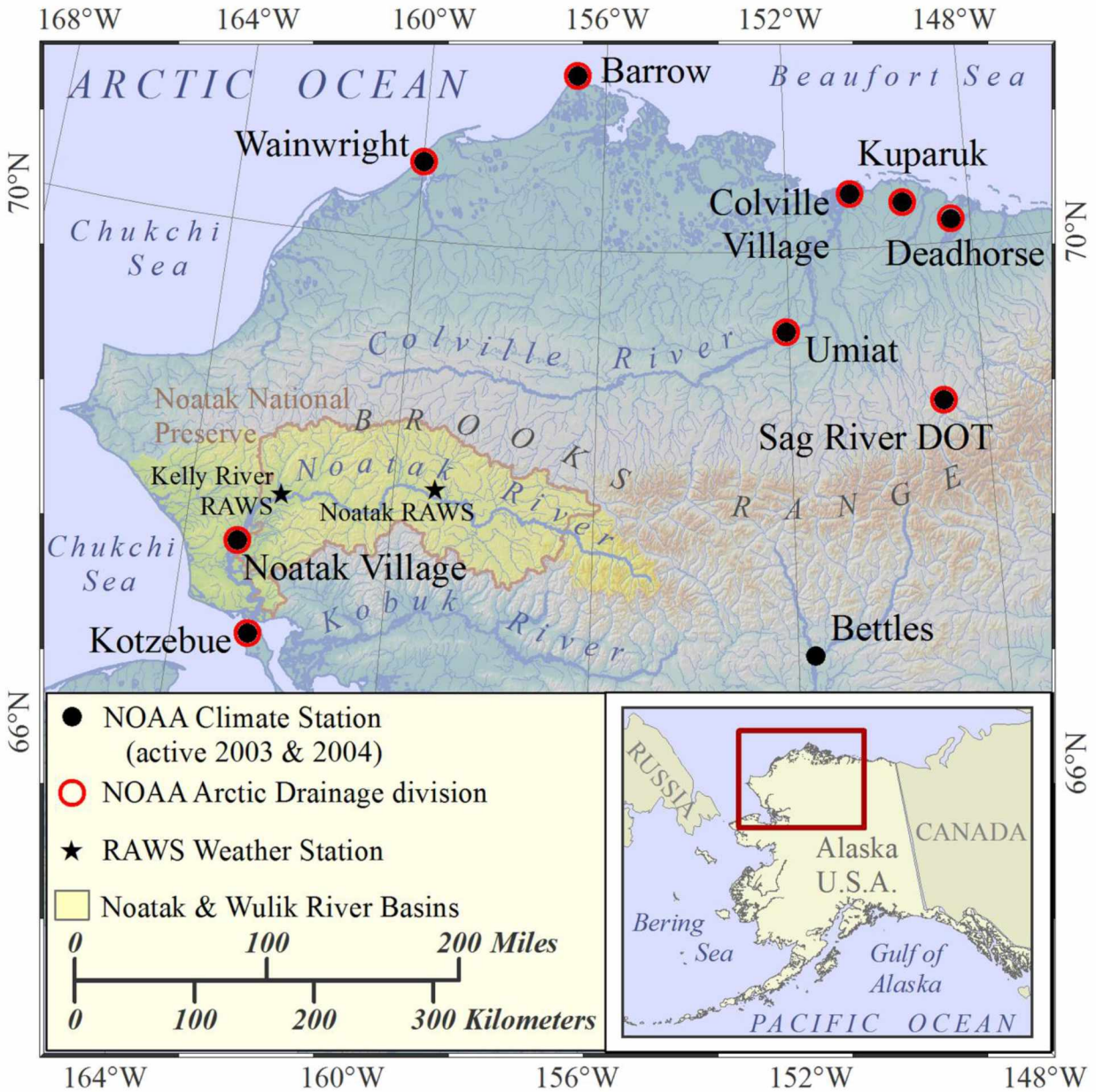


Figure 2.4. Locations of NOAA National Weather Service climate stations in northwest Alaska, active during 2003 and 2004. Data from stations within the Arctic Drainage division contributed to monthly mean values for temperature and precipitation reported for northern and northwest Alaska. Data from the Bettles station were also examined in this study due to its proximity to the upper Noatak Basin, representing a more continental climate in the interior.

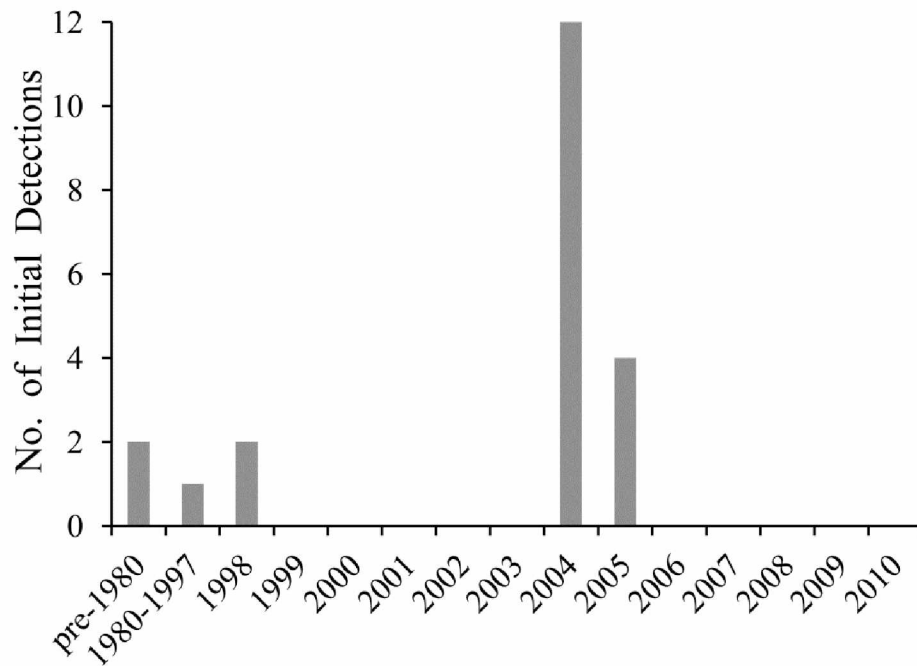


Figure 2.5. Year of first detection for 21 retrogressive thaw slumps in the Noatak Basin. Bars in this graph represent *only* the initial detection of each retrogressive thaw slump in the study. Every slump in the study was also detected in every subsequent year after initial detection, suggesting that all slumps remained active from time of initiation through at least 2010.

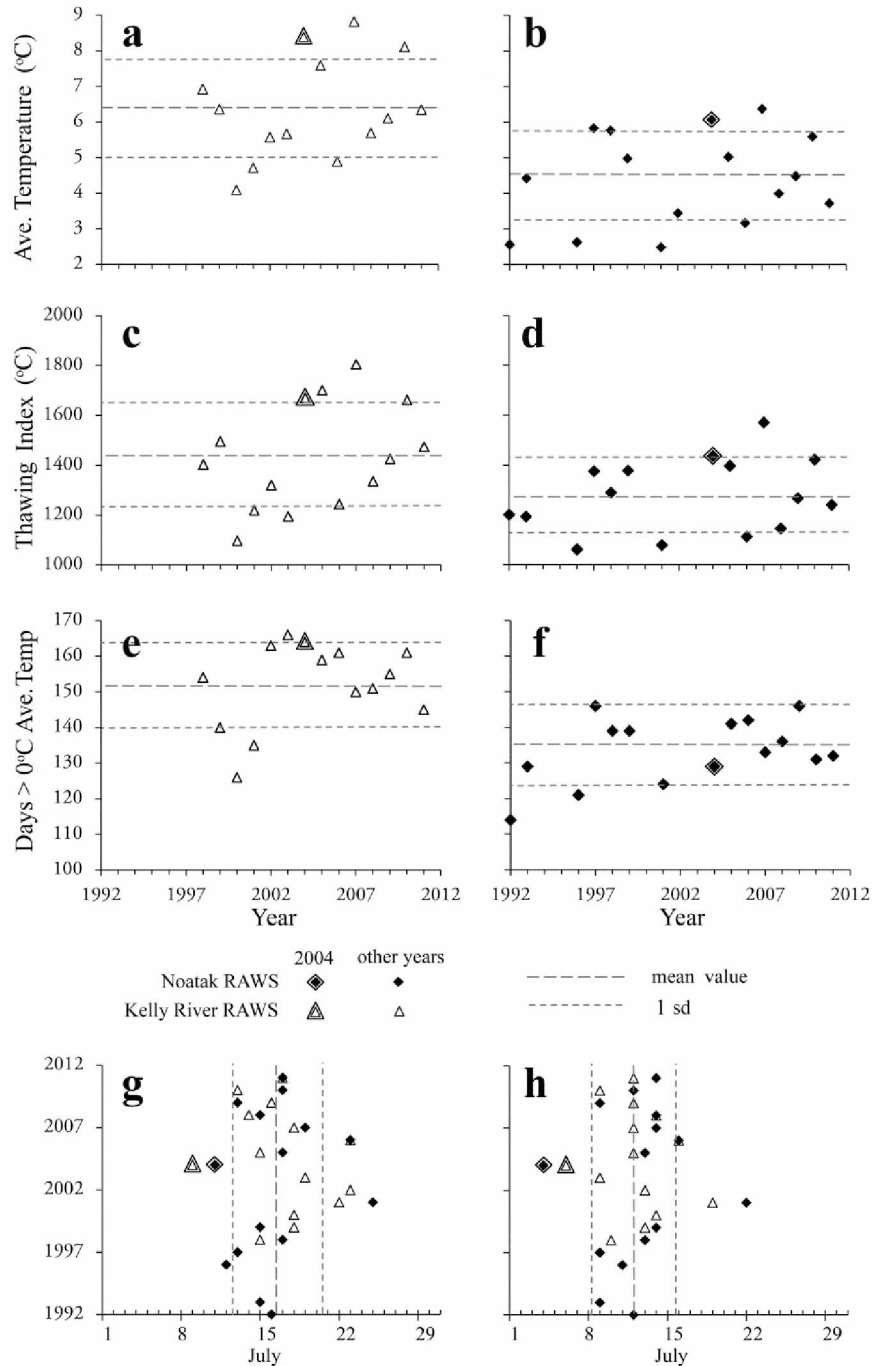


Figure 2.6. Average daily summer temperature, thawing index, number of days averaging above 0°C, and seasonal thawing temperature distribution (as center of mass, C_T) from two remote automated weather (RAW) stations in the Noatak basin, 1992-2011. Panels a. & b. show average daily air temperature (April 1 - September 30) 1992-2011 for the (a.) Kelly River and (b.) Noatak RAW Stations. Panels c. & d. show thawing index > 0°C (Van Everdingen 2005), April 1 - September 30; 1992-2011. Panels e. & f. show number of days with average daily temperature > 0°C, April 1 - September 30; 1992-2011. Panel g. depicts seasonal center of mass for daily average temperature (C_{Tave} , Eq. 2.1) in degrees Celsius, April 1 -

September 30; 1992-2011. Panel h. depicts seasonal center of Mass for daily maximum temperature ($C_{T_{max}}$, Eq. 2.1) in degrees Celsius, April 1 - September 30; 1992-2011.

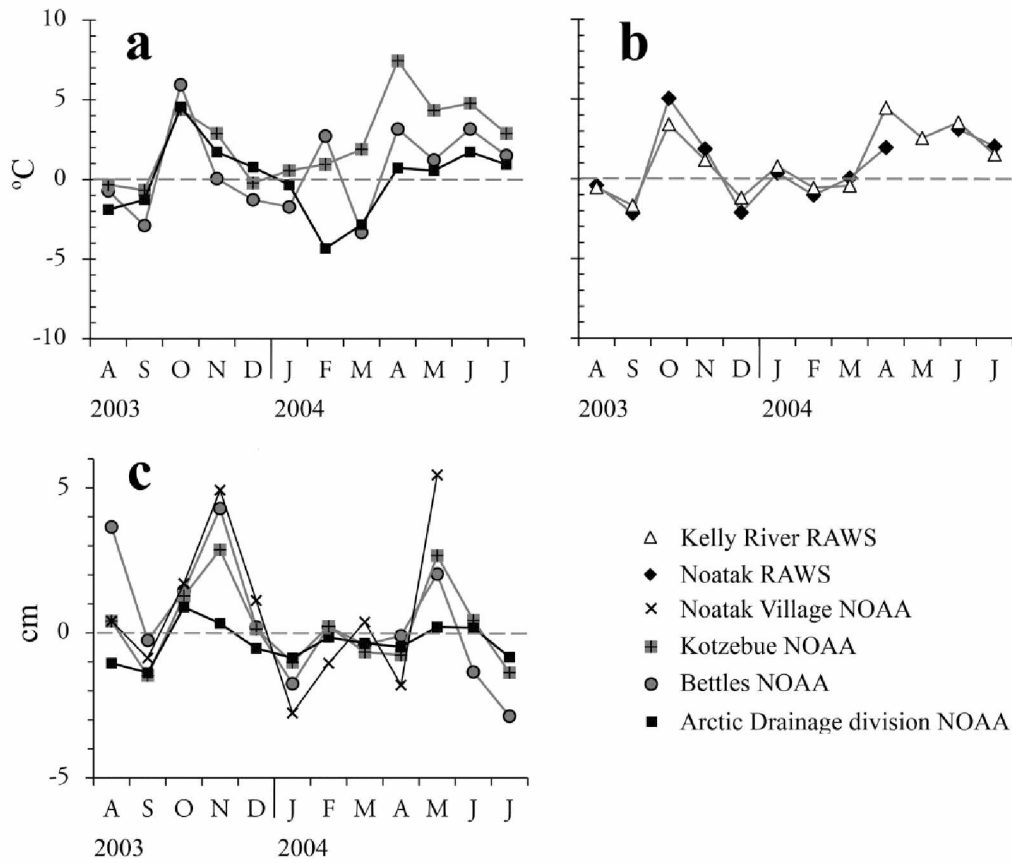


Figure 2.7. Monthly temperature and precipitation estimates as a departure from average, winter of 2003 through 2004. Panel a. shows estimates from NOAA National Weather Service climate stations at Kotzebue and Bettles, and for the Arctic Drainage division as a whole, while panel b. shows estimates from Kelly River and Noatak RAWs stations. Panel c. includes monthly precipitation estimates from NOAA climate stations as a departure from average. The data record begins in 1996 for Noatak Village, 1941 for Kotzebue, 1944 for Bettles, and in 1950 for the Arctic Drainage division NOAA stations. Data for June and July 2004 were unavailable for the Noatak Village station. Winter precipitation data for RAW stations are incomplete for most years and preclude calculating average statistics.

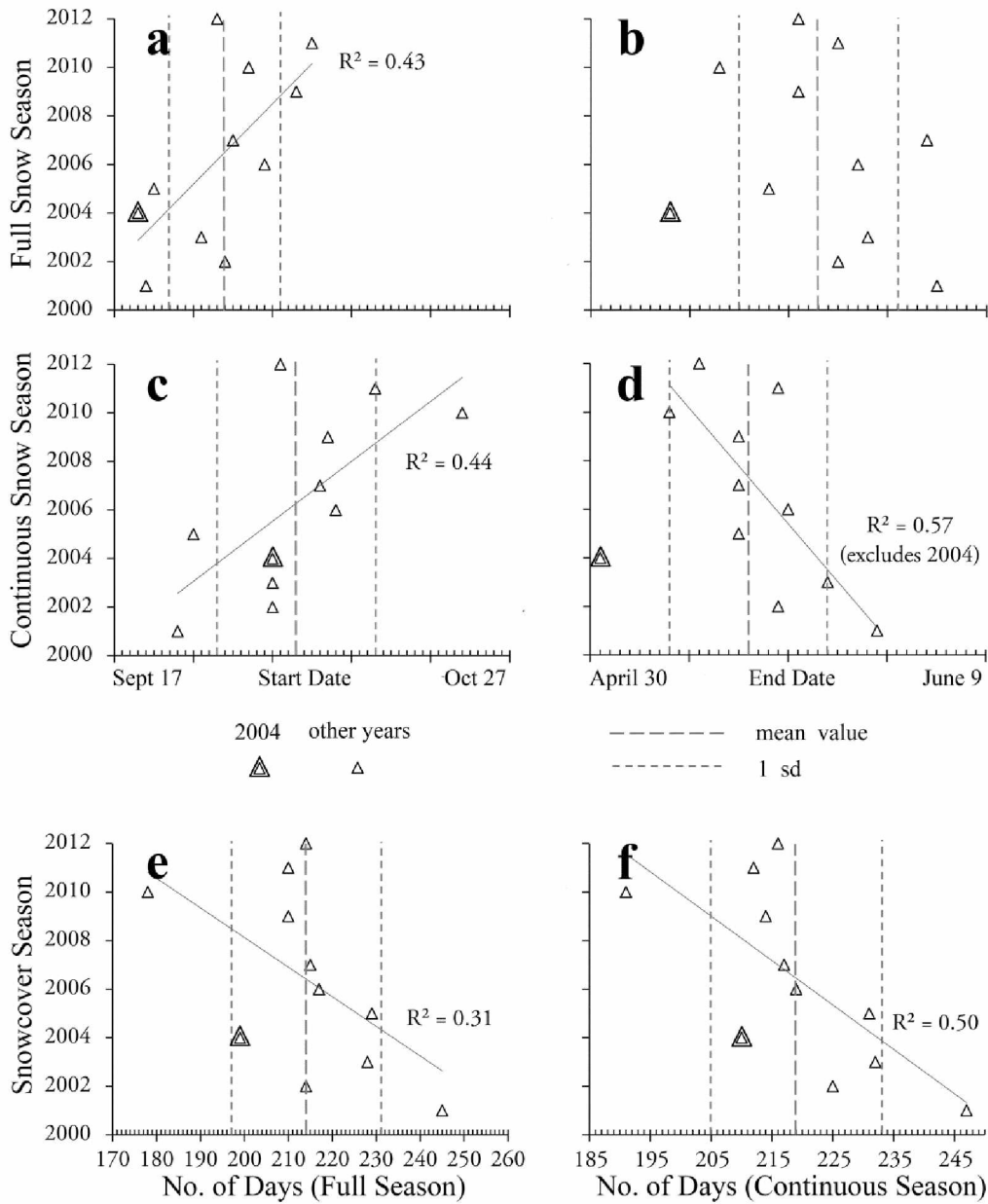


Figure 2.8. Snow cover metrics spatially clipped for the combined Noatak River and Wulik River watersheds (Figure 2.9), from the MODIS Snow Climatology (2001-2012) dataset. Panels a. & b. show start and end dates for the full snow season, by year. Panels c. & d. show start and end dates for the longest period of continuous snow cover, by year. Start and end dates are organized by contiguous snow year; e.g. start dates for the 2004 snow year occurred during the autumn of 2003, while end dates for the 2004 snow year occurred during the spring of 2004. Julian dates from original data have been converted to calendar dates to eliminate the effect of leap years within the figure, and for ease of interpretation. Panels e. & f. show total days of snow cover for the full snow season and the continuous snow season. Trend lines are significant at $p < 0.1$.

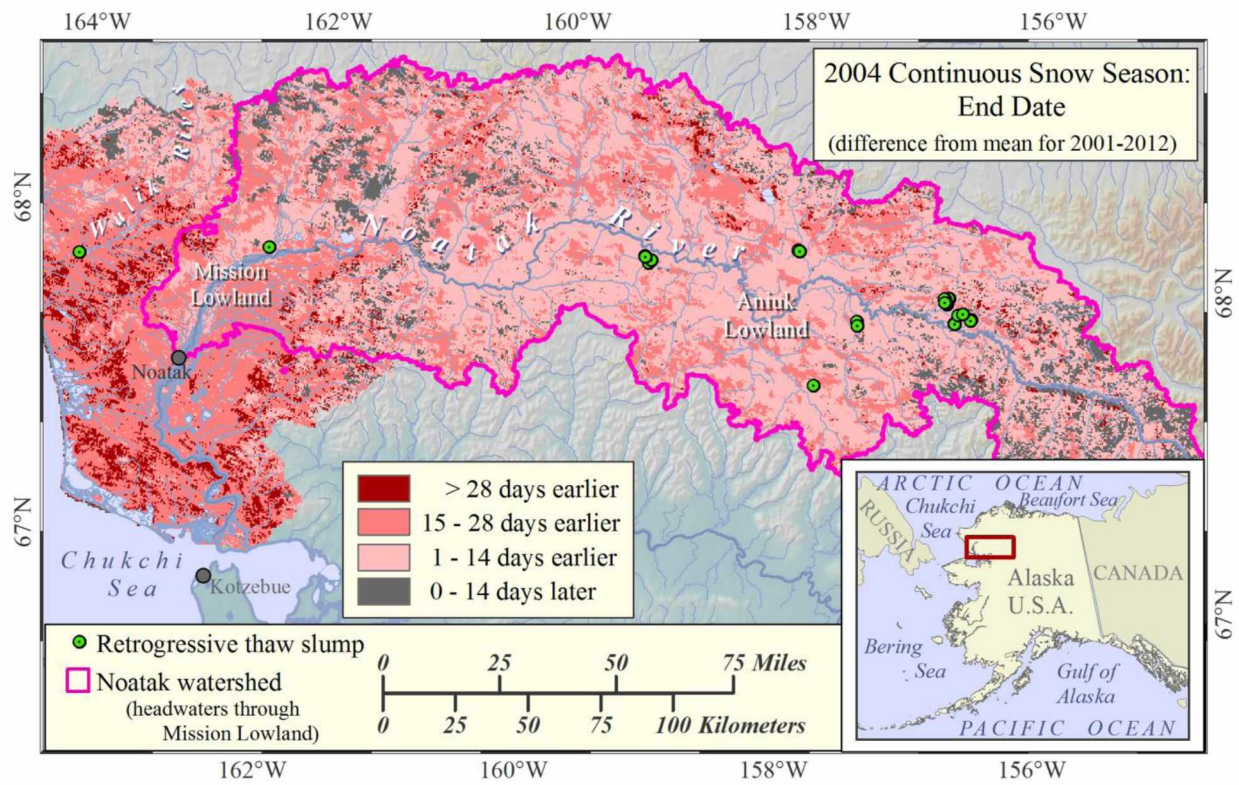


Figure 2.9. Spatial distribution of 2004 continuous snow season end date, as a difference from the mean end date for 2001 through 2012, calculated from the MODIS Snow Climatology (2001-2012) NASA dataset.

Table 2.1. Retrogressive thaw slump features in the Noatak Basin chosen for this study.

Physiographic provinces from Wahrhaftig (1965). 'NPS Code' cross links these data with the National Park Service database for the Arctic Network of Parks (Swanson and Hill 2010). 'ARCSS/TK Code' cross links these data with the NSF - ARCSS/Thermokarst project.

No.	Name	NPS Code	ARCSS/TK Code	Physiographic Province
1	Wulik	n/a	FT2010-16A	DeLong Mountains
2	Rainbucket	NOAT750	FT579A	Mission Lowland
3	Granddad	NOAT039	F35A	Aniuk Lowland
4	FT173Z	NOAT190	FT173Z	Aniuk Lowland
5	FT176Z	NOAT042	FT176Z	Aniuk Lowland
6	Okoklik	NOAT038	FT34A	Aniuk Lowland
7	Gavia Familia	NOAT262	FT2011-14A	Aniuk Lowland
8	Quebec	NOAT261	FT2011-15A	Aniuk Lowland
9	Cutler Ice N	NOAT148	FT2011-12A	Aniuk Lowland
10	Cutler Ice S	NOAT151	FT2011-16X	Aniuk Lowland
11	Cutler Hill	NOAT248	FT2012-2X	Cutler River Upland
12	Good Twin	NOAT068	FT2011-9A	Aniuk Lowland
13	Evil Twin	NOAT069	FT2011-20Z	Aniuk Lowland
14	Third Twin	NOAT070	FT2011-10A	Aniuk Lowland
15	Dropstone Lake S	NOAT071	FT2011-17X	Aniuk Lowland
16	Dropstone Lake NW	NOAT073	FT2011-18X	Aniuk Lowland
17	Dropstone Lake SW	NOAT072	FT2011-19X	Aniuk Lowland
18	Sock Lake 1	NOAT074	FT2012-3X	Central Brooks Range
19	Rico Lake 1	NOAT076	FT2012-4X	Central Brooks Range
20	Anvil Lake 1	NOAT159	FT104Z	Central Brooks Range
21	Aussie Lake 1	NOAT160	FT2012-5X	Central Brooks Range

Table 2.2. Maximum temperature and number of days with temperature above freezing for NOAA and RAWS stations proximal to the study area (Fig. 2.4).

Station	April		May		June	
	Max. Temp.	Max > 0°C	Max. Temp.	Max > 0°C	Max. Temp.	Max > 0°C
	°C	No. of days	°C	No. of days	°C	No. of days
Kotzebue NOAA	5.0	20	12.7	31 +	28.9	30 +
Kelly River RAWS	9.4	24	22.2	31	30.6	30
Noatak RAWS	10.7	18	29.4 *	31 *	34.5	30
Bettles NOAA	10.5	26	21.6	31 +	31.1	30 +

* includes some gap-filled values

+ includes multiple record high temperatures

Table 2.3. May 2004 precipitation at the NOAA and RAWS stations in the study area (Fig. 2.4).

	May 2004		total cm
	5/6 to 5/11 cm	5/22 to 5/24 cm	
Kotzebue NOAA	2.2	0.58	3.5 +
Kelly River RAWS	3.9	2.8	8.1
Noatak Village NOAA	3.5	1.8	6.9
Noatak RAWS	N/A	N/A	N/A
Bettles NOAA	1.2	0.2	4.2

+ includes record rainfall

Table 2.4. Full snow season (FSS) and continuous snow season (CSS) end date metrics for 2004 in the combined Noatak and Wulik River basin study area, and in the smaller subset of the Noatak River basin from the headwaters through the Mission Lowlands (Fig. 2.9).

Analysis Boundary	FSS End 2001-2012 mean date (sd, days)	FSS End 2004 Date (diff. from mean)	CSS End 2001-2012 mean date (sd, days)	CSS End 2004 Date (diff. from mean)
Noatak & Wulik	May 23 (8)	May 8 (-15)	May 16 (8)	May 1 (-15)
Noatak	May 25 (8)	May 12 (-13)	May 18 (7)	May 6 (-12)

Appendix 2. Retrogressive thaw slump features in the Noatak National Preserve from Chapter 2.

Table A2.1. Retrogressive thaw slump feature locations in the Noatak National Preserve. Data developed from ARCSS/TK aerial and field surveys conducted 2006-2011 (Balser et al. 2009), and from National Park Service(NPS) satellite image analysis (Swanson and Hill 2010) . 'NPS Code' cross links these data with the National Park Service database for the Arctic Network of Parks 'ARCSS/TK Code' cross links these data with the NSF - ARCSS/Thermokarst project.

NPS Code	ARCSS/TK Code	Latitude (NAD83)	Longitude (NAD83)
NOAT001	FT121Y	68.03334 °N	158.51775 °W
NOAT002	FT184Z	68.05279 °N	158.56249 °W
NOAT003	n/a	68.06853 °N	159.23989 °W
NOAT004	n/a	68.07031 °N	159.24418 °W
NOAT005	n/a	68.07269 °N	159.25147 °W
NOAT006	n/a	68.08330 °N	159.32616 °W
NOAT007	n/a	68.08189 °N	159.32315 °W
NOAT008	n/a	67.97844 °N	160.25284 °W
NOAT009	n/a	67.97282 °N	160.25395 °W
NOAT010	n/a	67.97141 °N	160.25249 °W
NOAT011	n/a	67.97087 °N	160.25234 °W
NOAT012	n/a	67.95385 °N	160.21667 °W
NOAT013	n/a	67.95436 °N	160.21585 °W
NOAT014	n/a	67.87646 °N	160.63092 °W
NOAT015	n/a	67.90887 °N	160.71330 °W
NOAT016	n/a	67.90904 °N	160.72318 °W
NOAT017	n/a	67.90082 °N	160.82549 °W
NOAT018	n/a	67.90226 °N	160.82915 °W
NOAT019	n/a	67.89851 °N	160.81624 °W
NOAT020	n/a	67.89949 °N	160.91541 °W
NOAT021	n/a	67.91995 °N	160.91194 °W
NOAT022	n/a	67.92061 °N	160.91425 °W
NOAT023	n/a	67.91768 °N	160.90648 °W
NOAT029	n/a	67.99699 °N	161.29088 °W
NOAT030	n/a	67.99772 °N	161.29939 °W
NOAT031	n/a	67.99794 °N	161.30280 °W
NOAT032	n/a	67.99809 °N	161.30445 °W
NOAT033	n/a	68.00434 °N	161.45043 °W
NOAT034	n/a	68.00362 °N	161.45283 °W
NOAT037	FT2007_22A	67.98678 °N	161.87443 °W
NOAT037	n/a	67.98526 °N	161.87393 °W
NOAT037	n/a	67.98639 °N	161.87164 °W
NOAT038	FT34A	68.01470 °N	159.25452 °W
NOAT039	FT35A	68.03589 °N	159.29135 °W

NOAT040	FT175Z	68.02665	°N	159.22937	°W
NOAT041	FT175Z	68.02721	°N	159.22966	°W
NOAT042	FT176Z	68.02386	°N	159.23461	°W
NOAT043	FT129Y	67.97465	°N	158.52016	°W
NOAT044	FT128Y	67.97390	°N	158.51884	°W
NOAT045	FT127Y	67.97275	°N	158.51785	°W
NOAT046	FT125Y	67.97129	°N	158.51487	°W
NOAT047	FT124Y	67.97029	°N	158.51184	°W
NOAT048	FT126Y	67.97181	°N	158.51739	°W
NOAT049	n/a	67.95465	°N	158.47456	°W
NOAT050	n/a	67.95610	°N	158.47488	°W
NOAT051	n/a	67.83972	°N	156.58271	°W
NOAT052	n/a	67.84914	°N	156.61588	°W
NOAT053	n/a	67.85062	°N	156.61327	°W
NOAT054	n/a	67.85100	°N	156.61317	°W
NOAT056	n/a	67.91812	°N	158.02284	°W
NOAT057	n/a	67.91715	°N	158.02288	°W
NOAT068	FT2011_9A	67.96099	°N	156.78836	°W
NOAT069	FT2011_20Z	67.96060	°N	156.79265	°W
NOAT070	FT2011_10A	67.95841	°N	156.82358	°W
NOAT070	FT2011_10B	67.95921	°N	156.82832	°W
NOAT071	FT2011_17X	67.94264	°N	156.80026	°W
NOAT072	FT2011_19X	67.94366	°N	156.80660	°W
NOAT073	FT2011_18X	67.94758	°N	156.81894	°W
NOAT074	FT2012_3X	67.89784	°N	156.60043	°W
NOAT075	n/a	67.89236	°N	156.59822	°W
NOAT076	FT2012_4X	67.89433	°N	156.60442	°W
NOAT077	n/a	67.89202	°N	156.57757	°W
NOAT079	n/a	67.96650	°N	156.84105	°W
NOAT080	n/a	67.96628	°N	157.09421	°W
NOAT081	FT2011_13A	67.98125	°N	157.07528	°W
NOAT082	n/a	67.89455	°N	157.25434	°W
NOAT082	n/a	67.89446	°N	157.25329	°W
NOAT083	n/a	67.89629	°N	157.24773	°W
NOAT084	n/a	67.90608	°N	156.69762	°W
NOAT085	n/a	67.90582	°N	156.69770	°W
NOAT086	n/a	67.90550	°N	156.69750	°W
NOAT087	n/a	67.90517	°N	156.69646	°W
NOAT088	n/a	67.89368	°N	156.62703	°W
NOAT089	n/a	67.89312	°N	156.62576	°W
NOAT090	n/a	67.89260	°N	156.62491	°W
NOAT091	n/a	67.89272	°N	156.62368	°W
NOAT092	n/a	67.89266	°N	156.62223	°W
NOAT093	n/a	67.89270	°N	156.62142	°W
NOAT094	n/a	67.89543	°N	156.60444	°W

NOAT095	n/a	67.98625	°N	157.68913	°W
NOAT108	n/a	67.90137	°N	157.41653	°W
NOAT095	n/a	67.98077	°N	157.41860	°W
NOAT176	n/a	67.98152	°N	157.41483	°W
NOAT096	n/a	67.98147	°N	157.41231	°W
NOAT097	n/a	67.98138	°N	157.42129	°W
NOAT098	n/a	67.98084	°N	157.42069	°W
NOAT099	n/a	68.05890	°N	157.76813	°W
NOAT104	FT10A	68.07933	°N	157.62717	°W
NOAT109	FT9A	68.07931	°N	157.62505	°W
NOAT110	FT8A	68.07904	°N	157.61800	°W
NOAT105	n/a	68.07893	°N	157.61612	°W
NOAT106	n/a	68.07867	°N	157.61316	°W
NOAT102	n/a	68.07753	°N	157.60869	°W
NOAT107	FT11A	68.07717	°N	157.56861	°W
NOAT111	n/a	68.07736	°N	157.57423	°W
NOAT112	n/a	68.07623	°N	157.57572	°W
NOAT113	FT12A	68.07662	°N	157.56633	°W
NOAT114	n/a	68.07347	°N	157.54499	°W
NOAT115	n/a	68.07494	°N	157.54430	°W
NOAT116	n/a	68.07608	°N	157.54599	°W
NOAT117	n/a	68.07486	°N	157.54758	°W
NOAT118	n/a	68.06585	°N	157.45293	°W
NOAT119	n/a	68.02436	°N	157.85493	°W
NOAT146	n/a	68.00267	°N	157.19802	°W
NOAT148	FT2011_12A	67.87676	°N	157.53235	°W
NOAT149	n/a	67.90181	°N	157.41200	°W
NOAT150	n/a	67.89925	°N	157.38847	°W
NOAT151	FT2011_16X	67.86285	°N	157.52668	°W
NOAT153	n/a	67.80366	°N	157.89732	°W
NOAT154	n/a	67.83530	°N	157.41018	°W
NOAT155	n/a	67.83603	°N	157.41232	°W
NOAT156	n/a	67.83473	°N	157.36882	°W
NOAT157	n/a	67.83254	°N	157.35241	°W
NOAT158	n/a	67.82688	°N	157.34956	°W
NOAT159	FT104Z	67.88304	°N	156.73583	°W
NOAT160	FT2012_5X	67.88113	°N	156.73525	°W
NOAT161	n/a	67.89352	°N	156.54770	°W
NOAT161	n/a	67.89301	°N	156.54582	°W
NOAT162	n/a	67.86172	°N	156.66156	°W
NOAT163	n/a	67.85773	°N	156.65427	°W
NOAT164	n/a	67.87380	°N	156.75980	°W
NOAT165	n/a	67.87432	°N	156.75221	°W
NOAT166	n/a	67.87405	°N	156.75833	°W
NOAT169	n/a	67.84408	°N	157.13806	°W

NOAT170	n/a	67.84225	°N	157.11533	°W
NOAT172	n/a	67.80643	°N	156.68164	°W
NOAT175	n/a	67.80098	°N	156.76809	°W
NOAT267	FT104ZC	67.88329	°N	156.73751	°W
NOAT177	n/a	67.94714	°N	156.81531	°W
NOAT178	n/a	67.94329	°N	156.80352	°W
NOAT180	n/a	68.05457	°N	159.64726	°W
NOAT180	n/a	68.05275	°N	159.64812	°W
NOAT183	FT2A	68.08785	°N	158.63906	°W
NOAT184	n/a	68.08701	°N	159.18238	°W
NOAT185	n/a	68.08767	°N	159.18178	°W
NOAT188	n/a	68.01996	°N	158.70861	°W
NOAT189	FT174Z	68.02809	°N	159.23927	°W
NOAT189	FT174Z	68.02844	°N	159.23732	°W
NOAT190	FT173Z	68.03361	°N	159.28723	°W
NOAT194	FT175Z	68.02782	°N	159.23027	°W
NOAT207	n/a	67.90050	°N	158.05920	°W
NOAT208	n/a	67.89910	°N	158.06268	°W
NOAT209	FT181Z	67.85119	°N	158.33407	°W
NOAT222	n/a	67.85694	°N	158.27643	°W
NOAT212	n/a	67.80501	°N	157.97156	°W
NOAT213	n/a	67.79261	°N	157.98444	°W
NOAT215	n/a	67.79747	°N	158.47198	°W
NOAT216	n/a	67.79189	°N	158.47167	°W
NOAT217	n/a	67.79056	°N	158.47154	°W
NOAT220	n/a	67.78388	°N	158.33236	°W
NOAT223	n/a	67.78138	°N	157.66112	°W
NOAT226	n/a	67.80153	°N	156.76805	°W
NOAT225	n/a	67.78753	°N	156.69310	°W
NOAT229	n/a	67.73322	°N	158.66719	°W
NOAT230	n/a	67.73044	°N	158.66659	°W
NOAT231	n/a	67.73203	°N	158.67144	°W
NOAT232	n/a	67.73148	°N	158.60186	°W
NOAT228	n/a	67.73367	°N	158.65859	°W
NOAT236	n/a	67.73333	°N	158.14458	°W
NOAT237	n/a	67.70493	°N	157.93539	°W
NOAT238	n/a	67.70405	°N	157.93604	°W
NOAT239	n/a	67.70571	°N	157.32923	°W
NOAT240	n/a	67.70551	°N	157.32699	°W
NOAT241	n/a	67.70294	°N	157.31894	°W
NOAT242	n/a	67.70203	°N	157.31464	°W
NOAT243	n/a	67.70243	°N	157.31290	°W
NOAT244	n/a	67.70069	°N	157.31179	°W
NOAT251	n/a	67.69133	°N	157.26403	°W
NOAT247	n/a	67.66974	°N	157.85169	°W

NOAT248	FT2012_2X	67.67070	°N	157.85285	°W
NOAT249	n/a	67.67169	°N	157.85449	°W
NOAT250	n/a	67.67228	°N	157.85321	°W
NOAT152	n/a	67.80435	°N	157.89493	°W
NOAT261	FT2011_12A	68.08791	°N	158.04023	°W
NOAT262	FT2011_14A	68.08375	°N	158.02692	°W
NOAT263	n/a	68.08242	°N	158.02099	°W
NOAT265	n/a	67.94688	°N	161.09126	°W
NOAT266	n/a	67.94850	°N	161.07638	°W
NOAT266	n/a	67.94741	°N	161.07644	°W
NOAT266	n/a	67.94765	°N	161.07468	°W
NOAT270	n/a	68.16894	°N	157.56485	°W
NOAT281	n/a	68.15882	°N	157.08467	°W
NOAT325	n/a	68.06351	°N	156.49344	°W
NOAT326	n/a	68.06398	°N	156.49405	°W
NOAT327	n/a	68.06448	°N	156.49490	°W
NOAT327	n/a	68.06467	°N	156.49572	°W
NOAT331	n/a	68.08817	°N	155.90028	°W
NOAT332	n/a	68.08753	°N	155.89988	°W
NOAT333	n/a	68.08328	°N	155.86213	°W
NOAT334	n/a	68.08030	°N	155.80049	°W
NOAT335	n/a	68.07969	°N	155.79896	°W
NOAT336	n/a	68.07921	°N	155.79826	°W
NOAT470	n/a	68.22815	°N	157.15002	°W
NOAT471	n/a	68.28109	°N	157.12691	°W
NOAT472	n/a	68.28237	°N	157.13269	°W
NOAT472	n/a	68.28243	°N	157.13399	°W
NOAT473	n/a	68.27850	°N	157.12403	°W
NOAT489	FT359X	68.27191	°N	157.88248	°W
NOAT490	FT299X	68.27429	°N	157.88515	°W
NOAT491	FT547X	68.27336	°N	157.88983	°W
NOAT492	n/a	68.27378	°N	157.87947	°W
NOAT505	FT377X	68.27889	°N	157.79493	°W
NOAT608	FT24A	68.23288	°N	158.33989	°W
NOAT609	FT25A	68.23102	°N	158.33418	°W
NOAT609	FT26A	68.23081	°N	158.33348	°W
NOAT610	FT167Z	68.19846	°N	159.47967	°W
NOAT611	FT168Z	68.20111	°N	159.47627	°W
NOAT612	FT169Z	68.20657	°N	159.46245	°W
NOAT613	FT170Z	68.20901	°N	159.45968	°W
NOAT631	n/a	68.53666	°N	160.10576	°W
NOAT644	FT14A	68.32479	°N	157.89185	°W
NOAT646	n/a	67.80498	°N	159.20327	°W
NOAT647	n/a	67.80441	°N	159.20169	°W
NOAT647	n/a	67.80359	°N	159.20258	°W

NOAT648	n/a	67.80167	°N	159.20583	°W
NOAT648	n/a	67.80132	°N	159.20652	°W
NOAT647	n/a	67.80382	°N	159.20521	°W
NOAT650	n/a	68.41579	°N	160.85692	°W
NOAT652	FT2007_18A	68.32304	°N	161.39026	°W
NOAT653	FT2007_1A	68.29209	°N	161.36458	°W
NOAT654	n/a	68.18955	°N	161.17762	°W
NOAT686	FT2007_8A	67.95591	°N	162.13584	°W
NOAT686	FT2007_9A	67.95618	°N	162.13618	°W
NOAT687	FT2007_20A	67.97359	°N	161.79731	°W
NOAT687	FT2007_20B	67.97370	°N	161.79612	°W
NOAT688	FT2007_20C	67.97498	°N	161.80024	°W
NOAT688	FT2007_20D	67.97490	°N	161.79904	°W
NOAT688	n/a	67.97465	°N	161.79826	°W
NOAT689	FT2007_21A	67.96973	°N	161.79829	°W
NOAT690	FT2007_21B	67.96881	°N	161.79856	°W
NOAT691	FT2007_21C	67.96829	°N	161.79847	°W
NOAT692	n/a	67.96802	°N	161.79787	°W
NOAT693	FT2007_19A	67.95938	°N	161.74303	°W
NOAT694	FT2007_19B	67.96068	°N	161.74355	°W
NOAT695	FT2007_19C	67.96096	°N	161.74364	°W
NOAT696	n/a	67.96658	°N	161.67807	°W
NOAT697	n/a	67.96681	°N	161.67888	°W
NOAT712	n/a	67.99308	°N	161.22251	°W
NOAT718	n/a	67.95998	°N	161.10841	°W
NOAT719	n/a	67.95384	°N	161.11060	°W
NOAT720	n/a	67.95324	°N	161.11110	°W
NOAT713	n/a	67.96606	°N	161.46904	°W
NOAT721	n/a	68.05971	°N	160.76811	°W
NOAT722	n/a	68.04412	°N	160.77664	°W
NOAT723	n/a	68.03463	°N	160.75558	°W
NOAT724	n/a	68.03699	°N	160.79310	°W
NOAT750	FT579A	67.94347	°N	162.35573	°W
NOAT754	FT2007_13A	67.56131	°N	161.77272	°W
NOAT767	FT2007_14A	67.58750	°N	161.61978	°W
NOAT767	FT2007_15A	67.58710	°N	161.61933	°W
NOAT778	FT2007_10A	67.61210	°N	161.57027	°W
NOAT779	FT2007_12A	67.60949	°N	161.53688	°W
NOAT782	FT2007_16A	67.59523	°N	161.59777	°W
NOAT788	FT578D	67.92763	°N	161.96554	°W
NOAT789	FT578C	67.92761	°N	161.97085	°W
NOAT790	FT578A	67.92805	°N	161.97232	°W
NOAT793	FT2007_2A	67.92566	°N	161.68138	°W
NOAT794	FT2007_3A	67.92613	°N	161.68129	°W
NOAT798	FT578B	67.92853	°N	161.96181	°W

NOAT809	n/a	67.91445	°N	160.90042	°W
NOAT842	n/a	67.88888	°N	160.82847	°W
NOAT842	n/a	67.88898	°N	160.82741	°W
NOAT842	n/a	67.88899	°N	160.82640	°W
NOAT842	n/a	67.88921	°N	160.82520	°W
NOAT842	n/a	67.88932	°N	160.82443	°W
NOAT265	n/a	67.94757	°N	161.09385	°W
NOAT265	n/a	67.94810	°N	161.09248	°W
NOAT265	n/a	67.94803	°N	161.09004	°W
NOAT265	n/a	67.94804	°N	161.09066	°W
NOAT265	n/a	67.94742	°N	161.09080	°W
NOAT265	n/a	67.94724	°N	161.09076	°W
NOAT265	FT2010_21A	67.94745	°N	161.09229	°W
NOAT265	FT2010_21B	67.94728	°N	161.09209	°W
NOAT265	n/a	67.94738	°N	161.09349	°W
NOAT845	n/a	67.90608	°N	160.46555	°W
NOAT846	n/a	67.90544	°N	160.46030	°W
NOAT847	n/a	67.90621	°N	160.78598	°W
NOAT847	n/a	67.90577	°N	160.78592	°W
NOAT848	n/a	67.88479	°N	160.35155	°W
NOAT852	FT2007_4A	67.85049	°N	161.33475	°W
NOAT853	FT2007_5A	67.85156	°N	161.32800	°W
NOAT854	FT569A	67.85891	°N	161.31608	°W
NOAT907	n/a	67.83676	°N	160.71961	°W
NOAT1140	n/a	67.78399	°N	160.70112	°W
NOAT1141	n/a	67.78742	°N	160.71386	°W
NOAT1142	n/a	67.78819	°N	160.71284	°W
NOAT1143	n/a	67.78558	°N	160.71948	°W
NOAT1131	n/a	67.80876	°N	160.58928	°W
NOAT1132	n/a	67.80865	°N	160.59132	°W
NOAT1133	n/a	67.81761	°N	160.61431	°W
NOAT1134	n/a	67.81760	°N	160.61171	°W
NOAT1135	n/a	67.81751	°N	160.61059	°W
NOAT1136	n/a	67.81648	°N	160.60323	°W
NOAT1137	n/a	67.81303	°N	160.57685	°W
NOAT983	FT2007_6A	67.67004	°N	161.57580	°W
NOAT1016	FT2010_15A	67.64841	°N	161.60614	°W
NOAT1021	FT2007_17A	67.58718	°N	161.59151	°W
NOAT1027	FT2007_7A	67.66096	°N	161.50148	°W
NOAT1045	FT2007_11A	67.60503	°N	161.52407	°W
NOAT1053	n/a	67.68936	°N	160.46550	°W
NOAT1100	n/a	67.93909	°N	160.22285	°W
NOAT1101	n/a	67.94431	°N	159.83957	°W
NOAT1102	n/a	67.92030	°N	159.83648	°W
NOAT1102	n/a	67.92008	°N	159.83878	°W

NOAT1102	n/a	67.91980	°N	159.83953	°W
NOAT1102	n/a	67.92018	°N	159.84003	°W
NOAT1104	n/a	67.94471	°N	159.69674	°W
NOAT1118	n/a	68.00343	°N	160.16666	°W
NOAT1119	n/a	67.99322	°N	160.17338	°W
NOAT1120	n/a	67.99219	°N	160.17853	°W
NOAT1121	n/a	67.96789	°N	160.24902	°W
NOAT1122	n/a	67.96819	°N	160.25019	°W
NOAT1127	FT165Z	68.19500	°N	159.54500	°W
NOAT1128	FT166Z	68.19534	°N	159.54512	°W
n/a	FT2010-16A	67.84741	°N	163.88147	°W

Balsler, A., M. N. Gooseff, J. Jones, and W. B. Bowden (2009), Thermokarst distribution and relationships to landscape characteristics in the Feniak Lake region, Noatak National Preserve, Alaska; Final Report to the National Park Service, Arctic Network (ARCN), Fairbanks, AK.

Swanson, D. K., and K. Hill (2010), Monitoring of Retrogressive Thaw Slumps in the Arctic Network, 2010 Baseline Data: Three-dimensional Modeling with Small-format Aerial Photographs, edited, p. 58, U.S. Department of the Interior, National Park Service, Natural Resource Data Series NPS/ARCN/NRDS—2010/123, Natural Resource Program Center, Fort Collins, CO.

Chapter 3. Relationship of Cryofacies, Surface and Subsurface Terrain Conditions in the Brooks Range and Foothills of Northern Alaska¹

3.0 Abstract

Permafrost landscape responses to climate change and disturbance impact local ecology and global greenhouse gas concentrations, but the nature and magnitude of response is linked with vegetation, terrain and permafrost properties which vary markedly across landscapes. As a subsurface property, permafrost conditions are difficult to characterize across landscapes, and modelled estimates rely upon relationships among permafrost characteristics and surface properties. While a general relationship among landscape and permafrost properties has been recognized throughout the arctic, the nature of these relationships is poorly documented in many regions, limiting modelling capability. We examined relationships among permafrost, terrain and vegetation within the Brooks Range and foothills of northern Alaska using field data from diverse sites within a multiple factor analysis ordination to identify and describe these relationships in this region, and to facilitate future modelling and ecological research. Terrain, vegetation and permafrost conditions were correlated throughout the region, with field sites falling into four statistically-separable groups based on ordination results. Our results identify index variables for honing field sampling and statistical analysis, illustrate the nature of relationships in the region, support future modelling of permafrost properties, and suggest a state factor approach for organizing data and ideas relevant for modelling of permafrost properties at a regional scale.

3.1 Introduction

Permafrost landscape responses are critical components of global climate change, but responses and feedbacks depend on ecosystem properties, which vary markedly throughout the arctic. Permafrost landscape structure develops through a complex interplay among climate, substrate, and surficial processes operating at multiple spatial and temporal scales (Shur and Jorgenson 2007). At the interface between the atmosphere and deep permafrost, processes of vegetation, soil, and upper-permafrost cryostructures respond to climate shifts and disturbance (Viereck 1973, ACIA 2005, Jorgenson et al. 2010a, Jorgenson et al. 2013), and mediate the influence of climate on deeper permafrost (Shur and Jorgenson 2007, French and Shur 2010). Vegetation and upper permafrost horizon development have been linked with terrain properties and climate (Kreig and Reger 1982, Shur 1988, Shur and Jorgenson 2007, Pastick et al. 2014), and are mutually influential at local and circumarctic scales, though the nature and extent of relationships among vegetation and permafrost is only partially understood (Raynolds and Walker 2008, Walker et al. 2008, French and Shur 2010, Lantz et al. 2010, Kokelj and Jorgenson 2013).

¹ Submitted to *Permafrost and Periglacial Processes*. Balsler, A. W., J. B. Jones, and M. T. Jorgenson, March 2015.

In the Brooks Range and foothills of northern Alaska, multiple modes of permafrost degradation appear to be accelerating (Jorgenson et al. 2006, Bowden et al. 2008, Jorgenson et al. 2008a, Balsler et al. 2009, Gooseff et al. 2009), but relationships among terrain properties, vegetation, and upper permafrost characteristics are weakly documented (Jorgenson et al. 2008b, Jorgenson et al. 2010b). Region-wide estimates of future landscape resilience and response to climate perturbation depend on spatially-explicit representations of conditions (Callaghan et al. 2004), but subsurface permafrost properties across the landscape are difficult to observe directly. Determination of permafrost properties in remote, northern Alaska depends on understanding these relationships, and applying them at a regional scale. Determining which specific terrain properties and groups of terrain properties are most correlated with vegetation and upper permafrost conditions within this region, and the degree to which correlations apply across diverse landscapes, is central to future estimates of resilience, responses, and feedbacks to climate in the Brooks Range and foothills of northern Alaska.

3.1.1 Responses and Feedbacks to Climate

Permafrost degradation rate has been increasing in recent decades throughout the circumarctic and is anticipated to continue or accelerate (ACIA 2005, Hinzman et al. 2005, Schuur and Abbott 2011). Marked impacts and feedbacks are expected across the cryosphere, with shifts in ecosystem structure and function (Callaghan et al. 2004, Osterkamp et al. 2009, Goetz et al. 2011, Myers-Smith et al. 2011), local and global hydrologic cycles (Peterson et al. 2002, Hinzman et al. 2006, Frey et al. 2007), and biogeochemistry and carbon release (Tamocai et al. 2009, Grosse et al. 2011, Schaefer et al. 2011).

Distinct modes of permafrost degradation correlate with specific combinations of surficial landscape properties, each with a different influence on ecological, hydrological, and biogeochemical shifts, and characterized by distinct morphologies and processes (Hinzman et al. 2005, Jorgenson et al. 2008a, Schuur et al. 2009, Lafreniere and Lamoureux 2013). Modes of permafrost degradation include active-layer deepening, as well as an array of subsidence features broadly termed ‘thermokarst’ (Hinzman et al. 2005, Jorgenson et al. 2008a). Each mode affects ecosystem properties and processes at different depths, rates, and scales, in turn driving the nature and magnitude of overall impacts (Jorgenson et al. 2013). Modes of permafrost degradation in response to climate perturbation or disturbance are coupled with local surficial conditions, including thermal properties, thaw stability, slope, hydrology and ground ice characteristics (Leibman et al. 2003, Lewkowicz and Harris 2005, Jorgenson et al. 2008a, Kokelj et al. 2009, Jorgenson et al. 2010a, Lantuit et al. 2012). Thermal properties, thaw stability, and hydrology, in turn, are influenced by cryostructure distribution and ground ice content, vegetation, and soil composition and organic layer development (Shur and Jorgenson 2007) .

3.1.2 Landscape Variability

Vegetation development on the surface and cryostructure development in the upper-permafrost are dynamically linked ecosystem processes organized in complex but potentially generalizable patterns across landscapes. Mutual influences between vegetation and permafrost (Raynolds and Walker 2008) are linked with terrain characteristics, surficial thermal properties, and hydrology (Shur and Jorgenson 2007, French and Shur 2010). These may be considered within the ‘state factor’ framework, which groups terrain properties within five umbrella categories: biota, parent material, topography, climate, and time (Jenny 1941, van Cleve et al. 1991, Jorgenson et al. 2013).

On newly deposited surfaces, topography, surficial geology, climate, and potential recruitment drive initial development of vegetation and new cryostructures, and influence the fate of pre-existing ground ice, such as relict glacial ice (Washburn 1980, Walker et al. 2008, French and Shur 2010). With time, vegetation and cryostructure development exert increasing influence at the surface, mediating heat flux, soil moisture, and decomposition rate of organic matter, which in turn feeds back on vegetation and cryostructure development (Davis 2001, Hobbie and Gough 2004, Walker et al. 2008). Vegetation, active-layer depth, and the nature and degree of permafrost and cryostructure development across heterogeneous landscapes are a product of these interactions (Shur and Jorgenson 2007, Raynolds and Walker 2008, Walker et al. 2008, French and Shur 2010, Walker et al. 2011). Correlations among vegetation and permafrost characteristics are recognized from studies at specific sites (Kreig and Reger 1982, Shur and Jorgenson 2007, Walker et al. 2008, Kanevskiy et al. 2011, Epstein et al. 2012), and from regional to circumarctic-scale studies (Raynolds and Walker 2008, Gruber 2012, Pastick et al. 2014).

3.1.3 Integrating Terrain Properties

A general approach describing relationships among terrain properties and permafrost, congruent with the state factor framework (Shur and Jorgenson 2007), has been developed to better estimate permafrost vulnerability among different landscapes. Terrain properties and permafrost characteristics co-vary, and consistency of associations among permafrost, terrain and vegetation enable landscape-scale analysis on that basis (Jorgenson and Kreig 1988, Raynolds and Walker 2008, Jorgenson et al. 2010a, Jorgenson et al. 2013, Pastick et al. 2014). While the importance of surficial deposits (Kreig and Reger 1982, Jorgenson et al. 2008b) and vegetation (Viereck 1973) to ground ice and permafrost development have long been recognized, landscape-scale methods for integrating terrain factors are not fully developed. Toward improved terrain factor integration, we hypothesized that: 1) vegetation and permafrost properties consistently correlate with specific terrain conditions across landscapes due to these relationships, 2) that diverse landscapes may fall into general groupings from statistical analysis of empirical field data for these combined properties, and 3) that these relationships can be used to help

identify which terrain factors, in combination, facilitate spatial characterization of surficial landscape properties in the Brooks Range and foothills of northern Alaska.

Our research tested these ideas statistically using ordination of empirical, field survey data collected from sites representing diverse landscapes in the Brooks Range and foothills of northern Alaska. Identifying statistically-supported linkages between permafrost properties including ground ice content and cryostructures, and terrain properties including vegetation and surficial geology, can facilitate regional scale estimation of permafrost vulnerability and estimation of ground ice conditions, and better inform models examining regional resilience, response and feedbacks to climate change.

3.2 Methods

3.2.1 Study Region

Our research spanned a gradient of arctic tundra and shrub landscapes within Alaska's Brooks Range and foothills, from the east-central portion of Alaska's North Slope westward through the Noatak Basin to the Mission Lowlands, near the Noatak delta (Figure 3.1). These periglacial landscapes are within the continuous permafrost zone (Jorgenson et al. 2008b) and are part of Arctic Bioclimate Subzone E (CAVM-Team 2003). The northeast portion of the study region was centered around Toolik Field Station on the north slope of Alaska, while the central and western study region followed the Noatak Basin from near its headwaters downstream to the Mission Lowlands, near the Noatak River delta.

Toolik Field Station is located in the northern Brooks Range foothills within a matrix of landscapes of varying glacial ages and ecotypes. Physiography ranges from low mountains at the edge of the Brooks Range to subtle foothills stretching more than 75 km from the mountains to the edge of the arctic coastal plain. Date since most recent glaciation ranges from early Pleistocene to Holocene for field sites surrounding Toolik Field Station, with acidic and nonacidic, graminoid and shrub tundra vegetation reflecting duration of ecosystem development and local site conditions (Walker et al. 1994, Walker et al. 1995, Hamilton 2003, Walker and Maier 2008). Lake and stream density is variable by landscape age-class and related with glacial and periglacial landforms (Hobbie et al. 1991, Kling 1995, Hamilton 2003).

The Noatak River flows 730 km along a westward course at approximately 67.5° N latitude (Figure 3.1). Most of the 33,100-km² basin falls within the Noatak National Preserve (U.S. National Park Service) and is recognized as a UNESCO Biosphere Reserve. The Noatak Basin was periodically glaciated throughout the Pleistocene and contains a patchwork of glacial and periglacial landforms ranging in age from early Pleistocene to contemporary (Hamilton 2010, Hamilton and Labay 2011). Physiographic provinces include high mountains of the east-central Brooks Range, through foothills and valley bottoms

to the Mission Lowlands at the arctic-boreal ecotone near the Noatak mouth (Wahrhaftig 1965, Young 1974). Land cover spans a gradient of ecotypes including arctic and alpine tundra, shrublands and lowland boreal forest (Young 1974, Viereck et al. 1992, Parker 2006, Jorgenson et al. 2010b).

Landscape conditions throughout this 500 km wide region represent a broad range of typical low-arctic landscapes (Figure 3.2). Alpine, foothill, and valley bottom settings include many characteristic ecotypes of the North American low arctic, a suite of periglacial landforms, diverse surficial geology and lithology, and a broad continuum of permafrost characteristics and cryostructures. While a geographic gap exists between the Toolik and Noatak subregions, substantial overlap among terrain properties and permafrost cryostratigraphy link them conceptually. Our study deliberately included a breadth of conditions over a large geographic area to represent a diversity of low-arctic landscapes in the region.

3.2.2 Field Surveys

Our regional survey identified areas of surface-exposed and degrading permafrost distributed among diverse landscapes, from which we selected field sites representing a range of low-arctic conditions. Aircraft-supported field campaigns and airphoto analysis in 2006, 2007, and 2008 were used to identify watersheds with actively degrading permafrost exposures representing different modes of degradation (and by proxy, differing ground-ice conditions). Several thousand permafrost degradation feature locations were recorded in an ArcGIS GeoDatabase, which was later expanded and augmented through a subsequent National Park Service survey which included both Gates of the Arctic National Park and Preserve and Noatak National Preserve, using high-resolution satellite imagery to census these features throughout both park units (Balsler et al. 2009, Swanson and Hill 2010). These data drove spatial analyses identifying diverse combinations of ecotype, lithology and surficial geology among subwatersheds accessible by helicopter from field camps at Kelly River, Feniak Lake, and Toolik Field Station (Figure 3.1). During subsequent helicopter-based visits in 2009, 2010, and 2011, field sites were chosen for detailed examination based on: 1) best accessibility to exposures of permafrost, and 2) inclusive representation among terrain properties including ecotype, lithology, and surficial geology.

At each field site, we measured and described general landscape characteristics and specific conditions at the site of permafrost exposure. A subset of categorical and quantitative data collection protocols and field codes (Appendix 3) were adopted from Jorgenson et al. (2010b) to characterize ambient surface properties (within approximately 100 m of the permafrost exposure) and to catalog the specific combination of vegetation, soil, surficial geology and cryostratigraphy immediately at the site of permafrost exposure (Table 3.1). Basic geomorphology, lithology, surficial geology, topography, and landforms were recorded to represent the area within approximately 100 m of the permafrost exposure.

Vegetation was recorded both by class (Viereck et al. 1992) and as a list of predominant overstory and understory species of vascular plants, and functional groups of bryophytes within 20 m of the permafrost exposure.

Permafrost profile exposures were described in detail to characterize and quantify live vegetation, contemporary soil (organic and mineral), parent material and archaic soils, coarse fraction, ice content, cryostratigraphy, and interpretations of mechanisms of cryogenesis. Permafrost exposures were predominantly comprised of vertical scarps at actively degrading edges of retrogressive thaw slumps, active layer detachment slides and thermo-erosional gullies (Figure 3.3). Permafrost exposures were prepared using hand tools to remove previously thawed material and expose an intact permafrost profile from the top (ground surface) down to the greatest accessible depth within the thaw feature (Figure 3.4). Exposures were prepared to a width of at least 1 m, with categorical and quantitative tabular data taken for each discernible layer in the profile (Figure 3.4) from vegetation at the surface to the bottom of the exposure. Data from each discernible subsurface layer were weighted by layer thickness and integrated to generate overall values for: a) contemporary soil; and b) archaic soil layers and parent material (Table 3.2). Hand-drawn cryostratigraphic maps roughly following Kanevskiy et al. (2011), and detail photos for each permafrost profile complement data and general site photos and were used for interpretation and summarization.

3.2.3 Data Analysis

3.2.3.1 Data Reduction

To statistically analyze our 46 field sites by terrain and permafrost properties, we began with data reduction to eliminate extraneous independent variables with minimal contribution to our model, and to reduce redundancy in the data. We employed Pearson (r) correlations in two separate steps to examine redundancy and to identify variables with minimal contribution to ordination results. In the first step, a Pearson correlation analysis of all variables against one another with R statistical software was used to examine inter-variable relationships and identify groups that might be represented by a single integrator variable. Where a set of variables was grouped by Pearson scores > 0.60 for all pairings, the group was considered a candidate for integration.

In the second step, all variables went through a pilot, three-axis non-metric multidimensional scaling (NMS) ordination with 50 runs of 250 iterations in PC-ORD to generate Pearson correlation values for each variable against each ordination axis. This ordination was used to examine the contribution of each variable to the ordination and eliminate those with minimal analytical value. For this analysis, categorical data were transformed to binary numbers for each categorical unit of each

categorical variable, while continuous and ordinal data were scaled 0 to 1 (precision to the hundredth) to conform with NMS analysis assumptions for a valid distance matrix (McCune and Grace 2002, McCune 2013). Those variables with NMS Pearson scores < 0.30 for each axis were deemed extraneous and excluded from subsequent ordination. From each grouping of highly correlated variables identified in step one, a single integrator variable was chosen from the group based on highest cumulative Pearson score across all axes in step two.

3.2.3.2 Multiple Factor Analysis Ordination

Relationships among permafrost and terrain properties were examined using multiple factor analysis (MFA) ordination of 46 surveyed field sites. Traditional ordination is conducted on datasets where all variables are comparable and of the same type (e.g., vegetative species by percent cover). While the goals of our analysis were similar to outcomes derived from traditional ordination (e.g., site similarity and clustering in multidimensional space as determined by a distance matrix), our dataset comprised different logical groupings of data for each site (e.g., ice, substrate and vegetation) and dissimilar data types, such as coarse fragment size class (ordinal), vegetation type (categorical), and ice percentage (continuous).

Multiple factor analysis (MFA), a recent adaptation of principal component analysis (PCA), was chosen for this application of ordination because it is designed to integrate dissimilar data types and different logical groupings of data (termed 'blocks') for each observation within a single ordination run (Escofier and Pagès 1994). While other ordination techniques, such as NMS, can also be applied after data transformation and scaling (McCune and Grace 2002, McCune 2013), MFA offers two distinct advantages over NMS and other ordination techniques under these conditions. First, end-user data transformation is unnecessary because MFA performs data normalization in an initial PCA step, using the square root of the first eigenvalue in a manner comparable to Z-score normalization (Abdi et al. 2013). These normalized data are then merged to form the analysis matrix, enabling valid distance matrices to be calculated from what were initially incongruous variables. Second, MFA provides the option to define blocks of data, which are conceptually coherent groups of variables pertaining to all observations (Abdi et al. 2013). The chief advantage of a block approach is that individual blocks of data (e.g., vegetation, substrate, ice) are inhibited from dominating the ordination results while other blocks become de-emphasized. MFA achieves this parity by normalizing the input data by block, and by handling each block as a sub-matrix of the whole. The first principal component of each block is scaled to 1 in the normalization step, which ensures that no block will dominate the model through disproportionate inertia in the final ordination (Abdi et al. 2013). Finally, each block must contain variables of the same data type

for the normalization step to produce valid results. Thus, conceptual blocks containing multiple data types were split by type.

Data were originally recorded by segment of the study site (Tables 3.1 and 3.2), but were reorganized for statistical analysis into response variables and independent variables, and by block. To effectively address the hypothesis that terrain properties consistently influence cryostructure, ground ice, and vegetation across sites, we divided the dataset into response variables and independent variables from the perspective of the current ecosystem. Site characteristics that predate and may potentially influence the current ecosystem (e.g., surficial geology) were classed as independent variables, while properties influenced by contemporary ecosystem processes (e.g., vegetation, microtopography and upper permafrost cryostructures) were classed as response variables and assigned to blocks. Response variables, termed 'active' variables in MFA, were the basis of ordination calculations. Potential explanatory or 'supplemental' variables were employed as overlays on graphs of analysis results to illustrate underlying drivers of statistically demonstrated relationships among permafrost, substrate and vegetation. The final set of variables, selected through Pearson score analyses and reorganized for MFA, were assigned to blocks (Table 3.3) and ordinated by MFA with three dimensions using the FactoMineR package within R statistical software (Le et al. 2008).

Finally, ordination results were used for hierarchic clustering in FactoMineR to produce a dendrogram depicting relative similarity/dissimilarity among sites, and to delineate statistical groupings of sites. Euclidean distance and Ward's method (0.75 inertia level) were used to generate the dendrogram and delineate groupings (Husson et al. 2010).

3.3 Results

MFA ordination revealed complex but consistent patterns of correlation among terrain and permafrost properties across sites, and subsequent hierarchical clustering analysis produced four primary groupings, two of which were further divided into subgroups based on subtle but consistent differences among sites. Correspondence among categorical variables within the ordination spanned across different MFA blocks (Figure 3.5), indicating that factors across the three blocks of vegetative, substrate, and permafrost/ice properties were co-varying among sites. Coarse and fine fraction (substrate), primary permafrost cryostructure (permafrost/ice), and ecotype (vegetative) all contributed to consistent, statistical separation among sites, while specific values for these variables were distributed across sites in complex combinations.

While co-varying, factors organized by block were not redundant in the ordination. Each of the first three ordination axes were driven by differential influences from each block, with axis one driven most by substrate then vegetation, axis two driven most by permafrost/ice then by vegetation, and axis three driven by roughly equivalent influence of all three blocks (Figure 3.6).

3.3.1. Hierarchically Clustered Groupings

Hierarchical clustering of ordination results produced four groupings from 46 sites in the study region (Figure 3.7). Group E1 contained six sites, E2 comprised 22 sites, E3 had five sites, and group E4 was made up of 13 sites. Groups E2 and E4 were further subdivided, based upon statistical differences driven by identifiable, single factors within the ordination. Each group was characterized by combinations of terrain and permafrost properties.

Group E1.

The E1 grouping was found on late-Pleistocene moraine deposits where: 1) carbonate lithologies comprise more than 10% of clast composition in the substrate, 2) the surface soils were well-drained, nonacidic, and had thin organic layers, and low percentages of massive and segregation ice, and 3) vegetation was dominated by calciphilic species (Table 3.4 and Figure 3.9). Substrates were characterized by glacial till overlain by silt, and are generally ice-poor throughout the profile, with low content of massive and segregation ice. Approaching the bottom of profile exposures, glacial till occasionally contained isolated masses of relict glacial ice, and rarely ice-wedges, with combined massive and segregated ice content generally less than 10 % by volume throughout the substrate profile. Clasts typically comprised more than 30% of the parent substrate, and often included stone to boulder size specimens (250 - 950 mm). Where proglacial lakes were once present, a mantle of glaciolacustrine deposits occasionally flanked the moraine atop the glacial till with increasing thickness from the moraine crest downward. Thin, post-glacial loess deposits comprised the uppermost substrate, with no evidence of colluvial re-deposition contributing to the profile at any of the sites examined, and minimal buried organic material (3.5% average, by volume). While the active layer was comparatively well drained, the upper permafrost horizon was typically saturated with pore ice. Small lenticular and thin lamellar cryostructures were usually present, though sparsely dispersed near the top of the permafrost. Total organic layer depth averaged 7.3 cm and was primarily composed of graminoid detritus.

Vegetation was dominated by upland and alpine graminoid dwarf shrub vegetation, and non-tussock forming sedges and *Dryas integrifolia* dominated all sites. Common calciphilic species included *Oxtripis nigrescens*, and the ericad *Rhododendron lapponicum*. *Eriophorum vaginatum* was present at

half of the sites but lacked tussock morphology. Dwarf willow species (primarily *Salix reticulata*), *Geum rossii*, *Astragalus umbellatus* and *Pedicularis capitata* were also prevalent at all sites.

Group E2.

E2 sites are found on mild hill slopes where drainage is moderate, uppermost substrates are more 90% silt, shallow surficial deposits overlie bedrock or till sheets, and acidic tundra is underlain by cryofacies assemblages of primarily syngenetic, segregated-ice cryostructures (Table 3.4 and Figure 3.9). Contemporary soils averaged 99% silt with minimal microtopography on slopes averaging 5° (sd = 2.5°). At least two landscape settings are associated with class E2: 1) mid and lower hill slope settings in broad valleys on glacial till sheets with a loess cap, and 2) on upper hill slope settings where a loess cap sits atop highly fractured, noncarbonate, near-surface bedrock. Primarily syngenetic cryofacies within the parent material occasionally included isolated lenses of intrusive, massive, or epigenetic cryostructures, or were (rarely) ice-poor. Upper substrates were greater than 90% silt regardless of setting or evidence of colluvial processes. Upper permafrost within loess contains 25 to 70% segregation ice by volume, primarily including reticulate, ataxitic, and bedded cryostructures, with occasional lenticular structures or veins.

Vegetation was dominated by moist acidic tundra (Walker and Maier 2008), almost exclusively of the Upland Dwarf Birch-Tussock Shrub ecotype, which has an average soil pH of 4.7 (0.7 standard deviation reported for sites in northern foothills of the Brooks Range in Alaska (Jorgenson et al. 2010b). Organic layer depth averaged 21 cm (min 15 cm, max 23 cm), with moss-dominated detritus. Dominant vegetation included *Eriophorum vaginatum*, *Betula nana* and dwarf and low willow and ericaceous species with a sphagnum and feathermoss understory.

Subgroups 'a' and 'b' are distinguished by total organic layer depth (O_a). Subgroup 'a' has an average total organic layer depth of 15 cm (sd = 4.5 cm) whereas subgroup 'b' averaged 22 cm (sd = 7.7 cm). The two subgroups partially coincide with regional geography (Figure 3.8) and strongly correlate with estimated time since last deglaciation. More than 85% of landscapes containing sites in subgroup 'a' sit atop surfaces estimated as late-Pleistocene/Holocene. Those of subgroup 'b' are atop mid to late-Pleistocene surfaces, with more than 40% estimated as mid-Pleistocene (Hamilton 2003, Hamilton 2010).

Group E3.

E3 occurred on thin deposits of silty colluvium over near-surface bedrock, typically on upper hill slopes near exposed-bedrock hilltops, where ambient slope averaged 5.4° (sd = 1.3°; Table 3.4 and Figure 3.9). Nonacidic, primarily herbaceous vegetation lay atop one to many deposits of colluvial material and syngenetic cryostructures, with interleaved layers or turbated fragments of relict vegetation. In contrast

with other groups, substrate composition was relatively similar and consistent among sites. Colluvial surficial deposits were an admixture of silt and gravels, with silt generally comprising most of the material in the contemporary soil (mean = 90 %; sd = 9 %) versus a more even proportion in the parent material (mean = 68 %; sd = 19 %). Most sites occurred on hill slopes below exposed outcrops of micaceous shales containing < 1 % quartzite in thin veins. The silt component frequently derived from some proportion of Pleistocene and Holocene loess (Hamilton 2010) mixed with silts from weathered shale, though the proportion is unknown either for any specific site or for these sites as a whole. Gravel clast lithology was a mixture of shale and quartzite. Generally, increased distance from exposed bedrock correlated with increased proportion of weathering-resistant fragments of quartzite. Permafrost profiles were almost exclusively comprised of syngenetic cryostructures, with an average 29 % (sd = 16 %) segregated ice by volume. Ataxitic and reticulate cryostructures were typically co-dominant, with ice-rich intermediate layers at both current and relict permafrost tables. Vegetation was nonacidic, with a community gradient appearing to correlate with surface hydrology. Communities situated near or within preferential surface flowpaths contained higher proportions non-tussock forming sedges (*Eriophorum angustifolium*, *Carex spp.*) with sparse cover of dwarf shrub (e.g., *Cassiope tetragona*, *Dryas spp.*, *Salix spp.*) and low shrub (*Salix spp.*), and an understory of unidentified feathermosses. The most hydric sites supported relatively deep surface organic layers of up to 33 cm of feathermoss-dominated material, with diffuse surface flow up to 20 cm deep. Dwarf shrub, forb and low shrub cover increases moving away from the hydric end of the gradient, with rapidly decreasing *E. angustifolium* cover. This group was distributed primarily in the Noatak Basin (Figure 3.8), with only one site found in the North Slope foothills.

Group E4.

Sites in group E4 were distributed across a highly variable suite of lowland sites where deep, ice-rich, non-carbonate glacial deposits underlay acidic or nonacidic low shrub communities. The most prominent common characteristic of this group was a deep deposit of ice-rich, diamictous, glacial till of primarily or exclusively noncarbonate lithology. At more than half of these sites, glacial till was overridden by, or interspersed with, glaciolacustrine, glaciofluvial, fluvial, or aeolian deposits, and typically appeared within kettle topography, on lower hill slopes, or along contemporary or relict river bluffs. The coarse fraction varied from 1 % to 75 % of the parent material by volume, including clast sizes from gravel to 2 m wide boulders (Table 3.4 and Figure 3.9). Massive ice was typically present in at least one form, including relict glacial ice, injection ice, and ice wedges. Ice wedges ranged from absent to dominant (> 90 % by volume) within the permafrost profile. Contemporary soils frequently included a loess cap, or less frequently appeared to develop directly from glacial deposits. Syngenetic cryostructures

were common in the upper permafrost horizon. Vegetation was typically low shrub dominated, with both acidic and nonacidic vegetation observed. While low shrubs tended to dominate across sites, community composition and organic layer depth varied markedly among these sites. Tussock cover ranged from absent to > 50 % cover.

Subgroupings were driven by outlier values for specific site properties. Subgroup ‘a’ represents the general characteristics of sites in this group. Subgroup ‘b’ included sites where ice wedges comprise > 40 % of the permafrost by volume. Subgroup ‘c’ was restricted to two sites within the same glacial deposit in the North Slope foothills containing > 75 % coarse fraction in the permafrost, with multiple boulder size clasts up to 1.9 m.

3.3.2 Relationships Among Sites and Groups

Spatial distribution of groups of sites partially corresponded with regional geography (Figure 3.8). While sites from all four groups occurred both on the North Slope and within the Noatak Basin, all groupings exhibited regional tendencies. E1 sites had the strongest geographic affiliation, with five out of six sites concentrated within a 25 km radius in the upper Noatak Basin. Sites grouped E2 were more common on the North Slope, with only two examples in the Noatak Basin, while E3 was distributed throughout the Noatak Basin, but occurred only once on the North Slope. E4 sites occurred across the study region, however only one of its three subgroups (E4a) was evenly distributed, with E4b primarily located in the Noatak Valley bottom, and E4c comprised of only two sites, both located within the same surficial geologic deposit on the North Slope.

The two sites grouped E4c behaved as outliers within the initial run of the MFA ordination, and were removed in the final ordination. These two sites were distinct in the sample, containing > 75% boulder-sized (600–1900mm) clasts by volume in the near-surface parent material, which was characteristic of that local moraine deposit. Removal of these two sites produced a more even spread of the remaining sites along graphed ordination axes, indicating a better representation of total variability among all sites. These two sites (36 and 38) were added back into the final grouping hierarchy as a subgroup, because all other site properties were comparable to those of the primary group with which they were associated in the pilot ordination.

3.4 Discussion

Broad scale modelling of permafrost and terrain properties is frequently limited by the variability of relationships among regions, which is difficult to quantify and describe due to the cost of field sampling to characterize conditions and relationships within regions (Riseborough et al. 2008). As a result, maps of

permafrost distribution and properties are either broad in scale but very general in content, or more specific in content but limited in spatial scale (Jorgenson et al. 2008b, Gruber 2012, Jorgenson et al. 2014, Pastick et al. 2014). Results from this study should support and inform future modelling of permafrost conditions in the central and western Brooks Range by providing further evidence of the relationship between permafrost conditions and landscape characteristics, and by illustrating the nature of these relationships for this region.

No single terrain factor emerged as the dominant driver of permafrost conditions in our study region. For example, while soil coarse fraction was a strongly influential factor driving the ordination, considered alone it failed to explain key differences among sites and groupings. Groups E1 and E3 (Figure 3.5) both comprised sites with gravelly surficial substrates, but sites grouped E1 occurred in xeric to mesic conditions with *Dryas*-dominated vegetation and ice-poor permafrost, while E3 sites were located in more hydric settings with wet sedge meadow vegetation and primarily reticulate and syngenetic cryostructures, frequently including an ice-rich intermediate layer. As no single factor was identified as a dominant driver of the ordination, estimation of upper permafrost conditions by proxy should incorporate multiple terrain factors.

Gradients and divisions among sites and site groupings were driven by terrain properties which generally correspond with state factors, suggesting that examination of properties organized by state factor may provide better insight and more complete, parsimonious information for estimating landscape permafrost conditions. MFA blocks representing vegetative and substrate factors were important, complementary drivers in the ordination, and correspond with two of the five state factors (biota and parent material). The data reduction step in our analyses revealed index variables in the data, which were correlated with multiple variables organized within logical data blocks. At landscape to regional scales, selection of the most statistically relevant and representative index variables from groups of variables defined by state factors may offer the most parsimonious method for analyzing terrain properties driving upper-permafrost characteristics. The complexity, broad diversity, and remote nature of landscapes throughout the low arctic present difficult challenges for estimating subsurface conditions such as permafrost, which are fundamental to landscape processes and critical to understanding climate change impacts and feedbacks at regional scales. Exploiting relationships among terrain and permafrost properties within a state factor framework may offer the most effective and efficient approach for estimation of permafrost-related properties and processes in remote, arctic regions.

Results of this analysis are also suggestive of the spatial distribution of prevalent ecological processes including paludification and development of the permafrost intermediate layer through quasi-

syngenetic permafrost aggradation (Shur 1988), and support the idea that these relationships may be modelled to better understand landscape distributions of cryofacies (French 1998, Shur and Jorgenson 2007, Jorgenson et al. 2014). Together, these provide insights for conceptual models of landscape development and response (Jorgenson et al. 2010a), which may in turn be empirically tested at landscape to regional scales using structural equation modeling, integrated terrain unit analysis, and other approaches which rely upon a-priori knowledge from which to construct initial models. Also, the results help identify which permafrost, vegetation and terrain properties may be most germane for modelling within this region, enabling more efficient and targeted field data collection.

Results of this study further support prior findings correlating permafrost properties and vegetation with terrain conditions, identifying which permafrost, vegetation and terrain factors are most closely correlated, and illustrating specific examples of these relationships from landscapes within our study region. The correlations of terrain conditions across a diversity of sites may provide for proxy estimation of certain permafrost properties within this region (Figures 3.5 - 3.7). Whereas our groupings of sites were at least partially a product of biased sampling, the groupings demonstrate that specific terrain properties are correlated with surficial conditions across a diversity of landscapes in the region, and that they likely influence surficial conditions in a generally consistent manner along landscape gradients. Relative estimates of some subsurface properties should therefore be possible across landscapes in the study region.

These results are generally consistent with those obtained from studies of other, differing permafrost regions and studies conducted at different scales, and offer detail for this region to support modelled estimates of permafrost properties. General relationships among terrain, vegetation, active layer and upper permafrost horizon properties and cryostructures have been described for regions throughout the arctic (Wolfe et al. 2001, Shur and Jorgenson 2007, Raynolds and Walker 2008, French and Shur 2010, Daanen et al. 2011, Jorgenson et al. 2013, Mishra and Riley 2014, Pastick et al. 2014) and for specific localities (Viereck 1973, Murton and French 1994, French 1998, Walker et al. 2008), and support early assertions of a general correlation between upper permafrost conditions and landscape characteristics throughout the arctic (Washburn 1980, Shur 1988). While inter-related correlations among terrain, vegetation, and permafrost have been found at broad scales throughout the arctic (Shur and Jorgenson 2007, Raynolds and Walker 2008, Kokelj and Jorgenson 2013), the nature and strength of relationships among terrain, vegetation and permafrost vary significantly by region (Shur and Jorgenson 2007, Jorgenson et al. 2010a, Pastick et al. 2014).

3.5 Conclusions

Correlations among terrain and permafrost properties offer opportunities to better understand distributions of ground ice and cryostructures, and provide evidence of cryogenic processes across landscape gradients. Statistically-supported groupings of sites across a broad diversity of landscapes suggest consistent, though complex, inter-relationships among terrain and permafrost properties in the study region. These are a potential basis for improved spatially-explicit, proxy estimations of conditions in upper permafrost horizons, and for identifying areas prone to particular modes of permafrost degradation in response to climate warming and disturbance across the study region. In the Brooks Range and foothills of northern Alaska, where diverse landscapes abutting the arctic-boreal ecotone may be especially prone to multiple modes of permafrost degradation with climate change, and where remote settings severely limit direct observation of permafrost properties, this approach facilitates better estimation of extents, trajectories and magnitudes of different permafrost degradation modes and their future impacts.

3.6 Acknowledgments

This work was supported by a University of Alaska Fairbanks Center for Global Change (CGC) Student Research Grant, by U.S. National Science Foundation grant ARC-0806465, and by U.S. Department of Energy Biological and Environmental Research Program grant 3ERKP818. A portion of this work was performed at Oak Ridge National Laboratory (ORNL). ORNL is managed by UT-Battelle, LLC, for the DOE under contract DE-AC05-00OR22725. We gratefully acknowledge Erin Trochim and Teresa Hollingsworth for discussion of statistical methods, and Steven B. Young for invaluable discussion of landscape development and for field expertise. The aviation skill and safety of pilots Tom George, Stan Hermens, Tommy Levanger, Christian Cabanilla, Terry Day, Jim Kincaid, and Buck Mackson were indispensable to the success of this research.

3.7 References

- Abdi, H., L. J. Williams, and D. Valentin. 2013. Multiple factor analysis: principal component analysis for multitable and multiblock data sets. *WIREs Computational Statistics*.
- ACIA. 2005. Arctic Climate Impact Assessment. Cambridge University Press.
- Balser, A., M. N. Gooseff, J. Jones, and W. B. Bowden. 2009. Thermokarst distribution and relationships to landscape characteristics in the Feniak Lake region, Noatak National Preserve, Alaska; Final Report to the National Park Service, Arctic Network (ARCN). Fairbanks, AK.

- Bowden, W. B., M. N. Gooseff, A. Balser, A. Green, B. J. Peterson, and J. Bradford. 2008. Sediment and nutrient delivery from thermokarst features in the foothills of the North Slope, Alaska: Potential impacts on headwater stream ecosystems. *Journal of Geophysical Research* 113. G02026. doi:10.1029/2007JG000470.
- Callaghan, T. V., L. O. Bjorn, Y. Chernov, T. Chapin, T. R. Christensen, B. Huntley, R. A. Ims, M. Johansson, D. Jolly, S. Jonasson, N. Matveyeva, N. Panikov, W. Oechel, G. Shaver, S. Schaphoff, and S. Sitch. 2004. Effects of changes in climate on landscape and regional processes, and feedbacks to the climate system. *Ambio* 33:459-468.
- CAVM-Team. 2003. Circumpolar Arctic Vegetation Map, Scale 1:7,500,000. Conservation of Arctic Flora and Fauna (CAFF) Map No. 1. U.S. Fish and Wildlife Service, Anchorage, Alaska.
- Daanen, R. P., T. Ingeman-Nielsen, S. S. Marchenko, V. E. Romanovsky, N. Foged, M. Stendel, J. H. Christensen, and K. H. Svendsen. 2011. Permafrost degradation risk zone assessment using simulation models. *The Cryosphere* 5:1043-1056.
- Davis, N. 2001. *Permafrost: A Guide to Frozen Ground in Transition*. University of Alaska Press, Fairbanks, AK.
- Epstein, H. E., M. K. Reynolds, D. A. Walker, U. S. Bhatt, C. J. Tucker, and J. E. Pinzon. 2012. Dynamics of aboveground phytomass of the circumpolar Arctic tundra during the past three decades. *Environmental Research Letters* 7.
- Escofier, B. and J. Pagès. 1994. Multiple factor analysis. *Computational Statistics & Data Analysis* 18:121-140.
- French, H. and Y. Shur. 2010. The principles of cryostratigraphy. *Earth-Science Reviews* 101:190-206.
- French, H. M. 1998. An appraisal of cryostratigraphy in north-west Arctic Canada. *Permafrost and Periglacial Processes* 9:297-312.
- Frey, K. E., J. W. McClelland, R. M. Holmes, and L. C. Smith. 2007. Impacts of climate warming and permafrost thaw on the riverine transport of nitrogen and phosphorus to the Kara Sea. *Journal of Geophysical Research G Biogeosciences [J Geophys Res (G Biogeosci)]* Vol 112.
- Goetz, S. J., H. E. Epstein, U. S. Bhatt, G. J. Jia, J. O. Kaplan, H. Lischke, Q. Yu, A. Bunn, A. H. Lloyd, D. Alcaraz-Segura, P. S. A. Beck, J. C. Comiso, M. K. Reynolds, and D. A. Walker. 2011. Recent Changes in Arctic Vegetation: Satellite Observations and Simulation Model Predictions.
- Gooseff, M., A. Balser, W. Bowden, and J. Jones. 2009. Effects of hillslope thermokarst in northern Alaska. , 90: 29-31. *Eos, Transactions of the American Geophysical Union* 90:29-31.

- Grosse, G., J. Harden, M. Turetsky, A. D. McGuire, P. Camill, C. Tamocai, S. Frolking, E. A. G. Schuur, T. Jorgenson, S. Marchenko, V. Romanovsky, K. P. Wickland, N. French, M. Waldrop, L. Bourgeau-Chavez, and R. G. Striegl. 2011. Vulnerability of high-latitude soil organic carbon in North America to disturbance. *J. Geophys. Res.* 116:G00K06.
- Gruber, S. 2012. Derivation and analysis of a high-resolution estimate of global permafrost zonation. *The Cryosphere* 6:221-233.
- Hamilton, T. D. 2003. Surficial geology of the Dalton Highway (Itkillik-Sagavanirktok rivers) area, southern Arctic foothills, Alaska: Alaska Division of Geological & Geophysical Surveys Professional Report 121. Pages 1-32. Alaska Division of Geological & Geophysical Surveys, Fairbanks, AK.
- Hamilton, T. D. 2010. Surficial Geologic Map of the Noatak National Preserve, Alaska. U.S. Geological Survey (in cooperation with U.S. National Park Service) Scientific Investigations Map 3036, 1 : 250,000 scale, and accompanying report:21p.
- Hamilton, T. D. and K. A. Labay. 2011. Surficial Geologic Map of the Gates of the Arctic National Park and Preserve, Alaska. U.S. Geological Survey (in cooperation with U.S. National Park Service) Scientific Investigations Map 3125, 1 : 300,000 scale, and accompanying report:19p.
- Hinzman, L., N. Bettez, W. Bolton, F. Chapin, M. Dyurgerov, C. Fastie, B. Griffith, R. Hollister, A. Hope, H. Huntington, A. Jensen, G. Jia, T. Jorgenson, D. Kane, D. Klein, G. Kofinas, A. Lynch, A. Lloyd, A. McGuire, F. Nelson, W. Oechel, T. Osterkamp, C. Racine, V. Romanovsky, R. Stone, D. Stow, M. Sturm, C. Tweedie, G. Vourlitis, M. Walker, D. Walker, P. Webber, J. Welker, K. Winker, and K. Yoshikawa. 2005. Evidence and Implications of Recent Climate Change in Northern Alaska and Other Arctic Regions. *Climatic Change* 72:251-298.
- Hinzman, L. D., W. R. Bolton, K. Petrone, J. Jones, K. Yoshikawa, and J. P. McNamara. 2006. Permafrost Degradation and Effects on Watershed Chemistry and Hydrology. *in American Geophysical Union Fall Meeting, San Francisco (USA), 11-15 Dec 2006.*
- Hobbie, J. E., B. J. Peterson, G. R. Shaver, and W. J. O'Brien. 1991. The Toolik Lake Project: terrestrial and freshwater research on change in the Arctic. Pages 378-383 *in* V. II, editor. Proceedings of the University of Alaska Conference, "International Conference on the Role of Polar Regions in Global Change", June 1990. University of Alaska, Fairbanks, Alaska.
- Hobbie, S. E. and L. Gough. 2004. Litter decomposition in moist acidic and non-acidic tundra with different glacial histories. *Oecologia* 140:113-124.
- Husson, F., J. Josse, and J. Pages. 2010. Principal component methods - hierarchical clustering - partitional clustering: why would we need to choose for visualizing data? , Applied Mathematics Department, Agro Campus Ouest, Rennes, France.

- Jenny, H. 1941. *Factors of Soil Formation: A System of Quantitative Pedology*. Dover Publications, Inc., New York, NY.
- Jorgenson, M. T., J. Harden, M. Kanevskiy, J. O'Donnell, K. P. Wickland, S. Ewing, K. L. Manies, Q. Zhuang, Y. Shur, R. G. Striegl, and J. Koch. 2013. Reorganization of vegetation, hydrology and soil carbon after permafrost degradation across heterogeneous boreal landscapes *Environmental Research Letters* 8:1-14.
- Jorgenson, M. T., M. Kanevskiy, Y. Shur, J. Grunblatt, C. Ping, and G. Michaelson. 2014. Permafrost Database Development, Characterization, and Mapping for Northern Alaska. U.S. Fish & Wildlife Service, Arctic Landscape Conservation Cooperative.
- Jorgenson, M. T. and R. A. Kreig. 1988. A Model for Mapping Permafrost Distribution Based on Landscape Component Maps and Climatic Variables. Pages 176-182 *in* 5th International Conference on Permafrost, August 2-5, 1988. Tapir Publishers, Trondheim, Norway.
- Jorgenson, M. T., V. Romanovsky, J. Harden, Y. Shur, J. O'Donnell, E. A. G. Schuur, M. Kanevskiy, and S. Marchenko. 2010a. Resilience and vulnerability of permafrost to climate change. *Canadian Journal of Forest Research-Revue Canadienne De Recherche Forestiere* 40:1219-1236.
- Jorgenson, M. T., J. E. Roth, P. F. Miller, M. J. Macander, M. S. Duffy, A. F. Wells, G. V. Frost, and E. R. Pullman. 2010b. An ecological land survey and landcover map of the Arctic Network. Natural Resource Technical Report NPS/ARC/NRTR—2009/270. National Park Service, Fort Collins, Colorado.
- Jorgenson, M. T., Y. L. Shur, and T. E. Osterkamp. 2008a. Thermokarst in Alaska. Pages 869-876 *in* Ninth International Conference on Permafrost. National Academy Press, Washington, DC, Fairbanks, AK.
- Jorgenson, M. T., Y. L. Shur, and E. R. Pullman. 2006. Abrupt increase in permafrost degradation in Arctic Alaska. *Geophysical Research Letters* 33:1 - 4.
- Jorgenson, T., K. Yoshikawa, V. Romanovsky, M. Kanevskiy, J. Brown, Y. Shur, S. Marchenko, G. Grosse, and B. Jones. 2008b. Map of Permafrost Characteristics in Alaska. Proceedings of the Ninth International Conference on Permafrost (NICOP), Fairbanks, AK June 30 - July 4, 2008.
- Kanevskiy, M., Y. Shur, D. Fortier, M. T. Jorgenson, and E. Stephani. 2011. Cryostratigraphy of late Pleistocene syngenetic permafrost (yedoma) in northern Alaska, Itkillik River exposure. *Quaternary Research* 75:584-596.
- Kling, G. W. 1995. Land-water linkages: the influence of terrestrial diversity on aquatic systems. Pages 297-310 *in* F. S. Chapin and C. Korner, editors. *The role of biodiversity in arctic and alpine tundra ecosystems*. Springer-Verlag, Berlin.

- Kokelj, S. V. and M. T. Jorgenson. 2013. Advances in Thermokarst Research. *Permafrost and Periglacial Processes* 24:108-119.
- Kokelj, S. V., T. C. Lantz, J. Kanigan, S. L. Smith, and R. Coutts. 2009. Origin and Polycyclic Behaviour of Tundra Thaw Slumps, Mackenzie Delta Region, Northwest Territories, Canada. *Permafrost and Periglacial Processes* 20:1-12.
- Kreig, R. A. and R. D. Reger. 1982. Airphoto Analysis and Summary of Landform Soil Properties along the Route of the Trans-Alaska Pipeline System, Geologic Report 66, Alaska Division of Geological and Geophysical Surveys. Page 149.
- Lafreniere, M. J. and S. F. Lamoureux. 2013. Thermal Perturbation and Rainfall Runoff have Greater Impact on Seasonal Solute Loads than Physical Disturbance of the Active Layer. *Permafrost and Periglacial Processes* 24:241-251.
- Lantuit, H., W. H. Pollard, N. Couture, M. Fritz, L. Schirmer, H. Meyer, and H. W. Hubberten. 2012. Modern and Late Holocene Retrogressive Thaw Slump Activity on the Yukon Coastal Plain and Herschel Island, Yukon Territory, Canada. *Permafrost and Periglacial Processes* 23:39-51.
- Lantz, T. C., S. E. Gergel, and S. V. Kokelj. 2010. Spatial Heterogeneity in the Shrub Tundra Ecotone in the Mackenzie Delta Region, Northwest Territories: Implications for Arctic Environmental Change. *Ecosystems* 13:194-204.
- Le, S., J. Josse, and F. Husson. 2008. FactoMineR: An R Package for Multivariate Analysis. *Journal of Statistical Software* 25:1-18.
- Leibman, M. O., A. I. Kizyakov, L. D. Sulerzhitsky, and N. E. Zaretskaya. 2003. Dynamics of the landslide slopes and mechanism of their development on Yamal peninsula, Russia. *in* Proceedings of the Eight International Conference on Permafrost. A.A.Balkema Publishers, Rotterdam, Netherlands Zurich 21-25 July 2003.
- Lewkowicz, A. G. and C. Harris. 2005. Morphology and geotechnique of active-layer detachment failures in discontinuous and continuous permafrost, northern Canada. *Geomorphology* 69:275-297.
- McCune, B. 2013. Non-metric multidimensional scaling analysis - personal communication.
- McCune, B. and J. B. Grace. 2002. Ch. 16: Nonmetric Multidimensional Scaling. Pages 125-142 in *Analysis of Ecological Communities*. MjM Software Design, Gleneden Beach, OR.
- Mishra, U. and W. J. Riley. 2014. Active-Layer Thickness across Alaska: Comparing Observation-Based Estimates with CMIP5 Earth System Model Predictions. *Soil Science Society of America Journal* 78:894-902.
- Murton, J. B. and H. M. French. 1994. CRYOSTRUCTURES IN PERMAFROST, TUKTOYAKTUK COASTLANDS, WESTERN ARCTIC CANADA. *Canadian Journal of Earth Sciences* 31:737-747.

- Myers-Smith, I. H., B. C. Forbes, M. Wilkming, M. Hallinger, T. Lantz, D. Blok, K. D. Tape, M. Macias-Fauria, U. Sass-Klaassen, E. Levesque, S. Boudreau, P. Ropars, L. Hermanutz, A. Trant, L. S. Collier, S. Weijers, J. Rozema, S. A. Rayback, N. M. Schmidt, G. Schaepman-Strub, S. Wipf, C. Rixen, C. B. Menard, S. Venn, S. Goetz, L. Andreu-Hayles, S. Elmendorf, V. Ravolainen, J. Welker, P. Grogan, H. E. Epstein, and D. S. Hik. 2011. Shrub expansion in tundra ecosystems: dynamics, impacts and research priorities. *Environmental Research Letters* 6.
- Osterkamp, T. E., M. T. Jorgenson, E. A. G. Schuur, Y. L. Shur, M. Z. Kanevskiy, J. G. Vogel, and V. E. Tumskoy. 2009. Physical and Ecological Changes Associated with Warming Permafrost and Thermokarst in Interior Alaska. *Permafrost and Periglacial Processes* 20:235-256.
- Parker, C. L. 2006. Vascular plant inventory of Alaska's Arctic National Parklands: Bering Land Bridge National Preserve, Cape Krusenstern National Monument, Gates of the Arctic National Park & Preserve, Kobuk Valley National Preserve, and Noatak National Preserve. ARCN I&M, National Park Service, Alaska Region Final Report:142p.
- Pastick, N. J., M. T. Jorgenson, B. K. Wylie, J. R. Rose, M. Rigge, and M. A. Walvoord. 2014. Spatial variability and landscape controls of near-surface permafrost within the Alaskan Yukon River Basin. *Journal of Geophysical Research-Biogeosciences* 119:1244-1265.
- Peterson, B. J., R. M. Holmes, J. W. McClelland, C. J. Vorosmarty, R. B. Lammers, A. I. Shiklomanov, I. A. Shiklomanov, and S. Rahmstorf. 2002. Increasing river discharge to the Arctic Ocean. *Science* 298:2171-2173.
- Raynolds, M. K. and D. A. Walker. 2008. Circumpolar Relationships Between Permafrost Characteristics, NDVI, and Arctic Vegetation Types. Pages 1469-1474 in D. Kane, editor. Ninth International Conference on Permafrost. National Academy Press, Washington, DC, Fairbanks, Alaska.
- Riseborough, D., N. Shiklomanov, B. Etzelmuller, S. Gruber, and S. Marchenko. 2008. Recent advances in permafrost modelling. *Permafrost and Periglacial Processes* 19:137-156.
- Schaefer, K., T. Zhang, L. Bruhwiler, and A. P. Barrett. 2011. Amount and timing of permafrost carbon release in response to climate warming. *Tellus Series B-Chemical and Physical Meteorology*:no-no.
- Schuur, E. A. G. and B. Abbott. 2011. Climate change: High risk of permafrost thaw. *Nature* 480:32-33.
- Schuur, E. A. G., J. G. Vogel, K. G. Crummer, H. Lee, J. O. Sickman, and T. E. Osterkamp. 2009. The effect of permafrost thaw on old carbon release and net carbon exchange from tundra. *Nature* 459:556-559.
- Shur, Y. L. 1988. The upper horizon of permafrost soil. Pages 867-871 in Proceedings of the Fifth Intern. Conf. on Permafrost. Tapir Publishers, Trondheim, Norway.

- Shur, Y. L. and M. T. Jorgenson. 2007. Patterns of Permafrost Formation and Degradation in Relation to Climate and Ecosystems. *Permafrost and Periglacial Processes* 18:7 - 19.
- Swanson, D. K. and K. Hill. 2010. Monitoring of Retrogressive Thaw Slumps in the Arctic Network, 2010 Baseline Data: Three-dimensional Modeling with Small-format Aerial Photographs. Page 58. U.S. Department of the Interior, National Park Service, Natural Resource Data Series NPS/ARC/NRDS—2010/123, Natural Resource Program Center, Fort Collins, CO.
- Tarnocai, C., J. G. Canadell, E. A. G. Schuur, P. Kuhry, G. Mazhitova, and S. Zimov. 2009. Soil organic carbon pools in the northern circumpolar permafrost region. *Global Biogeochemical Cycles* 23:1-11.
- van Cleve, K., F. S. Chapin, III, C. T. Dyrness, and L. A. Viereck. 1991. Element Cycling in Taiga Forests: State-Factor Control. *Bioscience* 41:78-88.
- Viereck, L. 1973. Ecological effects of river flooding and forest fires on permafrost in the taiga of Alaska. Pages 60-67 in *Permafrost: The North American contribution to the Second International Conference*. National Academy of Sciences, Yakutsk, USSR.
- Viereck, L. A., C. T. Dyrness, A. R. Batten, and K. J. Wenzlick. 1992. The Alaska Vegetation Classification. Page 278 in U. S. D. o. A. F. Service, editor. Gen. Tech. Rep. PNW-GTR-286, Portland, OR.
- Wahrhaftig, C. 1965. Physiographic Divisions of Alaska. U.S.G.S. Professional Paper 482. 52 pp.
- Walker, D. A., N. A. Auerbach, and M. M. Shippert. 1995. NDVI, biomass, and landscape evolution of glaciated terrain in northern Alaska. *Polar Record* 31:169-178.
- Walker, D. A., H. E. Epstein, V. E. Romanovsky, C. L. Ping, G. J. Michaelson, R. P. Daanen, Y. Shur, R. A. Peterson, W. B. Krantz, M. K. Reynolds, W. A. Gould, G. Gonzalez, D. J. Nicolsky, C. M. Vonlanthen, A. N. Kade, P. Kuss, A. M. Kelley, C. A. Munger, C. T. Tamocai, N. V. Matveyeva, and F. J. A. Daniels. 2008. Arctic patterned-ground ecosystems: A synthesis of field studies and models along a North American Arctic Transect. *Journal of Geophysical Research-Biogeosciences* 113.
- Walker, D. A., P. Kuss, H. E. Epstein, A. N. Kade, C. M. Vonlanthen, M. K. Reynolds, and F. J. A. Daniels. 2011. Vegetation of zonal patterned-ground ecosystems along the North America Arctic bioclimate gradient. *Applied Vegetation Science*:no-no.
- Walker, D. A. and H. A. Maier. 2008. Vegetation in the vicinity of the Toolik Field Station, Alaska. *Biological Papers of the University of Alaska*, No. 28, Institute of Arctic Biology, Fairbanks, AK.
- Walker, M. D., D. A. Walker, and N. A. Auerbach. 1994. PLANT-COMMUNITIES OF A TUSsock TUNDRA LANDSCAPE IN THE BROOKS RANGE FOOTHILLS, ALASKA. *Journal of Vegetation Science* 5:843-866.

- Washburn, A. L. 1980. *Geocryology: A survey of periglacial processes and environments*. Halsted Press, John Wiley & Sons, Inc., New York, USA.
- Wolfe, S. A., E. Kotler, and S. R. Dallimore. 2001. Surficial characteristics and the distribution of thaw landforms (1970-1999), Shingle Point to Kay Point, Yukon Territory. Geological Survey of Canada, Open File 4115, 2001.
- Young, S. B. 1974. The environment of the Noatak River basin, Alaska., Contributions of the Center for Northern Studies, Wolcott, VT.

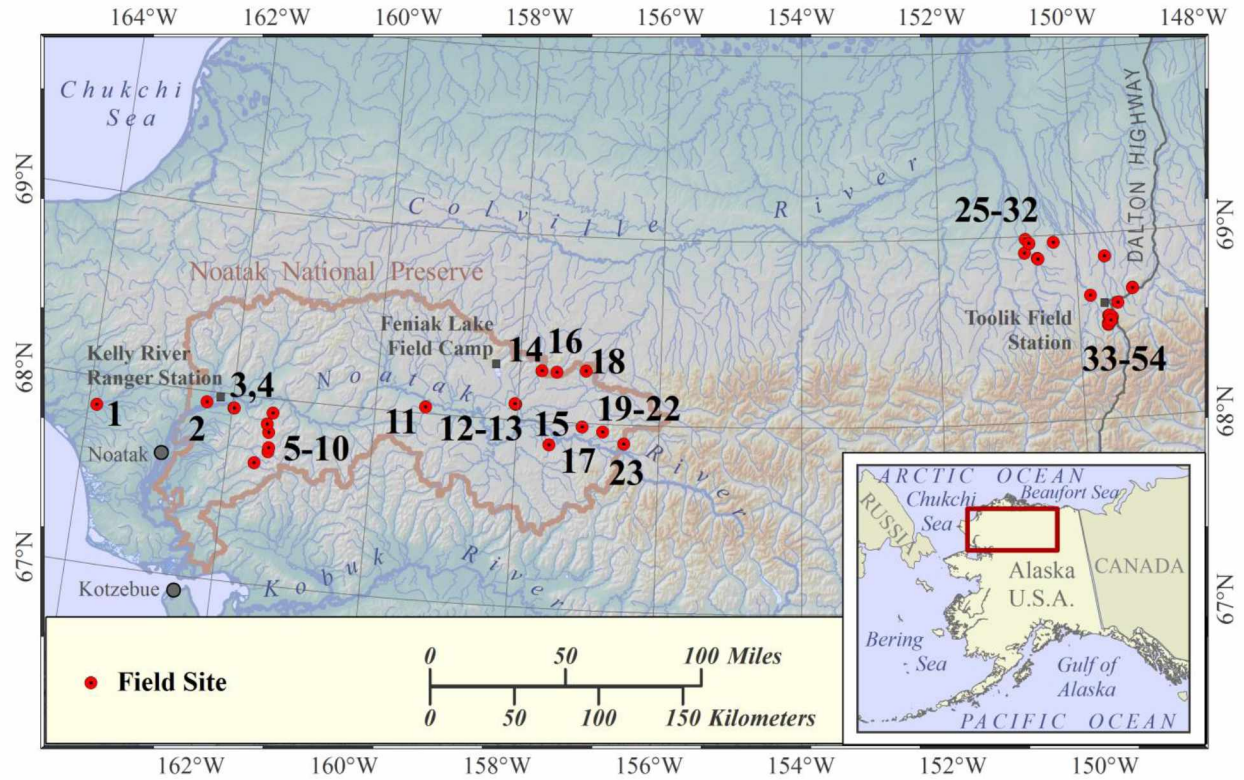


Figure 3.1. Study region in northern Alaska. Field sites were identified and selected through aerial survey, with ground visits by helicopter from Feniak Lake Camp and Kelly River Ranger Station in the Noatak National Preserve, and by helicopter and on foot from Toolik Field Station on Alaska's North Slope.

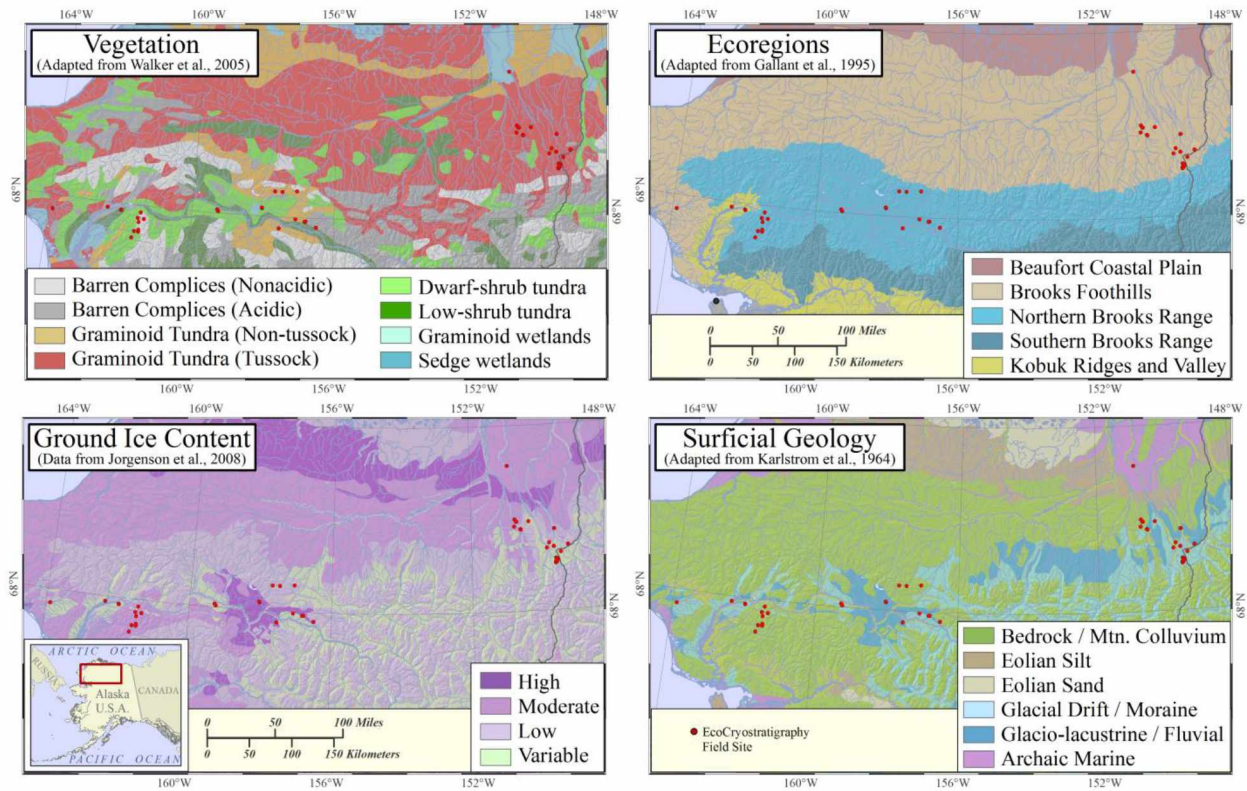


Figure 3.2. Generalized landscape characteristics of the study region. All field sites (red dots) are within the continuous permafrost zone (Jorgenson et al. 2008), within Arctic Bioclimate Subzone E (Walker et al. 2003), and are generally Climate-driven Ecosystem-modified permafrost landscapes (Shur and Jorgenson 2007). While these ancillary data sets provide valuable insight into regional landscape composition, this study is focused on terrain and upper permafrost horizon properties at finer scales.



Figure 3.3. Permafrost degradation features providing access to permafrost profile exposures. Photos show (a) general morphology from oblique airphotos and (b) unprepared permafrost exposures from ground photos. Retrogressive thaw slumps (1), thermo-erosional gullies (2) and active layer detachment slides (3) were the predominant permafrost degradation features in the study area and comprised all feature types examined in this study. Photos 2a and 2b courtesy W. B. Bowden, 2004.

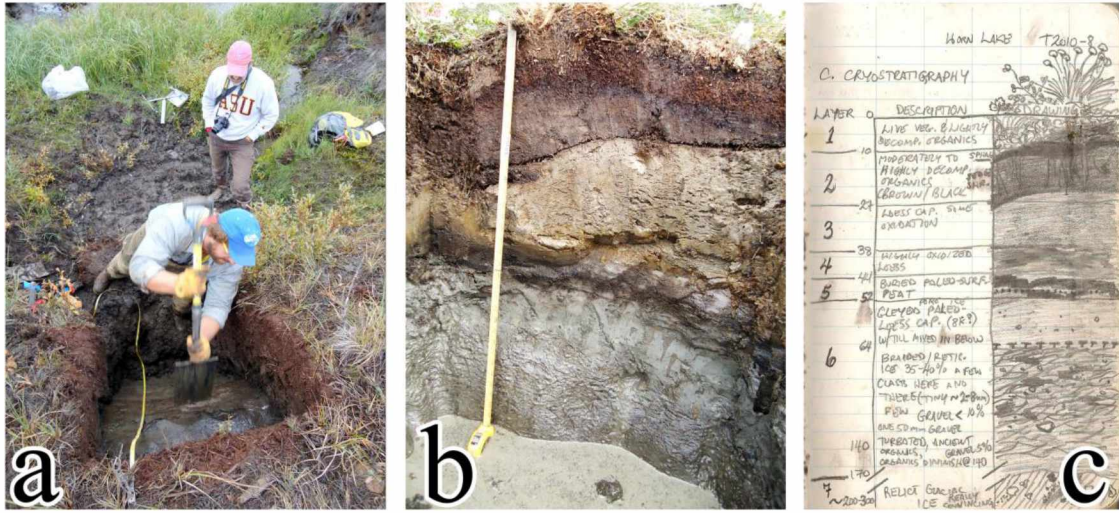


Figure 3.4. Upper permafrost profile exposure. Photos show (a) profile preparation, (b) a profile prepared for examination, and (c) schematic cryostratigraphic map of the permafrost profile, substrate and vegetation which complements tabular data for each profile layer.

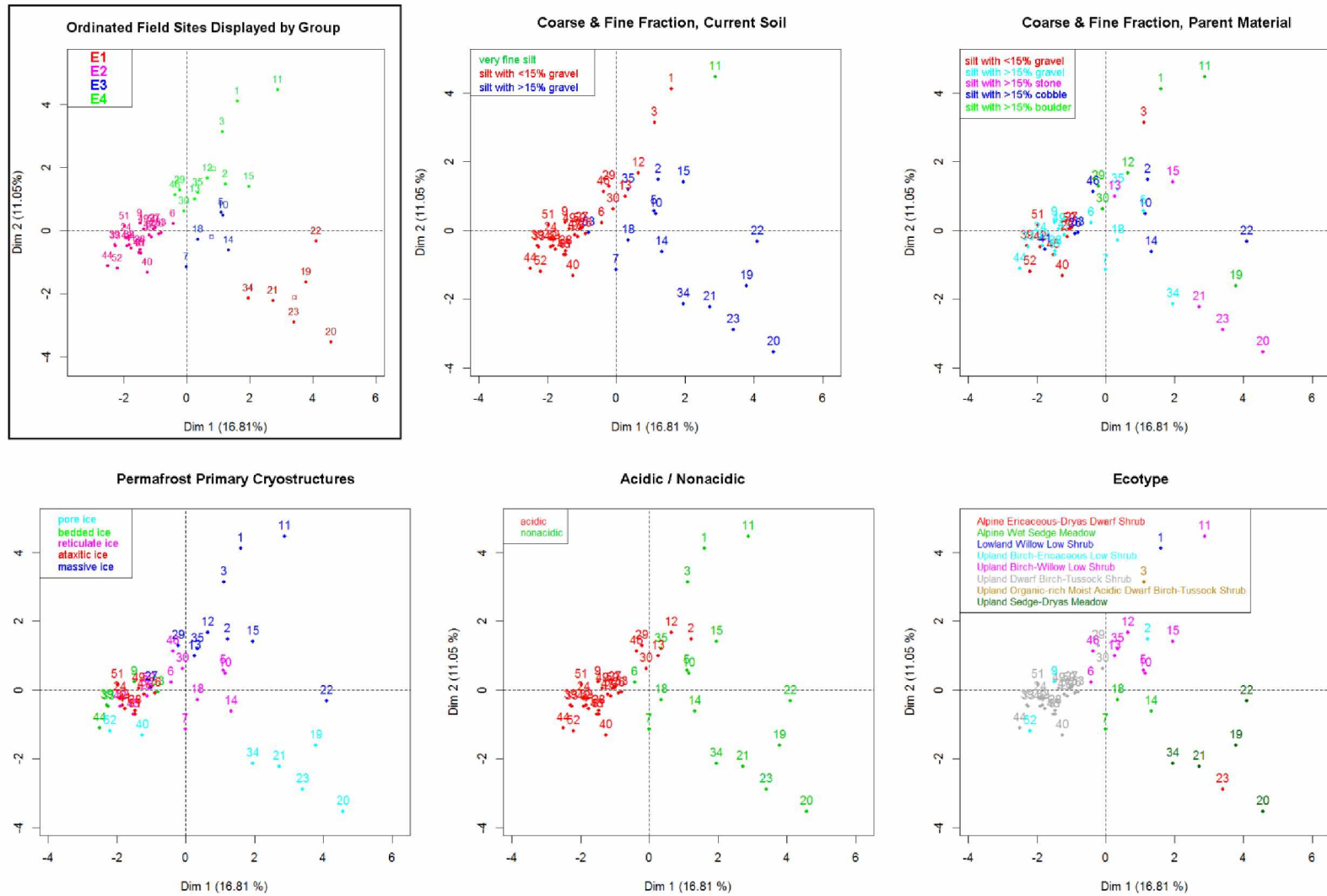


Figure 3.5. Field sites displayed by grouping and with active categorical variables overlain on graphed MFA results. Colors of groupings correspond with the dendrogram and map (Figures 3.8 & 3.8).

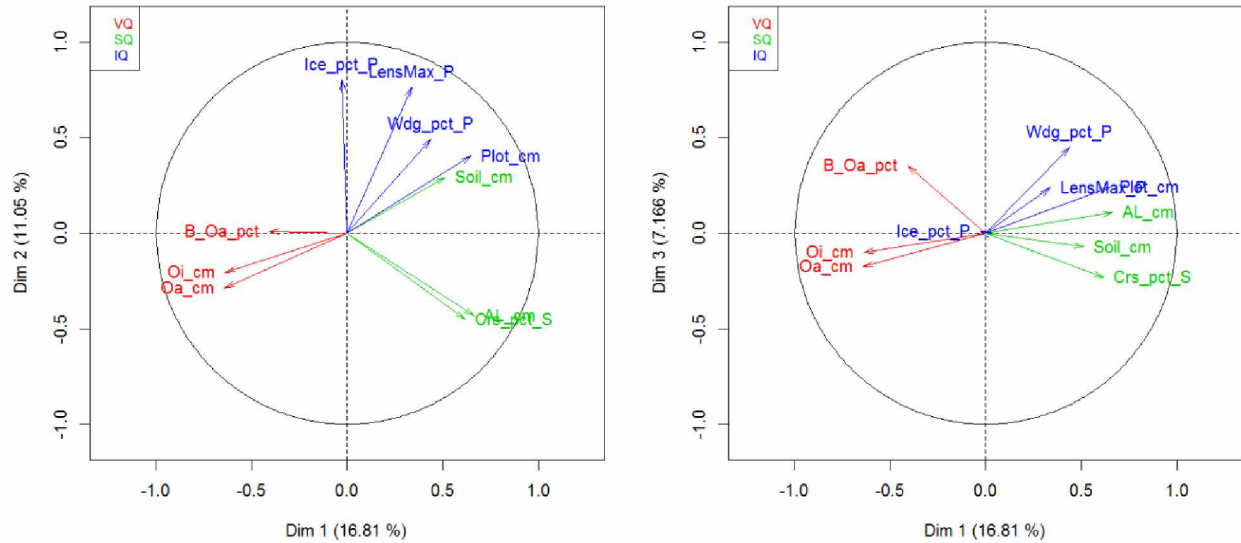


Figure 3.6. Influence of quantitative variables, shown by block, on the 3-dimensional MFA ordination driving clustered site groupings. Variables are shown by MFA block: VQ (red) = Vegetative, SQ (green) = substrate, IQ (blue) = Ice/Permafrost. Dimensions 1 and 2 are shown on left, dimensions 1 and 3 on the right.

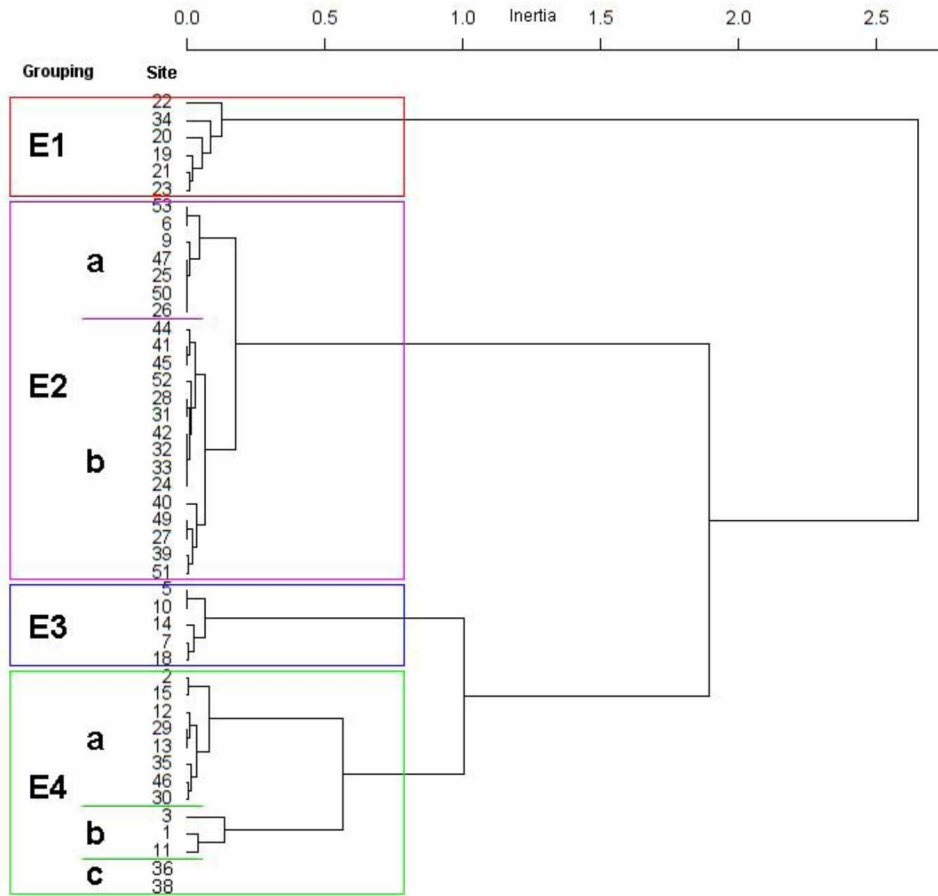


Figure 3.7. Dendrogram from hierarchic clustering of MFA results, showing groupings E1-E4. Colors correspond with ordination group overlay graph (Figure 3.5), and with map of sites by grouping (Figure 3.8).

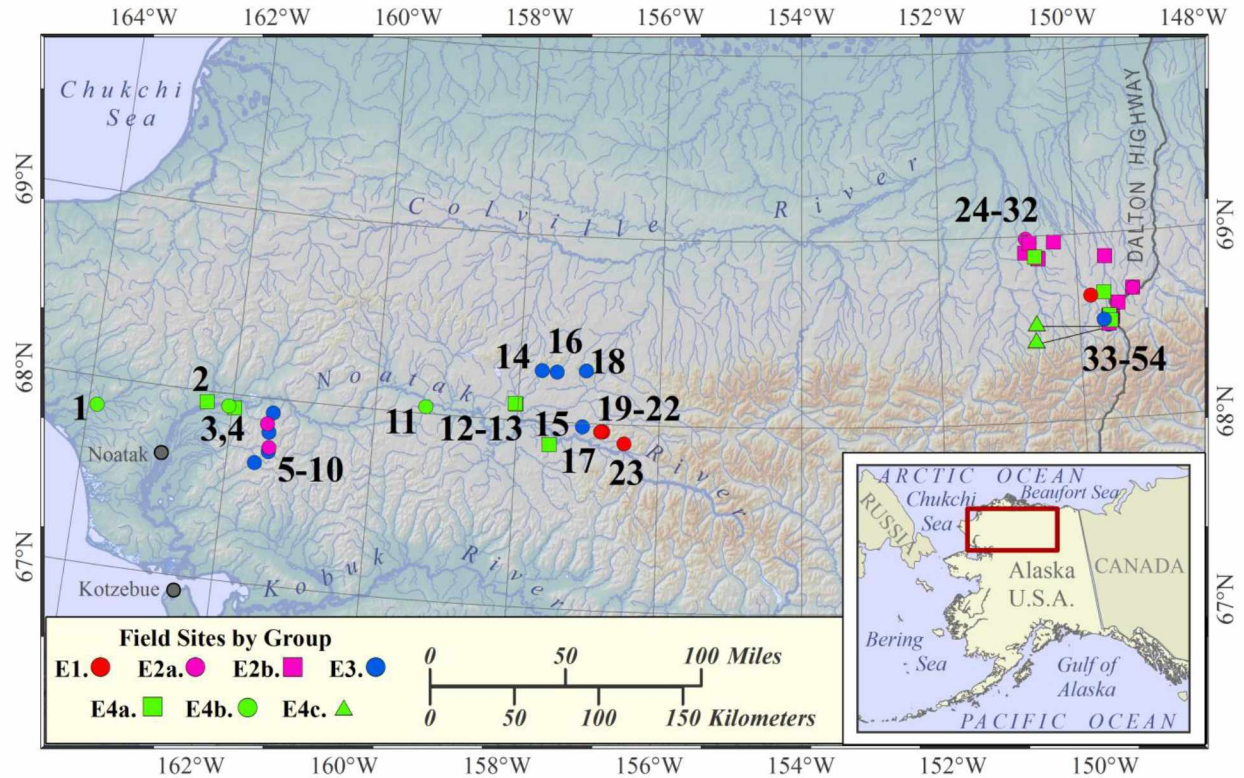
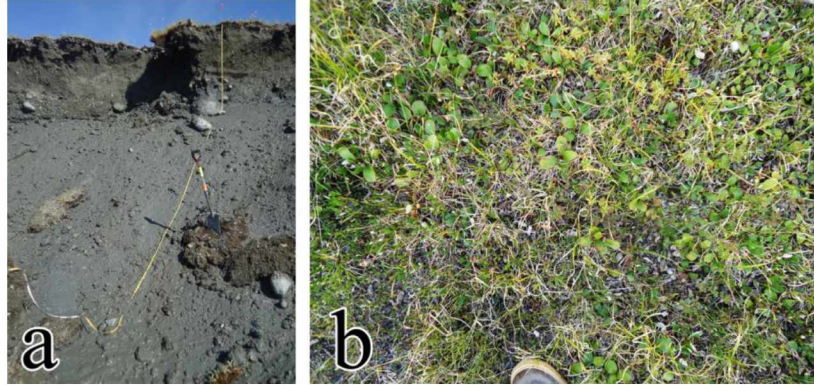
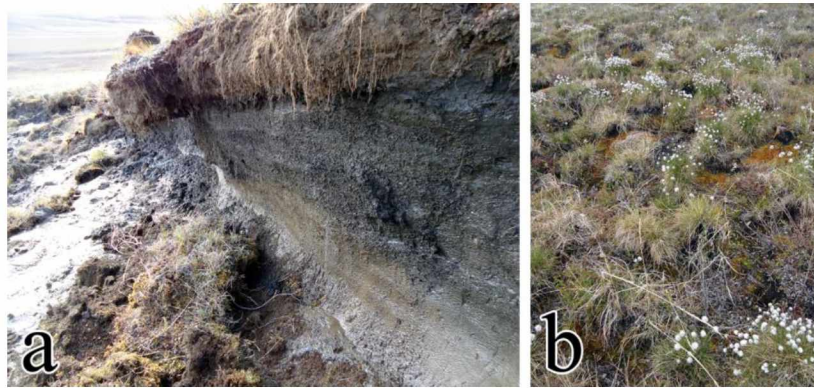


Figure 3.8. Distribution of field sites by grouping. E2a and E2b are similar sub-groups, differentiated mainly by the effects of a deeper organic horizon for E2a. E2 is found predominantly on the North Slope, with the two occurrences in the Noatak Basin of subtype 'a', possibly associated with warmer, drier conditions compared with a stronger maritime influence promoting cooler and damper summertime conditions on the north slope. E3 is found only once on the north slope, but is more common in the Noatak Basin associated with noncarbonate colluvial deposits prevalent on upper hill slopes there. We consider all of these sites to occur within Climate-Driven Ecosystem-Modified permafrost landscapes proposed by Shur and Jorgenson (2007), and all occur within Arctic Bioclimate Subzone E (CAVM-Team 2003).

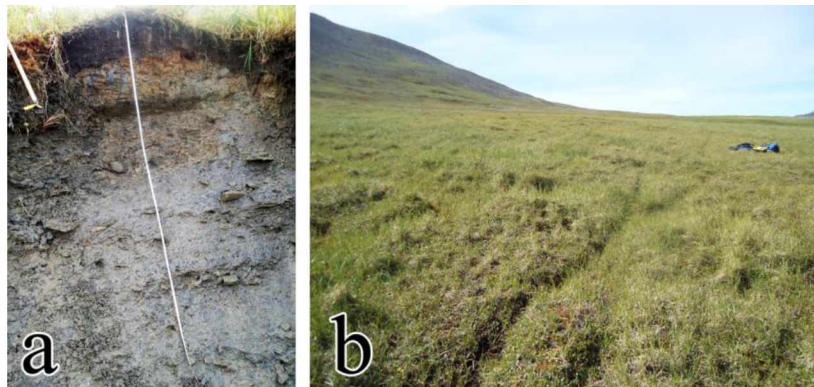
E1



E2



E3



E4

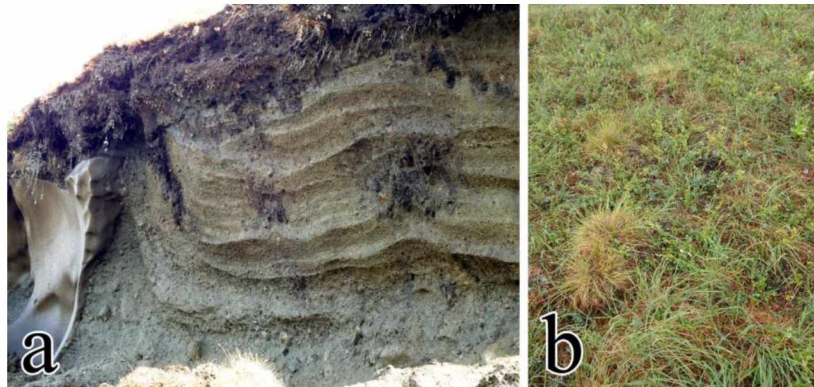


Figure 3.9. Photos of sites from groups E1, E2, E3 and E4. 'a' = substrate and upper permafrost profile, 'b' = vegetation. E1. Site 19; E2. Site 25; E3. Site 18; E4. Site 15.

Table 3.1. Variables characterizing conditions in the vicinity of each permafrost profile exposure.

Segment	Name	Type		Source
Landscape	Physiographic position	Categorical	*	Appendix. 2.; Jorgenson et al., (2010b)
Landscape	Surficial Geology	Categorical	*	Hamilton, (2003 & 2010)
Landscape	Lithology	Categorical	*	Appendix. 2.; Jorgenson et al., (2010b)
Landscape	Bedrock Geology	Categorical	§	Beikman (1982)
Landscape	Glacial Geology	Categorical	§	Hamilton, (2003 & 2010)
Site Surface	Elevation	Quantitative	*	Garmin eTrex GPS
Landscape	Elevation	Quantitative	§	ASTER DEM
Site Surface	Slope	Quantitative	*	Brunton inclinometer
Landscape	Slope	Quantitative	§	ASTER DEM
Site Surface	Aspect	Quantitative	*	Brunton compass (declination adjusted)
Landscape	Aspect	Quantitative	§	ASTER DEM
Landscape	Topographic Position Index	Quantitative	§	ASTER DEM, Jenness (2006)
Landscape	Macrotopography	Categorical	*	Appendix. 2.; Jorgenson et al., (2010b)
Site Surface	Microtopography	Categorical	*	Appendix. 2.; Jorgenson et al., (2010b)
Landscape	Geomorphic unit	Categorical	*	Appendix. 2.; Jorgenson et al., (2010b)
Site Surface	Permafrost degradation mode	Categorical	*	Jorgenson et al., (2008)
Site Surface	Vegetation	Categorical	*	Viereck et al., (1992); Jorgenson et al., (2010b)
Landscape	Vegetation complex	Categorical	§	Walker et al., (2002); Jorgenson et al., (2010b)
Site Surface	Dominant flora [over & understory]	Species	*	Hulten (1968) & Parker (2006)
Landscape	Summer Warmth Index	Quantitative	§	Raynolds et al., (2008)
Site Surface	Ecotype	Categorical	*	Jorgenson et al., (2010b)
Site Surface	Acidic (from mean pH per Ecotype)	Categorical	*	Jorgenson et al., (2010b)

* recorded in the field

§ derived from spatial (GIS & remote sensing) analyses

Table 3.2. Variables characterizing soil and permafrost properties in the vicinity of each permafrost profile exposure.

Name	Segment	Type	Integrator Variable	Units / Source
Depth of Active Layer	Profile	Quantitative		cm
Total Depth of Profile	Profile	Quantitative		cm
Wedge/Intrusive Ice Percentage	Profile	Quantitative		% of profile exposure
Litter Layer Thickness (O _l)	Soil	Quantitative		cm
Organic Layer Thickness (O _a)	Soil	Quantitative		cm
Depth of Contemporary Soil	Soil	Quantitative		cm
Coarse Fraction Percentage	Soil	Quantitative	§ Coarse & Fine Fraction	% of profile exposure
Maximum Clast Size	Soil	Quantitative	*	cm
Segregation Ice Percentage	Soil	Quantitative	*	% of profile exposure
Segregation Ice Max. Width	Soil	Quantitative	*	cm
Lithofacies	Soil	Categorical	§ Coarse & Fine Fraction	Appendix. 2; Jorgenson et al., (2010b)
Coarse & Fine Fraction	Soil	Categorical		Appendix. 2; Jorgenson et al., (2010b)
Coarse Fraction Shape	Soil	Ordinal	*	Appendix. 2; Jorgenson et al., (2010b)
Peat Type	Soil	Categorical	*	Appendix. 2; Jorgenson et al., (2010b)
Primary Cryostructures	Parent	Categorical		Appendix. 2; Jorgenson et al., (2010b)
Secondary Cryostructures	Parent	Categorical	*	Appendix. 2; Jorgenson et al., (2010b)
Lithofacies	Parent	Categorical	§ Coarse & Fine Fraction	Appendix. 2; Jorgenson et al., (2010b)
Coarse & Fine Fraction	Parent	Categorical		Appendix. 2; Jorgenson et al., (2010b)
Coarse Fraction Shape	Parent	Ordinal		Appendix. 2; Jorgenson et al., (2010b)
Buried Organics Percentage	Parent	Quantitative		% of profile exposure
Primary Cryostructures	Parent	Categorical		Appendix. 2; Jorgenson et al., (2010b)
Secondary Cryostructures	Parent	Categorical		Appendix. 2; Jorgenson et al., (2010b)
Coarse Fraction Percentage	Parent	Quantitative	§ Coarse & Fine Fraction	% of profile exposure
Maximum Clast Size	Parent	Quantitative	§ Coarse & Fine Fraction	cm
Segregation Ice Percentage	Parent	Quantitative		% of profile exposure
Segregation Ice Max. Width	Parent	Quantitative		cm

* excluded from MFA analysis; Pearson's $r < .300$ in pilot ordination

§ excluded from MFA analysis; information captured within a separate integrator variable (Pearson Correlation)

Table 3.3. Active (response) and supplemental (explanatory) variables used for statistical analysis, and subsequent grouping by hierarchical clustering. Active variables drive ordination results, while supplemental variables are used as overlays on ordination graphs to examine correspondence of that variable with ordination results.

Name	Block	Type	Class
Vegetation class	Vegetative	Categorical	Active
Acidic	Vegetative	Categorical	Active
Litter Layer Thickness (O _l)	Vegetative	Quantitative	Active
Organic Layer Thickness (O _a)	Vegetative	Quantitative	Active
Buried Organics Percentage	Vegetative	Quantitative	Active
Depth of Contemporary Soil	Substrate	Quantitative	Active
Depth of Active Layer	Substrate	Quantitative	Active
Coarse Fraction Percentage (contemporary soil)	Substrate	Quantitative	Active
Microtopography	Substrate	Categorical	Active
Coarse & Fine Fraction (contemporary soil)	Substrate	Categorical	Active
Coarse & Fine Fraction (archaic soil/parent material)	Substrate	Categorical	Active
Ice percentage	Ice	Quantitative	Active
Segregation Ice Maximum Lens Width	Ice	Quantitative	Active
Wedge/Intrusive Ice Percentage	Ice	Quantitative	Active
Total Depth of Profile	Ice	Quantitative	Active
Primary Cryostructures	Ice	Categorical	Active
Secondary Cryostructures	Ice	Categorical	Active
Acidity (mean Ecotype pH)	n/a	Quantitative	Supplemental
Elevation	n/a	Quantitative	Supplemental
Aspect	n/a	Quantitative	Supplemental
Topographic Position Index	n/a	Quantitative	Supplemental
Summer Warmth Index	n/a	Quantitative	Supplemental
Slope	n/a	Quantitative	Supplemental
Surficial Geology	n/a	Categorical	Supplemental
Bedrock Geology	n/a	Categorical	Supplemental
Glacial Geology	n/a	Categorical	Supplemental
Vegetation Complex	n/a	Categorical	Supplemental
Ecotype	n/a	Categorical	Supplemental
Lithology	n/a	Categorical	Supplemental
Macrotopography	n/a	Categorical	Supplemental
Permafrost Degradation Mode	n/a	Categorical	Supplemental
Lithofacies	n/a	Categorical	Supplemental

Table 3.4. Summary values for field-estimates characterizing soil and permafrost properties in the vicinity of each permafrost profile exposure, presented by grouping from hierarchical clustering of MFA ordination results.

	Units	Segment	E1		E2		E3		E4	
			mean	std	mean	std	mean	std	mean	std
Elevation	m	Site	576	70	633	240	657	167	469	314
Slope	°	Site	5.7	0.8	5.0	2.5	5.4	1.3	9.4	4.0
Aspect	°	Site	251	102	216	110	128	109	165	119
Depth of Active Layer	cm	Profile	156	55	58	16	82	21	64	23
Total Depth of Profile	cm	Profile	432	230	133	45	175	66	382	272
Wedge/Intrusive Ice	%	Profile	16	16	3	7	0	0	23	25
Litter Layer Thickness (O _i)	cm	Soil	1.5	0.5	9.3	5.6	6.1	4.6	3.9	2.1
Organic Layer Thickness (O _a)	cm	Soil	7.3	6.6	20.6	7.8	21.2	8.6	10.9	7.3
Depth of Contemporary Soil	cm	Soil	63	31	42	13	57	9	52	33
Coarse Fraction	%	Soil	15	9	1	3	10	9	9	20
Maximum Clast Size	cm	Soil	50	18	8	17	42	44	63	118
Segregation Ice	%	Soil	0	0	3	8	0	0	1	4
Segregation Ice Max.Width	mm	Soil	0	0	3	7	0	0	7	28
Buried Organics	%	Parent	3.5	6.2	8.8	6.9	7.0	8.7	6.3	7.3
Coarse Fraction	%	Parent	32	4	12	16	32	19	32	22
Maximum Clast Size	cm	Parent	501	332	41	41	88	46	559	483
Segregation Ice	%	Parent	9	15	29	19	29	16	56	24
Segregation Ice Max.Width	mm	Parent	75	86	65	107	52	55	947	1017

Table 3.5. Site groupings compared by permafrost degradation mode.

Site Grouping	Permafrost Degradation Mode				Total
	ALDS	Soil Pit	RTS	TEG	
E1	0	0	6	0	6
E2a	4	0	1	2	7
E2b	2	1	6	8	17
E3	7	0	2	0	9
E4a	0	0	3	0	3
E4b	0	0	9	1	10
E4c	0	0	2	0	2
Total	13	1	29	11	

ALDS = Active Layer Detachment Slide

RTS = Retrogressive Thaw Slump

TEG = Thermo-Erosional Gulley

Table 3.6. Field sites by group with ground coordinates (Geographic decimal degrees, NAD83).

Site	Name	Group	Subgroup	Latitude	Longitude
19	Third Twin A	E1		67.95835	-156.81985
20	Third Twin B	E1		67.95835	-156.81985
21	Third Twin C	E1		67.95835	-156.81985
22	Good Twin	E1		67.95929	-156.78624
23	Woodpile	E1		67.89927	-156.48472
34	Itkillik-2	E1		68.66615	-149.81720
6	Sushi	E2	a	67.86342	-161.48044
9	Bear Patch	E2	a	67.73697	-161.42747
25	Cotton Hollow	E2	a	68.98551	-150.71714
26	VoTK	E2	a	68.96278	-150.67086
47	GTH89	E2	a	68.52534	-149.54644
50	I-Minus-2 A	E2	a	68.54345	-149.52273
53	TRTK A	E2	a	68.69177	-149.20751
24	Helios	E2	b	68.91054	-150.74004
27	VoTK	E2	b	68.96067	-150.66970
28	VoTK Control	E2	b	68.96210	-150.66755
31	Ptarmigan Bluff	E2	b	68.87620	-150.54552
32	Horn Lake A	E2	b	68.96068	-150.31443
33	Horn Lake B	E2	b	68.96068	-150.31443
39	Nstk-3u A	E2	b	68.87147	-149.57768
40	Nstk-3u B	E2	b	68.87148	-149.57768
41	GTH88 A	E2	b	68.50785	-149.57474
42	GTH88 B	E2	b	68.50806	-149.57433
43	I-Minus-1 A	E2	b	68.55244	-149.57229
44	I-Minus-1 B	E2	b	68.55253	-149.57169
45	I-Minus-1 C	E2	b	68.55231	-149.57081
49	GTH89 A	E2	b	68.52510	-149.53815
51	I-Minus-2 B	E2	b	68.54337	-149.52260
52	GTH86	E2	b	68.61919	-149.42786
54	TRTK H	E2	b	68.69360	-149.20430
5	Remora	E3		67.64853	-161.60562
7	Saddle	E3		67.81790	-161.44655
8	Eli	E3		67.71618	-161.43026
10	Slopbucket	E3		67.92515	-161.41811
14	Old Ironslides	E3		68.27005	-157.68447
16	Mafic Monks	E3		68.26651	-157.47338
17	Jaded Plover	E3		67.98045	-157.07511
18	Bloodslide	E3		68.28070	-157.05966
37	GTH88 C	E3		68.50267	-149.58873
2	Rainbucket	E4	a	67.94305	-162.35649
4	Loon Lake A	E4	a	67.92730	-161.96506
12	Quebec	E4	a	68.08735	-158.04102
13	Gavia Familia	E4	a	68.08324	-158.02727
15	Cutler Ice	E4	a	67.87649	-157.53053
29	Lobelia A	E4	a	68.87938	-150.55647
30	Lobelia B	E4	a	68.87938	-150.55647
35	NE-14	E4	a	68.67904	-149.62320
46	I-Minus-1 D	E4	a	68.55272	-149.56517
48	GTH89 B	E4	a	68.52585	-149.54500
1	Wulik	E4	b	67.84770	-163.88159
3	Loon Lake B	E4	b	67.92794	-161.97230
11	Grandaddy	E4	b	68.03481	-159.29156
36	GTH88 D	E4	c	68.50268	-149.58901
38	GTH88 E	E4	c	68.51121	-149.58395

Appendix 3. Field Codes for Site Survey in Chapter 3

A3.1. Field Code Data Sheets used for Field Surveys in Chapter 3. The data sheets presented below are formatted for two-sided printing for lamination and field use. Codes were adapted from methods developed for the Ecological Land Survey and Landcover Map of the Arctic Network by M. Torre Jorgenson for Alaska Biological Research and Alaska EcoScience (Jorgenson et al. 2010).

Jorgenson, M. T., J. E. Roth, P. F. Miller, M. J. Macander, M. S. Duffy, A. F. Wells, G. V. Frost, and E. R. Pullman (2010), An ecological land survey and landcover map of the Arctic Network. Natural Resource Technical Report NPS/ARC/NRTR—2009/270., edited, National Park Service, Fort Collins, Colorado.

CODES USED FOR FIELD SURVEY – NORTHERN ALASKA 2009-2011

**AMBIENT SITE
CONDITIONS**

**I. ENVIRONMENTAL PLOT
DATA**

Lat(dd83):
 Long(dd83):
 ElevGPS(m):
Physiography:
 A Alpine
 U Upland
 L Lowland
 P Lacustrine (ponded)
 R Riverine
 C Coastal
Thaw Depth (cm):
 CryoTurb: Present or Absent
 SurfOrg: depth of top layer (cm)
 CumOrg40: total org in top 40
 DomMineral40: dominant mineral text.
 in top 40 cm
 B Bouldery (md, >15% crse ; >76 mm)
 K Blocky (ang., >76 mm)
 G Gravelly (rounded, 2-76 mm)
 R Rubbly (angular, >15% rocks)
 S Sandy (grSa to 1 Sa; <15% gravel)
 L Loamy (CL to SL)
 C Clayey (SC to C)
 O Organic-rich (20-40 cm org.)
 P Peat (>40 cm organics)
 DomText40: dominant text. (O or M) < 40cm
SurfaceFrag (%):
RockDepth(>15%): cm
SoilPH: to 0.1 units from paste
SoilEC: uS/cm from paste
SampDepth10:
SampMeth (Sampling Method):
 P pit
 L plug
 A auger
 C corer
 E bank exposure
 S surface
 M metal probe
 LM plug + probe
 LA plug + auger
FrostBoil(% cov): % cov. barren active
 frost boils

SoilClass: NRCS taxonomy 2003
VegClass(LIV): Viereck Level IV
EcoType: sequential coding for
 Physiograph, DomMin40, SoilMoist,
 Chemistry, Veg Structure

II. TERRAIN UNITS

COLLUVIAL DEPOSITS

C Colluvial Deposits
 Ch Hillslope Colluvium
 Cl Landslide Deposit
 Cs Solifluction Deposits

EOLIAN DEPOSITS

Esa Eolian Active Sand
 Essi Eolian Inactive Sand Sheet
 Essi Eolian Inactive Sand Sheet

FLUVIAL DEPOSITS

Fu Fluvial, undifferentiated

Fd Delta Floodplain

Fdra Delta Active Channel Deposit
 Fdri Delta Inactive Channel Deposit
 (High-water Channel)
 Fdoa Delta Active Overbank Deposit
 Fdoi Delta Inactive Overbank Deposit
 Fdob Delta Abandoned Overbank Dep
Fpm Meander Floodplain
 Fmr Meander Channel Dep (riverbed)
 Fmrac Meand Course Active Chan. Dep.
 Fmrif Meander Fine Inactive Chan Dep.
 Fmo Meander Overbank Deposit
 (complex)

Fmoa Meander Active Overbank Dep
 Fmoi Meander Inactive Overbank Dep
 Fmob Mean. Abandoned Overbank Dep

Fb Braided Floodplain

Fbr Braided Channel Dep (riverbed)
 Fbrac Braided Course Active ChanDep.
 Fbrif Braided Fine Inactive Chan Dep.
 Fbo Braided Overbank Dep (complex)
 Fboa Braided Active Overbank Deposit
 Fboi Braided Inactive Overbank Dep
 Fbob Braided Abandoned Ovrbank Dep
Fhl Headwater Lowland Floodplain
 Fto Old Terrace (lower terraces)

Ff Alluvial Fan

GLACIAL AND NON-G. DEPOSITS
 FGp Alluvial Plain Deposits
GLACIAL DEPOSITS
 Gmo Older Moraine

Gmy Younger Moraine
 Gto Older Till Sheet
 Gty Younger Till Sheet

GLACIOFLUVIAL DEPOSITS

GFO Glaciofluvial Outwash
 GFK Kame Deposits

GLACIOLACUSTRINE DEPOSITS

GL Glaciolacustrine Deposits

L LACUSTRINE DEPOSITS

Ltnu Ice-poor Thaw Basin (young)
 Lmc Ice-poor centers
 Ltm Ice-poor margins
 Ltiu Ice-rich Thaw Basin (old)
 Ltic Ice rich centers
 Ltim Ice rich margins
 Ltip Ice-rich-pingos

ORGANIC DEPOSITS (Org >40cm)

Of Organic Fens
 Ob Bogs

**III. MACROTOPOGRAPHY
CLASSES:**

C Top, Crest, Summit Or Ridge
 Fh Plateau (High Flats)

Sh Shoulder Slope

XP Pingo
Steep Slopes
 Sb Bluff or Bank (unconsolidated)
 Sbs Steep bluff south facing
 Sc Cliff (rocky)
 Sbr Riverbanks
Su UPPER SLOPE (convex, creep)
 Suc Concave (water gathering)
 Suv Convex (water shedding)

Sup Plane
Sl LOWER SLOPE (concave)
 Slc Concave (water gathering)

Slch Nivation hollows, Snowbanks,
 Slv Convex (water shedding)

Slp Plane
T TOE Slope
D Drainage or Water Track

B BASINS OR DEPRESSIONS

Bd Drained Basin
 Bk Kettle
F FLAT OR FLUV. RELATED
 Fn Nonpatterned
 Fm Flats margins (transition)
 Fc Channel, swale or gut,
 Fi Interfluv or flat bank
 Fl Levee
 Fb Bar (point, lateral, mid-channel)
 Fs Crevasse splay
 Ft Terrace
 Ff Flood Basin (behind levee)

**IV. MICROTOPOGRAPHY
CLASSES**

N NONPATTERNED

FROST FEATURES

Fh Hummocks (mineral cored)
 Fr Reticulate
 Ff Frost Scars and Boils
 Fc Circles (non-sorted, sorted)
 Fs Stripes (non-sorted, sorted)
 Fn Nets (non-sorted, sorted)
 Ft Steps (non-sorted, sorted)

Polygons

Pd Disjunct polygon rims
 Pll Low-cent., low-relief, low-density
 Pllh Low-cent., low-relief, high-density
 Pllh Low-cent., high-relief, high-density
 Pm Mixed high and low polygons
 Ph High-cent., low-relief (flat-cent.)
 Phh High-centered, high-relief

Thermokarst

Tm Mixed thermokarst pits and
 polygons
 Tb Beaded stream

MOUNDS (ice and peat related)

Mi Ice-cored mounds
 Mpm Peat mounds
 Ms String (strang)

Mg Gelifluction lobes (saturated flow)
 Mir Ice-shoved ridge
 Mid Ice-rafted debris
 Mrb Rocks, Blockfields
 Mrm Rocky Mounds (soil covered rocks)
 Mw Mounds caused by wildlife
 Mh Mounds caused by humans
 Mu Undifferentiated mounds (distinct)
DRAINAGE or EROSION RELATED
 Dt Water tracks (non-incised
 drainages)
 Df Feather pattern (in fens)
 Dr Ripples
 Dd Flow dunes
 Ds Scour channels-ridges

EOLIAN RELATED

Es Small dune
 Eb Scour depression
 X COMPLEXES

V. VEGETATION CLASSES

CLASS

(use Alaska Veg. Class; Level IV)

ECOTYPE VEG STRUCTURE

BP Barrens, Partially Vegetated
 FA Aquatic Forb
 SE Sedge Marsh
 GE Grass Marsh
 FE Forb Marsh
 SM Sedge Meadow
 GM Grass Meadow
 FM Forb Meadow
 TM Tussock
 KM Salt-killed Meadow
 DS Dwarf Shrub
 LS Low Shrub
 TS Tall Shrub
 Ow Open Water

** Coding system adopted from methods developed by Jorgenson et al. (2010)

CODES USED FOR FIELD SURVEY – NORTHERN ALASKA 2009-2011

PERMAFROST PROFILE

VI. SOIL LAYER

Lithofacies:

- B Blocky (angular > 380 mm, > 60%)
- R Rubble (ang, 2-380mm, > 60%)
- S Stony (rnd, > 250 mm, > 60%)
- Gm Gravel (md, massive, > 60%)
- Gfm Grav w/ fine, massive, 15-60%
- Gl Gravel (2-250 mm), layered
- Sm Sands, massive
- Si Sands, inclined
- Sl Sands, layered
- Soi Sands with org, inclined
- Sr Sands, rippled
- Sor Sands with org, inclined
- Sgm Sands w/tr gravel, massive
- Sgmt Sands w/tr gravel, turbated
- Om Organic, massive
- OI Organ., layered (> 10% org)
- Olt Organic, layered, turbated
- Oa Organic, limnic
- Fm Fines massive
- Fom Fines w/ organics, massive
- Fomt Fines with organics, massive, turbated
- Fgm Fines w/tr grav (tr-15% gr)
- Fl Fines, layered
- Fr Fines, rippled
- For Fines with organics, rippled
- Fcm Fines with clay, massive
- Fcl Fines with clay, layered
- Fa Fines with algae, limnic

Horizon: used NRCS codes

Master horizon:

O, A, AB, AE, A/B, A/E, A/C, AC, E, E/A, BA, B, BC, B/C, C, L, W, R,

Horizon suffixes:

a, b, c, co, d, di, e, f, ff, g, h, i, j, jj, k, m, ma, n, o, p, q, r, s, ss, t, v, w, y, z,

TopDepth: cm from surf (exc live moss)

BotDepth: cm

Coarse fragment content : (>2mm)

Combine content + size (sgr, xby)

- 0%, no crs frag modifier
- s trace to 15 % (grsil)
- 15 to 35 %; no modifier
- v 35 to 60 % (cbssil)
- x 60-90 % (grxSiL)
- >90%; use crs frg alone (eg. gr)

Crse fragment size class (>2mm); largest

- fl flagstones (flat, 150-380 mm)
- cn channery (flat, 2-150 mm)
- by boulder (round, > 600 mm)
- st stone (round, 250 – 600 mm)
- cb cobble (round, 75 – 250 mm)
- gr gravel (round, 2 – 75 mm)

Fine fraction (<2 mm) codes:

- s sand
- wcos very coarse sand (1-2 mm)
- cos coarse sand (0.5-1 mm)
- ms medium sand (0.25-0.5 mm)
- fs fine sand (0.1-.25 mm)
- vfs very fine sand (0.05-0.1 mm)
- lcos loamy coarse sand
- ls loamy sand
- lfs loamy fine sand
- lvfs loamy very fine sand
- cosl coarse sandy loam
- sl sandy loam
- fsl fine sandy loam
- vfsl very fine sandy loam
- l loam
- sil silt loam
- si silt (0.002-0.05 mm)
- scl sandy clay loam
- cl clay loam
- sicl silty clay loam
- sc sandy clay loam
- sic silty clay
- c clay (<0.02 mm)

Oasil Organic Silt (A horizon)

Organic Soils

- Oi slightly decomposed
- Oe intermediate decomposition.

- Oa highly decomposed
- mk mucky peat (>10% OM, <17% fibers)

Peat Types (Peat):

- G Graminoid or sedge
- Gf Gramin., fine (<2 mm wide)
- Gc Gram, coarse (>2 mm wide)
- H Herbaceous
- A Allochthonous (drifted)
- Mb Brown mosses (fens)
- Md dicranum/Polytrichum
- Mf feathermoss
- Ms Sphag
- Ml Live mosses
- W Woody
- S Sedimentary (algal, coprogen)

Coarse Fragment Content: %

Coarse Fragment Size: maximum (mm)

Coarse Fragment Shape:

- Av very angular,
- A angular,
- As subangular
- Rs subrounded,
- R rounded
- Rw well rounded

Ice Structure Vol: % visible

Primary (dominant) and Secondary (subordinate) Ice Structures:

Combine primary, secondary, and tertiary structures (Pnv, Abl, Mww)

Primary (continuity):

- P Pore (structureless)
- O Organic-matrix
- C Crustal
- V Vein (vertical)
- B Layered, Bedded (horizontal)
- L Lenticular

- R Reticulate
- A Ataxitic (50-95% ice)
- M Massive (solid) (>10 cm thick)

Secondary (shape or bedding):

- For Pore, Organic, Crustal, Vein,*
- n Nonvisible
- u Uniform
- i Irregular
- For Lenticular, Bedded*
- h Horizontal or planar
- w Wavy
- c Curved
- x Crossbedded or inclined
- For Reticulate:*
- t Trapezoidal (prismatic)
- l Lattice (regular, blocky)

For Ataxitic:

- r Round
- b Blocky or Angular
- p Platy

For Massive

- n Non-stratified, massive
- h Sheet, horizontally stratified,
- w Wedge, vertically stratified,
- v Vertically stratified
- i Irregularly stratified
- f Fractured
- d Discontinuous or porous
- c Columnar

Tertiary (size or clarity):

Ice thickness for Pore, Organic, Crustal, Vein, Bedded, Reticulate ice structures

- v Very fine (<0.5 mm)
- f Fine (0.5 - <1 mm)
- m Medium (1-3 mm)
- c Coarse (3-5 mm)
- l Large (5-10 mm)
- e Extremely large (>10 mm)

Soil width for ataxitic ice structure

Same sizes above

Clarity for massive ice

- c Clear
- s Clear soil inclusions
- w Opaque, clean, white,
- i Opaque, soil inclusions
- r Opaque, rock inclusions
- o Organic-rich, brown

Lens Thickness: maximum (mm)

**

Coding system adopted from methods developed by Jorgenson et al. (2010)

Chapter 4. Drivers and Estimates of Terrain Suitability for Active Layer Detachment Slides and Retrogressive Thaw Slumps in the Brooks Range and Foothills of Northwest Alaska¹

4.0 Abstract

Active layer detachment sliding and retrogressive thaw slumping are important modes of upland permafrost degradation and disturbance in permafrost regions, and have been linked with climate warming trends, ecosystem impacts, and permafrost carbon release. In the Brooks Range and foothills of northwest Alaska, these features are widespread, with distribution linked to multiple landscape properties. Inter-related and co-varying terrain properties, including surficial geology, topography, geomorphology, vegetation and hydrology, are generally considered key drivers of permafrost landscape characteristics and responses to climate perturbation. However, these inter-relationships as collective drivers of terrain suitability for active layer detachment and retrogressive thaw slump processes are poorly understood in this region. We empirically tested and refined a hypothetical model of terrain factors driving active layer detachment and retrogressive thaw slump terrain suitability, and used final model results to generate synoptic terrain suitability estimates across the study region. Spatial data for terrain properties were examined against locations of 2,492 observed active layer detachments and 805 observed retrogressive thaw slumps using structural equation modelling and integrated terrain unit analysis. Factors significant to achieving model fit were found to substantially hone and constrain region-wide terrain suitability estimates, suggesting that omission of relevant factors leads to broad overestimation of terrain suitability. Resulting probabilistic maps of terrain suitability, and a threshold-delineated mask of suitable terrain, were used to quantify and describe landscape settings typical of these features. 51% of the study region is estimated suitable terrain for retrogressive thaw slumps, compared with 35% for active layer detachment slides, while 29% of the study region is estimated suitable for both. Results improve current understanding of arctic landscape vulnerability and responses to climate warming, and enhance the capability to estimate quantities of permafrost carbon potentially subject to release through these modes of permafrost degradation.

4.1 Introduction

Permafrost degradation is widespread throughout the circumpolar north, occurring by multiple modes and mechanisms across diverse landscapes (Serreze et al. 2000, Hinzman et al. 2005, Anisimov and Reneva 2006, Jorgenson et al. 2008a). The pan-arctic rate of permafrost degradation is increasing, and permafrost carbon release will likely be a major contributor to atmospheric greenhouse gas

¹ Submitted to *Journal of Geophysical Research: Earth Surface*. Balser, A. W. and J. B. Jones, March 2015

concentrations in coming decades (Schuur et al. 2008, Grosse et al. 2011, Schaefer et al. 2011), yet spatial distribution and variability of these processes are poorly understood. Carbon and nitrogen released from frozen substrates may substantially contribute to atmospheric concentrations of CH₄, CO₂, and N₂O, and strongly affect global biogeochemistry and climate (Walter et al. 2006, Walter et al. 2007, Schuur et al. 2008, Desyatkin et al. 2009, Gooseff et al. 2009, Tarnocai et al. 2009, Grosse et al. 2011), with biogeochemical pathways and amplitudes for permafrost carbon and nitrogen flux potentially dependent upon mode of permafrost degradation (Abbott et al. 2014, Lamoureux and Lafreniere 2014). Locally, active layer detachment sliding and retrogressive thaw slumping mobilize previously frozen substrates, organic materials, and nutrients which alter the ecology of receiving streams (Bowden et al. 2008, Frey and McClelland 2009, Gooseff et al. 2009, Rozell 2009, Abbott et al. 2014, Lamoureux and Lafreniere 2014), impact sediment loads and productivity of streams and rivers (Walker et al. 1987, Walker and Hudson 2003, Gooseff et al. 2009, Bowden et al. 2012, Kokelj et al. 2013), and cause ecological and hydrobiogeochemical impacts to lake ecosystems (Thompson et al. 2008, Kokelj et al. 2009b, Mesquita et al. 2010, Bowden et al. 2012). Vegetation within and adjacent to these features is directly impacted through turbation, soil and hydrologic modification, and succession on altered surfaces (Leibman and Streletskaia 1997, Ukraintseva and Leibman 2007, Lantz and Kokelj 2008, Balser et al. 2009, Lantz et al. 2009, Bowden et al. 2012). An improved understanding of the extent and distribution of landscapes prone to these modes of permafrost degradation is needed to better estimate the nature and magnitude of ecological impacts both locally and within the global climate system.

Active layer detachment sliding (ALD) and retrogressive thaw slumping (RTS) are important permafrost degradation processes in which thaw of ice-rich permafrost on hill slopes or bluffs causes soil structural instability and mass-wasting subsidence (Burn and Lewkowicz 1990, Leibman 1995, Leibman et al. 2003, Lewkowicz and Harris 2005, Jorgenson et al. 2008a). ALDs occur on hill slopes where shear strength of active layer soils is exceeded by pore water pressures and the destabilized active layer slides down slope, exposing the permafrost table below (Figure 4.1; Jorgenson and Osterkamp 2005, Lewkowicz and Harris 2005, Lewkowicz 2007). Warm weather and precipitation can trigger sliding (Leibman et al. 2003, Lamoureux and Lafreniere 2009, Balser et al. 2014), particularly where warm air temperature pulses or rainfall accelerate thaw front advance through syngenetic cryofacies containing an ice-rich intermediate layer directly beneath the active layer (Shur 1988, French and Shur 2010). Active layer detachment sliding is episodic, with features often appearing clustered together in space and time, and with active degradation confined to one or two consecutive thawing seasons (Leibman 1995, Lamoureux and Lafreniere 2009, Lamoureux and Lafreniere 2014). In some settings, conditions at a prior

ALD site can redevelop over decades or centuries, with repeat initiation in response to triggering events (Leibman 1995, Khomutov 2012).

Retrogressive thaw slump formation can stem from several distinct mechanisms leading to exposure of ice-rich permafrost deposits (including pore, segregation, and massive ice). In coastal and riparian settings, lateral thermal erosion of protective overburden from adjacent bluffs can expose permafrost deposits rich with massive ice (Burn and Lewkowicz 1990, Lantuit et al. 2012, Kokelj and Jorgenson 2013). Wildfire that removes protective vegetation and organic layers, and promotes thaw front advance through the active layer may cause instability and disturbance (Lacelle et al. 2010). Channelized flow of surface water over networks of ice wedge polygons can melt ice wedges, creating thermo-erosion gullies with progressive downward and lateral thaw into the permafrost (Jorgenson and Osterkamp 2005). Intense precipitation may be a particular trigger for thermo-erosion gullies leading to RTS initiation (Bowden et al. 2008, Balsler et al. 2014). RTSs may develop from any of these exposures where conditions promote continued instability with downward subsidence of thawed material (Burn and Lewkowicz 1990, Jorgenson and Osterkamp 2005, Lacelle et al. 2010, Godin and Fortier 2012, Kokelj and Jorgenson 2013). Once initiated, RTSs continue to deepen and expand along the headwall, typically forming a steep headwall up to 20 m deep, an arcing headwall scarp, a floor of thawed and flowing debris, and a run out of re-stabilizing deposits (Figure 4.2; Burn and Lewkowicz 1990, Lacelle et al. 2010, Lantuit et al. 2012, Kokelj and Jorgenson 2013). Headwall retreat rate ranges from several to tens of meters annually, and is correlated with headwall height, ice content, and local climate (Kokelj and Jorgenson 2013). Expansion may continue for decades if thawed debris continues to subside and expose the headwall, and if newly exposed headwall deposits are ice rich and receive sufficient energy for thaw and subsidence (Lacelle et al. 2010). RTSs are frequently polycyclic, alternating between decades of stabilized, revegetated dormancy, and active degradation when slumps reinitiate within, or adjacent to, older slump scars. Re-initiation may be caused by mechanisms described above (Lantuit et al. 2012, Kokelj and Jorgenson 2013), with sublimic talik expansion as a significant additional driver in kettle lake basin settings (Kokelj et al. 2009a).

Active layer detachment sliding and retrogressive thaw slumping are widespread in the Brooks Range and foothills of northwest Alaska, and in this region are the most prominent of the nineteen described modes of permafrost degradation for Alaska (Jorgenson et al. 2008b). ALD and RTS features are linked with characteristic terrain properties which drive development of permafrost conditions associated with these modes and vulnerability to thaw (Jorgenson and Osterkamp 2005, Shur and Jorgenson 2007, Jorgenson et al. 2008a, Balsler et al. 2009, Jorgenson et al. 2010a). Terrain properties including parent material/surficial geology, topography, geomorphology, vegetation, hydrology, climate,

and time have been presented as co-varying factors controlling permafrost distribution and active layer thickness (Pastick et al. 2014b), permafrost evolution, ecosystem response to climate and fire disturbance (Shur and Jorgenson 2007, Jorgenson et al. 2013), active layer depth (Pastick et al. 2014b), and ALD and RTS distribution (Jorgenson et al. 2008a, Kokelj and Jorgenson 2013). Positive and negative feedbacks among multiple terrain properties have been identified as key determinants and mediators of landscape response to climate warming and disturbance, and to the distribution of ALD and RTS features (Jorgenson et al. 2008a, Kokelj and Jorgenson 2013) with particular influence on thermal properties of substrate profiles (Shur and Jorgenson 2007, Xie and Gough 2013). Terrain properties have been usefully grouped within a 'state factor' framework and applied to models of soil, permafrost, and vegetation development and distribution (Jenny 1941, van Cleve et al. 1991, Jorgenson et al. 2013). These principles are generally accepted, however the importance of, and relationships among, individual terrain properties and state factors as drivers of overall terrain suitability for ALD and RTS processes in the Brooks Range and foothills of northwest Alaska are not fully understood and have not been integrated to estimate terrain suitability focused on this region.

Inter-relationships among key terrain properties influencing permafrost distribution, characteristics, and degradation have been analyzed and modelled using both integrated terrain unit (ITU) approaches (Walker 1996, Jorgenson et al. 2010b, Jorgenson et al. 2014), and using statistical analyses of complex, causal linkages. Both of these approaches have advanced our understanding of terrain property relationships, ecological processes, and have contributed to predictive, spatial estimates of permafrost characteristics, distribution, and degradation at scales ranging from field sites of several square meters, to locales of several dozen square kilometers, up through regional and pan-arctic domains (Jorgenson et al. 2008b, Walker et al. 2008, Harris et al. 2009, Daanen et al. 2011, Gruber 2012, Khomutov 2012, Pastick et al. 2014a). Herein, we tested inter-relationships among specific terrain factors driving ALD and RTS distribution at a regional scale in the Brooks Range of northwest Alaska, and generated estimates of terrain suitability for ALD and RTS formation. We specifically chose the term 'suitability' to convey that these estimates are not hard spatial predictions of future feature occurrence, but rather a depiction of appropriateness of terrain. Suitability does not directly infer probability or vulnerability.

4.2 Methods

4.2.1 Study Region

Our study region spanned a gradient of arctic tundra and shrub landscapes abutting the forested, arctic-boreal ecotone, from the central portion of Alaska's Brooks Range mountains westward through the Noatak Basin to the Mission Lowlands, near the Noatak River delta (Figure 4.3). This periglacial

landscape is within the continuous permafrost zone (Jorgenson et al. 2008b) and is part of Arctic Bioclimate Subzone E (CAVM-Team 2003). The study region extended 63,707 km², which is slightly larger than the state of West Virginia, and covered Gates of the Arctic National Park and Preserve and Noatak National Preserve. Physiographic provinces include high mountains of the central Brooks Range, through foothills, valley bottoms and the Aniuk Lowland westward, entering the broad, Mission Lowland at the arctic/boreal ecotone near the Noatak mouth (Wahrhaftig 1965, Young 1974).

The study region is within the zone of climate-driven, ecosystem-modified permafrost (Shur and Jorgenson 2007), with ground ice conditions suitable for ALD and RTS processes distributed among landscapes throughout the region. Conditions differ markedly for alpine and lowland settings, with permafrost in the foothills comprising an intermingling of conditions characteristic of alpine and lowland landscapes. In alpine terrain, upper permafrost in thin soils over near-surface bedrock is primarily syngenetic (French and Shur 2010). Segregated ground ice exceeding 30% by volume, comprised mainly of ataxitic and reticulate cryostructures, has been observed in the top meter of permafrost in these locations (Balser et al. 2015). An ice-rich intermediate layer (Shur 1988, Shur et al. 2005), with an ice layer of several centimeters at the interface of the active layer and permafrost table may also be present across hill slopes (Balser et al. 2015). Episodes of solifluction and colluvial re-deposition contribute to successive syngenetic permafrost development above buried soil surfaces, thickening both overall soil and permafrost through time (Balser et al. 2015). Regional-scale ground ice estimates for these alpine areas range from low (<10%) to moderate (10%-40%) (Jorgenson et al. 2008b).

At low elevations, permafrost of glacial and glaciolacustrine origin includes extensive deposits of deep, ice-rich, syngenetic and epigenetic permafrost, with massive ice deposits (Balser et al. 2015). In the Mission and Aniuk Lowland, regional ground ice estimates range from moderate (10%-40%) to high (>40%) and include broad areas of active Holocene and inactive Pleistocene ice wedges (Young 1974, Jorgenson et al. 2008b, Balser et al. 2015) with deposits of relict glacial ice scattered throughout (Hamilton 2009, 2010). Syngenetic cryofacies at the top of the permafrost table have been observed in these lowlands, often within a loess cap up to several decimeters thick (Balser et al. 2015). Upper permafrost conditions may be highly variable, corresponding with surficial geology, landforms, vegetation, and glacial history (Hamilton 2009, 2010, Hamilton and Labay 2011, Balser et al. 2015). There is no permafrost borehole monitoring within the study region, but adjacent boreholes to the north and south report average annual temperatures of -5°C and 1°C respectively, while mean annual air temperature estimates for the study region are -7°C to -12°C (Jorgenson et al. 2008b).

Land cover comprises a broad suite of vegetation in various landscape settings including arctic and alpine tundra, shrublands, and lowland boreal forest along the arctic-boreal ecotone (Young 1974, Viereck et al. 1992, Parker 2006, Jorgenson et al. 2010b). Thirty-six ecotypes have been identified and mapped within our study region (Jorgenson et al. 2010b), with more than 50% of the land surface covered by shrub-graminoid ecotypes. Alpine and arctic dwarf shrub tundras are most prevalent at the highest elevations, and within north-draining watersheds, while low shrub, tall shrub, and tussock tundras are common in mid-elevation valleys and throughout the Noatak Basin. Lowland valleys within the southwest portion and along the southern boundary of the study region are part of the arctic-boreal ecotone, and include open and closed stands of conifer and broadleaf species along floodplains (Young 1974, Viereck et al. 1992, Parker 2006, Jorgenson et al. 2010b).

Generally, upland hill slopes with an ice-rich intermediate layer may be more favorable for active layer detachment sliding, while lowlands of glacial and glaciolacustrine origin offer prime settings for retrogressive thaw slump development, but these relationships are not obligate. RTSs are widespread along lowland lake margins, river banks, and bluffs. However, they can also occur in upland settings, often where an ALD has exposed the upper permafrost, and prior, episodic colluviation has accumulated a deeper layer of ice-rich, syngenetic, upper permafrost vulnerable to retrogressive thaw slumping (Hamilton 2009, Swanson 2010, Swanson and Hill 2010, Balsler et al. 2014). ALDs are most frequently found on broad, upland hill slopes, but have also been observed in lowlands, typically adjacent to river bluffs on mild slopes where an ice-rich intermediate layer has developed (Balsler et al. 2009, Gooseff et al. 2009, Swanson 2010, Balsler et al. 2014).

Conditions throughout the study region represent a broad range of typical low-arctic landscapes. Alpine, foothill, and valley bottom settings include many characteristic ecotypes of the North American low arctic, a suite of periglacial landforms, diverse lithologies, and a broad continuum of permafrost characteristics and cryofacies. Our study deliberately included this breadth of conditions to represent the diversity of landscapes within the region.

4.2.2 Analysis Overview

A conceptual diagram (Figure 4.4) depicts our initial, general hypothesis for inter-relationships among landscape characteristics of terrain suitability for ALD and RTS development in the central and western Brooks Range of northern Alaska. This diagram directed our approach and was iteratively tested and refined, with final terrain suitability estimates for the study region derived from the results.

Terrain suitability analysis and estimation involved four primary stages: 1) collection and preparation of input data, 2) integrated terrain unit (ITU) analysis, 3) structural equation modeling (SEM) analysis, and 4) terrain suitability estimation combining ITU and SEM results. Input data included a geodatabase of ALD and RTS locations (Table 4.1 and Appendix 5), and spatial data layers of categorical and continuous data covering the entire study region (Table 4.1). The study region boundary was defined by the geographic intersection of spatial data available for the region (Table 4.1 and Figure 4.3). All spatial data were clipped to the study region boundary, and landscape metrics were derived from continuous data (Table 4.2).

ITU and SEM analyses identified drivers, and relationships among drivers for terrain suitability, and were conducted separately for ALD and RTS features (Figure 4.5). ITU and SEM results were combined to produce a final dataset of estimated terrain suitability for each of the two feature types. Terrain suitability threshold values were calculated for each type of feature, and used to delineate areas of suitable and highly suitable terrain, by which landscape properties were summarized and tabulated from spatial data (Tables 1 and 2).

4.2.3. Steps for Terrain Suitability Analysis and Estimation

4.2.3.1 Collection and Preparation of Input Data

Feature Locations

Aircraft-supported field campaigns and airphoto surveys in 2006, 2007, 2010, and 2011 were used to map active layer detachment slides and retrogressive thaw slumps in the Noatak Basin. Initial fixed-wing surveys were used to identify the general distribution of RTSs and ALDs within the study area, and subsequent helicopter-supported surveys were used to mark the location of features in the field by GPS. Vertical aerial photography for areas with dense feature distributions was acquired using a Nikon D2X digital camera mounted beneath a small, fixed-wing aircraft. Airphoto lines were digitally stitched together, then manually georectified against pan-sharpened Landsat TM satellite ortho-imagery (Balser et al. 2009). Each feature location was manually marked within airphoto coverage. Our initial geodatabase of ALDs and RTSs in the Noatak Basin was expanded and augmented through a subsequent National Park Service survey, which included both Gates of the Arctic National Park and Preserve and Noatak National Preserve, using high-resolution satellite imagery to census these features throughout both park units (Figure 4.6; Balser et al. 2009, Swanson and Hill 2010). Randomly assigned control point locations were generated throughout the study region to represent areas without RTS or ALD features. Randomly generated points that fell within 200 m of mapped features were considered co-located with those features and were excluded. Separate datasets were constructed for ALDs and RTSs respectively, with each

dataset containing mapped feature locations and an equal number of randomly generated control point locations.

Landscape Properties and Metrics

We used thematic spatial datasets covering the entire study region that included both categorical and continuous data, deriving additional analysis variables from the continuous data (Table 4.1). Categorical data used in terrain unit analysis included lithology, surficial (glacial) geology, and ecotype. Lithology data were drawn from mapped eco-subsections for the region, following the National Hierarchical Framework for Ecological Units (ECOMAP 1993, Cleland et al. 1997, Jorgenson et al. 2001), and were grouped as either ‘carbonate’ or non-carbonate’ for analysis. Surficial geology was mapped at a scale of 1:250,000 from compiled reports and field surveys conducted throughout the study region over the course of several decades (Hamilton 2010, Hamilton and Labay 2011). For analysis, surficial geologic units were summarized by surficial deposit type (e.g. glacial drift, colluvium, alluvium) as presented by the authors. Ecotypes were mapped with Landsat ETM+ imagery from mapping algorithms trained and validated using extensive field data from the study region (Jorgenson et al. 2010b). Grid cells were resampled from their original 30 m cell size to 60 m cell size using the nearest neighbor method, but ecotype data were not thematically summarized for our analyses.

Two sources of continuous data were used to derive additional metrics used in SEM analysis (Table 4.1): 1) The National Elevation Dataset (NED) distributed by the U.S. Geological Survey (Gesch et al. 2002), and 2) monthly normalized difference vegetation index (NDVI) values, calculated from Moderate-resolution Imaging Spectrometer data by the U.S. Geological Survey for the 2000-2013 time span (Jenkerson et al. 2010). NED elevation was directly extracted, and geomorphologic, topographic and hydrologic derivatives were calculated from the NED (Table 4.2). Monthly NDVI data from 2000-2013 were analyzed first on an annual basis to extract peak growing season NDVI values for each pixel in the study region for each year. Next, these peak annual NDVI datasets were statistically summarized across all years (excluding 2000, which had incomplete data) to produce decadal values for peak growing season NDVI (Table 4.2). Variables were derived using ERDAS Imagine 2011, and using ArcGIS 9.3 and 10.1 software, including the “Geomorphometric and Gradient Metrics Toolbox” (Cushman et al. 2010, Evans et al. 2013). Values for derived variables were standardized prior to inclusion in SEM runs.

4.2.3.2 Integrated Terrain Unit Analysis

Integrated terrain unit analyses were conducted using ArcGIS 9.3 for ALD and RTS feature distribution among landscape units within lithology, ecotype and glacial geology data layers (Figure 4.5). Values for each landscape unit within each data layer were extracted using ALD and RTS locations from

the geodatabase, then tabulated to examine feature distribution among landscape units. Percentage feature distribution across units was compared with areal percentages of units within the study region, and a differential between them was calculated for each unit. Differentials were calculated as the percentage feature distribution for each unit divided by the study area percentage of that unit. These differentials informed weights assigned to each landscape unit within each data layer for ALD and RTS features, respectively. Landscape unit types consisting of exposed bedrock, open water, and snow from the ecotype layer, and active glacier/snowfield from the glacial geology layer, were considered obligate unsuitable for ALD and RTS features, and were automatically weighted to 0. Unit weights for ecotype, surficial geology and lithology were then combined with the result scaled 0 to 100, producing an ITU-derived terrain suitability estimate layer for ALD features and a separate ITU-derived terrain suitability estimate layer for RTS features throughout the study region.

4.2.3.3 Structural Equation Modelling

SEM was used to test and refine our hypothesized conceptual model of inter-relationships influencing terrain suitability, and incorporated both observed and latent variables (Grace 2006). In our models, all exogenous variables (those not a product of processes represented in the model) were observed, all endogenous variables (those influenced by processes within the model) were latent, and no composite variables were used.

Analyses were conducted separately for ALD and RTS datasets using the Lavaan 0.5-16 package written for R statistical software (Rosseel 2012). All variables used in SEM analyses were assessed against each other prior to SEM runs using Pearson correlation coefficients, calculated from all values throughout the study region (Table 4.3 and Figure 4.3). Pairs of variables with Pearson correlation coefficients greater than 0.7 were not used simultaneously in any of the analysis iterations. Each variable was also examined for statistical distribution (normal vs. non-normal) to determine the appropriate statistical estimator for analysis.

Numeric data for SEM runs (Tables 1 and 2) were extracted using locations in the feature and control point datasets. Feature and control locations were used as response variables, where features were assigned a value of 100, while control locations were assigned 0. The weighted least squares estimator, also known as asymptotically distribution free, was chosen as the estimator for all analyses in Lavaan due to non-normal distribution of several numeric variables. Our response variable was identified as ‘ordered’, and the orthogonal option was set to ‘false’, as no latent variables were exogenous within our models. No prior weighting of variables was used.

SEM runs testing ALD and RTS terrain suitability drivers used our hypothesized conceptual model (Figure 4.4) as the starting structural equation model. The model was iteratively refined using SEM fit metrics, and R^2 values generated for each variable (Joreskog and Sorbom 1996, Grace 2006, Hooper et al. 2008). Each model run was evaluated using recommended ‘good-fit’ thresholds for four fit metrics: 1) compound fit index, 2) Tucker-Lewis fit index, 3) root mean square error of approximation and 4) standardized root mean square residual (Hooper et al. 2008). Variables were placed within the model based upon their group (Figure 4.4 and Table 4.2). Model diagram structure and selection of variables used were refined through subsequent runs until all four fit metrics indicated good model fit, with the best fitting models used as the final models for ALDs and RTSs respectively. Final models were bootstrapped to confirm good fit, and to generate multi-run, averaged coefficients and intercepts for each exogenous and latent variable. Coefficients and intercepts were plugged into the final model diagram for each feature type, and run within ArcGIS 9.3 with data for the entire study region to produce SEM-based terrain suitability estimate layers, scaled 0 to 100, for ALD and RTS features separately.

4.2.3.4 Final Terrain Suitability Estimates (combined ITU and SEM results)

Terrain suitability estimates derived from independent ITU and SEM results were combined within ArcGIS 9.3 to create final terrain suitability estimates for ALD and RTS features (Figure 4.5). For each feature type, ITU-derived estimates were multiplied by SEM-derived estimates, and the result scaled 0 to 100. Numeric thresholds were used to delineate spatial masks of suitable and highly suitable terrain for each feature type, enabling calculations of areal extent and comparative summaries of landscape properties within suitable and highly suitable terrain for each feature type (Figure 4.5). Final terrain suitability estimate values for each feature type were extracted using the ALD and the RTS point location datasets. Mean and standard deviation of terrain suitability values were calculated for the extracted ALD and RTS feature locations. ‘Suitable terrain’ was defined as all terrain with values greater than or equal to one standard deviation below the mean value among feature locations, per feature type. ‘Highly suitable terrain’ was defined as terrain with values greater than or equal to the mean value for each feature type.

Suitable and highly suitable terrain areas were extracted as new spatial data layers from the final ALD and RTS terrain suitability datasets to characterize suitable landscapes (Figure 4.5). Areal extent for each suitability level was calculated, and the suitability data layers were used to clip thematic, spatial datasets used in the prior analyses, and also to clip ancillary datasets of soil carbon estimates (Hugelius et al. 2013) and decadal temperatures (SNAP 2014). Highly suitable terrain was extracted as a subset of suitable terrain, and did not represent additional area.

4.3 Results

4.3.1 Final Terrain Suitability Estimates

Terrain suitability estimates for feature formation in the study region (Figure 4.7) include large areas of terrain generally unsuited to either retrogressive thaw slump or active layer detachment processes, a significant area highly suited for both types of feature, and a continuum in between. Roughly half of the study region (51%) was estimated suitable for retrogressive thaw slumps, 35% was estimated suitable for active layer detachment slides, and 29% was estimated suitable for both, demonstrating significant overlap between RTS and ALD terrain suitability (Table 4.4 and Figure 4.8). Estimated area of highly suitable terrain was substantially lower than suitable terrain, at 24% for RTS features and 17% for ALD features (Table 4.4 and Figure 4.8), with 9% spatial overlap between highly suitable RTS and ALD terrain (Figures 8 and 9). ITU analyses produced slightly larger estimates of suitable terrain area than SEM analyses (Table 4.4 and Figure 4.8). The final model, combining ITU and SEM results, estimated less suitable terrain area than either ITU or SEM alone (Table 4.4 and Figure 4.8), with partial spatial correspondence between ITU-derived and SEM-derived estimated areas. Landscape properties related to vegetation, topography, hydrology, geomorphology, soil, and air temperature were correlated with observed ALD and RTS features, and also with estimated suitable terrain.

4.3.2 Active Layer Detachment Slide & Retrogressive Thaw Slump Terrain Descriptions

Active layer detachment slides and retrogressive thaw slumps both occur across gradients of landscape conditions, yet some typical settings can be identified for each. In uplands, the most suitable ALD terrain frequently occurs across broad, generally smooth hill slopes, and is sometimes concentrated along upper toe slopes beneath exposures of non-carbonate bedrock on rounded foothills (Figure 4.10), where ALD features frequently appear in clusters. Soils are typically thin, over near-surface bedrock, and in many places are subject to periodic colluvial re-deposition. With increasing distance downhill from the toe slope, ALD suitability remains high or mildly attenuates, while RTS suitability typically rises as colluvial deposits containing ice-rich, syngenetic permafrost become deeper, and hill slopes include more geomorphic variability. Toward valley bottoms, especially in larger valleys, ALD suitability attenuates more sharply as RTS suitability rises. This often reflects rougher geomorphological landscape texture, as well as shifts toward glacial drift and ice-contact features near valley bottoms, where ice-wedges and relict glacial ice may contribute to the ground-ice content of permafrost, where kettle topography often develops, and where soil physical properties are more variable. Both ALD and RTS suitability may drop markedly in upland drainage bottoms, where deposits of modern alluvium, fans, glacial outwash, and aeolian sands may include minimal topographic and geomorphic variability, and / or offer poor conditions for development of ice-rich cryofacies. As a general toposequence, vegetation grades from moderately

well-vegetated ericaceous and dryas dwarf shrub-graminoid tundras, through shrub-tussock and low shrub tundra on lower hillslopes, with riparian tall shrubs in valley bottoms. Small inclusions of wet-sedge meadow, coinciding with diffuse-flow watertracks, may be observed within larger patches of tundra ecotypes, primarily on mid and upper hillslopes, and have been noted as sites of ALD feature initiation (Balsler et al. 2009).

In lowland settings, ALD terrain suitability is highest on mild slopes on upper portions of rolling terrain, frequently underlain by glacial drift with a loess cap, where syngenetic cryostructures and an ice-rich intermediate layer may be prevalent near the permafrost table (Figure 4.11). Predominant ecotypes may include dwarf shrub tundra on hilltops flanked by low-shrub and shrub-tussock tundra on descending slopes. Inclusions of wet-sedge meadow within diffuse flow watertracks are rare or absent from these settings, though channelized-flow watertracks may be common. ALD suitability typically attenuates rapidly moving away downslope, though small patches of ALD terrain may sometimes be found near bluff tops. Suitable RTS terrain is widespread in lowland settings under a variety of conditions. On rolling, higher elevation terrain, patches of highly suitable RTS terrain appear where geomorphic features have begun forming from adjacent hydrothermal erosion, around margins of dispersed lakes, and in patches on mid-hillslopes. These high suitability terrain patches frequently occur atop glacial drift or lacustrine and glaciolacustrine surfaces. RTS suitability generally increases toward lower slopes and valley bottoms, where deposits may include glacial drift, lacustrine and glaciolacustrine surfaces, ice-contact features, and occasionally where inactive alluvial surfaces sit atop these deposits. Landscape rugosity is generally high in these settings compared with suitable terrain elsewhere in the study region, and is often the result of kettle-forming processes. Predominant ecotypes include low-shrub and shrub-tussock tundras, though more ecotype variability is evident within suitable RTS terrain in these settings, with isolated pockets of white spruce forest included in suitable terrain primarily in the Mission Lowland in southwest portion of the study region. Deep, ice-rich permafrost may be both extensive and heterogeneous in these areas, comprised of relict glacial ice, Pleistocene and Holocene ice-wedges, archaic syngenetic and epigenetic ice in lacustrine and glaciolacustrine sediments, cave ice, pore ice, and syngenetic cryofacies associated with contemporary soils and loess caps.

4.3.3 Integrated Terrain Unit Analysis Results

Distributions of ALD and RTS features within ecotype, glacial geology, and lithology units were disproportional to the areas of those landscape units within the study region (Table 4.5). Carbonate lithologies rarely contained features (< 2% of ALD features and < 1% of RTS features), though carbonate lithologies comprise > 10% of the landscape. More than 95% of ALD features occurred on only three

surficial geology units: thin soils over near-surface bedrock, colluvium, and glacial drift. Of these, occurrences within colluvium were the most disproportionate, containing 20% of ALD occurrences, while comprising only 7% of land area in the study region (Table 4.5). Disproportion of RTS feature distribution by glacial geology was slightly less pronounced, with 97% of features occurring across five glacial geology units: alluvium, thin soils over near-surface bedrock, colluvium, glacial drift, and lacustrine/glaciolacustrine. Of these, glacial drift was most disproportionate, hosting 46% of RTS features but comprising 16% of the land area in the study region (Table 4.5). ALD and RTS features were preferentially distributed among certain ecotypes as well, with the majority of both feature types occurring within three shrub tundra/shrub-tussock tundra ecotypes (Table 4.5). However, ALD and RTS features were more broadly distributed among ecotypes than among glacial geology or lithology units.

4.3.4 Structural Equation Modeling Results

Final SEM models incorporated geomorphologic, topographic, and vegetative factors for both ALD and RTS features. The model representing the original hypothesis fell short of recommended good fit values for both ALD and RTS analyses by all four fit measures used. However, refined, final models for both feature types were estimated to have good fit by all four SEM fit metrics (Table 4.6). For ALD features, the final model with best fit (Figure 4.12) incorporated the decadal average of inter-annual peak NDVI, the inter-annual variability of peak NDVI, heat load index, slope, slope position, topographic position index, and surface curvature. The strongest influences on ALD model fit were vegetative and topographic (Table 4.7 and Figure 4.12). The final model for RTS features (Figure 4.13) incorporated variability of inter-annual peak NDVI, topographic position index, dissection, compound topographic index, slope position and heat load index, where geomorphologic and topographic factors exerted greatest influence on the model (Table 4.7). This model also included a latent variable for upper permafrost and active layer conditions, comprised of both geomorphologic and vegetative factors. Within the final SEM results, the influence of each individual variable, and of each group of variables, differed appreciably. However, iterative testing revealed that good model fit could not be achieved for either ALD or RTS features in absence of any one of the variable groups of vegetation, topography or geomorphology; each was necessary in some form to support an explanatory relationship in the model.

4.3.5 Terrain Suitability Values and Thresholds

All terrain suitability estimates (ITU, SEM, and combined) included overlapping values between observed features and control point locations, with values at feature locations skewed toward higher suitability and with control point locations skewed toward low suitability. ITU-derived terrain suitability included an asymptotal distribution for the lowest suitability values of control point locations (Figure

4.14), mainly corresponding with areas masked as obligate unsuitable, while suitability values at ALD and RTS feature locations were normally distributed, and mainly within the highest 50% of estimated values (Figure 4.14). Estimated terrain suitability derived from SEM results was normally distributed for both feature locations and for control points, with feature locations skewed toward higher suitability values (Figure 4.14). Final, combined, ITU and SEM terrain suitability estimates produced clear separation between feature location and control point values, with ALD features showing especially stark separation from control point locations (Figure 4.14), where both ITU and SEM analyses contributed to separation from control for both ALD and RTS features (Figure 4.14). Thresholds for suitable and highly suitable terrain, as determined from the mean and standard deviation of values at observed feature locations, include overlap with values at control point locations (Figure 4.14).

4.3.6 Landscape Properties by Final Terrain Suitability

Values for individual landscape properties within suitable and highly suitable ALD and RTS estimated terrain, compared with the study region, ranged from very different to very similar, though no single factor emerged as dominant. Most numeric landscape values for both suitable ALD and suitable RTS terrain were consistently different from the mean value for the study region, but still within one standard deviation of the mean value for the study region (Table 4.8), and were generally comparable with values extracted from observed feature locations (Table 4.9). The suitable terrain area within individual landscape units was generally much less than the total area of those individual landscape units in the study region, with differing results between suitable ALD and RTS terrain. For example, thin soils over near-surface bedrock contained the single largest percentage of suitable terrain for both ALDs and RTSs, yet less than half of the total area of that unit within the study region was suitable for either feature type (Figure 4.15). Most of the total area of the upland dwarf birch tussock shrub ecotype was suitable for RTS features, but less than half of it was suitable for ALD features (Figure 4.15).

Suitable ALD terrain and suitable RTS terrain display separate trends toward certain combinations of landscape properties based on numeric variables representing geomorphology, topography and vegetation. Suitable ALD terrain (Table 4.8) tended toward mid-lower reaches of watersheds (slope position < 0), on well-vegetated surfaces with minimal inter-annual variability in peak growing-season greenness (inter-annual average peak NDVI > 0.7, inter-annual standard deviation of peak NDVI < 0.05), just below mid-hillslope locations (topographic position index just below 0.5), on very slightly concave surfaces (surface curvature just below 0) (McNab 1993).

Suitable RTS terrain (Table 4.8) occurred primarily in lower portions of watersheds (slope position < 0), on well-vegetated surfaces with minimal inter-annual variability in peak growing-season greenness

(inter-annual average peak NDVI > 0.7, inter-annual standard deviation of peak NDVI < 0.05), in lower portions of hillslope catenas with high soil wetness (high compound topographic index values), just below mid-hillslope locations (topographic position index at or just below 0.5), and at neither the top nor bottom of geomorphological features (dissection at or just below 0.5). Dissection and topographic position index (Table 4.2) shared a moderately strong, positive Pearson correlation coefficient across the entire study region (0.70; Table 4.3), but this positive correlation graded steadily downward through suitable RTS terrain (0.62), and highly suitable RTS terrain (0.58), to weakly negative when calculated only at RTS feature locations (-0.24).

4.4 Discussion

Both observed features and terrain suitability for active layer detachment slides and retrogressive thaw slumps are distributed across landscape gradients defined by multiple landscape properties. While specific terrain factors, and groups of factors, exerted varying influence on SEM results, no single landscape property was revealed as an obligate, or even dominant, positive indicator of suitable terrain. Landscape properties describing geomorphology, vegetation, topography, surficial geology and lithology all correlate with observed feature distribution (Balser et al. 2009), and are supported as drivers of suitable terrain conditions by these results. Adjacent regions in Alaska within different bioclimate subzones (Walker et al. 2005) exhibit similarly complex inter-relationships among multiple landscape properties and upper permafrost conditions (Jorgenson et al. 2014, Pastick et al. 2014a), as do landscapes elsewhere in the low arctic (Postoev et al. 2008, Khomutov 2012), though the nature of relationships varies among regions.

While meteorological and disturbance trigger events for ALD and RTS formation are not directly addressed in this study, they are relevant to the interpretation of our results, as the intensity of trigger events greatly influences feature initiation (Burn and Lewkowicz 1990, Leibman 1995, Lewkowicz and Harris 2005, Atkinson et al. 2006, Lamoureux and Lafreniere 2009, Balser et al. 2014). Trigger events vary in mode, duration and intensity, such that ALD and RTS formation is a function of both relative terrain suitability and strength of perturbation. Consequently, terrain suitability may best be considered on a continuous, relative basis, with threshold delineators beneficially employed for summary and comparative purposes, but not as means for definitive, positive designation as ‘suitable’. In the simplest terms, suitable terrain is comprised of three, basic conditions enabling thaw, melting and subsidence associated with ALD and RTS features: 1) adequate ground-ice concentration and distribution, 2) adequate topographic or geomorphic gradient, and, 3) adequate surface and upper-soil thermal properties.

A fourth condition, an adequate meteorological or disturbance trigger, is required for actual feature initiation.

‘Adequacy’ of any one of the conditions depends on the context of the others, and it appears likely, based on our cumulative results, that a suite of individual factors are co-contributing and / or mutually compensating as drivers of suitable terrain conditions. For example, within a particular surficial geology and ecotype, terrain with lower slope but higher ground ice percentage might be equally suitable to terrain with higher slope but lower ground ice percentage for RTS development. Adequacy of ground ice percentage in this example, then, is really a function of cumulative conditions. While this simplistic example illustrates the concept, our results strongly suggest that complex interactions, rather than simple pair-wise correlations, drive suitability.

Due to the complexity of interactions, considering all relevant factors in concert serves to improve and constrain spatial estimates of suitable terrain. The existence of co-contributing and mutually-compensating factors as terrain suitability drivers is supported by several aspects of our results. If interactions among factors were lacking, we might expect to see narrow ranges of values for each relevant factor describing suitable terrain. Instead, the distributions of observed features and suitable terrain were not associated with narrow value ranges for individual landscape variables. While the ranges of values we observed do tend to show consistent differences compared with the overall study region, they also tend to remain well within the standard deviations of study region values. However, suitable terrain area is only a subset of total area within any of these individual value ranges, and areal coverage of suitable terrain is substantially lower within the final, combined estimates, compared with ITU and SEM estimates separately. This suggests that: 1) while individual landscape properties may strongly contribute to suitability, relevant factors should be considered in concert for more accurate results, 2) suitability may range from low to high within any individual categorical landscape unit, and 3) there are no defining numeric values from individual landscape variables driving terrain suitability; values indicating suitability vary spatially depending on the context of other relevant variables.

We therefore expect that our estimates of terrain suitability would be further refined by the inclusion of both: a) additional factors, and b) more accurate and precise data for the study region. Several factors of known importance to permafrost development were not available as continuous data layers for the study region, including ground ice percentage, soil physical properties (e.g. percentages by clast size), and soil organic layer thickness. Some of these exist as estimated average values within other categorical datasets (Jorgenson et al. 2008b, Jorgenson et al. 2010b), but these were excluded from our analyses either because they were mapped at coarser scales than were appropriate for this work, or

because the value ranges reported were deemed too broad to be meaningful within these analyses. We also expect that a higher precision DEM would better resolve fine-scale geomorphology and increase the precision of terrain suitability estimates.

Results support a state factor framework (Jenny 1941, van Cleve et al. 1991) for assessing ALD and RTS terrain suitability at broad scales, at least within regions dominated by climate-driven, ecosystem-modified permafrost (Shur and Jorgenson 2007) to help ensure inclusion of relevant variables. In our models, each of three state factors (represented by groups of variables in our analyses: vegetation, parent material, and topography) contributed key explanatory information, and served to substantially hone terrain suitability estimates. The two other state factors, climate and time, were not explicitly included within the model. However, both were included implicitly, as feature occurrence itself within the study region indicates both climate drivers and time for permafrost terrain development. In a broad context of climate and time, expanses of suitable terrain might be considered a moving target; these areas have likely been shifting geographically over decadal to millennial timescales since the Pleistocene in response to shifting climate (ACIA 2005, Shur and Jorgenson 2007, Rowland et al. 2010, Aalto et al. 2014).

Given that shifting climate does not translate to wholesale geographic shifts of ecosystems in precise analog form, but rather involves adjustments in ecosystem structure and function (Callaghan et al. 2004, Jorgenson et al. 2010a), the relative importance of each contributing factor, and the particular factors best defining favorable conditions likely adjust through space and time as well. Also, suitable terrain within the study region may exist along a gradient between landscapes in warmer versus colder settings, possibly reflecting time and climate within an overall warming scenario. The warmest areas of the study region, defined by annual and seasonal air temperatures, may be approaching climate conditions warmer than what is most associated with current ALD and RTS feature distributions and may primarily represent suitable terrain of the past and present, while colder settings may become the focus of increased feature frequency in a future warming scenario.

As with trigger events for ALD and RTS formation, which vary in duration and intensity, terrain suitability in low arctic regions may best be considered on a continuous, relative basis, with value-threshold delineators used for comparative and summary purposes, but not as means for definitive, positive classification as ‘suitable’. Under this rubric, we posit that as much as 57% of the terrestrial landscape within the study region may be termed ‘suitable’ terrain for either ALD or RTS feature development, and as much as 29% may be ‘suitable’ for both, but that these estimates may vary depending upon the desired degree of sensitivity in interpretation. We further expect that future inclusion of measured or modelled values for additional factors, especially ground ice percentage, physical soil

characteristics, and organic layer properties, would likely refine analysis results to make these estimates more conservative, while higher resolution, higher accuracy continuous source data would add precision to analytical results.

4.5 Conclusions

ALD and RTS terrain suitability is determined by gradients defined across multiple landscape properties, where no single factor or group of factors, in isolation, emerges as a definitive indicator of suitable terrain. A suite of factors with co-contributing and mutually compensating interactions drive terrain suitability in the study region, such that modelling relevant factors in concert produces better estimates than analyzing individual factors and aggregating the results. Each relevant terrain factor serves to constrain suitability estimates; exclusion of relevant terrain factors from models generally causes overestimation of the spatial extent of suitable terrain. At least 32%, and up to 57% of the study region may be suitable terrain for either ALD or RTS formation, depending on the sensitivity of the chosen suitability threshold and the intensity of future trigger events. Similar proportions of suitable terrain may prevail in other low arctic regions. However, accurate estimates for other locales would likely require analogous, empirically modelled results to account for region-specific variability among terrain, vegetation and upper permafrost relationships. Modelled terrain suitability estimates enable better spatial quantification of permafrost degradation impacts, including vulnerable soil carbon stocks and ecological responses, and better identification of vulnerable ecosystems. Future addition of physical soil and soil organic layer properties, with further model refinement and field validation, might also produce reasonable, modelled spatial estimates of ground ice percentage and / or cryofacies distribution.

4.6 Acknowledgements

This work was supported by a University of Alaska Fairbanks Center for Global Change (CGC) Student Research grant, by U.S. National Science Foundation grant ARC-0806465, and by the National Park Service Arctic Network (ARCN). We gratefully acknowledge M. Torre Jorgenson, Michelle C. Mack, Steven B. Young, Amanda V. Bakian, W. Breck Bowden, Benjamin W. Abbott, Michael N. Gooseff, and Thomas D. Hamilton for invaluable discussion and / or assistance in the field. The aviation skill and safety of pilots Tom George, Stan Hermens, Tommy Levanger, Terry Day, Jim Kincaid, and Buck Mackson were indispensable to the success of this research.

4.7 References

- Aalto, J., A. Venäläinen, R. K. Heikkinen, and M. Luoto. 2014. Potential for extreme loss in high-latitude Earth surface processes due to climate change. *Geophysical Research Letters* 41:2014GL060095.
- Abbott, B. W., J. R. Larouche, J. B. Jones Jr., W. B. Bowden, and A. W. Balsler. 2014. Elevated dissolved organic carbon biodegradability from thawing and collapsing permafrost. *Journal of Geophysical Research: Biogeosciences* 119.
- ACIA. 2005. Arctic Climate Impact Assessment. Cambridge University Press.
- Anisimov, O. and S. Reneva. 2006. Permafrost and changing climate: The Russian perspective. *Ambio* 35:169-175.
- Atkinson, D., R. Brown, B. Alt, T. Agnew, J. Bourgeois, M. Burgess, C. Duguay, G. Henry, S. Jeffers, R. Koerner, A. Lewkowicz, S. McCourt, H. Melling, M. Sharp, S. Smith, A. Walker, K. Wilson, S. Wolfe, M.-K. Woo, and K. Young. 2006. Canadian cryospheric response to an anomalous warm summer: a synthesis of the Climate Change Action Fund project 'The state of the Arctic cryosphere during the extreme warm summer of 1998'. *Atmosphere-Ocean* 44:347-375.
- Balsler, A., M. N. Gooseff, J. Jones, and W. B. Bowden. 2009. Thermokarst distribution and relationships to landscape characteristics in the Feniak Lake region, Noatak National Preserve, Alaska; Final Report to the National Park Service, Arctic Network (ARCN). Fairbanks, AK.
- Balsler, A. W., J. B. Jones, and R. Gens. 2014. Timing of Retrogressive Thaw Slump Initiation in the Noatak Basin, Northwest Alaska, USA. *Journal of Geophysical Research: Earth Surface*:2013JF002889.
- Balsler, A. W., J. B. Jones, D. A. Walker, and M. T. Jorgenson. 2015. Relationship of Cryofacies, Surface and Subsurface Terrain Conditions in the Brooks Range and foothills of northern Alaska. PhD Dissertation, Chapter 3. University of Alaska Fairbanks, Fairbanks, AK.
- Bowden, W., J. R. Larouche, A. R. Pearce, B. T. Crosby, K. Krieger, M. B. Flinn, J. Kampman, M. N. Gooseff, S. E. Godsey, J. B. Jones, B. Abbott, M. T. Jorgenson, G. Kling, M. Mack, E. A. G. Schuur, A. F. Baron, and E. B. Rastetter. 2012. An Integrated Assessment of the Influences of Upland Thermal-Erosional Features on Landscape Structure and Function in the Foothills of the Brooks Range, Alaska. Pages 61-66 in *Tenth International Conference on Permafrost, Volume 1 - International Contributions*. The Northern Publisher, Salekhard, Russia.
- Bowden, W. B., M. N. Gooseff, A. Balsler, A. Green, B. J. Peterson, and J. Bradford. 2008. Sediment and nutrient delivery from thermokarst features in the foothills of the North Slope, Alaska: Potential impacts on headwater stream ecosystems. *Journal of Geophysical Research* 113. G02026. doi:10.1029/2007JG000470.

- Burn, C. R. and A. G. Lewkowicz. 1990. Retrogressive Thaw Slumps
The Canadian Geographer 34:273-276.
- Callaghan, T. V., L. O. Bjorn, Y. Chernov, T. Chapin, T. R. Christensen, B. Huntley, R. A. Ims, M. Johansson, D. Jolly, S. Jonasson, N. Matveyeva, N. Panikov, W. Oechel, G. Shaver, and H. Henttonen. 2004. Effects on the structure of arctic ecosystems in the short- and long-term perspectives. *Ambio* 33:436-447.
- CAVM-Team. 2003. Circumpolar Arctic Vegetation Map, Scale 1:7,500,000. Conservation of Arctic Flora and Fauna (CAFF) Map No. 1. U.S. Fish and Wildlife Service, Anchorage, Alaska.
- Cleland, D. T., P. E. Avers, W. H. McNab, M. E. Jensen, R. G. Bailey, T. King, and W. E. Russell. 1997. National Hierarchical Framework of Ecological Units. Pages 181-200 *in* M. S. Boyce and A. Haney, editors. *Ecosystem Management Applications for Sustainable Forest and Wildlife Resources*. Yale University Press, New Haven, CT.
- Cushman, S. A., K. Gutzweiler, J. S. Evans, and K. McGarigal. 2010. The Gradient Paradigm: A conceptual and analytical framework for landscape ecology (Chapter 5). Pages 83-108 *in* S. A. H. Cushman, F., editor. *Spatial complexity, informatics, and wildlife conservation*. Springer, New York.
- Daanen, R. P., T. Ingeman-Nielsen, S. S. Marchenko, V. E. Romanovsky, N. Foged, M. Stendel, J. H. Christensen, and K. H. Svendsen. 2011. Permafrost degradation risk zone assessment using simulation models. *The Cryosphere* 5:1043-1056.
- Desyatkin, A. R., F. Takakai, P. P. Fedorov, M. C. Nikolaeva, R. V. Desyatkin, and R. Hatano. 2009. CH₄ emission from different stages of thermokarst formation in Central Yakutia, East Siberia. *Soil Science and Plant Nutrition* 55:558-570.
- ECOMAP. 1993. National Hierarchical Framework of Ecological Units. Page 20 pp. USDA Forest Service, Washington, DC.
- Evans, J. S., J. Oakleaf, S. A. Cushman, and D. Theobald. 2013. A Toolbox for Surface Gradient Modeling, Available at: <http://evansmurphy.wix.com/evansspatial>. (in prep).
- French, H. and Y. Shur. 2010. The principles of cryostratigraphy. *Earth-Science Reviews* 101:190-206.
- Frey, K. E. and J. W. McClelland. 2009. Impacts of permafrost degradation on arctic river biogeochemistry. *Hydrological Processes* 23:169-182.
- Gesch, D., M. Oimoen, S. Greenlee, C. Nelson, M. Steuck, and D. Tyler. 2002. The National Elevation Dataset. *Photogrammetric Engineering and Remote Sensing* 68:5-+.
- Godin, E. and D. Fortier. 2012. Geomorphology of a thermo-erosion gully, Bylot Island, Nunavut, Canada. *Canadian Journal of Earth Sciences* 49:979-986.

- Gooseff, M., A. Balser, W. Bowden, and J. Jones. 2009. Effects of hillslope thermokarst in northern Alaska. , 90: 29-31. *Eos, Transactions of the American Geophysical Union* 90:29-31.
- Grace, J. B. 2006. *Structural Equation Modeling and Natural Systems*. 1st edition. Cambridge University Press, Cambridge, UK.
- Grosse, G., J. Harden, M. Turetsky, A. D. McGuire, P. Camill, C. Tarnocai, S. Frolking, E. A. G. Schuur, T. Jorgenson, S. Marchenko, V. Romanovsky, K. P. Wickland, N. French, M. Waldrop, L. Bourgeau-Chavez, and R. G. Striagl. 2011. Vulnerability of high-latitude soil organic carbon in North America to disturbance. *J. Geophys. Res.* 116:G00K06.
- Gruber, S. 2012. Derivation and analysis of a high-resolution estimate of global permafrost zonation. *The Cryosphere* 6:221-233.
- Hamilton, T. D. 2009. *Guide to surficial geology and river-bluff exposures, Noatak National Preserve, northwestern Alaska: U.S. Geological Survey Scientific Investigations Report 2008-5125*.
- Hamilton, T. D. 2010. *Surficial Geologic Map of the Noatak National Preserve, Alaska. U.S. Geological Survey (in cooperation with U.S. National Park Service) Scientific Investigations Map 3036, 1 : 250,000 scale, and accompanying report:21p*.
- Hamilton, T. D. and K. A. Labay. 2011. *Surficial Geologic Map of the Gates of the Arctic National Park and Preserve, Alaska. U.S. Geological Survey (in cooperation with U.S. National Park Service) Scientific Investigations Map 3125, 1 : 300,000 scale, and accompanying report:19p*.
- Harris, C., L. U. Arenson, H. H. Christiansen, B. Etzelmüller, R. Frauenfelder, S. Gruber, W. Haeberli, C. Hauck, M. Hölzle, O. Humlum, K. Isaksen, A. Kääb, M. A. Kern-Lütschg, M. Lehning, N. Matsuoka, J. B. Murton, J. Nötzli, M. Phillips, N. Ross, M. Seppälä, S. M. Springman, and D. Vonder Mühl. 2009. Permafrost and climate in Europe: Monitoring and modelling thermal, geomorphological and geotechnical responses. *Earth-Science Reviews* 92:117-171.
- Hinzman, L., N. Bettez, W. Bolton, F. Chapin, M. Dyurgerov, C. Fastie, B. Griffith, R. Hollister, A. Hope, H. Huntington, A. Jensen, G. Jia, T. Jorgenson, D. Kane, D. Klein, G. Kofinas, A. Lynch, A. Lloyd, A. McGuire, F. Nelson, W. Oechel, T. Osterkamp, C. Racine, V. Romanovsky, R. Stone, D. Stow, M. Sturm, C. Tweedie, G. Vourlitis, M. Walker, D. Walker, P. Webber, J. Welker, K. Winker, and K. Yoshikawa. 2005. Evidence and Implications of Recent Climate Change in Northern Alaska and Other Arctic Regions. *Climatic Change* 72:251-298.
- Hooper, D., J. Coughlan, and M. Mullen. 2008. Structural Equation Modelling: Guidelines for Determining Model Fit. *The Electronic Journal of Business Research Methods* 6:53-60.
- Hugelius, G., C. Tarnocai, G. Broll, J. G. Canadell, P. Kuhry, and D. K. Swanson. 2013. The Northern Circumpolar Soil Carbon Database: spatially distributed datasets of soil coverage and soil carbon storage in the northern permafrost regions. *Earth Syst. Sci. Data* 5:3-13.

- Jenkerson, C. B., T. Maiersperger, and G. Schmidt. 2010. eMODIS: A user-friendly data source: U.S. Geological Survey Open-File Report 2010–1055, 10 p.
- Jenny, H. 1941. *Factors of Soil Formation: A System of Quantitative Pedology*. Dover Publications, Inc., New York, NY.
- Joreskog, K. G. and D. Sorbom. 1996. LISREL8: User's Reference Guide. Scientific Software International, Chicago, IL.
- Jorgenson, M. T., J. Harden, M. Kanevskiy, J. O'Donnell, K. P. Wickland, S. Ewing, K. L. Manies, Q. Zhuang, Y. Shur, R. G. Striegl, and J. Koch. 2013. Reorganization of vegetation, hydrology and soil carbon after permafrost degradation across heterogeneous boreal landscapes *Environmental Research Letters* 8:1-14.
- Jorgenson, M. T., M. Kanevskiy, Y. Shur, J. Grunblatt, C. Ping, and G. Michaelson. 2014. Permafrost Database Development, Characterization, and Mapping for Northern Alaska. U.S. Fish & Wildlife Service, Arctic Landscape Conservation Cooperative.
- Jorgenson, M. T. and T. E. Osterkamp. 2005. Response of boreal ecosystems to varying modes of permafrost degradation. *Canadian Journal of Forest Research* 35:2100-2111.
- Jorgenson, M. T., V. Romanovsky, J. Harden, Y. Shur, J. O'Donnell, E. A. G. Schuur, M. Kanevskiy, and S. Marchenko. 2010a. Resilience and vulnerability of permafrost to climate change. *Canadian Journal of Forest Research-Revue Canadienne De Recherche Forestiere* 40:1219-1236.
- Jorgenson, M. T., J. E. Roth, P. F. Miller, M. J. Macander, M. S. Duffy, A. F. Wells, G. V. Frost, and E. R. Pullman. 2010b. An ecological land survey and landcover map of the Arctic Network. Natural Resource Technical Report NPS/ARC/NRTR—2009/270. National Park Service, Fort Collins, Colorado.
- Jorgenson, M. T., Y. L. Shur, and T. E. Osterkamp. 2008a. Thermokarst in Alaska. *in* Ninth International Conference on Permafrost. National Academy Press, Washington, DC, Fairbanks, AK.
- Jorgenson, M. T., D. K. Swanson, and M. Macander. 2001. Ecological subsections of Noatak National Preserve. Final Report to the U.S. National Park Service, Fairbanks, AK. 73. ABR Inc.
- Jorgenson, T., K. Yoshikawa, V. Romanovsky, M. Kanevskiy, J. Brown, Y. Shur, S. Marchenko, G. Grosse, and B. Jones. 2008b. Map of Permafrost Characteristics in Alaska. Proceedings of the Ninth International Conference on Permafrost (NICOP), Fairbanks, AK June 30 - July 4, 2008.
- Khomutov, A. V. 2012. Assessment of Landslide Geohazards in Typical Tundra of Central Yamal. Pages 157-162 *in* Tenth International Conference on Permafrost, Volume 2 - Translations of Russian Contributions. The Northern Publisher, Salekhard, Russia.
- Kokelj, S. V. and M. T. Jorgenson. 2013. Advances in Thermokarst Research. *Permafrost and Periglacial Processes* 24:108-119.

- Kokelj, S. V., D. Lacelle, T. C. Lantz, J. Tunnicliffe, L. Malone, I. D. Clark, and K. S. Chin. 2013. Thawing of massive ground ice in mega slumps drives increases in stream sediment and solute flux across a range of watershed scales. *Journal of Geophysical Research: Earth Surface* 118:681-692.
- Kokelj, S. V., T. C. Lantz, J. Kanigan, S. L. Smith, and R. Coutts. 2009a. Origin and Polycyclic Behaviour of Tundra Thaw Slumps, Mackenzie Delta Region, Northwest Territories, Canada. *Permafrost and Periglacial Processes* 20:1-12.
- Kokelj, S. V., B. Zajdlik, and M. S. Thompson. 2009b. The Impacts of Thawing Permafrost on the Chemistry of Lakes across the Subarctic Boreal-Tundra Transition, Mackenzie Delta Region, Canada. *Permafrost and Periglacial Processes* 20:1-15.
- Lacelle, D., J. Bjornson, and B. Lauriol. 2010. Climatic and Geomorphic Factors Affecting Contemporary (1950–2004) Activity of Retrogressive Thaw Slumps on the Aklavik Plateau, Richardson Mountains, NWT, Canada. *Permafrost and Periglacial Processes* 21.
- Lamoureux, S. F. and M. J. Lafreniere. 2009. Fluvial Impact of Extensive Active Layer Detachments, Cape Bounty, Melville Island, Canada. *Arctic, Antarctic, and Alpine Research* 41:59-68.
- Lamoureux, S. F. and M. J. Lafreniere. 2014. Seasonal fluxes and age of particulate organic carbon exported from Arctic catchments impacted by localized permafrost slope disturbances. *Environmental Research Letters* 9:10.
- Lantuit, H., W. H. Pollard, N. Couture, M. Fritz, L. Schirrmeister, H. Meyer, and H. W. Hubberten. 2012. Modern and Late Holocene Retrogressive Thaw Slump Activity on the Yukon Coastal Plain and Herschel Island, Yukon Territory, Canada. *Permafrost and Periglacial Processes* 23:39-51.
- Lantz, T. C. and S. V. Kokelj. 2008. Increasing rates of retrogressive thaw slump activity in the Mackenzie Delta region, NWT, Canada. *Geophysical Research Letters* 35.
- Lantz, T. C., S. V. Kokelj, S. E. Gergel, and G. H. R. Henry. 2009. Relative impacts of disturbance and temperature: persistent changes in microenvironment and vegetation in retrogressive thaw slumps. *Global Change Biology* 15:1664-1675.
- Leibman, M. O. 1995. Cryogenic Landslides on the Yamal Peninsula, Russia - Preliminary-Observations. *Permafrost and Periglacial Processes* 6:259-264.
- Leibman, M. O., A. I. Kizyakov, L. D. Sulerzhitsky, and N. E. Zaretskaya. 2003. Dynamics of the landslide slopes and mechanism of their development on Yamal peninsula, Russia. *in* Proceedings of the Eight International Conference on Permafrost. A.A.Balkema Publishers, Rotterdam, Netherlands Zurich 21-25 July 2003.

- Leibman, M. O. and I. D. Streletskaia. 1997. Land-slide induced changes in the chemical composition of active-layer soils and surface-water runoff, Yamal Peninsula, Russia. Pages 120-126 in Proceedings of the International Symposium on Physics, Chemistry and Ecology of Seasonally Frozen Soils. CRREL Special Report 97-10, Hanover, NH, Fairbanks, AK.
- Lewkowicz, A. G. 2007. Dynamics of Active-layer Detachment Failures, Fosheim Peninsula, Ellesmere Island, Nunavut, Canada. *Permafrost and Periglacial Processes* 18:89 - 103.
- Lewkowicz, A. G. and C. Harris. 2005. Morphology and geotechnique of active-layer detachment failures in discontinuous and continuous permafrost, northern Canada. *Geomorphology* 69:275-297.
- McNab, W. H. 1993. A topographic index to quantify the effect of mesoscale landform on site productivity. *Canadian Journal of Forest Research* 23:1100-1107.
- Mesquita, P. S., F. J. Wrona, and T. D. Prowse. 2010. Effects of retrogressive permafrost thaw slumping on sediment chemistry and submerged macrophytes in Arctic tundra lakes. *Freshwater Biology* 55:2347-2358.
- Parker, C. L. 2006. Vascular plant inventory of Alaska's Arctic National Parklands: Bering Land Bridge National Preserve, Cape Krusenstern National Monument, Gates of the Arctic National Park & Preserve, Kobuk Valley National Preserve, and Noatak National Preserve. ARCN I&M, National Park Service, Alaska Region Final Report:142p.
- Pastick, N. J., M. T. Jorgenson, B. K. Wylie, J. R. Rose, M. Rigge, and M. A. Walvoord. 2014a. Spatial variability and landscape controls of near-surface permafrost within the Alaskan Yukon River Basin. *Journal of Geophysical Research-Biogeosciences* 119:1244-1265.
- Pastick, N. J., M. Rigge, B. K. Wylie, M. T. Jorgenson, J. R. Rose, K. D. Johnson, and L. Ji. 2014b. Distribution and landscape controls of organic layer thickness and carbon within the Alaskan Yukon River Basin. *Geoderma* 230:79-94.
- Postoev, G. P., B. K. Lapochkin, A. I. Kazeev, and A. S. Nikulshin. 2008. Estimation of landslide hazard on construction sites. *Geokriologiya* 6:547-557.
- Rosseel, Y. 2012. lavaan: AN R Package for Structural Equation Modeling. *Journal of Statistical Software* 48:1-36.
- Rowland, J. C., C. E. Jones, G. Altmann, R. Bryan, B. T. Crosby, G. L. Geernaert, L. D. Hinzman, D. L. Kane, D. M. Lawrence, A. Mancino, P. Marsh, J. P. McNamara, V. E. Romanovsky, H. Toniolo, B. J. Travis, E. Trochim, and C. J. Wilson. 2010. Arctic landscapes in transition - Geomorphic responses to degrading permafrost. *EOS* 91:229-230.
- Rozell, N. 2009. Selawik Slump grows unabated, threatens fishery. Anchorage Daily News, Anchorage, AK.

- Schaefer, K., T. Zhang, L. Bruhwiler, and A. P. Barrett. 2011. Amount and timing of permafrost carbon release in response to climate warming. *Tellus Series B-Chemical and Physical Meteorology*:no-no.
- Schuur, E. A. G., J. Bockheim, J. G. Canadell, E. Euskirchen, C. B. Field, S. V. Goryachkin, S. Hagemann, P. Kuhry, P. M. Lafleur, H. Lee, G. Mazhitova, F. E. Nelson, A. Rinke, V. E. Romanovsky, N. Shiklomanov, C. Tarnocai, S. Venevsky, J. G. Vogel, and S. A. Zimov. 2008. Vulnerability of Permafrost Carbon to Climate Change: Implications for the Global Carbon Cycle. *Bioscience* 58:701-714.
- Serreze, M. C., J. E. Walsh, F. S. Chapin, T. Osterkamp, M. Dyrgerov, V. Romanovsky, W. C. Oechel, J. Morison, T. Zhang, and R. G. Barry. 2000. Observational Evidence of Recent Change in the Northern High-Latitude Environment. *Climatic Change* 46:159-207.
- Shur, Y. L. 1988. The upper horizon of permafrost soil. Pages 867-871 *in* Proceedings of the Fifth Intern. Conf. on Permafrost. Tapir Publishers, Trondheim, Norway.
- Shur, Y., K. M. Hinkel, and F. E. Nelson. 2005. The transient layer: implications for geocryology and climate-change science. *Permafrost and Periglacial Processes* 16:5-17.
- Shur, Y. L. and M. T. Jorgenson. 2007. Patterns of Permafrost Formation and Degradation in Relation to Climate and Ecosystems. *Permafrost and Periglacial Processes* 18:7 - 19.
- SNAP. 2014. Historical (1910–1999) derived temperature products from CRU TS 3.0 climate data, downscaled to 771m via the delta method. Retrieved from: <https://www.snap.uaf.edu/tools/data-downloads>. *in* U. o. Alaska, editor.
- Swanson, D. K. 2010. Mapping of erosion features related to thaw of permafrost in Bering Land Bridge National Preserve, Cape Krusenstern National Monument, and Kobuk Valley National Park. Natural Resource Data Series NPS/ARC/NRDS—2010/122. National Park Service, Fort Collins, Colorado.
- Swanson, D. K. and K. Hill. 2010. Monitoring of Retrogressive Thaw Slumps in the Arctic Network, 2010 Baseline Data: Three-dimensional Modeling with Small-format Aerial Photographs. Page 58. U.S. Department of the Interior, National Park Service, Natural Resource Data Series NPS/ARC/NRDS—2010/123, Natural Resource Program Center, Fort Collins, CO.
- Tarnocai, C., J. G. Canadell, E. A. G. Schuur, P. Kuhry, G. Mazhitova, and S. Zimov. 2009. Soil organic carbon pools in the northern circumpolar permafrost region. *Global Biogeochemical Cycles* 23:1-11.
- Thompson, M. S., S. V. Kokelj, T. D. Prowse, and F. J. White 2008. The impact of sediments derived from thawing permafrost on tundra lake water chemistry: An experimental approach. *in* Proceedings of the 9th Permafrost International Conference, Fairbanks, AK.

- Ukrainitseva, N. T. and M. O. Leibman. 2007. The effect of cryogenic landslides (active-layer detachments) on fertility of tundra soils on Yamal peninsula, Russia. Pages 1605-1615 *in* 1st North American Landslide Conference, Vail, CO.
- van Cleve, K., F. S. Chapin, III, C. T. Dyrness, and L. A. Viereck. 1991. Element Cycling in Taiga Forests: State-Factor Control. *Bioscience* 41:78-88.
- Viereck, L. A., C. T. Dyrness, A. R. Batten, and K. J. Wenzlick. 1992. The Alaska Vegetation Classification. Page 278 *in* U. S. D. o. A. F. Service, editor. Gen. Tech. Rep. PNW-GTR-286, Portland, OR.
- Wahrhaftig, C. 1965. Physiographic Divisions of Alaska. U.S.G.S. Professional Paper 482. 52 pp.
- Walker, D. A. 1996. Method for making an integrated vegetation map of northern Alaska (1:4,000,000 scale). Pages 54-61 *in* Second Circumpolar Arctic Vegetation Mapping Workshop, Arendal, Norway.
- Walker, D. A., H. E. Epstein, V. E. Romanovsky, C. L. Ping, G. J. Michaelson, R. P. Daanen, Y. Shur, R. A. Peterson, W. B. Krantz, M. K. Reynolds, W. A. Gould, G. Gonzalez, D. J. Nicolsky, C. M. Vonlanthen, A. N. Kade, P. Kuss, A. M. Kelley, C. A. Munger, C. T. Tamocai, N. V. Matveyeva, and F. J. A. Daniels. 2008. Arctic patterned-ground ecosystems: A synthesis of field studies and models along a North American Arctic Transect. *Journal of Geophysical Research-Biogeosciences* 113.
- Walker, D. A., M. K. Reynolds, F. J. A. Daniels, E. Einarsson, A. Elvebakk, W. A. Gould, A. E. Katenin, S. S. Kholod, C. J. Markon, E. S. Melnikov, N. G. Moskalenko, S. S. Talbot, B. A. Yurtsev, and C. Team. 2005. The Circumpolar Arctic vegetation map. *Journal of Vegetation Science* 16:267-282.
- Walker, H. J. and P. F. Hudson. 2003. Hydrologic and geomorphic processes in the Colville River delta, Alaska. *Geomorphology* 56:291-303.
- Walker, H. J., L. Arnborg, and J. Peippo. 1987. Riverbank Erosion in the Colville Delta, Alaska. *Geografiska Annaler Series a-Physical Geography* 69:61-70.
- Walter, K. M., M. E. Edwards, G. Grosse, S. A. Zimov, and F. S. Chapin. 2007. Thermokarst lakes as a source of atmospheric CH₄ during the last deglaciation. *Science* 318:633-636.
- Walter, K. M., S. A. Zimov, J. P. Chanton, D. Verbyla, and F. S. C. III. 2006. Methane bubbling from Siberian thaw lakes as a positive feedback to climate warming. *Nature* 443:71-75.
- Xie, C. and W. Gough. 2013. A Simple Thaw-Freezing Algorithm for a Multi-Layered Soil using the Stefan Equation. *Permafrost and Periglacial Processes* 24:252-260.
- Young, S. B. 1974. The environment of the Noatak River basin, Alaska., Contributions of the Center for Northern Studies, Wolcott, VT.

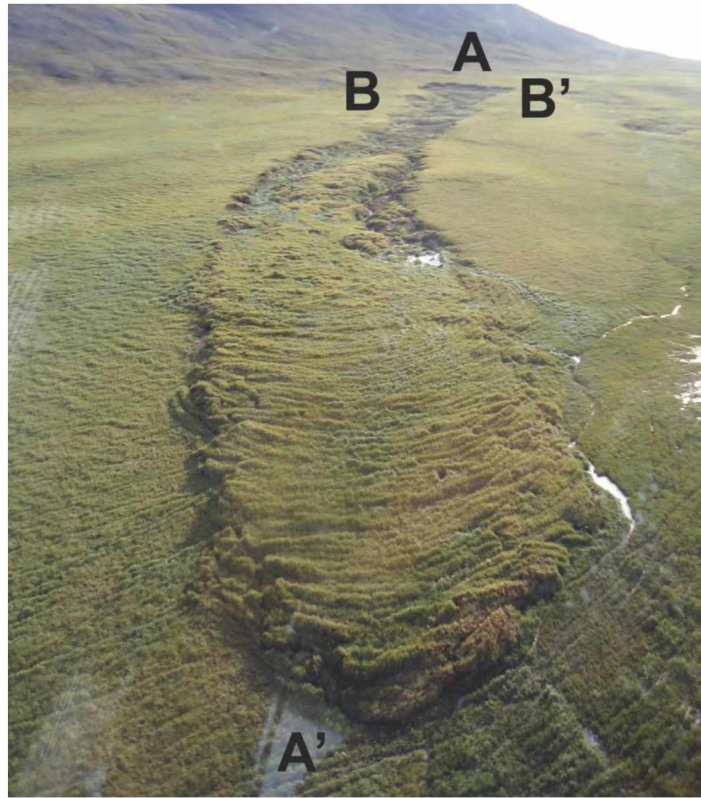


Figure 4.1. Active layer detachment, Noatak Basin, northwest Alaska. Active layer detachment slide on a northeast facing 6° slope on a deposit of colluvium and loess in the upper Fauna Creek drainage Noatak Basin, northwest Alaska. Length from headwall to end of overburden debris flow (A to A') is 483 m; width at widest point (B to B') is 58 m, as of July 2011. Deepest point was 3.5 m in the upper portion near the headwall. Photo: Andrew Balsler, 2011

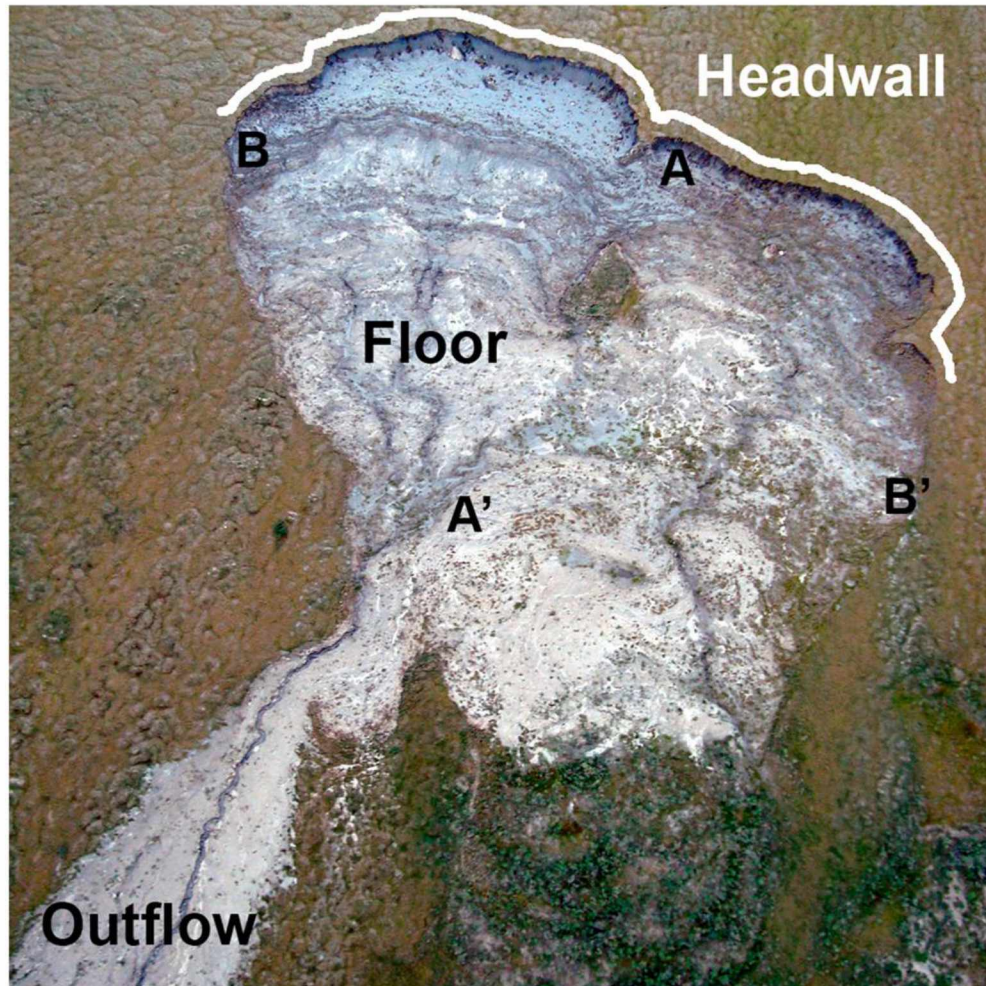


Figure 4.2. Retrogressive thaw slump, Noatak Basin, northwest Alaska. Retrogressive thaw slump on a west facing 6° slope on a late Pleistocene glaciolacustrine deposit in the upstream portion of the Aniuk Lowlands, Noatak Basin, Alaska. This slump is polycyclic, having initiated in 2004 from a previously re-stabilized and inactive retrogressive thaw slump. Length from headwall to beginning of outflow (A to A') is 181 m; width at widest point (B to B') is 287 m, as of July 2011. Deepest point was 14m at the base of the headwall near A. Photo: Andrew Balsler, 2011

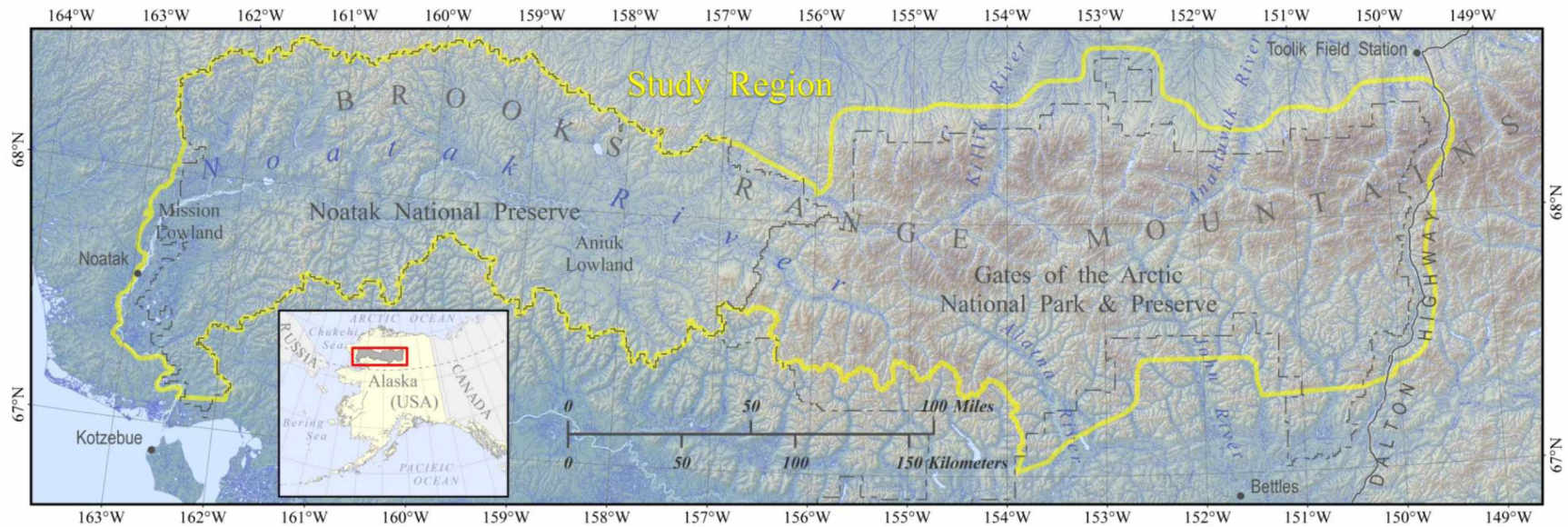


Figure 4.3. Map of the study region. The study region spans a physiographic gradient from the central portion of Alaska's Brooks Range mountains in Gates of the Arctic National Park and Preserve, westward through the Noatak River Basin in the Noatak National Preserve. Physiographic provinces include the high mountains of the Central Brooks Range in the eastern half of the study region through foothills and valley bottoms to the westward, with the broad, Mission Lowlands within the arctic/boreal ecotone near the Noatak mouth (Wahrhaftig, 1965). From the highest elevations (>2,000 m) in the Central Brooks Range, landscapes grade through foothills to glacially-sculpted valley bottoms containing major rivers emanating outward to the north, south and west. The study region boundary was determined by the geographic intersection of spatial datasets used in terrain suitability analyses.

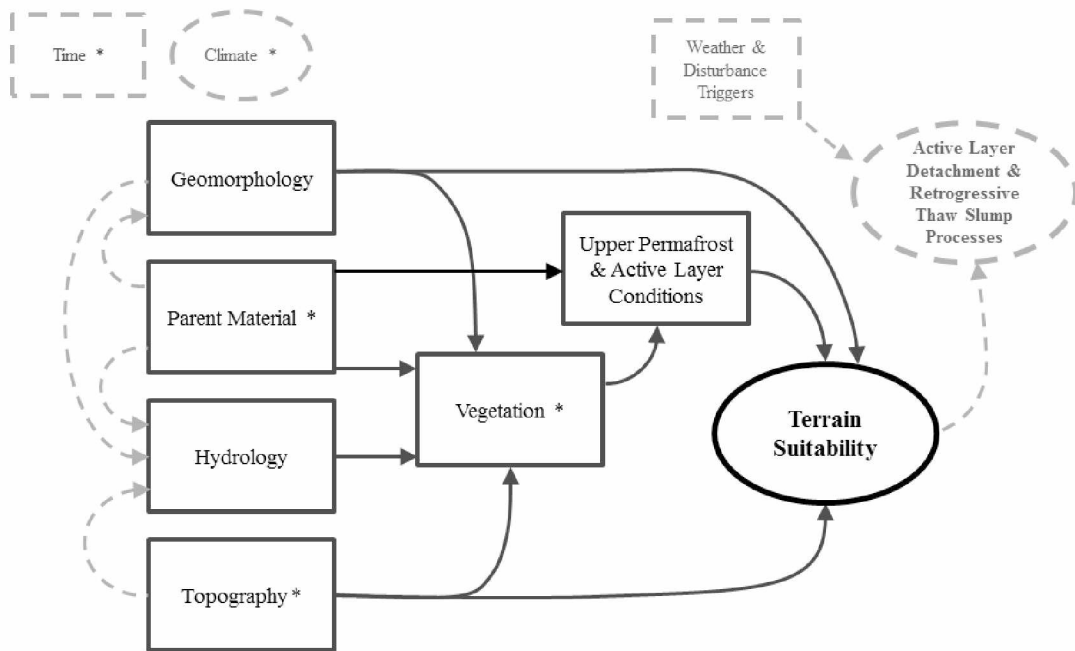


Figure 4.4. Initial conceptual model diagram of hypothesized landscape drivers of terrain suitability for active layer detachment slide (ALD) and retrogressive thaw slump (RTS) features. Boxes represent measurable variables; circles represent properties which include unknown factors. Dashed outlines and lines represent factors and relationships not included in the modeling analysis. Time and climate are considered drivers for all other properties and processes included in the diagram. The five State Factors (Jenny 1941, van Cleve et al. 1991); time, climate, parent material, topography, and biota are indicated with an *.

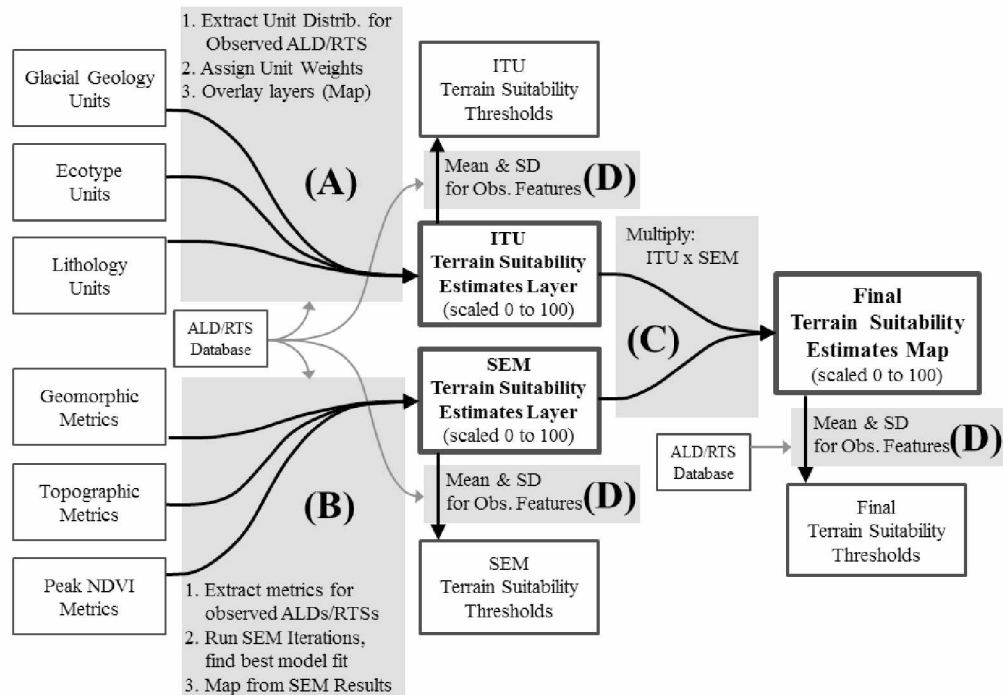


Figure 4.5. Overview of analysis approach for estimating active layer detachment slide (ALD) and retrogressive thaw slump (RTS) terrain suitability in the central and western Brooks Range, Alaska. Analysis included four general steps.

- A) Categorical landscape properties (glacial geology, ecotype and lithology) underwent point-in-polygon analysis with our database of observed ALD and RTS feature locations for integrated terrain unit (ITU) analysis within the study region. Analytical results were used to assign ALD and RTS weights to all categorical landscape units, which were then combined by overlay into two datasets: one for categorically-derived ALD terrain suitability estimates, and one for categorically-derived RTS terrain suitability estimates. Values were scaled 0 to 100, and the layers were rasterized to 60 m grid cells.
- B) Continuous, numeric variable values (derived from the National Elevation Dataset DEM and inter-annual MODIS NDVI data) were extracted for observed ALD and RTS locations, and for randomly-generated landscape control locations. These were run as structural equation model (SEM) iterations to find the model diagram with best fit for ALD and RTS features versus control respectively. Final SEM coefficients and intercepts were used to generate two datasets: one for SEM-derived ALD terrain suitability, and one for SEM-derived RTS terrain suitability.
- C) For each feature type (ALD vs RTS), terrain suitability results from A) ITU analysis and B) SEM analysis were scaled 0 to 100, then multiplied together. The resulting, combined (final) terrain suitability datasets (one for ALD and one for RTS) were then scaled 0 to 100.
- D) Estimated terrain suitability values from each raster dataset (ITU, SEM and combined; for ALD and RTS respectively), were extracted using observed feature locations. Mean and standard deviation of values at observed features were used to define suitability thresholds. ‘Suitable terrain’ was defined by values greater than one standard deviation below the mean for each feature type. ‘Highly suitable terrain’ was defined by values greater than the mean for each feature type.

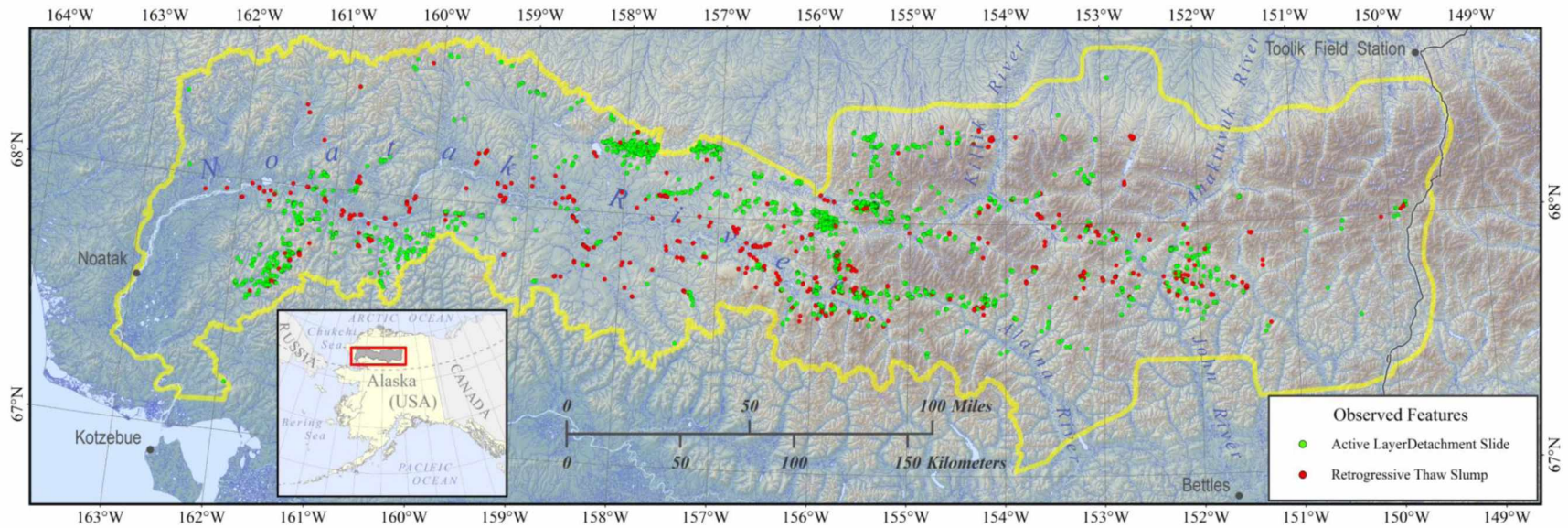


Figure 4.6. Map of observed active layer detachment slides and retrogressive thaw slumps within the study region in the western Brooks Range and foothills of northern Alaska. Feature locations derive from aerial photo analysis, and airborne and ground based field reconnaissance (Balser et al., 2009; Balser et al., 2014) and from high-resolution satellite image analysis by the National Park Service (Swanson & Hill, 2010). The analysis dataset contained 2492 active layer detachment slides and 805 retrogressive thaw slumps.

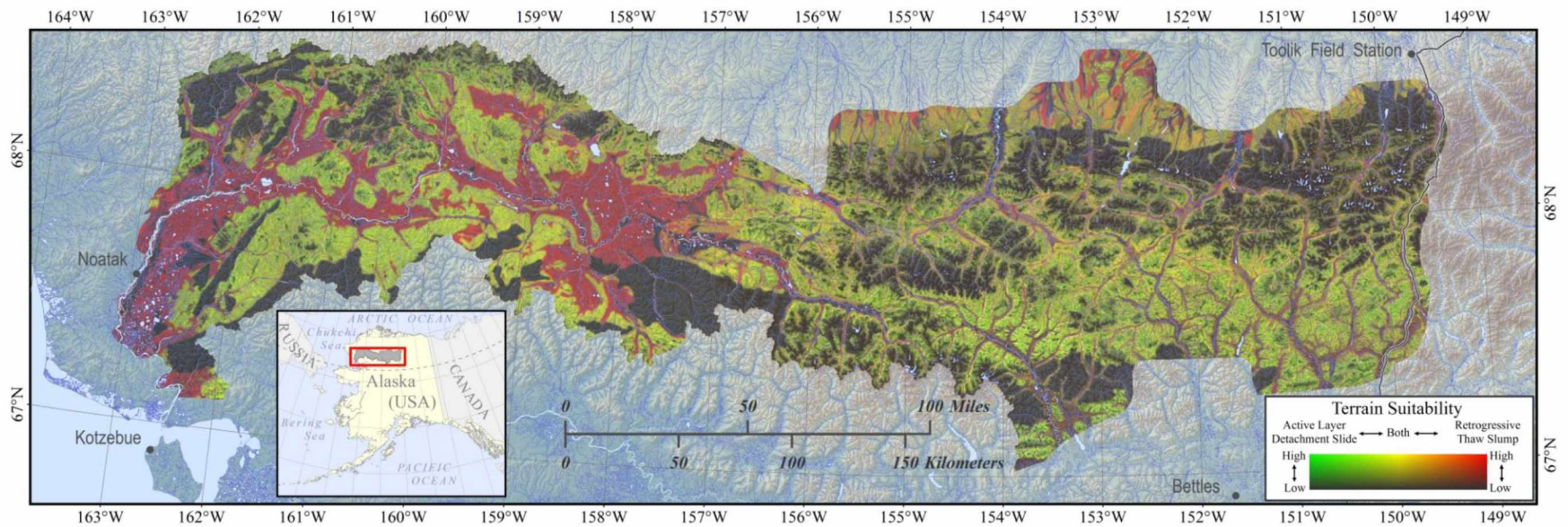


Figure 4.7. Map of estimated terrain suitability for active layer detachment slides (green) and retrogressive thaw slumps (red) for the study region in the western Brooks Range of northern Alaska.

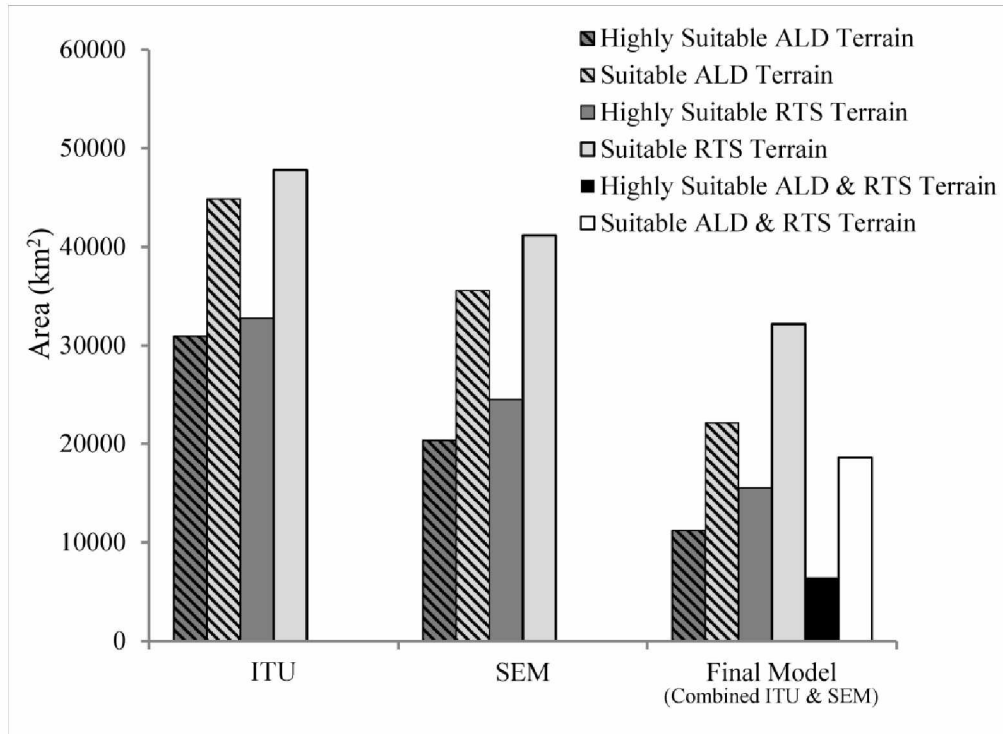


Figure 4.8. Areal estimates of suitability for active layer detachment (ALD) and retrogressive thaw slump (RTS) terrain from integrated terrain unit (ITU) analysis, structural equation modeling (SEM) analysis, and from the final, combined model. Estimated values at observed active layer detachment slide and retrogressive thaw slump features were used to define “suitable” and “highly suitable” terrain. “Suitable” was defined as estimated values greater than or equal to one standard deviation below the mean. “Highly suitable” was defined as estimated values greater than or equal to the mean. ALD and RTS terrain share significant overlap, as shown by bars representing terrain which is suitable/highly suitable for both ALD and RTS.

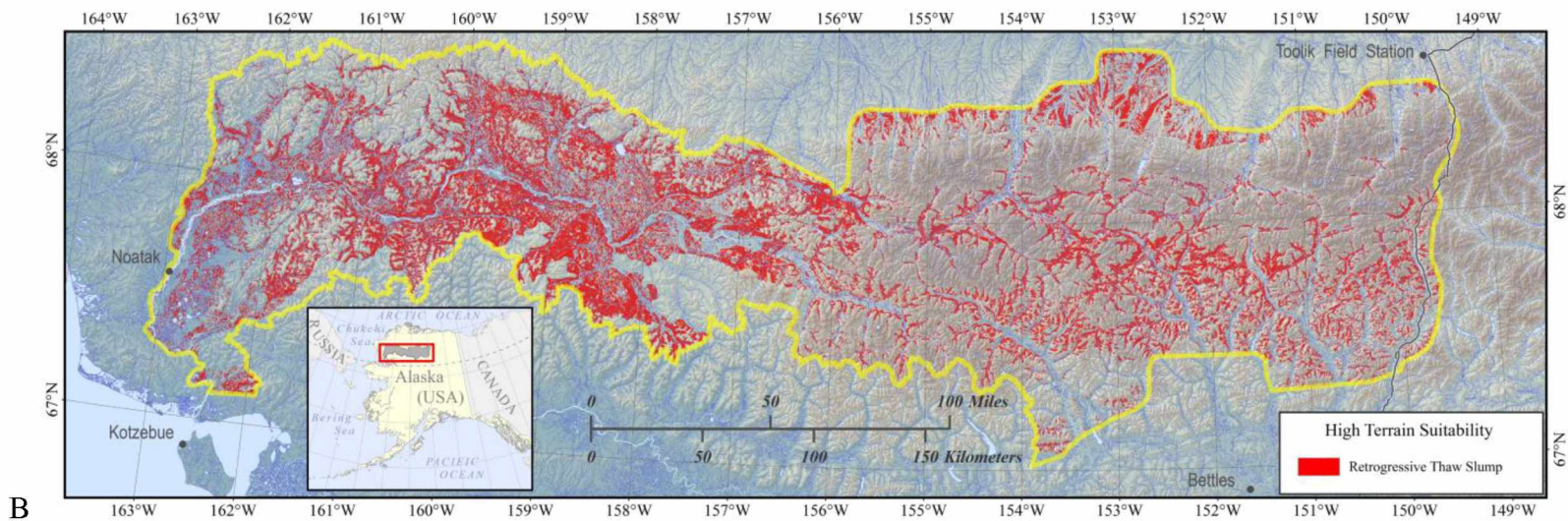
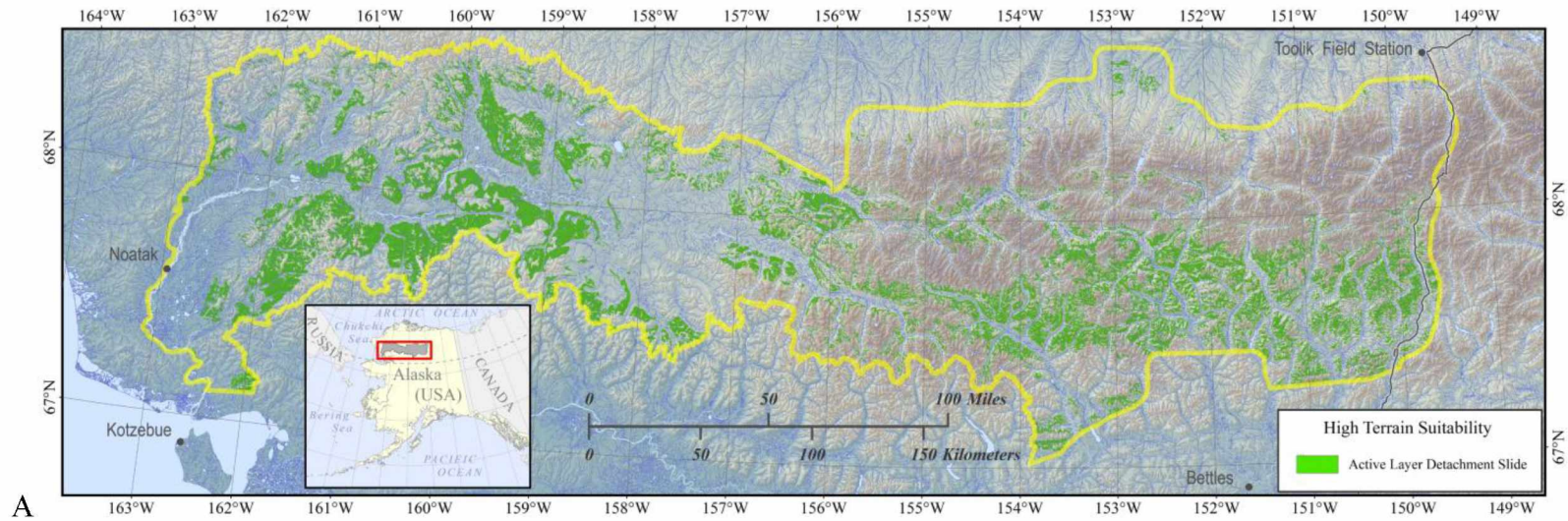


Figure 4.9. Areas estimated as highly suitable terrain for A) active layer detachment slides (green) and B) retrogressive thaw slumps (red) for the study region in the western Brooks Range of northern Alaska.

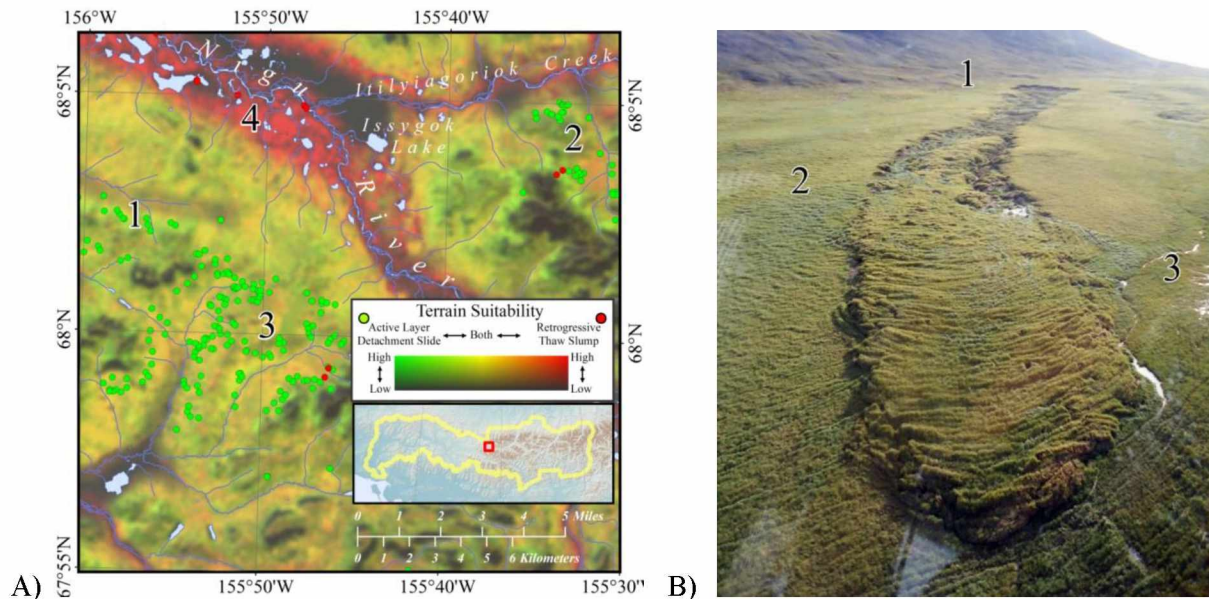


Figure 4.10. Active layer detachment slide and retrogressive thaw slump terrain suitability in an upland setting.

A) Estimated terrain suitability for active layer detachment slides (green) and retrogressive thaw slumps (red) and for both (yellow) near the headwaters of the Nigu River in the northwest portion of Gates of the Arctic National Park and Preserve, west-central Brooks Range, northern Alaska; (1) A cluster of active layer detachment slides within colluvial deposits (s), upslope of late-Pleistocene outwash deposits (io_1) (Hamilton, 2011), along a toe slope beneath exposed and partially-exposed, non-carbonate bedrock (Jorgenson et al. 2001), (dark, upland features on the map). The surface is generally smooth latitudinally across the hillslope, with some convexity longitudinally down the hillslope, where slope angle decreases slightly at the toe below exposed bedrock. Predominant ecotypes include upland birch-ericaceous-willow low shrub, upland dwarf birch-tussock shrub, and alpine ericaceous dwarf shrub (Jorgenson et al. 2010b); (2) Similar conditions to (1), but the presence of several RTS features suggest locally deeper, ice-rich colluvial deposits where permafrost exposed by active layer detachment sliding is vulnerable to retrogressive thaw slumping; (3) Similar geomorphic conditions to (1) and (2), but underlain by a combination of thin soils over near-surface bedrock and late-Pleistocene glacial drift (id_1) (Hamilton, 2011), and with primarily alpine dryas dwarf shrub and upland birch-ericaceous-willow low shrub ecotypes (Jorgenson et al, 2010b); (4) Retrogressive thaw slumps within valley-bottom, ice-contact, kame and kame terrace deposits (ik_3) and glacial drift (id_3), both of the late-Pleistocene (Hamilton, 2011). Small, mild hills interspersed with ponds and lakes characterize this kettle-lake area. Predominant ecotypes include upland dwarf birch-tussock tundra, upland birch-ericaceous-willow low shrub, lowland birch-ericaceous-willow low shrub and lowland sedge fen (Jorgenson et al. 2010b).

B) Active layer detachment slides in thin deposits of upper hillslope colluvium, along (1) a toe slope below non-carbonate, exposed bedrock (micaeous shale) 50 km west of the map frame (A) in the upper Fauna Creek drainage in the Noatak Basin, northwest Alaska. The hill is a smooth, 6° slope, with tracks from migrating caribou visible across the hillslope at the bottom of the image. (2) Predominantly upland birch-ericaceous-willow low shrub, with graminoid cover $> 50\%$ over much of the area. (3) Wet sedge meadow along a watertrack below the feature. This active layer detachment is 483 m long from the headwall to the bottom of the run out, 58 m wide at the widest point, near the headwall, and 3.5 m deep at the deepest point, also near the headwall. Recorded at the headwall, the active layer depth was 110 cm deep, including a 33 cm organic layer, loess from 33 to 60 cm, and colluvially re-transported gravel (55%) and silt (45%) from 60 to 100 cm. Below the permafrost table, ice-rich, syngenetic permafrost is composed of segregated ice (50 to 70%, ataxitic and reticulate), gravel (25 to 35%), and silt (15 to 25%). These conditions continued to the bottom of the headwall profile at 248 cm. Photo: Andrew Balsler, 2011.

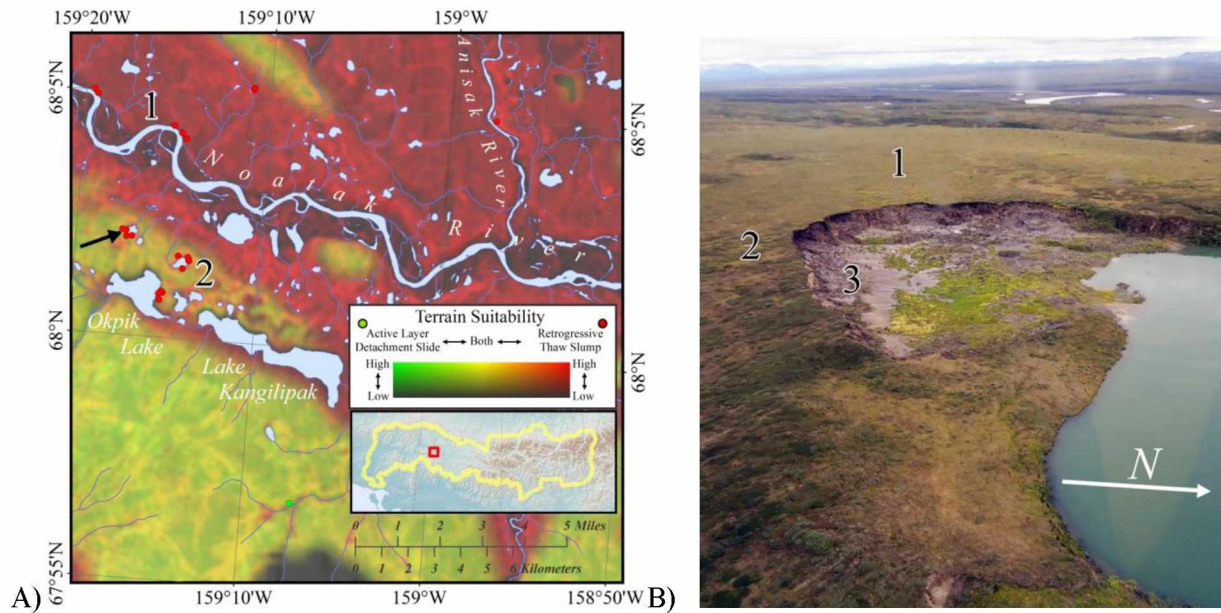


Figure 4.11. Active layer detachment slide and retrogressive thaw slump terrain suitability in a lowland setting.

A) Estimated terrain suitability for active layer detachment slides (green) and retrogressive thaw slumps (red) and both (yellow) at the western edge of the Aniak Lowland, adjacent to the mainstem Noatak River in the Noatak National Preserve, northwest Alaska. (1) Retrogressive thaw slumps along a bluff adjacent to the Noatak River, within late-Pleistocene glaciolacustrine deposits ($ig1_{1B}$ and $ig2$) which over-drape late-Pleistocene glacial drift deposits (id_{1B}) (Hamilton, 2010). Progressive down-cutting and hydro-thermal erosion since the Pleistocene have left a bluff complex 15 – 80 m tall (Hamilton, 2009) containing ice-rich, deep permafrost. Behind the bluff are mild hills and smaller geomorphic features among small ponds and lakes. Predominant ecotypes are upland dwarf birch-tussock shrub and upland birch-ericaceous-willow low shrub (Jorgenson et al. 2010b). These conditions cover the majority of terrain north of the Noatak River within the map frame. (2) Retrogressive thaw slumps on the margins of kettle lakes within late-Pleistocene glacial drift deposits (id_{1B}). A patch of suitable ALD terrain is visible on a bluff top on the south side of the Noatak River, north of Lake Kangilipak and east of several, smaller lakes. Surface conditions include mild hills and smaller geomorphic features among small ponds and lakes, and predominant ecotypes are upland dwarf birch-tussock shrub and upland birch-ericaceous-willow low shrub (Jorgenson et al. 2010b).

B) A retrogressive thaw slump on a kettle lake within a glacial drift deposit (id_{1B}), indicated by an arrow on the map (A). (1) Gently sloped hilltop just upslope of the retrogressive thaw slump with primarily dwarf and low shrub-tussock tundra ecotypes (Jorgenson et al. 2010b). Geomorphic features become more pronounced approaching the Noatak River bluffs in the distance. (2) Mixed low shrub and dwarf shrub tundra ecotypes along a mid-hillslope with moderate, meso-scale geomorphic variability. Hill slope is roughly 9° . (3) Retrogressive thaw slump which has been active since at least 1980 (Balser et al., 2014). Dimensions were 191 m at the widest point, 122 m long from the apex of the headwall to the end of the run out fan, and 18 m deep at the deepest location along the headwall, with the headwall retreating roughly 12 m between the summers of 2006 and 2011. Deposits within the headwall are comprised of 60% massive ice, where roughly two thirds are Pleistocene and Holocene ice wedges, and roughly one third is relict glacial ice. The widest deposit of massive ice was 2.5 m across. The glacial drift included up to 55% angular and sub-angular coarse fragments, at clast sizes from gravel up to boulders of over 50 cm. Within 1 m of the surface, deposits were composed of Aeolian loess and sand (> 1 m), active layer depth of roughly 45 cm, with primarily pore and lenticular ice and occasional pockets of reticulate ice below the permafrost table. The surface was covered with a relatively thin organic layer (roughly 4 cm) (Balser et al., 2015). Photo: Andrew Balser, 2010.

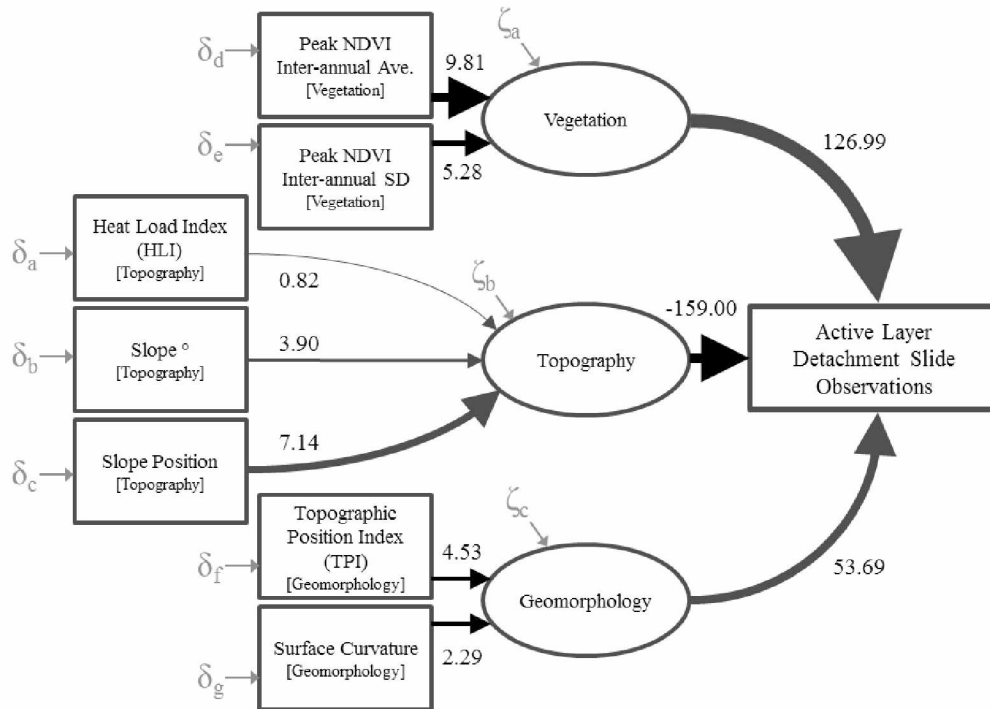


Figure 4.12. Final, fitted structural equation model (SEM) diagram for active layer detachment slide (ALD) terrain suitability (as represented by field observations versus randomly generated control point locations for model fitting). Bracketed labels refer to boxes in the original hypothesis and conceptual model hypothesis diagram (Figure 4.4). Boxes represent observed, exogenous variables, while circles represent latent, endogenous variables. Line weights represent the strength of the modeled causal relationship. Numbers next to lines are final model coefficients, averaged from ten bootstrapped model runs using standardized data. δ represents unknown measurement error for observed, exogenous variables. ζ represents unknown error for latent, endogenous variables.

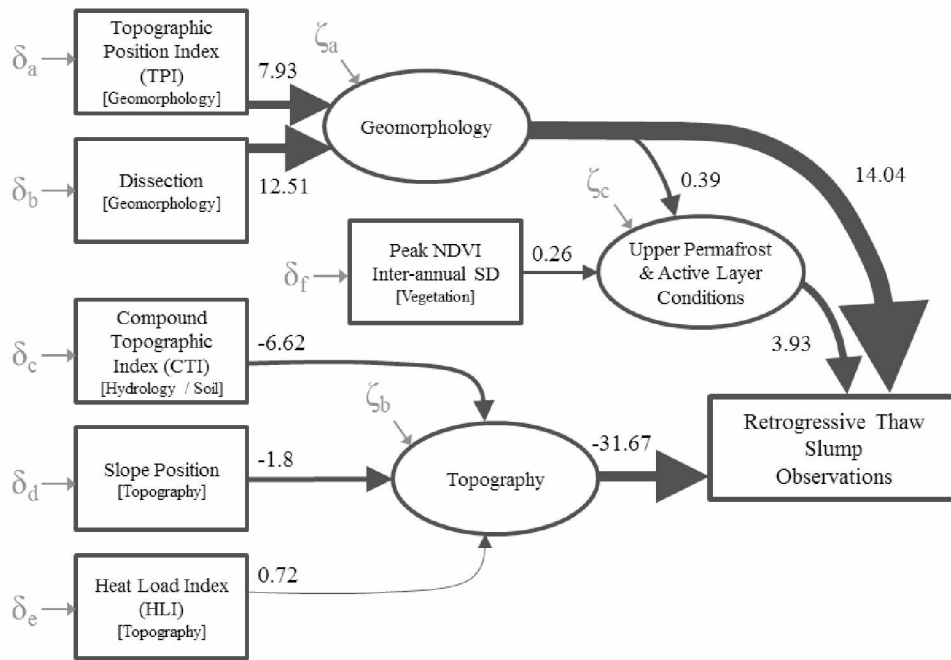


Figure 4.13. Final, fitted structural equation model (SEM) diagram for retrogressive thaw slump (RTS) terrain suitability (as represented by field observations versus randomly generated control point locations for model fitting). Bracketed labels refer to boxes in the original hypothesis and conceptual model hypothesis diagram (Figure 4.4). Boxes represent observed, exogenous variables, while circles represent latent, endogenous variables. Line weights represent the strength of the modeled causal relationship. Numbers next to lines are final model coefficients, averaged from ten bootstrapped model runs using standardized data. δ represents unknown measurement error for observed, exogenous variables. ζ represents unknown error for latent, endogenous variables.

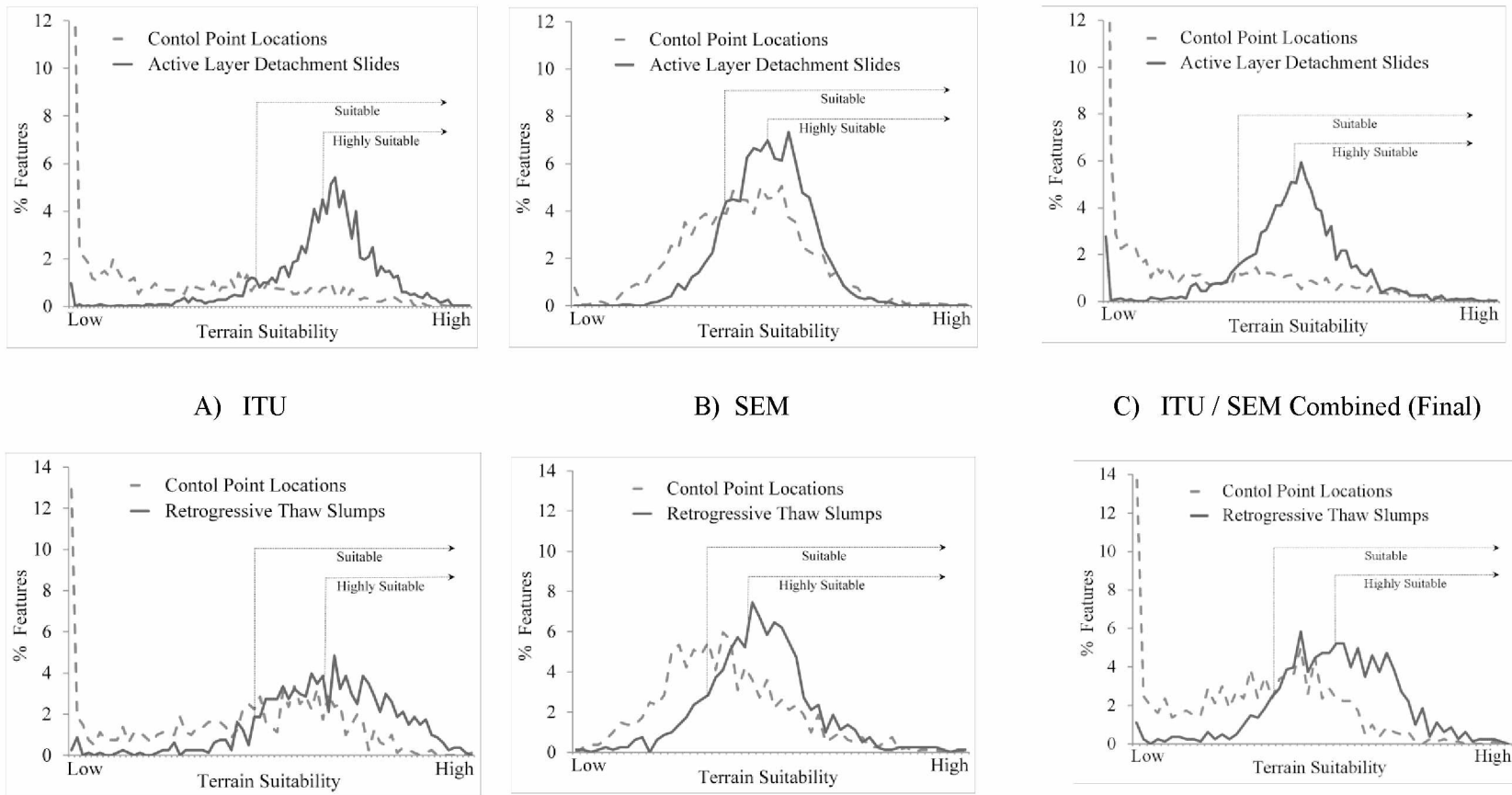


Figure 4.14. Frequency distributions of estimated terrain suitability for active layer detachment slide features, retrogressive thaw slump features, and randomly generated landscape control points within the study region in the central and western Brooks Range, Alaska. A) Terrain suitability estimated with integrated terrain unit (ITU) analysis of categorical variables. B) Terrain suitability estimated using structural equation modeling analysis coefficients of numeric landscape variables. C) Final estimates of terrain suitability combining results from A. and B. Estimated values at observed active layer detachment slide and retrogressive thaw slump features were used to define “suitable” and “highly suitable” terrain. “Suitable” was defined as estimated values greater than or equal to one standard deviation below the mean. “Highly suitable” was defined as estimated values greater than or equal to the mean.

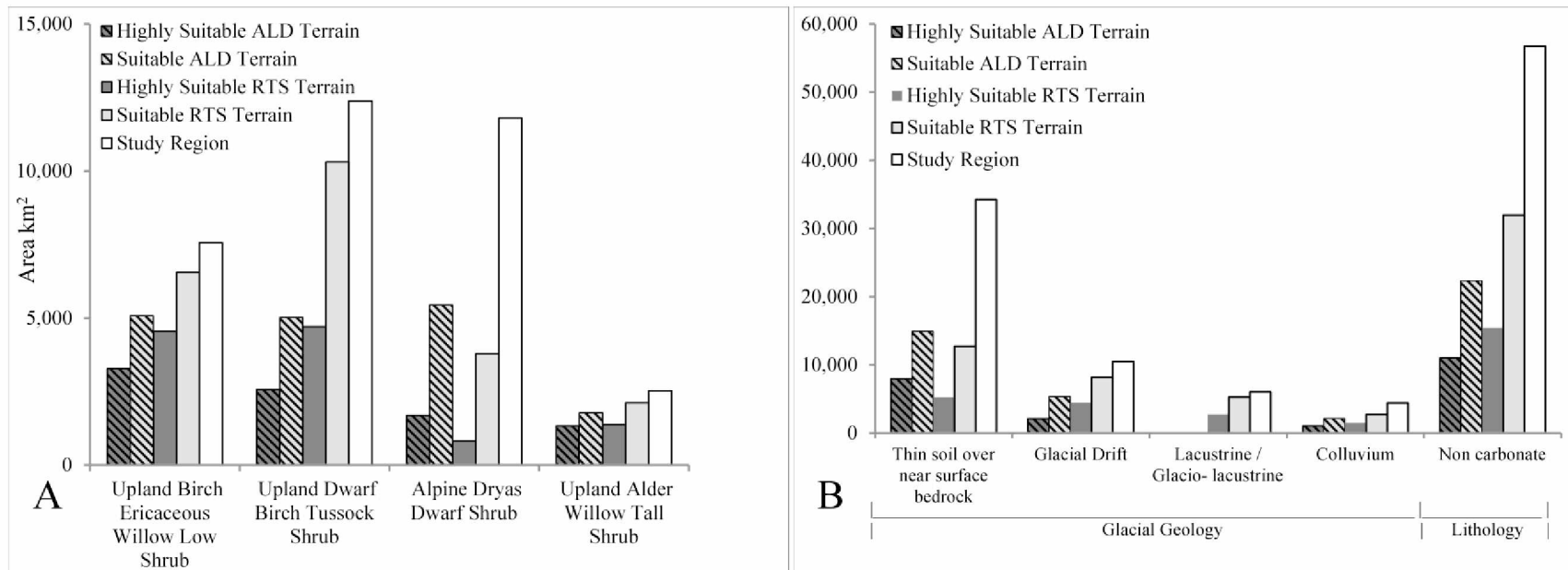


Figure 4.15. Areal extent of categorical landscape properties by active layer detachment slide (ALD) and retrogressive thaw slump (RTS) terrain suitability, and for the study region in the central and western Brooks Range, Alaska. A) Distribution among the four most prevalent ecotypes within suitable terrain. B) Distribution among the four most prevalent glacial geology units within suitable terrain, and distribution of noncarbonate lithology. Estimated values at observed active layer detachment slide and retrogressive thaw slump features (i.e. excluding the randomly generated control point locations) were used to define “suitable” and “highly suitable” terrain. “Suitable” was defined as estimated values greater than or equal to one standard deviation below the mean. “Highly suitable” was defined as estimated values greater than or equal to the mean.

Table 4.1. Input data sets used for terrain suitability analyses for active layer detachment slides (ALD) and retrogressive thaw slumps (RTS) within the study region in the central and western Brooks Range of northern Alaska.

Dataset	Cell Size	Source	Type	Reference
ALD and RTS Feature Locations	n / a	University of Alaska Fairbanks / U.S. National Park Service (Arctic Network)	ArcGIS point geodatabase	(Balsler 2009; Swanson and Hill, 2010)
Glacial / Surficial Geology	n / a	U.S. Geological Survey, Alaska Science Center	ArcGIS polygon geodatabase	(Hamilton, 2010; Hamilton and Labay 2011)
Lithology	n / a	Alaska Biological Research Inc. / U.S. National Park Service, Arctic Network	ArcGIS polygon shapefile	(Jorgenson et al., 2001)
Ecotype	30m	Alaska Biological Research Inc. / U.S. National Park Service, Arctic Network	ArcGIS raster geodatabase	(Jorgenson et al., 2010b)
National Elevation Dataset (NED)	60m	U.S. Geological Survey, EROS Data Center	ArcGIS raster image	(Gesch et al., 2002)
2001 - 2012 Normalized Difference Vegetation Index (NDVI), Moderate-resolution Imaging Spectrometer (MODIS)	250m	U.S. Geological Survey, EROS Data Center	ArcGIS raster image	(Jenkerson et al., 2010)

Table 4.2. Derived variables used in structural equation model (SEM) analyses. All variables derive from either A) National Elevation Dataset (NED) data from the U.S. Geological Survey, or B) Moderate-resolution Imaging Spectrometer (MODIS) 2001-2012 monthly Normalized Difference Vegetation Index (NDVI) data (Table 1). ‘Group’ refers to boxes in Figure U. * resampling was conducted after calculation of statistical values using the ‘cubic convolution’ method.

Variable	Group	Calculation	Source Data Cell Size (m)	Derived Variable Cell Size (m)	Cell Neighborhood of Calculation
Compound Topographic Index (CTI)	Hydrology	$\ln(F_{acc} / \tan(\text{slope}_{rad}))$, where: F_{acc} = flow accumulation slope_{rad} = slope in radians	60	60	Contributing watershed (values smoothed using 3 x 3 focalmean kernel)
Surface Curvature	Geomorphology	Concavity / Convexity (Bolstad’s Variant)	60	60	5 x 5
Dissection (m)	Geomorphology	$(z - z_{min}) / (z_{max} - z_{min})$, where: z = cell elevation z_{max} = neighborhood max. elev. z_{min} = neighborhood min. elev.	60	60	3 x 3
Topographic Position Index (TPI)(m)	Geomorphology	$(z_{mean} - z_{min}) / (z_{max} - z_{min})$, where: z_{mean} = neighborhood mean elev. z_{max} = neighborhood max. elev. z_{min} = neighborhood min. elev.	60	60	5 x 5
Elevation (m)	Topography	Data value from NED dataset	60	60	not derived
Heat Load Index (HLI)	Topography	$(1 - \cos(\text{aspect} - 45)) / 2$, where: Aspect = degrees from north	60	60	3 x 3
Slope °	Topography	$(\arctan(\text{Rise} / \text{Run}) \times 57.29578)$	60	60	3 x 3
Slope Position (m)	Topography	$z - z_{mean}$ where: z = cell elevation z_{mean} = neighborhood mean elev.	60	60	500 x 500
NDVI Annual Peak, 2001-2013	Vegetation	Maximum NDVI per pixel, per year	250		1 x 1
- Average		Average peak value among years		60*	
- Maximum		Maximum peak value among years		60*	
- Minimum		Minimum peak value among years		60*	
- Standard Deviation		SD of peak values among years		60*	
- Range		Range of peak values among years		60*	

Table 4.3. Pearson correlation coefficients for variables tested with structural equation modeling, calculated for the entire study region. Values greater than 0.5 or less than -0.5 are shown in bold.

		Hydrology, Topography and Geomorphology								NDVI Annual Peak 2001-2012				
		CTI	Curv.	Diss.	Elev.	HLI	Slope °	Slope Pos.	TPI	Ave	Max	Min	Range	Std.
Hyd. Topo. & Geom.	CTI	1.00												
	Curv.	-0.30	1.00											
	Diss.	-0.42	0.52	1.00										
	Elev.	-0.57	0.12	0.17	1.00									
	HLI	-0.08	0.00	0.01	0.07	1.00								
	Slope °	-0.76	0.05	0.13	0.64	0.10	1.00							
	SPos.	-0.49	0.23	0.24	0.57	0.06	0.48	1.00						
	TPI	-0.35	0.27	0.70	0.18	0.01	0.13	0.28	1.00					
NDVI Ann. Peak 2001- 2012	Ave	0.34	-0.05	-0.07	-0.61	-0.09	-0.45	-0.57	-0.08	1.00				
	Max	0.20	-0.01	-0.04	-0.37	-0.09	-0.27	-0.36	-0.06	0.70	1.00			
	Min	0.37	-0.07	-0.08	-0.66	-0.06	-0.51	-0.60	-0.09	0.97	0.63	1.00		
	Range	-0.32	0.09	0.06	0.52	-0.02	0.44	0.44	0.06	-0.54	-0.02	-0.68	1.00	
	Std.	-0.32	0.10	0.07	0.51	-0.03	0.44	0.44	0.07	-0.52	-0.03	-0.66	0.96	1.00

158

Table 4.4. Areal estimates of active layer detachment slide (ALD) and retrogressive thaw slump (RTS) terrain suitability for integrated terrain unit (ITU) and structural equation model (SEM) analyses, and for the final model which combines ITU and SEM results.

	ITU		SEM		Final (Combined ITU & SEM)	
	Highly Suitable	Suitable	Highly Suitable	Suitable	Highly Suitable	Suitable
	km ² (% study region)	km ² (% study region)	km ² (% study region)	km ² (% study region)	km ² (% study region)	km ² (% study region)
ALD Terrain	30,937 (49)	44,843 (70)	20,346 (32)	35,549 (56)	11,046 (17)	22,464 (35)
RTS Terrain	32,757 (51)	47,760 (75)	24,513 (38)	41,156 (65)	15,537 (24)	32,174 (51)
ALD & RTS Terrain	n/a	n/a	n/a	n/a	5,841 (9)	18,235 (29)

Table 4.5. Categorical landscape properties as a percentage study region, by percentage retrogressive thaw slump (RTS) and active layer detachment slide (ALD) distribution, and differential (Feature % / Study Area %). Ecotypes which are present within the study region but comprise less than 0.5% feature distribution are excluded from this table.

Ecotype	% of Study Region	% of RTS Features	% Differential	% of ALD Features	% Differential
Alpine Dryas Dwarf Shrub	19.0	15.7	0.8	20.0	1.1
Alpine Ericaceous Dwarf Shrub	0.0	0.0	0.0	5.0	2.5
Alpine Ericaceous Dwarf Shrub	2.0	2.8	1.4	0.0	0.0
Alpine Wet Sedge Meadow	1.0	1.0	1.0	1.0	1.5
Lowland Birch-Ericaceous-Willow Low Shrub	3.0	2.4	0.8	0.0	0.0
Lowland Sedge Fen	1.0	2.8	2.8	0.0	0.0
Riverine Alder or Willow Tall Shrub	1.0	1.6	1.6	0.0	0.0
Riverine Birch-Willow Low Shrub	1.0	2.0	2.0	0.0	0.0
Riverine Wet Sedge Meadow	1.0	1.2	1.2	0.0	0.0
Riverine Willow Low Shrub	1.0	0.9	0.9	0.0	0.0
Upland Alder-Willow Tall Shrub	4.0	6.8	1.7	9.0	2.3
Upland Birch-Ericaceous-Willow Low Shrub	12.0	23.7	2.0	23.0	1.9
Upland Dwarf Birch-Tussock Shrub	19.0	19.2	1.0	29.0	1.5
Upland Sedge-Dryas Meadow	6.0	9.6	1.6	6.0	1.0
Upland White Spruce Forest	4.0	3.0	0.8	1.0	0.3
Upland Willow Low Shrub	0.0	0.0	0.0	3.0	1.5
Upland Willow Low Shrub	2.0	2.9	1.4	0.0	0.0
Glacial Geology	% of Study Region	% of RTS Features	% Differential	% of ALD Features	% Differential
Alluvium	6.1	7.0	1.1	1.0	0.2
Thin Soil over Near-surface Bedrock	53.8	26.0	0.5	54.0	1.0
Colluvium	6.9	7.0	1.0	20.0	2.9
Glacial Drift	16.4	46.0	2.8	22.0	1.3
Fan Deposits	1.8	0.3	0.2	0.2	0.1
Gravel	0.1	0.1	0.7	0.0	0.0
Ice Contact	0.5	1.0	2.1	0.0	0.1
Inwash / Outwash	1.5	0.4	0.3	0.1	0.1
Lacustrine / Glaciolacustrine	9.4	11.0	1.2	2.0	0.2
Organic	0.0	0.0	0.0	0.0	0.0
Other (Active Glacier / Snowfield)	0.7	0.0	0.0	0.5	0.7
Sand	0.6	0.2	0.3	0.0	0.0
Silt	1.0	0.0	0.0	0.0	0.0
Terrace	1.2	1.0	0.8	0.0	0.0
Lithology	% of Study Region	% of RTS Features	% Differential	% of ALD Features	% Differential
Noncarbonate	89.8	99.2	1.1	98.3	1.1
Carbonate	10.2	0.8	0.1	1.7	0.2

Table 4.6. Structural equation model fit metrics (Hooper et al., 2008) from ten bootstrapped model runs for active layer detachment slide (ALD) and ten bootstrapped model runs for retrogressive thaw slump (RTS) terrain suitability in the central and western Brooks Range, Alaska. The ALD model uses 2492 observed ALD feature locations, and an equal number of randomly generated, non-ALD control locations. The model uses 805 observed RTS feature locations, and an equal number of randomly generated, non-RTS control locations. Coefficients and intercepts from the ten bootstrap runs were used to produce ALD and RTS terrain suitability estimates, mapped for the study region (Figure 8). Mean values for the ten runs shown in bold.

SEM ALD Bootstrap Run											
Fit metric; recommended threshold value for good fit	1	2	3	4	5	6	7	8	9	10	mean
Comparative Fit Index (CFI); > 0.950	0.977	0.970	0.977	0.973	0.972	0.971	0.979	0.976	0.971	0.978	0.974
Tucker-Lewis Index (TLI); > 0.950	0.958	0.952	0.959	0.953	0.942†	0.955	0.946†	0.959	0.948†	0.957	0.953
Root mean square error of approximation (RMSEA); < 0.07	0.037	0.036	0.037	0.033	0.037	0.030	0.035	0.035	0.037	0.036	0.035
Standardized Root Mean Square Residual (SRMR); < 0.50	0.029	0.029	0.033	0.029	0.032	0.032	0.031	0.031	0.028	0.032	0.031
SEM RTS Bootstrap Run											
Fit metric; recommended threshold value for good fit	1	2	3	4	5	6	7	8	9	10	mean
Comparative Fit Index (CFI); > 0.950	0.994	0.991	0.982	0.990	0.990	0.991	0.983	0.977	0.988	0.983	0.987
Tucker-Lewis Index (TLI); > 0.950	0.980	0.968	0.979	0.974	0.980	0.972	0.986	0.967	0.976	0.975	0.976
Root mean square error of approximation (RMSEA); < 0.07	0.027	0.030	0.032	0.034	0.033	0.049	0.038	0.044	0.063	0.043	0.039
Standardized Root Mean Square Residual (SRMR); < 0.50	0.019	0.036	0.031	0.026	0.030	0.030	0.023	0.031	0.026	0.028	0.028

† does not meet recommended value for good fit

Table 4.7. Structural equation model R^2 values from ten bootstrapped model runs for active layer detachment slide (ALD) and ten bootstrapped model runs for retrogressive thaw slump (RTS) terrain suitability in the central and western Brooks Range, Alaska. R^2 represents the variation among endogenous variables in the model explained by that factor (Joreskog and Sorbom, 1996). The ALD model uses 2492 observed ALD feature locations, and an equal number of randomly generated, non-ALD control locations. The RTS model uses 805 observed RTS feature locations, and an equal number of randomly generated, non-RTS control locations. Mean values for the ten runs shown in bold.

SEM ALD Bootstrap Run R^2 Values											
Variable	1	2	3	4	5	6	7	8	9	10	mean
Peak NDVI Inter-annual average	0.61	0.59	0.61	0.59	0.59	0.60	0.60	0.60	0.56	0.54	0.59
Peak NDVI Inter-annual standard deviation	0.35	0.40	0.37	0.41	0.42	0.41	0.43	0.43	0.40	0.42	0.40
Curvature	0.29	0.35	0.29	0.27	0.28	0.32	0.33	0.30	0.34	0.38	0.31
Topographic Position Index (TPI)	0.29	0.24	0.26	0.28	0.30	0.27	0.29	0.29	0.24	0.24	0.27
Slope Position	0.50	0.52	0.52	0.50	0.52	0.54	0.51	0.48	0.51	0.51	0.51
Heat Load Index (HLI)	0.00	0.01	0.00	0.01	0.00	0.01	0.00	0.00	0.01	0.00	0.00
Slope (°)	0.17	0.18	0.18	0.19	0.19	0.17	0.16	0.17	0.17	0.19	0.18
SEM RTS Bootstrap Run R^2 Values											
Variable	1	2	3	4	5	6	7	8	9	10	mean
Peak NDVI Inter-annual standard deviation	0.07	0.05	0.08	0.06	0.06	0.04	0.07	0.09	0.06	0.05	0.06
Topographic Position Index (TPI)	0.68	0.63	0.74	0.71	0.72	0.68	0.70	0.74	0.66	0.70	0.69
Dissection	0.88	0.88	0.83	0.84	0.80	0.79	0.73	0.82	0.85	0.80	0.82
Slope Position	0.39	0.36	0.48	0.40	0.44	0.33	0.37	0.39	0.46	0.40	0.40
Heat Load Index (HLI)	0.00	0.01	0.00	0.00	0.00	0.00	0.00	0.00	0.00	0.01	0.00
Compound Topographic Index (CTI)	0.35	0.39	0.35	0.42	0.34	0.40	0.37	0.37	0.34	0.34	0.37

Table 4.8. Numeric landscape properties within the study region, and by terrain suitability for active layer detachment slides and retrogressive thaw slumps. Original source data from: * (Hugelius et al., 2013), and † (Jorgenson et al., 2010b).

Landscape Property	Study Region		Active Layer Detachment Slide Terrain				Retrogressive Thaw Slump Terrain			
	mean	std	Highly Suitable		Suitable		Highly Suitable		Suitable	
			mean	std	mean	std	mean	std	mean	std
Peak NDVI Inter-annual Ave. †	0.700	0.155	0.801	0.046	0.777	0.061	0.790	0.048	0.780	0.056
Peak NDVI Inter-annual SD †	0.062	0.033	0.175	0.045	0.048	0.016	0.046	0.014	0.049	0.015
Heat Load Index (HLI) †	5,257	1,320	5,276	1,266	5,254	1,248	5,090	842	5,144	940
Topographic Position Index (TPI) †	0.47	0.10	0.48	0.07	0.48	0.08	0.50	0.09	0.49	0.09
Dissection †	0.47	0.16	0.49	0.11	0.49	0.12	0.50	0.15	0.48	0.15
Compound Topographic Index (CTI) †	7.1	1.9	6.8	1.3	6.8	1.3	7.8	1.5	7.6	1.5
Surface Curvature †	0.01	2.10	-0.12	1.53	-0.09	1.68	-0.16	1.09	-0.17	1.26
Slope (°) †	13.1	10.9	13.2	8.0	13.0	8.4	7.7	6.9	8.7	7.7
Slope Position †	0.4	217.0	8.5	143.2	-5.1	159.5	-83.7	133.4	-73.1	146.8
Soil Organic Carbon Top 2m (kg/m ²) *	10.2	10.5	8.9	8.8	8.8	9.3	8.7	8.7	8.6	9.2
Soil Organic Carbon Top 3m (kg/m ²) *	11.2	11.5	9.9	9.6	9.7	10.1	9.6	9.4	9.4	10.0
Surface Organic Depth (cm) †	9.6	7.0	10.9	4.4	10.2	4.8	13.5	5.2	13.1	5.8
pH †	5.5	0.9	5.1	0.3	5.2	0.4	5.2	0.6	5.2	0.6

† Included in structural equation modelling (SEM)

Table 4.9. Numeric landscape properties for randomly-assigned control locations, and for observed active layer detachment slide and retrogressive thaw slump features. Original source data from: * (Hugelius et al., 2013), and † (Jorgenson et al., 2010b).

Landscape Property	Control		Active Layer Detachment Slides		Retrogressive Thaw Slumps	
	mean	std	mean	std	mean	std
Peak NDVI Inter-annual Ave. †	0.700	0.157	0.776	0.051	0.768	0.050
Peak NDVI Inter-annual SD †	0.062	0.035	0.048	0.015	0.051	0.018
Heat Load Index (HLI) †	5,253	1,322	5,228	1,143	5,103	998
Topographic Position Index (TPI) †	0.47	0.11	0.47	0.06	0.47	0.09
Dissection †	0.47	0.16	0.47	0.08	0.47	0.14
Compound Topographic Index (CTI) †	7.1	1.9	7.3	1.1	7.6	1.1
Surface Curvature †	-0.01	2.12	-0.42	0.92	-0.37	0.98
Slope (°)†	13.2	10.9	11.9	7.1	9.8	5.6
Slope Position †	0.2	216.3	-44.2	133.9	-113.6	126.2
Soil Organic Carbon Top 2m (kg/m ²) *	7.3	9.8	5.3	6.6	10.0	10.1
Soil Organic Carbon Top 3m (kg/m ²) *	8.1	11.1	5.9	7.2	11.1	11.0
Surface Organic Depth (cm) †	9.0	5.7	10.9	4.4	11.3	4.7
pH †	5.4	0.9	5.1	0.4	5.4	0.6

† Included in structural equation modelling (SEM)

Appendix 4. Extended Methods and Results for Chapter 4

A4.1 Extended Methods

A4.1.1 Study Region

Our study region spanned a gradient of arctic tundra and shrub landscapes abutting the forested, arctic-boreal ecotone, from the central portion of Alaska's Brooks Range mountains westward through the Noatak Basin to the Mission Lowlands, near the Noatak River delta (Figure A4.1.1). This periglacial landscape is within the continuous permafrost zone (Jorgenson et al. 2008) and is part of Arctic Bioclimate Subzone E (CAVM-Team 2003). The study region extended 63,707 km², which is slightly larger than the state of West Virginia, and covered Gates of the Arctic National Park and Preserve and Noatak National Preserve.

The central Brooks Range transitions from Mt. Igikpak (2523 m), through mountains and foothills, to glacially-sculpted valley bottoms containing major rivers flowing radially outward to the north, south, and west. The Noatak River Basin begins in the central Brooks Range and flows 730 km along a westward course at approximately 67.5° N latitude within the western sub-ranges of the Brooks Range (Figure A4.1.1), and is recognized as a UNESCO Biosphere Reserve. Physiographic provinces include high mountains of the central Brooks Range, through foothills, valley bottoms and the Aniuk Lowland westward, entering the broad, Mission Lowland at the arctic/boreal ecotone near the Noatak mouth (Wahrhaftig 1965, Young 1974).

The study region was periodically glaciated throughout the Pleistocene and contains a patchwork of glacial and periglacial landscapes dating from early Pleistocene to present times (Hamilton 2010, Hamilton and Labay 2011). Alpine physiographic provinces contain significant expanses of exposed bedrock at high elevations, with upper toe slopes covered by thin, often colluvially mixed and re-deposited soils derived from loess, weathered bedrock, and drift, with local pockets of active solifluction (Young 1974, Jorgenson et al. 2010, Hamilton and Labay 2011). Mountain valley bottoms are primarily underlain by late Pleistocene glacial drift deposits with adjacent ice-contact features, terraces, glacial inwash and outwash. Areas of solifluction become larger and more common with decreasing elevation, and modern alluvium prevails along narrow, contemporary river corridors at lower elevations where mountains grade to foothills (Hamilton 2010, Hamilton and Labay 2011). Rounded foothills interspersed with upland valleys, most of which were overtopped by Pleistocene glaciers, contain a mixture of thin soil deposits over near-surface bedrock on hilltops, below which are loess and middle and late Pleistocene glacial drift, with glacial outwash common at drift deposit margins (Young 1974, Hamilton 2010, Jorgenson et al. 2010, Hamilton and Labay 2011). Lowland physiographic provinces (Wahrhaftig 1965)

are characterized by extensive lateral, recessional, and terminal ice-cored moraines, as well as kettle topography, all associated with middle and late Pleistocene glacial drift surfaces. Lowland valley bottoms are commonly over-draped with expansive, deep, ice-rich glaciolacustrine deposits from extensive and long-lived, Pleistocene proglacial lakes (Hamilton 2009, 2010, Balsler et al. 2015). Glaciolacustrine deposits become thinner along a gradient from lowland valley bottoms rising toward glacially rounded foothills, and large outwash deposits may abut terminal and recessional moraines. Modern alluvium covers broad, meandering river corridors, frequently bounded by bluffs of glacial drift and glaciolacustrine deposits exposed through millennia of erosional down-cutting (Hamilton 2009, 2010). A loess cap of variable thickness is common throughout these landscapes (Jorgenson et al. 2010, Balsler et al. 2015).

The study region is within the zone of climate-driven, ecosystem-modified permafrost (Shur and Jorgenson 2007), with ground ice conditions suitable for ALD and RTS processes dispersed among landscapes throughout the region. In alpine terrain, upper permafrost in thin soils over near-surface bedrock is primarily syngenetic (French and Shur 2010). Segregated ground ice exceeding 30% by volume, comprised mainly of ataxitic and reticulate cryostructures, has been observed in the top meter of permafrost in these locations (Balsler et al. 2015). An ice-rich intermediate layer (Shur 1988, Shur et al. 2005), with an ice layer of several centimeters at the interface of the active layer and permafrost table may also be present across hill slopes (Balsler et al. 2015). Episodes of solifluction and colluvial re-deposition contribute to successive syngenetic permafrost development above buried soil surfaces, thickening both overall soil and permafrost through time (Balsler et al. 2015). Regional-scale ground ice estimates for these alpine areas range from low (<10%) to moderate (10%-40%) (Jorgenson et al. 2008).

At low elevations, permafrost of glacial and glaciolacustrine origin includes extensive deposits of deep, ice-rich, syngenetic and epigenetic permafrost, with massive ice deposits (Balsler et al. 2015). In the Mission and Aniuk Lowland, regional ground ice estimates range from moderate (10%-40%) to high (>40%) and include broad areas of active Holocene and inactive Pleistocene ice wedges (Young 1974, Jorgenson et al. 2008, Balsler et al. 2015) with deposits of relict glacial ice scattered throughout (Hamilton 2009, 2010). Late-Pleistocene glaciolacustrine deposits can be especially ice-rich (Balsler et al. 2015), as is common across the low arctic (Shur and Zhestkova 2003). Syngenetic cryofacies at the top of the permafrost table have been observed in these lowlands, often within a loess cap up to several decimeters thick (Balsler et al. 2015). Upper permafrost conditions may be highly variable, corresponding with surficial geology, landforms, vegetation, and glacial history (Hamilton 2009, 2010, Hamilton and Labay 2011, Balsler et al. 2015).

Permafrost in the foothills comprises an intermingling of conditions characteristic of alpine and lowland landscapes. Upper hill slopes include predominantly syngenetic cryofacies, periodically overtopped by solifluction and colluviation resulting in progressive permafrost aggradation, while lower slope positions may also include some ice wedges, relict glacial ice within Pleistocene drift, and older syngenetic permafrost associated with Pleistocene glaciolacustrine deposits (Young 1974, Balsler et al. 2015). There is no permafrost borehole monitoring within the study region, but adjacent boreholes to the north and south report average annual temperatures of -5°C and 1°C respectively, while mean annual air temperature estimates for the study region are -7°C to -12°C (Jorgenson et al. 2008).

Land cover comprises a broad suite of vegetation in various landscape settings including arctic and alpine tundra, shrublands, and lowland boreal forest along the arctic-boreal ecotone (Young 1974, Viereck et al. 1992, Parker 2006, Jorgenson et al. 2010). Thirty-six ecotypes have been identified and mapped within our study region (Jorgenson et al. 2010), with more than 50% of the land surface covered by shrub-graminoid ecotypes. Alpine and arctic dwarf shrub tundras are most prevalent at the highest elevations, and within north-draining watersheds, while low shrub, tall shrub, and tussock tundras are common in mid-elevation valleys and throughout the Noatak Basin. Lowland valleys within the southwest portion and along the southern boundary of the study region are part of the arctic-boreal ecotone, and include open and closed stands of conifer and broadleaf species along floodplains (Young 1974, Viereck et al. 1992, Parker 2006, Jorgenson et al. 2010).

Differing lithologies have been strongly linked with soil properties within the study region. Carbonate, non-carbonate, mafic and ultramafic lithologies are correlated with differences in soil development, soil chemistry, and grain size proportions (Jorgenson et al. 2010). These are in turn linked with vegetation, and with surface organic depth (Jorgenson et al. 2010). These factors are known to influence permafrost characteristics (Davis 2001, Shur and Jorgenson 2007), though the full extent of these influences has not been reported for the study region. We suspect that lithology exerts more influence in upland settings where a larger proportion of surfaces derive from the adjacent and underlying bedrock, compared with lowlands containing extensive deposits mixed origin transported from elsewhere through glacial and periglacial processes.

Generally, upland hill slopes with an ice-rich intermediate layer may be more favorable for active layer detachment sliding, while lowlands of glacial and glaciolacustrine origin offer prime settings for retrogressive thaw slump development, but these relationships are not obligate. RTSs are widespread along lowland lake margins, river banks, and bluffs. However, they can also occur in upland settings, often where an ALD has exposed the upper permafrost, and prior, episodic colluviation has accumulated a

layer of ice-rich, syngenetic, upper permafrost which is more than 2 m deep and vulnerable to sustained, retrogressive thaw slumping (Hamilton 2009, Swanson 2010, Swanson and Hill 2010, Balsler et al. 2014). ALDs are most frequently found on broad, upland hill slopes, but have also been observed in lowlands, typically adjacent to river bluffs on mild slopes where an ice-rich intermediate layer has developed (Balsler et al. 2009, Gooseff et al. 2009, Swanson 2010, Balsler et al. 2014).

Overall, conditions throughout the study region represent a broad range of typical low-arctic landscapes. Alpine, foothill, and valley bottom settings include many characteristic ecotypes of the North American low arctic, a suite of periglacial landforms, diverse lithologies, and a broad continuum of permafrost characteristics and cryofacies. Our study deliberately included this breadth of conditions over a large geographic area to represent a diversity of low-arctic landscapes.

A4.1.2 Overview of terrain suitability analysis

A conceptual diagram (Figure A4.1.2) depicts our initial, general hypothesis for inter-relationships among landscape characteristics of terrain suitability for ALD and RTS development in the central and western Brooks Range of northern Alaska. This diagram directed our approach and was iteratively tested and refined, with final terrain suitability estimates for the study region derived from the results.

Terrain suitability analysis and estimation involved four primary stages: 1) collection and preparation of input data, 2) integrated terrain unit (ITU) analysis, 3) structural equation modeling (SEM) analysis, and 4) terrain suitability estimation combining ITU and SEM results. Input data included a geodatabase of ALD and RTS locations (Table A4.1.1 and Appendix 5), and spatial data layers of categorical and continuous data covering the entire study region (Table A4.1.1). The study region boundary was defined by the geographic intersection of spatial data available for the region (Table A4.1.1 and Figure A4.1.1). All spatial data were clipped to the study region boundary, and landscape metrics were derived from continuous data (Table A4.1.2).

ITU and SEM analyses identified drivers, and relationships among drivers for terrain suitability, and were conducted separately for ALD and RTS features (Figure A4.1.3). The combined ITU and SEM results were used to produce a final dataset of estimated terrain suitability for each of the two feature types. Terrain suitability threshold values were calculated for each type of feature, and used to delineate areas of suitable and highly suitable terrain, by which landscape properties were summarized and tabulated from spatial data (Table A4.1.1 and Table A4.1.2).

A4.1.3. Steps for terrain suitability analysis and estimation

A4.1.3.1 Collection and preparation of input data

Feature locations

Aircraft-supported field campaigns and airphoto surveys in 2006, 2007, 2010, and 2011 were used to map active layer detachment slides and retrogressive thaw slumps in the Noatak Basin. Initial fixed-wing surveys were used to identify the general distribution of RTSs and ALDs within the study area, and subsequent helicopter-supported surveys were used to mark the location of features in the field by GPS. Vertical aerial photography for areas with dense feature distributions was acquired using a Nikon D2X digital camera mounted beneath a small, fixed-wing aircraft. Airphoto lines were digitally stitched together, then manually georectified against pan-sharpened Landsat TM satellite ortho-imagery (Balser et al. 2009). Each feature location was manually marked within airphoto coverage. Our initial geodatabase of ALDs and RTSs in the Noatak Basin was expanded and augmented through a subsequent National Park Service survey, which included both Gates of the Arctic National Park and Preserve and Noatak National Preserve, using high-resolution satellite imagery to census these features throughout both park units (Figure A4.1.4; Balser et al. 2009, Swanson and Hill 2010). Randomly assigned control point locations were generated throughout the study region to represent areas without RTS or ALD features. Randomly generated points that fell within 200 m of mapped features were considered co-located with those features and were excluded. Separate datasets were constructed for ALDs and RTSs respectively, with each dataset containing mapped feature locations and an equal number of randomly generated control point locations.

Landscape properties and metrics

We used thematic spatial datasets covering the entire study region that included both categorical and continuous data, deriving additional analysis variables from the continuous data (Table A4.1.1). Categorical data used in terrain unit analysis included lithology, surficial (glacial) geology, and ecotype. Lithology data were drawn from mapped eco-subsections for the region, following the National Hierarchical Framework for Ecological Units (ECOMAP 1993, Cleland et al. 1997, Jorgenson et al. 2001), and were grouped as either ‘carbonate’ or non-carbonate’ for analysis. Glacial (surficial) geology was mapped at a scale of 1:250,000 from compiled reports and field surveys conducted throughout the study region over the course of several decades (Hamilton 2010, Hamilton and Labay 2011). For analysis, surficial geologic units were summarized by surficial deposit type (e.g. glacial drift, colluvium, alluvium) as presented by the authors. Ecotypes were mapped with Landsat ETM+ imagery from mapping algorithms trained and validated using extensive field data from the study region (Jorgenson et

al. 2010). Grid cells were resampled from their original 30 m cell size to 60 m cell size using the nearest neighbor method, but ecotype data were not thematically summarized for our analyses.

Two sources of continuous data were used to derive additional metrics used in SEM analysis (Table A4.1.1): 1) The National Elevation Dataset (NED) distributed by the U.S. Geological Survey (Gesch et al. 2002), and 2) monthly normalized difference vegetation index (NDVI) values, calculated from Moderate-resolution Imaging Spectrometer data by the U.S. Geological Survey for the 2000-2013 timespan (Jenkerson et al. 2010). Geomorphologic, topographic and hydrologic derivatives were calculated from the NED (Table A4.1.2), and included compound topographic index (Moore et al. 1993), surface curvature (McNab 1993), dissection (Evans 1972), topographic position index (Jenness 2006), heat load index (McCune and Keon 2002), and slope position. Elevation, not derived but taken directly from the NED data, was also used. Monthly NDVI data from 2000-2013 were first analyzed on an annual basis to extract peak growing season NDVI values for each pixel in the study region for each year. Next, these annual peak NDVI datasets were statistically summarized across all years (excluding 2000, which had incomplete data) to produce decadal values for peak growing season NDVI (Table A4.1.2). Variables were derived using ERDAS Imagine 2011, and using ArcGIS 9.3 and 10.1 software, including the “Geomorphometric and Gradient Metrics Toolbox” (Cushman et al. 2010, Evans et al. 2013). Values for derived variables were standardized prior to inclusion in SEM runs.

A4.1.3.2 Integrated terrain unit analysis

Integrated terrain unit analyses were conducted using ArcGIS 9.3 for ALD and RTS feature distribution among landscape units within lithology, ecotype and glacial geology data layers (Figure A4.1.3). Values for each landscape unit within each data layer were extracted using ALD and RTS locations from the geodatabase, then tabulated to examine feature distribution among landscape units. Percentage feature distribution across units was compared with areal percentages of units within the study region, and a differential between them was calculated for each unit. Differentials were calculated as the percentage feature distribution of each unit divided by the study area percentage of that unit. These differentials informed unit weights assigned to each landscape unit within each data layer for ALD and RTS features, respectively (Table A4.1.3). Landscape unit types consisting of exposed bedrock, open water, and snow from the ecotype layer, and active glacier/snowfield from the glacial geology layer, were considered obligate unsuitable for ALD and RTS features, and were automatically weighted to 0. The unit weights for ecotype, surficial geology and lithology were then combined with the result scaled 0 to 100, producing an ITU-derived terrain suitability estimate layer for ALD features and a separate ITU-derived terrain suitability estimate layer for RTS features throughout the study region.

A4.1.3.3 Structural equation modelling

SEM was used to test and refine our hypothesized conceptual model of inter-relationships influencing terrain suitability, and incorporated both observed and latent variables (Grace 2006). Structural equation modeling (SEM) was used to iteratively test hypothesized relationships among numeric landscape variables as drivers of terrain suitability for ALD and RTS processes (Figure A4.1.3). SEM is a statistically rigorous method designed to test and refine hypothesized complex, causal inter-relationships in cases where measured observations may not be available for all factors perceived relevant in the modeled relationships (Grace 2006). The technique has been employed effectively in ecosystems research including spatially explicit applications, and within arctic and boreal settings (Johnstone et al. 2009, Lamb et al. 2014). Factors not fully defined by existing measurements are termed ‘latent variables’ (Grace 2006). These may either be single, well-defined factors for which measurements are not available, or they may comprise combined landscape properties (e.g. permafrost conditions) where some contributing factors are both measured and known, while others may be known but unmeasured, or if it is suspected that factors beyond those identified may be relevant. It should be noted that this is distinct from what are termed ‘composite’ variables; variables comprised of multiple properties for which all properties are known, measured and accounted for. This approach allows a conceptual hypothesis to be tested and modified in the absence of complete data for all relevant factors (Grace 2006). In our models, all exogenous variables (those not a product of processes represented in the model) were observed, all endogenous variables (those influenced by processes within the model) were latent, and no composite variables were used.

Analyses were conducted separately for ALD and RTS datasets using the Lavaan 0.5-16 package written for R statistical software (Rosseel 2012). All variables used in SEM analyses were assessed against each other prior to SEM runs using Pearson correlation coefficients, calculated from all values throughout the study region (Table A4.1.4 and Figure A4.1.1). Pairs of variables with Pearson correlation coefficients greater than 0.7 were not used simultaneously in any of the analysis iterations. Each variable was also examined for statistical distribution (normal vs. non-normal) to determine the appropriate statistical estimator for analysis.

Numeric data for SEM runs (Table A4.1.1 and Table A4.1.2) were extracted using locations in the feature and control point datasets. Feature and control locations were used as response variables, where features were assigned a value of 100, while control locations were assigned 0. The weighted least squares estimator, also known as asymptotically distribution free, was chosen as the estimator for all analyses in Lavaan due to non-normal distribution of several numeric variables. Our response variable

was identified as ‘ordered’, the orthogonal option was set to ‘false’, as no latent variables were exogenous within our models. No prior weighting of variables was used.

SEM runs testing ALD and RTS terrain suitability drivers used our hypothesized conceptual model (Figure A4.1.2) as the starting structural equation model. The model was iteratively refined using output fit metrics, and R^2 values generated for each variable (Joreskog and Sorbom 1996, Grace 2006, Hooper et al. 2008). Each model run was evaluated using recommended ‘good-fit’ thresholds for four SEM fit metrics: 1) compound fit index, 2) Tucker-Lewis fit index, 3) root mean square error of approximation and 4) standardized root mean square residual (Hooper et al. 2008). Variables were placed within the model based upon their group (Figure A4.1.2 and Table A4.1.2). Selection of variables used in models and in model diagrams was refined through subsequent runs until all four fit metrics indicated good model fit, with the best fitting model used as the final model for ALDs and RTSs respectively. Final models were bootstrapped to confirm good model fit, and to generate multi-run, averaged coefficients and intercepts for each exogenous and latent variable. Coefficients and intercepts were plugged into the final model diagram for each feature type, and run within ArcGIS 9.3 with data for the entire study region to produce SEM-based terrain suitability estimate layers, scaled 0 to 100, for ALD and RTS features separately.

A4.1.3.4 Final terrain suitability estimates (combined ITU and SEM results)

Terrain suitability estimates derived from independent ITU and SEM results were combined within ArcGIS 9.3 to create final terrain suitability estimates for ALD and RTS features (Figure A4.1.3). For each feature type, ITU-derived estimates were multiplied by SEM-derived estimates, and the result scaled 0 to 100. These final estimates were packaged as a two-band image for color composite display, with ALD terrain suitability as band 1, and RTS terrain suitability as band 2.

A4.1.3.5 Terrain suitability thresholds

Numeric thresholds were used to delineate areas of suitable and highly suitable terrain for each feature type, enabling calculations of areal extent and comparative summaries of landscape properties within suitable and highly suitable terrain for each feature type (Figure A4.1.3). Final terrain suitability estimate values for each feature type were extracted using the ALD and the RTS point location datasets. Mean and standard deviation of terrain suitability values were calculated for the extracted ALD and RTS feature locations. ‘Suitable terrain’ was defined as all terrain with values greater than or equal to one standard deviation below the mean value at feature locations, per feature type. ‘Highly suitable terrain’ was defined as terrain with values greater than or equal to the mean value for each feature type.

A4.1.4 Landscape properties by terrain suitability

Suitable and highly suitable terrain areas were extracted as new spatial data layers from the final ALD and RTS terrain suitability datasets to characterize suitable landscapes (Figure A4.1.3). Areal extent for each suitability level was calculated, and the suitability data layers were used to clip thematic, spatial datasets used in the prior analyses, and also to clip ancillary datasets of soil carbon estimates (Hugelius et al. 2013) and decadal temperatures (SNAP 2014). Highly suitable terrain was extracted as a subset of suitable terrain, and does not represent additional area.

A4.2. Extended results

A4.2.1 Final terrain suitability estimates

Terrain suitability estimates for feature formation in the study region (Figure A4.2.5) include large areas of terrain generally unsuited to either retrogressive thaw slump or active layer detachment processes, a significant area highly suited for both types of feature, and a continuum in between. Roughly half of the study region (51%) was estimated suitable for retrogressive thaw slumps, 35% was estimated suitable for active layer detachment slides, and 29% was estimated suitable for both, demonstrating significant overlap between RTS and ALD terrain suitability (Table A4.2.5 and Figure A4.2.6). Estimated area of highly suitable terrain was substantially lower than suitable terrain, at 24% for RTS features and 17% for ALD features (Table A4.2.5 and Figure A4.2.6), with 9% spatial overlap between highly suitable RTS and ALD terrain (Figures A4.2.6 and A4.2.7). ITU analyses produced slightly larger estimates of suitable terrain area than SEM analyses (Table A4.2.5 and Figure A4.2.6). The final model, combining ITU and SEM results, estimated significantly less suitable terrain area than either ITU or SEM alone (Table A4.2.5 and Figure A4.2.6), with partial spatial correspondence between ITU-derived and SEM-derived estimated areas (Table A4.2.6). Landscape properties related to vegetation, topography, hydrology, geomorphology, soil, and air temperature were correlated with observed ALD and RTS features, and also with estimated suitable terrain.

A4.2.2 Active layer detachment slide and retrogressive thaw slump terrain descriptions

Active layer detachment slides and retrogressive thaw slumps both occur across gradients of landscape conditions, yet some typical settings can be identified for each. In uplands, the most suitable ALD terrain frequently occurs across broad, generally smooth hill slopes, and is sometimes concentrated along upper toe slopes beneath exposures of non-carbonate bedrock on rounded foothills (Figure A4.2.8), where ALD features frequently appear in clusters. Soils are typically thin, over near-surface bedrock, and are frequently subject to periodic colluvial re-deposition. With increasing distance from the toe slope,

ALD suitability remains high or mildly attenuates, while RTS suitability typically rises as colluvial deposits containing ice-rich, syngenetic permafrost become deeper, and hill slopes include more geomorphic variability. Toward valley bottoms, especially in larger valleys, ALD suitability attenuates more sharply as RTS suitability rises. This often reflects rougher geomorphological landscape texture, as well as shifts toward glacial drift and ice-contact features near valley bottoms, where ice-wedges and relict glacial ice may contribute to the ground-ice content of permafrost, where kettle topography often develops, and where soil physical properties are more variable. Both ALD and RTS suitability may drop markedly in upland drainage bottoms, where deposits of modern alluvium, fans, glacial outwash, and aeolian sands may include minimal topographic and geomorphic variability, and / or offer poor conditions for development of ice-rich cryofacies. As a general toposequence, vegetation grades from moderately well-vegetated ericaceous and dryas dwarf shrub-graminoid tundras, through shrub-tussock and low shrub tundra on lower hillslopes, with riparian tall shrubs in valley bottoms. Small inclusions of wet-sedge meadow, coinciding with diffuse-flow watertracks, may be observed within larger patches of tundra ecotypes, primarily on mid and upper hillslopes, and have been noted as sites of ALD feature initiation (Balsler et al. 2009).

In lowland settings, ALD terrain suitability is highest on mild slopes on upper portions of rolling terrain, frequently underlain by glacial drift with a loess cap, where syngenetic cryostructures and an ice-rich intermediate layer may be prevalent near the permafrost table (Figure A4.2.9). Predominant ecotypes may include dwarf shrub tundra on hilltops flanked by low-shrub and shrub-tussock tundra on descending slopes. Inclusions of wet-sedge meadow within diffuse flow watertracks are rare or absent from these settings, though channelized-flow watertracks may be common. ALD suitability typically attenuates rapidly moving away downslope, though small patches of ALD terrain may sometimes be found near bluff tops. Suitable RTS terrain is widespread in lowland settings under a variety of conditions. On rolling, higher elevation terrain, patches of highly suitable RTS terrain appear where geomorphic features have begun forming from adjacent hydrothermal erosion, around margins of dispersed lakes, and in patches on mid-hillslopes. These patches frequently occur atop glacial drift or lacustrine and glaciolacustrine surfaces. RTS suitability generally increases toward lower slopes and valley bottoms, where deposits may include glacial drift, lacustrine and glaciolacustrine surfaces, ice-contact features, and occasionally where inactive alluvial surfaces sit atop these deposits. Landscape rugosity is generally high in these settings compared with suitable terrain elsewhere in the study region, and is often the result of kettle-forming processes. Predominant ecotypes include low-shrub and shrub-tussock tundras, though more ecotype variability is evident within suitable RTS terrain in these settings, with isolated pockets of white spruce forest included in suitable terrain primarily in the Mission Lowland in southwest portion of

the study region. Deep, ice-rich permafrost may be both extensive and heterogeneous in these areas, comprised of relict glacial ice, Pleistocene and Holocene ice-wedges, archaic syngenetic and epigenetic ice in lacustrine and glaciolacustrine sediments, cave ice, pore ice, and syngenetic cryofacies associated with contemporary soils and loess caps.

A4.2.3 Integrated terrain unit (ITU) analysis results

Distributions of ALD and RTS features within ecotype, glacial geology, and lithology units were disproportional to the areas of those landscape units within the study region (Table A4.2.7). Carbonate lithologies rarely contained features (< 2% of ALD features and < 1% of RTS features), though carbonate lithologies comprise > 10% of the landscape. Ultramafic lithologies were found to correspond with an analogous, exposed bedrock unit from the ecotype layer, which had already been masked out, and were thus excluded from further analysis as a discreet lithology unit. More than 95% of ALD features occurred on only three surficial geology units: thin soils over near-surface bedrock, colluvium, and glacial drift. Of these, occurrences within colluvium were the most disproportionate, containing 20% of ALD occurrences, while comprising only 7% of land area in the study region (Table A4.2.7). Disproportion of RTS feature distribution by glacial geology was slightly less pronounced, with 97% of features occurring across five glacial geology units: alluvium, thin soils over near-surface bedrock, colluvium, glacial drift, and lacustrine/glaciolacustrine. Of these, glacial drift was most disproportionate, hosting 46% of RTS features but comprising 16% of the land area in the study region (Table A4.2.7). ALD and RTS features were preferentially distributed among certain ecotypes as well, with the majority of both feature types occurring in three shrub tundra/shrub-tussock tundra units (Table A4.2.7). However, ALD and RTS features were more broadly distributed among ecotypes than among glacial geology or lithology units.

A4.2.4 Structural equation modeling (SEM) analysis results

Final SEM models, refined from the original hypothesis describing relationships influencing terrain suitability, incorporated geomorphological, topographic, and vegetative factors for both ALD and RTS features. The model representing the original hypothesis fell short of recommended good fit values for both ALD and RTS analyses by all four fit measures used. However, refined, final models for both feature types were estimated to have good fit by all four SEM fit metrics. For ALD features, the final model with best fit (Figure A4.2.10) incorporated the decadal average of inter-annual peak NDVI, the inter-annual variability of peak NDVI, heat load index, slope, slope position, topographic position index, and surface curvature. This model performed consistently well across ten bootstrap runs, with only three individual fit values below the recommended good fit threshold, and all mean values across runs exceeding the threshold for good fit (Table A4.2.8). The strongest influences on ALD model fit were

vegetative (average and variability of inter-annual peak NDVI) and topographic (slope position; Table A4.2.9 and Figure A4.2.10). The final model for RTS features (Figure A4.2.11) incorporated variability of inter-annual peak NDVI, topographic position index, dissection, compound topographic index, slope position and heat load index. This model also incorporated a latent variable for upper permafrost and active layer conditions, comprised of both geomorphological and vegetative factors. The final RTS model produced good fit values across all metrics for all bootstrap runs, with mean fit values well in excess of recommended thresholds (Table A4.2.8). Geomorphologic (dissection and topographic position index) and topographic (slope position) factors exerted greatest influence on the model (Table A4.2.9). Within the final SEM results, the influence of each individual variable, and of each groups of variables, differed appreciably. However, iterative testing revealed that good model fit could not be achieved for either ALD or RTS features in absence of any one of the variable groups of vegetation, topography or geomorphology; each was necessary in some form to support an explanatory relationship in the model.

A4.2.5 Terrain suitability values and thresholds

All terrain suitability estimates (ITU, SEM and combined) included overlapping values between observed features and control point locations, with values at feature locations skewed toward higher suitability and with control point locations skewed toward low suitability. ITU-derived terrain suitability included an asymptotal distribution for the lowest suitability values of control point locations (Figure A4.2.12), mainly corresponding with areas masked as obligate unsuitable, while suitability values at ALD and RTS feature locations were normally distributed, and mainly within the highest 50% of estimated values (Figure A4.2.12). Estimated terrain suitability derived from SEM results was normally distributed for both feature locations and for control points, with feature locations skewed toward higher suitability values (Figure A4.2.12). Final, combined ITU and SEM terrain suitability estimates produced clear separation between feature location and control point values, with ALD features showing especially stark separation from control point locations (Figure A4.2.12). ITU analyses produced greater separation between features and control than SEM analyses for ALD features, while the opposite was true for RTS features. However, both ITU and SEM analyses contributed to separation from control for both ALD and RTS features (Figure A4.2.12). Thresholds for suitable and highly suitable terrain, as determined from the mean and standard deviation of values at observed feature locations, include overlap with values at control point locations (Figure A4.2.12).

A4.2.6 Landscape properties by final terrain suitability

Values for individual landscape properties, within suitable and highly suitable ALD and RTS estimated terrain, ranged from very different to very similar when compared with the entire study region,

though no single factor emerged as dominant. Glacial geology and lithology both contained landscape units disproportionately represented in suitable terrain compared with the study region (Table A4.2.10). Nearly all suitable and highly suitable terrain for both feature types occurred within non-carbonate lithologies, while three glacial geology units (thin soils over near-surface bedrock, colluvium and drift) accounted for almost all suitable ALD terrain, and four glacial geology units (thin soils over near-surface bedrock, colluvium, drift and lacustrine/glaciolacustrine) comprised 88% of suitable RTS terrain (Table A4.2.10). Over 90% of suitable ALD terrain falls within seven ecotypes, while 90% suitable RTS terrain occurs within eight ecotypes, of which more than 50% is within either dwarf shrub-tussock or low shrub tundra ecotypes (Table A4.2.11).

The suitable terrain area within individual landscape units was generally much less than the total area of those individual landscape units in the study region, with differing results between suitable ALD and RTS terrain. For example, thin soils over near-surface bedrock contained the single largest percentage of suitable terrain for both ALDs and RTSs, yet less than half of the total area of that unit within the study region was suitable for either feature type (Table A4.2.10 and Figure A4.2.13). Most of the total area of the upland dwarf birch tussock shrub ecotype was suitable for RTS features, but less than half of it was suitable for ALD features (Table A4.2.11 and Figure A4.2.13). For one landscape unit, the upland alder-willow tall shrub ecotype, more than half of the total area within the study region was not only suitable, but highly suitable, for both feature types, though this ecotype covered 2,528 km², comprising only 4% of the study region (Table A4.2.11 and Figure A4.2.13).

Suitable ALD terrain and suitable RTS terrain display separate trends toward certain combinations of landscape properties based on numeric variables representing geomorphology, topography and vegetation. Suitable ALD terrain (Table A4.2.12) tended toward mid-lower reaches of watersheds (slope position < 0), on well-vegetated surfaces with minimal inter-annual variability in peak growing-season greenness (inter-annual average peak NDVI > 0.7, inter-annual standard deviation of peak NDVI < 0.05), just below mid-hillslope locations (topographic position index just below 0.5), on very slightly concave surfaces (surface curvature just below 0). The subset of highly suitable ALD terrain shows sharp trends toward higher inter-annual variability in peak growing-season greenness, slope positions higher up in watersheds (slope position > 0), and mild trends toward more concave surfaces (Table A4.2.12). The trend toward higher peak NDVI variability is most likely driven by mixed pixels, since much of the most suitable ALD terrain occurs on well-vegetated surfaces immediately below exposed bedrock. The high variability then, is more a function of intra-sample mixing than of inter-annual variability in the vigor of the vegetation.

Suitable RTS terrain (Table A4.2.12) occurred primarily in lower portions of watersheds (slope position < 0), on well-vegetated surfaces with minimal inter-annual variability in peak growing-season greenness (inter-annual average peak NDVI > 0.7, inter-annual standard deviation of peak NDVI < 0.05), in lower portions of hillslope catenas with high soil wetness (high compound topographic index values), just below mid-hillslope locations (topographic position index at or just below 0.5), and at neither the top nor bottom of geomorphological features (dissection at or just below 0.5). The smaller subset of highly suitable RTS terrain included slightly higher values for NDVI, topographic position index, dissection and compound topographic index, and a significantly lower slope position (Table A4.2.12). Dissection and topographic position index (Table A4.1.2) shared a moderately strong, positive Pearson correlation coefficient across the entire study region (0.70; Table A4.1.4), but this positive correlation graded steadily downward through suitable RTS terrain (0.62), and highly suitable RTS terrain (0.58), to weakly negative when calculated only at RTS feature locations (-0.24). Most numeric landscape values for both suitable ALD and suitable RTS terrain were consistently different from the mean value for the study region, but still within one standard deviation of the mean value for the study region (Table A4.2.12), and were generally comparable with values extracted from observed feature locations (Table A4.2.13).

A4.3 References for extended methods and results

- Balser, A., M. N. Gooseff, J. Jones, and W. B. Bowden. 2009. Thermokarst distribution and relationships to landscape characteristics in the Feniak Lake region, Noatak National Preserve, Alaska; Final Report to the National Park Service, Arctic Network (ARCN). Fairbanks, AK.
- Balser, A. W., J. B. Jones, and R. Gens. 2014. Timing of Retrogressive Thaw Slump Initiation in the Noatak Basin, Northwest Alaska, USA. *Journal of Geophysical Research: Earth Surface*:2013JF002889.
- Balser, A. W., J. B. Jones, D. A. Walker, and M. T. Jorgenson. 2015. Relationship of Cryofacies, Surface and Subsurface Terrain Conditions in the Brooks Range and foothills of northern Alaska. PhD Dissertation, Chapter 3. University of Alaska Fairbanks, Fairbanks, AK.
- CAVM-Team. 2003. Circumpolar Arctic Vegetation Map, Scale 1:7,500,000. Conservation of Arctic Flora and Fauna (CAFF) Map No. 1. U.S. Fish and Wildlife Service, Anchorage, Alaska.
- Cleland, D. T., P. E. Avers, W. H. McNab, M. E. Jensen, R. G. Bailey, T. King, and W. E. Russell. 1997. National Hierarchical Framework of Ecological Units. Pages 181-200 in M. S. Boyce and A. Haney, editors. *Ecosystem Management Applications for Sustainable Forest and Wildlife Resources*. Yale University Press, New Haven, CT.

- Cushman, S. A., K. Gutzweiler, J. S. Evans, and K. McGarigal. 2010. The Gradient Paradigm: A conceptual and analytical framework for landscape ecology (Chapter 5). Pages 83-108 in S. A. H. Cushman, F., editor. *Spatial complexity, informatics, and wildlife conservation*. Springer, New York.
- Davis, N. 2001. *Permafrost: A Guide to Frozen Ground in Transition*. University of Alaska Press, Fairbanks, AK.
- ECOMAP. 1993. National Hierarchical Framework of Ecological Units. Page 20 pp. USDA Forest Service, Washington, DC.
- Evans, I. S. 1972. General geomorphometry, derivatives of altitude, and descriptive statistics. Pages 17-90 in R. J. Chorley, editor. *Spatial Analysis in Geomorphology*. Harper & Row, New York.
- Evans, J. S., J. Oakleaf, S. A. Cushman, and D. Theobald. 2013. A Toolbox for Surface Gradient Modeling, Available at: <http://evansmurphy.wix.com/evansspatial>. (in prep).
- French, H. and Y. Shur. 2010. The principles of cryostratigraphy. *Earth-Science Reviews* 101:190-206.
- Gesch, D., M. Oimoen, S. Greenlee, C. Nelson, M. Steuck, and D. Tyler. 2002. The National Elevation Dataset. *Photogrammetric Engineering and Remote Sensing* 68:5-+.
- Gooseff, M., A. Balser, W. Bowden, and J. Jones. 2009. Effects of hillslope thermokarst in northern Alaska. , 90: 29-31. *Eos, Transactions of the American Geophysical Union* 90:29-31.
- Grace, J. B. 2006. *Structural Equation Modeling and Natural Systems*. 1st edition. Cambridge University Press, Cambridge, UK.
- Hamilton, T. D. 2009. Guide to surficial geology and river-bluff exposures, Noatak National Preserve, northwestern Alaska: U.S. Geological Survey Scientific Investigations Report 2008-5125.
- Hamilton, T. D. 2010. Surficial Geologic Map of the Noatak National Preserve, Alaska. U.S. Geological Survey (in cooperation with U.S. National Park Service) Scientific Investigations Map 3036, 1 : 250,000 scale, and accompanying report:21p.
- Hamilton, T. D. and K. A. Labay. 2011. Surficial Geologic Map of the Gates of the Arctic National Park and Preserve, Alaska. U.S. Geological Survey (in cooperation with U.S. National Park Service) Scientific Investigations Map 3125, 1 : 300,000 scale, and accompanying report:19p.
- Hooper, D., J. Coughlan, and M. Mullen. 2008. Structural Equation Modelling: Guidelines for Determining Model Fit. *The Electronic Journal of Business Research Methods* 6:53-60.
- Hugelius, G., C. Tamocai, G. Broll, J. G. Canadell, P. Kuhry, and D. K. Swanson. 2013. The Northern Circumpolar Soil Carbon Database: spatially distributed datasets of soil coverage and soil carbon storage in the northern permafrost regions. *Earth Syst. Sci. Data* 5:3-13.
- Jenkerson, C. B., T. Maiersperger, and G. Schmidt. 2010. eMODIS: A user-friendly data source: U.S. Geological Survey Open-File Report 2010-1055, 10 p.

- Jenness, J. 2006. Topographic Position Index (tpi_jen.avx) extension for ArcView.
<http://www.jennessent.com/arcview/tpi.htm>.
- Johnstone, J., L. Boby, E. Tissier, M. Mack, D. Verbyla, and X. Walker. 2009. Postfire seed rain of black spruce, a semiserotinous conifer, in forests of interior Alaska. *Canadian Journal of Forest Research-Revue Canadienne De Recherche Forestiere* 39:1575-1588.
- Joreskog, K. G. and D. Sorbom. 1996. LISREL8: User's Reference Guide. Scientific Software International, Chicago, IL.
- Jorgenson, M. T., J. E. Roth, P. F. Miller, M. J. Macander, M. S. Duffy, A. F. Wells, G. V. Frost, and E. R. Pullman. 2010. An ecological land survey and landcover map of the Arctic Network. Natural Resource Technical Report NPS/ARC/NRTR—2009/270. National Park Service, Fort Collins, Colorado.
- Jorgenson, M. T., D. K. Swanson, and M. Macander. 2001. Ecological subsections of Noatak National Preserve. Final Report to the U.S. National Park Service, Fairbanks, AK. 73. ABR Inc.
- Jorgenson, T., K. Yoshikawa, V. Romanovsky, M. Kanevskiy, J. Brown, Y. Shur, S. Marchenko, G. Grosse, and B. Jones. 2008. Map of Permafrost Characteristics in Alaska. Proceedings of the Ninth International Conference on Permafrost (NICOP), Fairbanks, AK June 30 - July 4, 2008.
- Lamb, E. G., K. L. Mengersen, K. J. Stewart, U. Attanayake, and S. D. Siciliano. 2014. Spatially explicit structural equation modeling. *Ecology* 95:2434-2442.
- McCune, B. and D. Keon. 2002. Equations for potential annual direct incident radiation and heat load. *Journal of Vegetation Science* 13:603-606.
- McNab, W. H. 1993. A topographic index to quantify the effect of mesoscale landform on site productivity. *Canadian Journal of Forest Research* 23:1100-1107.
- Moore, I. D., P. E. Gessler, G. A. Nielsen, and G. A. Petersen. 1993. Terrain attributes: estimation methods and scale effects. Pages 189-214 *in* M. B. B. A.J. Jakeman, and M. McAleer, editor. *Modeling Change in Environmental Systems*. Wiley, London.
- Parker, C. L. 2006. Vascular plant inventory of Alaska's Arctic National Parklands: Bering Land Bridge National Preserve, Cape Krusenstern National Monument, Gates of the Arctic National Park & Preserve, Kobuk Valley National Preserve, and Noatak National Preserve. ARC/N I&M, National Park Service, Alaska Region Final Report:142p.
- Rosseel, Y. 2012. lavaan: AN R Package for Structural Equation Modeling. *Journal of Statistical Software* 48:1-36.
- Shur, Y., K. M. Hinkel, and F. E. Nelson. 2005. The transient layer: implications for geocryology and climate-change science. *Permafrost and Periglacial Processes* 16:5-17.
- Shur, Y. and T. Zhestkova. 2003. Cryogenic structure of a glacio-lacustrine deposit.

- Shur, Y. L. and M. T. Jorgenson. 2007. Patterns of Permafrost Formation and Degradation in Relation to Climate and Ecosystems. *Permafrost and Periglacial Processes* 18:7 - 19.
- SNAP. 2014. Historical (1910–1999) derived temperature products from CRU TS 3.0 climate data, downscaled to 771m via the delta method. Retrieved from: <https://www.snap.uaf.edu/tools/data-downloads>. *in* U. o. Alaska, editor.
- Swanson, D. K. 2010. Mapping of erosion features related to thaw of permafrost in Bering Land Bridge National Preserve, Cape Krusenstern National Monument, and Kobuk Valley National Park. Natural Resource Data Series NPS/ARC/NRDS—2010/122. National Park Service, Fort Collins, Colorado.
- Swanson, D. K. and K. Hill. 2010. Monitoring of Retrogressive Thaw Slumps in the Arctic Network, 2010 Baseline Data: Three-dimensional Modeling with Small-format Aerial Photographs. Page 58. U.S. Department of the Interior, National Park Service, Natural Resource Data Series NPS/ARC/NRDS—2010/123, Natural Resource Program Center, Fort Collins, CO.
- Viereck, L. A., C. T. Dyrness, A. R. Batten, and K. J. Wenzlick. 1992. The Alaska Vegetation Classification. Page 278 *in* U. S. D. o. A. F. Service, editor. Gen. Tech. Rep. PNW-GTR-286, Portland, OR.
- Wahrhaftig, C. 1965. Physiographic Divisions of Alaska. U.S.G.S. Professional Paper 482. 52 pp.
- Young, S. B. 1974. The environment of the Noatak River basin, Alaska., Contributions of the Center for Northern Studies, Wolcott, VT.

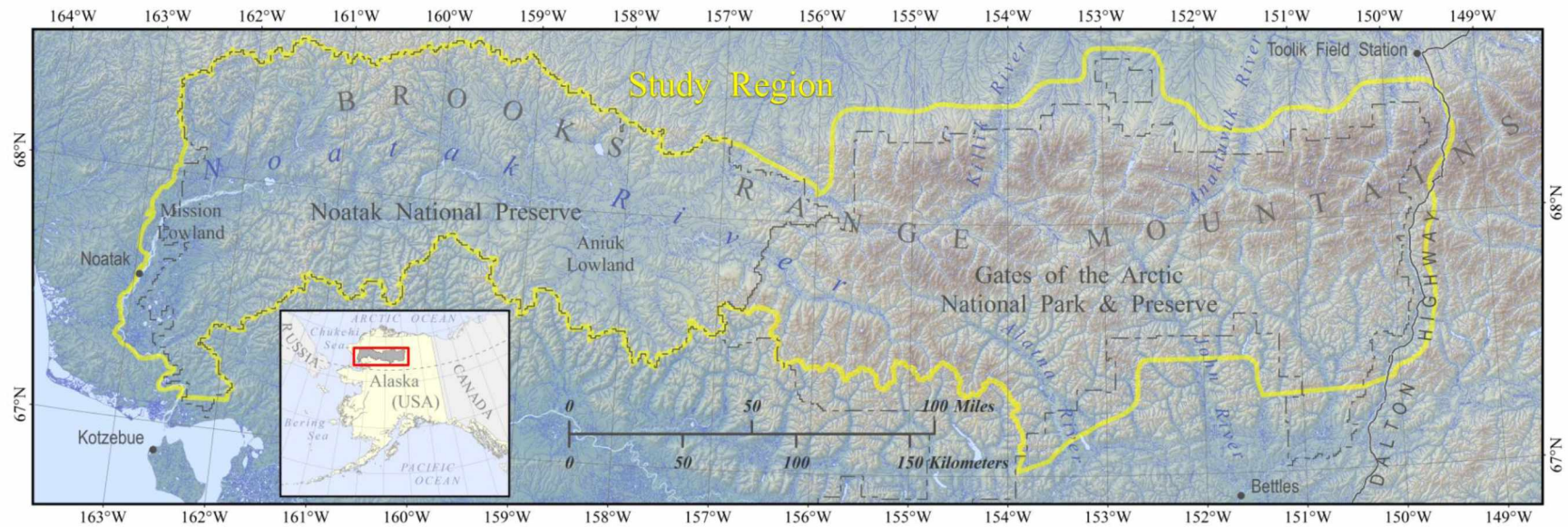


Figure A4.1.1. Map of the study region. The study region spans a physiographic gradient from the central portion of Alaska's Brooks Range mountains in Gates of the Arctic National Park and Preserve, westward through the Noatak River Basin in the Noatak National Preserve. Physiographic provinces include the high mountains of the Central Brooks Range in the eastern half of the study region through foothills and valley bottoms to the westward, with the broad, Mission Lowlands within the arctic/boreal ecotone near the Noatak mouth (Wahrhaftig, 1965). From the highest elevations (>2,000 m) in the Central Brooks Range, landscapes grade through foothills to glacially-sculpted valley bottoms containing major rivers emanating outward to the north, south and west. The study region boundary was determined by the geographic intersection of spatial datasets used in terrain suitability analyses.

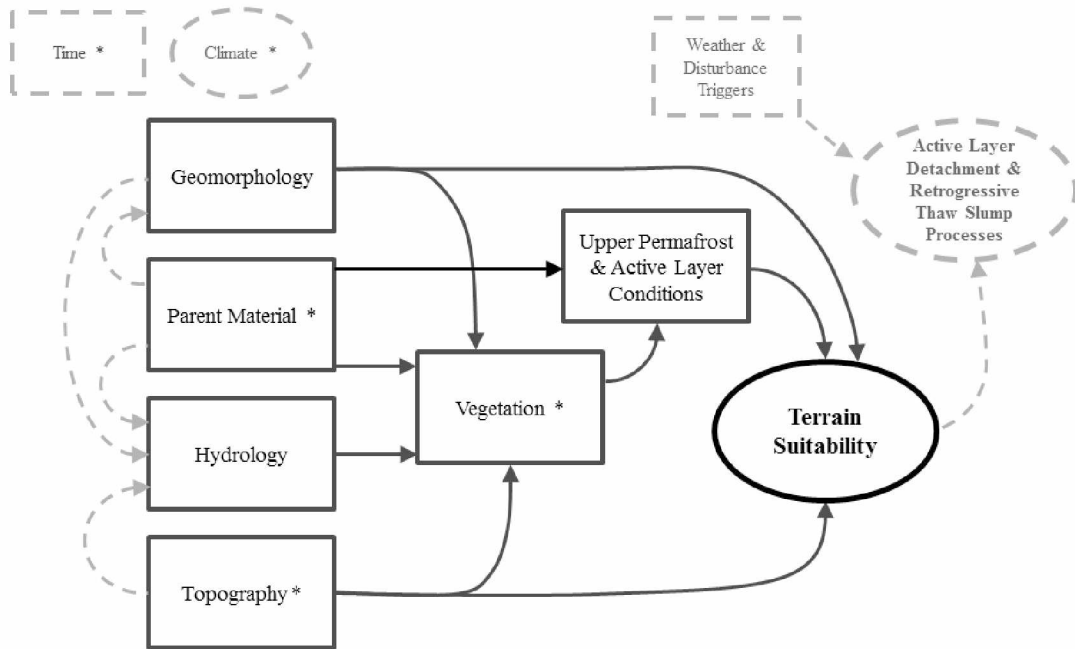


Figure A4.1.2. Conceptual Model. Initial conceptual model diagram of hypothesized landscape drivers of terrain suitability for active layer detachment slide (ALD) and retrogressive thaw slump (RTS) features. Boxes represent measurable variables; circles represent properties which include unknown factors. Dashed outlines and lines represent factors and relationships not included in the modeling analysis. Time and climate are considered drivers for all other properties and processes included in the diagram. The five State Factors (Jenny 1941); time, climate, parent material, topography, and biota are indicated with an *.

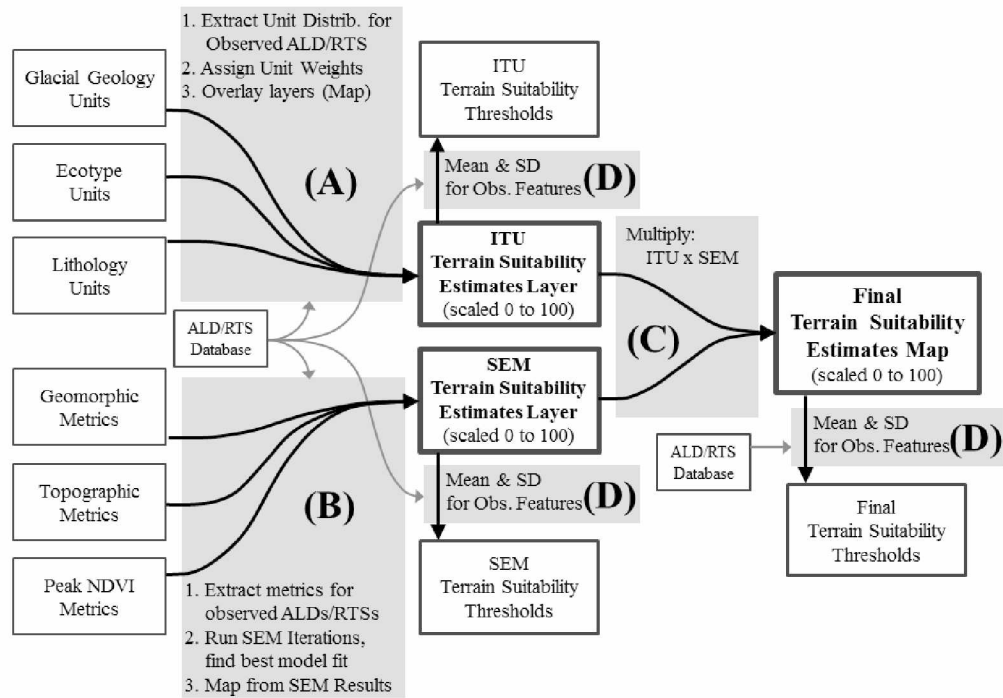


Figure A4.1.3. Overview of analysis approach for estimating active layer detachment slide (ALD) and retrogressive thaw slump (RTS) terrain suitability in the central and western Brooks Range, Alaska. Analysis included four general steps.

- E) Categorical landscape properties (glacial geology, ecotype and lithology) underwent point-in-polygon analysis with our database of observed ALD and RTS feature locations for integrated terrain unit (ITU) analysis within the study region. Analytical results were used to assign ALD and RTS weights to all categorical landscape units, which were then combined by overlay into two datasets: one for categorically-derived ALD terrain suitability estimates, and one for categorically-derived RTS terrain suitability estimates. Values were scaled 0 to 100, and the layers were rasterized to 60 m grid cells.
- F) Continuous, numeric variable values (derived from the National Elevation Dataset DEM and inter-annual MODIS NDVI data) were extracted for observed ALD and RTS locations, and for randomly-generated landscape control locations. These were run as structural equation model (SEM) iterations to find the model diagram with best fit for ALD and RTS features versus control respectively. Final SEM coefficients and intercepts were used to generate two datasets: one for SEM-derived ALD terrain suitability, and one for SEM-derived RTS terrain suitability.
- G) For each feature type (ALD vs RTS), terrain suitability results from A) ITU analysis and B) SEM analysis were scaled 0 to 100, then multiplied together. The resulting, combined (final) terrain suitability datasets (one for ALD and one for RTS) were then scaled 0 to 100.
- H) Estimated terrain suitability values from each raster dataset (ITU, SEM and combined; for ALD and RTS respectively), were extracted using observed feature locations. Mean and standard deviation of values at observed features were used to define suitability thresholds. ‘Suitable terrain’ was defined by values greater than one standard deviation below the mean for each feature type. ‘Highly suitable terrain’ was defined by values greater than the mean for each feature type.

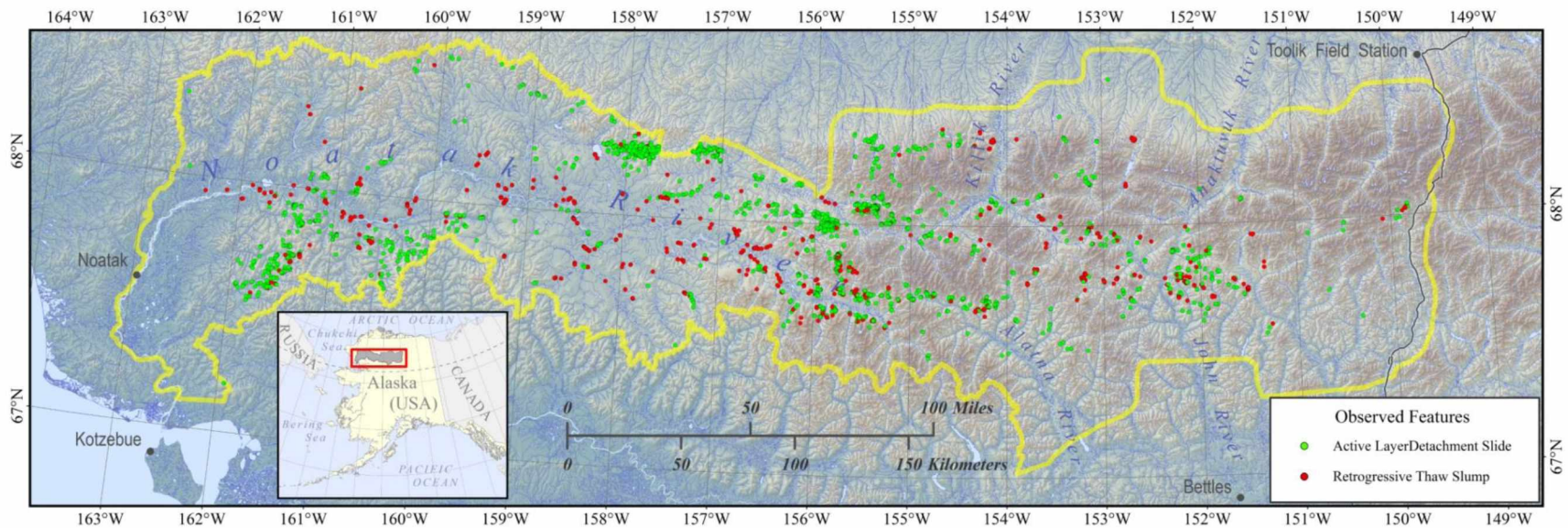


Figure A4.1.4. Observed active layer detachment slides and retrogressive thaw slumps within the study region in the western Brooks Range and foothills of northern Alaska. Feature locations derive from aerial photo analysis, and airborne and ground based field reconnaissance (Balser et al., 2009; Balser et al., 2014) and from high-resolution satellite image analysis by the National Park Service (Swanson & Hill, 2010). The analysis dataset contained 2492 active layer detachment slides and 805 retrogressive thaw slumps.

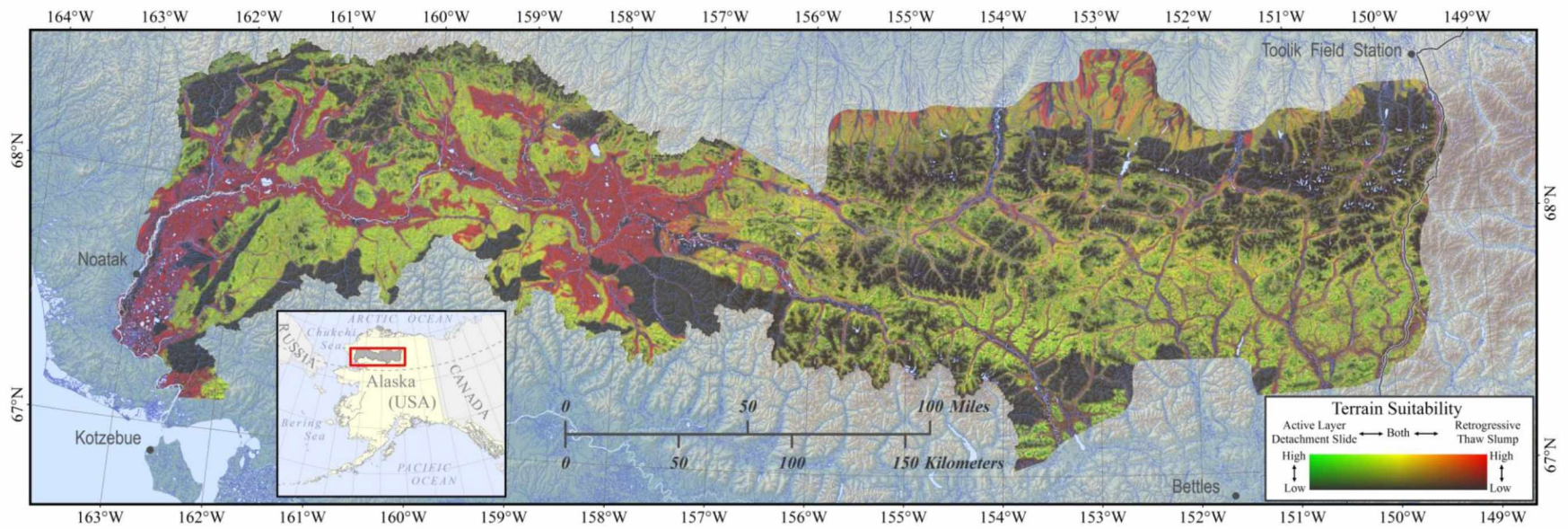


Figure A4.2.5. Estimated terrain suitability for active layer detachment slides (green) and retrogressive thaw slumps (red) for the study region in the western Brooks Range of northern Alaska.

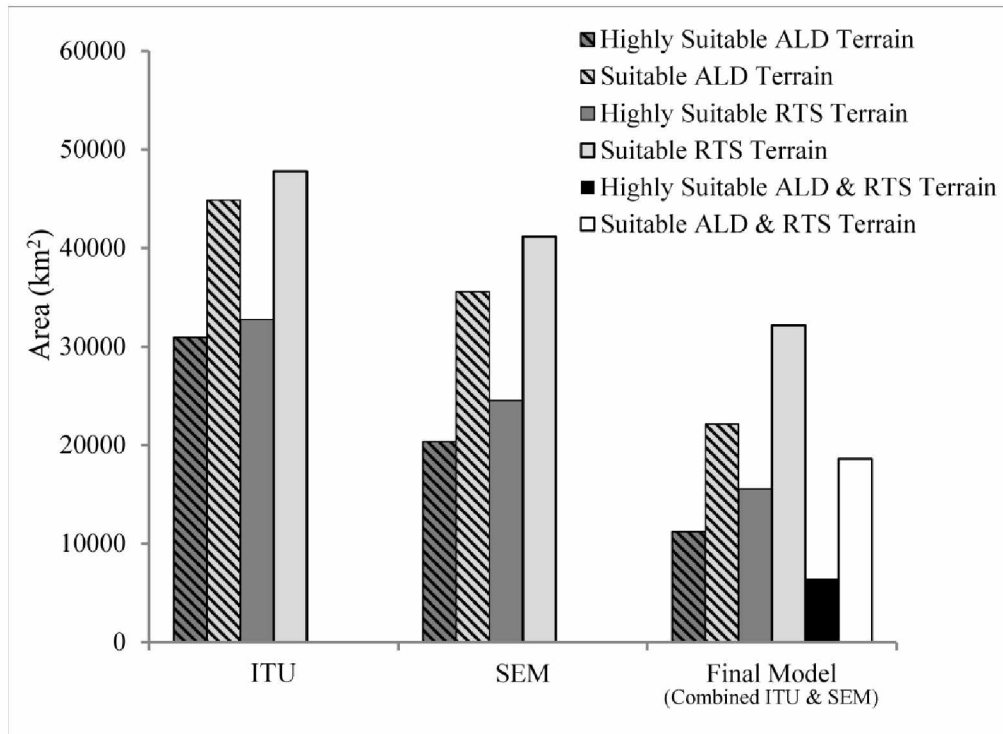


Figure A4.2.6. Areal estimates of suitability for active layer detachment (ALD) and retrogressive thaw slump (RTS) terrain from integrated terrain unit (ITU) analysis, structural equation modeling (SEM) analysis, and from the final, combined model. Estimated values at observed active layer detachment slide and retrogressive thaw slump features were used to define “suitable” and “highly suitable” terrain. “Suitable” was defined as estimated values greater than or equal to one standard deviation below the mean. “Highly suitable” was defined as estimated values greater than or equal to the mean. ALD and RTS terrain share significant overlap, as shown by bars representing terrain which is suitable/highly suitable for both ALD and RTS.

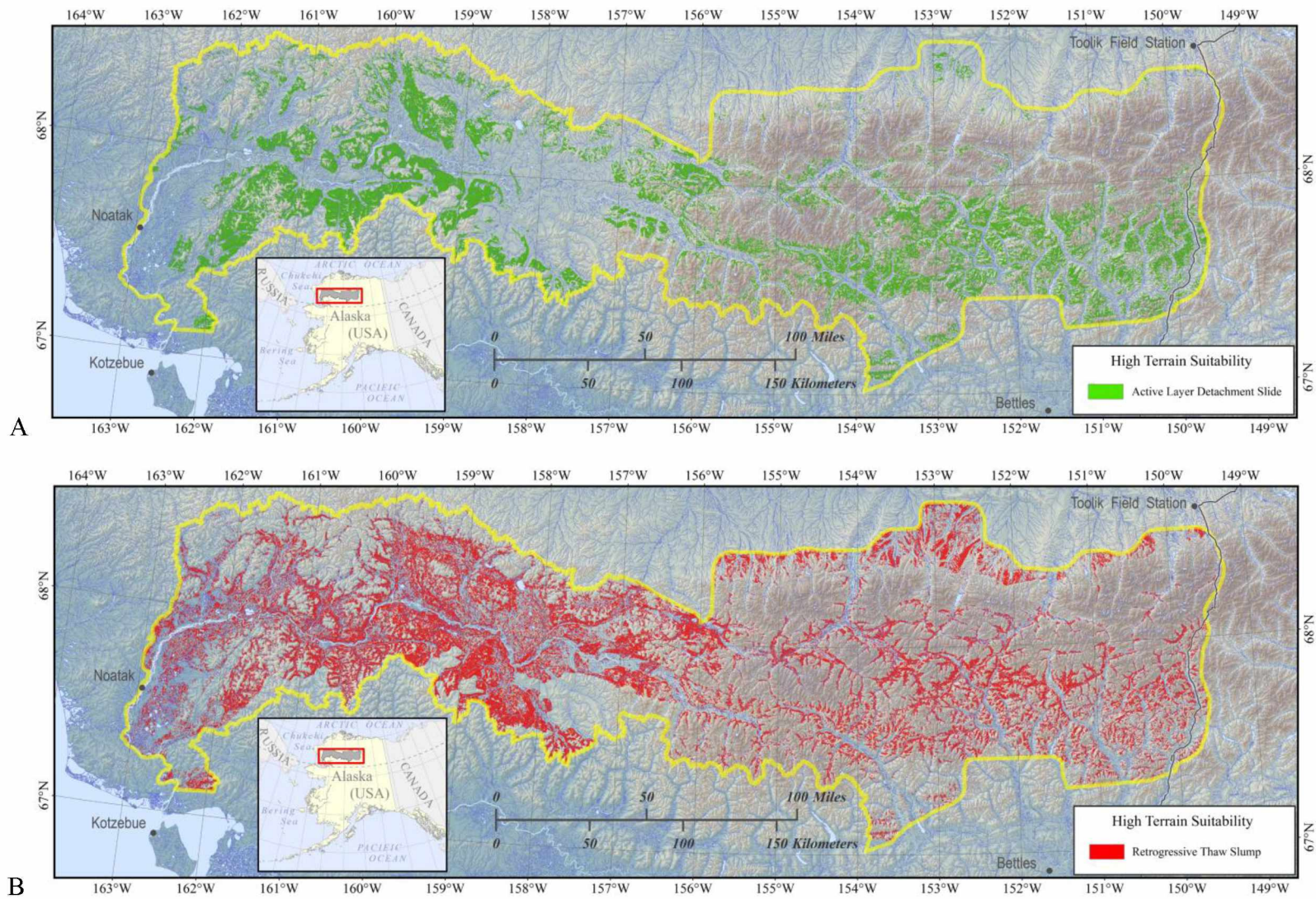


Figure A4.2.7. Areas estimated as highly suitable terrain for A) active layer detachment slides (green) and B) retrogressive thaw slumps (red) for the study region in the western Brooks Range of northern Alaska.

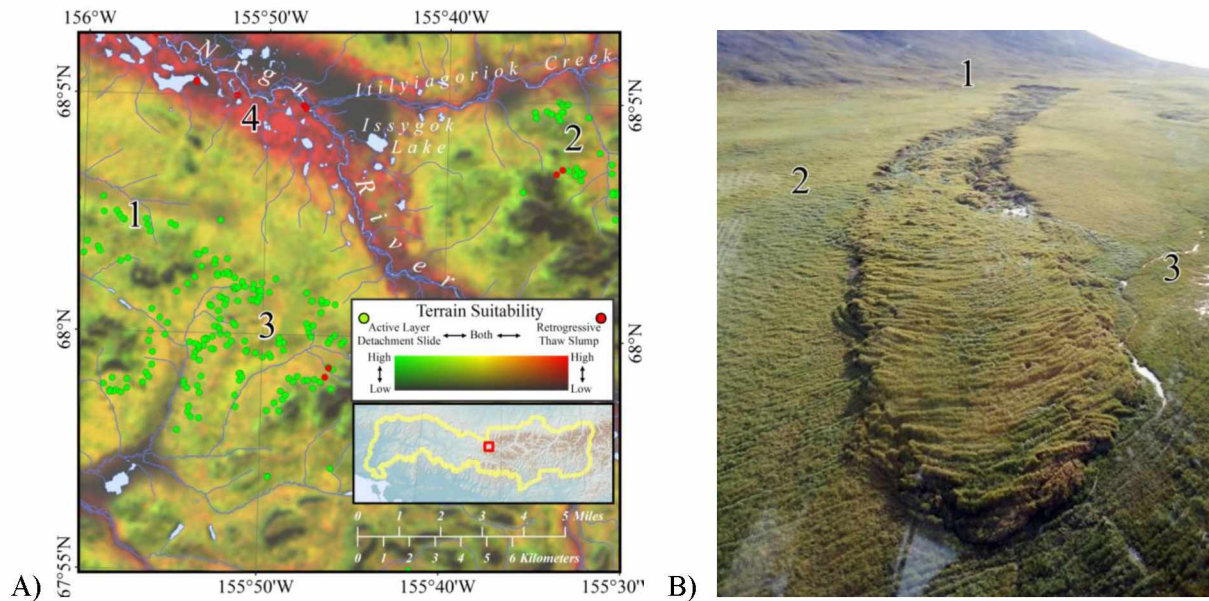


Figure A4.2.8. Active layer detachment slide (ALD) and retrogressive thaw slump (RTS) terrain suitability in an upland setting.

C) Estimated terrain suitability for active layer detachment slides (green) and retrogressive thaw slumps (red) and for both (yellow) near the headwaters of the Nigu River in the northwest portion of Gates of the Arctic National Park and Preserve, west-central Brooks Range, northern Alaska; (1) A cluster of active layer detachment slides within colluvial deposits (s), upslope of late-Pleistocene outwash deposits (io_1) (Hamilton, 2011), along a toe slope beneath exposed and partially-exposed, non-carbonate bedrock (Jorgenson et al., 2001), (dark, upland features on the map). The surface is generally smooth latitudinally across the hillslope, with some concavity longitudinally down the hillslope, where slope angle decreases slightly at the toe below exposed bedrock. Predominant ecotypes include upland birch-ericaceous-willow low shrub, upland dwarf birch-tussock shrub, and alpine ericaceous dwarf shrub (Jorgenson et al., 2010); (2) Similar conditions to (1), but the presence of several RTS features suggest locally deeper, ice-rich colluvial deposits where permafrost exposed by active layer detachment sliding is vulnerable to retrogressive thaw slumping; (3) Similar geomorphic conditions to (1) and (2), but underlain by a combination of thin soils over near-surface bedrock and late-Pleistocene glacial drift (id_1) (Hamilton, 2011), and with primarily alpine dryas dwarf shrub and upland birch-ericaceous-willow low shrub ecotypes (Jorgenson et al., 2010); (4) Retrogressive thaw slumps within valley-bottom, ice-contact, kame and kame terrace deposits (ik_3) and glacial drift (id_3), both of the late-Pleistocene (Hamilton, 2011). Small, mild hills interspersed with ponds and lakes characterize this kettle-lake area. Predominant ecotypes include upland dwarf birch-tussock tundra, upland birch-ericaceous-willow low shrub, lowland birch-ericaceous-willow low shrub and lowland sedge fen (Jorgenson et al., 2010).

D) Active layer detachment slides in thin deposits of upper hillslope colluvium, along (1) a toe slope below non-carbonate, exposed bedrock (micaeous shale) 50 km west of the map frame (A) in the upper Fauna Creek drainage in the Noatak Basin, northwest Alaska. The hill is a smooth, 6° slope, with tracks from migrating caribou visible across the hillslope at the bottom of the image. (2) Predominantly upland birch-ericaceous-willow low shrub, with graminoid cover $> 50\%$ over much of the area. (3) Wet sedge meadow along a watertrack below the feature. This active layer detachment is 483 m long from the headwall to the bottom of the run out, 58 m wide at the widest point, near the headwall, and 3.5 m deep at the deepest point, also near the headwall. Recorded at the headwall, the active layer depth was 110 cm deep, including a 33 cm organic layer, loess from 33 to 60 cm, and colluvially re-transported gravel (55%) and silt (45%) from 60 to 100 cm. Below the permafrost table, ice-rich, syngenetic permafrost is composed of segregated ice (50 to 70%, ataxitic and reticulate), gravel (25 to 35%), and silt (15 to 25%). These conditions continued to the bottom of the headwall profile at 248 cm. Photo: Andrew Balsler, 2011.

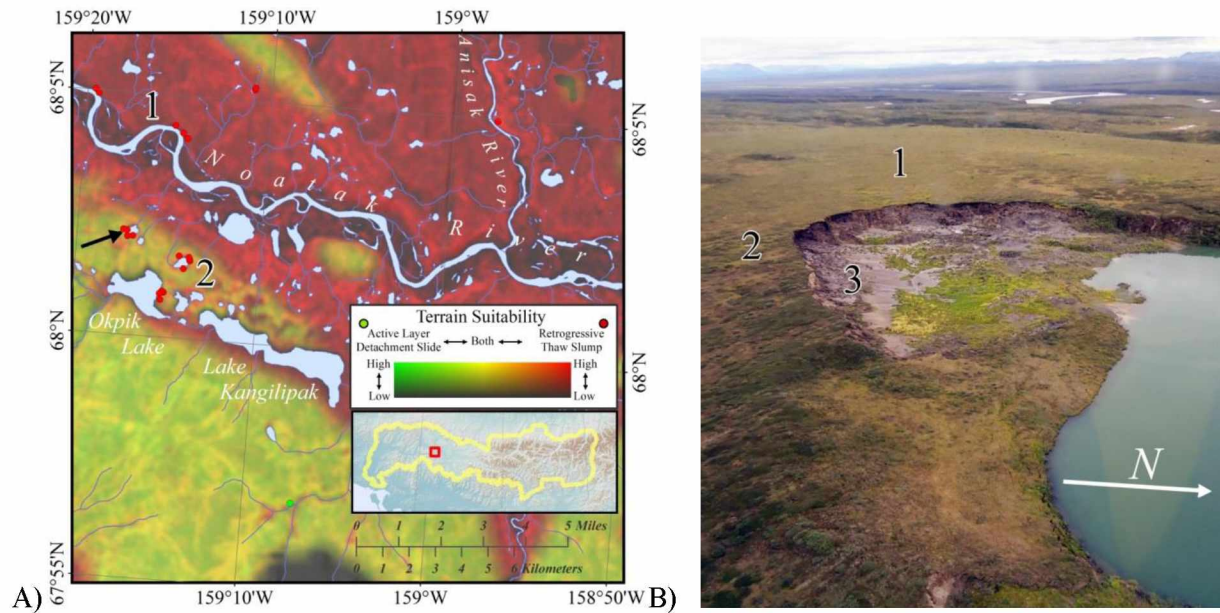


Figure A4.2.9. Active layer detachment slide (ALD) and retrogressive thaw slump (RTS) terrain suitability in a lowland setting.

A) Estimated terrain suitability for active layer detachment slides (green) and retrogressive thaw slumps (red) and both (yellow) at the western edge of the Aniuk Lowland, adjacent to the mainstem Noatak River in the Noatak National Preserve, northwest Alaska. (1) Retrogressive thaw slumps along a bluff adjacent to the Noatak River, within late-Pleistocene glaciolacustrine deposits (igl_{1B} and igl_2) which over-drape late-Pleistocene glacial drift deposits (id_{1B}) (Hamilton, 2010). Progressive down-cutting and hydro-thermal erosion since the Pleistocene have left a bluff complex 15 – 80 m tall (Hamilton, 2009) containing ice-rich, deep permafrost. Behind the bluff are mild hills and smaller geomorphic features among small ponds and lakes. Predominant ecotypes are upland dwarf birch-tussock shrub and upland birch-ericaceous-willow low shrub (Jorgenson et al., 2010). These conditions cover the majority of terrain north of the Noatak River within the map frame. (2) Retrogressive thaw slumps on the margins of kettle lakes within late-Pleistocene glacial drift deposits (id_{1B}). A patch of suitable ALD terrain is visible on a bluff top on the south side of the Noatak River, north of Lake Kangilipak and east of several, smaller lakes. Surface conditions include mild hills and smaller geomorphic features among small ponds and lakes, and predominant ecotypes are upland dwarf birch-tussock shrub and upland birch-ericaceous-willow low shrub (Jorgenson et al., 2010).

B) A retrogressive thaw slump on a kettle lake within a glacial drift deposit (id_{1B}), indicated by an arrow on the map (A). (1) Gently sloped hilltop just upslope of the retrogressive thaw slump with primarily dwarf and low shrub-tussock tundra ecotypes (Jorgenson et al., 2010). Geomorphic features become more pronounced approaching the Noatak River bluffs in the distance. (2) Mixed low shrub and dwarf shrub tundra ecotypes along a mid-hillslope with moderate, meso-scale geomorphic variability. Hill slope is roughly 9° . (3) Retrogressive thaw slump which has been active since at least 1980 (Balsler et al., 2014). Dimensions were 191 m at the widest point, 122 m long from the apex of the headwall to the end of the run out fan, and 18 m deep at the deepest location along the headwall, with the headwall retreating roughly 12 m between the summers of 2006 and 2011. Deposits within the headwall are comprised of 60% massive ice, where roughly two thirds are Pleistocene and Holocene ice wedges, and roughly one third is relict glacial ice. The widest deposit of massive ice was 2.5 m across. The glacial drift included up to 55% angular and sub-angular coarse fragments, at clast sizes from gravel up to boulders of over 50 cm. Within 1 m of the surface, deposits were composed of Aeolian loess and sand (> 1 m), active layer depth of roughly 45 cm, with primarily pore and lenticular ice and occasional pockets of reticulate ice below the permafrost table. The surface was covered with a relatively thin organic layer (roughly 4 cm) (Balsler et al., 2015). Photo: Andrew Balsler, 2010.

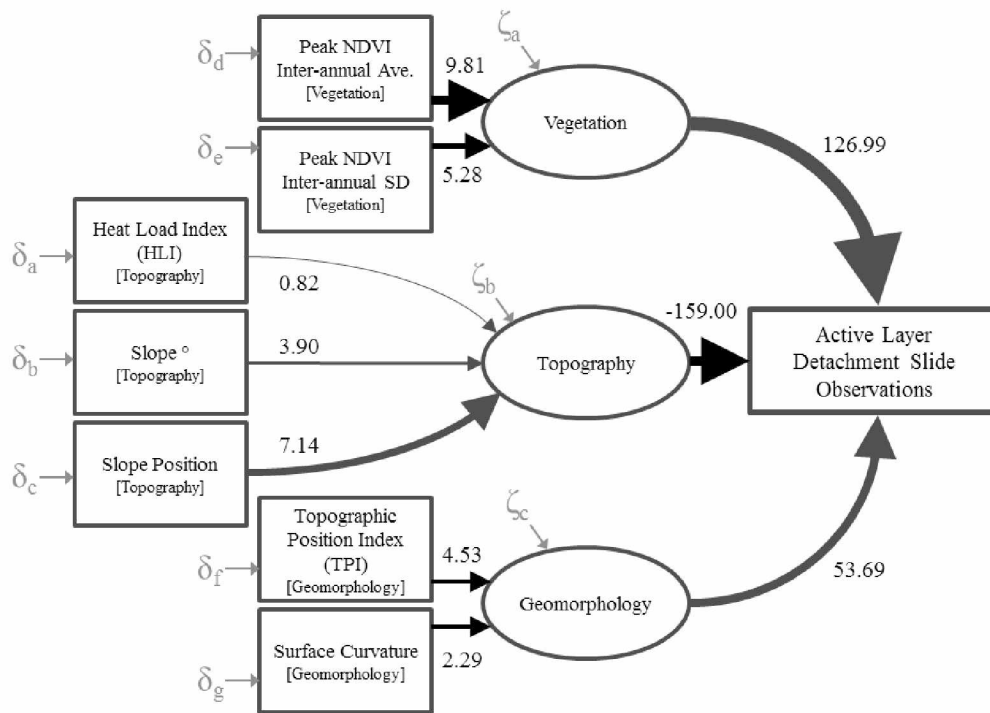


Figure A4.2.10. Final, fitted structural equation model (SEM) diagram for active layer detachment slide (ALD) terrain suitability (as represented by field observations versus randomly generated control point locations for model fitting). Bracketed labels refer to boxes in the original hypothesis and conceptual model hypothesis diagram (Figure A4.1.2). Boxes represent observed, exogenous variables, while circles represent latent, endogenous variables. Line weights represent the strength of the modeled causal relationship. Numbers next to lines are final model coefficients, averaged from ten bootstrapped model runs using standardized data. δ represents unknown measurement error for observed, exogenous variables. ζ represents unknown error for latent, endogenous variables.

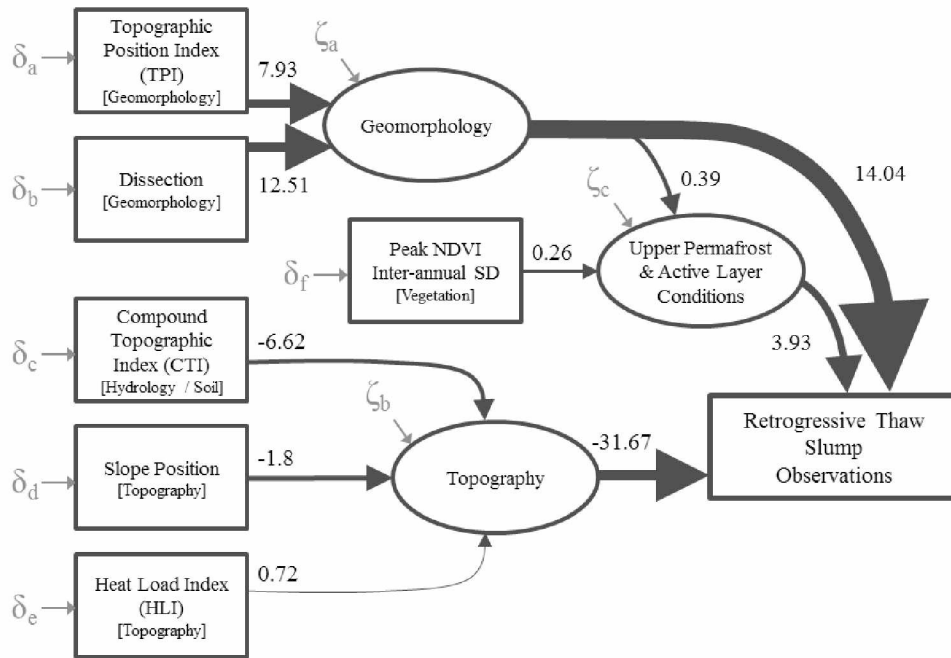


Figure A4.2.11. Final, fitted structural equation model (SEM) diagram for retrogressive thaw slump (RTS) terrain suitability (as represented by field observations versus randomly generated control point locations for model fitting). Bracketed labels refer to boxes in the original hypothesis and conceptual model hypothesis diagram (Figure A4.1.2). Boxes represent observed, exogenous variables, while circles represent latent, endogenous variables. Line weights represent the strength of the modeled causal relationship. Numbers next to lines are final model coefficients, averaged from ten bootstrapped model runs using standardized data. δ represents unknown measurement error for observed, exogenous variables. ζ represents unknown error for latent, endogenous variables.

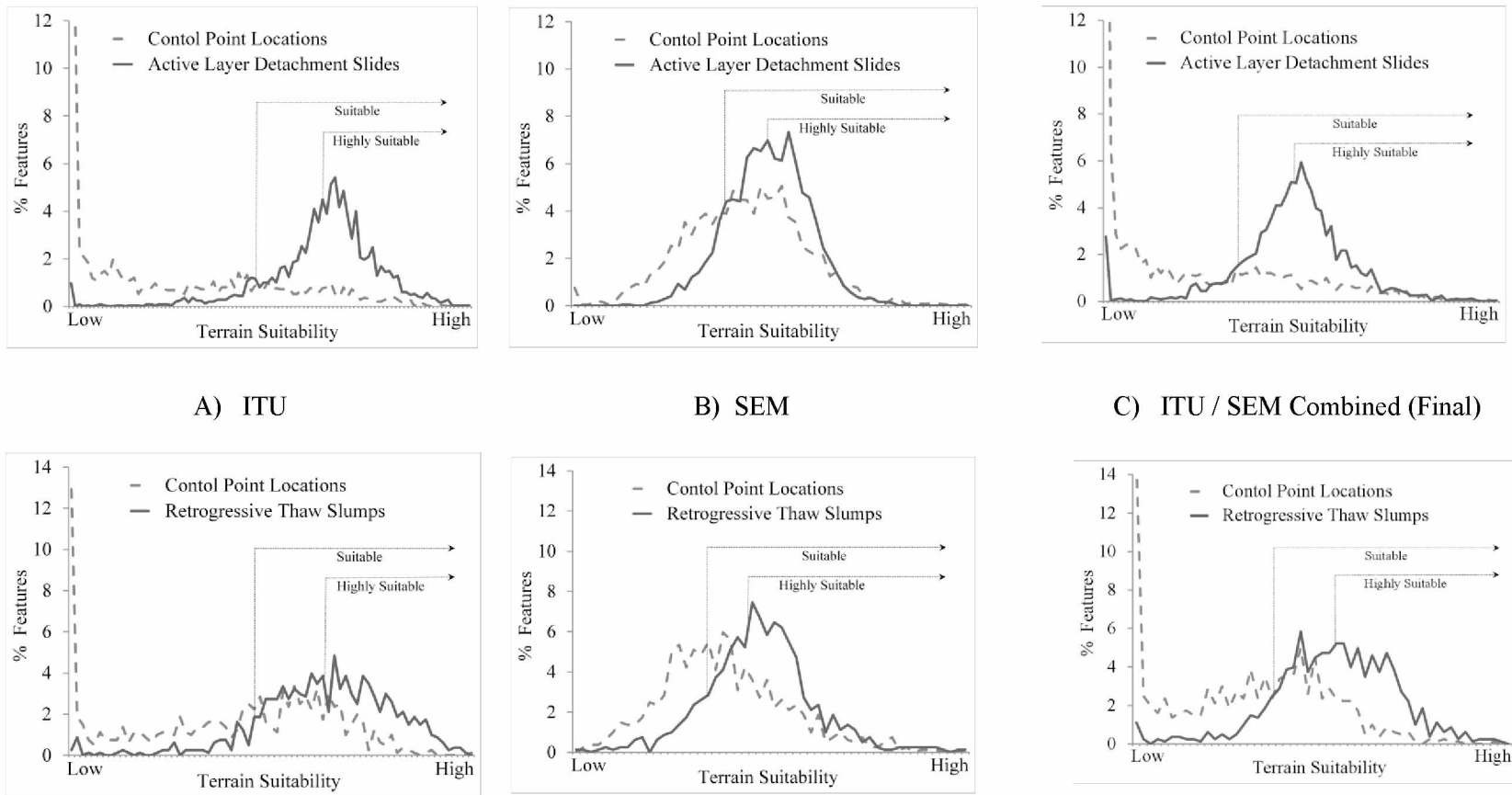


Figure A4.2.12. Frequency distributions of estimated terrain suitability for active layer detachment slide features, retrogressive thaw slump features, and randomly generated landscape control points within the study region in the central and western Brooks Range, Alaska. A) Terrain suitability estimated with integrated terrain unit (ITU) analysis of categorical variables. B) Terrain suitability estimated using structural equation modeling analysis coefficients of numeric landscape variables. C) Final estimates of terrain suitability combining results from A. and B. Estimated values at observed active layer detachment slide and retrogressive thaw slump features were used to define “suitable” and “highly suitable” terrain. “Suitable” was defined as estimated values greater than or equal to one standard deviation below the mean. “Highly suitable” was defined as estimated values greater than or equal to the mean.

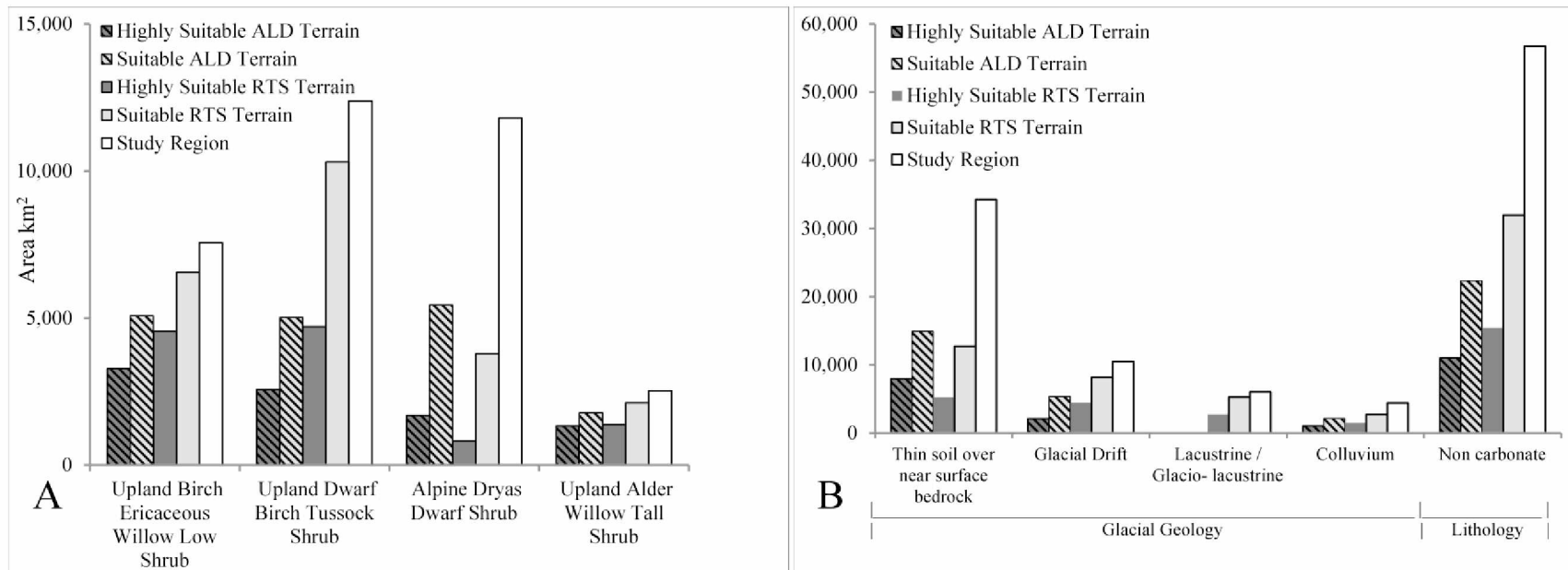


Figure A4.2.13. Areal extent of categorical landscape properties by active layer detachment slide (ALD) and retrogressive thaw slump (RTS) terrain suitability, and for the study region in the central and western Brooks Range, Alaska. A) Distribution among the four most prevalent ecotypes within suitable terrain. B) Distribution among the four most prevalent glacial geology units within suitable terrain, and distribution of noncarbonate lithology. Estimated values at observed active layer detachment slide and retrogressive thaw slump features (i.e. excluding the randomly generated control point locations) were used to define “suitable” and “highly suitable” terrain. “Suitable” was defined as estimated values greater than or equal to one standard deviation below the mean. “Highly suitable” was defined as estimated values greater than or equal to the mean.

Table A4.1.1. Input data sets used for terrain suitability analyses for active layer detachment slides (ALD) and retrogressive thaw slumps (RTS) within the study region in the central and western Brooks Range of northern Alaska.

Dataset	Cell Size	Source	Type	Reference
ALD and RTS Feature Locations	n / a	University of Alaska Fairbanks / U.S. National Park Service (Arctic Network)	ArcGIS point geodatabase	(Balsler, 2009; Swanson and Hill, 2010)
Glacial / Surficial Geology	n / a	U.S. Geological Survey, Alaska Science Center	ArcGIS polygon geodatabase	(Hamilton, 2010; Hamilton and Labay 2011)
Lithology	n / a	Alaska Biological Research Inc. / U.S. National Park Service, Arctic Network	ArcGIS polygon shapefile	(Jorgenson et al., 2001)
Ecotype	30m	Alaska Biological Research Inc. / U.S. National Park Service, Arctic Network	ArcGIS raster geodatabase	(Jorgenson et al., 2010)
National Elevation Dataset (NED)	60m	U.S. Geological Survey, EROS Data Center	ArcGIS raster image	(Gesch et al., 2002)
2001 - 2012 Normalized Difference Vegetation Index (NDVI), Moderate-resolution Imaging Spectrometer (MODIS)	250m	U.S. Geological Survey, EROS Data Center	ArcGIS raster image	(Jenkerson et al., 2010)

Table A4.1.2. Derived variables used in structural equation model (SEM) analyses. All variables derive from either A) National Elevation Dataset (NED) data from the U.S. Geological Survey, or B) Moderate-resolution Imaging Spectrometer (MODIS) 2001-2012 monthly Normalized Difference Vegetation Index (NDVI) data (Table A4.1.1). ‘Group’ refers to boxes in Figure A4.1.2. * resampling was conducted after calculation of statistical values using the ‘cubic convolution’ method.

Variable	Group	Calculation	Source Data Cell Size (m)	Derived Variable Cell Size (m)	Cell Neighborhood of Calculation
Compound Topographic Index (CTI) (Moore et al., 1993)	Hydrology	$\ln(F_{acc} / \tan(\text{slope}_{rad}))$, where: F_{acc} = flow accumulation slope_{rad} = slope in radians	60	60	Contributing watershed (values smoothed using 3 x 3 focalmean kernel)
Surface Curvature (McNab, 1993)	Geomorphology	Concavity / Convexity (Bolstad’s Variant)	60	60	5 x 5
Dissection (m) (Evans, 1972)	Geomorphology	$(z - z_{min}) / (z_{max} - z_{min})$, where: z = cell elevation z_{max} = neighborhood max. elev. z_{min} = neighborhood min. elev.	60	60	3 x 3
Topographic Position Index (TPI)(m) (Jenness, 2006)	Geomorphology	$(z_{mean} - z_{min}) / (z_{max} - z_{min})$, where: z_{mean} = neighborhood mean elev. z_{max} = neighborhood max. elev. z_{min} = neighborhood min. elev.	60	60	5 x 5
Elevation (m)	Topography	Data value from NED dataset	60	60	not derived
Heat Load Index (HLI) (McCune & Keon, 2002)	Topography	$(1 - \cos(\text{aspect} - 45)) / 2$, where: Aspect = degrees from north	60	60	3 x 3
Slope °	Topography	$(\arctan(\text{Rise} / \text{Run}) \times 57.29578)$	60	60	3 x 3
Slope Position (m)	Topography	$z - z_{mean}$, where: z = cell elevation z_{mean} = neighborhood mean elev.	60	60	500 x 500
NDVI Annual Peak, 2001-2013	Vegetation	Maximum NDVI per pixel, per year	250		1 x 1
- Average		Average peak value among years		60*	
- Maximum		Maximum peak value among years		60*	
- Minimum		Minimum peak value among years		60*	
- Standard Deviation		SD of peak values among years		60*	
- Range		Range of peak values among years		60*	

Table A4.1.3. Variables and values used for categorical analysis of terrain suitability for the study region in the central and western Brooks Range, Alaska. Numeric values were assigned based on point-in-polygon overlay analyses using points from our active layer detachment slide (ALD)/retrogressive thaw slump (RTS) GIS database, and using GIS datasets available for the study region (as cited below).

		ALD	RTS
Lithology *	Noncarbonate	1	1
	Carbonate	0.02	0.02
Glacial Geology †	Alluvium	0.02	1
	Near-surface Bedrock	1	1
	Colluvium	1	1
	Glacial Drift	1	1
	Fan Deposits	0.02	0.02
	Gravel	0.02	0.02
	Ice Contact	0.02	1
	Inwash / Outwash	0.02	0.02
	Lacustrine / Glaciolacustrine	0.02	1
	Organic	0.02	1
	Other (Active Glacier / Snowfield)	0	0
	Sand	0.02	0.02
	Silt	0.02	0.02
	Terrace	0.02	0.02
Ecotype ‡	Alpine Lake	0.0	0.0
	Alpine Rocky Circumneutral Wet Sedge Meadow	1.5	1.0
	Alpine Rocky Dry Acidic Barrens	0.1	0.0
	Alpine Rocky Dry Alkaline Barrens	0.0	0.0
	Alpine Rocky Dry Dryas Dwarf Shrub	1.1	0.8
	Alpine Rocky Dry Mafic Barrens	0.0	0.0
	Alpine Rocky Moist Ericaceous Dwarf Shrub	2.5	1.4
	Lowland Acidic Ericaceous Shrub Bog	0.0	0.2
	Lowland Circumacidic Sedge Fen	0.0	2.8
	Lowland Lake	0.0	0.0
	Lowland Moist Dwarf Birch-Ericaceous-Willow Low Shrub	0.0	0.8
	Lowland Moist Sedge-Dryas Meadow	0.0	0.2
	Lowland Organic-rich Wet Acidic Black Spruce Forest	0.0	0.2
	Lowland Organic-rich Wet Circumacidic Alder Tall Shrub	0.0	0.2
	Lowland Organic-rich Wet Circumacidic Willow Low Shrub	0.0	0.2
	Riverine Gravelly Dry Alkaline Dryas Dwarf Shrub	0.0	0.2
	Riverine Gravelly Moist Circumalkaline Barrens	0.0	0.0
	Riverine Gravelly-loamy Moist Circumalkaline Poplar Forest	0.0	0.2
	Riverine Gravelly-loamy Moist Circumalkaline White Spruce-Poplar Forest	0.0	0.2
	Riverine Gravelly-loamy Moist Circumalkaline White Spruce-Willow Forest	0.0	0.2
	Riverine Gravelly-loamy Moist Circumalkaline Willow Low Shrub	0.0	0.9

Ecotype †	Riverine Loamy Moist Alder or Willow Tall Shrub	0.0	1.6
	Riverine Loamy Moist Circumacidic Birch-Willow Low Shrub	0.0	2.0
	Riverine Loamy Wet Circumacidic Wet Sedge Meadow	0.0	0.2
	Riverine Water	0.0	0.0
	Shadow/Indeterminate	0.0	0.0
	Snow	0.0	0.0
	Upland Loamy Moist Circumalkaline Willow Low Shrub	1.5	1.4
	Upland Moist Dwarf Birch-Ericaceous-Willow Low Shrub	1.9	2.0
	Upland Organic-rich Moist Acidic Dwarf Birch-Tussock Shrub	1.5	1.0
	Upland Rocky-loamy Moist Alkaline Sedge-Dryas Meadow	1.0	1.6
	Upland Rocky-loamy Moist Circumacidic Alder-Willow Tall Shrub	2.3	1.7
	Upland Rocky-loamy Moist Circumacidic Birch Forest	0.0	0.2
	Upland Rocky-loamy Moist Circumacidic Spruce-Birch Forest	0.0	0.2
	Upland Rocky-loamy Moist White Spruce Forest	0.3	0.8
	Upland Sandy Dry Acidic White Spruce-Lichen Woodland	0.0	0.2

* (Jorgenson et al., 2001)

† (Hamilton & Labay, 2011; Hamilton, 2010)

‡ (Jorgenson et al., 2010)

Table A4.1.4. Pearson correlation coefficients for variables tested with structural equation modeling, calculated for the entire study region. Values greater than 0.5 or less than -0.5 are shown in bold.

		Hydrology, Topography and Geomorphology								NDVI Annual Peak 2001-2012				
		CTI	Curv.	Diss.	Elev.	HLI	Slope °	Slope Pos.	TPI	Ave	Max	Min	Range	Std.
Hyd. Topo. & Geom.	CTI	1.00												
	Curv.	-0.30	1.00											
	Diss.	-0.42	0.52	1.00										
	Elev.	-0.57	0.12	0.17	1.00									
	HLI	-0.08	0.00	0.01	0.07	1.00								
	Slope °	-0.76	0.05	0.13	0.64	0.10	1.00							
	SPos.	-0.49	0.23	0.24	0.57	0.06	0.48	1.00						
	TPI	-0.35	0.27	0.70	0.18	0.01	0.13	0.28	1.00					
NDVI Ann. Peak 2001- 2012	Ave	0.34	-0.05	-0.07	-0.61	-0.09	-0.45	-0.57	-0.08	1.00				
	Max	0.20	-0.01	-0.04	-0.37	-0.09	-0.27	-0.36	-0.06	0.70	1.00			
	Min	0.37	-0.07	-0.08	-0.66	-0.06	-0.51	-0.60	-0.09	0.97	0.63	1.00		
	Range	-0.32	0.09	0.06	0.52	-0.02	0.44	0.44	0.06	-0.54	-0.02	-0.68	1.00	
	Std.	-0.32	0.10	0.07	0.51	-0.03	0.44	0.44	0.07	-0.52	-0.03	-0.66	0.96	1.00

179

Table A4.2.5. Areal estimates of active layer detachment slide (ALD) and retrogressive thaw slump (RTS) terrain suitability for integrated terrain unit (ITU) and structural equation model (SEM) analyses, and for the final model which combines ITU and SEM results.

	ITU		SEM		Final (Combined ITU & SEM)	
	Highly Suitable	Suitable	Highly Suitable	Suitable	Highly Suitable	Suitable
	km ² (% study region)	km ² (% study region)	km ² (% study region)	km ² (% study region)	km ² (% study region)	km ² (% study region)
ALD Terrain	30,937 (49)	44,843 (70)	20,346 (32)	35,549 (56)	11,046 (17)	22,464 (35)
RTS Terrain	32,757 (51)	47,760 (75)	24,513 (38)	41,156 (65)	15,537 (24)	32,174 (51)
ALD & RTS Terrain	n/a	n/a	n/a	n/a	5,841 (9)	18,235 (29)

Table A4.2.6. Pearson correlations for active layer detachment slide (ALD) and retrogressive thaw slump (RTS) terrain suitability estimates from integrated terrain unit (ITU) and structural equation model (SEM) analyses.

		ITU		SEM	
		ALD	RTS	ALD	RTS
ITU	ALD	1			
	RTS	0.695	1		
SEM	ALD	0.440	0.461	1	
	RTS	0.007	0.289	-0.063	1

Table A4.2.7. Categorical landscape properties as a percentage study region, by percentage retrogressive thaw slump (RTS) and active layer detachment slide (ALD) distribution, and differential (Feature % / Study Area %). Ecotypes which are present within the study region but comprise less than 0.5% feature distribution are excluded from this table.

Ecotype	% of Study Region	% of RTS Features	% Differential	% of ALD Features	% Differential
Alpine Dryas Dwarf Shrub	19.0	15.7	0.8	20.0	1.1
Alpine Ericaceous Dwarf Shrub	0.0	0.0	0.0	5.0	2.5
Alpine Ericaceous Dwarf Shrub	2.0	2.8	1.4	0.0	0.0
Alpine Wet Sedge Meadow	1.0	1.0	1.0	1.0	1.5
Lowland Birch-Ericaceous-Willow Low Shrub	3.0	2.4	0.8	0.0	0.0
Lowland Sedge Fen	1.0	2.8	2.8	0.0	0.0
Riverine Alder or Willow Tall Shrub	1.0	1.6	1.6	0.0	0.0
Riverine Birch-Willow Low Shrub	1.0	2.0	2.0	0.0	0.0
Riverine Wet Sedge Meadow	1.0	1.2	1.2	0.0	0.0
Riverine Willow Low Shrub	1.0	0.9	0.9	0.0	0.0
Upland Alder-Willow Tall Shrub	4.0	6.8	1.7	9.0	2.3
Upland Birch-Ericaceous-Willow Low Shrub	12.0	23.7	2.0	23.0	1.9
Upland Dwarf Birch-Tussock Shrub	19.0	19.2	1.0	29.0	1.5
Upland Sedge-Dryas Meadow	6.0	9.6	1.6	6.0	1.0
Upland White Spruce Forest	4.0	3.0	0.8	1.0	0.3
Upland Willow Low Shrub	0.0	0.0	0.0	3.0	1.5
Upland Willow Low Shrub	2.0	2.9	1.4	0.0	0.0
Glacial Geology	% of Study Region	% of RTS Features	% Differential	% of ALD Features	% Differential
Alluvium	6.1	7.0	1.1	1.0	0.2
Thin Soil over Near-surface Bedrock	53.8	26.0	0.5	54.0	1.0
Colluvium	6.9	7.0	1.0	20.0	2.9
Glacial Drift	16.4	46.0	2.8	22.0	1.3
Fan Deposits	1.8	0.3	0.2	0.2	0.1
Gravel	0.1	0.1	0.7	0.0	0.0
Ice Contact	0.5	1.0	2.1	0.0	0.1
Inwash / Outwash	1.5	0.4	0.3	0.1	0.1
Lacustrine / Glaciolacustrine	9.4	11.0	1.2	2.0	0.2
Organic	0.0	0.0	0.0	0.0	0.0
Other (Active Glacier / Snowfield)	0.7	0.0	0.0	0.5	0.7
Sand	0.6	0.2	0.3	0.0	0.0
Silt	1.0	0.0	0.0	0.0	0.0
Terrace	1.2	1.0	0.8	0.0	0.0
Lithology	% of Study Region	% of RTS Features	% Differential	% of ALD Features	% Differential
Noncarbonate	89.8	99.2	1.1	98.3	1.1
Carbonate	10.2	0.8	0.1	1.7	0.2

Table A4.2.8. Structural equation model fit metrics (Hooper et al., 2008) from ten bootstrapped model runs for active layer detachment slide (ALD) and ten bootstrapped model runs for retrogressive thaw slump (RTS) terrain suitability in the central and western Brooks Range, Alaska. The ALD model uses 2492 observed ALD feature locations, and an equal number of randomly generated, non-ALD control locations. The model uses 805 observed RTS feature locations, and an equal number of randomly generated, non-RTS control locations. Coefficients and intercepts from the ten bootstrap runs were used to produce ALD and RTS terrain suitability estimates, mapped for the study region (Figure A4.2.5). Mean values for the ten runs shown in bold.

SEM ALD Bootstrap Run											
Fit metric; recommended threshold value for good fit	1	2	3	4	5	6	7	8	9	10	mean
Comparative Fit Index (CFI); > 0.950	0.977	0.970	0.977	0.973	0.972	0.971	0.979	0.976	0.971	0.978	0.974
Tucker-Lewis Index (TLI); > 0.950	0.958	0.952	0.959	0.953	0.942†	0.955	0.946†	0.959	0.948†	0.957	0.953
Root mean square error of approximation (RMSEA); < 0.07	0.037	0.036	0.037	0.033	0.037	0.030	0.035	0.035	0.037	0.036	0.035
Standardized Root Mean Square Residual (SRMR); < 0.50	0.029	0.029	0.033	0.029	0.032	0.032	0.031	0.031	0.028	0.032	0.031
SEM RTS Bootstrap Run											
Fit metric; recommended threshold value for good fit	1	2	3	4	5	6	7	8	9	10	mean
Comparative Fit Index (CFI); > 0.950	0.994	0.991	0.982	0.990	0.990	0.991	0.983	0.977	0.988	0.983	0.987
Tucker-Lewis Index (TLI); > 0.950	0.980	0.968	0.979	0.974	0.980	0.972	0.986	0.967	0.976	0.975	0.976
Root mean square error of approximation (RMSEA); < 0.07	0.027	0.030	0.032	0.034	0.033	0.049	0.038	0.044	0.063	0.043	0.039
Standardized Root Mean Square Residual (SRMR); < 0.50	0.019	0.036	0.031	0.026	0.030	0.030	0.023	0.031	0.026	0.028	0.028

† does not meet recommended value for good fit

Table A4.2.9. Structural equation model R^2 values from ten bootstrapped model runs for active layer detachment slide (ALD) and ten bootstrapped model runs for retrogressive thaw slump (RTS) terrain suitability in the central and western Brooks Range, Alaska. R^2 represents the variation among endogenous variables in the model explained by that factor (Joreskog and Sorbom, 1996). The ALD model uses 2492 observed ALD feature locations, and an equal number of randomly generated, non-ALD control locations. The RTS model uses 805 observed RTS feature locations, and an equal number of randomly generated, non-RTS control locations. Mean values for the ten runs shown in bold.

SEM ALD Bootstrap Run R^2 Values											
Variable	1	2	3	4	5	6	7	8	9	10	mean
Peak NDVI Inter-annual average	0.61	0.59	0.61	0.59	0.59	0.60	0.60	0.60	0.56	0.54	0.59
Peak NDVI Inter-annual standard deviation	0.35	0.40	0.37	0.41	0.42	0.41	0.43	0.43	0.40	0.42	0.40
Curvature	0.29	0.35	0.29	0.27	0.28	0.32	0.33	0.30	0.34	0.38	0.31
Topographic Position Index (TPI)	0.29	0.24	0.26	0.28	0.30	0.27	0.29	0.29	0.24	0.24	0.27
Slope Position	0.50	0.52	0.52	0.50	0.52	0.54	0.51	0.48	0.51	0.51	0.51
Heat Load Index (HLI)	0.00	0.01	0.00	0.01	0.00	0.01	0.00	0.00	0.01	0.00	0.00
Slope (°)	0.17	0.18	0.18	0.19	0.19	0.17	0.16	0.17	0.17	0.19	0.18
SEM RTS Bootstrap Run R^2 Values											
Variable	1	2	3	4	5	6	7	8	9	10	mean
Peak NDVI Inter-annual standard deviation	0.07	0.05	0.08	0.06	0.06	0.04	0.07	0.09	0.06	0.05	0.06
Topographic Position Index (TPI)	0.68	0.63	0.74	0.71	0.72	0.68	0.70	0.74	0.66	0.70	0.69
Dissection	0.88	0.88	0.83	0.84	0.80	0.79	0.73	0.82	0.85	0.80	0.82
Slope Position	0.39	0.36	0.48	0.40	0.44	0.33	0.37	0.39	0.46	0.40	0.40
Heat Load Index (HLI)	0.00	0.01	0.00	0.00	0.00	0.00	0.00	0.00	0.00	0.01	0.00
Compound Topographic Index (CTI)	0.35	0.39	0.35	0.42	0.34	0.40	0.37	0.37	0.34	0.34	0.37

Table A4.2.10. Areal extent of glacial geology units and noncarbonate lithologies within the study region, and by terrain suitability for active layer detachment slides (ALD) and retrogressive thaw slumps (RTS) in the central and western Brooks Range, Alaska. * (Hamilton, 2009; Hamilton and Labay, 2010), † (Jorgenson et al., 2001)

Glacial Geology*	Study Region		Active Layer Detachment Slide Terrain				Retrogressive Thaw Slump Terrain			
	km ²	%	Highly Suitable		Suitable		Highly Suitable		Suitable	
			km ²	%	km ²	%	km ²	%	km ²	%
Alluvium	3,899	6	1	0	19	0	801	5	1,732	5
Thin soils over near-surface bedrock	34,244	54	7,916	72	14,908	66	5,263	34	12,705	39
Colluvium	4,388	7	1,041	9	2,135	10	1,471	9	2,716	8
Drift	10,464	16	2,085	19	5,353	24	4,462	29	8,144	25
Fan	1,121	2	1	0	17	0	12	0	107	0
Gravel	86	0	0	0	2	0	1	0	11	0
Ice contact	308	0	0	0	2	0	130	1	235	1
Inwash / outwash	985	2	0	0	9	0	8	0	89	0
Lacustrine / glaciolacustrine	5,998	9	0	0	11	0	2,709	17	5,254	16
Organic	8	0	0	0	0	0	1	0	1	0
Other	552	1	0	0	0	0	0	0	0	0
Sand	367	1	0	0	0	0	0	0	4	0
Silt	634	1	0	0	5	0	293	2	525	2
Terrace	755	1	0	0	3	0	386	2	642	2
Total	63,707	100	11,046	100	22,464	100	15,536	100	32,166	100
Lithology†										
Noncarbonate	57,336	90	10,988	100	22,343	100	15,443	100	31,970	100
Carbonate	6,371	10	1	0	5	0	1	0	6	0
Total	63,707	100	10,989	100	22,348	100	15,444	100	31,976	100

Table A4.2.11. Areal extent of ecotypes within the study region, and by terrain suitability for active layer detachment slides and retrogressive thaw slumps. Ecotypes which are present in the study region but comprised less than 1% of suitable terrain are excluded from this table. * (Jorgenson et al., 2010)

Ecotype*	Study Region		Active Layer Detachment Slide Terrain				Retrogressive Thaw Slump Terrain			
	km ²	%	Highly Suitable		Suitable		Highly Suitable		Suitable	
			km ²	%	km ²	%	km ²	%	km ²	%
Upland Birch-Ericaceous-Willow Low Shrub	7,560	12	3,271	30	5,080	23	4,549	29	6,555	20
Upland Dwarf Birch-Tussock Shrub	12,375	19	2,567	23	5,022	22	4,705	30	10,306	32
Alpine Dryas Dwarf Shrub	11,806	19	1,688	15	5,443	24	816	5	3,786	12
Upland Alder-Willow Tall Shrub	2,528	4	1,332	12	1,778	8	1,374	9	2,116	7
Alpine Ericaceous Dwarf Shrub	1,583	2	706	6	1,165	5	142	1	715	2
Upland Willow Low Shrub	1,221	2	446	4	694	3	644	4	983	3
Upland Sedge-Dryas Meadow	3,555	6	442	4	1,388	6	1,451	9	2,580	8
Upland White Spruce Forest	2,813	4	289	3	755	3	370	2	1,579	5
Alpine Wet Sedge Meadow	538	1	120	1	292	1	78	1	243	1
Alpine Acidic Barrens	6,950	11	95	1	465	2	36	0	217	1
Lowland Birch-Ericaceous-Willow Low Shrub	1,750	3	17	0	100	0	443	3	1,122	3
Lowland Alder Tall Shrub	323	1	10	0	28	0	71	0	181	1
Lowland Willow Low Shrub	262	0	4	0	16	0	68	0	163	1
Lowland Sedge Fen	684	1	3	0	21	0	330	2	470	1
Lowland Ericaceous Shrub Bog	333	1	0	0	3	0	96	1	176	1
Riverine Birch-Willow Low Shrub	437	1	0	0	0	0	154	1	271	1
Total	54,717	87	10,990	99	22,251	99	15,328	99	31,462	98

Table A4.2.12 Numeric landscape properties within the study region, and by terrain suitability for active layer detachment slides and retrogressive thaw slumps. Original source data from: * (Hugelius et al., 2013), and † (Jorgenson et al., 2010).

Landscape Property	Study Region		Active Layer Detachment Slide Terrain				Retrogressive Thaw Slump Terrain			
	mean	std	Highly Suitable		Suitable		Highly Suitable		Suitable	
			mean	std	mean	std	mean	std	mean	std
Peak NDVI Inter-annual Ave. †	0.700	0.155	0.801	0.046	0.777	0.061	0.790	0.048	0.780	0.056
Peak NDVI Inter-annual SD †	0.062	0.033	0.175	0.045	0.048	0.016	0.046	0.014	0.049	0.015
Heat Load Index (HLI) †	5,257	1,320	5,276	1,266	5,254	1,248	5,090	842	5,144	940
Topographic Position Index (TPI) †	0.47	0.10	0.48	0.07	0.48	0.08	0.50	0.09	0.49	0.09
Dissection †	0.47	0.16	0.49	0.11	0.49	0.12	0.50	0.15	0.48	0.15
Compound Topographic Index (CTI) †	7.1	1.9	6.8	1.3	6.8	1.3	7.8	1.5	7.6	1.5
Surface Curvature †	0.01	2.10	-0.12	1.53	-0.09	1.68	-0.16	1.09	-0.17	1.26
Slope (°) †	13.1	10.9	13.2	8.0	13.0	8.4	7.7	6.9	8.7	7.7
Slope Position †	0.4	217.0	8.5	143.2	-5.1	159.5	-83.7	133.4	-73.1	146.8
Soil Organic Carbon Top 2m (kg/m ²) *	10.2	10.5	8.9	8.8	8.8	9.3	8.7	8.7	8.6	9.2
Soil Organic Carbon Top 3m (kg/m ²) *	11.2	11.5	9.9	9.6	9.7	10.1	9.6	9.4	9.4	10.0
Surface Organic Depth (cm) †	9.6	7.0	10.9	4.4	10.2	4.8	13.5	5.2	13.1	5.8
pH †	5.5	0.9	5.1	0.3	5.2	0.4	5.2	0.6	5.2	0.6

† Included in structural equation modelling (SEM)

Table A4.2.13. Numeric landscape properties for randomly-assigned control locations, and for observed active layer detachment slide and retrogressive thaw slump features. Original source data from: * (Hugelius et al., 2013), and † (Jorgenson et al., 2010).

Landscape Property	Control		Active Layer Detachment Slides		Retrogressive Thaw Slumps	
	mean	std	mean	std	mean	std
Peak NDVI Inter-annual Ave. †	0.700	0.157	0.776	0.051	0.768	0.050
Peak NDVI Inter-annual SD †	0.062	0.035	0.048	0.015	0.051	0.018
Heat Load Index (HLI) †	5,253	1,322	5,228	1,143	5,103	998
Topographic Position Index (TPI) †	0.47	0.11	0.47	0.06	0.47	0.09
Dissection †	0.47	0.16	0.47	0.08	0.47	0.14
Compound Topographic Index (CTI) †	7.1	1.9	7.3	1.1	7.6	1.1
Surface Curvature †	-0.01	2.12	-0.42	0.92	-0.37	0.98
Slope (°)†	13.2	10.9	11.9	7.1	9.8	5.6
Slope Position †	0.2	216.3	-44.2	133.9	-113.6	126.2
Soil Organic Carbon Top 2m (kg/m ²) *	7.3	9.8	5.3	6.6	10.0	10.1
Soil Organic Carbon Top 3m (kg/m ²) *	8.1	11.1	5.9	7.2	11.1	11.0
Surface Organic Depth (cm) †	9.0	5.7	10.9	4.4	11.3	4.7
pH †	5.4	0.9	5.1	0.4	5.4	0.6

† Included in structural equation modelling (SEM)

Table A4.2.14. Area of suitable climate conditions for active layer detachment slides and retrogressive thaw slumps for the 1910-1919 and 1990-1999 timeframes: within the study region, and by terrain suitability for active layer detachment slides (ALD) and retrogressive thaw slumps (RTS). Original climate source data from SNAP (2014).

Climate Metric	Study Region km2	Active Layer Detachment Slide Terrain		Retrogressive Thaw Slump Terrain	
		Highly Suitable km2	Suitable km2	Highly Suitable km2	Suitable km2
Suitable Climate Conditions ALD 1990-1999 km2	39,402	5,538	11,614		
Suitable Climate Conditions ALD 1910-1919 km2	35,107	5,669	11,638		
Suitable Climate Conditions RTS 1990-1999 km2	28,029			6,186	12,394
Suitable Climate Conditions RTS 1910-1919 km2	22,636			5,247	11,104

Table A4.2.15. Climate metrics for randomly-assigned control locations, and for observed active layer detachment slide and retrogressive thaw slump features. Original climate source data from SNAP (2014).

Climate Metric	Control		Active Layer Detachment Slides		Retrogressive Thaw Slumps	
	mean	std	mean	std	mean	std
Summer Warmth Index (SWI)	29.2	5.1	28.4	2.1	29.5	3.0
Mean Annual Air Temperature (MAAT) °C, 1910-1999	-7.8	1.7	-8.4	1.7	-7.6	1.3
Mean Annual Air Temperature (MAAT) °C, 1910-1919	-8.1	1.7	-8.8	1.7	-8.0	1.3
Mean Annual Air Temperature (MAAT) °C, 1910-1939	-8.0	1.7	-8.6	1.7	-7.8	1.3
Mean Annual Air Temperature (MAAT) °C, 1970-1999	-7.5	1.7	-8.1	1.7	-7.3	1.3
Mean Annual Air Temperature (MAAT) °C, 1990-1999	-7.0	1.7	-7.6	1.7	-6.8	1.3
Mean Annual Air Temperature Increase (MAAT) °C, 1990-1999 vs 1910-1919	1.08	0.32	1.19	0.29	1.18	0.26
Mean Annual Air Temperature Increase (MAAT) °C, 1970-1999 vs 1930-1939	0.50	0.40	0.50	0.04	0.50	0.03

Table A4.2.16. Climate metrics within the study region, and by terrain suitability for active layer detachment slides and retrogressive thaw slumps. Original climate source data from SNAP (2014).

Climate Metric	Study Region		Active Layer Detachment Slide Terrain				Retrogressive Thaw Slump Terrain			
	mean	std	Highly Suitable		Suitable		Highly Suitable		Suitable	
			mean	std	mean	std	mean	std	mean	std
Summer Warmth Index (SWI)	27.9	7.9	29.5	6.5	28.6	6.4	30.6	6.8	30.5	6.9
Mean Annual Air Temperature (MAAT) °C, 1910-1999	-7.8	1.7	-7.5	1.8	-7.7	1.8	-7.8	1.7	-7.8	1.7
Mean Annual Air Temperature (MAAT) °C, 1910-1919	-8.1	1.7	-7.8	1.8	-8.0	1.8	-8.1	1.7	-8.1	1.7
Mean Annual Air Temperature (MAAT) °C, 1910-1939	-8.0	1.7	-7.7	1.9	-7.9	1.8	-8.0	1.7	-8.0	1.8
Mean Annual Air Temperature (MAAT) °C, 1970-1999	-7.5	1.7	-7.2	1.9	-7.4	1.8	-7.5	1.7	-7.5	1.8
Mean Annual Air Temperature (MAAT) °C, 1990-1999	-7.1	1.7	-6.8	1.9	-6.9	1.9	-7.1	1.7	-7.0	1.8
Mean Annual Air Temperature Increase (MAAT) °C, 1990-1999 vs 1910-1919	1.09	0.32	1.06	0.30	1.10	0.29	1.05	0.30	1.06	0.31
Mean Annual Air Temperature Increase (MAAT) °C, 1970-1999 vs 1930-1939	0.50	0.03	0.51	0.03	0.50	0.03	0.51	0.03	0.50	0.03

Chapter 5. Conclusions

5.1 Summary

Roughly half the surface terrain in the central and western Brooks Range and foothills of northern Alaska is suitable for active layer detachment sliding and retrogressive thaw slumping, which is widespread and has become more common in recent decades. Understanding and representing complex, co-varying relationships among terrain and permafrost properties is necessary to accurately estimate the spatial distribution of terrain suitable for these permafrost mass-wasting disturbances. No single landscape property is a definitive indicator of terrain suitability, and each relevant property serves to constrain spatial estimates and increase overall model accuracy. A bottom-up approach using empirically-driven modelling enables us to scale estimates of vulnerable area up from regions to the pan-arctic, and enhances our ability to spatially quantify impacts from and feedbacks to ecosystems, permafrost carbon stocks, weather and climate. Specific weather events and patterns, in conjunction with a general warming press, determine initiation of active layer detachment slides and retrogressive thaw slumps, such that future change trajectories may hinge largely on the timing of weather events and on seasonal shifts. Forecasting future conditions in the cryosphere depends on synthesizing weather and climate patterns with spatially explicit information on terrain and permafrost relationships.

5.2 Synthesis

Forecasting potential future conditions throughout the cryosphere depends upon understanding complex interactions among terrain conditions, weather events, and climate patterns at relatively short time intervals for small areas, and then scaling that knowledge across broad regions of highly diverse landscapes in context of weather events and seasonal shifts which are superimposed over climate changes occurring at decadal to millennial time scales. Effects of any given weather event or climate trend vary greatly by location. A seasonal weather shift which simultaneously triggers widespread permafrost mass-wasting on some landscapes may have little impact elsewhere, while a steady warming trend may deepen the active layer enough to catalyze a marked vegetation shift on some landscapes but leave carbon stocks in the permafrost relatively unaffected. Understanding how different combinations of surface and subsurface conditions respond to each type of perturbation, and how these combinations are arrayed across landscapes, enables better quantification of impacts and feedbacks at regional and global scales and aids better forecasting for trajectories of changing conditions in the cryosphere.

In Alaska's central and western Brooks Range, increased frequency of active layer detachment sliding and retrogressive thaw slumping is widespread, but is tied with particular weather events and terrain settings. General climate warming likely serves as a preconditioning agent, warming upper

permafrost and enhancing the potential for weather events and seasonal shifts to accelerate thaw front advance through the active layer, melting ground ice in the upper permafrost and leading to active layer detachment sliding and retrogressive thaw slumping. Early thawing-season warmth and snowmelt, linked with slump initiation, may be a critical factor in landscape to regional-scale change trajectories, impacts, and feedbacks from retrogressive thaw slumps. Active layer deepening, which occurs with general climate warming, is at least partially reversible with subsequent cooling. Deeper degradation and mobilization of upper permafrost layers, as with retrogressive thaw slumping, may release frozen soil carbon and be a more permanent phenomenon with differing and stronger impacts locally and globally. The temporal pattern of climate change may therefore be critical in determining rate of retrogressive thaw slump initiation and associated impacts and feedbacks, with potentially very different outcomes depending upon future changes in the timing of weather events, as well as their magnitude.

A bottom-up approach to understanding relationships among terrain and permafrost properties provides the opportunity to characterize conditions across regions, and eventually link different types of landscapes with impacts from, and feedbacks to, climate and weather shifts. Broad scale modelling of permafrost and terrain properties is limited by the variability of relationships among regions, which are difficult to quantify and describe due to the cost of field sampling to characterize conditions and relationships within regions. As a result, maps of permafrost distribution and properties are either broad in spatial scale but very general in content, or more specific in content but limited in scale. Assessing relationships among terrain and permafrost conditions across diverse sites within a region facilitates an understanding of the gradients within that region, providing better modelling capacity for that area and evidence of prevalent landscape dynamics and processes. As an overall strategy, assessing regions separately and then scaling up to global models by aggregating regional results is more time consuming and costly, but may reduce error and imprecision inherent to coarser scale approaches which may identify trends incorrectly for constituent regions.

Across diverse Brooks Range landscapes, statistically-supported groupings of sites suggest consistent, though complex, inter-relationships among terrain and permafrost properties in the study region. These are a potential basis for improved spatially-explicit, proxy estimations of conditions in upper permafrost horizons, and for identifying areas prone to particular modes of permafrost degradation, including active layer detachment sliding and retrogressive thaw slumping. In this region, where diverse landscapes abutting the arctic-boreal ecotone may be especially prone to multiple modes of permafrost degradation with climate change, and where remote settings severely limit direct observation of permafrost properties, this approach facilitates better estimation of extents, trajectories and magnitudes of different permafrost degradation modes and their future impacts.

Spatial distribution of groups of sites partially corresponded with regional geography in the central and western Brooks Range. While sites from all groups occurred both on the North Slope and within the Noatak Basin, all groupings exhibited regional tendencies. One group had a strong geographic affiliation, with five out of six sites concentrated within a 25 km radius in the upper Noatak Basin. Two groups were more common either on the North Slope or in the Noatak Basin but were widely distributed, while a final group was distributed throughout the study region, but exhibited differences in particular terrain properties corresponding with local geography.

Gradients and divisions among sites and site groupings were driven by terrain properties which generally correspond with state factors, suggesting that examination of properties organized by state factor may provide better insight and more complete, parsimonious information for estimating permafrost conditions across landscapes. At landscape to regional scales, selection of the most statistically relevant and representative index variables from groups of variables defined by state factors may offer the most parsimonious method for analyzing terrain properties driving upper-permafrost characteristics, and for identifying the most effective and efficient field sampling strategy for estimation of permafrost-related properties and processes in remote, arctic regions.

Identifying which terrain properties are relevant is critical to constrain spatial estimates of suitable terrain for active layer detachment slides and retrogressive thaw slumps. Both observed features and terrain suitability for active layer detachment slides and retrogressive thaw slumps are spatially distributed across landscape gradients defined by multiple landscape properties. While specific terrain factors, and groups of factors, exerted varying influence on overall terrain suitability, no single landscape property emerged as an obligate, or even dominant, positive indicator of suitable terrain. Landscape properties describing geomorphology, vegetation, topography, surficial geology and lithology all correlate with observed feature distribution, and are supported as drivers of suitable terrain conditions in the central and western Brooks Range. A complex but coherent combination of co-varying relationships determines terrain suitability for active layer detachment slides and retrogressive thaw slumps, such that individual landscape properties are only truly relevant when considered in concert with, and in context of, all other relevant properties.

At least 32%, and up to 57% of central and western Brooks Range landscape area is suitable terrain for either active layer detachment sliding or retrogressive thaw slumping, depending on the sensitivity of the chosen suitability threshold and the intensity of trigger events. Similar proportions of suitable terrain may prevail in other low arctic regions. Future feature initiation on these surfaces is uncertain, depending on future trends and shifts in weather and climate. Similar proportions of suitable terrain may prevail in

other low arctic regions. However, accurate estimates for other locales would likely require analogous, empirically modelled results to account for region-specific variability among terrain, vegetation and upper permafrost relationships. Modelled terrain suitability estimates enable better spatial quantification of permafrost degradation impacts, including vulnerable soil carbon stocks and ecological responses, and better identification of vulnerable ecosystems. Future addition of physical soil and soil organic layer properties, with further model refinement and field validation, might also produce reasonable, modelled spatial estimates of ground ice percentage and / or cryofacies distribution.

5.3 References

- Abbott, B. W. 2014. Permafrost in a Warmer World: Net Ecosystem Carbon Imbalance. PhD. University of Alaska Fairbanks, Fairbanks, AK.
- ACIA. 2005. Arctic Climate Impact Assessment. Cambridge University Press.
- Anisimov, O. and S. Reneva. 2006. Permafrost and changing climate: The Russian perspective. *Ambio* 35:169-175.
- Balser, A., M. N. Gooseff, J. Jones, and W. B. Bowden. 2009. Thermokarst distribution and relationships to landscape characteristics in the Feniak Lake region, Noatak National Preserve, Alaska; Final Report to the National Park Service, Arctic Network (ARCN). Fairbanks, AK.
- Balser, A. W., J. B. Jones, and R. Gens. 2014. Timing of Retrogressive Thaw Slump Initiation in the Noatak Basin, Northwest Alaska, USA. *Journal of Geophysical Research: Earth Surface*:2013JF002889.
- Balser, A. W., J. B. Jones, D. A. Walker, and M. T. Jorgenson. 2015. Relationship of Cryofacies, Surface and Subsurface Terrain Conditions in the Brooks Range and foothills of northern Alaska. PhD Dissertation, Chapter 3. University of Alaska Fairbanks, Fairbanks, AK.
- Bowden, W. B., A. W. Balser, A. D. Huryn, C. Luecke, D. M. Sanzone, B. Peterson, G. Burkart, J. Larouche, and S. M. Parker. 2007. Aquatic biodiversity, community composition and ecosystem processes in the Noatak River Watershed. NPS/AKRARC/NRTR-2006/01, US National Park Service, DOI.
- Bowden, W. B., M. N. Gooseff, A. Balser, A. Green, B. J. Peterson, and J. Bradford. 2008. Sediment and nutrient delivery from thermokarst features in the foothills of the North Slope, Alaska: Potential impacts on headwater stream ecosystems. *Journal of Geophysical Research* 113. G02026. doi:10.1029/2007JG000470.
- Burn, C. R. and A. G. Lewkowicz. 1990. Retrogressive Thaw Slumps *The Canadian Geographer* 34:273-276.

- CAVM-Team. 2003. Circumpolar Arctic Vegetation Map, Scale 1:7,500,000. Conservation of Arctic Flora and Fauna (CAFF) Map No. 1. U.S. Fish and Wildlife Service, Anchorage, Alaska.
- Daanen, R. P., T. Ingeman-Nielsen, S. S. Marchenko, V. E. Romanovsky, N. Foged, M. Stendel, J. H. Christensen, and K. H. Svendsen. 2011. Permafrost degradation risk zone assessment using simulation models. *The Cryosphere* 5:1043-1056.
- Davis, N. 2001. *Permafrost: A Guide to Frozen Ground in Transition*. University of Alaska Press, Fairbanks, AK.
- Desyatkin, A. R., F. Takakai, P. P. Fedorov, M. C. Nikolaeva, R. V. Desyatkin, and R. Hatano. 2009. CH₄ emission from different stages of thermokarst formation in Central Yakutia, East Siberia. *Soil Science and Plant Nutrition* 55:558-570.
- French, H. and Y. Shur. 2010. The principles of cryostratigraphy. *Earth-Science Reviews* 101:190-206.
- Frey, K. E. and J. W. McClelland. 2009. Impacts of permafrost degradation on arctic river biogeochemistry. *Hydrological Processes* 23:169-182.
- Godin, E. and D. Fortier. 2012. Geomorphology of a thermo-erosion gully, Bylot Island, Nunavut, Canada. *Canadian Journal of Earth Sciences* 49:979-986.
- Gooseff, M., A. Balser, W. Bowden, and J. Jones. 2009. Effects of hillslope thermokarst in northern Alaska. , 90: 29-31. *Eos, Transactions of the American Geophysical Union* 90:29-31.
- Grosse, G., J. Harden, M. Turetsky, A. D. McGuire, P. Camill, C. Tarnocai, S. Frolking, E. A. G. Schuur, T. Jorgenson, S. Marchenko, V. Romanovsky, K. P. Wickland, N. French, M. Waldrop, L. Bourgeau-Chavez, and R. G. Striegl. 2011. Vulnerability of high-latitude soil organic carbon in North America to disturbance. *J. Geophys. Res.* 116:G00K06.
- Gruber, S. 2012. Derivation and analysis of a high-resolution estimate of global permafrost zonation. *The Cryosphere* 6:221-233.
- Hamilton, T. D. 2003. Surficial geology of the Dalton Highway (Itkillik-Sagavanirktok rivers) area, southern Arctic foothills, Alaska: Alaska Division of Geological & Geophysical Surveys Professional Report 121. Pages 1-32. Alaska Division of Geological & Geophysical Surveys, Fairbanks, AK.
- Hamilton, T. D. 2009. Guide to surficial geology and river-bluff exposures, Noatak National Preserve, northwestern Alaska: U.S. Geological Survey Scientific Investigations Report 2008-5125.
- Hamilton, T. D. 2010. Surficial Geologic Map of the Noatak National Preserve, Alaska. U.S. Geological Survey (in cooperation with U.S. National Park Service) Scientific Investigations Map 3036, 1 : 250,000 scale, and accompanying report:21p.

- Hamilton, T. D. and K. A. Labay. 2011. Surficial Geologic Map of the Gates of the Arctic National Park and Preserve, Alaska. U.S. Geological Survey (in cooperation with U.S. National Park Service) Scientific Investigations Map 3125, 1 : 300,000 scale, and accompanying report:19p.
- Harris, C., L. U. Arenson, H. H. Christiansen, B. Etzelmüller, R. Frauenfelder, S. Gruber, W. Haeberli, C. Hauck, M. Hölzle, O. Humlum, K. Isaksen, A. Kääb, M. A. Kern-Lütschg, M. Lehning, N. Matsuoka, J. B. Murton, J. Nötzli, M. Phillips, N. Ross, M. Seppälä, S. M. Springman, and D. Vonder Mühl. 2009. Permafrost and climate in Europe: Monitoring and modelling thermal, geomorphological and geotechnical responses. *Earth-Science Reviews* 92:117-171.
- Hinzman, L., N. Bettez, W. Bolton, F. Chapin, M. Dyurgerov, C. Fastie, B. Griffith, R. Hollister, A. Hope, H. Huntington, A. Jensen, G. Jia, T. Jorgenson, D. Kane, D. Klein, G. Kofinas, A. Lynch, A. Lloyd, A. McGuire, F. Nelson, W. Oechel, T. Osterkamp, C. Racine, V. Romanovsky, R. Stone, D. Stow, M. Sturm, C. Tweedie, G. Vourlitis, M. Walker, D. Walker, P. Webber, J. Welker, K. Winker, and K. Yoshikawa. 2005. Evidence and Implications of Recent Climate Change in Northern Alaska and Other Arctic Regions. *Climatic Change* 72:251-298.
- Hobbie, J. E., B. J. Peterson, G. R. Shaver, and W. J. O'Brien. 1991. The Toolik Lake Project: terrestrial and freshwater research on change in the Arctic. Pages 378-383 *in* V. II, editor. Proceedings of the University of Alaska Conference, "International Conference on the Role of Polar Regions in Global Change", June 1990. University of Alaska, Fairbanks, Alaska.
- Jenny, H. 1941. *Factors of Soil Formation: A System of Quantitative Pedology*. Dover Publications, Inc., New York, NY.
- Jorgenson, M. T., J. Harden, M. Kanevskiy, J. O'Donnell, K. P. Wickland, S. Ewing, K. L. Manies, Q. Zhuang, Y. Shur, R. G. Striegl, and J. Koch. 2013. Reorganization of vegetation, hydrology and soil carbon after permafrost degradation across heterogeneous boreal landscapes *Environmental Research Letters* 8:1-14.
- Jorgenson, M. T. and R. A. Kreig. 1988. A Model for Mapping Permafrost Distribution Based on Landscape Component Maps and Climatic Variables. Pages 176-182 *in* 5th International Conference on Permafrost, August 2-5, 1988. Tapir Publishers, Trondheim, Norway.
- Jorgenson, M. T. and T. E. Osterkamp. 2005. Response of boreal ecosystems to varying modes of permafrost degradation. *Canadian Journal of Forest Research* 35:2100-2111.
- Jorgenson, M. T., V. Romanovsky, J. Harden, Y. Shur, J. O'Donnell, E. A. G. Schuur, M. Kanevskiy, and S. Marchenko. 2010a. Resilience and vulnerability of permafrost to climate change. *Canadian Journal of Forest Research-Revue Canadienne De Recherche Forestiere* 40:1219-1236.

- Jorgenson, M. T., J. E. Roth, P. F. Miller, M. J. Macander, M. S. Duffy, A. F. Wells, G. V. Frost, and E. R. Pullman. 2010b. An ecological land survey and landcover map of the Arctic Network. Natural Resource Technical Report NPS/ARC/NRTR—2009/270. National Park Service, Fort Collins, Colorado.
- Jorgenson, M. T., Y. L. Shur, and T. E. Osterkamp. 2008a. Thermokarst in Alaska. Pages 869-876 *in* Ninth International Conference on Permafrost. National Academy Press, Washington, DC, Fairbanks, AK.
- Jorgenson, T., K. Yoshikawa, V. Romanovsky, M. Kanevskiy, J. Brown, Y. Shur, S. Marchenko, G. Grosse, and B. Jones. 2008b. Map of Permafrost Characteristics in Alaska. Proceedings of the Ninth International Conference on Permafrost (NICOP), Fairbanks, AK June 30 - July 4, 2008.
- Khomutov, A. V. 2012. Assessment of Landslide Geohazards in Typical Tundra of Central Yamal. Pages 157-162 *in* Tenth International Conference on Permafrost, Volume 2 - Translations of Russian Contributions. The Northern Publisher, Salekhard, Russia.
- Kling, G. W. 1995. Land-water linkages: the influence of terrestrial diversity on aquatic systems. Pages 297-310 *in* F. S. Chapin and C. Körner, editors. The role of biodiversity in arctic and alpine tundra ecosystems. Springer-Verlag, Berlin.
- Kokelj, S. V., R. E. Jenkins, D. Milburn, C. R. Burn, and N. Snow. 2005. The influence of thermokarst disturbance on the water quality of small upland lakes, Mackenzie Delta Region, Northwest Territories, Canada. *Permafrost and Periglacial Processes* 16:343-353.
- Kokelj, S. V. and M. T. Jorgenson. 2013. Advances in Thermokarst Research. *Permafrost and Periglacial Processes* 24:108-119.
- Kokelj, S. V., T. C. Lantz, J. Kanigan, S. L. Smith, and R. Coutts. 2009a. Origin and Polycyclic Behaviour of Tundra Thaw Slumps, Mackenzie Delta Region, Northwest Territories, Canada. *Permafrost and Periglacial Processes* 20:1-12.
- Kokelj, S. V., B. Zajdlik, and M. S. Thompson. 2009b. The Impacts of Thawing Permafrost on the Chemistry of Lakes across the Subarctic Boreal-Tundra Transition, Mackenzie Delta Region, Canada. *Permafrost and Periglacial Processes* 20:1-15.
- Kreig, R. A. and R. D. Reger. 1982. Airphoto Analysis and Summary of Landform Soil Properties along the Route of the Trans-Alaska Pipeline System, Geologic Report 66, Alaska Division of Geological and Geophysical Surveys. Page 149.
- Lacelle, D., J. Bjornson, and B. Lauriol. 2010. Climatic and Geomorphic Factors Affecting Contemporary (1950–2004) Activity of Retrogressive Thaw Slumps on the Aklavik Plateau, Richardson Mountains, NWT, Canada. *Permafrost and Periglacial Processes* 21.

- Lafreniere, M. J. and S. F. Lamoureux. 2013. Thermal Perturbation and Rainfall Runoff have Greater Impact on Seasonal Solute Loads than Physical Disturbance of the Active Layer. *Permafrost and Periglacial Processes* 24:241-251.
- Lamoureux, S. F. and M. J. Lafreniere. 2009. Fluvial Impact of Extensive Active Layer Detachments, Cape Bounty, Melville Island, Canada. *Arctic, Antarctic, and Alpine Research* 41:59-68.
- Lamoureux, S. F. and M. J. Lafreniere. 2014. Seasonal fluxes and age of particulate organic carbon exported from Arctic catchments impacted by localized permafrost slope disturbances. *Environmental Research Letters* 9:10.
- Lantuit, H. and W. H. Pollard. 2008. Fifty years of coastal erosion and retrogressive thaw slump activity on Herschel Island, southern Beaufort Sea, Yukon Territory, Canada. *Geomorphology* [Geomorphology]. Vol. 95: no. 1-2.
- Lantuit, H., W. H. Pollard, N. Couture, M. Fritz, L. Schirmer, H. Meyer, and H. W. Hubberten. 2012. Modern and Late Holocene Retrogressive Thaw Slump Activity on the Yukon Coastal Plain and Herschel Island, Yukon Territory, Canada. *Permafrost and Periglacial Processes* 23:39-51.
- Lantz, T. C., S. E. Gergel, and S. V. Kokelj. 2010. Spatial Heterogeneity in the Shrub Tundra Ecotone in the Mackenzie Delta Region, Northwest Territories: Implications for Arctic Environmental Change. *Ecosystems* 13:194-204.
- Lantz, T. C. and S. V. Kokelj. 2008. Increasing rates of retrogressive thaw slump activity in the Mackenzie Delta region, NWT, Canada. *Geophysical Research Letters* 35.
- Lantz, T. C., S. V. Kokelj, S. E. Gergel, and G. H. R. Henry. 2009. Relative impacts of disturbance and temperature: persistent changes in microenvironment and vegetation in retrogressive thaw slumps. *Global Change Biology* 15:1664-1675.
- Leibman, M. O. 1995. Cryogenic Landslides on the Yamal Peninsula, Russia - Preliminary-Observations. *Permafrost and Periglacial Processes* 6:259-264.
- Leibman, M. O., A. I. Kizyakov, L. D. Sulerzhitsky, and N. E. Zaretskaya. 2003. Dynamics of the landslide slopes and mechanism of their development on Yamal peninsula, Russia. *in* Proceedings of the Eight International Conference on Permafrost. A.A. Balkema Publishers, Rotterdam, Netherlands Zurich 21-25 July 2003.
- Lewkowicz, A. G. 1991. Climate Change and the Permafrost Landscape. Pages 91-104 *in* Arctic Environment: Past, Present and Future, McMaster University, Hamilton, ON.
- Lewkowicz, A. G. 1992. Climatic Change and the Permafrost Landscape. Pages 91-104 *in* M. Woo, D. Gregor, editor. Arctic Environment: Past, Present and Future. McMaster University, Hamilton, ON.

- Lewkowicz, A. G. 2007. Dynamics of Active-layer Detachment Failures, Fosheim Peninsula, Ellesmere Island, Nunavut, Canada. *Permafrost and Periglacial Processes* 18:89 - 103.
- Lewkowicz, A. G. and C. Harris. 2005. Morphology and geotechnique of active-layer detachment failures in discontinuous and continuous permafrost, northern Canada. *Geomorphology* 69:275-297.
- Mesquita, P. S., F. J. Wrona, and T. D. Prowse. 2010. Effects of retrogressive permafrost thaw slumping on sediment chemistry and submerged macrophytes in Arctic tundra lakes. *Freshwater Biology* 55:2347-2358.
- Parker, C. L. 2006. Vascular plant inventory of Alaska's Arctic National Parklands: Bering Land Bridge National Preserve, Cape Krusenstern National Monument, Gates of the Arctic National Park & Preserve, Kobuk Valley National Preserve, and Noatak National Preserve. ARCN I&M, National Park Service, Alaska Region Final Report:142p.
- Pastick, N. J., M. T. Jorgenson, B. K. Wylie, J. R. Rose, M. Rigge, and M. A. Walvoord. 2014a. Spatial variability and landscape controls of near-surface permafrost within the Alaskan Yukon River Basin. *Journal of Geophysical Research-Biogeosciences* 119:1244-1265.
- Pastick, N. J., M. Rigge, B. K. Wylie, M. T. Jorgenson, J. R. Rose, K. D. Johnson, and L. Ji. 2014b. Distribution and landscape controls of organic layer thickness and carbon within the Alaskan Yukon River Basin. *Geoderma* 230:79-94.
- Raynolds, M. K. and D. A. Walker. 2008. Circumpolar Relationships Between Permafrost Characteristics, NDVI, and Arctic Vegetation Types. Pages 1469-1474 *in* D. Kane, editor. Ninth International Conference on Permafrost. National Academy Press, Washington, DC, Fairbanks, Alaska.
- Rozell, N. 2009. Selawik Slump grows unabated, threatens fishery. Anchorage Daily News, Anchorage, AK.
- Schaefer, K., H. Lantuit, V. E. Romanovsky, E. A. G. Schuur, and R. Witt. 2014. The impact of the permafrost carbon feedback on global climate. *Environmental Research Letters* 9.
- Schaefer, K., T. Zhang, L. Bruhwiler, and A. P. Barrett. 2011. Amount and timing of permafrost carbon release in response to climate warming. *Tellus Series B-Chemical and Physical Meteorology*:no-no.
- Schuur, E. A. G., J. Bockheim, J. G. Canadell, E. Euskirchen, C. B. Field, S. V. Goryachkin, S. Hagemann, P. Kuhry, P. M. Lafleur, H. Lee, G. Mazhitova, F. E. Nelson, A. Rinke, V. E. Romanovsky, N. Shiklomanov, C. Tarnocai, S. Venevsky, J. G. Vogel, and S. A. Zimov. 2008. Vulnerability of Permafrost Carbon to Climate Change: Implications for the Global Carbon Cycle. *Bioscience* 58:701-714.

- Schuur, E. A. G., J. G. Vogel, K. G. Crummer, H. Lee, J. O. Sickman, and T. E. Osterkamp. 2009. The effect of permafrost thaw on old carbon release and net carbon exchange from tundra. *Nature* 459:556-559.
- Serreze, M. C., J. E. Walsh, F. S. Chapin, T. Osterkamp, M. Dyurgerov, V. Romanovsky, W. C. Oechel, J. Morison, T. Zhang, and R. G. Barry. 2000. Observational Evidence of Recent Change in the Northern High-Latitude Environment. *Climatic Change* 46:159-207.
- Shur, Y., K. M. Hinkel, and F. E. Nelson. 2005. The transient layer: implications for geocryology and climate-change science. *Permafrost and Periglacial Processes* 16:5-17.
- Shur, Y. and T. Zhestkova. 2003. Cryogenic structure of a glacio-lacustrine deposit.
- Shur, Y. L. 1988. The upper horizon of permafrost soil. Pages 867-871 *in* Proceedings of the Fifth Intern. Conf. on Permafrost. Tapir Publishers, Trondheim, Norway.
- Shur, Y. L. and M. T. Jorgenson. 2007. Patterns of Permafrost Formation and Degradation in Relation to Climate and Ecosystems. *Permafrost and Periglacial Processes* 18:7 - 19.
- Slater, A. G. and D. M. Lawrence. 2013. Diagnosing Present and Future Permafrost from Climate Models. *Journal of Climate* 26:5608-5623.
- Stewart, I. T., D. R. Cayan, and M. D. Dettinger. 2005. Changes toward earlier streamflow timing across western North America. *Journal of Climate* 18:1136-1155.
- Swanson, D. K. 2010. Mapping of erosion features related to thaw of permafrost in Bering Land Bridge National Preserve, Cape Krusenstern National Monument, and Kobuk Valley National Park. Natural Resource Data Series NPS/ARCN/NRDS—2010/122. National Park Service, Fort Collins, Colorado.
- Swanson, D. K. and K. Hill. 2010. Monitoring of Retrogressive Thaw Slumps in the Arctic Network, 2010 Baseline Data: Three-dimensional Modeling with Small-format Aerial Photographs. Page 58. U.S. Department of the Interior, National Park Service, Natural Resource Data Series NPS/ARCN/NRDS—2010/123, Natural Resource Program Center, Fort Collins, CO.
- Tarnocai, C., J. G. Canadell, E. A. G. Schuur, P. Kuhry, G. Mazhitova, and S. Zimov. 2009. Soil organic carbon pools in the northern circumpolar permafrost region. *Global Biogeochemical Cycles* 23:1-11.
- Thompson, M. S., S. V. Kokelj, T. D. Prowse, and F. J. W. . 2008. The impact of sediments derived from thawing permafrost on tundra lake water chemistry: An experimental approach. *in* Proceedings of the 9th Permafrost International Conference, Fairbanks, AK.
- van Cleve, K., F. S. Chapin, III, C. T. Dyrness, and L. A. Viereck. 1991. Element Cycling in Taiga Forests: State-Factor Control. *Bioscience* 41:78-88.

- Viereck, L. 1973. Ecological effects of river flooding and forest fires on permafrost in the taiga of Alaska. Pages 60-67 in *Permafrost: The North American contribution to the Second International Conference*. National Academy of Sciences, Yakutsk, USSR.
- Viereck, L. A., C. T. Dyrness, A. R. Batten, and K. J. Wenzlick. 1992. The Alaska Vegetation Classification. Page 278 in U. S. D. o. A. F. Service, editor. Gen. Tech. Rep. PNW-GTR-286, Portland, OR.
- Wahrhaftig, C. 1965. Physiographic Divisions of Alaska. U.S.G.S. Professional Paper 482. 52 pp.
- Walker, D. A., N. A. Auerbach, and M. M. Shippert. 1995. NDVI, biomass, and landscape evolution of glaciated terrain in northern Alaska. *Polar Record* 31:169-178.
- Walker, D. A., H. E. Epstein, V. E. Romanovsky, C. L. Ping, G. J. Michaelson, R. P. Daanen, Y. Shur, R. A. Peterson, W. B. Krantz, M. K. Reynolds, W. A. Gould, G. Gonzalez, D. J. Nicolsky, C. M. Vonlanthen, A. N. Kade, P. Kuss, A. M. Kelley, C. A. Munger, C. T. Tamocai, N. V. Matveyeva, and F. J. A. Daniels. 2008. Arctic patterned-ground ecosystems: A synthesis of field studies and models along a North American Arctic Transect. *Journal of Geophysical Research-Biogeosciences* 113.
- Walker, D. A. and H. A. Maier. 2008. Vegetation in the vicinity of the Toolik Field Station, Alaska. *Biological Papers of the University of Alaska*, No. 28, Insitute of Arctic Biology, Fairbanks, AK.
- Walker, H. J. and P. F. Hudson. 2003. Hydrologic and geomorphic processes in the Colville River delta, Alaska. *Geomorphology* 56:291-303.
- Walker, J., L. Amborg, and J. Peippo. 1987. Riverbank Erosion in the Colville Delta, Alaska. *Geografiska Annaler Series a-Physical Geography* 69:61-70.
- Walker, M. D., D. A. Walker, and N. A. Auerbach. 1994. PLANT-COMMUNITIES OF A TUSsock TUNDRA LANDSCAPE IN THE BROOKS RANGE FOOTHILLS, ALASKA. *Journal of Vegetation Science* 5:843-866.
- Walter, K. M., M. E. Edwards, G. Grosse, S. A. Zimov, and F. S. Chapin. 2007. Thermokarst lakes as a source of atmospheric CH₄ during the last deglaciation. *Science* 318:633-636.
- Walter, K. M., S. A. Zimov, J. P. Chanton, D. Verbyla, and F. S. C. III. 2006. Methane bubbling from Siberian thaw lakes as a positive feedback to climate warming. *Nature* 443:71-75.
- Xie, C. and W. Gough. 2013. A Simple Thaw-Freeze Algorithm for a Multi-Layered Soil using the Stefan Equation. *Permafrost and Periglacial Processes* 24:252-260.
- Young, S. B. 1974. The environment of the Noatak River basin, Alaska., *Contributions of the Center for Northern Studies*, Wolcott, VT.

- Zimov, N. S., S. A. Zimov, A. E. Zimova, G. M. Zimova, V. I. Chuprynin, and F. S. Chapin, III. 2009. Carbon storage in permafrost and soils of the mammoth tundra-steppe biome: Role in the global carbon budget. *Geophysical Research Letters* 36.
- Zimov, S. A., S. P. Davydov, G. M. Zimova, A. I. Davydova, E. A. G. Schuur, K. Dutta, and I. F. S. Chapin. 2006. Permafrost carbon: Stock and decomposability of a globally significant carbon pool. *Geophysical Research Letters* 33.

Appendices

Appendix A. Active layer detachment slide and retrogressive thaw slump locations within the study region.

Locations for features are given in geographic coordinates, NAD83. Initial location data were developed through the University of Alaska Fairbanks (Balser et al. 2009, Gooseff et al. 2009 and Balser et al. 2014), and were significantly expanded by the U.S. National Park Service (Swanson and Hill 2010).

Balser, A., M. N. Gooseff, J. Jones, and W. B. Bowden (2009), Thermokarst distribution and relationships to landscape characteristics in the Feniak Lake region, Noatak National Preserve, Alaska; Final Report to the National Park Service, Arctic Network (ARCN), Fairbanks, AK.

Balser, A. W., J. B. Jones, and R. Gens (2014), Timing of Retrogressive Thaw Slump Initiation in the Noatak Basin, Northwest Alaska, USA, *Journal of Geophysical Research: Earth Surface*, 2013JF002889.

Gooseff, M., A. Balser, W. Bowden, and J. Jones (2009), Effects of hillslope thermokarst in northern Alaska. , 90: 29-31., *Eos, Transactions of the American Geophysical Union*, 90(4), 29-31.

Swanson, D. K., and K. Hill (2010), Monitoring of Retrogressive Thaw Slumps in the Arctic Network, 2010 Baseline Data: Three-dimensional Modeling with Small-format Aerial Photographs, edited, p. 58, U.S. Department of the Interior, National Park Service, Natural Resource Data Series NPS/ARCN/NRDS—2010/123, Natural Resource Program Center, Fort Collins, CO.

Table AA.1. Active layer detachment slides and retrogressive thaw slump locations within the study region; central and western Brooks Range, Alaska.

Database ID (ARCSS-TK / NPS)	Feature Type	Source	Group	Year (GPS / Imagery)	Latitude	Longitude
FT104Z	Active Layer Detachment Slide	Field GPS	U. of Alaska Fairbanks	2006	67.88324	-156.73721
FT105Z	Active Layer Detachment Slide	Field GPS	U. of Alaska Fairbanks	2006	67.76704	-156.34677
FT107Z	Active Layer Detachment Slide	Field GPS	U. of Alaska Fairbanks	2006	67.67092	-155.91830
FT110Z	Active Layer Detachment Slide	Field GPS	U. of Alaska Fairbanks	2006	68.23462	-157.71762
FT111Z	Active Layer Detachment Slide	Field GPS	U. of Alaska Fairbanks	2006	68.23590	-157.72273
FT114Y	Active Layer Detachment Slide	Field GPS	U. of Alaska Fairbanks	2006	68.48897	-159.14814
FT115Y	Active Layer Detachment Slide	Field GPS	U. of Alaska Fairbanks	2006	68.48937	-159.14649
FT116Y	Active Layer Detachment Slide	Field GPS	U. of Alaska Fairbanks	2006	68.48831	-159.14861
FT118Y	Retrogressive Thaw Slump	Field GPS	U. of Alaska Fairbanks	2006	68.03853	-158.52225
FT119Y	Retrogressive Thaw Slump	Field GPS	U. of Alaska Fairbanks	2006	68.03749	-158.51876
FT120Y	Retrogressive Thaw Slump	Field GPS	U. of Alaska Fairbanks	2006	68.03631	-158.51643
FT121Y	Retrogressive Thaw Slump	Field GPS	U. of Alaska Fairbanks	2006	68.03515	-158.51538
FT122Y	Retrogressive Thaw Slump	Field GPS	U. of Alaska Fairbanks	2006	68.04035	-158.52200
FT123Y	Retrogressive Thaw Slump	Field GPS	U. of Alaska Fairbanks	2006	68.04149	-158.52456
FT124Y	Retrogressive Thaw Slump	Field GPS	U. of Alaska Fairbanks	2006	67.97018	-158.50768
FT125Y	Retrogressive Thaw Slump	Field GPS	U. of Alaska Fairbanks	2006	67.97085	-158.50967
FT126Y	Retrogressive Thaw Slump	Field GPS	U. of Alaska Fairbanks	2006	67.97189	-158.51258
FT127Y	Retrogressive Thaw Slump	Field GPS	U. of Alaska Fairbanks	2006	67.97379	-158.51672
FT128Y	Retrogressive Thaw Slump	Field GPS	U. of Alaska Fairbanks	2006	67.97453	-158.51822
FT129Y	Retrogressive Thaw Slump	Field GPS	U. of Alaska Fairbanks	2006	67.97603	-158.51927
FT130Y	Retrogressive Thaw Slump	Field GPS	U. of Alaska Fairbanks	2006	67.85559	-158.35374
FT131Y	Retrogressive Thaw Slump	Field GPS	U. of Alaska Fairbanks	2006	67.86143	-158.38172
FT132Y	Retrogressive Thaw Slump	Field GPS	U. of Alaska Fairbanks	2006	67.86491	-158.39166
FT133Y	Retrogressive Thaw Slump	Field GPS	U. of Alaska Fairbanks	2006	67.86445	-158.38743
FT134Y	Retrogressive Thaw Slump	Field GPS	U. of Alaska Fairbanks	2006	67.86398	-158.38569
FT135Y	Retrogressive Thaw Slump	Field GPS	U. of Alaska Fairbanks	2006	67.86355	-158.38528
FT136Y	Retrogressive Thaw Slump	Field GPS	U. of Alaska Fairbanks	2006	67.86301	-158.38411

FT137Y	Retrogressive Thaw Slump	Field GPS
FT138Y	Retrogressive Thaw Slump	Field GPS
FT139Y	Retrogressive Thaw Slump	Field GPS
FT140Y	Retrogressive Thaw Slump	Field GPS
FT142Y	Active Layer Detachment Slide	Field GPS
FT146Y	Active Layer Detachment Slide	Field GPS
FT147Y	Active Layer Detachment Slide	Field GPS
FT148Y	Active Layer Detachment Slide	Field GPS
FT149Z	Active Layer Detachment Slide	Field GPS
FT154Z	Active Layer Detachment Slide	Field GPS
FT159Z	Active Layer Detachment Slide	Field GPS
FT160Z	Active Layer Detachment Slide	Field GPS
FT161Z	Active Layer Detachment Slide	Field GPS
FT162Z	Active Layer Detachment Slide	Field GPS
FT165Z	Retrogressive Thaw Slump	Field GPS
FT167Z	Retrogressive Thaw Slump	Field GPS
FT171Z	Active Layer Detachment Slide	Field GPS
FT172Z	Retrogressive Thaw Slump	Field GPS
FT173Z	Retrogressive Thaw Slump	Field GPS
FT178Z	Active Layer Detachment Slide	Field GPS
FT181Z	Retrogressive Thaw Slump	Field GPS
FT183Z	Retrogressive Thaw Slump	Field GPS
FT184Z	Retrogressive Thaw Slump	Field GPS
FT185Z	Retrogressive Thaw Slump	Field GPS
FT187Z	Retrogressive Thaw Slump	Field GPS
FT188Z	Retrogressive Thaw Slump	Field GPS
FT189Z	Active Layer Detachment Slide	Field GPS
FT190Z	Active Layer Detachment Slide	Field GPS
FT191Z	Retrogressive Thaw Slump	Field GPS
FT192Z	Retrogressive Thaw Slump	Field GPS
FT195Z	Active Layer Detachment Slide	Field GPS
FT196Z	Active Layer Detachment Slide	Field GPS

U. of Alaska Fairbanks	2006	67.85766	-158.36826
U. of Alaska Fairbanks	2006	67.85784	-158.37111
U. of Alaska Fairbanks	2006	67.85852	-158.37321
U. of Alaska Fairbanks	2006	67.85891	-158.37519
U. of Alaska Fairbanks	2006	68.26778	-157.30949
U. of Alaska Fairbanks	2006	68.26728	-157.31006
U. of Alaska Fairbanks	2006	68.26808	-157.30991
U. of Alaska Fairbanks	2006	68.26861	-157.30958
U. of Alaska Fairbanks	2006	68.25142	-157.90627
U. of Alaska Fairbanks	2006	68.26370	-157.29374
U. of Alaska Fairbanks	2006	68.45438	-158.97491
U. of Alaska Fairbanks	2006	68.45168	-158.97390
U. of Alaska Fairbanks	2006	68.45534	-159.05866
U. of Alaska Fairbanks	2006	68.47945	-159.17736
U. of Alaska Fairbanks	2006	68.16111	-159.55474
U. of Alaska Fairbanks	2006	68.15463	-159.57100
U. of Alaska Fairbanks	2006	68.05341	-159.64712
U. of Alaska Fairbanks	2006	68.01296	-159.25386
U. of Alaska Fairbanks	2006	68.03417	-159.28272
U. of Alaska Fairbanks	2006	68.17480	-158.56306
U. of Alaska Fairbanks	2006	67.84861	-158.33163
U. of Alaska Fairbanks	2006	68.00376	-158.47685
U. of Alaska Fairbanks	2006	68.04581	-158.58311
U. of Alaska Fairbanks	2006	68.00185	-158.58830
U. of Alaska Fairbanks	2006	68.04343	-158.63505
U. of Alaska Fairbanks	2006	68.13034	-158.72775
U. of Alaska Fairbanks	2006	68.16480	-158.70499
U. of Alaska Fairbanks	2006	68.19123	-158.64402
U. of Alaska Fairbanks	2006	68.08284	-158.96152
U. of Alaska Fairbanks	2006	68.11407	-158.96053
U. of Alaska Fairbanks	2006	68.25162	-157.97818
U. of Alaska Fairbanks	2006	68.14685	-157.43647

FT198Z	Active Layer Detachment Slide	Field GPS
FT199Z	Active Layer Detachment Slide	Field GPS
FT200X	Active Layer Detachment Slide	Airphoto(AHAP)
FT201X	Active Layer Detachment Slide	Airphoto(AHAP)
FT202X	Active Layer Detachment Slide	Airphoto(AHAP)
FT203X	Active Layer Detachment Slide	Airphoto(AHAP)
FT204X	Active Layer Detachment Slide	Airphoto(AHAP)
FT205X	Active Layer Detachment Slide	Airphoto(AHAP)
FT206X	Active Layer Detachment Slide	Airphoto(AHAP)
FT208X	Retrogressive Thaw Slump	Airphoto(AHAP)
FT209X	Active Layer Detachment Slide	Airphoto(AHAP)
FT210X	Active Layer Detachment Slide	Airphoto(AHAP)
FT211X	Retrogressive Thaw Slump	Airphoto(AHAP)
FT212X	Retrogressive Thaw Slump	Airphoto(AHAP)
FT213X	Active Layer Detachment Slide	Airphoto(AHAP)
FT214X	Active Layer Detachment Slide	Airphoto(AHAP)
FT215X	Active Layer Detachment Slide	Airphoto(AHAP)
FT216X	Active Layer Detachment Slide	Airphoto(AHAP)
FT217X	Active Layer Detachment Slide	Airphoto(AHAP)
FT218X	Active Layer Detachment Slide	Airphoto(AHAP)
FT219X	Active Layer Detachment Slide	Airphoto(AHAP)
FT220X	Retrogressive Thaw Slump	Airphoto(AHAP)
FT221X	Retrogressive Thaw Slump	Airphoto(AHAP)
FT222X	Active Layer Detachment Slide	Airphoto(AHAP)
FT224X	Retrogressive Thaw Slump	Airphoto(AHAP)
FT225X	Retrogressive Thaw Slump	Airphoto(AHAP)
FT226X	Retrogressive Thaw Slump	Airphoto(AHAP)
FT227X	Retrogressive Thaw Slump	Airphoto(AHAP)
FT228X	Retrogressive Thaw Slump	Airphoto(AHAP)
FT229X	Active Layer Detachment Slide	Airphoto(AHAP)
FT230X	Active Layer Detachment Slide	Airphoto(AHAP)
FT231X	Active Layer Detachment Slide	Airphoto(AHAP)

U. of Alaska Fairbanks	2006	68.16018	-157.98005
U. of Alaska Fairbanks	2006	68.19228	-158.03011
U. of Alaska Fairbanks	1978	68.24374	-157.81451
U. of Alaska Fairbanks	1978	68.24313	-157.81479
U. of Alaska Fairbanks	1978	68.24188	-157.81536
U. of Alaska Fairbanks	1978	68.24461	-157.79860
U. of Alaska Fairbanks	1978	68.24119	-157.79776
U. of Alaska Fairbanks	1978	68.24198	-157.79926
U. of Alaska Fairbanks	1978	68.25346	-157.79999
U. of Alaska Fairbanks	1978	68.24900	-157.76760
U. of Alaska Fairbanks	1978	68.24152	-157.78810
U. of Alaska Fairbanks	1978	68.24413	-157.79234
U. of Alaska Fairbanks	1978	68.24736	-157.76669
U. of Alaska Fairbanks	1978	68.24624	-157.76585
U. of Alaska Fairbanks	1978	68.22581	-157.76864
U. of Alaska Fairbanks	1978	68.22496	-157.76614
U. of Alaska Fairbanks	1978	68.22443	-157.76551
U. of Alaska Fairbanks	1978	68.22432	-157.76268
U. of Alaska Fairbanks	1978	68.22526	-157.75619
U. of Alaska Fairbanks	1978	68.22671	-157.75946
U. of Alaska Fairbanks	1978	68.22740	-157.76113
U. of Alaska Fairbanks	1978	68.23982	-157.79417
U. of Alaska Fairbanks	1978	68.23970	-157.79278
U. of Alaska Fairbanks	1978	68.24069	-157.79121
U. of Alaska Fairbanks	1978	68.23863	-157.80087
U. of Alaska Fairbanks	1978	68.23876	-157.80276
U. of Alaska Fairbanks	1978	68.23887	-157.79766
U. of Alaska Fairbanks	1978	68.23897	-157.79556
U. of Alaska Fairbanks	1978	68.23901	-157.79856
U. of Alaska Fairbanks	1978	68.25167	-157.94785
U. of Alaska Fairbanks	1978	68.25327	-157.94596
U. of Alaska Fairbanks	1978	68.25341	-157.94770

FT232X	Active Layer Detachment Slide	Airphoto(AHAP)
FT233X	Active Layer Detachment Slide	Airphoto(AHAP)
FT234X	Active Layer Detachment Slide	Airphoto(AHAP)
FT235X	Active Layer Detachment Slide	Airphoto(AHAP)
FT236X	Active Layer Detachment Slide	Airphoto(AHAP)
FT237X	Active Layer Detachment Slide	Airphoto(AHAP)
FT238X	Active Layer Detachment Slide	Airphoto(AHAP)
FT239X	Active Layer Detachment Slide	Airphoto(AHAP)
FT240X	Active Layer Detachment Slide	Airphoto(AHAP)
FT241X	Active Layer Detachment Slide	Airphoto(AHAP)
FT242X	Retrogressive Thaw Slump	Airphoto(AHAP)
FT243X	Active Layer Detachment Slide	Airphoto(AHAP)
FT244X	Active Layer Detachment Slide	Airphoto(AHAP)
FT245X	Active Layer Detachment Slide	Airphoto(AHAP)
FT246X	Active Layer Detachment Slide	Airphoto(AHAP)
FT247X	Active Layer Detachment Slide	Airphoto(AHAP)
FT250X	Active Layer Detachment Slide	Airphoto(AHAP)
FT252X	Active Layer Detachment Slide	Airphoto(AHAP)
FT253X	Active Layer Detachment Slide	Airphoto(AHAP)
FT254X	Active Layer Detachment Slide	Airphoto(AHAP)
FT255X	Active Layer Detachment Slide	Airphoto(AHAP)
FT256X	Active Layer Detachment Slide	Airphoto(AHAP)
FT257X	Active Layer Detachment Slide	Airphoto(AHAP)
FT258X	Active Layer Detachment Slide	Airphoto(AHAP)
FT259X	Active Layer Detachment Slide	Airphoto(AHAP)
FT260X	Active Layer Detachment Slide	Airphoto(AHAP)
FT261X	Active Layer Detachment Slide	Airphoto(AHAP)
FT262X	Active Layer Detachment Slide	Airphoto(AHAP)
FT263X	Active Layer Detachment Slide	Airphoto(AHAP)
FT264X	Active Layer Detachment Slide	Airphoto(AHAP)
FT265X	Active Layer Detachment Slide	Airphoto(AHAP)
FT266X	Active Layer Detachment Slide	Airphoto(AHAP)

U. of Alaska Fairbanks	1978	68.25239	-157.94823
U. of Alaska Fairbanks	1978	68.25412	-157.89484
U. of Alaska Fairbanks	1978	68.24992	-157.90883
U. of Alaska Fairbanks	1978	68.24989	-157.92408
U. of Alaska Fairbanks	1978	68.25073	-157.95475
U. of Alaska Fairbanks	1978	68.24961	-157.95889
U. of Alaska Fairbanks	1978	68.25105	-157.95266
U. of Alaska Fairbanks	1978	68.25056	-157.95387
U. of Alaska Fairbanks	1978	68.25048	-157.94994
U. of Alaska Fairbanks	1978	68.24321	-157.92735
U. of Alaska Fairbanks	1978	68.24602	-157.91152
U. of Alaska Fairbanks	1978	68.24452	-157.89454
U. of Alaska Fairbanks	1978	68.24467	-157.89578
U. of Alaska Fairbanks	1978	68.25016	-157.90132
U. of Alaska Fairbanks	1978	68.23882	-157.88194
U. of Alaska Fairbanks	1978	68.24644	-157.87995
U. of Alaska Fairbanks	1978	68.24508	-157.87710
U. of Alaska Fairbanks	1978	68.25043	-157.87115
U. of Alaska Fairbanks	1978	68.24985	-157.87240
U. of Alaska Fairbanks	1978	68.25000	-157.87204
U. of Alaska Fairbanks	1978	68.25275	-157.87388
U. of Alaska Fairbanks	1978	68.25048	-157.85776
U. of Alaska Fairbanks	1978	68.25067	-157.85709
U. of Alaska Fairbanks	1978	68.25357	-157.83788
U. of Alaska Fairbanks	1978	68.25252	-157.83833
U. of Alaska Fairbanks	1978	68.25159	-157.83858
U. of Alaska Fairbanks	1978	68.25310	-157.84052
U. of Alaska Fairbanks	1978	68.25614	-157.84351
U. of Alaska Fairbanks	1978	68.25490	-157.84377
U. of Alaska Fairbanks	1978	68.24817	-157.83473
U. of Alaska Fairbanks	1978	68.24545	-157.83141
U. of Alaska Fairbanks	1978	68.24752	-157.83984

FT267X	Active Layer Detachment Slide	Airphoto(AHAP)
FT268X	Active Layer Detachment Slide	Airphoto(AHAP)
FT269X	Active Layer Detachment Slide	Airphoto(AHAP)
FT270X	Active Layer Detachment Slide	Airphoto(AHAP)
FT271X	Active Layer Detachment Slide	Airphoto(AHAP)
FT272X	Active Layer Detachment Slide	Airphoto(AHAP)
FT273X	Active Layer Detachment Slide	Airphoto(AHAP)
FT274X	Active Layer Detachment Slide	Airphoto(AHAP)
FT275X	Active Layer Detachment Slide	Airphoto(AHAP)
FT276X	Active Layer Detachment Slide	Airphoto(AHAP)
FT277X	Active Layer Detachment Slide	Airphoto(AHAP)
FT278X	Active Layer Detachment Slide	Airphoto(AHAP)
FT279X	Active Layer Detachment Slide	Airphoto(AHAP)
FT280X	Active Layer Detachment Slide	Airphoto(AHAP)
FT281X	Active Layer Detachment Slide	Airphoto(AHAP)
FT282X	Active Layer Detachment Slide	Airphoto(AHAP)
FT283X	Active Layer Detachment Slide	Airphoto(AHAP)
FT284X	Active Layer Detachment Slide	Airphoto(AHAP)
FT285X	Active Layer Detachment Slide	Airphoto(AHAP)
FT286X	Active Layer Detachment Slide	Airphoto(AHAP)
FT287X	Active Layer Detachment Slide	Airphoto(AHAP)
FT288X	Active Layer Detachment Slide	Airphoto(AHAP)
FT289X	Active Layer Detachment Slide	Airphoto(AHAP)
FT292X	Retrogressive Thaw Slump	Airphoto(AHAP)
FT293X	Active Layer Detachment Slide	Airphoto(AHAP)
FT294X	Active Layer Detachment Slide	Airphoto(AHAP)
FT295X	Active Layer Detachment Slide	Airphoto(AHAP)
FT296X	Active Layer Detachment Slide	Airphoto(AHAP)
FT297X	Active Layer Detachment Slide	Airphoto(AHAP)
FT298X	Active Layer Detachment Slide	Airphoto(AHAP)
FT299X	Active Layer Detachment Slide	Airphoto(AHAP)
FT303X	Active Layer Detachment Slide	Airphoto(AHAP)

U. of Alaska Fairbanks	1978	68.24529	-157.83440
U. of Alaska Fairbanks	1978	68.24379	-157.81763
U. of Alaska Fairbanks	1978	68.24433	-157.81664
U. of Alaska Fairbanks	1978	68.24413	-157.82076
U. of Alaska Fairbanks	1978	68.24369	-157.82281
U. of Alaska Fairbanks	1978	68.24451	-157.82297
U. of Alaska Fairbanks	1978	68.24427	-157.81916
U. of Alaska Fairbanks	1978	68.24272	-157.81884
U. of Alaska Fairbanks	1978	68.24272	-157.82325
U. of Alaska Fairbanks	1978	68.24458	-157.82805
U. of Alaska Fairbanks	1978	68.24947	-157.86284
U. of Alaska Fairbanks	1978	68.24318	-157.86216
U. of Alaska Fairbanks	1978	68.23606	-157.84473
U. of Alaska Fairbanks	1978	68.23505	-157.83078
U. of Alaska Fairbanks	1978	68.23428	-157.83133
U. of Alaska Fairbanks	1978	68.23407	-157.83303
U. of Alaska Fairbanks	1978	68.24107	-157.82654
U. of Alaska Fairbanks	1978	68.25563	-157.74648
U. of Alaska Fairbanks	1978	68.25444	-157.69488
U. of Alaska Fairbanks	1978	68.25707	-157.68690
U. of Alaska Fairbanks	1978	68.25349	-157.69308
U. of Alaska Fairbanks	1978	68.25472	-157.68615
U. of Alaska Fairbanks	1985	68.27034	-158.08197
U. of Alaska Fairbanks	1985	68.26975	-158.12172
U. of Alaska Fairbanks	1985	68.25659	-158.06031
U. of Alaska Fairbanks	1985	68.25950	-158.03684
U. of Alaska Fairbanks	1985	68.25962	-158.03592
U. of Alaska Fairbanks	1985	68.25980	-158.03183
U. of Alaska Fairbanks	1985	68.25528	-158.05220
U. of Alaska Fairbanks	1985	68.25537	-158.05599
U. of Alaska Fairbanks	1985	68.26131	-157.90704
U. of Alaska Fairbanks	1985	68.26681	-157.99564

FT304X	Active Layer Detachment Slide	Airphoto(AHAP)
FT305X	Active Layer Detachment Slide	Airphoto(AHAP)
FT306X	Active Layer Detachment Slide	Airphoto(AHAP)
FT307X	Active Layer Detachment Slide	Airphoto(AHAP)
FT308X	Active Layer Detachment Slide	Airphoto(AHAP)
FT309X	Active Layer Detachment Slide	Airphoto(AHAP)
FT310X	Active Layer Detachment Slide	Airphoto(AHAP)
FT311X	Active Layer Detachment Slide	Airphoto(AHAP)
FT312X	Active Layer Detachment Slide	Airphoto(AHAP)
FT313X	Active Layer Detachment Slide	Airphoto(AHAP)
FT323X	Active Layer Detachment Slide	Airphoto(TT)
FT324X	Active Layer Detachment Slide	Airphoto(TT)
FT325X	Active Layer Detachment Slide	Airphoto(TT)
FT326X	Active Layer Detachment Slide	Airphoto(TT)
FT327X	Active Layer Detachment Slide	Airphoto(TT)
FT328X	Active Layer Detachment Slide	Airphoto(TT)
FT329X	Active Layer Detachment Slide	Airphoto(TT)
FT330X	Active Layer Detachment Slide	Airphoto(TT)
FT331X	Active Layer Detachment Slide	Airphoto(TT)
FT332X	Active Layer Detachment Slide	Airphoto(TT)
FT333X	Active Layer Detachment Slide	Airphoto(TT)
FT334X	Active Layer Detachment Slide	Airphoto(TT)
FT335X	Active Layer Detachment Slide	Airphoto(TT)
FT336X	Active Layer Detachment Slide	Airphoto(TT)
FT337X	Active Layer Detachment Slide	Airphoto(TT)
FT338X	Active Layer Detachment Slide	Airphoto(TT)
FT339X	Active Layer Detachment Slide	Airphoto(TT)
FT340X	Active Layer Detachment Slide	Airphoto(TT)
FT343X	Active Layer Detachment Slide	Airphoto(TT)
FT344X	Active Layer Detachment Slide	Airphoto(TT)
FT345X	Active Layer Detachment Slide	Airphoto(TT)
FT346X	Active Layer Detachment Slide	Airphoto(TT)

U. of Alaska Fairbanks	1985	68.26329	-157.99109
U. of Alaska Fairbanks	1985	68.25666	-157.93146
U. of Alaska Fairbanks	1985	68.25809	-157.93253
U. of Alaska Fairbanks	1985	68.25799	-157.92656
U. of Alaska Fairbanks	1985	68.25624	-157.92813
U. of Alaska Fairbanks	1985	68.25653	-157.92666
U. of Alaska Fairbanks	1985	68.25867	-157.92875
U. of Alaska Fairbanks	1985	68.25737	-157.93432
U. of Alaska Fairbanks	1985	68.25792	-157.92973
U. of Alaska Fairbanks	1985	68.26774	-157.71379
U. of Alaska Fairbanks	2006	68.25728	-157.97759
U. of Alaska Fairbanks	2006	68.25972	-157.96862
U. of Alaska Fairbanks	2006	68.26012	-157.93282
U. of Alaska Fairbanks	2006	68.26153	-157.92475
U. of Alaska Fairbanks	2006	68.26184	-157.92052
U. of Alaska Fairbanks	2006	68.25884	-157.93292
U. of Alaska Fairbanks	2006	68.25770	-157.93206
U. of Alaska Fairbanks	2006	68.25849	-157.92576
U. of Alaska Fairbanks	2006	68.25406	-157.92832
U. of Alaska Fairbanks	2006	68.25299	-157.92977
U. of Alaska Fairbanks	2006	68.24986	-157.95498
U. of Alaska Fairbanks	2006	68.24334	-157.95452
U. of Alaska Fairbanks	2006	68.24528	-157.91670
U. of Alaska Fairbanks	2006	68.24118	-157.88893
U. of Alaska Fairbanks	2006	68.24231	-157.90763
U. of Alaska Fairbanks	2006	68.24422	-157.89726
U. of Alaska Fairbanks	2006	68.24370	-157.89394
U. of Alaska Fairbanks	2006	68.24384	-157.89297
U. of Alaska Fairbanks	2006	68.24050	-157.87341
U. of Alaska Fairbanks	2006	68.23943	-157.86403
U. of Alaska Fairbanks	2006	68.24068	-157.87293
U. of Alaska Fairbanks	2006	68.24549	-157.87433

FT349X	Active Layer Detachment Slide	Airphoto(TT)
FT350X	Active Layer Detachment Slide	Airphoto(TT)
FT351X	Active Layer Detachment Slide	Airphoto(TT)
FT352X	Active Layer Detachment Slide	Airphoto(TT)
FT353X	Active Layer Detachment Slide	Airphoto(TT)
FT354X	Active Layer Detachment Slide	Airphoto(TT)
FT355X	Active Layer Detachment Slide	Airphoto(TT)
FT356X	Active Layer Detachment Slide	Airphoto(TT)
FT357X	Active Layer Detachment Slide	Airphoto(TT)
FT358X	Active Layer Detachment Slide	Airphoto(TT)
FT359X	Active Layer Detachment Slide	Airphoto(TT)
FT360X	Active Layer Detachment Slide	Airphoto(TT)
FT361X	Active Layer Detachment Slide	Airphoto(TT)
FT362X	Active Layer Detachment Slide	Airphoto(TT)
FT363X	Active Layer Detachment Slide	Airphoto(TT)
FT364X	Active Layer Detachment Slide	Airphoto(TT)
FT365X	Active Layer Detachment Slide	Airphoto(TT)
FT366X	Active Layer Detachment Slide	Airphoto(TT)
FT367X	Active Layer Detachment Slide	Airphoto(TT)
FT368X	Active Layer Detachment Slide	Airphoto(TT)
FT369X	Active Layer Detachment Slide	Airphoto(TT)
FT370X	Active Layer Detachment Slide	Airphoto(TT)
FT371X	Active Layer Detachment Slide	Airphoto(TT)
FT372X	Active Layer Detachment Slide	Airphoto(TT)
FT373X	Active Layer Detachment Slide	Airphoto(TT)
FT374X	Active Layer Detachment Slide	Airphoto(TT)
FT375X	Active Layer Detachment Slide	Airphoto(TT)
FT376X	Active Layer Detachment Slide	Airphoto(TT)
FT377X	Active Layer Detachment Slide	Airphoto(TT)
FT378X	Active Layer Detachment Slide	Airphoto(TT)
FT379X	Active Layer Detachment Slide	Airphoto(TT)
FT380X	Active Layer Detachment Slide	Airphoto(TT)

U. of Alaska Fairbanks	2006	68.25022	-157.86837
U. of Alaska Fairbanks	2006	68.24980	-157.86178
U. of Alaska Fairbanks	2006	68.25015	-157.86224
U. of Alaska Fairbanks	2006	68.25005	-157.87503
U. of Alaska Fairbanks	2006	68.25110	-157.87448
U. of Alaska Fairbanks	2006	68.25126	-157.87420
U. of Alaska Fairbanks	2006	68.25171	-157.86606
U. of Alaska Fairbanks	2006	68.25155	-157.86777
U. of Alaska Fairbanks	2006	68.25019	-157.86660
U. of Alaska Fairbanks	2006	68.25655	-157.87332
U. of Alaska Fairbanks	2006	68.25712	-157.87097
U. of Alaska Fairbanks	2006	68.25482	-157.86756
U. of Alaska Fairbanks	2006	68.25373	-157.86976
U. of Alaska Fairbanks	2006	68.25329	-157.87174
U. of Alaska Fairbanks	2006	68.25267	-157.87415
U. of Alaska Fairbanks	2006	68.25185	-157.85336
U. of Alaska Fairbanks	2006	68.25373	-157.85847
U. of Alaska Fairbanks	2006	68.25064	-157.85467
U. of Alaska Fairbanks	2006	68.25137	-157.83456
U. of Alaska Fairbanks	2006	68.24923	-157.83782
U. of Alaska Fairbanks	2006	68.24328	-157.83046
U. of Alaska Fairbanks	2006	68.24471	-157.85855
U. of Alaska Fairbanks	2006	68.23430	-157.85424
U. of Alaska Fairbanks	2006	68.23357	-157.83444
U. of Alaska Fairbanks	2006	68.23707	-157.82703
U. of Alaska Fairbanks	2006	68.23153	-157.83696
U. of Alaska Fairbanks	2006	68.23509	-157.83193
U. of Alaska Fairbanks	2006	68.25732	-158.00647
U. of Alaska Fairbanks	2006	68.27298	-157.74122
U. of Alaska Fairbanks	2006	68.27361	-157.73190
U. of Alaska Fairbanks	2006	68.27443	-157.74045
U. of Alaska Fairbanks	2006	68.27466	-157.72863

FT381X	Active Layer Detachment Slide	Airphoto(TT)
FT382X	Active Layer Detachment Slide	Airphoto(TT)
FT383X	Active Layer Detachment Slide	Airphoto(TT)
FT384X	Active Layer Detachment Slide	Airphoto(TT)
FT385X	Active Layer Detachment Slide	Airphoto(TT)
FT386X	Active Layer Detachment Slide	Airphoto(TT)
FT388X	Active Layer Detachment Slide	Airphoto(TT)
FT389X	Active Layer Detachment Slide	Airphoto(TT)
FT392X	Active Layer Detachment Slide	Airphoto(TT)
FT393X	Active Layer Detachment Slide	Airphoto(TT)
FT394X	Active Layer Detachment Slide	Airphoto(TT)
FT395X	Active Layer Detachment Slide	Airphoto(TT)
FT396X	Active Layer Detachment Slide	Airphoto(TT)
FT397X	Active Layer Detachment Slide	Airphoto(TT)
FT398X	Active Layer Detachment Slide	Airphoto(TT)
FT399X	Active Layer Detachment Slide	Airphoto(TT)
FT400X	Active Layer Detachment Slide	Airphoto(TT)
FT401X	Active Layer Detachment Slide	Airphoto(TT)
FT453X	Active Layer Detachment Slide	Airphoto(TT)
FT454X	Active Layer Detachment Slide	Airphoto(TT)
FT455X	Active Layer Detachment Slide	Airphoto(TT)
FT456X	Active Layer Detachment Slide	Airphoto(TT)
FT457X	Active Layer Detachment Slide	Airphoto(TT)
FT458X	Active Layer Detachment Slide	Airphoto(TT)
FT459X	Active Layer Detachment Slide	Airphoto(TT)
FT460X	Active Layer Detachment Slide	Airphoto(TT)
FT461X	Active Layer Detachment Slide	Airphoto(TT)
FT466X	Active Layer Detachment Slide	Airphoto(TT)
FT467X	Active Layer Detachment Slide	Airphoto(TT)
FT468X	Active Layer Detachment Slide	Airphoto(TT)
FT469X	Active Layer Detachment Slide	Airphoto(TT)
FT470X	Active Layer Detachment Slide	Airphoto(TT)

U. of Alaska Fairbanks	2006	68.27920	-157.68623
U. of Alaska Fairbanks	2006	68.27595	-157.68426
U. of Alaska Fairbanks	2006	68.27603	-157.68347
U. of Alaska Fairbanks	2006	68.27982	-157.67118
U. of Alaska Fairbanks	2006	68.27765	-157.67320
U. of Alaska Fairbanks	2006	68.27795	-157.66911
U. of Alaska Fairbanks	2006	68.27730	-157.67040
U. of Alaska Fairbanks	2006	68.27865	-157.67291
U. of Alaska Fairbanks	2006	68.26107	-157.75232
U. of Alaska Fairbanks	2006	68.26128	-157.75052
U. of Alaska Fairbanks	2006	68.26222	-157.75238
U. of Alaska Fairbanks	2006	68.26337	-157.74980
U. of Alaska Fairbanks	2006	68.26355	-157.74671
U. of Alaska Fairbanks	2006	68.25806	-157.74124
U. of Alaska Fairbanks	2006	68.25552	-157.74238
U. of Alaska Fairbanks	2006	68.26168	-157.72437
U. of Alaska Fairbanks	2006	68.25175	-157.71757
U. of Alaska Fairbanks	2006	68.26341	-157.70030
U. of Alaska Fairbanks	2006	68.26563	-157.67298
U. of Alaska Fairbanks	2006	68.26526	-157.67013
U. of Alaska Fairbanks	2006	68.24360	-157.79245
U. of Alaska Fairbanks	2006	68.24311	-157.81226
U. of Alaska Fairbanks	2006	68.25072	-157.79591
U. of Alaska Fairbanks	2006	68.25188	-157.79721
U. of Alaska Fairbanks	2006	68.24512	-157.73977
U. of Alaska Fairbanks	2006	68.24100	-157.72506
U. of Alaska Fairbanks	2006	68.23686	-157.72490
U. of Alaska Fairbanks	2006	68.22362	-157.75857
U. of Alaska Fairbanks	2006	68.22299	-157.75843
U. of Alaska Fairbanks	2006	68.22246	-157.75773
U. of Alaska Fairbanks	2006	68.22235	-157.75622
U. of Alaska Fairbanks	2006	68.22243	-157.75703

FT471X	Active Layer Detachment Slide	Airphoto(TT)
FT472X	Active Layer Detachment Slide	Airphoto(TT)
FT473X	Active Layer Detachment Slide	Airphoto(TT)
FT474X	Active Layer Detachment Slide	Airphoto(TT)
FT475X	Active Layer Detachment Slide	Airphoto(TT)
FT476X	Active Layer Detachment Slide	Airphoto(TT)
FT477X	Active Layer Detachment Slide	Airphoto(TT)
FT478X	Active Layer Detachment Slide	Airphoto(TT)
FT479X	Active Layer Detachment Slide	Airphoto(TT)
FT480X	Active Layer Detachment Slide	Airphoto(TT)
FT481X	Active Layer Detachment Slide	Airphoto(TT)
FT482X	Active Layer Detachment Slide	Airphoto(TT)
FT483X	Active Layer Detachment Slide	Airphoto(TT)
FT484X	Active Layer Detachment Slide	Airphoto(TT)
FT485X	Active Layer Detachment Slide	Airphoto(TT)
FT486X	Active Layer Detachment Slide	Airphoto(TT)
FT487X	Active Layer Detachment Slide	Airphoto(TT)
FT488X	Active Layer Detachment Slide	Airphoto(TT)
FT489X	Active Layer Detachment Slide	Airphoto(TT)
FT490X	Active Layer Detachment Slide	Airphoto(TT)
FT491X	Active Layer Detachment Slide	Airphoto(TT)
FT492X	Active Layer Detachment Slide	Airphoto(TT)
FT493X	Active Layer Detachment Slide	Airphoto(TT)
FT494X	Active Layer Detachment Slide	Airphoto(TT)
FT495X	Active Layer Detachment Slide	Airphoto(TT)
FT496X	Active Layer Detachment Slide	Airphoto(TT)
FT497X	Active Layer Detachment Slide	Airphoto(TT)
FT498X	Active Layer Detachment Slide	Airphoto(TT)
FT499X	Active Layer Detachment Slide	Airphoto(TT)
FT500X	Active Layer Detachment Slide	Airphoto(TT)
FT501X	Active Layer Detachment Slide	Airphoto(TT)
FT502X	Active Layer Detachment Slide	Airphoto(TT)

U. of Alaska Fairbanks	2006	68.24088	-157.78491
U. of Alaska Fairbanks	2006	68.23298	-157.77241
U. of Alaska Fairbanks	2006	68.24019	-157.79631
U. of Alaska Fairbanks	2006	68.27414	-158.22880
U. of Alaska Fairbanks	2006	68.27416	-158.22829
U. of Alaska Fairbanks	2006	68.27714	-158.22060
U. of Alaska Fairbanks	2006	68.27975	-158.21656
U. of Alaska Fairbanks	2006	68.27985	-158.21616
U. of Alaska Fairbanks	2006	68.27976	-158.21445
U. of Alaska Fairbanks	2006	68.27954	-158.21357
U. of Alaska Fairbanks	2006	68.27757	-158.25533
U. of Alaska Fairbanks	2006	68.27748	-158.25343
U. of Alaska Fairbanks	2006	68.27734	-158.25318
U. of Alaska Fairbanks	2006	68.28205	-158.19622
U. of Alaska Fairbanks	2006	68.28178	-158.19288
U. of Alaska Fairbanks	2006	68.28122	-158.18930
U. of Alaska Fairbanks	2006	68.28962	-158.16656
U. of Alaska Fairbanks	2006	68.27448	-158.17344
U. of Alaska Fairbanks	2006	68.26827	-158.14978
U. of Alaska Fairbanks	2006	68.26743	-158.15012
U. of Alaska Fairbanks	2006	68.26244	-158.13630
U. of Alaska Fairbanks	2006	68.25847	-157.93904
U. of Alaska Fairbanks	2006	68.25811	-157.94277
U. of Alaska Fairbanks	2006	68.25509	-157.94986
U. of Alaska Fairbanks	2006	68.25252	-157.94717
U. of Alaska Fairbanks	2006	68.25427	-157.94638
U. of Alaska Fairbanks	2006	68.25349	-157.94195
U. of Alaska Fairbanks	2006	68.25251	-157.90695
U. of Alaska Fairbanks	2006	68.25229	-157.90563
U. of Alaska Fairbanks	2006	68.25277	-157.90295
U. of Alaska Fairbanks	2006	68.25162	-157.90076
U. of Alaska Fairbanks	2006	68.25395	-157.90165

FT503X	Active Layer Detachment Slide	Airphoto(TT)
FT504X	Active Layer Detachment Slide	Airphoto(TT)
FT505X	Active Layer Detachment Slide	Airphoto(TT)
FT506X	Active Layer Detachment Slide	Airphoto(TT)
FT507X	Active Layer Detachment Slide	Airphoto(TT)
FT508X	Retrogressive Thaw Slump	Airphoto(TT)
FT509X	Active Layer Detachment Slide	Airphoto(TT)
FT510X	Active Layer Detachment Slide	Airphoto(TT)
FT513X	Active Layer Detachment Slide	Airphoto(TT)
FT514X	Active Layer Detachment Slide	Airphoto(TT)
FT515X	Active Layer Detachment Slide	Airphoto(TT)
FT516X	Active Layer Detachment Slide	Airphoto(TT)
FT517X	Active Layer Detachment Slide	Airphoto(TT)
FT518X	Active Layer Detachment Slide	Airphoto(TT)
FT519X	Active Layer Detachment Slide	Airphoto(TT)
FT520X	Active Layer Detachment Slide	Airphoto(TT)
FT521X	Active Layer Detachment Slide	Airphoto(TT)
FT522X	Active Layer Detachment Slide	Airphoto(TT)
FT523X	Active Layer Detachment Slide	Airphoto(TT)
FT524X	Active Layer Detachment Slide	Airphoto(TT)
FT525X	Active Layer Detachment Slide	Airphoto(TT)
FT526X	Active Layer Detachment Slide	Airphoto(TT)
FT527X	Active Layer Detachment Slide	Airphoto(TT)
FT528X	Active Layer Detachment Slide	Airphoto(TT)
FT529X	Active Layer Detachment Slide	Airphoto(TT)
FT530X	Active Layer Detachment Slide	Airphoto(TT)
FT531X	Active Layer Detachment Slide	Airphoto(TT)
FT532X	Active Layer Detachment Slide	Airphoto(TT)
FT533X	Active Layer Detachment Slide	Airphoto(TT)
FT534X	Retrogressive Thaw Slump	Airphoto(TT)
FT535X	Active Layer Detachment Slide	Airphoto(TT)
FT536X	Active Layer Detachment Slide	Airphoto(TT)

U. of Alaska Fairbanks	2006	68.25489	-157.90526
U. of Alaska Fairbanks	2006	68.27043	-158.08345
U. of Alaska Fairbanks	2006	68.26803	-158.08388
U. of Alaska Fairbanks	2006	68.26989	-158.07852
U. of Alaska Fairbanks	2006	68.26903	-158.07882
U. of Alaska Fairbanks	2006	68.26972	-158.06987
U. of Alaska Fairbanks	2006	68.27032	-158.08291
U. of Alaska Fairbanks	2006	68.26954	-158.08257
U. of Alaska Fairbanks	2006	68.27329	-158.12741
U. of Alaska Fairbanks	2006	68.27332	-158.12500
U. of Alaska Fairbanks	2006	68.27356	-158.12373
U. of Alaska Fairbanks	2006	68.25756	-158.08706
U. of Alaska Fairbanks	2006	68.25670	-158.07040
U. of Alaska Fairbanks	2006	68.25623	-158.06203
U. of Alaska Fairbanks	2006	68.25477	-158.05930
U. of Alaska Fairbanks	2006	68.25691	-158.05934
U. of Alaska Fairbanks	2006	68.26094	-158.04535
U. of Alaska Fairbanks	2006	68.26025	-158.04985
U. of Alaska Fairbanks	2006	68.26014	-158.05128
U. of Alaska Fairbanks	2006	68.25942	-158.03487
U. of Alaska Fairbanks	2006	68.25958	-158.03316
U. of Alaska Fairbanks	2006	68.25881	-158.03474
U. of Alaska Fairbanks	2006	68.25981	-158.03976
U. of Alaska Fairbanks	2006	68.25505	-158.05801
U. of Alaska Fairbanks	2006	68.26112	-158.04329
U. of Alaska Fairbanks	2006	68.26411	-158.05361
U. of Alaska Fairbanks	2006	68.26360	-158.04949
U. of Alaska Fairbanks	2006	68.26330	-158.05227
U. of Alaska Fairbanks	2006	68.26587	-158.04929
U. of Alaska Fairbanks	2006	68.27914	-158.07297
U. of Alaska Fairbanks	2006	68.27424	-158.02457
U. of Alaska Fairbanks	2006	68.27391	-158.02692

FT537X	Active Layer Detachment Slide	Airphoto(TT)
FT538X	Active Layer Detachment Slide	Airphoto(TT)
FT539X	Active Layer Detachment Slide	Airphoto(TT)
FT540X	Active Layer Detachment Slide	Airphoto(TT)
FT541X	Active Layer Detachment Slide	Airphoto(TT)
FT542X	Active Layer Detachment Slide	Airphoto(TT)
FT543X	Active Layer Detachment Slide	Airphoto(TT)
FT544X	Active Layer Detachment Slide	Airphoto(TT)
FT545X	Active Layer Detachment Slide	Airphoto(TT)
FT546X	Active Layer Detachment Slide	Airphoto(TT)
FT547X	Active Layer Detachment Slide	Airphoto(TT)
FT548X	Active Layer Detachment Slide	Airphoto(TT)
FT549X	Active Layer Detachment Slide	Airphoto(TT)
FT550X	Active Layer Detachment Slide	Airphoto(TT)
FT551X	Active Layer Detachment Slide	Airphoto(TT)
FT552X	Active Layer Detachment Slide	Airphoto(TT)
FT553X	Active Layer Detachment Slide	Airphoto(TT)
FT554X	Active Layer Detachment Slide	Airphoto(TT)
FT555X	Active Layer Detachment Slide	Airphoto(TT)
FT556X	Active Layer Detachment Slide	Airphoto(TT)
FT557X	Active Layer Detachment Slide	Airphoto(TT)
FT558X	Active Layer Detachment Slide	Airphoto(TT)
FT10A	Retrogressive Thaw Slump	Field GPS
FT11A	Retrogressive Thaw Slump	Field GPS
FT11B	Retrogressive Thaw Slump	Field GPS
FT11C	Retrogressive Thaw Slump	Field GPS
FT12A	Retrogressive Thaw Slump	Field GPS
FT13A	Active Layer Detachment Slide	Field GPS
FT13B	Active Layer Detachment Slide	Field GPS
FT14A	Active Layer Detachment Slide	Field GPS
FT15A	Active Layer Detachment Slide	Field GPS
FT15B	Active Layer Detachment Slide	Field GPS

U. of Alaska Fairbanks	2006	68.27098	-158.02245
U. of Alaska Fairbanks	2006	68.26624	-158.02110
U. of Alaska Fairbanks	2006	68.26706	-158.00826
U. of Alaska Fairbanks	2006	68.26698	-158.00973
U. of Alaska Fairbanks	2006	68.26721	-158.01028
U. of Alaska Fairbanks	2006	68.26279	-158.03207
U. of Alaska Fairbanks	2006	68.25164	-157.92939
U. of Alaska Fairbanks	2006	68.26080	-157.92085
U. of Alaska Fairbanks	2006	68.26128	-157.92225
U. of Alaska Fairbanks	2006	68.26091	-157.91153
U. of Alaska Fairbanks	2006	68.26048	-157.90810
U. of Alaska Fairbanks	2006	68.24975	-157.95180
U. of Alaska Fairbanks	2006	68.24913	-157.94657
U. of Alaska Fairbanks	2006	68.25930	-158.02905
U. of Alaska Fairbanks	2006	68.25873	-158.03084
U. of Alaska Fairbanks	2006	68.25732	-158.03257
U. of Alaska Fairbanks	2006	68.26331	-157.99166
U. of Alaska Fairbanks	2006	68.26528	-157.99419
U. of Alaska Fairbanks	2006	68.27208	-158.00762
U. of Alaska Fairbanks	2006	68.27047	-157.97173
U. of Alaska Fairbanks	2006	68.26586	-157.97094
U. of Alaska Fairbanks	2006	68.26703	-157.96607
U. of Alaska Fairbanks	2006	68.07963	-157.62363
U. of Alaska Fairbanks	2006	68.07708	-157.56521
U. of Alaska Fairbanks	2006	68.07835	-157.56649
U. of Alaska Fairbanks	2006	68.07894	-157.56718
U. of Alaska Fairbanks	2006	68.07707	-157.56278
U. of Alaska Fairbanks	2006	68.25406	-158.19807
U. of Alaska Fairbanks	2006	68.24789	-158.20479
U. of Alaska Fairbanks	2006	68.32557	-157.88768
U. of Alaska Fairbanks	2006	68.31688	-157.92696
U. of Alaska Fairbanks	2006	68.31575	-157.92589

FT16B	Active Layer Detachment Slide	Field GPS
FT17A	Active Layer Detachment Slide	Field GPS
FT17B	Active Layer Detachment Slide	Field GPS
FT17C	Active Layer Detachment Slide	Field GPS
FT19A	Active Layer Detachment Slide	Field GPS
FT1A	Retrogressive Thaw Slump	Field GPS
FT20A	Active Layer Detachment Slide	Field GPS
FT21A	Active Layer Detachment Slide	Field GPS
FT24A	Retrogressive Thaw Slump	Field GPS
FT25A	Retrogressive Thaw Slump	Field GPS
FT26A	Retrogressive Thaw Slump	Field GPS
FT29A	Retrogressive Thaw Slump	Field GPS
FT2A	Retrogressive Thaw Slump	Field GPS
FT30A	Retrogressive Thaw Slump	Field GPS
FT31A	Active Layer Detachment Slide	Field GPS
FT32A	Active Layer Detachment Slide	Field GPS
FT33A	Active Layer Detachment Slide	Field GPS
FT34A	Retrogressive Thaw Slump	Field GPS
FT34B	Retrogressive Thaw Slump	Field GPS
FT35A	Retrogressive Thaw Slump	Field GPS
FT4A	Active Layer Detachment Slide	Field GPS
FT4B	Active Layer Detachment Slide	Field GPS
FT4C	Active Layer Detachment Slide	Field GPS
FT4D	Active Layer Detachment Slide	Field GPS
FT6A	Active Layer Detachment Slide	Field GPS
FT7A	Active Layer Detachment Slide	Field GPS
FT8A	Retrogressive Thaw Slump	Field GPS
FT9A	Retrogressive Thaw Slump	Field GPS
FT581A	Active Layer Detachment Slide	Field GPS
FT582A	Active Layer Detachment Slide	Field GPS
GAAR0001	Retrogressive Thaw Slump	IKONOS/Geoeye/Worldview
GAAR0002	Retrogressive Thaw Slump	IKONOS/Geoeye/Worldview

U. of Alaska Fairbanks	2006	68.31568	-157.92555
U. of Alaska Fairbanks	2006	68.23682	-157.84747
U. of Alaska Fairbanks	2006	68.23651	-157.84581
U. of Alaska Fairbanks	2006	68.23510	-157.84294
U. of Alaska Fairbanks	2006	68.23860	-157.82732
U. of Alaska Fairbanks	2006	68.21769	-158.31030
U. of Alaska Fairbanks	2006	68.23858	-157.82441
U. of Alaska Fairbanks	2006	68.23771	-157.81593
U. of Alaska Fairbanks	2006	68.23364	-158.33745
U. of Alaska Fairbanks	2006	68.23275	-158.33302
U. of Alaska Fairbanks	2006	68.23186	-158.33097
U. of Alaska Fairbanks	2006	68.46083	-158.99083
U. of Alaska Fairbanks	2006	68.08833	-158.63656
U. of Alaska Fairbanks	2006	68.45888	-158.99104
U. of Alaska Fairbanks	2006	68.18636	-158.55246
U. of Alaska Fairbanks	2006	68.21260	-158.52734
U. of Alaska Fairbanks	2006	68.18139	-158.55370
U. of Alaska Fairbanks	2006	68.01547	-159.25122
U. of Alaska Fairbanks	2006	68.01592	-159.25282
U. of Alaska Fairbanks	2006	68.03597	-159.28823
U. of Alaska Fairbanks	2006	68.23937	-158.09557
U. of Alaska Fairbanks	2006	68.24388	-158.09712
U. of Alaska Fairbanks	2006	68.24615	-158.09665
U. of Alaska Fairbanks	2006	68.24605	-158.10187
U. of Alaska Fairbanks	2006	67.70168	-155.56229
U. of Alaska Fairbanks	2006	68.08998	-157.51568
U. of Alaska Fairbanks	2006	68.07917	-157.62093
U. of Alaska Fairbanks	2006	68.07983	-157.62222
U. of Alaska Fairbanks	2010	67.71954	-161.54893
U. of Alaska Fairbanks	2010	67.71978	-161.54877
NPS	2010	67.81390	-156.50759
NPS	2010	67.80429	-156.50043

GAAR0003	Active Layer Detachment Slide	IKONOS/Geoeye/Worldview
GAAR0004	Active Layer Detachment Slide	IKONOS/Geoeye/Worldview
GAAR0005	Active Layer Detachment Slide	IKONOS/Geoeye/Worldview
GAAR0006	Active Layer Detachment Slide	IKONOS/Geoeye/Worldview
GAAR0007	Retrogressive Thaw Slump	IKONOS/Geoeye/Worldview
GAAR0008	Retrogressive Thaw Slump	IKONOS/Geoeye/Worldview
GAAR0009	Retrogressive Thaw Slump	IKONOS/Geoeye/Worldview
GAAR0010	Retrogressive Thaw Slump	IKONOS/Geoeye/Worldview
GAAR0011	Retrogressive Thaw Slump	IKONOS/Geoeye/Worldview
GAAR0012	Retrogressive Thaw Slump	IKONOS/Geoeye/Worldview
GAAR0013	Retrogressive Thaw Slump	IKONOS/Geoeye/Worldview
GAAR0014	Active Layer Detachment Slide	IKONOS/Geoeye/Worldview
GAAR0015	Active Layer Detachment Slide	IKONOS/Geoeye/Worldview
GAAR0016	Active Layer Detachment Slide	IKONOS/Geoeye/Worldview
GAAR0017	Active Layer Detachment Slide	IKONOS/Geoeye/Worldview
GAAR0018	Active Layer Detachment Slide	IKONOS/Geoeye/Worldview
GAAR0019	Active Layer Detachment Slide	IKONOS/Geoeye/Worldview
GAAR0020	Active Layer Detachment Slide	IKONOS/Geoeye/Worldview
GAAR0021	Active Layer Detachment Slide	IKONOS/Geoeye/Worldview
GAAR0022	Active Layer Detachment Slide	IKONOS/Geoeye/Worldview
GAAR0023	Active Layer Detachment Slide	IKONOS/Geoeye/Worldview
GAAR0024	Active Layer Detachment Slide	IKONOS/Geoeye/Worldview
GAAR0025	Active Layer Detachment Slide	IKONOS/Geoeye/Worldview
GAAR0026	Active Layer Detachment Slide	IKONOS/Geoeye/Worldview
GAAR0027	Active Layer Detachment Slide	IKONOS/Geoeye/Worldview
GAAR0028	Retrogressive Thaw Slump	IKONOS/Geoeye/Worldview
GAAR0029	Retrogressive Thaw Slump	IKONOS/Geoeye/Worldview
GAAR0030	Retrogressive Thaw Slump	IKONOS/Geoeye/Worldview
GAAR0031	Retrogressive Thaw Slump	IKONOS/Geoeye/Worldview
GAAR0032	Active Layer Detachment Slide	IKONOS/Geoeye/Worldview
GAAR0033	Active Layer Detachment Slide	IKONOS/Geoeye/Worldview
GAAR0034	Retrogressive Thaw Slump	IKONOS/Geoeye/Worldview

NPS	2010	67.80929	-156.56505
NPS	2010	67.80906	-156.56687
NPS	2010	67.81051	-156.56492
NPS	2010	67.81426	-156.57417
NPS	2010	67.72229	-156.04237
NPS	2010	67.90101	-156.48631
NPS	2010	67.89789	-156.49960
NPS	2010	68.38353	-154.68033
NPS	2010	67.65837	-155.89169
NPS	2010	67.66913	-155.96046
NPS	2010	67.66596	-155.95914
NPS	2010	67.67293	-155.92891
NPS	2010	67.67253	-155.92664
NPS	2010	67.67302	-155.92405
NPS	2010	67.67299	-155.92067
NPS	2010	67.67308	-155.91776
NPS	2010	67.66144	-155.88922
NPS	2010	67.66251	-155.89171
NPS	2010	67.66356	-155.88796
NPS	2010	67.66445	-155.89063
NPS	2010	67.65394	-155.88881
NPS	2010	67.65269	-155.89518
NPS	2010	67.65420	-155.89245
NPS	2010	67.64981	-155.89319
NPS	2010	67.64931	-155.89457
NPS	2010	67.66258	-155.78181
NPS	2010	67.65936	-155.78507
NPS	2010	67.65909	-155.78681
NPS	2010	67.65695	-155.78553
NPS	2010	67.62245	-155.52941
NPS	2010	67.62483	-155.53306
NPS	2010	67.62351	-155.47903

GAAR0035	Retrogressive Thaw Slump	IKONOS/Geoeye/Worldview
GAAR0036	Retrogressive Thaw Slump	IKONOS/Geoeye/Worldview
GAAR0037	Retrogressive Thaw Slump	IKONOS/Geoeye/Worldview
GAAR0038	Active Layer Detachment Slide	IKONOS/Geoeye/Worldview
GAAR0039	Active Layer Detachment Slide	IKONOS/Geoeye/Worldview
GAAR0040	Active Layer Detachment Slide	IKONOS/Geoeye/Worldview
GAAR0041	Active Layer Detachment Slide	IKONOS/Geoeye/Worldview
GAAR0042	Active Layer Detachment Slide	IKONOS/Geoeye/Worldview
GAAR0043	Active Layer Detachment Slide	IKONOS/Geoeye/Worldview
GAAR0044	Active Layer Detachment Slide	IKONOS/Geoeye/Worldview
GAAR0045	Active Layer Detachment Slide	IKONOS/Geoeye/Worldview
GAAR0046	Active Layer Detachment Slide	IKONOS/Geoeye/Worldview
GAAR0047	Active Layer Detachment Slide	IKONOS/Geoeye/Worldview
GAAR0048	Active Layer Detachment Slide	IKONOS/Geoeye/Worldview
GAAR0049	Active Layer Detachment Slide	IKONOS/Geoeye/Worldview
GAAR0050	Active Layer Detachment Slide	IKONOS/Geoeye/Worldview
GAAR0051	Active Layer Detachment Slide	IKONOS/Geoeye/Worldview
GAAR0052	Active Layer Detachment Slide	IKONOS/Geoeye/Worldview
GAAR0053	Active Layer Detachment Slide	IKONOS/Geoeye/Worldview
GAAR0054	Active Layer Detachment Slide	IKONOS/Geoeye/Worldview
GAAR0055	Active Layer Detachment Slide	IKONOS/Geoeye/Worldview
GAAR0056	Active Layer Detachment Slide	IKONOS/Geoeye/Worldview
GAAR0057	Active Layer Detachment Slide	IKONOS/Geoeye/Worldview
GAAR0058	Active Layer Detachment Slide	IKONOS/Geoeye/Worldview
GAAR0059	Active Layer Detachment Slide	IKONOS/Geoeye/Worldview
GAAR0061	Active Layer Detachment Slide	IKONOS/Geoeye/Worldview
GAAR0062	Active Layer Detachment Slide	IKONOS/Geoeye/Worldview
GAAR0063	Active Layer Detachment Slide	IKONOS/Geoeye/Worldview
GAAR0067	Retrogressive Thaw Slump	IKONOS/Geoeye/Worldview
GAAR0068	Retrogressive Thaw Slump	IKONOS/Geoeye/Worldview
GAAR0069	Retrogressive Thaw Slump	IKONOS/Geoeye/Worldview
GAAR0070	Retrogressive Thaw Slump	IKONOS/Geoeye/Worldview

NPS	2010	67.62270	-155.47906
NPS	2010	67.72061	-155.00326
NPS	2010	67.72001	-155.00390
NPS	2010	67.71737	-155.00897
NPS	2010	67.71735	-155.01060
NPS	2010	67.71582	-155.01167
NPS	2010	67.71411	-155.00792
NPS	2010	67.71441	-155.00627
NPS	2010	67.71504	-155.00288
NPS	2010	67.71919	-155.00500
NPS	2010	67.72118	-155.00980
NPS	2010	67.72081	-155.01148
NPS	2010	67.71504	-154.99674
NPS	2010	68.10528	-154.16550
NPS	2010	68.10348	-154.15890
NPS	2010	68.10107	-154.16036
NPS	2010	68.10133	-154.16185
NPS	2010	68.10024	-154.16274
NPS	2010	68.09811	-154.16003
NPS	2010	68.09680	-154.16061
NPS	2010	68.09645	-154.15920
NPS	2010	67.96868	-154.80121
NPS	2010	67.96641	-154.80518
NPS	2010	67.97450	-154.78071
NPS	2010	67.96229	-154.81591
NPS	2010	67.96399	-154.82001
NPS	2010	67.95920	-154.85164
NPS	2010	68.36228	-154.50716
NPS	2010	68.34595	-153.89835
NPS	2010	68.33888	-152.65234
NPS	2010	68.33700	-152.65465
NPS	2010	68.33675	-152.65619

GAAR0071	Retrogressive Thaw Slump	IKONOS/Geoeye/Worldview
GAAR0072	Retrogressive Thaw Slump	IKONOS/Geoeye/Worldview
GAAR0073	Retrogressive Thaw Slump	IKONOS/Geoeye/Worldview
GAAR0074	Retrogressive Thaw Slump	IKONOS/Geoeye/Worldview
GAAR0075	Retrogressive Thaw Slump	IKONOS/Geoeye/Worldview
GAAR0076	Retrogressive Thaw Slump	IKONOS/Geoeye/Worldview
GAAR0077	Retrogressive Thaw SlumpN	IKONOS/Geoeye/Worldview
GAAR0078	Retrogressive Thaw SlumpN	IKONOS/Geoeye/Worldview
GAAR0079	Active Layer Detachment Slide	IKONOS/Geoeye/Worldview
GAAR0080	Active Layer Detachment Slide	IKONOS/Geoeye/Worldview
GAAR0081	Active Layer Detachment Slide	IKONOS/Geoeye/Worldview
GAAR0082	Active Layer Detachment Slide	IKONOS/Geoeye/Worldview
GAAR0083	Active Layer Detachment Slide	IKONOS/Geoeye/Worldview
GAAR0084	Active Layer Detachment Slide	IKONOS/Geoeye/Worldview
GAAR0085	Active Layer Detachment Slide	IKONOS/Geoeye/Worldview
GAAR0086	Active Layer Detachment Slide	IKONOS/Geoeye/Worldview
GAAR0087	Active Layer Detachment Slide	IKONOS/Geoeye/Worldview
GAAR0088	Active Layer Detachment Slide	IKONOS/Geoeye/Worldview
GAAR0089	Active Layer Detachment Slide	IKONOS/Geoeye/Worldview
GAAR0090	Active Layer Detachment Slide	IKONOS/Geoeye/Worldview
GAAR0091	Active Layer Detachment Slide	IKONOS/Geoeye/Worldview
GAAR0092	Active Layer Detachment Slide	IKONOS/Geoeye/Worldview
GAAR0093	Active Layer Detachment Slide	IKONOS/Geoeye/Worldview
GAAR0094	Active Layer Detachment Slide	IKONOS/Geoeye/Worldview
GAAR0095	Active Layer Detachment Slide	IKONOS/Geoeye/Worldview
GAAR0096	Active Layer Detachment Slide	IKONOS/Geoeye/Worldview
GAAR0097	Active Layer Detachment Slide	IKONOS/Geoeye/Worldview
GAAR0098	Active Layer Detachment Slide	IKONOS/Geoeye/Worldview
GAAR0099	Active Layer Detachment Slide	IKONOS/Geoeye/Worldview
GAAR0100	Active Layer Detachment Slide	IKONOS/Geoeye/Worldview
GAAR0101	Active Layer Detachment Slide	IKONOS/Geoeye/Worldview
GAAR0102	Active Layer Detachment Slide	IKONOS/Geoeye/Worldview

NPS	2010	68.33559	-152.65778
NPS	2010	68.33599	-152.66039
NPS	2010	68.34815	-152.68018
NPS	2010	68.34423	-152.68281
NPS	2010	67.96246	-155.00330
NPS	2010	68.30825	-154.18560
NPS	2010	68.30746	-154.18750
NPS	2010	68.30703	-154.18829
NPS	2010	68.02330	-155.89103
NPS	2010	68.02426	-155.87870
NPS	2010	68.02078	-155.87035
NPS	2010	68.02089	-155.87613
NPS	2010	68.02129	-155.86573
NPS	2010	68.02153	-155.86706
NPS	2010	68.02061	-155.86563
NPS	2010	68.02579	-155.87858
NPS	2010	68.02612	-155.86735
NPS	2010	68.01956	-155.86010
NPS	2010	68.01830	-155.85309
NPS	2010	68.01181	-155.86746
NPS	2010	68.01258	-155.87148
NPS	2010	68.01267	-155.87363
NPS	2010	68.01015	-155.86862
NPS	2010	68.00992	-155.88255
NPS	2010	68.00950	-155.88112
NPS	2010	68.00779	-155.87440
NPS	2010	68.00494	-155.87287
NPS	2010	68.00373	-155.86072
NPS	2010	68.00299	-155.85867
NPS	2010	68.01148	-155.85673
NPS	2010	68.00229	-155.87482
NPS	2010	68.00248	-155.87759

NPS	2010	68.00152	-155.87296
NPS	2010	67.99962	-155.86547
NPS	2010	67.99436	-155.87785
NPS	2010	67.99878	-155.87916
NPS	2010	67.99825	-155.88515
NPS	2010	67.99733	-155.86199
NPS	2010	67.99553	-155.88717
NPS	2010	67.99583	-155.86557
NPS	2010	67.99316	-155.89456
NPS	2010	67.99449	-155.89157
NPS	2010	67.99481	-155.89148
NPS	2010	67.99553	-155.89172
NPS	2010	67.99622	-155.89486
NPS	2010	67.99768	-155.88431
NPS	2010	67.99773	-155.88677
NPS	2010	67.99671	-155.90017
NPS	2010	67.99907	-155.92277
NPS	2010	67.99674	-155.93761
NPS	2010	68.00022	-155.93650
NPS	2010	68.00312	-155.92096
NPS	2010	68.00800	-155.93564
NPS	2010	68.00495	-155.92811
NPS	2010	68.01432	-155.91338
NPS	2010	68.01709	-155.90349
NPS	2010	68.01961	-155.89715
NPS	2010	68.01607	-155.86090
NPS	2010	68.01565	-155.85947
NPS	2010	68.01649	-155.86034
NPS	2010	68.01601	-155.85806
NPS	2010	68.01615	-155.85674
NPS	2010	68.01654	-155.85040
NPS	2010	68.01743	-155.84240

NPS	2010	68.01578	-155.84309
NPS	2010	68.01194	-155.84443
NPS	2010	68.01198	-155.84156
NPS	2010	68.01226	-155.83886
NPS	2010	68.01134	-155.83865
NPS	2010	68.01300	-155.83670
NPS	2010	68.01470	-155.83804
NPS	2010	68.01409	-155.83583
NPS	2010	68.01532	-155.83768
NPS	2010	68.01541	-155.83589
NPS	2010	68.01805	-155.83475
NPS	2010	68.01473	-155.82813
NPS	2010	67.99889	-155.77090
NPS	2010	68.01491	-155.79358
NPS	2010	68.01215	-155.78868
NPS	2010	68.00810	-155.78015
NPS	2010	67.99757	-155.77278
NPS	2010	68.01134	-155.77926
NPS	2010	68.01110	-155.76718
NPS	2010	68.01156	-155.77480
NPS	2010	68.01242	-155.77963
NPS	2010	68.00410	-155.79304
NPS	2010	68.00346	-155.78695
NPS	2010	68.00240	-155.79123
NPS	2010	68.00060	-155.79058
NPS	2010	67.99953	-155.78850
NPS	2010	67.99729	-155.81402
NPS	2010	67.99691	-155.81791
NPS	2010	67.99873	-155.81770
NPS	2010	67.99458	-155.81361
NPS	2010	67.99316	-155.82662
NPS	2010	67.99427	-155.84735

GAAR0169	Active Layer Detachment Slide	IKONOS/Geoeye/Worldview
GAAR0170	Active Layer Detachment Slide	IKONOS/Geoeye/Worldview
GAAR0171	Active Layer Detachment Slide	IKONOS/Geoeye/Worldview
GAAR0172	Active Layer Detachment Slide	IKONOS/Geoeye/Worldview
GAAR0173	Active Layer Detachment Slide	IKONOS/Geoeye/Worldview
GAAR0174	Active Layer Detachment Slide	IKONOS/Geoeye/Worldview
GAAR0175	Active Layer Detachment Slide	IKONOS/Geoeye/Worldview
GAAR0176	Active Layer Detachment Slide	IKONOS/Geoeye/Worldview
GAAR0177	Active Layer Detachment Slide	IKONOS/Geoeye/Worldview
GAAR0178	Active Layer Detachment Slide	IKONOS/Geoeye/Worldview
GAAR0179	Active Layer Detachment Slide	IKONOS/Geoeye/Worldview
GAAR0180	Active Layer Detachment Slide	IKONOS/Geoeye/Worldview
GAAR0181	Active Layer Detachment Slide	IKONOS/Geoeye/Worldview
GAAR0182	Active Layer Detachment Slide	IKONOS/Geoeye/Worldview
GAAR0183	Active Layer Detachment Slide	IKONOS/Geoeye/Worldview
GAAR0184	Active Layer Detachment Slide	IKONOS/Geoeye/Worldview
GAAR0185	Retrogressive Thaw Slump	IKONOS/Geoeye/Worldview
GAAR0186	Retrogressive Thaw Slump	IKONOS/Geoeye/Worldview
GAAR0187	Active Layer Detachment Slide	IKONOS/Geoeye/Worldview
GAAR0188	Active Layer Detachment Slide	IKONOS/Geoeye/Worldview
GAAR0189	Retrogressive Thaw Slump	IKONOS/Geoeye/Worldview
GAAR0190	Retrogressive Thaw Slump	IKONOS/Geoeye/Worldview
GAAR0191	Retrogressive Thaw Slump	IKONOS/Geoeye/Worldview
GAAR0192	Retrogressive Thaw Slump	IKONOS/Geoeye/Worldview
GAAR0193	Retrogressive Thaw Slump	IKONOS/Geoeye/Worldview
GAAR0194	Retrogressive Thaw Slump	IKONOS/Geoeye/Worldview
GAAR0198	Active Layer Detachment Slide	IKONOS/Geoeye/Worldview
GAAR0199	Active Layer Detachment Slide	IKONOS/Geoeye/Worldview
GAAR0200	Retrogressive Thaw Slump	IKONOS/Geoeye/Worldview
GAAR0201	Active Layer Detachment Slide	IKONOS/Geoeye/Worldview
GAAR0202	Retrogressive Thaw Slump	IKONOS/Geoeye/Worldview
GAAR0203	Active Layer Detachment Slide	IKONOS/Geoeye/Worldview

NPS	2010	67.99384	-155.84805
NPS	2010	67.99744	-155.84945
NPS	2010	67.99338	-155.83955
NPS	2010	68.01960	-155.82244
NPS	2010	68.08001	-155.58716
NPS	2010	68.08050	-155.57639
NPS	2010	68.07965	-155.57215
NPS	2010	68.08378	-155.56509
NPS	2010	68.08048	-155.56122
NPS	2010	68.08306	-155.56304
NPS	2010	68.08302	-155.56161
NPS	2010	68.08290	-155.55872
NPS	2010	68.08314	-155.55704
NPS	2010	68.07755	-155.56423
NPS	2010	68.08478	-155.48909
NPS	2010	68.07925	-155.45700
NPS	2010	68.08031	-155.45005
NPS	2010	68.08094	-155.44865
NPS	2010	67.92850	-154.88488
NPS	2010	67.93861	-154.90222
NPS	2010	68.33567	-152.66361
NPS	2010	68.33960	-152.65070
NPS	2010	68.34092	-152.64753
NPS	2010	68.34280	-152.64866
NPS	2010	68.34406	-152.65069
NPS	2010	68.33693	-152.66688
NPS	2010	67.96713	-156.44476
NPS	2010	67.97062	-156.43312
NPS	2010	67.97802	-156.31366
NPS	2010	67.95508	-156.31269
NPS	2010	67.93656	-156.12115
NPS	2010	67.93438	-156.11892

GAAR0204	Retrogressive Thaw Slump	IKONOS/Geoeye/Worldview
GAAR0205	Retrogressive Thaw Slump	IKONOS/Geoeye/Worldview
GAAR0206	Active Layer Detachment Slide	IKONOS/Geoeye/Worldview
GAAR0207	Active Layer Detachment Slide	IKONOS/Geoeye/Worldview
GAAR0208	Active Layer Detachment Slide	IKONOS/Geoeye/Worldview
GAAR0209	Active Layer Detachment Slide	IKONOS/Geoeye/Worldview
GAAR0210	Active Layer Detachment Slide	IKONOS/Geoeye/Worldview
GAAR0211	Active Layer Detachment Slide	IKONOS/Geoeye/Worldview
GAAR0212	Active Layer Detachment Slide	IKONOS/Geoeye/Worldview
GAAR0213	Active Layer Detachment Slide	IKONOS/Geoeye/Worldview
GAAR0214	Active Layer Detachment Slide	IKONOS/Geoeye/Worldview
GAAR0215	Active Layer Detachment Slide	IKONOS/Geoeye/Worldview
GAAR0216	Active Layer Detachment Slide	IKONOS/Geoeye/Worldview
GAAR0217	Active Layer Detachment Slide	IKONOS/Geoeye/Worldview
GAAR0218	Active Layer Detachment Slide	IKONOS/Geoeye/Worldview
GAAR0219	Active Layer Detachment Slide	IKONOS/Geoeye/Worldview
GAAR0220	Active Layer Detachment Slide	IKONOS/Geoeye/Worldview
GAAR0221	Active Layer Detachment Slide	IKONOS/Geoeye/Worldview
GAAR0222	Active Layer Detachment Slide	IKONOS/Geoeye/Worldview
GAAR0223	Active Layer Detachment Slide	IKONOS/Geoeye/Worldview
GAAR0224	Active Layer Detachment Slide	IKONOS/Geoeye/Worldview
GAAR0225	Active Layer Detachment Slide	IKONOS/Geoeye/Worldview
GAAR0226	Active Layer Detachment Slide	IKONOS/Geoeye/Worldview
GAAR0227	Active Layer Detachment Slide	IKONOS/Geoeye/Worldview
GAAR0228	Active Layer Detachment Slide	IKONOS/Geoeye/Worldview
GAAR0229	Active Layer Detachment Slide	IKONOS/Geoeye/Worldview
GAAR0230	Active Layer Detachment Slide	IKONOS/Geoeye/Worldview
GAAR0231	Active Layer Detachment Slide	IKONOS/Geoeye/Worldview
GAAR0232	Active Layer Detachment Slide	IKONOS/Geoeye/Worldview
GAAR0233	Active Layer Detachment Slide	IKONOS/Geoeye/Worldview
GAAR0234	Active Layer Detachment Slide	IKONOS/Geoeye/Worldview
GAAR0235	Active Layer Detachment Slide	IKONOS/Geoeye/Worldview

NPS	2010	67.93276	-156.12150
NPS	2010	67.90580	-156.45720
NPS	2010	67.91447	-156.24293
NPS	2010	67.98317	-155.95660
NPS	2010	67.98009	-155.95664
NPS	2010	67.97848	-155.96183
NPS	2010	67.98135	-155.97819
NPS	2010	67.98216	-155.94227
NPS	2010	67.97918	-155.96658
NPS	2010	67.97862	-155.96894
NPS	2010	67.97919	-155.97237
NPS	2010	67.97860	-155.97238
NPS	2010	67.98349	-155.97020
NPS	2010	67.99289	-155.93385
NPS	2010	67.98844	-155.93438
NPS	2010	67.98552	-155.93937
NPS	2010	67.98419	-155.93698
NPS	2010	67.99033	-155.89065
NPS	2010	67.98480	-155.88878
NPS	2010	67.98138	-155.89198
NPS	2010	67.97907	-155.89011
NPS	2010	67.98287	-155.90442
NPS	2010	67.98165	-155.90423
NPS	2010	67.98049	-155.90139
NPS	2010	67.99146	-155.89569
NPS	2010	67.97054	-155.89741
NPS	2010	67.96584	-155.90989
NPS	2010	67.98618	-155.85246
NPS	2010	67.98606	-155.85387
NPS	2010	67.98368	-155.85342
NPS	2010	67.98493	-155.85096
NPS	2010	67.97845	-155.85717

GAAR0236	Active Layer Detachment Slide	IKONOS/Geoeye/Worldview
GAAR0237	Active Layer Detachment Slide	IKONOS/Geoeye/Worldview
GAAR0238	Active Layer Detachment Slide	IKONOS/Geoeye/Worldview
GAAR0239	Active Layer Detachment Slide	IKONOS/Geoeye/Worldview
GAAR0240	Active Layer Detachment Slide	IKONOS/Geoeye/Worldview
GAAR0241	Active Layer Detachment Slide	IKONOS/Geoeye/Worldview
GAAR0242	Active Layer Detachment Slide	IKONOS/Geoeye/Worldview
GAAR0243	Active Layer Detachment Slide	IKONOS/Geoeye/Worldview
GAAR0244	Active Layer Detachment Slide	IKONOS/Geoeye/Worldview
GAAR0245	Active Layer Detachment Slide	IKONOS/Geoeye/Worldview
GAAR0246	Active Layer Detachment Slide	IKONOS/Geoeye/Worldview
GAAR0247	Active Layer Detachment Slide	IKONOS/Geoeye/Worldview
GAAR0248	Active Layer Detachment Slide	IKONOS/Geoeye/Worldview
GAAR0249	Active Layer Detachment Slide	IKONOS/Geoeye/Worldview
GAAR0250	Retrogressive Thaw Slump	IKONOS/Geoeye/Worldview
GAAR0251	Active Layer Detachment Slide	IKONOS/Geoeye/Worldview
GAAR0252	Active Layer Detachment Slide	IKONOS/Geoeye/Worldview
GAAR0254	Active Layer Detachment Slide	IKONOS/Geoeye/Worldview
GAAR0255	Active Layer Detachment Slide	IKONOS/Geoeye/Worldview
GAAR0256	Active Layer Detachment Slide	IKONOS/Geoeye/Worldview
GAAR0257	Active Layer Detachment Slide	IKONOS/Geoeye/Worldview
GAAR0258	Active Layer Detachment Slide	IKONOS/Geoeye/Worldview
GAAR0259	Active Layer Detachment Slide	IKONOS/Geoeye/Worldview
GAAR0260	Active Layer Detachment Slide	IKONOS/Geoeye/Worldview
GAAR0261	Retrogressive Thaw Slump	IKONOS/Geoeye/Worldview
GAAR0262	Retrogressive Thaw Slump	IKONOS/Geoeye/Worldview
GAAR0263	Retrogressive Thaw Slump	IKONOS/Geoeye/Worldview
GAAR0264	Active Layer Detachment Slide	IKONOS/Geoeye/Worldview
GAAR0265	Active Layer Detachment Slide	IKONOS/Geoeye/Worldview
GAAR0266	Active Layer Detachment Slide	IKONOS/Geoeye/Worldview
GAAR0267	Active Layer Detachment Slide	IKONOS/Geoeye/Worldview
GAAR0268	Active Layer Detachment Slide	IKONOS/Geoeye/Worldview

NPS	2010	67.97612	-155.82095
NPS	2010	67.97441	-155.85668
NPS	2010	67.97330	-155.82782
NPS	2010	67.99203	-155.83258
NPS	2010	67.99203	-155.82506
NPS	2010	67.98484	-155.80805
NPS	2010	67.98374	-155.80418
NPS	2010	67.98560	-155.80018
NPS	2010	67.97738	-155.81334
NPS	2010	67.97894	-155.81051
NPS	2010	67.98026	-155.81552
NPS	2010	67.97342	-155.81661
NPS	2010	67.98929	-155.77244
NPS	2010	67.98832	-155.76782
NPS	2010	67.98874	-155.77161
NPS	2010	67.98417	-155.79398
NPS	2010	67.98428	-155.79080
NPS	2010	67.98380	-155.77936
NPS	2010	67.98164	-155.78578
NPS	2010	67.98152	-155.76922
NPS	2010	67.95355	-155.76802
NPS	2010	67.95033	-155.82520
NPS	2010	67.95015	-155.82530
NPS	2010	67.93243	-156.02273
NPS	2010	67.94863	-156.02549
NPS	2010	67.94692	-156.03359
NPS	2010	67.94702	-156.03542
NPS	2010	67.89363	-156.06929
NPS	2010	67.89593	-156.08329
NPS	2010	67.89158	-156.07433
NPS	2010	67.89292	-156.07244
NPS	2010	67.89530	-156.00818

GAAR0269	Active Layer Detachment Slide	IKONOS/Geoeye/Worldview
GAAR0270	Active Layer Detachment Slide	IKONOS/Geoeye/Worldview
GAAR0271	Active Layer Detachment Slide	IKONOS/Geoeye/Worldview
GAAR0272	Active Layer Detachment Slide	IKONOS/Geoeye/Worldview
GAAR0273	Retrogressive Thaw Slump	IKONOS/Geoeye/Worldview
GAAR0274	Retrogressive Thaw Slump	IKONOS/Geoeye/Worldview
GAAR0275	Retrogressive Thaw Slump	IKONOS/Geoeye/Worldview
GAAR0276	Retrogressive Thaw Slump	IKONOS/Geoeye/Worldview
GAAR0277	Active Layer Detachment Slide	IKONOS/Geoeye/Worldview
GAAR0278	Active Layer Detachment Slide	IKONOS/Geoeye/Worldview
GAAR0279	Active Layer Detachment Slide	IKONOS/Geoeye/Worldview
GAAR0280	Retrogressive Thaw Slump	IKONOS/Geoeye/Worldview
GAAR0281	Retrogressive Thaw Slump	IKONOS/Geoeye/Worldview
GAAR0282	Active Layer Detachment Slide	IKONOS/Geoeye/Worldview
GAAR0283	Active Layer Detachment Slide	IKONOS/Geoeye/Worldview
GAAR0284	Active Layer Detachment Slide	IKONOS/Geoeye/Worldview
GAAR0285	Active Layer Detachment Slide	IKONOS/Geoeye/Worldview
GAAR0286	Active Layer Detachment Slide	IKONOS/Geoeye/Worldview
GAAR0287	Active Layer Detachment Slide	IKONOS/Geoeye/Worldview
GAAR0288	Active Layer Detachment Slide	IKONOS/Geoeye/Worldview
GAAR0289	Active Layer Detachment Slide	IKONOS/Geoeye/Worldview
GAAR0290	Active Layer Detachment Slide	IKONOS/Geoeye/Worldview
GAAR0291	Active Layer Detachment Slide	IKONOS/Geoeye/Worldview
GAAR0292	Active Layer Detachment Slide	IKONOS/Geoeye/Worldview
GAAR0293	Active Layer Detachment Slide	IKONOS/Geoeye/Worldview
GAAR0294	Active Layer Detachment Slide	IKONOS/Geoeye/Worldview
GAAR0295	Active Layer Detachment Slide	IKONOS/Geoeye/Worldview
GAAR0296	Active Layer Detachment Slide	IKONOS/Geoeye/Worldview
GAAR0297	Active Layer Detachment Slide	IKONOS/Geoeye/Worldview
GAAR0298	Active Layer Detachment Slide	IKONOS/Geoeye/Worldview
GAAR0299	Active Layer Detachment Slide	IKONOS/Geoeye/Worldview
GAAR0300	Active Layer Detachment Slide	IKONOS/Geoeye/Worldview

NPS	2010	67.97014	-155.88985
NPS	2010	67.97221	-155.90036
NPS	2010	67.97416	-155.89913
NPS	2010	67.80454	-155.75067
NPS	2010	67.74285	-155.75184
NPS	2010	67.74401	-155.73400
NPS	2010	67.74453	-155.72468
NPS	2010	67.74521	-155.72246
NPS	2010	67.73957	-155.71868
NPS	2010	67.73976	-155.71924
NPS	2010	67.73733	-155.71837
NPS	2010	67.75860	-155.95220
NPS	2010	67.77836	-155.96006
NPS	2010	67.74866	-155.95699
NPS	2010	67.73845	-155.92417
NPS	2010	67.73786	-155.92926
NPS	2010	67.73803	-155.93122
NPS	2010	67.73816	-155.93275
NPS	2010	67.73914	-155.94670
NPS	2010	67.72756	-155.96979
NPS	2010	67.72460	-155.97426
NPS	2010	67.72412	-155.97425
NPS	2010	67.72435	-155.97523
NPS	2010	67.72505	-155.97490
NPS	2010	67.72531	-155.97525
NPS	2010	67.72432	-155.97623
NPS	2010	67.72326	-155.97563
NPS	2010	67.72575	-155.97646
NPS	2010	67.72540	-155.97724
NPS	2010	67.72507	-155.97734
NPS	2010	67.72350	-155.97758
NPS	2010	67.72598	-155.98093

NPS	2010	67.72559	-155.98093
NPS	2010	67.72536	-155.98049
NPS	2010	67.72555	-155.98404
NPS	2010	67.72666	-155.98340
NPS	2010	67.72124	-155.97451
NPS	2010	67.72111	-155.97423
NPS	2010	67.72035	-155.97345
NPS	2010	67.72087	-155.97292
NPS	2010	67.72079	-155.97083
NPS	2010	67.72849	-155.98472
NPS	2010	67.72535	-155.98929
NPS	2010	67.72722	-155.98658
NPS	2010	67.72368	-155.96021
NPS	2010	67.72344	-155.95998
NPS	2010	67.72282	-155.95915
NPS	2010	67.72216	-155.96112
NPS	2010	67.72066	-155.96326
NPS	2010	67.71978	-155.96566
NPS	2010	67.71960	-155.96267
NPS	2010	67.72004	-155.96107
NPS	2010	67.71897	-155.96144
NPS	2010	67.71977	-155.96015
NPS	2010	67.72067	-155.95049
NPS	2010	67.72100	-155.95301
NPS	2010	67.72092	-155.95379
NPS	2010	67.72081	-155.95607
NPS	2010	67.72075	-155.95697
NPS	2010	67.72090	-155.95698
NPS	2010	67.72116	-155.95733
NPS	2010	67.72113	-155.95781
NPS	2010	67.72135	-155.95819
NPS	2010	67.82493	-156.57117

GAAR0333	Active Layer Detachment Slide	IKONOS/Geoeye/Worldview
GAAR0334	Active Layer Detachment Slide	IKONOS/Geoeye/Worldview
GAAR0335	Active Layer Detachment Slide	IKONOS/Geoeye/Worldview
GAAR0336	Retrogressive Thaw Slump	IKONOS/Geoeye/Worldview
GAAR0337	Active Layer Detachment Slide	IKONOS/Geoeye/Worldview
GAAR0338	Active Layer Detachment Slide	IKONOS/Geoeye/Worldview
GAAR0339	Active Layer Detachment Slide	IKONOS/Geoeye/Worldview
GAAR0340	Retrogressive Thaw Slump	IKONOS/Geoeye/Worldview
GAAR0341	Retrogressive Thaw Slump	IKONOS/Geoeye/Worldview
GAAR0342	Retrogressive Thaw Slump	IKONOS/Geoeye/Worldview
GAAR0343	Retrogressive Thaw Slump	IKONOS/Geoeye/Worldview
GAAR0344	Active Layer Detachment Slide	IKONOS/Geoeye/Worldview
GAAR0345	Retrogressive Thaw Slump	IKONOS/Geoeye/Worldview
GAAR0346	Active Layer Detachment Slide	IKONOS/Geoeye/Worldview
GAAR0347	Active Layer Detachment Slide	IKONOS/Geoeye/Worldview
GAAR0348	Active Layer Detachment Slide	IKONOS/Geoeye/Worldview
GAAR0349	Active Layer Detachment Slide	IKONOS/Geoeye/Worldview
GAAR0350	Active Layer Detachment Slide	IKONOS/Geoeye/Worldview
GAAR0351	Active Layer Detachment Slide	IKONOS/Geoeye/Worldview
GAAR0352	Active Layer Detachment Slide	IKONOS/Geoeye/Worldview
GAAR0353	Active Layer Detachment Slide	IKONOS/Geoeye/Worldview
GAAR0354	Active Layer Detachment Slide	IKONOS/Geoeye/Worldview
GAAR0355	Active Layer Detachment Slide	IKONOS/Geoeye/Worldview
GAAR0356	Active Layer Detachment Slide	IKONOS/Geoeye/Worldview
GAAR0357	Active Layer Detachment Slide	IKONOS/Geoeye/Worldview
GAAR0358	Active Layer Detachment Slide	IKONOS/Geoeye/Worldview
GAAR0359	Active Layer Detachment Slide	IKONOS/Geoeye/Worldview
GAAR0360	Active Layer Detachment Slide	IKONOS/Geoeye/Worldview
GAAR0362	Active Layer Detachment Slide	IKONOS/Geoeye/Worldview
GAAR0363	Active Layer Detachment Slide	IKONOS/Geoeye/Worldview
GAAR0364	Active Layer Detachment Slide	IKONOS/Geoeye/Worldview
GAAR0365	Active Layer Detachment Slide	IKONOS/Geoeye/Worldview

NPS	2010	67.82298	-156.55310
NPS	2010	67.82259	-156.55123
NPS	2010	67.82156	-156.57265
NPS	2010	67.80337	-156.50574
NPS	2010	67.80616	-156.51962
NPS	2010	67.80526	-156.51897
NPS	2010	67.81018	-156.51396
NPS	2010	67.81320	-156.50801
NPS	2010	67.81755	-156.50300
NPS	2010	67.81783	-156.50163
NPS	2010	67.81801	-156.50038
NPS	2010	67.80195	-156.62383
NPS	2010	67.87978	-156.17850
NPS	2010	67.86228	-155.83443
NPS	2010	67.88734	-155.84861
NPS	2010	67.88272	-155.84428
NPS	2010	67.86996	-155.77829
NPS	2010	67.86506	-155.78124
NPS	2010	67.86173	-155.77255
NPS	2010	67.86471	-155.76834
NPS	2010	67.86535	-155.76317
NPS	2010	67.86285	-155.76433
NPS	2010	67.86811	-155.78007
NPS	2010	67.86721	-155.76905
NPS	2010	67.86764	-155.76704
NPS	2010	67.86865	-155.76378
NPS	2010	67.86897	-155.76073
NPS	2010	67.86948	-155.76401
NPS	2010	67.87693	-155.75954
NPS	2010	67.84908	-155.75822
NPS	2010	67.84830	-155.75833
NPS	2010	67.84723	-155.76577

GAAR0366	Active Layer Detachment Slide	IKONOS/Geoeye/Worldview
GAAR0367	Active Layer Detachment Slide	IKONOS/Geoeye/Worldview
GAAR0368	Active Layer Detachment Slide	IKONOS/Geoeye/Worldview
GAAR0369	Active Layer Detachment Slide	IKONOS/Geoeye/Worldview
GAAR0370	Active Layer Detachment Slide	IKONOS/Geoeye/Worldview
GAAR0371	Active Layer Detachment Slide	IKONOS/Geoeye/Worldview
GAAR0372	Active Layer Detachment Slide	IKONOS/Geoeye/Worldview
GAAR0373	Active Layer Detachment Slide	IKONOS/Geoeye/Worldview
GAAR0374	Active Layer Detachment Slide	IKONOS/Geoeye/Worldview
GAAR0375	Retrogressive Thaw Slump	IKONOS/Geoeye/Worldview
GAAR0376	Retrogressive Thaw Slump	IKONOS/Geoeye/Worldview
GAAR0377	Active Layer Detachment Slide	IKONOS/Geoeye/Worldview
GAAR0378	Active Layer Detachment Slide	IKONOS/Geoeye/Worldview
GAAR0379	Active Layer Detachment Slide	IKONOS/Geoeye/Worldview
GAAR0380	Active Layer Detachment Slide	IKONOS/Geoeye/Worldview
GAAR0381	Active Layer Detachment Slide	IKONOS/Geoeye/Worldview
GAAR0382	Active Layer Detachment Slide	IKONOS/Geoeye/Worldview
GAAR0383	Active Layer Detachment Slide	IKONOS/Geoeye/Worldview
GAAR0384	Active Layer Detachment Slide	IKONOS/Geoeye/Worldview
GAAR0385	Active Layer Detachment Slide	IKONOS/Geoeye/Worldview
GAAR0386	Active Layer Detachment Slide	IKONOS/Geoeye/Worldview
GAAR0387	Retrogressive Thaw Slump	IKONOS/Geoeye/Worldview
GAAR0388	Retrogressive Thaw Slump	IKONOS/Geoeye/Worldview
GAAR0389	Retrogressive Thaw Slump	IKONOS/Geoeye/Worldview
GAAR0390	Retrogressive Thaw Slump	IKONOS/Geoeye/Worldview
GAAR0391	Active Layer Detachment Slide	IKONOS/Geoeye/Worldview
GAAR0392	Active Layer Detachment Slide	IKONOS/Geoeye/Worldview
GAAR0393	Active Layer Detachment Slide	IKONOS/Geoeye/Worldview
GAAR0394	Retrogressive Thaw Slump	IKONOS/Geoeye/Worldview
GAAR0395	Retrogressive Thaw Slump	IKONOS/Geoeye/Worldview
GAAR0396	Retrogressive Thaw Slump	IKONOS/Geoeye/Worldview
GAAR0397	Retrogressive Thaw Slump	IKONOS/Geoeye/Worldview

NPS	2010	67.84636	-155.76153
NPS	2010	67.84609	-155.76483
NPS	2010	67.82209	-155.75580
NPS	2010	67.82351	-155.76052
NPS	2010	67.82531	-155.76594
NPS	2010	67.81957	-155.77241
NPS	2010	67.82017	-155.76954
NPS	2010	67.82359	-155.75421
NPS	2010	67.82029	-155.76282
NPS	2010	67.73169	-156.57990
NPS	2010	67.79161	-156.37607
NPS	2010	67.79864	-156.15555
NPS	2010	67.79748	-156.15559
NPS	2010	67.79800	-156.15173
NPS	2010	67.79397	-156.14959
NPS	2010	67.79501	-156.15631
NPS	2010	67.79271	-156.15450
NPS	2010	67.79171	-156.15110
NPS	2010	67.79220	-156.15717
NPS	2010	67.79065	-156.15801
NPS	2010	67.78755	-156.08665
NPS	2010	67.75380	-156.09539
NPS	2010	67.75100	-156.09751
NPS	2010	67.75063	-156.09645
NPS	2010	67.75007	-156.09638
NPS	2010	67.76012	-156.14391
NPS	2010	67.76044	-156.14396
NPS	2010	67.75989	-156.14063
NPS	2010	67.77900	-156.35507
NPS	2010	67.77566	-156.35424
NPS	2010	67.76396	-156.33643
NPS	2010	67.74745	-156.35986

GAAR0398	Retrogressive Thaw Slump	IKONOS/Geoeye/Worldview
GAAR0399	Active Layer Detachment Slide	IKONOS/Geoeye/Worldview
GAAR0400	Retrogressive Thaw Slump	IKONOS/Geoeye/Worldview
GAAR0401	Active Layer Detachment Slide	IKONOS/Geoeye/Worldview
GAAR0402	Active Layer Detachment Slide	IKONOS/Geoeye/Worldview
GAAR0403	Retrogressive Thaw Slump	IKONOS/Geoeye/Worldview
GAAR0404	Retrogressive Thaw Slump	IKONOS/Geoeye/Worldview
GAAR0405	Retrogressive Thaw Slump	IKONOS/Geoeye/Worldview
GAAR0406	Active Layer Detachment Slide	IKONOS/Geoeye/Worldview
GAAR0407	Retrogressive Thaw Slump	IKONOS/Geoeye/Worldview
GAAR0408	Retrogressive Thaw Slump	IKONOS/Geoeye/Worldview
GAAR0409	Retrogressive Thaw Slump	IKONOS/Geoeye/Worldview
GAAR0410	Active Layer Detachment Slide	IKONOS/Geoeye/Worldview
GAAR0411	Retrogressive Thaw Slump	IKONOS/Geoeye/Worldview
GAAR0412	Retrogressive Thaw Slump	IKONOS/Geoeye/Worldview
GAAR0413	Active Layer Detachment Slide	IKONOS/Geoeye/Worldview
GAAR0414	Active Layer Detachment Slide	IKONOS/Geoeye/Worldview
GAAR0415	Active Layer Detachment Slide	IKONOS/Geoeye/Worldview
GAAR0416	Active Layer Detachment Slide	IKONOS/Geoeye/Worldview
GAAR0417	Active Layer Detachment Slide	IKONOS/Geoeye/Worldview
GAAR0418	Active Layer Detachment Slide	IKONOS/Geoeye/Worldview
GAAR0419	Active Layer Detachment Slide	IKONOS/Geoeye/Worldview
GAAR0420	Active Layer Detachment Slide	IKONOS/Geoeye/Worldview
GAAR0421	Active Layer Detachment Slide	IKONOS/Geoeye/Worldview
GAAR0422	Active Layer Detachment Slide	IKONOS/Geoeye/Worldview
GAAR0423	Retrogressive Thaw Slump	IKONOS/Geoeye/Worldview
GAAR0424	Active Layer Detachment Slide	IKONOS/Geoeye/Worldview
GAAR0425	Retrogressive Thaw Slump	IKONOS/Geoeye/Worldview
GAAR0426	Active Layer Detachment Slide	IKONOS/Geoeye/Worldview
GAAR0427	Active Layer Detachment Slide	IKONOS/Geoeye/Worldview
GAAR0428	Active Layer Detachment Slide	IKONOS/Geoeye/Worldview
GAAR0429	Active Layer Detachment Slide	IKONOS/Geoeye/Worldview

NPS	2010	67.75069	-156.37111
NPS	2010	67.72394	-156.32856
NPS	2010	67.72191	-156.32009
NPS	2010	67.72473	-156.30998
NPS	2010	67.72687	-156.31159
NPS	2010	67.73008	-156.01464
NPS	2010	67.73270	-156.02318
NPS	2010	67.72331	-155.77905
NPS	2010	67.67046	-155.77533
NPS	2010	67.67060	-155.78705
NPS	2010	67.67092	-155.78788
NPS	2010	67.67344	-155.79393
NPS	2010	67.67261	-155.78915
NPS	2010	67.67139	-155.79679
NPS	2010	67.65939	-155.76018
NPS	2010	67.66120	-155.76943
NPS	2010	67.65680	-155.76194
NPS	2010	67.65470	-155.78459
NPS	2010	67.65451	-155.78270
NPS	2010	67.65470	-155.77912
NPS	2010	67.65187	-155.77876
NPS	2010	67.65168	-155.77232
NPS	2010	67.65037	-155.78887
NPS	2010	67.65043	-155.79389
NPS	2010	67.65275	-155.79951
NPS	2010	67.63752	-155.79324
NPS	2010	67.69255	-156.21993
NPS	2010	67.65517	-156.19903
NPS	2010	67.65259	-156.20432
NPS	2010	67.67384	-156.15801
NPS	2010	67.67418	-156.15626
NPS	2010	67.65849	-156.19208

GAAR0430	Active Layer Detachment Slide	IKONOS/Geoeye/Worldview
GAAR0431	Active Layer Detachment Slide	IKONOS/Geoeye/Worldview
GAAR0432	Active Layer Detachment Slide	IKONOS/Geoeye/Worldview
GAAR0433	Active Layer Detachment Slide	IKONOS/Geoeye/Worldview
GAAR0434	Active Layer Detachment Slide	IKONOS/Geoeye/Worldview
GAAR0435	Active Layer Detachment Slide	IKONOS/Geoeye/Worldview
GAAR0436	Active Layer Detachment Slide	IKONOS/Geoeye/Worldview
GAAR0437	Active Layer Detachment Slide	IKONOS/Geoeye/Worldview
GAAR0438	Active Layer Detachment Slide	IKONOS/Geoeye/Worldview
GAAR0439	Active Layer Detachment Slide	IKONOS/Geoeye/Worldview
GAAR0440	Active Layer Detachment Slide	IKONOS/Geoeye/Worldview
GAAR0441	Active Layer Detachment Slide	IKONOS/Geoeye/Worldview
GAAR0442	Active Layer Detachment Slide	IKONOS/Geoeye/Worldview
GAAR0443	Active Layer Detachment Slide	IKONOS/Geoeye/Worldview
GAAR0444	Retrogressive Thaw Slump	IKONOS/Geoeye/Worldview
GAAR0445	Retrogressive Thaw Slump	IKONOS/Geoeye/Worldview
GAAR0446	Active Layer Detachment Slide	IKONOS/Geoeye/Worldview
GAAR0447	Active Layer Detachment Slide	IKONOS/Geoeye/Worldview
GAAR0448	Active Layer Detachment Slide	IKONOS/Geoeye/Worldview
GAAR0449	Active Layer Detachment Slide	IKONOS/Geoeye/Worldview
GAAR0450	Retrogressive Thaw Slump	IKONOS/Geoeye/Worldview
GAAR0451	Retrogressive Thaw Slump	IKONOS/Geoeye/Worldview
GAAR0452	Active Layer Detachment Slide	IKONOS/Geoeye/Worldview
GAAR0453	Active Layer Detachment Slide	IKONOS/Geoeye/Worldview
GAAR0454	Active Layer Detachment Slide	IKONOS/Geoeye/Worldview
GAAR0455	Retrogressive Thaw Slump	IKONOS/Geoeye/Worldview
GAAR0456	Retrogressive Thaw Slump	IKONOS/Geoeye/Worldview
GAAR0457	Retrogressive Thaw Slump	IKONOS/Geoeye/Worldview
GAAR0458	Retrogressive Thaw Slump	IKONOS/Geoeye/Worldview
GAAR0459	Active Layer Detachment Slide	IKONOS/Geoeye/Worldview
GAAR0460	Active Layer Detachment Slide	IKONOS/Geoeye/Worldview
GAAR0461	Active Layer Detachment Slide	IKONOS/Geoeye/Worldview

NPS	2010	67.66042	-156.18852
NPS	2010	67.66002	-156.18597
NPS	2010	67.66400	-156.18127
NPS	2010	67.66425	-156.17897
NPS	2010	67.68711	-156.23300
NPS	2010	67.68749	-156.23125
NPS	2010	67.68782	-156.22907
NPS	2010	67.64491	-156.21734
NPS	2010	67.71297	-155.95974
NPS	2010	67.71393	-155.94205
NPS	2010	67.66487	-155.88954
NPS	2010	67.66312	-155.89412
NPS	2010	67.66347	-155.89340
NPS	2010	67.66446	-155.89368
NPS	2010	67.62476	-156.11540
NPS	2010	67.61468	-155.93873
NPS	2010	67.63271	-155.91549
NPS	2010	67.63153	-155.91992
NPS	2010	67.63069	-155.91914
NPS	2010	67.63019	-155.91831
NPS	2010	67.64356	-155.89622
NPS	2010	67.64541	-155.89137
NPS	2010	67.63564	-155.85084
NPS	2010	67.63648	-155.85426
NPS	2010	67.63568	-155.85298
NPS	2010	67.62912	-155.84993
NPS	2010	67.62863	-155.84653
NPS	2010	67.62854	-155.85011
NPS	2010	67.62971	-155.85592
NPS	2010	67.63302	-155.97815
NPS	2010	67.63387	-155.97931
NPS	2010	67.63476	-155.97486

GAAR0462	Active Layer Detachment Slide	IKONOS/Geoeye/Worldview
GAAR0463	Active Layer Detachment Slide	IKONOS/Geoeye/Worldview
GAAR0464	Active Layer Detachment Slide	IKONOS/Geoeye/Worldview
GAAR0465	Active Layer Detachment Slide	IKONOS/Geoeye/Worldview
GAAR0466	Retrogressive Thaw Slump	IKONOS/Geoeye/Worldview
GAAR0467	Active Layer Detachment Slide	IKONOS/Geoeye/Worldview
GAAR0468	Active Layer Detachment Slide	IKONOS/Geoeye/Worldview
GAAR0469	Active Layer Detachment Slide	IKONOS/Geoeye/Worldview
GAAR0470	Active Layer Detachment Slide	IKONOS/Geoeye/Worldview
GAAR0471	Active Layer Detachment Slide	IKONOS/Geoeye/Worldview
GAAR0472	Active Layer Detachment Slide	IKONOS/Geoeye/Worldview
GAAR0473	Active Layer Detachment Slide	IKONOS/Geoeye/Worldview
GAAR0474	Active Layer Detachment Slide	IKONOS/Geoeye/Worldview
GAAR0475	Active Layer Detachment Slide	IKONOS/Geoeye/Worldview
GAAR0476	Active Layer Detachment Slide	IKONOS/Geoeye/Worldview
GAAR0477	Active Layer Detachment Slide	IKONOS/Geoeye/Worldview
GAAR0478	Active Layer Detachment Slide	IKONOS/Geoeye/Worldview
GAAR0479	Active Layer Detachment Slide	IKONOS/Geoeye/Worldview
GAAR0480	Active Layer Detachment Slide	IKONOS/Geoeye/Worldview
GAAR0481	Active Layer Detachment Slide	IKONOS/Geoeye/Worldview
GAAR0482	Active Layer Detachment Slide	IKONOS/Geoeye/Worldview
GAAR0483	Active Layer Detachment Slide	IKONOS/Geoeye/Worldview
GAAR0484	Active Layer Detachment Slide	IKONOS/Geoeye/Worldview
GAAR0485	Active Layer Detachment Slide	IKONOS/Geoeye/Worldview
GAAR0486	Active Layer Detachment Slide	IKONOS/Geoeye/Worldview
GAAR0487	Active Layer Detachment Slide	IKONOS/Geoeye/Worldview
GAAR0488	Active Layer Detachment Slide	IKONOS/Geoeye/Worldview
GAAR0489	Active Layer Detachment Slide	IKONOS/Geoeye/Worldview
GAAR0490	Active Layer Detachment Slide	IKONOS/Geoeye/Worldview
GAAR0491	Active Layer Detachment Slide	IKONOS/Geoeye/Worldview
GAAR0492	Active Layer Detachment Slide	IKONOS/Geoeye/Worldview
GAAR0493	Active Layer Detachment Slide	IKONOS/Geoeye/Worldview

NPS	2010	67.63468	-155.98523
NPS	2010	67.63258	-155.97729
NPS	2010	67.58924	-156.29240
NPS	2010	67.59293	-156.29072
NPS	2010	67.60264	-156.12083
NPS	2010	68.35104	-153.40141
NPS	2010	68.35005	-153.39924
NPS	2010	68.34905	-153.39910
NPS	2010	68.34630	-153.39789
NPS	2010	68.33860	-153.37545
NPS	2010	68.33714	-153.05028
NPS	2010	68.33564	-153.05118
NPS	2010	68.33396	-153.04916
NPS	2010	67.58952	-153.57199
NPS	2010	67.57574	-153.62965
NPS	2010	67.53129	-153.45354
NPS	2010	67.53847	-153.42554
NPS	2010	67.51269	-153.34180
NPS	2010	67.51327	-153.34301
NPS	2010	67.51312	-153.38380
NPS	2010	67.49470	-153.98626
NPS	2010	67.50480	-153.16783
NPS	2010	68.19903	-153.48582
NPS	2010	68.20432	-153.24359
NPS	2010	68.21662	-153.20926
NPS	2010	68.18999	-153.17154
NPS	2010	68.19022	-153.17960
NPS	2010	68.19107	-153.17283
NPS	2010	68.19163	-153.08307
NPS	2010	68.19247	-153.07563
NPS	2010	68.19736	-153.10235
NPS	2010	68.16260	-153.12382

NPS	2010	68.16369	-153.13662
NPS	2010	68.16472	-153.13930
NPS	2010	68.16486	-153.13850
NPS	2010	68.16597	-153.14077
NPS	2010	68.16890	-153.14629
NPS	2010	68.16745	-153.14580
NPS	2010	68.16828	-153.14759
NPS	2010	68.17785	-153.16192
NPS	2010	68.17562	-153.17103
NPS	2010	68.07819	-155.58623
NPS	2010	68.08040	-155.56267
NPS	2010	68.07886	-155.56605
NPS	2010	68.07872	-155.53774
NPS	2010	68.08114	-155.48597
NPS	2010	68.08317	-155.49168
NPS	2010	68.08417	-155.49473
NPS	2010	68.08171	-155.49544
NPS	2010	68.08237	-155.49502
NPS	2010	68.08505	-155.48624
NPS	2010	68.07601	-155.50497
NPS	2010	68.07668	-155.50599
NPS	2010	68.07901	-155.50315
NPS	2010	68.07905	-155.50016
NPS	2010	68.07675	-155.49091
NPS	2010	68.07667	-155.49474
NPS	2010	68.08080	-155.48877
NPS	2010	68.07499	-155.43259
NPS	2010	68.07421	-155.43525
NPS	2010	68.07470	-155.43731
NPS	2010	68.07511	-155.43703
NPS	2010	68.07551	-155.43489
NPS	2010	68.07574	-155.43553

GAAR0526	Active Layer Detachment Slide	IKONOS/Geoeye/Worldview
GAAR0527	Active Layer Detachment Slide	IKONOS/Geoeye/Worldview
GAAR0528	Active Layer Detachment Slide	IKONOS/Geoeye/Worldview
GAAR0529	Active Layer Detachment Slide	IKONOS/Geoeye/Worldview
GAAR0530	Active Layer Detachment Slide	IKONOS/Geoeye/Worldview
GAAR0531	Active Layer Detachment Slide	IKONOS/Geoeye/Worldview
GAAR0532	Active Layer Detachment Slide	IKONOS/Geoeye/Worldview
GAAR0533	Active Layer Detachment Slide	IKONOS/Geoeye/Worldview
GAAR0534	Active Layer Detachment Slide	IKONOS/Geoeye/Worldview
GAAR0535	Active Layer Detachment Slide	IKONOS/Geoeye/Worldview
GAAR0536	Active Layer Detachment Slide	IKONOS/Geoeye/Worldview
GAAR0537	Active Layer Detachment Slide	IKONOS/Geoeye/Worldview
GAAR0538	Active Layer Detachment Slide	IKONOS/Geoeye/Worldview
GAAR0539	Active Layer Detachment Slide	IKONOS/Geoeye/Worldview
GAAR0540	Active Layer Detachment Slide	IKONOS/Geoeye/Worldview
GAAR0541	Active Layer Detachment Slide	IKONOS/Geoeye/Worldview
GAAR0542	Active Layer Detachment Slide	IKONOS/Geoeye/Worldview
GAAR0543	Active Layer Detachment Slide	IKONOS/Geoeye/Worldview
GAAR0544	Active Layer Detachment Slide	IKONOS/Geoeye/Worldview
GAAR0545	Active Layer Detachment Slide	IKONOS/Geoeye/Worldview
GAAR0546	Active Layer Detachment Slide	IKONOS/Geoeye/Worldview
GAAR0547	Active Layer Detachment Slide	IKONOS/Geoeye/Worldview
GAAR0548	Active Layer Detachment Slide	IKONOS/Geoeye/Worldview
GAAR0549	Active Layer Detachment Slide	IKONOS/Geoeye/Worldview
GAAR0550	Active Layer Detachment Slide	IKONOS/Geoeye/Worldview
GAAR0551	Active Layer Detachment Slide	IKONOS/Geoeye/Worldview
GAAR0552	Active Layer Detachment Slide	IKONOS/Geoeye/Worldview
GAAR0553	Active Layer Detachment Slide	IKONOS/Geoeye/Worldview
GAAR0554	Active Layer Detachment Slide	IKONOS/Geoeye/Worldview
GAAR0555	Active Layer Detachment Slide	IKONOS/Geoeye/Worldview
GAAR0556	Active Layer Detachment Slide	IKONOS/Geoeye/Worldview
GAAR0557	Active Layer Detachment Slide	IKONOS/Geoeye/Worldview

NPS	2010	68.07532	-155.43792
NPS	2010	68.07573	-155.43841
NPS	2010	68.07473	-155.44238
NPS	2010	68.07657	-155.44292
NPS	2010	68.07660	-155.44232
NPS	2010	68.07764	-155.44550
NPS	2010	68.07822	-155.43927
NPS	2010	68.07871	-155.44083
NPS	2010	68.07916	-155.44362
NPS	2010	68.10326	-155.39581
NPS	2010	68.07910	-155.38594
NPS	2010	68.07800	-155.38474
NPS	2010	68.07831	-155.38023
NPS	2010	68.07717	-155.37742
NPS	2010	68.07851	-155.37336
NPS	2010	68.07758	-155.37157
NPS	2010	68.07670	-155.37334
NPS	2010	68.07629	-155.37566
NPS	2010	68.07588	-155.37694
NPS	2010	68.07490	-155.37339
NPS	2010	68.07412	-155.37173
NPS	2010	68.07411	-155.37440
NPS	2010	68.07416	-155.37506
NPS	2010	68.07297	-155.37595
NPS	2010	68.07495	-155.37561
NPS	2010	68.07434	-155.37605
NPS	2010	68.07401	-155.37619
NPS	2010	68.07459	-155.37806
NPS	2010	68.07458	-155.37919
NPS	2010	68.07589	-155.38118
NPS	2010	68.07595	-155.38259
NPS	2010	68.07593	-155.38330

GAAR0558	Active Layer Detachment Slide	IKONOS/Geoeye/Worldview
GAAR0559	Active Layer Detachment Slide	IKONOS/Geoeye/Worldview
GAAR0560	Active Layer Detachment Slide	IKONOS/Geoeye/Worldview
GAAR0561	Active Layer Detachment Slide	IKONOS/Geoeye/Worldview
GAAR0562	Active Layer Detachment Slide	IKONOS/Geoeye/Worldview
GAAR0563	Active Layer Detachment Slide	IKONOS/Geoeye/Worldview
GAAR0564	Active Layer Detachment Slide	IKONOS/Geoeye/Worldview
GAAR0565	Active Layer Detachment Slide	IKONOS/Geoeye/Worldview
GAAR0566	Active Layer Detachment Slide	IKONOS/Geoeye/Worldview
GAAR0567	Active Layer Detachment Slide	IKONOS/Geoeye/Worldview
GAAR0568	Active Layer Detachment Slide	IKONOS/Geoeye/Worldview
GAAR0569	Active Layer Detachment Slide	IKONOS/Geoeye/Worldview
GAAR0570	Active Layer Detachment Slide	IKONOS/Geoeye/Worldview
GAAR0571	Active Layer Detachment Slide	IKONOS/Geoeye/Worldview
GAAR0572	Active Layer Detachment Slide	IKONOS/Geoeye/Worldview
GAAR0573	Active Layer Detachment Slide	IKONOS/Geoeye/Worldview
GAAR0574	Active Layer Detachment Slide	IKONOS/Geoeye/Worldview
GAAR0575	Active Layer Detachment Slide	IKONOS/Geoeye/Worldview
GAAR0576	Active Layer Detachment Slide	IKONOS/Geoeye/Worldview
GAAR0577	Active Layer Detachment Slide	IKONOS/Geoeye/Worldview
GAAR0578	Active Layer Detachment Slide	IKONOS/Geoeye/Worldview
GAAR0579	Active Layer Detachment Slide	IKONOS/Geoeye/Worldview
GAAR0580	Active Layer Detachment Slide	IKONOS/Geoeye/Worldview
GAAR0581	Retrogressive Thaw Slump	IKONOS/Geoeye/Worldview
GAAR0582	Active Layer Detachment Slide	IKONOS/Geoeye/Worldview
GAAR0583	Active Layer Detachment Slide	IKONOS/Geoeye/Worldview
GAAR0584	Active Layer Detachment Slide	IKONOS/Geoeye/Worldview
GAAR0585	Active Layer Detachment Slide	IKONOS/Geoeye/Worldview
GAAR0586	Active Layer Detachment Slide	IKONOS/Geoeye/Worldview
GAAR0587	Active Layer Detachment Slide	IKONOS/Geoeye/Worldview
GAAR0588	Active Layer Detachment Slide	IKONOS/Geoeye/Worldview
GAAR0589	Active Layer Detachment Slide	IKONOS/Geoeye/Worldview

NPS	2010	68.07586	-155.38566
NPS	2010	68.07485	-155.38268
NPS	2010	68.07416	-155.38395
NPS	2010	68.07687	-155.39341
NPS	2010	68.07689	-155.39547
NPS	2010	68.07336	-155.39130
NPS	2010	68.07288	-155.39651
NPS	2010	68.08176	-155.44097
NPS	2010	68.07680	-155.34589
NPS	2010	68.10842	-155.30001
NPS	2010	68.10711	-155.30748
NPS	2010	68.10836	-155.31567
NPS	2010	68.10538	-155.31548
NPS	2010	68.10337	-155.31045
NPS	2010	68.10456	-155.30990
NPS	2010	68.10486	-155.30887
NPS	2010	68.10405	-155.30693
NPS	2010	68.10588	-155.30465
NPS	2010	68.10435	-155.31940
NPS	2010	68.10386	-155.32143
NPS	2010	68.08631	-155.28830
NPS	2010	68.08280	-155.24005
NPS	2010	68.08161	-155.24027
NPS	2010	68.08028	-155.24568
NPS	2010	68.07830	-155.24456
NPS	2010	68.07585	-155.24882
NPS	2010	68.04723	-155.20061
NPS	2010	68.04622	-155.20106
NPS	2010	68.04561	-155.19995
NPS	2010	68.04164	-155.20319
NPS	2010	68.04105	-155.20762
NPS	2010	68.03985	-155.19839

GAAR0590	Active Layer Detachment Slide	IKONOS/Geoeye/Worldview
GAAR0591	Active Layer Detachment Slide	IKONOS/Geoeye/Worldview
GAAR0592	Active Layer Detachment Slide	IKONOS/Geoeye/Worldview
GAAR0593	Active Layer Detachment Slide	IKONOS/Geoeye/Worldview
GAAR0594	Active Layer Detachment Slide	IKONOS/Geoeye/Worldview
GAAR0595	Active Layer Detachment Slide	IKONOS/Geoeye/Worldview
GAAR0596	Active Layer Detachment Slide	IKONOS/Geoeye/Worldview
GAAR0597	Active Layer Detachment Slide	IKONOS/Geoeye/Worldview
GAAR0598	Active Layer Detachment Slide	IKONOS/Geoeye/Worldview
GAAR0599	Active Layer Detachment Slide	IKONOS/Geoeye/Worldview
GAAR0600	Active Layer Detachment Slide	IKONOS/Geoeye/Worldview
GAAR0601	Active Layer Detachment Slide	IKONOS/Geoeye/Worldview
GAAR0602	Active Layer Detachment Slide	IKONOS/Geoeye/Worldview
GAAR0603	Active Layer Detachment Slide	IKONOS/Geoeye/Worldview
GAAR0604	Active Layer Detachment Slide	IKONOS/Geoeye/Worldview
GAAR0605	Active Layer Detachment Slide	IKONOS/Geoeye/Worldview
GAAR0606	Active Layer Detachment Slide	IKONOS/Geoeye/Worldview
GAAR0607	Active Layer Detachment Slide	IKONOS/Geoeye/Worldview
GAAR0608	Retrogressive Thaw Slump	IKONOS/Geoeye/Worldview
GAAR0609	Active Layer Detachment Slide	IKONOS/Geoeye/Worldview
GAAR0610	Active Layer Detachment Slide	IKONOS/Geoeye/Worldview
GAAR0611	Retrogressive Thaw Slump	IKONOS/Geoeye/Worldview
GAAR0612	Active Layer Detachment Slide	IKONOS/Geoeye/Worldview
GAAR0613	Active Layer Detachment Slide	IKONOS/Geoeye/Worldview
GAAR0614	Active Layer Detachment Slide	IKONOS/Geoeye/Worldview
GAAR0615	Active Layer Detachment Slide	IKONOS/Geoeye/Worldview
GAAR0616	Active Layer Detachment Slide	IKONOS/Geoeye/Worldview
GAAR0617	Active Layer Detachment Slide	IKONOS/Geoeye/Worldview
GAAR0618	Retrogressive Thaw Slump	IKONOS/Geoeye/Worldview
GAAR0619	Active Layer Detachment Slide	IKONOS/Geoeye/Worldview
GAAR0620	Active Layer Detachment Slide	IKONOS/Geoeye/Worldview
GAAR0621	Active Layer Detachment Slide	IKONOS/Geoeye/Worldview

NPS	2010	68.04113	-155.20310
NPS	2010	68.06844	-155.34746
NPS	2010	68.06868	-155.34709
NPS	2010	68.07048	-155.34122
NPS	2010	68.07067	-155.34217
NPS	2010	68.07119	-155.34673
NPS	2010	68.06218	-155.35206
NPS	2010	68.06295	-155.35521
NPS	2010	68.06338	-155.35647
NPS	2010	68.06411	-155.35775
NPS	2010	68.06429	-155.35885
NPS	2010	68.06454	-155.35960
NPS	2010	68.06466	-155.36019
NPS	2010	68.06416	-155.35636
NPS	2010	68.06278	-155.35839
NPS	2010	68.06434	-155.36393
NPS	2010	68.06498	-155.36274
NPS	2010	68.06583	-155.36145
NPS	2010	68.06626	-155.35946
NPS	2010	68.06322	-155.35880
NPS	2010	68.06284	-155.35953
NPS	2010	68.06537	-155.35652
NPS	2010	68.06713	-155.35565
NPS	2010	68.06671	-155.35836
NPS	2010	68.06697	-155.35820
NPS	2010	68.06790	-155.36194
NPS	2010	68.06777	-155.36175
NPS	2010	68.06660	-155.36255
NPS	2010	68.06676	-155.36396
NPS	2010	68.06808	-155.35683
NPS	2010	68.06962	-155.35784
NPS	2010	68.06955	-155.36066

GAAR0622	Active Layer Detachment Slide	IKONOS/Geoeye/Worldview
GAAR0623	Active Layer Detachment Slide	IKONOS/Geoeye/Worldview
GAAR0624	Active Layer Detachment Slide	IKONOS/Geoeye/Worldview
GAAR0625	Active Layer Detachment Slide	IKONOS/Geoeye/Worldview
GAAR0626	Active Layer Detachment Slide	IKONOS/Geoeye/Worldview
GAAR0627	Active Layer Detachment Slide	IKONOS/Geoeye/Worldview
GAAR0628	Active Layer Detachment Slide	IKONOS/Geoeye/Worldview
GAAR0629	Active Layer Detachment Slide	IKONOS/Geoeye/Worldview
GAAR0630	Active Layer Detachment Slide	IKONOS/Geoeye/Worldview
GAAR0631	Active Layer Detachment Slide	IKONOS/Geoeye/Worldview
GAAR0632	Active Layer Detachment Slide	IKONOS/Geoeye/Worldview
GAAR0633	Active Layer Detachment Slide	IKONOS/Geoeye/Worldview
GAAR0634	Active Layer Detachment Slide	IKONOS/Geoeye/Worldview
GAAR0635	Retrogressive Thaw Slump	IKONOS/Geoeye/Worldview
GAAR0636	Active Layer Detachment Slide	IKONOS/Geoeye/Worldview
GAAR0637	Active Layer Detachment Slide	IKONOS/Geoeye/Worldview
GAAR0638	Retrogressive Thaw Slump	IKONOS/Geoeye/Worldview
GAAR0639	Active Layer Detachment Slide	IKONOS/Geoeye/Worldview
GAAR0640	Active Layer Detachment Slide	IKONOS/Geoeye/Worldview
GAAR0641	Active Layer Detachment Slide	IKONOS/Geoeye/Worldview
GAAR0642	Active Layer Detachment Slide	IKONOS/Geoeye/Worldview
GAAR0643	Active Layer Detachment Slide	IKONOS/Geoeye/Worldview
GAAR0644	Active Layer Detachment Slide	IKONOS/Geoeye/Worldview
GAAR0645	Active Layer Detachment Slide	IKONOS/Geoeye/Worldview
GAAR0646	Active Layer Detachment Slide	IKONOS/Geoeye/Worldview
GAAR0647	Active Layer Detachment Slide	IKONOS/Geoeye/Worldview
GAAR0648	Active Layer Detachment Slide	IKONOS/Geoeye/Worldview
GAAR0649	Active Layer Detachment Slide	IKONOS/Geoeye/Worldview
GAAR0650	Active Layer Detachment Slide	IKONOS/Geoeye/Worldview
GAAR0651	Active Layer Detachment Slide	IKONOS/Geoeye/Worldview
GAAR0652	Active Layer Detachment Slide	IKONOS/Geoeye/Worldview
GAAR0653	Active Layer Detachment Slide	IKONOS/Geoeye/Worldview

NPS	2010	68.06867	-155.36422
NPS	2010	68.06942	-155.36573
NPS	2010	68.06942	-155.36846
NPS	2010	68.06845	-155.36692
NPS	2010	68.06711	-155.36507
NPS	2010	68.06229	-155.38399
NPS	2010	68.06135	-155.38307
NPS	2010	68.06145	-155.38623
NPS	2010	68.06156	-155.38788
NPS	2010	68.06350	-155.38896
NPS	2010	68.06232	-155.39292
NPS	2010	68.06852	-155.38554
NPS	2010	68.06494	-155.39740
NPS	2010	68.04819	-155.37824
NPS	2010	68.05404	-155.37844
NPS	2010	68.05298	-155.38115
NPS	2010	68.05206	-155.38147
NPS	2010	68.05194	-155.38402
NPS	2010	68.04579	-155.36607
NPS	2010	68.04473	-155.36486
NPS	2010	68.04489	-155.36710
NPS	2010	68.04564	-155.37080
NPS	2010	68.06118	-155.44887
NPS	2010	68.05770	-155.46099
NPS	2010	68.05873	-155.46323
NPS	2010	68.06176	-155.46924
NPS	2010	68.06195	-155.46658
NPS	2010	68.06207	-155.46427
NPS	2010	68.06138	-155.46414
NPS	2010	68.06014	-155.46603
NPS	2010	68.05660	-155.47681
NPS	2010	68.05475	-155.47399

GAAR0654	Active Layer Detachment Slide	IKONOS/Geoeye/Worldview
GAAR0655	Active Layer Detachment Slide	IKONOS/Geoeye/Worldview
GAAR0656	Active Layer Detachment Slide	IKONOS/Geoeye/Worldview
GAAR0657	Active Layer Detachment Slide	IKONOS/Geoeye/Worldview
GAAR0658	Retrogressive Thaw Slump	IKONOS/Geoeye/Worldview
GAAR0659	Active Layer Detachment Slide	IKONOS/Geoeye/Worldview
GAAR0660	Active Layer Detachment Slide	IKONOS/Geoeye/Worldview
GAAR0661	Active Layer Detachment Slide	IKONOS/Geoeye/Worldview
GAAR0662	Active Layer Detachment Slide	IKONOS/Geoeye/Worldview
GAAR0663	Active Layer Detachment Slide	IKONOS/Geoeye/Worldview
GAAR0664	Retrogressive Thaw Slump	IKONOS/Geoeye/Worldview
GAAR0665	Active Layer Detachment Slide	IKONOS/Geoeye/Worldview
GAAR0666	Active Layer Detachment Slide	IKONOS/Geoeye/Worldview
GAAR0667	Active Layer Detachment Slide	IKONOS/Geoeye/Worldview
GAAR0668	Active Layer Detachment Slide	IKONOS/Geoeye/Worldview
GAAR0669	Retrogressive Thaw Slump	IKONOS/Geoeye/Worldview
GAAR0670	Active Layer Detachment Slide	IKONOS/Geoeye/Worldview
GAAR0671	Active Layer Detachment Slide	IKONOS/Geoeye/Worldview
GAAR0672	Active Layer Detachment Slide	IKONOS/Geoeye/Worldview
GAAR0673	Active Layer Detachment Slide	IKONOS/Geoeye/Worldview
GAAR0678	Active Layer Detachment Slide	IKONOS/Geoeye/Worldview
GAAR0679	Active Layer Detachment Slide	IKONOS/Geoeye/Worldview
GAAR0680	Active Layer Detachment Slide	IKONOS/Geoeye/Worldview
GAAR0681	Active Layer Detachment Slide	IKONOS/Geoeye/Worldview
GAAR0682	Active Layer Detachment Slide	IKONOS/Geoeye/Worldview
GAAR0683	Active Layer Detachment Slide	IKONOS/Geoeye/Worldview
GAAR0684	Active Layer Detachment Slide	IKONOS/Geoeye/Worldview
GAAR0685	Active Layer Detachment Slide	IKONOS/Geoeye/Worldview
GAAR0686	Active Layer Detachment Slide	IKONOS/Geoeye/Worldview
GAAR0687	Active Layer Detachment Slide	IKONOS/Geoeye/Worldview
GAAR0688	Active Layer Detachment Slide	IKONOS/Geoeye/Worldview
GAAR0689	Active Layer Detachment Slide	IKONOS/Geoeye/Worldview

NPS	2010	68.05391	-155.47163
NPS	2010	68.05314	-155.47172
NPS	2010	68.05448	-155.45529
NPS	2010	68.05478	-155.45473
NPS	2010	68.05337	-155.46942
NPS	2010	68.05601	-155.44862
NPS	2010	68.05391	-155.44298
NPS	2010	68.05462	-155.44747
NPS	2010	68.05338	-155.46439
NPS	2010	68.05162	-155.45989
NPS	2010	68.05554	-155.47083
NPS	2010	68.05321	-155.47498
NPS	2010	68.05766	-155.48302
NPS	2010	68.05910	-155.48554
NPS	2010	68.05911	-155.48393
NPS	2010	68.05862	-155.47979
NPS	2010	68.05081	-155.50227
NPS	2010	68.05197	-155.50681
NPS	2010	68.05287	-155.51068
NPS	2010	68.05286	-155.51439
NPS	2010	68.05036	-155.50284
NPS	2010	68.05346	-155.49626
NPS	2010	68.05196	-155.51080
NPS	2010	68.05198	-155.51434
NPS	2010	68.05905	-155.49531
NPS	2010	68.05989	-155.50059
NPS	2010	68.05929	-155.51528
NPS	2010	68.04310	-155.51122
NPS	2010	68.06235	-155.51527
NPS	2010	68.05660	-155.54362
NPS	2010	68.05923	-155.54139
NPS	2010	68.05884	-155.54413

GAAR0690	Active Layer Detachment Slide	IKONOS/Geoeye/Worldview
GAAR0691	Active Layer Detachment Slide	IKONOS/Geoeye/Worldview
GAAR0692	Active Layer Detachment Slide	IKONOS/Geoeye/Worldview
GAAR0693	Active Layer Detachment Slide	IKONOS/Geoeye/Worldview
GAAR0694	Retrogressive Thaw Slump	IKONOS/Geoeye/Worldview
GAAR0695	Retrogressive Thaw Slump	IKONOS/Geoeye/Worldview
GAAR0696	Active Layer Detachment Slide	IKONOS/Geoeye/Worldview
GAAR0697	Active Layer Detachment Slide	IKONOS/Geoeye/Worldview
GAAR0698	Active Layer Detachment Slide	IKONOS/Geoeye/Worldview
GAAR0699	Active Layer Detachment Slide	IKONOS/Geoeye/Worldview
GAAR0700	Active Layer Detachment Slide	IKONOS/Geoeye/Worldview
GAAR0701	Active Layer Detachment Slide	IKONOS/Geoeye/Worldview
GAAR0702	Active Layer Detachment Slide	IKONOS/Geoeye/Worldview
GAAR0703	Active Layer Detachment Slide	IKONOS/Geoeye/Worldview
GAAR0704	Active Layer Detachment Slide	IKONOS/Geoeye/Worldview
GAAR0705	Active Layer Detachment Slide	IKONOS/Geoeye/Worldview
GAAR0706	Active Layer Detachment Slide	IKONOS/Geoeye/Worldview
GAAR0707	Active Layer Detachment Slide	IKONOS/Geoeye/Worldview
GAAR0708	Active Layer Detachment Slide	IKONOS/Geoeye/Worldview
GAAR0709	Active Layer Detachment Slide	IKONOS/Geoeye/Worldview
GAAR0710	Active Layer Detachment Slide	IKONOS/Geoeye/Worldview
GAAR0711	Active Layer Detachment Slide	IKONOS/Geoeye/Worldview
GAAR0713	Active Layer Detachment Slide	IKONOS/Geoeye/Worldview
GAAR0714	Active Layer Detachment Slide	IKONOS/Geoeye/Worldview
GAAR0715	Active Layer Detachment Slide	IKONOS/Geoeye/Worldview
GAAR0716	Active Layer Detachment Slide	IKONOS/Geoeye/Worldview
GAAR0717	Active Layer Detachment Slide	IKONOS/Geoeye/Worldview
GAAR0718	Active Layer Detachment Slide	IKONOS/Geoeye/Worldview
GAAR0719	Active Layer Detachment Slide	IKONOS/Geoeye/Worldview
GAAR0720	Active Layer Detachment Slide	IKONOS/Geoeye/Worldview
GAAR0722	Active Layer Detachment Slide	IKONOS/Geoeye/Worldview
GAAR0723	Active Layer Detachment Slide	IKONOS/Geoeye/Worldview

NPS	2010	68.05962	-155.54613
NPS	2010	68.05827	-155.54895
NPS	2010	68.05986	-155.55473
NPS	2010	68.06086	-155.54804
NPS	2010	68.06007	-155.56065
NPS	2010	68.05852	-155.56618
NPS	2010	68.06631	-155.52659
NPS	2010	68.06417	-155.50216
NPS	2010	68.03336	-155.34762
NPS	2010	68.01957	-155.24199
NPS	2010	68.05203	-155.59679
NPS	2010	68.05974	-154.90944
NPS	2010	68.05953	-154.90120
NPS	2010	68.05498	-154.93965
NPS	2010	68.01771	-155.19519
NPS	2010	68.01359	-155.18695
NPS	2010	68.01629	-155.18252
NPS	2010	68.01555	-155.17830
NPS	2010	68.01543	-155.18744
NPS	2010	68.01376	-155.17501
NPS	2010	68.01967	-155.18866
NPS	2010	68.02000	-155.18810
NPS	2010	68.02023	-155.18721
NPS	2010	68.01999	-155.18540
NPS	2010	68.02329	-155.18853
NPS	2010	68.02264	-155.19007
NPS	2010	68.02805	-155.02913
NPS	2010	68.02309	-155.02541
NPS	2010	68.02244	-155.02472
NPS	2010	68.02264	-155.02107
NPS	2010	68.02170	-155.02244
NPS	2010	68.02193	-155.02509

GAAR0724	Active Layer Detachment Slide	IKONOS/Geoeye/Worldview
GAAR0726	Active Layer Detachment Slide	IKONOS/Geoeye/Worldview
GAAR0727	Active Layer Detachment Slide	IKONOS/Geoeye/Worldview
GAAR0728	Active Layer Detachment Slide	IKONOS/Geoeye/Worldview
GAAR0729	Active Layer Detachment Slide	IKONOS/Geoeye/Worldview
GAAR0730	Active Layer Detachment Slide	IKONOS/Geoeye/Worldview
GAAR0731	Active Layer Detachment Slide	IKONOS/Geoeye/Worldview
GAAR0732	Active Layer Detachment Slide	IKONOS/Geoeye/Worldview
GAAR0733	Active Layer Detachment Slide	IKONOS/Geoeye/Worldview
GAAR0735	Active Layer Detachment Slide	IKONOS/Geoeye/Worldview
GAAR0736	Active Layer Detachment Slide	IKONOS/Geoeye/Worldview
GAAR0738	Active Layer Detachment Slide	IKONOS/Geoeye/Worldview
GAAR0739	Active Layer Detachment Slide	IKONOS/Geoeye/Worldview
GAAR0740	Active Layer Detachment Slide	IKONOS/Geoeye/Worldview
GAAR0741	Active Layer Detachment Slide	IKONOS/Geoeye/Worldview
GAAR0742	Active Layer Detachment Slide	IKONOS/Geoeye/Worldview
GAAR0743	Active Layer Detachment Slide	IKONOS/Geoeye/Worldview
GAAR0744	Active Layer Detachment Slide	IKONOS/Geoeye/Worldview
GAAR0745	Active Layer Detachment Slide	IKONOS/Geoeye/Worldview
GAAR0746	Active Layer Detachment Slide	IKONOS/Geoeye/Worldview
GAAR0747	Active Layer Detachment Slide	IKONOS/Geoeye/Worldview
GAAR0748	Retrogressive Thaw Slump	IKONOS/Geoeye/Worldview
GAAR0749	Retrogressive Thaw Slump	IKONOS/Geoeye/Worldview
GAAR0750	Retrogressive Thaw Slump	IKONOS/Geoeye/Worldview
GAAR0751	Retrogressive Thaw Slump	IKONOS/Geoeye/Worldview
GAAR0752	Retrogressive Thaw Slump	IKONOS/Geoeye/Worldview
GAAR0753	Retrogressive Thaw Slump	IKONOS/Geoeye/Worldview
GAAR0754	Retrogressive Thaw Slump	IKONOS/Geoeye/Worldview
GAAR0755	Active Layer Detachment Slide	IKONOS/Geoeye/Worldview
GAAR0756	Active Layer Detachment Slide	IKONOS/Geoeye/Worldview
GAAR0757	Active Layer Detachment Slide	IKONOS/Geoeye/Worldview
GAAR0758	Active Layer Detachment Slide	IKONOS/Geoeye/Worldview

NPS	2010	68.02019	-155.02516
NPS	2010	68.02894	-155.07503
NPS	2010	68.09365	-154.57392
NPS	2010	68.06385	-154.67515
NPS	2010	68.09876	-154.16860
NPS	2010	68.09798	-154.16786
NPS	2010	68.09683	-154.16163
NPS	2010	68.09899	-154.16181
NPS	2010	68.10027	-154.16332
NPS	2010	68.10323	-154.16022
NPS	2010	68.10649	-154.16689
NPS	2010	68.09266	-154.11441
NPS	2010	68.09302	-154.11075
NPS	2010	68.09345	-154.10963
NPS	2010	68.08470	-154.11562
NPS	2010	68.08525	-154.11328
NPS	2010	68.07132	-154.06242
NPS	2010	68.05806	-154.07759
NPS	2010	68.05757	-154.07763
NPS	2010	68.06031	-154.26447
NPS	2010	68.06509	-154.27003
NPS	2010	68.07070	-154.17789
NPS	2010	68.07126	-154.18324
NPS	2010	68.07262	-154.18483
NPS	2010	68.07313	-154.18555
NPS	2010	68.07460	-154.18855
NPS	2010	68.04652	-154.27437
NPS	2010	68.04610	-154.27398
NPS	2010	68.03622	-154.31106
NPS	2010	68.35876	-155.60566
NPS	2010	68.35402	-155.60818
NPS	2010	68.35460	-155.38960

GAAR0759	Active Layer Detachment Slide	IKONOS/Geoeye/Worldview
GAAR0760	Active Layer Detachment Slide	IKONOS/Geoeye/Worldview
GAAR0761	Active Layer Detachment Slide	IKONOS/Geoeye/Worldview
GAAR0762	Active Layer Detachment Slide	IKONOS/Geoeye/Worldview
GAAR0763	Active Layer Detachment Slide	IKONOS/Geoeye/Worldview
GAAR0764	Active Layer Detachment Slide	IKONOS/Geoeye/Worldview
GAAR0765	Active Layer Detachment Slide	IKONOS/Geoeye/Worldview
GAAR0766	Active Layer Detachment Slide	IKONOS/Geoeye/Worldview
GAAR0767	Active Layer Detachment Slide	IKONOS/Geoeye/Worldview
GAAR0768	Active Layer Detachment Slide	IKONOS/Geoeye/Worldview
GAAR0769	Active Layer Detachment Slide	IKONOS/Geoeye/Worldview
GAAR0770	Active Layer Detachment Slide	IKONOS/Geoeye/Worldview
GAAR0771	Active Layer Detachment Slide	IKONOS/Geoeye/Worldview
GAAR0772	Active Layer Detachment Slide	IKONOS/Geoeye/Worldview
GAAR0773	Active Layer Detachment Slide	IKONOS/Geoeye/Worldview
GAAR0774	Active Layer Detachment Slide	IKONOS/Geoeye/Worldview
GAAR0775	Active Layer Detachment Slide	IKONOS/Geoeye/Worldview
GAAR0776	Active Layer Detachment Slide	IKONOS/Geoeye/Worldview
GAAR0777	Active Layer Detachment Slide	IKONOS/Geoeye/Worldview
GAAR0778	Active Layer Detachment Slide	IKONOS/Geoeye/Worldview
GAAR0779	Active Layer Detachment Slide	IKONOS/Geoeye/Worldview
GAAR0780	Active Layer Detachment Slide	IKONOS/Geoeye/Worldview
GAAR0781	Active Layer Detachment Slide	IKONOS/Geoeye/Worldview
GAAR0782	Active Layer Detachment Slide	IKONOS/Geoeye/Worldview
GAAR0783	Active Layer Detachment Slide	IKONOS/Geoeye/Worldview
GAAR0784	Active Layer Detachment Slide	IKONOS/Geoeye/Worldview
GAAR0785	Active Layer Detachment Slide	IKONOS/Geoeye/Worldview
GAAR0786	Active Layer Detachment Slide	IKONOS/Geoeye/Worldview
GAAR0787	Active Layer Detachment Slide	IKONOS/Geoeye/Worldview
GAAR0788	Active Layer Detachment Slide	IKONOS/Geoeye/Worldview
GAAR0789	Active Layer Detachment Slide	IKONOS/Geoeye/Worldview
GAAR0790	Active Layer Detachment Slide	IKONOS/Geoeye/Worldview

NPS	2010	68.35423	-155.39567
NPS	2010	68.34708	-155.39065
NPS	2010	68.34438	-155.41960
NPS	2010	68.34107	-155.40520
NPS	2010	68.34094	-155.44194
NPS	2010	68.33962	-155.48607
NPS	2010	68.33496	-155.50124
NPS	2010	68.31229	-154.99093
NPS	2010	68.30029	-155.04220
NPS	2010	68.30108	-155.04517
NPS	2010	68.30985	-155.15724
NPS	2010	68.29933	-155.17578
NPS	2010	68.30386	-155.18263
NPS	2010	68.31259	-155.30898
NPS	2010	68.30791	-155.33251
NPS	2010	68.30787	-155.32636
NPS	2010	68.30798	-155.32953
NPS	2010	68.30895	-155.33001
NPS	2010	68.30661	-155.33588
NPS	2010	68.31211	-155.32937
NPS	2010	68.30087	-155.36334
NPS	2010	68.30135	-155.36926
NPS	2010	68.30055	-155.37138
NPS	2010	68.30078	-155.36741
NPS	2010	68.30065	-155.36686
NPS	2010	68.30254	-155.35853
NPS	2010	68.30321	-155.35736
NPS	2010	68.30386	-155.42107
NPS	2010	68.30378	-155.41841
NPS	2010	68.30319	-155.41314
NPS	2010	68.30326	-155.42089
NPS	2010	68.32642	-155.41866

GAAR0791	Active Layer Detachment Slide	IKONOS/Geoeye/Worldview
GAAR0792	Active Layer Detachment Slide	IKONOS/Geoeye/Worldview
GAAR0793	Active Layer Detachment Slide	IKONOS/Geoeye/Worldview
GAAR0794	Active Layer Detachment Slide	IKONOS/Geoeye/Worldview
GAAR0795	Active Layer Detachment Slide	IKONOS/Geoeye/Worldview
GAAR0796	Active Layer Detachment Slide	IKONOS/Geoeye/Worldview
GAAR0797	Active Layer Detachment Slide	IKONOS/Geoeye/Worldview
GAAR0798	Active Layer Detachment Slide	IKONOS/Geoeye/Worldview
GAAR0799	Active Layer Detachment Slide	IKONOS/Geoeye/Worldview
GAAR0800	Active Layer Detachment Slide	IKONOS/Geoeye/Worldview
GAAR0801	Active Layer Detachment Slide	IKONOS/Geoeye/Worldview
GAAR0802	Active Layer Detachment Slide	IKONOS/Geoeye/Worldview
GAAR0803	Active Layer Detachment Slide	IKONOS/Geoeye/Worldview
GAAR0804	Active Layer Detachment Slide	IKONOS/Geoeye/Worldview
GAAR0805	Active Layer Detachment Slide	IKONOS/Geoeye/Worldview
GAAR0806	Active Layer Detachment Slide	IKONOS/Geoeye/Worldview
GAAR0807	Active Layer Detachment Slide	IKONOS/Geoeye/Worldview
GAAR0808	Active Layer Detachment Slide	IKONOS/Geoeye/Worldview
GAAR0809	Active Layer Detachment Slide	IKONOS/Geoeye/Worldview
GAAR0810	Active Layer Detachment Slide	IKONOS/Geoeye/Worldview
GAAR0811	Active Layer Detachment Slide	IKONOS/Geoeye/Worldview
GAAR0812	Active Layer Detachment Slide	IKONOS/Geoeye/Worldview
GAAR0813	Active Layer Detachment Slide	IKONOS/Geoeye/Worldview
GAAR0814	Active Layer Detachment Slide	IKONOS/Geoeye/Worldview
GAAR0815	Active Layer Detachment Slide	IKONOS/Geoeye/Worldview
GAAR0816	Active Layer Detachment Slide	IKONOS/Geoeye/Worldview
GAAR0817	Active Layer Detachment Slide	IKONOS/Geoeye/Worldview
GAAR0818	Active Layer Detachment Slide	IKONOS/Geoeye/Worldview
GAAR0819	Active Layer Detachment Slide	IKONOS/Geoeye/Worldview
GAAR0820	Active Layer Detachment Slide	IKONOS/Geoeye/Worldview
GAAR0821	Active Layer Detachment Slide	IKONOS/Geoeye/Worldview
GAAR0822	Active Layer Detachment Slide	IKONOS/Geoeye/Worldview

NPS	2010	68.33207	-155.44861
NPS	2010	68.33157	-155.44871
NPS	2010	68.33054	-155.45881
NPS	2010	68.33055	-155.46189
NPS	2010	68.33102	-155.46123
NPS	2010	68.30627	-154.95687
NPS	2010	68.30437	-154.94904
NPS	2010	68.30613	-154.93599
NPS	2010	68.31507	-154.96477
NPS	2010	68.30933	-154.86279
NPS	2010	68.30888	-154.86113
NPS	2010	68.30723	-154.86144
NPS	2010	68.30502	-154.92011
NPS	2010	68.30507	-154.91763
NPS	2010	68.30509	-154.92162
NPS	2010	68.32139	-154.79537
NPS	2010	68.31814	-154.61334
NPS	2010	68.32376	-154.60694
NPS	2010	68.32308	-154.60829
NPS	2010	68.32553	-154.60644
NPS	2010	68.32475	-154.60972
NPS	2010	68.36169	-154.67683
NPS	2010	68.36669	-154.68528
NPS	2010	68.36944	-154.68849
NPS	2010	68.36928	-154.69000
NPS	2010	68.34067	-154.49500
NPS	2010	68.33171	-154.49715
NPS	2010	68.32440	-154.50712
NPS	2010	68.32341	-154.51702
NPS	2010	68.32515	-154.51415
NPS	2010	68.32503	-154.51949
NPS	2010	68.32179	-154.51739

GAAR0823	Active Layer Detachment Slide	IKONOS/Geoeye/Worldview
GAAR0824	Active Layer Detachment Slide	IKONOS/Geoeye/Worldview
GAAR0825	Active Layer Detachment Slide	IKONOS/Geoeye/Worldview
GAAR0826	Retrogressive Thaw Slump	IKONOS/Geoeye/Worldview
GAAR0830	Active Layer Detachment Slide	IKONOS/Geoeye/Worldview
GAAR0835	Active Layer Detachment Slide	IKONOS/Geoeye/Worldview
GAAR0836	Active Layer Detachment Slide	IKONOS/Geoeye/Worldview
GAAR0837	Active Layer Detachment Slide	IKONOS/Geoeye/Worldview
GAAR0838	Retrogressive Thaw Slump	IKONOS/Geoeye/Worldview
GAAR0839	Retrogressive Thaw Slump	IKONOS/Geoeye/Worldview
GAAR0840	Retrogressive Thaw Slump	IKONOS/Geoeye/Worldview
GAAR0841	Retrogressive Thaw Slump	IKONOS/Geoeye/Worldview
GAAR0842	Active Layer Detachment Slide	IKONOS/Geoeye/Worldview
GAAR0843	Active Layer Detachment Slide	IKONOS/Geoeye/Worldview
GAAR0844	Active Layer Detachment Slide	IKONOS/Geoeye/Worldview
GAAR0845	Active Layer Detachment Slide	IKONOS/Geoeye/Worldview
GAAR0846	Active Layer Detachment Slide	IKONOS/Geoeye/Worldview
GAAR0847	Retrogressive Thaw Slump	IKONOS/Geoeye/Worldview
GAAR0848	Retrogressive Thaw Slump	IKONOS/Geoeye/Worldview
GAAR0849	Retrogressive Thaw Slump	IKONOS/Geoeye/Worldview
GAAR0850	Active Layer Detachment Slide	IKONOS/Geoeye/Worldview
GAAR0851	Retrogressive Thaw Slump	IKONOS/Geoeye/Worldview
GAAR0852	Active Layer Detachment Slide	IKONOS/Geoeye/Worldview
GAAR0853	Active Layer Detachment Slide	IKONOS/Geoeye/Worldview
GAAR0854	Retrogressive Thaw Slump	IKONOS/Geoeye/Worldview
GAAR0855	Retrogressive Thaw Slump	IKONOS/Geoeye/Worldview
GAAR0856	Retrogressive Thaw Slump	IKONOS/Geoeye/Worldview
GAAR0858	Active Layer Detachment Slide	IKONOS/Geoeye/Worldview
GAAR0859	Active Layer Detachment Slide	IKONOS/Geoeye/Worldview
GAAR0860	Retrogressive Thaw Slump	IKONOS/Geoeye/Worldview
GAAR0861	Retrogressive Thaw Slump	IKONOS/Geoeye/Worldview
GAAR0862	Retrogressive Thaw Slump	IKONOS/Geoeye/Worldview

NPS	2010	68.32196	-154.52285
NPS	2010	68.32084	-154.34602
NPS	2010	68.32222	-154.34065
NPS	2010	68.31885	-154.34130
NPS	2010	68.43398	-153.44594
NPS	2010	67.77990	-155.70872
NPS	2010	67.77822	-155.70876
NPS	2010	67.78278	-155.70952
NPS	2010	67.77530	-155.66634
NPS	2010	67.80924	-155.55149
NPS	2010	67.73836	-155.47050
NPS	2010	67.73796	-155.46804
NPS	2010	67.73922	-155.46267
NPS	2010	67.73900	-155.46665
NPS	2010	67.74996	-155.70216
NPS	2010	67.75044	-155.70167
NPS	2010	67.75029	-155.69960
NPS	2010	67.74212	-155.55050
NPS	2010	67.74097	-155.55254
NPS	2010	67.74174	-155.55834
NPS	2010	67.73299	-155.59348
NPS	2010	67.73417	-155.59621
NPS	2010	67.72834	-155.59961
NPS	2010	67.73320	-155.58113
NPS	2010	67.73243	-155.57574
NPS	2010	67.73212	-155.57170
NPS	2010	67.73231	-155.57111
NPS	2010	67.74159	-155.72363
NPS	2010	67.74296	-155.72890
NPS	2010	67.98970	-153.50628
NPS	2010	67.98904	-153.50439
NPS	2010	67.98943	-153.49539

GAAR0863	Retrogressive Thaw Slump	IKONOS/Geoeye/Worldview
GAAR0864	Active Layer Detachment Slide	IKONOS/Geoeye/Worldview
GAAR0865	Active Layer Detachment Slide	IKONOS/Geoeye/Worldview
GAAR0866	Active Layer Detachment Slide	IKONOS/Geoeye/Worldview
GAAR0867	Retrogressive Thaw Slump	IKONOS/Geoeye/Worldview
GAAR0868	Retrogressive Thaw Slump	IKONOS/Geoeye/Worldview
GAAR0869	Active Layer Detachment Slide	IKONOS/Geoeye/Worldview
GAAR0870	Retrogressive Thaw Slump	IKONOS/Geoeye/Worldview
GAAR0871	Retrogressive Thaw Slump	IKONOS/Geoeye/Worldview
GAAR0872	Retrogressive Thaw Slump	IKONOS/Geoeye/Worldview
GAAR0873	Retrogressive Thaw Slump	IKONOS/Geoeye/Worldview
GAAR0874	Retrogressive Thaw Slump	IKONOS/Geoeye/Worldview
GAAR0875	Retrogressive Thaw Slump	IKONOS/Geoeye/Worldview
GAAR0876	Retrogressive Thaw Slump	IKONOS/Geoeye/Worldview
GAAR0877	Active Layer Detachment Slide	IKONOS/Geoeye/Worldview
GAAR0878	Retrogressive Thaw Slump	IKONOS/Geoeye/Worldview
GAAR0879	Retrogressive Thaw Slump	IKONOS/Geoeye/Worldview
GAAR0880	Retrogressive Thaw Slump	IKONOS/Geoeye/Worldview
GAAR0881	Retrogressive Thaw Slump	IKONOS/Geoeye/Worldview
GAAR0882	Active Layer Detachment Slide	IKONOS/Geoeye/Worldview
GAAR0883	Active Layer Detachment Slide	IKONOS/Geoeye/Worldview
GAAR0884	Retrogressive Thaw Slump	IKONOS/Geoeye/Worldview
GAAR0885	Retrogressive Thaw Slump	IKONOS/Geoeye/Worldview
GAAR0886	Retrogressive Thaw Slump	IKONOS/Geoeye/Worldview
GAAR0887	Retrogressive Thaw Slump	IKONOS/Geoeye/Worldview
GAAR0888	Active Layer Detachment Slide	IKONOS/Geoeye/Worldview
GAAR0889	Active Layer Detachment Slide	IKONOS/Geoeye/Worldview
GAAR0890	Retrogressive Thaw Slump	IKONOS/Geoeye/Worldview
GAAR0891	Active Layer Detachment Slide	IKONOS/Geoeye/Worldview
GAAR0892	Active Layer Detachment Slide	IKONOS/Geoeye/Worldview
GAAR0893	Active Layer Detachment Slide	IKONOS/Geoeye/Worldview
GAAR0894	Retrogressive Thaw Slump	IKONOS/Geoeye/Worldview

NPS	2010	68.00812	-153.43701
NPS	2010	68.00694	-153.44182
NPS	2010	67.97557	-153.40631
NPS	2010	67.94270	-153.37800
NPS	2010	67.93116	-153.58926
NPS	2010	67.93267	-153.59207
NPS	2010	68.00963	-153.13760
NPS	2010	67.99208	-153.14926
NPS	2010	67.98572	-153.14964
NPS	2010	67.98505	-153.14765
NPS	2010	67.98474	-153.14978
NPS	2010	67.98465	-153.15166
NPS	2010	67.98405	-153.14990
NPS	2010	67.98368	-153.15398
NPS	2010	68.00255	-153.11761
NPS	2010	67.99485	-153.11606
NPS	2010	67.95534	-153.03041
NPS	2010	67.95430	-153.03409
NPS	2010	67.97001	-153.04874
NPS	2010	67.96923	-153.05667
NPS	2010	67.96991	-153.06120
NPS	2010	67.96889	-153.05983
NPS	2010	67.98100	-153.14563
NPS	2010	67.98090	-153.15035
NPS	2010	67.97953	-153.15071
NPS	2010	67.98157	-153.15487
NPS	2010	67.98084	-153.15587
NPS	2010	67.97441	-153.16039
NPS	2010	67.97632	-153.16376
NPS	2010	67.97568	-153.16441
NPS	2010	67.97073	-153.16956
NPS	2010	67.94990	-153.22799

GAAR0895	Retrogressive Thaw Slump	IKONOS/Geoeye/Worldview
GAAR0896	Active Layer Detachment Slide	IKONOS/Geoeye/Worldview
GAAR0897	Active Layer Detachment Slide	IKONOS/Geoeye/Worldview
GAAR0898	Active Layer Detachment Slide	IKONOS/Geoeye/Worldview
GAAR0899	Active Layer Detachment Slide	IKONOS/Geoeye/Worldview
GAAR0900	Active Layer Detachment Slide	IKONOS/Geoeye/Worldview
GAAR0901	Active Layer Detachment Slide	IKONOS/Geoeye/Worldview
GAAR0902	Active Layer Detachment Slide	IKONOS/Geoeye/Worldview
GAAR0903	Active Layer Detachment Slide	IKONOS/Geoeye/Worldview
GAAR0904	Active Layer Detachment Slide	IKONOS/Geoeye/Worldview
GAAR0905	Active Layer Detachment Slide	IKONOS/Geoeye/Worldview
GAAR0906	Active Layer Detachment Slide	IKONOS/Geoeye/Worldview
GAAR0907	Retrogressive Thaw Slump	IKONOS/Geoeye/Worldview
GAAR0908	Active Layer Detachment Slide	IKONOS/Geoeye/Worldview
GAAR0909	Active Layer Detachment Slide	IKONOS/Geoeye/Worldview
GAAR0910	Active Layer Detachment Slide	IKONOS/Geoeye/Worldview
GAAR0911	Active Layer Detachment Slide	IKONOS/Geoeye/Worldview
GAAR0912	Active Layer Detachment Slide	IKONOS/Geoeye/Worldview
GAAR0913	Active Layer Detachment Slide	IKONOS/Geoeye/Worldview
GAAR0914	Active Layer Detachment Slide	IKONOS/Geoeye/Worldview
GAAR0915	Retrogressive Thaw Slump	IKONOS/Geoeye/Worldview
GAAR0916	Active Layer Detachment Slide	IKONOS/Geoeye/Worldview
GAAR0917	Active Layer Detachment Slide	IKONOS/Geoeye/Worldview
GAAR0918	Active Layer Detachment Slide	IKONOS/Geoeye/Worldview
GAAR0919	Retrogressive Thaw Slump	IKONOS/Geoeye/Worldview
GAAR0920	Retrogressive Thaw Slump	IKONOS/Geoeye/Worldview
GAAR0921	Retrogressive Thaw Slump	IKONOS/Geoeye/Worldview
GAAR0922	Retrogressive Thaw Slump	IKONOS/Geoeye/Worldview
GAAR0923	Retrogressive Thaw Slump	IKONOS/Geoeye/Worldview
GAAR0924	Retrogressive Thaw Slump	IKONOS/Geoeye/Worldview
GAAR0925	Retrogressive Thaw Slump	IKONOS/Geoeye/Worldview
GAAR0926	Retrogressive Thaw Slump	IKONOS/Geoeye/Worldview

NPS	2010	67.92917	-153.10955
NPS	2010	67.92756	-153.11547
NPS	2010	67.92785	-153.11583
NPS	2010	67.92797	-153.11614
NPS	2010	67.92821	-153.11640
NPS	2010	67.92423	-153.02537
NPS	2010	67.92509	-153.02663
NPS	2010	67.92197	-152.97653
NPS	2010	67.94691	-152.96531
NPS	2010	68.09738	-153.94306
NPS	2010	68.09863	-153.93713
NPS	2010	68.09862	-153.93224
NPS	2010	68.09905	-153.92816
NPS	2010	68.10380	-153.92744
NPS	2010	68.10327	-153.92751
NPS	2010	68.10397	-153.92050
NPS	2010	68.10422	-153.91785
NPS	2010	68.08838	-153.78699
NPS	2010	68.09844	-153.78659
NPS	2010	68.12119	-153.65523
NPS	2010	68.12248	-153.62998
NPS	2010	68.12172	-153.65265
NPS	2010	68.12244	-153.65151
NPS	2010	68.11418	-153.67950
NPS	2010	68.03865	-153.66824
NPS	2010	68.04068	-153.66774
NPS	2010	68.03985	-153.66890
NPS	2010	68.03951	-153.67156
NPS	2010	68.02674	-153.64092
NPS	2010	68.02735	-153.62066
NPS	2010	68.02644	-153.61942
NPS	2010	68.03128	-153.64408

GAAR0927	Active Layer Detachment Slide	IKONOS/Geoeye/Worldview
GAAR0928	Retrogressive Thaw Slump	IKONOS/Geoeye/Worldview
GAAR0929	Retrogressive Thaw Slump	IKONOS/Geoeye/Worldview
GAAR0930	Retrogressive Thaw Slump	IKONOS/Geoeye/Worldview
GAAR0931	Retrogressive Thaw Slump	IKONOS/Geoeye/Worldview
GAAR0932	Retrogressive Thaw Slump	IKONOS/Geoeye/Worldview
GAAR0933	Active Layer Detachment Slide	IKONOS/Geoeye/Worldview
GAAR0934	Retrogressive Thaw Slump	IKONOS/Geoeye/Worldview
GAAR0935	Retrogressive Thaw Slump	IKONOS/Geoeye/Worldview
GAAR0936	Retrogressive Thaw Slump	IKONOS/Geoeye/Worldview
GAAR0937	Retrogressive Thaw Slump	IKONOS/Geoeye/Worldview
GAAR0938	Retrogressive Thaw Slump	IKONOS/Geoeye/Worldview
GAAR0939	Retrogressive Thaw Slump	IKONOS/Geoeye/Worldview
GAAR0940	Retrogressive Thaw Slump	IKONOS/Geoeye/Worldview
GAAR0941	Retrogressive Thaw Slump	IKONOS/Geoeye/Worldview
GAAR0942	Retrogressive Thaw Slump	IKONOS/Geoeye/Worldview
GAAR0943	Retrogressive Thaw Slump	IKONOS/Geoeye/Worldview
GAAR0944	Retrogressive Thaw Slump	IKONOS/Geoeye/Worldview
GAAR0945	Retrogressive Thaw Slump	IKONOS/Geoeye/Worldview
GAAR0946	Retrogressive Thaw Slump	IKONOS/Geoeye/Worldview
GAAR0947	Retrogressive Thaw Slump	IKONOS/Geoeye/Worldview
GAAR0948	Retrogressive Thaw Slump	IKONOS/Geoeye/Worldview
GAAR0949	Retrogressive Thaw Slump	IKONOS/Geoeye/Worldview
GAAR0950	Retrogressive Thaw Slump	IKONOS/Geoeye/Worldview
GAAR0951	Retrogressive Thaw Slump	IKONOS/Geoeye/Worldview
GAAR0952	Retrogressive Thaw Slump	IKONOS/Geoeye/Worldview
GAAR0953	Retrogressive Thaw Slump	IKONOS/Geoeye/Worldview
GAAR0954	Retrogressive Thaw Slump	IKONOS/Geoeye/Worldview
GAAR0955	Retrogressive Thaw Slump	IKONOS/Geoeye/Worldview
GAAR0956	Retrogressive Thaw Slump	IKONOS/Geoeye/Worldview
GAAR0957	Retrogressive Thaw Slump	IKONOS/Geoeye/Worldview
GAAR0958	Retrogressive Thaw Slump	IKONOS/Geoeye/Worldview

NPS	2010	68.03295	-153.63866
NPS	2010	68.03260	-153.64292
NPS	2010	68.02995	-153.64072
NPS	2010	68.03027	-153.63615
NPS	2010	68.03784	-153.44396
NPS	2010	68.03689	-153.44271
NPS	2010	67.77651	-153.99163
NPS	2010	67.77424	-153.78874
NPS	2010	67.76797	-153.78520
NPS	2010	67.76783	-153.78830
NPS	2010	67.76846	-153.78550
NPS	2010	67.79232	-153.21769
NPS	2010	67.79199	-153.21673
NPS	2010	67.79186	-153.21408
NPS	2010	67.79230	-153.21115
NPS	2010	67.79017	-153.21726
NPS	2010	67.78945	-153.21964
NPS	2010	67.78942	-153.22058
NPS	2010	67.78898	-153.22179
NPS	2010	67.78868	-153.21970
NPS	2010	67.79297	-153.22132
NPS	2010	67.79402	-153.22839
NPS	2010	67.79574	-153.22822
NPS	2010	67.79579	-153.23031
NPS	2010	67.78983	-153.20844
NPS	2010	67.78901	-153.20991
NPS	2010	67.78874	-153.21162
NPS	2010	67.78801	-153.21309
NPS	2010	67.78795	-153.21044
NPS	2010	67.78788	-153.21964
NPS	2010	67.78719	-153.21563
NPS	2010	67.79016	-153.21021

GAAR0959	Retrogressive Thaw Slump	IKONOS/Geoeye/Worldview
GAAR0960	Retrogressive Thaw Slump	IKONOS/Geoeye/Worldview
GAAR0961	Retrogressive Thaw Slump	IKONOS/Geoeye/Worldview
GAAR0962	Active Layer Detachment Slide	IKONOS/Geoeye/Worldview
GAAR0963	Active Layer Detachment Slide	IKONOS/Geoeye/Worldview
GAAR0964	Retrogressive Thaw Slump	IKONOS/Geoeye/Worldview
GAAR0965	Retrogressive Thaw Slump	IKONOS/Geoeye/Worldview
GAAR0966	Retrogressive Thaw Slump	IKONOS/Geoeye/Worldview
GAAR0967	Retrogressive Thaw Slump	IKONOS/Geoeye/Worldview
GAAR0968	Retrogressive Thaw Slump	IKONOS/Geoeye/Worldview
GAAR0969	Retrogressive Thaw Slump	IKONOS/Geoeye/Worldview
GAAR0970	Retrogressive Thaw Slump	IKONOS/Geoeye/Worldview
GAAR0971	Retrogressive Thaw Slump	IKONOS/Geoeye/Worldview
GAAR0972	Retrogressive Thaw Slump	IKONOS/Geoeye/Worldview
GAAR0973	Retrogressive Thaw Slump	IKONOS/Geoeye/Worldview
GAAR0974	Active Layer Detachment Slide	IKONOS/Geoeye/Worldview
GAAR0975	Retrogressive Thaw Slump	IKONOS/Geoeye/Worldview
GAAR0976	Active Layer Detachment Slide	IKONOS/Geoeye/Worldview
GAAR0977	Retrogressive Thaw Slump	IKONOS/Geoeye/Worldview
GAAR0978	Retrogressive Thaw Slump	IKONOS/Geoeye/Worldview
GAAR0979	Retrogressive Thaw Slump	IKONOS/Geoeye/Worldview
GAAR0980	Active Layer Detachment Slide	IKONOS/Geoeye/Worldview
GAAR0981	Retrogressive Thaw Slump	IKONOS/Geoeye/Worldview
GAAR0982	Retrogressive Thaw Slump	IKONOS/Geoeye/Worldview
GAAR0983	Active Layer Detachment Slide	IKONOS/Geoeye/Worldview
GAAR0984	Active Layer Detachment Slide	IKONOS/Geoeye/Worldview
GAAR0985	Active Layer Detachment Slide	IKONOS/Geoeye/Worldview
GAAR0986	Active Layer Detachment Slide	IKONOS/Geoeye/Worldview
GAAR0987	Active Layer Detachment Slide	IKONOS/Geoeye/Worldview
GAAR0988	Active Layer Detachment Slide	IKONOS/Geoeye/Worldview
GAAR0989	Active Layer Detachment Slide	IKONOS/Geoeye/Worldview
GAAR0990	Active Layer Detachment Slide	IKONOS/Geoeye/Worldview

NPS	2010	67.78797	-153.20193
NPS	2010	67.78664	-153.20267
NPS	2010	67.78721	-153.20076
NPS	2010	67.78533	-153.20137
NPS	2010	67.78815	-153.19611
NPS	2010	67.78494	-153.20482
NPS	2010	67.78514	-153.20981
NPS	2010	67.78384	-153.20330
NPS	2010	67.78384	-153.20116
NPS	2010	67.78539	-153.19091
NPS	2010	67.78545	-153.19599
NPS	2010	67.79220	-153.20359
NPS	2010	67.79446	-153.21156
NPS	2010	67.79060	-153.20014
NPS	2010	67.78145	-153.19916
NPS	2010	67.77803	-153.20947
NPS	2010	67.80517	-153.19429
NPS	2010	67.79945	-153.15119
NPS	2010	67.78437	-153.00252
NPS	2010	67.77529	-152.99174
NPS	2010	67.77602	-152.99330
NPS	2010	67.71140	-153.27445
NPS	2010	67.74528	-153.19422
NPS	2010	67.70594	-153.27757
NPS	2010	67.62600	-153.91381
NPS	2010	67.62780	-153.91475
NPS	2010	67.62983	-153.91376
NPS	2010	67.62952	-153.90842
NPS	2010	67.62270	-153.89244
NPS	2010	67.67200	-153.54912
NPS	2010	67.67072	-153.55125
NPS	2010	67.67268	-153.54875

GAAR0991	Active Layer Detachment Slide	IKONOS/Geoeye/Worldview
GAAR0992	Active Layer Detachment Slide	IKONOS/Geoeye/Worldview
GAAR0993	Retrogressive Thaw Slump	IKONOS/Geoeye/Worldview
GAAR0994	Retrogressive Thaw Slump	IKONOS/Geoeye/Worldview
GAAR0995	Retrogressive Thaw Slump	IKONOS/Geoeye/Worldview
GAAR0996	Retrogressive Thaw Slump	IKONOS/Geoeye/Worldview
GAAR0997	Retrogressive Thaw Slump	IKONOS/Geoeye/Worldview
GAAR0998	Retrogressive Thaw Slump	IKONOS/Geoeye/Worldview
GAAR0999	Retrogressive Thaw Slump	IKONOS/Geoeye/Worldview
GAAR1000	Retrogressive Thaw Slump	IKONOS/Geoeye/Worldview
GAAR1001	Retrogressive Thaw Slump	IKONOS/Geoeye/Worldview
GAAR1002	Active Layer Detachment Slide	IKONOS/Geoeye/Worldview
GAAR1003	Retrogressive Thaw Slump	IKONOS/Geoeye/Worldview
GAAR1004	Active Layer Detachment Slide	IKONOS/Geoeye/Worldview
GAAR1005	Retrogressive Thaw Slump	IKONOS/Geoeye/Worldview
GAAR1006	Retrogressive Thaw Slump	IKONOS/Geoeye/Worldview
GAAR1007	Retrogressive Thaw Slump	IKONOS/Geoeye/Worldview
GAAR1008	Retrogressive Thaw Slump	IKONOS/Geoeye/Worldview
GAAR1009	Retrogressive Thaw Slump	IKONOS/Geoeye/Worldview
GAAR1010	Retrogressive Thaw Slump	IKONOS/Geoeye/Worldview
GAAR1011	Retrogressive Thaw Slump	IKONOS/Geoeye/Worldview
GAAR1012	Retrogressive Thaw Slump	IKONOS/Geoeye/Worldview
GAAR1013	Active Layer Detachment Slide	IKONOS/Geoeye/Worldview
GAAR1014	Active Layer Detachment Slide	IKONOS/Geoeye/Worldview
GAAR1015	Active Layer Detachment Slide	IKONOS/Geoeye/Worldview
GAAR1016	Active Layer Detachment Slide	IKONOS/Geoeye/Worldview
GAAR1017	Active Layer Detachment Slide	IKONOS/Geoeye/Worldview
GAAR1018	Active Layer Detachment Slide	IKONOS/Geoeye/Worldview
GAAR1019	Active Layer Detachment Slide	IKONOS/Geoeye/Worldview
GAAR1020	Active Layer Detachment Slide	IKONOS/Geoeye/Worldview
GAAR1021	Active Layer Detachment Slide	IKONOS/Geoeye/Worldview
GAAR1022	Active Layer Detachment Slide	IKONOS/Geoeye/Worldview

NPS	2010	67.61165	-153.55956
NPS	2010	67.60771	-153.56220
NPS	2010	67.91493	-153.59502
NPS	2010	67.82910	-153.68872
NPS	2010	67.82877	-153.68901
NPS	2010	67.82876	-153.68538
NPS	2010	67.82589	-153.68951
NPS	2010	67.82592	-153.68765
NPS	2010	67.82953	-153.71928
NPS	2010	67.81322	-153.70811
NPS	2010	67.81360	-153.70895
NPS	2010	67.81868	-153.70833
NPS	2010	67.81386	-153.71114
NPS	2010	67.81356	-153.70167
NPS	2010	67.81204	-153.19555
NPS	2010	67.81215	-153.19178
NPS	2010	67.81104	-153.18937
NPS	2010	67.80643	-153.19441
NPS	2010	67.80791	-153.18815
NPS	2010	67.81153	-153.18957
NPS	2010	67.80747	-153.18624
NPS	2010	67.80742	-153.18296
NPS	2010	67.48573	-154.80763
NPS	2010	67.48656	-154.80351
NPS	2010	67.47408	-154.80349
NPS	2010	67.47237	-154.80409
NPS	2010	67.48656	-154.04970
NPS	2010	68.27024	-155.59950
NPS	2010	68.27040	-155.59589
NPS	2010	68.26974	-155.59406
NPS	2010	68.26447	-155.37799
NPS	2010	68.26294	-155.36684

GAAR1023	Active Layer Detachment Slide	IKONOS/Geoeye/Worldview
GAAR1024	Active Layer Detachment Slide	IKONOS/Geoeye/Worldview
GAAR1025	Active Layer Detachment Slide	IKONOS/Geoeye/Worldview
GAAR1026	Active Layer Detachment Slide	IKONOS/Geoeye/Worldview
GAAR1027	Active Layer Detachment Slide	IKONOS/Geoeye/Worldview
GAAR1028	Active Layer Detachment Slide	IKONOS/Geoeye/Worldview
GAAR1029	Active Layer Detachment Slide	IKONOS/Geoeye/Worldview
GAAR1030	Active Layer Detachment Slide	IKONOS/Geoeye/Worldview
GAAR1031	Retrogressive Thaw Slump	IKONOS/Geoeye/Worldview
GAAR1032	Active Layer Detachment Slide	IKONOS/Geoeye/Worldview
GAAR1033	Active Layer Detachment Slide	IKONOS/Geoeye/Worldview
GAAR1034	Active Layer Detachment Slide	IKONOS/Geoeye/Worldview
GAAR1035	Active Layer Detachment Slide	IKONOS/Geoeye/Worldview
GAAR1036	Active Layer Detachment Slide	IKONOS/Geoeye/Worldview
GAAR1037	Retrogressive Thaw Slump	IKONOS/Geoeye/Worldview
GAAR1038	Retrogressive Thaw Slump	IKONOS/Geoeye/Worldview
GAAR1039	Retrogressive Thaw Slump	IKONOS/Geoeye/Worldview
GAAR1040	Retrogressive Thaw Slump	IKONOS/Geoeye/Worldview
GAAR1041	Retrogressive Thaw Slump	IKONOS/Geoeye/Worldview
GAAR1042	Active Layer Detachment Slide	IKONOS/Geoeye/Worldview
GAAR1043	Active Layer Detachment Slide	IKONOS/Geoeye/Worldview
GAAR1044	Active Layer Detachment Slide	IKONOS/Geoeye/Worldview
GAAR1045	Retrogressive Thaw Slump	IKONOS/Geoeye/Worldview
GAAR1046	Retrogressive Thaw Slump	IKONOS/Geoeye/Worldview
GAAR1047	Retrogressive Thaw Slump	IKONOS/Geoeye/Worldview
GAAR1048	Retrogressive Thaw Slump	IKONOS/Geoeye/Worldview
GAAR1049	Retrogressive Thaw Slump	IKONOS/Geoeye/Worldview
GAAR1050	Retrogressive Thaw Slump	IKONOS/Geoeye/Worldview
GAAR1051	Retrogressive Thaw Slump	IKONOS/Geoeye/Worldview
GAAR1052	Retrogressive Thaw Slump	IKONOS/Geoeye/Worldview
GAAR1053	Active Layer Detachment Slide	IKONOS/Geoeye/Worldview
GAAR1054	Active Layer Detachment Slide	IKONOS/Geoeye/Worldview

NPS	2010	68.26325	-155.37413
NPS	2010	68.24630	-155.39548
NPS	2010	68.24948	-155.39065
NPS	2010	68.23016	-155.34615
NPS	2010	68.23425	-155.35324
NPS	2010	68.22383	-155.41435
NPS	2010	68.22468	-155.40680
NPS	2010	68.28100	-155.19953
NPS	2010	68.28064	-155.13530
NPS	2010	68.29771	-155.03075
NPS	2010	68.26963	-154.89252
NPS	2010	67.72641	-155.72548
NPS	2010	67.72664	-155.71780
NPS	2010	67.72643	-155.70751
NPS	2010	67.72227	-155.69515
NPS	2010	67.72178	-155.69375
NPS	2010	67.72168	-155.69303
NPS	2010	67.72165	-155.69253
NPS	2010	67.72116	-155.68726
NPS	2010	67.72462	-155.69294
NPS	2010	67.72519	-155.69461
NPS	2010	67.72512	-155.68821
NPS	2010	67.72378	-155.55154
NPS	2010	67.72222	-155.54745
NPS	2010	67.72437	-155.56295
NPS	2010	67.72109	-155.54203
NPS	2010	67.72116	-155.53846
NPS	2010	67.71790	-155.55056
NPS	2010	67.71742	-155.54686
NPS	2010	67.71813	-155.54340
NPS	2010	67.71998	-155.53915
NPS	2010	67.70592	-155.52972

GAAR1055	Active Layer Detachment Slide	IKONOS/Geoeye/Worldview
GAAR1056	Active Layer Detachment Slide	IKONOS/Geoeye/Worldview
GAAR1057	Active Layer Detachment Slide	IKONOS/Geoeye/Worldview
GAAR1058	Active Layer Detachment Slide	IKONOS/Geoeye/Worldview
GAAR1059	Active Layer Detachment Slide	IKONOS/Geoeye/Worldview
GAAR1060	Active Layer Detachment Slide	IKONOS/Geoeye/Worldview
GAAR1061	Active Layer Detachment Slide	IKONOS/Geoeye/Worldview
GAAR1062	Active Layer Detachment Slide	IKONOS/Geoeye/Worldview
GAAR1063	Retrogressive Thaw Slump	IKONOS/Geoeye/Worldview
GAAR1064	Retrogressive Thaw Slump	IKONOS/Geoeye/Worldview
GAAR1065	Retrogressive Thaw Slump	IKONOS/Geoeye/Worldview
GAAR1066	Retrogressive Thaw Slump	IKONOS/Geoeye/Worldview
GAAR1067	Retrogressive Thaw Slump	IKONOS/Geoeye/Worldview
GAAR1068	Active Layer Detachment Slide	IKONOS/Geoeye/Worldview
GAAR1069	Active Layer Detachment Slide	IKONOS/Geoeye/Worldview
GAAR1070	Active Layer Detachment Slide	IKONOS/Geoeye/Worldview
GAAR1071	Active Layer Detachment Slide	IKONOS/Geoeye/Worldview
GAAR1072	Active Layer Detachment Slide	IKONOS/Geoeye/Worldview
GAAR1073	Active Layer Detachment Slide	IKONOS/Geoeye/Worldview
GAAR1074	Active Layer Detachment Slide	IKONOS/Geoeye/Worldview
GAAR1075	Active Layer Detachment Slide	IKONOS/Geoeye/Worldview
GAAR1076	Active Layer Detachment Slide	IKONOS/Geoeye/Worldview
GAAR1077	Retrogressive Thaw Slump	IKONOS/Geoeye/Worldview
GAAR1078	Active Layer Detachment Slide	IKONOS/Geoeye/Worldview
GAAR1079	Active Layer Detachment Slide	IKONOS/Geoeye/Worldview
GAAR1080	Active Layer Detachment Slide	IKONOS/Geoeye/Worldview
GAAR1081	Active Layer Detachment Slide	IKONOS/Geoeye/Worldview
GAAR1082	Active Layer Detachment Slide	IKONOS/Geoeye/Worldview
GAAR1083	Active Layer Detachment Slide	IKONOS/Geoeye/Worldview
GAAR1084	Active Layer Detachment Slide	IKONOS/Geoeye/Worldview
GAAR1085	Active Layer Detachment Slide	IKONOS/Geoeye/Worldview
GAAR1086	Active Layer Detachment Slide	IKONOS/Geoeye/Worldview

NPS	2010	67.70570	-155.52565
NPS	2010	67.69871	-155.52024
NPS	2010	67.69988	-155.51750
NPS	2010	67.70587	-155.50948
NPS	2010	67.70375	-155.50384
NPS	2010	67.71470	-155.47851
NPS	2010	67.71499	-155.47581
NPS	2010	67.71377	-155.47805
NPS	2010	67.72139	-155.46440
NPS	2010	67.72030	-155.46214
NPS	2010	67.71514	-155.45737
NPS	2010	67.72183	-155.45543
NPS	2010	67.72285	-155.45295
NPS	2010	67.71909	-155.43436
NPS	2010	67.71850	-155.42673
NPS	2010	67.71992	-155.42714
NPS	2010	67.72104	-155.42533
NPS	2010	67.71974	-155.43494
NPS	2010	67.71222	-155.43793
NPS	2010	67.70853	-155.45209
NPS	2010	67.70903	-155.44406
NPS	2010	67.70909	-155.44598
NPS	2010	67.71109	-155.45348
NPS	2010	67.72736	-155.42663
NPS	2010	67.72598	-155.43429
NPS	2010	67.72045	-155.40931
NPS	2010	67.72012	-155.40565
NPS	2010	67.72235	-155.37648
NPS	2010	67.72308	-155.40487
NPS	2010	67.69314	-155.42912
NPS	2010	67.69014	-155.43511
NPS	2010	67.68848	-155.43212

GAAR1087	Active Layer Detachment Slide	IKONOS/Geoeye/Worldview
GAAR1088	Active Layer Detachment Slide	IKONOS/Geoeye/Worldview
GAAR1089	Active Layer Detachment Slide	IKONOS/Geoeye/Worldview
GAAR1090	Active Layer Detachment Slide	IKONOS/Geoeye/Worldview
GAAR1091	Active Layer Detachment Slide	IKONOS/Geoeye/Worldview
GAAR1092	Retrogressive Thaw Slump	IKONOS/Geoeye/Worldview
GAAR1093	Retrogressive Thaw Slump	IKONOS/Geoeye/Worldview
GAAR1094	Active Layer Detachment Slide	IKONOS/Geoeye/Worldview
GAAR1095	Active Layer Detachment Slide	IKONOS/Geoeye/Worldview
GAAR1096	Active Layer Detachment Slide	IKONOS/Geoeye/Worldview
GAAR1097	Active Layer Detachment Slide	IKONOS/Geoeye/Worldview
GAAR1098	Active Layer Detachment Slide	IKONOS/Geoeye/Worldview
GAAR1099	Active Layer Detachment Slide	IKONOS/Geoeye/Worldview
GAAR1100	Active Layer Detachment Slide	IKONOS/Geoeye/Worldview
GAAR1101	Active Layer Detachment Slide	IKONOS/Geoeye/Worldview
GAAR1102	Active Layer Detachment Slide	IKONOS/Geoeye/Worldview
GAAR1103	Active Layer Detachment Slide	IKONOS/Geoeye/Worldview
GAAR1104	Active Layer Detachment Slide	IKONOS/Geoeye/Worldview
GAAR1105	Active Layer Detachment Slide	IKONOS/Geoeye/Worldview
GAAR1106	Active Layer Detachment Slide	IKONOS/Geoeye/Worldview
GAAR1107	Active Layer Detachment Slide	IKONOS/Geoeye/Worldview
GAAR1108	Active Layer Detachment Slide	IKONOS/Geoeye/Worldview
GAAR1109	Active Layer Detachment Slide	IKONOS/Geoeye/Worldview
GAAR1110	Active Layer Detachment Slide	IKONOS/Geoeye/Worldview
GAAR1111	Active Layer Detachment Slide	IKONOS/Geoeye/Worldview
GAAR1112	Active Layer Detachment Slide	IKONOS/Geoeye/Worldview
GAAR1113	Active Layer Detachment Slide	IKONOS/Geoeye/Worldview
GAAR1114	Active Layer Detachment Slide	IKONOS/Geoeye/Worldview
GAAR1115	Active Layer Detachment Slide	IKONOS/Geoeye/Worldview
GAAR1116	Retrogressive Thaw Slump	IKONOS/Geoeye/Worldview
GAAR1117	Retrogressive Thaw Slump	IKONOS/Geoeye/Worldview
GAAR1118	Active Layer Detachment Slide	IKONOS/Geoeye/Worldview

NPS	2010	67.68749	-155.43385
NPS	2010	67.68811	-155.43338
NPS	2010	67.68771	-155.43266
NPS	2010	67.64997	-155.62031
NPS	2010	67.64734	-155.61758
NPS	2010	67.64526	-155.61472
NPS	2010	67.64454	-155.61347
NPS	2010	67.64374	-155.53492
NPS	2010	67.64117	-155.55538
NPS	2010	67.63379	-155.52000
NPS	2010	67.63510	-155.51996
NPS	2010	67.63568	-155.51900
NPS	2010	67.63847	-155.51905
NPS	2010	67.63759	-155.45013
NPS	2010	67.63572	-155.45762
NPS	2010	67.63411	-155.46076
NPS	2010	67.63354	-155.47171
NPS	2010	67.72001	-155.30240
NPS	2010	67.71986	-155.30116
NPS	2010	67.72089	-155.29083
NPS	2010	67.72171	-155.29066
NPS	2010	67.72209	-155.28893
NPS	2010	67.72092	-155.29340
NPS	2010	67.71347	-155.21202
NPS	2010	67.71631	-155.22499
NPS	2010	67.71663	-155.22528
NPS	2010	67.71746	-155.22619
NPS	2010	67.71772	-155.22580
NPS	2010	67.71746	-155.22861
NPS	2010	67.70112	-155.11714
NPS	2010	67.70310	-155.11654
NPS	2010	67.70687	-155.12387

GAAR1119	Active Layer Detachment Slide	IKONOS/Geoeye/Worldview
GAAR1120	Active Layer Detachment Slide	IKONOS/Geoeye/Worldview
GAAR1121	Active Layer Detachment Slide	IKONOS/Geoeye/Worldview
GAAR1122	Active Layer Detachment Slide	IKONOS/Geoeye/Worldview
GAAR1123	Active Layer Detachment Slide	IKONOS/Geoeye/Worldview
GAAR1124	Active Layer Detachment Slide	IKONOS/Geoeye/Worldview
GAAR1125	Active Layer Detachment Slide	IKONOS/Geoeye/Worldview
GAAR1126	Active Layer Detachment Slide	IKONOS/Geoeye/Worldview
GAAR1127	Active Layer Detachment Slide	IKONOS/Geoeye/Worldview
GAAR1128	Active Layer Detachment Slide	IKONOS/Geoeye/Worldview
GAAR1129	Active Layer Detachment Slide	IKONOS/Geoeye/Worldview
GAAR1130	Retrogressive Thaw Slump	IKONOS/Geoeye/Worldview
GAAR1131	Retrogressive Thaw Slump	IKONOS/Geoeye/Worldview
GAAR1132	Retrogressive Thaw Slump	IKONOS/Geoeye/Worldview
GAAR1133	Active Layer Detachment Slide	IKONOS/Geoeye/Worldview
GAAR1134	Active Layer Detachment Slide	IKONOS/Geoeye/Worldview
GAAR1135	Active Layer Detachment Slide	IKONOS/Geoeye/Worldview
GAAR1136	Active Layer Detachment Slide	IKONOS/Geoeye/Worldview
GAAR1137	Active Layer Detachment Slide	IKONOS/Geoeye/Worldview
GAAR1138	Active Layer Detachment Slide	IKONOS/Geoeye/Worldview
GAAR1139	Active Layer Detachment Slide	IKONOS/Geoeye/Worldview
GAAR1140	Active Layer Detachment Slide	IKONOS/Geoeye/Worldview
GAAR1141	Active Layer Detachment Slide	IKONOS/Geoeye/Worldview
GAAR1142	Active Layer Detachment Slide	IKONOS/Geoeye/Worldview
GAAR1143	Active Layer Detachment Slide	IKONOS/Geoeye/Worldview
GAAR1144	Active Layer Detachment Slide	IKONOS/Geoeye/Worldview
GAAR1145	Active Layer Detachment Slide	IKONOS/Geoeye/Worldview
GAAR1146	Active Layer Detachment Slide	IKONOS/Geoeye/Worldview
GAAR1147	Active Layer Detachment Slide	IKONOS/Geoeye/Worldview
GAAR1148	Active Layer Detachment Slide	IKONOS/Geoeye/Worldview
GAAR1149	Active Layer Detachment Slide	IKONOS/Geoeye/Worldview
GAAR1150	Active Layer Detachment Slide	IKONOS/Geoeye/Worldview

NPS	2010	67.70728	-155.12251
NPS	2010	67.70625	-155.12499
NPS	2010	67.70586	-155.12293
NPS	2010	67.70542	-155.12441
NPS	2010	67.71794	-155.01242
NPS	2010	67.72283	-154.99835
NPS	2010	67.71040	-154.96901
NPS	2010	67.70977	-154.96662
NPS	2010	67.70839	-154.97265
NPS	2010	67.70345	-154.97492
NPS	2010	67.70698	-154.97867
NPS	2010	67.70795	-154.95798
NPS	2010	67.70673	-154.95921
NPS	2010	67.70614	-154.95867
NPS	2010	67.70800	-154.96085
NPS	2010	67.71656	-154.88417
NPS	2010	67.71615	-154.88555
NPS	2010	67.71613	-154.89036
NPS	2010	67.66547	-155.18682
NPS	2010	67.66409	-155.19380
NPS	2010	67.68403	-155.19600
NPS	2010	67.69084	-155.19224
NPS	2010	67.66258	-155.18296
NPS	2010	67.72575	-154.82310
NPS	2010	67.72303	-154.82137
NPS	2010	67.72310	-154.81709
NPS	2010	67.72295	-154.81581
NPS	2010	67.72401	-154.82313
NPS	2010	67.71934	-154.77464
NPS	2010	67.72066	-154.77661
NPS	2010	67.72122	-154.77688
NPS	2010	67.71844	-154.78120

GAAR1151	Active Layer Detachment Slide	IKONOS/Geoeye/Worldview
GAAR1152	Active Layer Detachment Slide	IKONOS/Geoeye/Worldview
GAAR1153	Active Layer Detachment Slide	IKONOS/Geoeye/Worldview
GAAR1154	Active Layer Detachment Slide	IKONOS/Geoeye/Worldview
GAAR1155	Active Layer Detachment Slide	IKONOS/Geoeye/Worldview
GAAR1156	Active Layer Detachment Slide	IKONOS/Geoeye/Worldview
GAAR1157	Retrogressive Thaw Slump	IKONOS/Geoeye/Worldview
GAAR1158	Active Layer Detachment Slide	IKONOS/Geoeye/Worldview
GAAR1159	Active Layer Detachment Slide	IKONOS/Geoeye/Worldview
GAAR1160	Active Layer Detachment Slide	IKONOS/Geoeye/Worldview
GAAR1161	Active Layer Detachment Slide	IKONOS/Geoeye/Worldview
GAAR1162	Active Layer Detachment Slide	IKONOS/Geoeye/Worldview
GAAR1163	Active Layer Detachment Slide	IKONOS/Geoeye/Worldview
GAAR1164	Active Layer Detachment Slide	IKONOS/Geoeye/Worldview
GAAR1165	Retrogressive Thaw Slump	IKONOS/Geoeye/Worldview
GAAR1166	Active Layer Detachment Slide	IKONOS/Geoeye/Worldview
GAAR1167	Active Layer Detachment Slide	IKONOS/Geoeye/Worldview
GAAR1168	Active Layer Detachment Slide	IKONOS/Geoeye/Worldview
GAAR1169	Active Layer Detachment Slide	IKONOS/Geoeye/Worldview
GAAR1170	Active Layer Detachment Slide	IKONOS/Geoeye/Worldview
GAAR1171	Active Layer Detachment Slide	IKONOS/Geoeye/Worldview
GAAR1172	Active Layer Detachment Slide	IKONOS/Geoeye/Worldview
GAAR1173	Active Layer Detachment Slide	IKONOS/Geoeye/Worldview
GAAR1174	Active Layer Detachment Slide	IKONOS/Geoeye/Worldview
GAAR1175	Active Layer Detachment Slide	IKONOS/Geoeye/Worldview
GAAR1176	Active Layer Detachment Slide	IKONOS/Geoeye/Worldview
GAAR1177	Active Layer Detachment Slide	IKONOS/Geoeye/Worldview
GAAR1178	Active Layer Detachment Slide	IKONOS/Geoeye/Worldview
GAAR1179	Active Layer Detachment Slide	IKONOS/Geoeye/Worldview
GAAR1180	Active Layer Detachment Slide	IKONOS/Geoeye/Worldview
GAAR1181	Retrogressive Thaw Slump	IKONOS/Geoeye/Worldview
GAAR1182	Active Layer Detachment Slide	IKONOS/Geoeye/Worldview

NPS	2010	67.71791	-154.77402
NPS	2010	67.72271	-154.74737
NPS	2010	67.72202	-154.75395
NPS	2010	67.72097	-154.75132
NPS	2010	67.72602	-154.74937
NPS	2010	67.72658	-154.74629
NPS	2010	67.72132	-154.76195
NPS	2010	67.71276	-154.56135
NPS	2010	67.71418	-154.55673
NPS	2010	67.71643	-154.57635
NPS	2010	67.71791	-154.57277
NPS	2010	67.70757	-154.59559
NPS	2010	67.70502	-154.59054
NPS	2010	67.70225	-154.58335
NPS	2010	67.70169	-154.57613
NPS	2010	67.70797	-154.45938
NPS	2010	67.71181	-154.45093
NPS	2010	67.71252	-154.44568
NPS	2010	67.71328	-154.45096
NPS	2010	67.71398	-154.45086
NPS	2010	67.68087	-154.43685
NPS	2010	67.67656	-154.44526
NPS	2010	67.66254	-154.61320
NPS	2010	67.66293	-154.61341
NPS	2010	67.66185	-154.61714
NPS	2010	67.66313	-154.60861
NPS	2010	67.66274	-154.60634
NPS	2010	67.64840	-154.69772
NPS	2010	67.71698	-154.59722
NPS	2010	67.70293	-154.24716
NPS	2010	67.70581	-154.21492
NPS	2010	67.72056	-154.20657

GAAR1183	Active Layer Detachment Slide	IKONOS/Geoeye/Worldview
GAAR1184	Active Layer Detachment Slide	IKONOS/Geoeye/Worldview
GAAR1185	Active Layer Detachment Slide	IKONOS/Geoeye/Worldview
GAAR1186	Active Layer Detachment Slide	IKONOS/Geoeye/Worldview
GAAR1187	Active Layer Detachment Slide	IKONOS/Geoeye/Worldview
GAAR1188	Active Layer Detachment Slide	IKONOS/Geoeye/Worldview
GAAR1189	Active Layer Detachment Slide	IKONOS/Geoeye/Worldview
GAAR1190	Active Layer Detachment Slide	IKONOS/Geoeye/Worldview
GAAR1191	Active Layer Detachment Slide	IKONOS/Geoeye/Worldview
GAAR1192	Active Layer Detachment Slide	IKONOS/Geoeye/Worldview
GAAR1193	Active Layer Detachment Slide	IKONOS/Geoeye/Worldview
GAAR1194	Retrogressive Thaw Slump	IKONOS/Geoeye/Worldview
GAAR1195	Active Layer Detachment Slide	IKONOS/Geoeye/Worldview
GAAR1196	Active Layer Detachment Slide	IKONOS/Geoeye/Worldview
GAAR1197	Retrogressive Thaw Slump	IKONOS/Geoeye/Worldview
GAAR1198	Active Layer Detachment Slide	IKONOS/Geoeye/Worldview
GAAR1199	Active Layer Detachment Slide	IKONOS/Geoeye/Worldview
GAAR1200	Active Layer Detachment Slide	IKONOS/Geoeye/Worldview
GAAR1201	Active Layer Detachment Slide	IKONOS/Geoeye/Worldview
GAAR1202	Active Layer Detachment Slide	IKONOS/Geoeye/Worldview
GAAR1203	Active Layer Detachment Slide	IKONOS/Geoeye/Worldview
GAAR1204	Active Layer Detachment Slide	IKONOS/Geoeye/Worldview
GAAR1205	Active Layer Detachment Slide	IKONOS/Geoeye/Worldview
GAAR1206	Active Layer Detachment Slide	IKONOS/Geoeye/Worldview
GAAR1207	Active Layer Detachment Slide	IKONOS/Geoeye/Worldview
GAAR1208	Retrogressive Thaw Slump	IKONOS/Geoeye/Worldview
GAAR1209	Retrogressive Thaw Slump	IKONOS/Geoeye/Worldview
GAAR1210	Retrogressive Thaw Slump	IKONOS/Geoeye/Worldview
GAAR1211	Retrogressive Thaw Slump	IKONOS/Geoeye/Worldview
GAAR1212	Retrogressive Thaw Slump	IKONOS/Geoeye/Worldview
GAAR1213	Retrogressive Thaw Slump	IKONOS/Geoeye/Worldview
GAAR1214	Retrogressive Thaw Slump	IKONOS/Geoeye/Worldview

NPS	2010	67.71923	-154.20817
NPS	2010	67.69977	-154.21221
NPS	2010	67.70162	-154.21525
NPS	2010	67.69959	-154.21359
NPS	2010	67.69870	-154.21513
NPS	2010	67.69549	-154.21470
NPS	2010	67.69490	-154.21335
NPS	2010	67.69325	-154.21501
NPS	2010	67.70085	-154.18028
NPS	2010	67.70121	-154.17893
NPS	2010	67.70028	-154.18338
NPS	2010	67.69924	-154.10782
NPS	2010	67.69965	-154.11240
NPS	2010	67.69980	-154.11012
NPS	2010	67.69228	-154.10312
NPS	2010	67.69178	-154.10329
NPS	2010	67.71637	-154.03845
NPS	2010	67.72026	-154.00055
NPS	2010	67.67746	-154.11494
NPS	2010	67.67797	-154.11884
NPS	2010	67.68613	-154.12196
NPS	2010	67.68543	-154.11973
NPS	2010	67.68749	-154.12540
NPS	2010	67.68927	-154.12290
NPS	2010	67.69003	-154.12430
NPS	2010	67.68188	-154.20154
NPS	2010	67.68216	-154.20095
NPS	2010	67.68233	-154.20118
NPS	2010	67.68259	-154.20080
NPS	2010	67.68298	-154.20009
NPS	2010	67.68342	-154.19964
NPS	2010	67.68439	-154.19880

GAAR1215	Retrogressive Thaw Slump	IKONOS/Geoeye/Worldview
GAAR1216	Active Layer Detachment Slide	IKONOS/Geoeye/Worldview
GAAR1217	Active Layer Detachment Slide	IKONOS/Geoeye/Worldview
GAAR1218	Active Layer Detachment Slide	IKONOS/Geoeye/Worldview
GAAR1219	Active Layer Detachment Slide	IKONOS/Geoeye/Worldview
GAAR1220	Active Layer Detachment Slide	IKONOS/Geoeye/Worldview
GAAR1221	Active Layer Detachment Slide	IKONOS/Geoeye/Worldview
GAAR1222	Active Layer Detachment Slide	IKONOS/Geoeye/Worldview
GAAR1223	Retrogressive Thaw Slump	IKONOS/Geoeye/Worldview
GAAR1224	Retrogressive Thaw Slump	IKONOS/Geoeye/Worldview
GAAR1225	Retrogressive Thaw Slump	IKONOS/Geoeye/Worldview
GAAR1226	Active Layer Detachment Slide	IKONOS/Geoeye/Worldview
GAAR1227	Active Layer Detachment Slide	IKONOS/Geoeye/Worldview
GAAR1228	Active Layer Detachment Slide	IKONOS/Geoeye/Worldview
GAAR1229	Active Layer Detachment Slide	IKONOS/Geoeye/Worldview
GAAR1230	Retrogressive Thaw Slump	IKONOS/Geoeye/Worldview
GAAR1231	Active Layer Detachment Slide	IKONOS/Geoeye/Worldview
GAAR1232	Retrogressive Thaw Slump	IKONOS/Geoeye/Worldview
GAAR1233	Retrogressive Thaw Slump	IKONOS/Geoeye/Worldview
GAAR1234	Retrogressive Thaw Slump	IKONOS/Geoeye/Worldview
GAAR1235	Active Layer Detachment Slide	IKONOS/Geoeye/Worldview
GAAR1236	Active Layer Detachment Slide	IKONOS/Geoeye/Worldview
GAAR1237	Retrogressive Thaw Slump	IKONOS/Geoeye/Worldview
GAAR1238	Retrogressive Thaw Slump	IKONOS/Geoeye/Worldview
GAAR1239	Retrogressive Thaw Slump	IKONOS/Geoeye/Worldview
GAAR1240	Active Layer Detachment Slide	IKONOS/Geoeye/Worldview
GAAR1241	Active Layer Detachment Slide	IKONOS/Geoeye/Worldview
GAAR1242	Retrogressive Thaw Slump	IKONOS/Geoeye/Worldview
GAAR1243	Active Layer Detachment Slide	IKONOS/Geoeye/Worldview
GAAR1244	Active Layer Detachment Slide	IKONOS/Geoeye/Worldview
GAAR1245	Active Layer Detachment Slide	IKONOS/Geoeye/Worldview
GAAR1246	Active Layer Detachment Slide	IKONOS/Geoeye/Worldview

NPS	2010	67.68384	-154.19681
NPS	2010	67.67817	-154.19429
NPS	2010	67.67723	-154.18753
NPS	2010	67.67739	-154.18723
NPS	2010	67.67884	-154.18815
NPS	2010	67.67989	-154.18459
NPS	2010	67.68026	-154.18885
NPS	2010	67.68142	-154.18506
NPS	2010	67.66784	-154.23636
NPS	2010	67.66828	-154.24590
NPS	2010	67.66847	-154.24555
NPS	2010	67.67413	-154.22730
NPS	2010	67.67460	-154.22789
NPS	2010	67.67209	-154.23374
NPS	2010	67.67210	-154.23298
NPS	2010	67.67197	-154.23205
NPS	2010	67.67305	-154.30201
NPS	2010	67.66785	-154.30220
NPS	2010	67.67053	-154.29225
NPS	2010	67.66879	-154.30870
NPS	2010	67.66466	-154.28947
NPS	2010	67.66500	-154.29496
NPS	2010	67.66030	-154.32127
NPS	2010	67.66508	-154.32423
NPS	2010	67.66020	-154.32754
NPS	2010	67.67235	-154.41242
NPS	2010	67.68806	-154.38043
NPS	2010	67.64124	-154.22933
NPS	2010	67.62656	-155.52680
NPS	2010	67.62694	-155.52230
NPS	2010	67.62694	-155.51946
NPS	2010	67.62865	-155.52465

GAAR1247	Active Layer Detachment Slide	IKONOS/Geoeye/Worldview
GAAR1249	Active Layer Detachment Slide	IKONOS/Geoeye/Worldview
GAAR1250	Active Layer Detachment Slide	IKONOS/Geoeye/Worldview
GAAR1251	Active Layer Detachment Slide	IKONOS/Geoeye/Worldview
GAAR1252	Active Layer Detachment Slide	IKONOS/Geoeye/Worldview
GAAR1253	Active Layer Detachment Slide	IKONOS/Geoeye/Worldview
GAAR1254	Active Layer Detachment Slide	IKONOS/Geoeye/Worldview
GAAR1255	Active Layer Detachment Slide	IKONOS/Geoeye/Worldview
GAAR1256	Active Layer Detachment Slide	IKONOS/Geoeye/Worldview
GAAR1257	Active Layer Detachment Slide	IKONOS/Geoeye/Worldview
GAAR1258	Active Layer Detachment Slide	IKONOS/Geoeye/Worldview
GAAR1259	Active Layer Detachment Slide	IKONOS/Geoeye/Worldview
GAAR1260	Active Layer Detachment Slide	IKONOS/Geoeye/Worldview
GAAR1261	Active Layer Detachment Slide	IKONOS/Geoeye/Worldview
GAAR1262	Active Layer Detachment Slide	IKONOS/Geoeye/Worldview
GAAR1263	Active Layer Detachment Slide	IKONOS/Geoeye/Worldview
GAAR1264	Retrogressive Thaw Slump	IKONOS/Geoeye/Worldview
GAAR1265	Active Layer Detachment Slide	IKONOS/Geoeye/Worldview
GAAR1266	Active Layer Detachment Slide	IKONOS/Geoeye/Worldview
GAAR1267	Retrogressive Thaw Slump	IKONOS/Geoeye/Worldview
GAAR1268	Retrogressive Thaw Slump	IKONOS/Geoeye/Worldview
GAAR1269	Retrogressive Thaw Slump	IKONOS/Geoeye/Worldview
GAAR1270	Retrogressive Thaw Slump	IKONOS/Geoeye/Worldview
GAAR1271	Retrogressive Thaw Slump	IKONOS/Geoeye/Worldview
GAAR1272	Retrogressive Thaw Slump	IKONOS/Geoeye/Worldview
GAAR1273	Active Layer Detachment Slide	IKONOS/Geoeye/Worldview
GAAR1274	Active Layer Detachment Slide	IKONOS/Geoeye/Worldview
GAAR1275	Active Layer Detachment Slide	IKONOS/Geoeye/Worldview
GAAR1276	Active Layer Detachment Slide	IKONOS/Geoeye/Worldview
GAAR1277	Retrogressive Thaw Slump	IKONOS/Geoeye/Worldview
GAAR1278	Retrogressive Thaw Slump	IKONOS/Geoeye/Worldview
GAAR1279	Retrogressive Thaw Slump	IKONOS/Geoeye/Worldview

NPS	2010	67.62869	-155.51700
NPS	2010	67.62468	-155.52224
NPS	2010	67.62481	-155.52196
NPS	2010	67.62606	-155.52163
NPS	2010	67.62526	-155.52102
NPS	2010	67.62546	-155.52271
NPS	2010	67.62518	-155.52172
NPS	2010	67.62743	-155.52008
NPS	2010	67.62766	-155.52011
NPS	2010	67.62855	-155.52104
NPS	2010	67.62958	-155.52043
NPS	2010	67.62945	-155.51618
NPS	2010	67.62964	-155.51482
NPS	2010	67.62947	-155.51512
NPS	2010	67.61449	-155.54253
NPS	2010	67.61639	-155.53981
NPS	2010	67.61532	-155.52988
NPS	2010	67.59332	-155.40937
NPS	2010	67.59390	-155.40875
NPS	2010	67.61872	-155.38775
NPS	2010	67.62220	-155.38055
NPS	2010	67.62418	-155.37394
NPS	2010	67.61833	-155.37764
NPS	2010	67.61817	-155.37155
NPS	2010	67.61883	-155.36364
NPS	2010	67.62165	-155.36231
NPS	2010	67.62181	-155.36840
NPS	2010	67.62089	-155.37173
NPS	2010	67.61946	-155.37470
NPS	2010	67.61298	-155.21022
NPS	2010	67.59219	-155.25681
NPS	2010	67.59178	-155.25515

GAAR1280	Retrogressive Thaw Slump	IKONOS/Geoeye/Worldview
GAAR1281	Active Layer Detachment Slide	IKONOS/Geoeye/Worldview
GAAR1282	Active Layer Detachment Slide	IKONOS/Geoeye/Worldview
GAAR1283	Active Layer Detachment Slide	IKONOS/Geoeye/Worldview
GAAR1284	Active Layer Detachment Slide	IKONOS/Geoeye/Worldview
GAAR1285	Active Layer Detachment Slide	IKONOS/Geoeye/Worldview
GAAR1286	Active Layer Detachment Slide	IKONOS/Geoeye/Worldview
GAAR1287	Active Layer Detachment Slide	IKONOS/Geoeye/Worldview
GAAR1288	Active Layer Detachment Slide	IKONOS/Geoeye/Worldview
GAAR1289	Active Layer Detachment Slide	IKONOS/Geoeye/Worldview
GAAR1290	Active Layer Detachment Slide	IKONOS/Geoeye/Worldview
GAAR1291	Retrogressive Thaw Slump	IKONOS/Geoeye/Worldview
GAAR1292	Active Layer Detachment Slide	IKONOS/Geoeye/Worldview
GAAR1293	Active Layer Detachment Slide	IKONOS/Geoeye/Worldview
GAAR1294	Active Layer Detachment Slide	IKONOS/Geoeye/Worldview
GAAR1295	Active Layer Detachment Slide	IKONOS/Geoeye/Worldview
GAAR1296	Active Layer Detachment Slide	IKONOS/Geoeye/Worldview
GAAR1297	Active Layer Detachment Slide	IKONOS/Geoeye/Worldview
GAAR1298	Active Layer Detachment Slide	IKONOS/Geoeye/Worldview
GAAR1299	Active Layer Detachment Slide	IKONOS/Geoeye/Worldview
GAAR1300	Active Layer Detachment Slide	IKONOS/Geoeye/Worldview
GAAR1301	Active Layer Detachment Slide	IKONOS/Geoeye/Worldview
GAAR1302	Active Layer Detachment Slide	IKONOS/Geoeye/Worldview
GAAR1303	Active Layer Detachment Slide	IKONOS/Geoeye/Worldview
GAAR1304	Active Layer Detachment Slide	IKONOS/Geoeye/Worldview
GAAR1305	Active Layer Detachment Slide	IKONOS/Geoeye/Worldview
GAAR1306	Active Layer Detachment Slide	IKONOS/Geoeye/Worldview
GAAR1307	Active Layer Detachment Slide	IKONOS/Geoeye/Worldview
GAAR1308	Active Layer Detachment Slide	IKONOS/Geoeye/Worldview
GAAR1309	Active Layer Detachment Slide	IKONOS/Geoeye/Worldview
GAAR1310	Active Layer Detachment Slide	IKONOS/Geoeye/Worldview
GAAR1311	Active Layer Detachment Slide	IKONOS/Geoeye/Worldview

NPS	2010	67.59136	-155.25595
NPS	2010	67.59921	-155.25005
NPS	2010	67.57977	-154.86566
NPS	2010	67.57905	-154.86416
NPS	2010	67.57500	-154.40140
NPS	2010	68.18903	-155.42044
NPS	2010	68.20728	-155.42222
NPS	2010	68.19888	-155.21142
NPS	2010	68.19445	-155.21415
NPS	2010	68.19317	-155.21395
NPS	2010	68.15438	-155.55532
NPS	2010	68.12526	-155.62328
NPS	2010	68.11985	-155.62410
NPS	2010	68.11494	-155.51827
NPS	2010	68.11461	-155.38656
NPS	2010	68.11385	-155.38958
NPS	2010	68.11347	-155.39048
NPS	2010	68.11245	-155.39011
NPS	2010	68.12309	-155.30348
NPS	2010	68.11342	-155.31267
NPS	2010	68.11428	-155.31073
NPS	2010	68.11199	-155.31049
NPS	2010	68.11311	-155.30346
NPS	2010	68.11475	-155.31793
NPS	2010	68.11452	-155.31833
NPS	2010	68.11104	-155.33395
NPS	2010	68.11071	-155.33821
NPS	2010	68.10868	-155.32790
NPS	2010	68.11208	-155.39806
NPS	2010	68.11032	-155.39864
NPS	2010	68.17761	-155.18408
NPS	2010	68.15920	-155.12888

GAAR1312	Active Layer Detachment Slide	IKONOS/Geoeye/Worldview
GAAR1313	Active Layer Detachment Slide	IKONOS/Geoeye/Worldview
GAAR1314	Active Layer Detachment Slide	IKONOS/Geoeye/Worldview
GAAR1315	Active Layer Detachment Slide	IKONOS/Geoeye/Worldview
GAAR1316	Active Layer Detachment Slide	IKONOS/Geoeye/Worldview
GAAR1317	Active Layer Detachment Slide	IKONOS/Geoeye/Worldview
GAAR1318	Active Layer Detachment Slide	IKONOS/Geoeye/Worldview
GAAR1319	Active Layer Detachment Slide	IKONOS/Geoeye/Worldview
GAAR1320	Active Layer Detachment Slide	IKONOS/Geoeye/Worldview
GAAR1321	Active Layer Detachment Slide	IKONOS/Geoeye/Worldview
GAAR1322	Active Layer Detachment Slide	IKONOS/Geoeye/Worldview
GAAR1323	Active Layer Detachment Slide	IKONOS/Geoeye/Worldview
GAAR1324	Active Layer Detachment Slide	IKONOS/Geoeye/Worldview
GAAR1325	Active Layer Detachment Slide	IKONOS/Geoeye/Worldview
GAAR1326	Active Layer Detachment Slide	IKONOS/Geoeye/Worldview
GAAR1327	Active Layer Detachment Slide	IKONOS/Geoeye/Worldview
GAAR1328	Active Layer Detachment Slide	IKONOS/Geoeye/Worldview
GAAR1329	Active Layer Detachment Slide	IKONOS/Geoeye/Worldview
GAAR1330	Active Layer Detachment Slide	IKONOS/Geoeye/Worldview
GAAR1331	Active Layer Detachment Slide	IKONOS/Geoeye/Worldview
GAAR1332	Active Layer Detachment Slide	IKONOS/Geoeye/Worldview
GAAR1333	Active Layer Detachment Slide	IKONOS/Geoeye/Worldview
GAAR1334	Active Layer Detachment Slide	IKONOS/Geoeye/Worldview
GAAR1335	Active Layer Detachment Slide	IKONOS/Geoeye/Worldview
GAAR1336	Active Layer Detachment Slide	IKONOS/Geoeye/Worldview
GAAR1337	Active Layer Detachment Slide	IKONOS/Geoeye/Worldview
GAAR1338	Retrogressive Thaw Slump	IKONOS/Geoeye/Worldview
GAAR1339	Active Layer Detachment Slide	IKONOS/Geoeye/Worldview
GAAR1340	Active Layer Detachment Slide	IKONOS/Geoeye/Worldview
GAAR1341	Active Layer Detachment Slide	IKONOS/Geoeye/Worldview
GAAR1342	Active Layer Detachment Slide	IKONOS/Geoeye/Worldview
GAAR1343	Active Layer Detachment Slide	IKONOS/Geoeye/Worldview

NPS	2010	68.14702	-154.77981
NPS	2010	68.12426	-154.70597
NPS	2010	68.00028	-155.76681
NPS	2010	67.99837	-155.75830
NPS	2010	67.99723	-155.76068
NPS	2010	67.97438	-155.57609
NPS	2010	67.96585	-155.56966
NPS	2010	67.96541	-155.56558
NPS	2010	67.91722	-155.69259
NPS	2010	67.91625	-155.69776
NPS	2010	67.91449	-155.69294
NPS	2010	67.91853	-155.69390
NPS	2010	68.00569	-155.31056
NPS	2010	68.00575	-155.30838
NPS	2010	68.00542	-155.30623
NPS	2010	68.00572	-155.29969
NPS	2010	68.00440	-155.30816
NPS	2010	68.00442	-155.31065
NPS	2010	68.00422	-155.30830
NPS	2010	68.00384	-155.30798
NPS	2010	68.00359	-155.30997
NPS	2010	68.00106	-155.30912
NPS	2010	68.00265	-155.25247
NPS	2010	68.00829	-155.25710
NPS	2010	68.00803	-155.25591
NPS	2010	68.00774	-155.25669
NPS	2010	68.00805	-155.21825
NPS	2010	68.00321	-155.21992
NPS	2010	68.00541	-155.22294
NPS	2010	67.99072	-155.04333
NPS	2010	67.98788	-155.03504
NPS	2010	67.98824	-155.03833

GAAR1344	Active Layer Detachment Slide	IKONOS/Geoeye/Worldview
GAAR1345	Active Layer Detachment Slide	IKONOS/Geoeye/Worldview
GAAR1346	Active Layer Detachment Slide	IKONOS/Geoeye/Worldview
GAAR1347	Active Layer Detachment Slide	IKONOS/Geoeye/Worldview
GAAR1348	Active Layer Detachment Slide	IKONOS/Geoeye/Worldview
GAAR1349	Retrogressive Thaw Slump	IKONOS/Geoeye/Worldview
GAAR1350	Retrogressive Thaw Slump	IKONOS/Geoeye/Worldview
GAAR1351	Active Layer Detachment Slide	IKONOS/Geoeye/Worldview
GAAR1352	Active Layer Detachment Slide	IKONOS/Geoeye/Worldview
GAAR1353	Active Layer Detachment Slide	IKONOS/Geoeye/Worldview
GAAR1354	Active Layer Detachment Slide	IKONOS/Geoeye/Worldview
GAAR1355	Active Layer Detachment Slide	IKONOS/Geoeye/Worldview
GAAR1356	Active Layer Detachment Slide	IKONOS/Geoeye/Worldview
GAAR1357	Active Layer Detachment Slide	IKONOS/Geoeye/Worldview
GAAR1358	Active Layer Detachment Slide	IKONOS/Geoeye/Worldview
GAAR1359	Active Layer Detachment Slide	IKONOS/Geoeye/Worldview
GAAR1360	Retrogressive Thaw Slump	IKONOS/Geoeye/Worldview
GAAR1361	Active Layer Detachment Slide	IKONOS/Geoeye/Worldview
GAAR1362	Active Layer Detachment Slide	IKONOS/Geoeye/Worldview
GAAR1363	Active Layer Detachment Slide	IKONOS/Geoeye/Worldview
GAAR1364	Active Layer Detachment Slide	IKONOS/Geoeye/Worldview
GAAR1365	Retrogressive Thaw Slump	IKONOS/Geoeye/Worldview
GAAR1366	Active Layer Detachment Slide	IKONOS/Geoeye/Worldview
GAAR1367	Active Layer Detachment Slide	IKONOS/Geoeye/Worldview
GAAR1368	Active Layer Detachment Slide	IKONOS/Geoeye/Worldview
GAAR1369	Active Layer Detachment Slide	IKONOS/Geoeye/Worldview
GAAR1370	Active Layer Detachment Slide	IKONOS/Geoeye/Worldview
GAAR1371	Active Layer Detachment Slide	IKONOS/Geoeye/Worldview
GAAR1372	Active Layer Detachment Slide	IKONOS/Geoeye/Worldview
GAAR1373	Active Layer Detachment Slide	IKONOS/Geoeye/Worldview
GAAR1374	Active Layer Detachment Slide	IKONOS/Geoeye/Worldview
GAAR1375	Active Layer Detachment Slide	IKONOS/Geoeye/Worldview

NPS	2010	67.98669	-155.04165
NPS	2010	67.99005	-155.02978
NPS	2010	67.91049	-155.09509
NPS	2010	68.00012	-154.87301
NPS	2010	67.94976	-154.53077
NPS	2010	67.96754	-154.58587
NPS	2010	67.96055	-154.58883
NPS	2010	67.94509	-154.52890
NPS	2010	67.94167	-154.63111
NPS	2010	67.94330	-154.61441
NPS	2010	67.95157	-154.69888
NPS	2010	67.95917	-154.85574
NPS	2010	67.95866	-154.85986
NPS	2010	67.96097	-154.78815
NPS	2010	67.96123	-154.78962
NPS	2010	67.95668	-154.85523
NPS	2010	67.94595	-154.27422
NPS	2010	67.92103	-154.34179
NPS	2010	67.92030	-154.34418
NPS	2010	67.91667	-154.34286
NPS	2010	67.91272	-154.34303
NPS	2010	67.92667	-154.18438
NPS	2010	67.88122	-155.73360
NPS	2010	67.88044	-155.73092
NPS	2010	67.88147	-155.73024
NPS	2010	67.88608	-155.73112
NPS	2010	67.88281	-155.73113
NPS	2010	67.84662	-155.62152
NPS	2010	67.84642	-155.62164
NPS	2010	67.88488	-155.74339
NPS	2010	67.88156	-155.75641
NPS	2010	67.88140	-155.75415

GAAR1376	Active Layer Detachment Slide	IKONOS/Geoeye/Worldview
GAAR1377	Active Layer Detachment Slide	IKONOS/Geoeye/Worldview
GAAR1378	Retrogressive Thaw Slump	IKONOS/Geoeye/Worldview
GAAR1379	Retrogressive Thaw Slump	IKONOS/Geoeye/Worldview
GAAR1380	Retrogressive Thaw Slump	IKONOS/Geoeye/Worldview
GAAR1381	Retrogressive Thaw Slump	IKONOS/Geoeye/Worldview
GAAR1382	Retrogressive Thaw Slump	IKONOS/Geoeye/Worldview
GAAR1383	Active Layer Detachment Slide	IKONOS/Geoeye/Worldview
GAAR1384	Active Layer Detachment Slide	IKONOS/Geoeye/Worldview
GAAR1385	Active Layer Detachment Slide	IKONOS/Geoeye/Worldview
GAAR1386	Active Layer Detachment Slide	IKONOS/Geoeye/Worldview
GAAR1387	Active Layer Detachment Slide	IKONOS/Geoeye/Worldview
GAAR1388	Retrogressive Thaw Slump	IKONOS/Geoeye/Worldview
GAAR1389	Active Layer Detachment Slide	IKONOS/Geoeye/Worldview
GAAR1390	Active Layer Detachment Slide	IKONOS/Geoeye/Worldview
GAAR1391	Active Layer Detachment Slide	IKONOS/Geoeye/Worldview
GAAR1392	Retrogressive Thaw Slump	IKONOS/Geoeye/Worldview
GAAR1393	Retrogressive Thaw Slump	IKONOS/Geoeye/Worldview
GAAR1394	Active Layer Detachment Slide	IKONOS/Geoeye/Worldview
GAAR1395	Active Layer Detachment Slide	IKONOS/Geoeye/Worldview
GAAR1396	Active Layer Detachment Slide	IKONOS/Geoeye/Worldview
GAAR1397	Active Layer Detachment Slide	IKONOS/Geoeye/Worldview
GAAR1398	Active Layer Detachment Slide	IKONOS/Geoeye/Worldview
GAAR1399	Active Layer Detachment Slide	IKONOS/Geoeye/Worldview
GAAR1400	Active Layer Detachment Slide	IKONOS/Geoeye/Worldview
GAAR1401	Active Layer Detachment Slide	IKONOS/Geoeye/Worldview
GAAR1402	Active Layer Detachment Slide	IKONOS/Geoeye/Worldview
GAAR1403	Retrogressive Thaw Slump	IKONOS/Geoeye/Worldview
GAAR1404	Retrogressive Thaw Slump	IKONOS/Geoeye/Worldview
GAAR1405	Active Layer Detachment Slide	IKONOS/Geoeye/Worldview
GAAR1406	Active Layer Detachment Slide	IKONOS/Geoeye/Worldview
GAAR1407	Retrogressive Thaw Slump	IKONOS/Geoeye/Worldview

NPS	2010	67.88074	-155.75392
NPS	2010	67.88004	-155.75358
NPS	2010	67.87908	-155.75235
NPS	2010	67.87924	-155.75579
NPS	2010	67.87738	-155.74823
NPS	2010	67.87623	-155.74853
NPS	2010	67.87503	-155.73843
NPS	2010	67.83962	-155.72529
NPS	2010	67.83607	-155.73985
NPS	2010	67.83491	-155.73980
NPS	2010	67.83423	-155.74025
NPS	2010	67.83097	-155.74772
NPS	2010	67.83439	-155.72355
NPS	2010	67.82366	-155.74683
NPS	2010	67.82296	-155.75058
NPS	2010	67.82662	-155.75050
NPS	2010	67.87104	-155.74443
NPS	2010	67.87166	-155.74922
NPS	2010	67.86998	-155.75171
NPS	2010	67.87714	-155.75813
NPS	2010	67.87715	-155.75706
NPS	2010	67.87497	-155.75745
NPS	2010	67.87394	-155.75553
NPS	2010	67.87375	-155.75472
NPS	2010	67.86707	-155.75678
NPS	2010	67.86663	-155.75706
NPS	2010	67.86646	-155.75707
NPS	2010	67.86551	-155.75224
NPS	2010	67.86535	-155.75588
NPS	2010	67.85389	-155.75566
NPS	2010	67.85263	-155.73608
NPS	2010	67.85539	-155.74556

GAAR1408	Active Layer Detachment Slide	IKONOS/Geoeye/Worldview
GAAR1409	Active Layer Detachment Slide	IKONOS/Geoeye/Worldview
GAAR1410	Retrogressive Thaw Slump	IKONOS/Geoeye/Worldview
GAAR1411	Active Layer Detachment Slide	IKONOS/Geoeye/Worldview
GAAR1412	Active Layer Detachment Slide	IKONOS/Geoeye/Worldview
GAAR1413	Active Layer Detachment Slide	IKONOS/Geoeye/Worldview
GAAR1414	Active Layer Detachment Slide	IKONOS/Geoeye/Worldview
GAAR1415	Active Layer Detachment Slide	IKONOS/Geoeye/Worldview
GAAR1416	Active Layer Detachment Slide	IKONOS/Geoeye/Worldview
GAAR1417	Retrogressive Thaw Slump	IKONOS/Geoeye/Worldview
GAAR1418	Retrogressive Thaw Slump	IKONOS/Geoeye/Worldview
GAAR1419	Retrogressive Thaw Slump	IKONOS/Geoeye/Worldview
GAAR1420	Retrogressive Thaw Slump	IKONOS/Geoeye/Worldview
GAAR1421	Retrogressive Thaw Slump	IKONOS/Geoeye/Worldview
GAAR1422	Retrogressive Thaw Slump	IKONOS/Geoeye/Worldview
GAAR1423	Retrogressive Thaw Slump	IKONOS/Geoeye/Worldview
GAAR1424	Retrogressive Thaw Slump	IKONOS/Geoeye/Worldview
GAAR1425	Active Layer Detachment Slide	IKONOS/Geoeye/Worldview
GAAR1426	Active Layer Detachment Slide	IKONOS/Geoeye/Worldview
GAAR1427	Active Layer Detachment Slide	IKONOS/Geoeye/Worldview
GAAR1428	Retrogressive Thaw Slump	IKONOS/Geoeye/Worldview
GAAR1429	Retrogressive Thaw Slump	IKONOS/Geoeye/Worldview
GAAR1430	Retrogressive Thaw Slump	IKONOS/Geoeye/Worldview
GAAR1431	Active Layer Detachment Slide	IKONOS/Geoeye/Worldview
GAAR1432	Active Layer Detachment Slide	IKONOS/Geoeye/Worldview
GAAR1433	Active Layer Detachment Slide	IKONOS/Geoeye/Worldview
GAAR1434	Active Layer Detachment Slide	IKONOS/Geoeye/Worldview
GAAR1435	Retrogressive Thaw Slump	IKONOS/Geoeye/Worldview
GAAR1436	Active Layer Detachment Slide	IKONOS/Geoeye/Worldview
GAAR1437	Active Layer Detachment Slide	IKONOS/Geoeye/Worldview
GAAR1438	Active Layer Detachment Slide	IKONOS/Geoeye/Worldview
GAAR1439	Active Layer Detachment Slide	IKONOS/Geoeye/Worldview

NPS	2010	67.85399	-155.73475
NPS	2010	67.85056	-155.74986
NPS	2010	67.84885	-155.74781
NPS	2010	67.84790	-155.74968
NPS	2010	67.84454	-155.74997
NPS	2010	67.84600	-155.75463
NPS	2010	67.84308	-155.74455
NPS	2010	67.84280	-155.74287
NPS	2010	67.81073	-155.75073
NPS	2010	67.81618	-155.73295
NPS	2010	67.81552	-155.72402
NPS	2010	67.81635	-155.72135
NPS	2010	67.82976	-155.62576
NPS	2010	67.82721	-155.63745
NPS	2010	67.82217	-155.60382
NPS	2010	67.82264	-155.60167
NPS	2010	67.81902	-155.59376
NPS	2010	67.81836	-155.64010
NPS	2010	67.81870	-155.63992
NPS	2010	67.81865	-155.62887
NPS	2010	67.81057	-155.59326
NPS	2010	67.81441	-155.57221
NPS	2010	67.81346	-155.57571
NPS	2010	67.89381	-154.35492
NPS	2010	67.89306	-154.35492
NPS	2010	67.89061	-154.35878
NPS	2010	67.90363	-154.30331
NPS	2010	67.86733	-154.23609
NPS	2010	67.76239	-155.03618
NPS	2010	67.76330	-155.04339
NPS	2010	67.76385	-155.03537
NPS	2010	67.76229	-155.03186

GAAR1440	Active Layer Detachment Slide	IKONOS/Geoeye/Worldview
GAAR1441	Retrogressive Thaw Slump	IKONOS/Geoeye/Worldview
GAAR1442	Retrogressive Thaw Slump	IKONOS/Geoeye/Worldview
GAAR1443	Active Layer Detachment Slide	IKONOS/Geoeye/Worldview
GAAR1444	Active Layer Detachment Slide	IKONOS/Geoeye/Worldview
GAAR1445	Active Layer Detachment Slide	IKONOS/Geoeye/Worldview
GAAR1446	Active Layer Detachment Slide	IKONOS/Geoeye/Worldview
GAAR1447	Active Layer Detachment Slide	IKONOS/Geoeye/Worldview
GAAR1448	Active Layer Detachment Slide	IKONOS/Geoeye/Worldview
GAAR1449	Active Layer Detachment Slide	IKONOS/Geoeye/Worldview
GAAR1450	Active Layer Detachment Slide	IKONOS/Geoeye/Worldview
GAAR1451	Active Layer Detachment Slide	IKONOS/Geoeye/Worldview
GAAR1452	Active Layer Detachment Slide	IKONOS/Geoeye/Worldview
GAAR1453	Active Layer Detachment Slide	IKONOS/Geoeye/Worldview
GAAR1454	Active Layer Detachment Slide	IKONOS/Geoeye/Worldview
GAAR1455	Active Layer Detachment Slide	IKONOS/Geoeye/Worldview
GAAR1456	Active Layer Detachment Slide	IKONOS/Geoeye/Worldview
GAAR1457	Active Layer Detachment Slide	IKONOS/Geoeye/Worldview
GAAR1458	Active Layer Detachment Slide	IKONOS/Geoeye/Worldview
GAAR1459	Active Layer Detachment Slide	IKONOS/Geoeye/Worldview
GAAR1460	Active Layer Detachment Slide	IKONOS/Geoeye/Worldview
GAAR1461	Active Layer Detachment Slide	IKONOS/Geoeye/Worldview
GAAR1462	Active Layer Detachment Slide	IKONOS/Geoeye/Worldview
GAAR1463	Active Layer Detachment Slide	IKONOS/Geoeye/Worldview
GAAR1464	Active Layer Detachment Slide	IKONOS/Geoeye/Worldview
GAAR1465	Retrogressive Thaw Slump	IKONOS/Geoeye/Worldview
GAAR1466	Retrogressive Thaw Slump	IKONOS/Geoeye/Worldview
GAAR1467	Retrogressive Thaw Slump	IKONOS/Geoeye/Worldview
GAAR1468	Active Layer Detachment Slide	IKONOS/Geoeye/Worldview
GAAR1470	Active Layer Detachment Slide	IKONOS/Geoeye/Worldview
GAAR1471	Active Layer Detachment Slide	IKONOS/Geoeye/Worldview
GAAR1472	Retrogressive Thaw Slump	IKONOS/Geoeye/Worldview

NPS	2010	67.76616	-155.04728
NPS	2010	67.75301	-155.22124
NPS	2010	67.74942	-155.22127
NPS	2010	67.73376	-155.23370
NPS	2010	67.74361	-154.91626
NPS	2010	67.74263	-154.91223
NPS	2010	67.74284	-154.90940
NPS	2010	67.73166	-154.93264
NPS	2010	67.73701	-154.83410
NPS	2010	67.73667	-154.83428
NPS	2010	67.73649	-154.83418
NPS	2010	67.73596	-154.83404
NPS	2010	67.73229	-154.82761
NPS	2010	67.73237	-154.82635
NPS	2010	67.73174	-154.82659
NPS	2010	67.73002	-154.82747
NPS	2010	67.73307	-154.75438
NPS	2010	67.73031	-154.75422
NPS	2010	67.73029	-154.75930
NPS	2010	67.73053	-154.76146
NPS	2010	67.72956	-154.74920
NPS	2010	67.72977	-154.74409
NPS	2010	67.81894	-153.94366
NPS	2010	67.81447	-153.93314
NPS	2010	68.58079	-152.92321
NPS	2010	68.02588	-149.83747
NPS	2010	68.02700	-149.83732
NPS	2010	68.02547	-149.84847
NPS	2010	68.03114	-149.84039
NPS	2010	68.02981	-149.84348
NPS	2010	68.03125	-149.82445
NPS	2010	68.03275	-149.82387

GAAR1473	Active Layer Detachment Slide	IKONOS/Geoeye/Worldview
GAAR1474	Retrogressive Thaw Slump	IKONOS/Geoeye/Worldview
GAAR1475	Active Layer Detachment Slide	IKONOS/Geoeye/Worldview
GAAR1476	Active Layer Detachment Slide	IKONOS/Geoeye/Worldview
GAAR1477	Active Layer Detachment Slide	IKONOS/Geoeye/Worldview
GAAR1478	Retrogressive Thaw Slump	IKONOS/Geoeye/Worldview
GAAR1479	Active Layer Detachment Slide	IKONOS/Geoeye/Worldview
GAAR1480	Active Layer Detachment Slide	IKONOS/Geoeye/Worldview
GAAR1481	Active Layer Detachment Slide	IKONOS/Geoeye/Worldview
GAAR1482	Active Layer Detachment Slide	IKONOS/Geoeye/Worldview
GAAR1483	Active Layer Detachment Slide	IKONOS/Geoeye/Worldview
GAAR1486	Retrogressive Thaw Slump	IKONOS/Geoeye/Worldview
GAAR1487	Retrogressive Thaw Slump	IKONOS/Geoeye/Worldview
GAAR1488	Retrogressive Thaw Slump	IKONOS/Geoeye/Worldview
GAAR1489	Active Layer Detachment Slide	IKONOS/Geoeye/Worldview
GAAR1490	Active Layer Detachment Slide	IKONOS/Geoeye/Worldview
GAAR1491	Active Layer Detachment Slide	IKONOS/Geoeye/Worldview
GAAR1492	Active Layer Detachment Slide	IKONOS/Geoeye/Worldview
GAAR1493	Active Layer Detachment Slide	IKONOS/Geoeye/Worldview
GAAR1494	Active Layer Detachment Slide	IKONOS/Geoeye/Worldview
GAAR1495	Active Layer Detachment Slide	IKONOS/Geoeye/Worldview
GAAR1496	Active Layer Detachment Slide	IKONOS/Geoeye/Worldview
GAAR1497	Active Layer Detachment Slide	IKONOS/Geoeye/Worldview
GAAR1498	Active Layer Detachment Slide	IKONOS/Geoeye/Worldview
GAAR1499	Active Layer Detachment Slide	IKONOS/Geoeye/Worldview
GAAR1500	Active Layer Detachment Slide	IKONOS/Geoeye/Worldview
GAAR1501	Active Layer Detachment Slide	IKONOS/Geoeye/Worldview
GAAR1502	Active Layer Detachment Slide	IKONOS/Geoeye/Worldview
GAAR1503	Retrogressive Thaw Slump	IKONOS/Geoeye/Worldview
GAAR1504	Active Layer Detachment Slide	IKONOS/Geoeye/Worldview
GAAR1505	Active Layer Detachment Slide	IKONOS/Geoeye/Worldview
GAAR1506	Active Layer Detachment Slide	IKONOS/Geoeye/Worldview

NPS	2010	68.02985	-149.81693
NPS	2010	68.04245	-149.82151
NPS	2010	68.04494	-149.81974
NPS	2010	68.01937	-149.92702
NPS	2010	68.01961	-149.92300
NPS	2010	68.01571	-149.87445
NPS	2010	68.09711	-151.54755
NPS	2010	68.09485	-151.54702
NPS	2010	68.09162	-151.55836
NPS	2010	68.09284	-151.55891
NPS	2010	68.09422	-151.56283
NPS	2010	68.15536	-152.75295
NPS	2010	68.15596	-152.75867
NPS	2010	68.16517	-152.75545
NPS	2010	68.13759	-151.99232
NPS	2010	68.13603	-151.97817
NPS	2010	67.90248	-151.90215
NPS	2010	67.90199	-151.90135
NPS	2010	67.90155	-151.90007
NPS	2010	67.90031	-151.89687
NPS	2010	67.90074	-151.90284
NPS	2010	67.90351	-151.89467
NPS	2010	67.88977	-151.91507
NPS	2010	67.89162	-151.90952
NPS	2010	67.88803	-151.91354
NPS	2010	67.87935	-151.90052
NPS	2010	67.74400	-151.65694
NPS	2010	67.74166	-151.62628
NPS	2010	67.75459	-151.55575
NPS	2010	67.71455	-151.54556
NPS	2010	67.71528	-151.54664
NPS	2010	67.71588	-151.54980

GAAR1507	Retrogressive Thaw Slump	IKONOS/Geoeye/Worldview
GAAR1508	Retrogressive Thaw Slump	IKONOS/Geoeye/Worldview
GAAR1509	Active Layer Detachment Slide	IKONOS/Geoeye/Worldview
GAAR1510	Active Layer Detachment Slide	IKONOS/Geoeye/Worldview
GAAR1511	Active Layer Detachment Slide	IKONOS/Geoeye/Worldview
GAAR1512	Active Layer Detachment Slide	IKONOS/Geoeye/Worldview
GAAR1513	Active Layer Detachment Slide	IKONOS/Geoeye/Worldview
GAAR1514	Retrogressive Thaw Slump	IKONOS/Geoeye/Worldview
GAAR1515	Retrogressive Thaw Slump	IKONOS/Geoeye/Worldview
GAAR1516	Retrogressive Thaw Slump	IKONOS/Geoeye/Worldview
GAAR1517	Retrogressive Thaw Slump	IKONOS/Geoeye/Worldview
GAAR1518	Retrogressive Thaw Slump	IKONOS/Geoeye/Worldview
GAAR1519	Retrogressive Thaw Slump	IKONOS/Geoeye/Worldview
GAAR1520	Retrogressive Thaw Slump	IKONOS/Geoeye/Worldview
GAAR1521	Retrogressive Thaw Slump	IKONOS/Geoeye/Worldview
GAAR1522	Retrogressive Thaw Slump	IKONOS/Geoeye/Worldview
GAAR1523	Retrogressive Thaw Slump	IKONOS/Geoeye/Worldview
GAAR1524	Retrogressive Thaw Slump	IKONOS/Geoeye/Worldview
GAAR1525	Retrogressive Thaw Slump	IKONOS/Geoeye/Worldview
GAAR1526	Retrogressive Thaw Slump	IKONOS/Geoeye/Worldview
GAAR1527	Retrogressive Thaw Slump	IKONOS/Geoeye/Worldview
GAAR1528	Retrogressive Thaw Slump	IKONOS/Geoeye/Worldview
GAAR1529	Retrogressive Thaw Slump	IKONOS/Geoeye/Worldview
GAAR1530	Active Layer Detachment Slide	IKONOS/Geoeye/Worldview
GAAR1531	Retrogressive Thaw Slump	IKONOS/Geoeye/Worldview
GAAR1532	Active Layer Detachment Slide	IKONOS/Geoeye/Worldview
GAAR1533	Active Layer Detachment Slide	IKONOS/Geoeye/Worldview
GAAR1534	Active Layer Detachment Slide	IKONOS/Geoeye/Worldview
GAAR1535	Retrogressive Thaw Slump	IKONOS/Geoeye/Worldview
GAAR1536	Retrogressive Thaw Slump	IKONOS/Geoeye/Worldview
GAAR1537	Retrogressive Thaw Slump	IKONOS/Geoeye/Worldview
GAAR1538	Active Layer Detachment Slide	IKONOS/Geoeye/Worldview

NPS	2010	67.71223	-151.88049
NPS	2010	67.70855	-151.85808
NPS	2010	67.67845	-151.82806
NPS	2010	67.67884	-151.82853
NPS	2010	67.67916	-151.82870
NPS	2010	67.67809	-151.85260
NPS	2010	67.67845	-151.84910
NPS	2010	67.73261	-151.51325
NPS	2010	67.73241	-151.50811
NPS	2010	67.73236	-151.50676
NPS	2010	67.73135	-151.51210
NPS	2010	67.73096	-151.51112
NPS	2010	67.73040	-151.51292
NPS	2010	67.73367	-151.51465
NPS	2010	67.73724	-151.51814
NPS	2010	67.74120	-151.50571
NPS	2010	67.74083	-151.50791
NPS	2010	67.74110	-151.50874
NPS	2010	67.74160	-151.50875
NPS	2010	67.73847	-151.51043
NPS	2010	67.73812	-151.50868
NPS	2010	67.73878	-151.50589
NPS	2010	67.73991	-151.50648
NPS	2010	67.71666	-150.67338
NPS	2010	67.59310	-151.27165
NPS	2010	67.60869	-150.34131
NPS	2010	67.57948	-151.30766
NPS	2010	67.55796	-151.32628
NPS	2010	67.95236	-151.43832
NPS	2010	67.95258	-151.46398
NPS	2010	67.94928	-151.44665
NPS	2010	67.94651	-150.87089

GAAR1539	Active Layer Detachment Slide	IKONOS/Geoeye/Worldview
GAAR1540	Active Layer Detachment Slide	IKONOS/Geoeye/Worldview
GAAR1541	Active Layer Detachment Slide	IKONOS/Geoeye/Worldview
GAAR1542	Retrogressive Thaw Slump	IKONOS/Geoeye/Worldview
GAAR1543	Active Layer Detachment Slide	IKONOS/Geoeye/Worldview
GAAR1544	Active Layer Detachment Slide	IKONOS/Geoeye/Worldview
GAAR1545	Retrogressive Thaw Slump	IKONOS/Geoeye/Worldview
GAAR1546	Active Layer Detachment Slide	IKONOS/Geoeye/Worldview
GAAR1547	Active Layer Detachment Slide	IKONOS/Geoeye/Worldview
GAAR1548	Active Layer Detachment Slide	IKONOS/Geoeye/Worldview
GAAR1549	Retrogressive Thaw Slump	IKONOS/Geoeye/Worldview
GAAR1550	Retrogressive Thaw Slump	IKONOS/Geoeye/Worldview
GAAR1551	Retrogressive Thaw Slump	IKONOS/Geoeye/Worldview
GAAR1552	Active Layer Detachment Slide	IKONOS/Geoeye/Worldview
GAAR1553	Active Layer Detachment Slide	IKONOS/Geoeye/Worldview
GAAR1554	Active Layer Detachment Slide	IKONOS/Geoeye/Worldview
GAAR1555	Retrogressive Thaw Slump	IKONOS/Geoeye/Worldview
GAAR1556	Retrogressive Thaw Slump	IKONOS/Geoeye/Worldview
GAAR1557	Retrogressive Thaw Slump	IKONOS/Geoeye/Worldview
GAAR1558	Retrogressive Thaw Slump	IKONOS/Geoeye/Worldview
GAAR1559	Retrogressive Thaw Slump	IKONOS/Geoeye/Worldview
GAAR1560	Retrogressive Thaw Slump	IKONOS/Geoeye/Worldview
GAAR1561	Active Layer Detachment Slide	IKONOS/Geoeye/Worldview
GAAR1562	Active Layer Detachment Slide	IKONOS/Geoeye/Worldview
GAAR1563	Retrogressive Thaw Slump	IKONOS/Geoeye/Worldview
GAAR1564	Retrogressive Thaw Slump	IKONOS/Geoeye/Worldview
GAAR1565	Retrogressive Thaw Slump	IKONOS/Geoeye/Worldview
GAAR1566	Retrogressive Thaw Slump	IKONOS/Geoeye/Worldview
GAAR1567	Retrogressive Thaw Slump	IKONOS/Geoeye/Worldview
GAAR1568	Retrogressive Thaw Slump	IKONOS/Geoeye/Worldview
GAAR1569	Retrogressive Thaw Slump	IKONOS/Geoeye/Worldview
GAAR1570	Retrogressive Thaw Slump	IKONOS/Geoeye/Worldview

NPS	2010	67.98206	-150.48803
NPS	2010	67.97963	-150.48985
NPS	2010	67.95034	-150.50117
NPS	2010	67.98699	-150.08379
NPS	2010	67.98622	-149.94448
NPS	2010	67.99056	-149.90448
NPS	2010	68.02668	-149.84198
NPS	2010	67.97383	-152.91672
NPS	2010	67.97067	-152.90710
NPS	2010	67.96933	-152.89868
NPS	2010	67.96698	-152.88543
NPS	2010	67.96421	-152.88272
NPS	2010	67.96259	-152.88271
NPS	2010	67.95326	-152.86062
NPS	2010	67.95057	-152.85256
NPS	2010	67.94899	-152.83666
NPS	2010	67.94048	-152.85439
NPS	2010	67.95125	-152.61797
NPS	2010	67.95384	-152.61154
NPS	2010	67.95457	-152.61177
NPS	2010	67.93412	-152.49982
NPS	2010	67.98984	-152.14247
NPS	2010	67.97746	-152.11869
NPS	2010	67.91647	-152.16616
NPS	2010	67.77909	-152.99361
NPS	2010	67.77690	-152.99545
NPS	2010	67.79142	-152.85827
NPS	2010	67.78991	-152.86133
NPS	2010	67.78977	-152.86300
NPS	2010	67.78732	-152.85966
NPS	2010	67.78681	-152.86104
NPS	2010	67.78816	-152.86766

GAAR1571	Retrogressive Thaw Slump	IKONOS/Geoeye/Worldview
GAAR1572	Active Layer Detachment Slide	IKONOS/Geoeye/Worldview
GAAR1573	Retrogressive Thaw Slump	IKONOS/Geoeye/Worldview
GAAR1574	Retrogressive Thaw Slump	IKONOS/Geoeye/Worldview
GAAR1575	Active Layer Detachment Slide	IKONOS/Geoeye/Worldview
GAAR1576	Active Layer Detachment Slide	IKONOS/Geoeye/Worldview
GAAR1577	Active Layer Detachment Slide	IKONOS/Geoeye/Worldview
GAAR1578	Active Layer Detachment Slide	IKONOS/Geoeye/Worldview
GAAR1579	Active Layer Detachment Slide	IKONOS/Geoeye/Worldview
GAAR1580	Active Layer Detachment Slide	IKONOS/Geoeye/Worldview
GAAR1581	Active Layer Detachment Slide	IKONOS/Geoeye/Worldview
GAAR1582	Active Layer Detachment Slide	IKONOS/Geoeye/Worldview
GAAR1583	Retrogressive Thaw Slump	IKONOS/Geoeye/Worldview
GAAR1584	Retrogressive Thaw Slump	IKONOS/Geoeye/Worldview
GAAR1585	Retrogressive Thaw Slump	IKONOS/Geoeye/Worldview
GAAR1586	Retrogressive Thaw Slump	IKONOS/Geoeye/Worldview
GAAR1587	Retrogressive Thaw Slump	IKONOS/Geoeye/Worldview
GAAR1588	Active Layer Detachment Slide	IKONOS/Geoeye/Worldview
GAAR1589	Active Layer Detachment Slide	IKONOS/Geoeye/Worldview
GAAR1590	Retrogressive Thaw Slump	IKONOS/Geoeye/Worldview
GAAR1591	Retrogressive Thaw Slump	IKONOS/Geoeye/Worldview
GAAR1592	Active Layer Detachment Slide	IKONOS/Geoeye/Worldview
GAAR1593	Active Layer Detachment Slide	IKONOS/Geoeye/Worldview
GAAR1594	Retrogressive Thaw Slump	IKONOS/Geoeye/Worldview
GAAR1595	Retrogressive Thaw Slump	IKONOS/Geoeye/Worldview
GAAR1596	Retrogressive Thaw Slump	IKONOS/Geoeye/Worldview
GAAR1597	Retrogressive Thaw Slump	IKONOS/Geoeye/Worldview
GAAR1598	Active Layer Detachment Slide	IKONOS/Geoeye/Worldview
GAAR1599	Active Layer Detachment Slide	IKONOS/Geoeye/Worldview
GAAR1600	Active Layer Detachment Slide	IKONOS/Geoeye/Worldview
GAAR1601	Retrogressive Thaw Slump	IKONOS/Geoeye/Worldview
GAAR1602	Active Layer Detachment Slide	IKONOS/Geoeye/Worldview

NPS	2010	67.78726	-152.87086
NPS	2010	67.80000	-152.70242
NPS	2010	67.80412	-152.67844
NPS	2010	67.80099	-152.68203
NPS	2010	67.74331	-152.65276
NPS	2010	67.72916	-152.79623
NPS	2010	67.72982	-152.79517
NPS	2010	67.74055	-152.80150
NPS	2010	67.73972	-152.79603
NPS	2010	67.74217	-152.80205
NPS	2010	67.71614	-152.84502
NPS	2010	67.74370	-152.80414
NPS	2010	67.70912	-152.72179
NPS	2010	67.70939	-152.72216
NPS	2010	67.71049	-152.72004
NPS	2010	67.70818	-152.72434
NPS	2010	67.70778	-152.72412
NPS	2010	67.74712	-152.62726
NPS	2010	67.74662	-152.63458
NPS	2010	67.79531	-152.62261
NPS	2010	67.78643	-152.36628
NPS	2010	67.78367	-152.24281
NPS	2010	67.80293	-152.25586
NPS	2010	67.72834	-152.31356
NPS	2010	67.72910	-152.31398
NPS	2010	67.76029	-152.34176
NPS	2010	67.76109	-152.34777
NPS	2010	67.74222	-152.31785
NPS	2010	67.74496	-152.32465
NPS	2010	67.74436	-152.31158
NPS	2010	67.80331	-152.22549
NPS	2010	67.80284	-152.22162

GAAR1603	Active Layer Detachment Slide	IKONOS/Geoeye/Worldview
GAAR1604	Active Layer Detachment Slide	IKONOS/Geoeye/Worldview
GAAR1605	Active Layer Detachment Slide	IKONOS/Geoeye/Worldview
GAAR1606	Active Layer Detachment Slide	IKONOS/Geoeye/Worldview
GAAR1607	Active Layer Detachment Slide	IKONOS/Geoeye/Worldview
GAAR1608	Active Layer Detachment Slide	IKONOS/Geoeye/Worldview
GAAR1609	Active Layer Detachment Slide	IKONOS/Geoeye/Worldview
GAAR1610	Retrogressive Thaw Slump	IKONOS/Geoeye/Worldview
GAAR1611	Retrogressive Thaw Slump	IKONOS/Geoeye/Worldview
GAAR1612	Active Layer Detachment Slide	IKONOS/Geoeye/Worldview
GAAR1613	Retrogressive Thaw Slump	IKONOS/Geoeye/Worldview
GAAR1614	Active Layer Detachment Slide	IKONOS/Geoeye/Worldview
GAAR1615	Active Layer Detachment Slide	IKONOS/Geoeye/Worldview
GAAR1616	Retrogressive Thaw Slump	IKONOS/Geoeye/Worldview
GAAR1617	Active Layer Detachment Slide	IKONOS/Geoeye/Worldview
GAAR1618	Retrogressive Thaw Slump	IKONOS/Geoeye/Worldview
GAAR1619	Active Layer Detachment Slide	IKONOS/Geoeye/Worldview
GAAR1620	Retrogressive Thaw Slump	IKONOS/Geoeye/Worldview
GAAR1621	Retrogressive Thaw Slump	IKONOS/Geoeye/Worldview
GAAR1622	Retrogressive Thaw Slump	IKONOS/Geoeye/Worldview
GAAR1623	Retrogressive Thaw Slump	IKONOS/Geoeye/Worldview
GAAR1624	Retrogressive Thaw Slump	IKONOS/Geoeye/Worldview
GAAR1625	Retrogressive Thaw Slump	IKONOS/Geoeye/Worldview
GAAR1626	Active Layer Detachment Slide	IKONOS/Geoeye/Worldview
GAAR1627	Active Layer Detachment Slide	IKONOS/Geoeye/Worldview
GAAR1628	Active Layer Detachment Slide	IKONOS/Geoeye/Worldview
GAAR1629	Active Layer Detachment Slide	IKONOS/Geoeye/Worldview
GAAR1630	Active Layer Detachment Slide	IKONOS/Geoeye/Worldview
GAAR1631	Active Layer Detachment Slide	IKONOS/Geoeye/Worldview
GAAR1632	Retrogressive Thaw Slump	IKONOS/Geoeye/Worldview
GAAR1633	Retrogressive Thaw Slump	IKONOS/Geoeye/Worldview
GAAR1634	Retrogressive Thaw Slump	IKONOS/Geoeye/Worldview

NPS	2010	67.80177	-152.23368
NPS	2010	67.80076	-152.23139
NPS	2010	67.80018	-152.23285
NPS	2010	67.80320	-152.23655
NPS	2010	67.80207	-152.23709
NPS	2010	67.80113	-152.22880
NPS	2010	67.80191	-152.22945
NPS	2010	67.79822	-152.24023
NPS	2010	67.80058	-152.19164
NPS	2010	67.79280	-152.18668
NPS	2010	67.78861	-152.18809
NPS	2010	67.80446	-152.20940
NPS	2010	67.78452	-152.21059
NPS	2010	67.78733	-152.20495
NPS	2010	67.78978	-152.21099
NPS	2010	67.77702	-152.23629
NPS	2010	67.77315	-152.17069
NPS	2010	67.77313	-152.16249
NPS	2010	67.77387	-152.16580
NPS	2010	67.79164	-152.14499
NPS	2010	67.78685	-152.11149
NPS	2010	67.78856	-152.11378
NPS	2010	67.78903	-152.11183
NPS	2010	67.78358	-151.94903
NPS	2010	67.80143	-151.88437
NPS	2010	67.78651	-151.87839
NPS	2010	67.78125	-151.88302
NPS	2010	67.78139	-151.88011
NPS	2010	67.77581	-151.87652
NPS	2010	67.74668	-151.97394
NPS	2010	67.74825	-151.97673
NPS	2010	67.74399	-151.96927

GAAR1635	Retrogressive Thaw Slump	IKONOS/Geoeye/Worldview
GAAR1636	Active Layer Detachment Slide	IKONOS/Geoeye/Worldview
GAAR1637	Active Layer Detachment Slide	IKONOS/Geoeye/Worldview
GAAR1638	Active Layer Detachment Slide	IKONOS/Geoeye/Worldview
GAAR1639	Retrogressive Thaw Slump	IKONOS/Geoeye/Worldview
GAAR1640	Active Layer Detachment Slide	IKONOS/Geoeye/Worldview
GAAR1641	Retrogressive Thaw Slump	IKONOS/Geoeye/Worldview
GAAR1642	Retrogressive Thaw Slump	IKONOS/Geoeye/Worldview
GAAR1643	Retrogressive Thaw Slump	IKONOS/Geoeye/Worldview
GAAR1644	Retrogressive Thaw Slump	IKONOS/Geoeye/Worldview
GAAR1645	Retrogressive Thaw Slump	IKONOS/Geoeye/Worldview
GAAR1646	Retrogressive Thaw Slump	IKONOS/Geoeye/Worldview
GAAR1647	Retrogressive Thaw Slump	IKONOS/Geoeye/Worldview
GAAR1648	Retrogressive Thaw Slump	IKONOS/Geoeye/Worldview
GAAR1649	Active Layer Detachment Slide	IKONOS/Geoeye/Worldview
GAAR1650	Active Layer Detachment Slide	IKONOS/Geoeye/Worldview
GAAR1651	Active Layer Detachment Slide	IKONOS/Geoeye/Worldview
GAAR1652	Active Layer Detachment Slide	IKONOS/Geoeye/Worldview
GAAR1653	Active Layer Detachment Slide	IKONOS/Geoeye/Worldview
GAAR1654	Active Layer Detachment Slide	IKONOS/Geoeye/Worldview
GAAR1655	Active Layer Detachment Slide	IKONOS/Geoeye/Worldview
GAAR1656	Active Layer Detachment Slide	IKONOS/Geoeye/Worldview
GAAR1657	Active Layer Detachment Slide	IKONOS/Geoeye/Worldview
GAAR1658	Active Layer Detachment Slide	IKONOS/Geoeye/Worldview
GAAR1659	Active Layer Detachment Slide	IKONOS/Geoeye/Worldview
GAAR1660	Active Layer Detachment Slide	IKONOS/Geoeye/Worldview
GAAR1661	Active Layer Detachment Slide	IKONOS/Geoeye/Worldview
GAAR1662	Active Layer Detachment Slide	IKONOS/Geoeye/Worldview
GAAR1663	Active Layer Detachment Slide	IKONOS/Geoeye/Worldview
GAAR1664	Active Layer Detachment Slide	IKONOS/Geoeye/Worldview
GAAR1665	Retrogressive Thaw Slump	IKONOS/Geoeye/Worldview
GAAR1666	Retrogressive Thaw Slump	IKONOS/Geoeye/Worldview

NPS	2010	67.74427	-151.96929
NPS	2010	67.74076	-152.03895
NPS	2010	67.73896	-152.03968
NPS	2010	67.73953	-152.03910
NPS	2010	67.75792	-151.99124
NPS	2010	67.76053	-151.98260
NPS	2010	67.75578	-152.06472
NPS	2010	67.75651	-152.06615
NPS	2010	67.75455	-152.06318
NPS	2010	67.76488	-152.15041
NPS	2010	67.76577	-152.14430
NPS	2010	67.77011	-152.14597
NPS	2010	67.76911	-152.14136
NPS	2010	67.76889	-152.13952
NPS	2010	67.76895	-152.13840
NPS	2010	67.76947	-152.14027
NPS	2010	67.76854	-152.13445
NPS	2010	67.76763	-152.13080
NPS	2010	67.73121	-152.21613
NPS	2010	67.72068	-152.22525
NPS	2010	67.72081	-152.22427
NPS	2010	67.72064	-152.22139
NPS	2010	67.72127	-152.22212
NPS	2010	67.72082	-152.21417
NPS	2010	67.72447	-152.21847
NPS	2010	67.72120	-152.20265
NPS	2010	67.72209	-152.20125
NPS	2010	67.71117	-152.23113
NPS	2010	67.71107	-152.22938
NPS	2010	67.70984	-152.23036
NPS	2010	67.71124	-152.22466
NPS	2010	67.71236	-152.22472

GAAR1667	Retrogressive Thaw Slump	IKONOS/Geoeye/Worldview
GAAR1668	Retrogressive Thaw Slump	IKONOS/Geoeye/Worldview
GAAR1669	Retrogressive Thaw Slump	IKONOS/Geoeye/Worldview
GAAR1670	Retrogressive Thaw Slump	IKONOS/Geoeye/Worldview
GAAR1671	Active Layer Detachment Slide	IKONOS/Geoeye/Worldview
GAAR1672	Active Layer Detachment Slide	IKONOS/Geoeye/Worldview
GAAR1673	Active Layer Detachment Slide	IKONOS/Geoeye/Worldview
GAAR1674	Active Layer Detachment Slide	IKONOS/Geoeye/Worldview
GAAR1675	Active Layer Detachment Slide	IKONOS/Geoeye/Worldview
GAAR1676	Active Layer Detachment Slide	IKONOS/Geoeye/Worldview
GAAR1677	Active Layer Detachment Slide	IKONOS/Geoeye/Worldview
GAAR1678	Active Layer Detachment Slide	IKONOS/Geoeye/Worldview
GAAR1679	Active Layer Detachment Slide	IKONOS/Geoeye/Worldview
GAAR1680	Active Layer Detachment Slide	IKONOS/Geoeye/Worldview
GAAR1681	Active Layer Detachment Slide	IKONOS/Geoeye/Worldview
GAAR1682	Active Layer Detachment Slide	IKONOS/Geoeye/Worldview
GAAR1683	Active Layer Detachment Slide	IKONOS/Geoeye/Worldview
GAAR1684	Retrogressive Thaw Slump	IKONOS/Geoeye/Worldview
GAAR1685	Active Layer Detachment Slide	IKONOS/Geoeye/Worldview
GAAR1686	Active Layer Detachment Slide	IKONOS/Geoeye/Worldview
GAAR1687	Active Layer Detachment Slide	IKONOS/Geoeye/Worldview
GAAR1688	Active Layer Detachment Slide	IKONOS/Geoeye/Worldview
GAAR1689	Active Layer Detachment Slide	IKONOS/Geoeye/Worldview
GAAR1690	Active Layer Detachment Slide	IKONOS/Geoeye/Worldview
GAAR1691	Active Layer Detachment Slide	IKONOS/Geoeye/Worldview
GAAR1692	Active Layer Detachment Slide	IKONOS/Geoeye/Worldview
GAAR1693	Active Layer Detachment Slide	IKONOS/Geoeye/Worldview
GAAR1694	Active Layer Detachment Slide	IKONOS/Geoeye/Worldview
GAAR1695	Active Layer Detachment Slide	IKONOS/Geoeye/Worldview
GAAR1696	Retrogressive Thaw Slump	IKONOS/Geoeye/Worldview
GAAR1697	Active Layer Detachment Slide	IKONOS/Geoeye/Worldview
GAAR1698	Active Layer Detachment Slide	IKONOS/Geoeye/Worldview

NPS	2010	67.71017	-152.22795
NPS	2010	67.70784	-152.22777
NPS	2010	67.70679	-151.88183
NPS	2010	67.69524	-152.13995
NPS	2010	67.67396	-152.73128
NPS	2010	67.70153	-152.71640
NPS	2010	67.70445	-152.70969
NPS	2010	67.70031	-152.71027
NPS	2010	67.69613	-152.68864
NPS	2010	67.63780	-152.80688
NPS	2010	67.63800	-152.80615
NPS	2010	67.63931	-152.80959
NPS	2010	67.68659	-152.06965
NPS	2010	67.67439	-151.99648
NPS	2010	67.67880	-152.00872
NPS	2010	67.68103	-152.01033
NPS	2010	67.68128	-152.01079
NPS	2010	67.66171	-151.92755
NPS	2010	67.66291	-151.93346
NPS	2010	67.64130	-151.95985
NPS	2010	67.64998	-152.13109
NPS	2010	67.65534	-152.19372
NPS	2010	67.61471	-151.97466
NPS	2010	67.81207	-151.81969
NPS	2010	67.80644	-151.81410
NPS	2010	67.80935	-151.80642
NPS	2010	67.77851	-151.63776
NPS	2010	67.77764	-151.64016
NPS	2010	67.77739	-151.64040
NPS	2010	67.77338	-151.64392
NPS	2010	67.76629	-151.80930
NPS	2010	67.75451	-151.70924

GAAR1699	Active Layer Detachment Slide	IKONOS/Geoeye/Worldview
GAAR1700	Retrogressive Thaw Slump	IKONOS/Geoeye/Worldview
GAAR1701	Retrogressive Thaw Slump	IKONOS/Geoeye/Worldview
GAAR1702	Retrogressive Thaw Slump	IKONOS/Geoeye/Worldview
GAAR1703	Retrogressive Thaw Slump	IKONOS/Geoeye/Worldview
GAAR1704	Active Layer Detachment Slide	IKONOS/Geoeye/Worldview
GAAR1705	Active Layer Detachment Slide	IKONOS/Geoeye/Worldview
GAAR1706	Active Layer Detachment Slide	IKONOS/Geoeye/Worldview
GAAR1707	Active Layer Detachment Slide	IKONOS/Geoeye/Worldview
GAAR1708	Active Layer Detachment Slide	IKONOS/Geoeye/Worldview
GAAR1709	Active Layer Detachment Slide	IKONOS/Geoeye/Worldview
GAAR1710	Active Layer Detachment Slide	IKONOS/Geoeye/Worldview
GAAR1711	Active Layer Detachment Slide	IKONOS/Geoeye/Worldview
GAAR1712	Active Layer Detachment Slide	IKONOS/Geoeye/Worldview
GAAR1713	Active Layer Detachment Slide	IKONOS/Geoeye/Worldview
GAAR1714	Active Layer Detachment Slide	IKONOS/Geoeye/Worldview
GAAR1715	Active Layer Detachment Slide	IKONOS/Geoeye/Worldview
GAAR1716	Retrogressive Thaw Slump	IKONOS/Geoeye/Worldview
GAAR1717	Active Layer Detachment Slide	IKONOS/Geoeye/Worldview
GAAR1718	Retrogressive Thaw Slump	IKONOS/Geoeye/Worldview
GAAR1719	Active Layer Detachment Slide	IKONOS/Geoeye/Worldview
GAAR1720	Active Layer Detachment Slide	IKONOS/Geoeye/Worldview
GAAR1721	Active Layer Detachment Slide	IKONOS/Geoeye/Worldview
GAAR1722	Active Layer Detachment Slide	IKONOS/Geoeye/Worldview
GAAR1723	Active Layer Detachment Slide	IKONOS/Geoeye/Worldview
GAAR1724	Active Layer Detachment Slide	IKONOS/Geoeye/Worldview
GAAR1725	Active Layer Detachment Slide	IKONOS/Geoeye/Worldview
GAAR1726	Active Layer Detachment Slide	IKONOS/Geoeye/Worldview
GAAR1727	Active Layer Detachment Slide	IKONOS/Geoeye/Worldview
GAAR1728	Active Layer Detachment Slide	IKONOS/Geoeye/Worldview
GAAR1729	Active Layer Detachment Slide	IKONOS/Geoeye/Worldview
GAAR1730	Active Layer Detachment Slide	IKONOS/Geoeye/Worldview

NPS	2010	67.75319	-151.71174
NPS	2010	67.77888	-151.65737
NPS	2010	67.77863	-151.65823
NPS	2010	67.84016	-151.33621
NPS	2010	67.81933	-151.33683
NPS	2010	67.88655	-152.74091
NPS	2010	67.88366	-152.73807
NPS	2010	67.88306	-152.73819
NPS	2010	67.88439	-152.72134
NPS	2010	67.85849	-152.73061
NPS	2010	67.85954	-152.71922
NPS	2010	67.92928	-152.64484
NPS	2010	67.89010	-152.28777
NPS	2010	67.89060	-152.28227
NPS	2010	67.86051	-152.57416
NPS	2010	67.85793	-152.56491
NPS	2010	67.85515	-152.56671
NPS	2010	67.89181	-151.93155
NPS	2010	67.89247	-152.07510
NPS	2010	67.91433	-152.10653
NPS	2010	67.89587	-152.22379
NPS	2010	67.89953	-152.27141
NPS	2010	67.89916	-152.27856
NPS	2010	67.89818	-152.27943
NPS	2010	67.89759	-152.27944
NPS	2010	67.89721	-152.27762
NPS	2010	67.89772	-152.26985
NPS	2010	67.89668	-152.27382
NPS	2010	67.89672	-152.27521
NPS	2010	67.89087	-152.27799
NPS	2010	67.89334	-152.28268
NPS	2010	67.89338	-152.28449

GAAR1731	Active Layer Detachment Slide	IKONOS/Geoeye/Worldview
GAAR1732	Active Layer Detachment Slide	IKONOS/Geoeye/Worldview
GAAR1733	Active Layer Detachment Slide	IKONOS/Geoeye/Worldview
GAAR1734	Active Layer Detachment Slide	IKONOS/Geoeye/Worldview
GAAR1735	Active Layer Detachment Slide	IKONOS/Geoeye/Worldview
GAAR1736	Active Layer Detachment Slide	IKONOS/Geoeye/Worldview
GAAR1737	Active Layer Detachment Slide	IKONOS/Geoeye/Worldview
GAAR1738	Retrogressive Thaw Slump	IKONOS/Geoeye/Worldview
GAAR1739	Active Layer Detachment Slide	IKONOS/Geoeye/Worldview
GAAR1740	Active Layer Detachment Slide	IKONOS/Geoeye/Worldview
GAAR1741	Active Layer Detachment Slide	IKONOS/Geoeye/Worldview
GAAR1742	Active Layer Detachment Slide	IKONOS/Geoeye/Worldview
GAAR1743	Retrogressive Thaw Slump	IKONOS/Geoeye/Worldview
GAAR1744	Retrogressive Thaw Slump	IKONOS/Geoeye/Worldview
GAAR1745	Active Layer Detachment Slide	IKONOS/Geoeye/Worldview
GAAR1746	Active Layer Detachment Slide	IKONOS/Geoeye/Worldview
GAAR1747	Active Layer Detachment Slide	IKONOS/Geoeye/Worldview
GAAR1748	Active Layer Detachment Slide	IKONOS/Geoeye/Worldview
GAAR1749	Active Layer Detachment Slide	IKONOS/Geoeye/Worldview
GAAR1750	Active Layer Detachment Slide	IKONOS/Geoeye/Worldview
GAAR1751	Active Layer Detachment Slide	IKONOS/Geoeye/Worldview
GAAR1752	Retrogressive Thaw SlumpO	IKONOS/Geoeye/Worldview
GAAR1753	Retrogressive Thaw SlumpO	IKONOS/Geoeye/Worldview
GAAR1754	Retrogressive Thaw SlumpO	IKONOS/Geoeye/Worldview
GAAR1755	Retrogressive Thaw SlumpO	IKONOS/Geoeye/Worldview
GAAR1756	Retrogressive Thaw SlumpO	IKONOS/Geoeye/Worldview
GAAR1757	Retrogressive Thaw SlumpO	IKONOS/Geoeye/Worldview
GAAR1758	Retrogressive Thaw SlumpO	IKONOS/Geoeye/Worldview
GAAR1759	Retrogressive Thaw SlumpO	IKONOS/Geoeye/Worldview
GAAR1760	Retrogressive Thaw SlumpO	IKONOS/Geoeye/Worldview
GAAR1761	Retrogressive Thaw SlumpO	IKONOS/Geoeye/Worldview
GAAR1762	Retrogressive Thaw SlumpO	IKONOS/Geoeye/Worldview

NPS	2010	67.89317	-152.28463
NPS	2010	67.86503	-152.12250
NPS	2010	67.85845	-152.07397
NPS	2010	67.85694	-152.05909
NPS	2010	67.86208	-152.03804
NPS	2010	67.86841	-152.00897
NPS	2010	67.86991	-151.98977
NPS	2010	67.83381	-152.85415
NPS	2010	67.87625	-151.93917
NPS	2010	67.81975	-151.94736
NPS	2010	67.82811	-152.00614
NPS	2010	67.84439	-152.01020
NPS	2010	67.82786	-152.03941
NPS	2010	67.84794	-152.09638
NPS	2010	67.81673	-152.12691
NPS	2010	67.81685	-152.12082
NPS	2010	67.81938	-152.12295
NPS	2010	67.82618	-152.21227
NPS	2010	67.82602	-152.23411
NPS	2010	67.82499	-152.23214
NPS	2010	67.81005	-152.04019
NPS	2010	68.37533	-154.28520
NPS	2010	68.36954	-154.28445
NPS	2010	68.33694	-154.13685
NPS	2010	68.33762	-154.14609
NPS	2010	68.33787	-154.15086
NPS	2010	68.33771	-154.15562
NPS	2010	68.33982	-154.15767
NPS	2010	68.33928	-154.16657
NPS	2010	68.33519	-154.16773
NPS	2010	68.33302	-154.15349
NPS	2010	68.34510	-154.14707

GAAR1763	Retrogressive Thaw SlumpO	IKONOS/Geoeye/Worldview
GAAR1764	Retrogressive Thaw SlumpO	IKONOS/Geoeye/Worldview
GAAR1765	Active Layer Detachment Slide	IKONOS/Geoeye/Worldview
GAAR1766	Retrogressive Thaw Slump	IKONOS/Geoeye/Worldview
GAAR1767	Active Layer Detachment Slide	IKONOS/Geoeye/Worldview
GAAR1768	Retrogressive Thaw Slump	IKONOS/Geoeye/Worldview
GAAR1769	Retrogressive Thaw Slump	IKONOS/Geoeye/Worldview
GAAR1770	Retrogressive Thaw Slump	IKONOS/Geoeye/Worldview
GAAR1771	Active Layer Detachment Slide	IKONOS/Geoeye/Worldview
GAAR1772	Active Layer Detachment Slide	IKONOS/Geoeye/Worldview
GAAR1773	Active Layer Detachment Slide	IKONOS/Geoeye/Worldview
GAAR1774	Active Layer Detachment Slide	IKONOS/Geoeye/Worldview
GAAR1775	Active Layer Detachment Slide	IKONOS/Geoeye/Worldview
GAAR1776	Active Layer Detachment Slide	IKONOS/Geoeye/Worldview
GAAR1777	Active Layer Detachment Slide	IKONOS/Geoeye/Worldview
GAAR1778	Active Layer Detachment Slide	IKONOS/Geoeye/Worldview
GAAR1779	Retrogressive Thaw Slump	IKONOS/Geoeye/Worldview
GAAR1780	Active Layer Detachment Slide	IKONOS/Geoeye/Worldview
GAAR1781	Retrogressive Thaw Slump	IKONOS/Geoeye/Worldview
GAAR1782	Retrogressive Thaw Slump	IKONOS/Geoeye/Worldview
GAAR1783	Active Layer Detachment Slide	IKONOS/Geoeye/Worldview
GAAR1784	Active Layer Detachment Slide	IKONOS/Geoeye/Worldview
GAAR1785	Retrogressive Thaw Slump	IKONOS/Geoeye/Worldview
GAAR1786	Active Layer Detachment Slide	IKONOS/Geoeye/Worldview
GAAR1787	Active Layer Detachment Slide	IKONOS/Geoeye/Worldview
GAAR1788	Retrogressive Thaw Slump	IKONOS/Geoeye/Worldview
GAAR1789	Active Layer Detachment Slide	IKONOS/Geoeye/Worldview
GAAR1790	Retrogressive Thaw Slump	IKONOS/Geoeye/Worldview
GAAR1791	Active Layer Detachment Slide	IKONOS/Geoeye/Worldview
GAAR1792	Active Layer Detachment Slide	IKONOS/Geoeye/Worldview
GAAR1793	Retrogressive Thaw Slump	IKONOS/Geoeye/Worldview
NOAT0001	Retrogressive Thaw Slump	IKONOS/Geoeye/Worldview

NPS	2010	68.34397	-154.15086
NPS	2010	68.30972	-154.17877
NPS	2010	67.60938	-156.24250
NPS	2010	67.94046	-152.85239
NPS	2010	68.10984	-155.39271
NPS	2010	67.76954	-152.89616
NPS	2010	67.78670	-152.87150
NPS	2010	68.05857	-155.45446
NPS	2010	67.95726	-154.85327
NPS	2010	67.93739	-152.88779
NPS	2010	67.69028	-155.35173
NPS	2010	67.71659	-152.84486
NPS	2010	68.04606	-154.63955
NPS	2010	67.96507	-154.81233
NPS	2010	67.74283	-152.80302
NPS	2010	67.72208	-155.40653
NPS	2010	67.66517	-155.95666
NPS	2010	67.98465	-155.78432
NPS	2010	67.77464	-155.97676
NPS	2010	67.77561	-155.97252
NPS	2010	68.02017	-155.87608
NPS	2010	67.99979	-155.87208
NPS	2010	67.98559	-155.77489
NPS	2010	67.99454	-155.88009
NPS	2010	67.65304	-156.20439
NPS	2010	67.65624	-156.19993
NPS	2010	67.65742	-155.76761
NPS	2010	67.82922	-155.63658
NPS	2010	67.76282	-152.33352
NPS	2010	67.76878	-152.13617
NPS	2010	68.05465	-155.48802
NPS	2010	68.03367	-158.51800

NOAT0002	Retrogressive Thaw Slump	IKONOS/Geoeye/Worldview
NOAT0003	Retrogressive Thaw Slump	IKONOS/Geoeye/Worldview
NOAT0004	Retrogressive Thaw Slump	IKONOS/Geoeye/Worldview
NOAT0005	Retrogressive Thaw Slump	IKONOS/Geoeye/Worldview
NOAT0006	Retrogressive Thaw Slump	IKONOS/Geoeye/Worldview
NOAT0007	Retrogressive Thaw Slump	IKONOS/Geoeye/Worldview
NOAT0008	Retrogressive Thaw Slump	IKONOS/Geoeye/Worldview
NOAT0009	Retrogressive Thaw Slump	IKONOS/Geoeye/Worldview
NOAT0010	Retrogressive Thaw Slump	IKONOS/Geoeye/Worldview
NOAT0011	Retrogressive Thaw Slump	IKONOS/Geoeye/Worldview
NOAT0012	Retrogressive Thaw Slump	IKONOS/Geoeye/Worldview
NOAT0013	Retrogressive Thaw Slump	IKONOS/Geoeye/Worldview
NOAT0014	Retrogressive Thaw Slump	IKONOS/Geoeye/Worldview
NOAT0015	Retrogressive Thaw Slump	IKONOS/Geoeye/Worldview
NOAT0016	Retrogressive Thaw Slump	IKONOS/Geoeye/Worldview
NOAT0017	Retrogressive Thaw Slump	IKONOS/Geoeye/Worldview
NOAT0018	Retrogressive Thaw Slump	IKONOS/Geoeye/Worldview
NOAT0019	Retrogressive Thaw Slump	IKONOS/Geoeye/Worldview
NOAT0020	Retrogressive Thaw Slump	IKONOS/Geoeye/Worldview
NOAT0021	Retrogressive Thaw Slump	IKONOS/Geoeye/Worldview
NOAT0022	Retrogressive Thaw Slump	IKONOS/Geoeye/Worldview
NOAT0023	Retrogressive Thaw Slump	IKONOS/Geoeye/Worldview
NOAT0024	Active Layer Detachment Slide	IKONOS/Geoeye/Worldview
NOAT0025	Active Layer Detachment Slide	IKONOS/Geoeye/Worldview
NOAT0026	Active Layer Detachment Slide	IKONOS/Geoeye/Worldview
NOAT0027	Active Layer Detachment Slide	IKONOS/Geoeye/Worldview
NOAT0028	Active Layer Detachment Slide	IKONOS/Geoeye/Worldview
NOAT0029	Retrogressive Thaw Slump	IKONOS/Geoeye/Worldview
NOAT0030	Retrogressive Thaw Slump	IKONOS/Geoeye/Worldview
NOAT0031	Retrogressive Thaw Slump	IKONOS/Geoeye/Worldview
NOAT0032	Retrogressive Thaw Slump	IKONOS/Geoeye/Worldview
NOAT0033	Retrogressive Thaw Slump	IKONOS/Geoeye/Worldview

NPS	2010	68.05311	-158.56274
NPS	2010	68.06885	-159.24018
NPS	2010	68.07064	-159.24448
NPS	2010	68.07301	-159.25176
NPS	2010	68.08363	-159.32645
NPS	2010	68.08221	-159.32345
NPS	2010	67.97876	-160.25319
NPS	2010	67.97314	-160.25430
NPS	2010	67.97173	-160.25284
NPS	2010	67.97119	-160.25269
NPS	2010	67.95417	-160.21701
NPS	2010	67.95468	-160.21619
NPS	2010	67.87677	-160.63129
NPS	2010	67.90918	-160.71368
NPS	2010	67.90935	-160.72356
NPS	2010	67.90114	-160.82587
NPS	2010	67.90257	-160.82953
NPS	2010	67.89882	-160.81661
NPS	2010	67.89981	-160.91579
NPS	2010	67.92027	-160.91233
NPS	2010	67.92092	-160.91463
NPS	2010	67.91800	-160.90686
NPS	2010	67.96446	-161.10893
NPS	2010	67.97686	-161.14081
NPS	2010	67.99884	-161.20776
NPS	2010	68.00047	-161.21091
NPS	2010	68.00094	-161.21193
NPS	2010	67.99730	-161.29128
NPS	2010	67.99804	-161.29980
NPS	2010	67.99825	-161.30321
NPS	2010	67.99840	-161.30486
NPS	2010	68.00466	-161.45085

NOAT0034	Retrogressive Thaw Slump	IKONOS/Geoeye/Worldview
NOAT0035	Active Layer Detachment Slide	IKONOS/Geoeye/Worldview
NOAT0036	Active Layer Detachment Slide	IKONOS/Geoeye/Worldview
NOAT0037	Retrogressive Thaw Slump	IKONOS/Geoeye/Worldview
NOAT0038	Retrogressive Thaw Slump	IKONOS/Geoeye/Worldview
NOAT0039	Retrogressive Thaw Slump	IKONOS/Geoeye/Worldview
NOAT0040	Retrogressive Thaw Slump	IKONOS/Geoeye/Worldview
NOAT0041	Retrogressive Thaw Slump	IKONOS/Geoeye/Worldview
NOAT0042	Retrogressive Thaw Slump	IKONOS/Geoeye/Worldview
NOAT0043	Retrogressive Thaw Slump	IKONOS/Geoeye/Worldview
NOAT0044	Retrogressive Thaw Slump	IKONOS/Geoeye/Worldview
NOAT0045	Retrogressive Thaw Slump	IKONOS/Geoeye/Worldview
NOAT0046	Retrogressive Thaw Slump	IKONOS/Geoeye/Worldview
NOAT0047	Retrogressive Thaw Slump	IKONOS/Geoeye/Worldview
NOAT0048	Retrogressive Thaw Slump	IKONOS/Geoeye/Worldview
NOAT0049	Retrogressive Thaw Slump	IKONOS/Geoeye/Worldview
NOAT0050	Retrogressive Thaw Slump	IKONOS/Geoeye/Worldview
NOAT0051	Retrogressive Thaw Slump	IKONOS/Geoeye/Worldview
NOAT0052	Retrogressive Thaw Slump	IKONOS/Geoeye/Worldview
NOAT0055	Active Layer Detachment Slide	IKONOS/Geoeye/Worldview
NOAT0056	Retrogressive Thaw Slump	IKONOS/Geoeye/Worldview
NOAT0057	Retrogressive Thaw Slump	IKONOS/Geoeye/Worldview
NOAT0058	Active Layer Detachment Slide	IKONOS/Geoeye/Worldview
NOAT0059	Active Layer Detachment Slide	IKONOS/Geoeye/Worldview
NOAT0060	Active Layer Detachment Slide	IKONOS/Geoeye/Worldview
NOAT0061	Active Layer Detachment Slide	IKONOS/Geoeye/Worldview
NOAT0062	Active Layer Detachment Slide	IKONOS/Geoeye/Worldview
NOAT0063	Active Layer Detachment Slide	IKONOS/Geoeye/Worldview
NOAT0064	Active Layer Detachment Slide	IKONOS/Geoeye/Worldview
NOAT0065	Active Layer Detachment Slide	IKONOS/Geoeye/Worldview
NOAT0066	Active Layer Detachment Slide	IKONOS/Geoeye/Worldview
NOAT0067	Active Layer Detachment Slide	IKONOS/Geoeye/Worldview

NPS	2010	68.00394	-161.45324
NPS	2010	67.95394	-161.63501
NPS	2010	67.95368	-161.63448
NPS	2010	67.98710	-161.87486
NPS	2010	68.01502	-159.25482
NPS	2010	68.03621	-159.29165
NPS	2010	68.02698	-159.22966
NPS	2010	68.02754	-159.22996
NPS	2010	68.02418	-159.23490
NPS	2010	67.97497	-158.52041
NPS	2010	67.97422	-158.51909
NPS	2010	67.97307	-158.51810
NPS	2010	67.97161	-158.51512
NPS	2010	67.97061	-158.51210
NPS	2010	67.97213	-158.51765
NPS	2010	67.95497	-158.47481
NPS	2010	67.95642	-158.47513
NPS	2010	67.84003	-156.58286
NPS	2010	67.84946	-156.61602
NPS	2010	67.91311	-156.95429
NPS	2010	67.91844	-158.02307
NPS	2010	67.91747	-158.02310
NPS	2010	67.88192	-158.21464
NPS	2010	67.88145	-158.21603
NPS	2010	67.88129	-158.21679
NPS	2010	67.88012	-158.22628
NPS	2010	67.86920	-158.24945
NPS	2010	67.87346	-158.24809
NPS	2010	67.87742	-158.24687
NPS	2010	67.91551	-158.35599
NPS	2010	67.91621	-158.35649
NPS	2010	67.91819	-158.35720

NOAT0068	Retrogressive Thaw Slump	IKONOS/Geoeye/Worldview
NOAT0069	Retrogressive Thaw Slump	IKONOS/Geoeye/Worldview
NOAT0070	Retrogressive Thaw Slump	IKONOS/Geoeye/Worldview
NOAT0071	Retrogressive Thaw Slump	IKONOS/Geoeye/Worldview
NOAT0072	Retrogressive Thaw Slump	IKONOS/Geoeye/Worldview
NOAT0073	Retrogressive Thaw Slump	IKONOS/Geoeye/Worldview
NOAT0074	Retrogressive Thaw Slump	IKONOS/Geoeye/Worldview
NOAT0075	Retrogressive Thaw Slump	IKONOS/Geoeye/Worldview
NOAT0076	Retrogressive Thaw Slump	IKONOS/Geoeye/Worldview
NOAT0077	Retrogressive Thaw Slump	IKONOS/Geoeye/Worldview
NOAT0078	Retrogressive Thaw Slump	IKONOS/Geoeye/Worldview
NOAT0079	Retrogressive Thaw Slump	IKONOS/Geoeye/Worldview
NOAT0080	Retrogressive Thaw Slump	IKONOS/Geoeye/Worldview
NOAT0081	Retrogressive Thaw Slump	IKONOS/Geoeye/Worldview
NOAT0082	Retrogressive Thaw Slump	IKONOS/Geoeye/Worldview
NOAT0083	Retrogressive Thaw Slump	IKONOS/Geoeye/Worldview
NOAT0084	Retrogressive Thaw Slump	IKONOS/Geoeye/Worldview
NOAT0085	Retrogressive Thaw Slump	IKONOS/Geoeye/Worldview
NOAT0086	Retrogressive Thaw Slump	IKONOS/Geoeye/Worldview
NOAT0087	Retrogressive Thaw Slump	IKONOS/Geoeye/Worldview
NOAT0088	Retrogressive Thaw Slump	IKONOS/Geoeye/Worldview
NOAT0089	Retrogressive Thaw Slump	IKONOS/Geoeye/Worldview
NOAT0090	Retrogressive Thaw Slump	IKONOS/Geoeye/Worldview
NOAT0091	Retrogressive Thaw Slump	IKONOS/Geoeye/Worldview
NOAT0092	Retrogressive Thaw Slump	IKONOS/Geoeye/Worldview
NOAT0093	Retrogressive Thaw Slump	IKONOS/Geoeye/Worldview
NOAT0094	Retrogressive Thaw Slump	IKONOS/Geoeye/Worldview
NOAT0095	Retrogressive Thaw Slump	IKONOS/Geoeye/Worldview
NOAT0096	Retrogressive Thaw Slump	IKONOS/Geoeye/Worldview
NOAT0097	Retrogressive Thaw Slump	IKONOS/Geoeye/Worldview
NOAT0098	Retrogressive Thaw Slump	IKONOS/Geoeye/Worldview
NOAT0099	Retrogressive Thaw Slump	IKONOS/Geoeye/Worldview

NPS	2010	67.96132	-156.78851
NPS	2010	67.96093	-156.79281
NPS	2010	67.95953	-156.82848
NPS	2010	67.94296	-156.80042
NPS	2010	67.94399	-156.80676
NPS	2010	67.94791	-156.81910
NPS	2010	67.89817	-156.60057
NPS	2010	67.89268	-156.59836
NPS	2010	67.89466	-156.60457
NPS	2010	67.89234	-156.57772
NPS	2010	67.96564	-156.83869
NPS	2010	67.96682	-156.84121
NPS	2010	67.96660	-157.09439
NPS	2010	67.98158	-157.07546
NPS	2010	67.89478	-157.25347
NPS	2010	67.89661	-157.24791
NPS	2010	67.90640	-156.69777
NPS	2010	67.90614	-156.69785
NPS	2010	67.90582	-156.69765
NPS	2010	67.90549	-156.69661
NPS	2010	67.89400	-156.62718
NPS	2010	67.89344	-156.62591
NPS	2010	67.89293	-156.62506
NPS	2010	67.89304	-156.62383
NPS	2010	67.89298	-156.62238
NPS	2010	67.89303	-156.62156
NPS	2010	67.89576	-156.60459
NPS	2010	67.98658	-157.68934
NPS	2010	67.98180	-157.41250
NPS	2010	67.98171	-157.42148
NPS	2010	67.98116	-157.42088
NPS	2010	68.05923	-157.76834

NOAT0100	Active Layer Detachment Slide	IKONOS/Geoeye/Worldview
NOAT0101	Active Layer Detachment Slide	IKONOS/Geoeye/Worldview
NOAT0102	Retrogressive Thaw Slump	IKONOS/Geoeye/Worldview
NOAT0103	Active Layer Detachment Slide	IKONOS/Geoeye/Worldview
NOAT0104	Retrogressive Thaw Slump	IKONOS/Geoeye/Worldview
NOAT0105	Retrogressive Thaw Slump	IKONOS/Geoeye/Worldview
NOAT0106	Retrogressive Thaw Slump	IKONOS/Geoeye/Worldview
NOAT0107	Retrogressive Thaw Slump	IKONOS/Geoeye/Worldview
NOAT0108	Retrogressive Thaw Slump	IKONOS/Geoeye/Worldview
NOAT0109	Retrogressive Thaw Slump	IKONOS/Geoeye/Worldview
NOAT0110	Retrogressive Thaw Slump	IKONOS/Geoeye/Worldview
NOAT0111	Retrogressive Thaw Slump	IKONOS/Geoeye/Worldview
NOAT0112	Retrogressive Thaw Slump	IKONOS/Geoeye/Worldview
NOAT0113	Retrogressive Thaw Slump	IKONOS/Geoeye/Worldview
NOAT0114	Retrogressive Thaw Slump	IKONOS/Geoeye/Worldview
NOAT0115	Retrogressive Thaw Slump	IKONOS/Geoeye/Worldview
NOAT0116	Retrogressive Thaw Slump	IKONOS/Geoeye/Worldview
NOAT0117	Retrogressive Thaw Slump	IKONOS/Geoeye/Worldview
NOAT0118	Retrogressive Thaw Slump	IKONOS/Geoeye/Worldview
NOAT0119	Retrogressive Thaw Slump	IKONOS/Geoeye/Worldview
NOAT0120	Active Layer Detachment Slide	IKONOS/Geoeye/Worldview
NOAT0121	Active Layer Detachment Slide	IKONOS/Geoeye/Worldview
NOAT0122	Active Layer Detachment Slide	IKONOS/Geoeye/Worldview
NOAT0123	Active Layer Detachment Slide	IKONOS/Geoeye/Worldview
NOAT0124	Active Layer Detachment Slide	IKONOS/Geoeye/Worldview
NOAT0125	Active Layer Detachment Slide	IKONOS/Geoeye/Worldview
NOAT0126	Active Layer Detachment Slide	IKONOS/Geoeye/Worldview
NOAT0127	Active Layer Detachment Slide	IKONOS/Geoeye/Worldview
NOAT0128	Active Layer Detachment Slide	IKONOS/Geoeye/Worldview
NOAT0129	Active Layer Detachment Slide	IKONOS/Geoeye/Worldview
NOAT0130	Active Layer Detachment Slide	IKONOS/Geoeye/Worldview
NOAT0131	Active Layer Detachment Slide	IKONOS/Geoeye/Worldview

NPS	2010	68.07215	-157.73918
NPS	2010	68.07490	-157.64906
NPS	2010	68.07786	-157.60890
NPS	2010	68.07969	-157.62370
NPS	2010	68.07966	-157.62737
NPS	2010	68.07926	-157.61632
NPS	2010	68.07900	-157.61336
NPS	2010	68.07749	-157.56881
NPS	2010	67.90169	-157.41672
NPS	2010	68.07963	-157.62526
NPS	2010	68.07937	-157.61820
NPS	2010	68.07769	-157.57443
NPS	2010	68.07656	-157.57592
NPS	2010	68.07694	-157.56653
NPS	2010	68.07380	-157.54519
NPS	2010	68.07526	-157.54450
NPS	2010	68.07640	-157.54619
NPS	2010	68.07519	-157.54778
NPS	2010	68.06618	-157.45312
NPS	2010	68.02468	-157.85515
NPS	2010	68.08944	-156.93590
NPS	2010	68.08913	-156.92858
NPS	2010	68.08914	-156.91848
NPS	2010	68.06552	-156.73625
NPS	2010	68.06356	-156.73248
NPS	2010	68.06006	-156.73234
NPS	2010	68.06025	-156.73678
NPS	2010	68.06046	-156.73020
NPS	2010	68.06332	-156.73933
NPS	2010	68.06760	-156.73876
NPS	2010	68.07023	-156.61586
NPS	2010	68.06979	-156.61443

NOAT0132	Active Layer Detachment Slide	IKONOS/Geoeye/Worldview
NOAT0133	Active Layer Detachment Slide	IKONOS/Geoeye/Worldview
NOAT0134	Active Layer Detachment Slide	IKONOS/Geoeye/Worldview
NOAT0136	Active Layer Detachment Slide	IKONOS/Geoeye/Worldview
NOAT0137	Active Layer Detachment Slide	IKONOS/Geoeye/Worldview
NOAT0138	Active Layer Detachment Slide	IKONOS/Geoeye/Worldview
NOAT0139	Active Layer Detachment Slide	IKONOS/Geoeye/Worldview
NOAT0140	Active Layer Detachment Slide	IKONOS/Geoeye/Worldview
NOAT0141	Active Layer Detachment Slide	IKONOS/Geoeye/Worldview
NOAT0142	Active Layer Detachment Slide	IKONOS/Geoeye/Worldview
NOAT0145	Active Layer Detachment Slide	IKONOS/Geoeye/Worldview
NOAT0146	Retrogressive Thaw Slump	IKONOS/Geoeye/Worldview
NOAT0147	Active Layer Detachment Slide	IKONOS/Geoeye/Worldview
NOAT0148	Retrogressive Thaw Slump	IKONOS/Geoeye/Worldview
NOAT0149	Retrogressive Thaw Slump	IKONOS/Geoeye/Worldview
NOAT0150	Retrogressive Thaw Slump	IKONOS/Geoeye/Worldview
NOAT0151	Retrogressive Thaw Slump	IKONOS/Geoeye/Worldview
NOAT0152	Retrogressive Thaw Slump	IKONOS/Geoeye/Worldview
NOAT0153	Retrogressive Thaw Slump	IKONOS/Geoeye/Worldview
NOAT0154	Retrogressive Thaw Slump	IKONOS/Geoeye/Worldview
NOAT0155	Retrogressive Thaw Slump	IKONOS/Geoeye/Worldview
NOAT0156	Retrogressive Thaw Slump	IKONOS/Geoeye/Worldview
NOAT0157	Retrogressive Thaw Slump	IKONOS/Geoeye/Worldview
NOAT0158	Retrogressive Thaw Slump	IKONOS/Geoeye/Worldview
NOAT0159	Retrogressive Thaw Slump	IKONOS/Geoeye/Worldview
NOAT0160	Retrogressive Thaw Slump	IKONOS/Geoeye/Worldview
NOAT0161	Retrogressive Thaw Slump	IKONOS/Geoeye/Worldview
NOAT0162	Retrogressive Thaw Slump	IKONOS/Geoeye/Worldview
NOAT0163	Retrogressive Thaw Slump	IKONOS/Geoeye/Worldview
NOAT0164	Retrogressive Thaw Slump	IKONOS/Geoeye/Worldview
NOAT0165	Retrogressive Thaw Slump	IKONOS/Geoeye/Worldview
NOAT0166	Retrogressive Thaw Slump	IKONOS/Geoeye/Worldview

NPS	2010	68.07331	-156.69854
NPS	2010	68.07476	-156.69652
NPS	2010	68.07397	-156.69605
NPS	2010	68.08431	-156.59221
NPS	2010	68.05131	-156.68777
NPS	2010	68.03103	-156.74664
NPS	2010	68.03010	-156.74416
NPS	2010	68.02698	-156.73944
NPS	2010	68.04715	-156.77572
NPS	2010	68.03345	-156.82210
NPS	2010	68.03772	-157.09267
NPS	2010	68.00299	-157.19820
NPS	2010	68.02185	-156.51960
NPS	2010	67.87708	-157.53254
NPS	2010	67.90213	-157.41219
NPS	2010	67.89957	-157.38866
NPS	2010	67.86317	-157.52687
NPS	2010	67.80467	-157.89514
NPS	2010	67.80398	-157.89753
NPS	2010	67.83562	-157.41037
NPS	2010	67.83635	-157.41251
NPS	2010	67.83505	-157.36900
NPS	2010	67.83286	-157.35259
NPS	2010	67.82720	-157.34974
NPS	2010	67.88336	-156.73598
NPS	2010	67.88145	-156.73540
NPS	2010	67.89384	-156.54784
NPS	2010	67.86204	-156.66171
NPS	2010	67.85805	-156.65442
NPS	2010	67.87412	-156.75995
NPS	2010	67.87464	-156.75236
NPS	2010	67.87437	-156.75848

NOAT0168	Active Layer Detachment Slide	IKONOS/Geoeye/Worldview
NOAT0169	Retrogressive Thaw Slump	IKONOS/Geoeye/Worldview
NOAT0170	Retrogressive Thaw Slump	IKONOS/Geoeye/Worldview
NOAT0171	Active Layer Detachment Slide	IKONOS/Geoeye/Worldview
NOAT0172	Retrogressive Thaw Slump	IKONOS/Geoeye/Worldview
NOAT0175	Retrogressive Thaw Slump	IKONOS/Geoeye/Worldview
NOAT0176	Retrogressive Thaw Slump	IKONOS/Geoeye/Worldview
NOAT0177	Retrogressive Thaw Slump	IKONOS/Geoeye/Worldview
NOAT0178	Retrogressive Thaw Slump	IKONOS/Geoeye/Worldview
NOAT0180	Retrogressive Thaw Slump	IKONOS/Geoeye/Worldview
NOAT0182	Active Layer Detachment Slide	IKONOS/Geoeye/Worldview
NOAT0183	Retrogressive Thaw Slump	IKONOS/Geoeye/Worldview
NOAT0184	Retrogressive Thaw Slump	IKONOS/Geoeye/Worldview
NOAT0185	Retrogressive Thaw Slump	IKONOS/Geoeye/Worldview
NOAT0186	Active Layer Detachment Slide	IKONOS/Geoeye/Worldview
NOAT0187	Active Layer Detachment Slide	IKONOS/Geoeye/Worldview
NOAT0188	Retrogressive Thaw Slump	IKONOS/Geoeye/Worldview
NOAT0189	Retrogressive Thaw Slump	IKONOS/Geoeye/Worldview
NOAT0190	Retrogressive Thaw Slump	IKONOS/Geoeye/Worldview
NOAT0191	Active Layer Detachment Slide	IKONOS/Geoeye/Worldview
NOAT0192	Active Layer Detachment Slide	IKONOS/Geoeye/Worldview
NOAT0193	Active Layer Detachment Slide	IKONOS/Geoeye/Worldview
NOAT0194	Retrogressive Thaw Slump	IKONOS/Geoeye/Worldview
NOAT0195	Active Layer Detachment Slide	IKONOS/Geoeye/Worldview
NOAT0196	Active Layer Detachment Slide	IKONOS/Geoeye/Worldview
NOAT0197	Active Layer Detachment Slide	IKONOS/Geoeye/Worldview
NOAT0198	Active Layer Detachment Slide	IKONOS/Geoeye/Worldview
NOAT0199	Active Layer Detachment Slide	IKONOS/Geoeye/Worldview
NOAT0200	Active Layer Detachment Slide	IKONOS/Geoeye/Worldview
NOAT0201	Active Layer Detachment Slide	IKONOS/Geoeye/Worldview
NOAT0202	Active Layer Detachment Slide	IKONOS/Geoeye/Worldview
NOAT0203	Active Layer Detachment Slide	IKONOS/Geoeye/Worldview

NPS	2010	67.85701	-157.13277
NPS	2010	67.84440	-157.13824
NPS	2010	67.84257	-157.11551
NPS	2010	67.81636	-157.17243
NPS	2010	67.80675	-156.68179
NPS	2010	67.80130	-156.76825
NPS	2010	67.98185	-157.41502
NPS	2010	67.94747	-156.81547
NPS	2010	67.94361	-156.80368
NPS	2010	68.05308	-159.64844
NPS	2010	68.00451	-158.57965
NPS	2010	68.08817	-158.63931
NPS	2010	68.08734	-159.18267
NPS	2010	68.08799	-159.18207
NPS	2010	68.00199	-158.58436
NPS	2010	68.00686	-158.64983
NPS	2010	68.02029	-158.70887
NPS	2010	68.02841	-159.23956
NPS	2010	68.03394	-159.28752
NPS	2010	67.95098	-159.65669
NPS	2010	67.95278	-159.65472
NPS	2010	67.95425	-159.82655
NPS	2010	68.02814	-159.23056
NPS	2010	67.94934	-159.47097
NPS	2010	67.95072	-159.46705
NPS	2010	67.95122	-159.46197
NPS	2010	67.95159	-159.45955
NPS	2010	67.95025	-159.46196
NPS	2010	67.94949	-159.46005
NPS	2010	67.94818	-159.46151
NPS	2010	67.94856	-159.46198
NPS	2010	67.94809	-159.48703

NOAT0204	Active Layer Detachment Slide	IKONOS/Geoeye/Worldview
NOAT0205	Active Layer Detachment Slide	IKONOS/Geoeye/Worldview
NOAT0206	Active Layer Detachment Slide	IKONOS/Geoeye/Worldview
NOAT0207	Retrogressive Thaw Slump	IKONOS/Geoeye/Worldview
NOAT0208	Retrogressive Thaw Slump	IKONOS/Geoeye/Worldview
NOAT0209	Retrogressive Thaw Slump	IKONOS/Geoeye/Worldview
NOAT0210	Active Layer Detachment Slide	IKONOS/Geoeye/Worldview
NOAT0212	Retrogressive Thaw Slump	IKONOS/Geoeye/Worldview
NOAT0213	Retrogressive Thaw Slump	IKONOS/Geoeye/Worldview
NOAT0214	Active Layer Detachment Slide	IKONOS/Geoeye/Worldview
NOAT0215	Retrogressive Thaw Slump	IKONOS/Geoeye/Worldview
NOAT0216	Retrogressive Thaw Slump	IKONOS/Geoeye/Worldview
NOAT0217	Retrogressive Thaw Slump	IKONOS/Geoeye/Worldview
NOAT0218	Active Layer Detachment Slide	IKONOS/Geoeye/Worldview
NOAT0219	Active Layer Detachment Slide	IKONOS/Geoeye/Worldview
NOAT0220	Retrogressive Thaw Slump	IKONOS/Geoeye/Worldview
NOAT0221	Active Layer Detachment Slide	IKONOS/Geoeye/Worldview
NOAT0222	Retrogressive Thaw Slump	IKONOS/Geoeye/Worldview
NOAT0223	Retrogressive Thaw Slump	IKONOS/Geoeye/Worldview
NOAT0224	Active Layer Detachment Slide	IKONOS/Geoeye/Worldview
NOAT0225	Retrogressive Thaw Slump	IKONOS/Geoeye/Worldview
NOAT0226	Retrogressive Thaw Slump	IKONOS/Geoeye/Worldview
NOAT0227	Active Layer Detachment Slide	IKONOS/Geoeye/Worldview
NOAT0228	Retrogressive Thaw Slump	IKONOS/Geoeye/Worldview
NOAT0229	Retrogressive Thaw Slump	IKONOS/Geoeye/Worldview
NOAT0230	Retrogressive Thaw Slump	IKONOS/Geoeye/Worldview
NOAT0231	Retrogressive Thaw Slump	IKONOS/Geoeye/Worldview
NOAT0232	Retrogressive Thaw Slump	IKONOS/Geoeye/Worldview
NOAT0233	Active Layer Detachment Slide	IKONOS/Geoeye/Worldview
NOAT0234	Active Layer Detachment Slide	IKONOS/Geoeye/Worldview
NOAT0236	Retrogressive Thaw Slump	IKONOS/Geoeye/Worldview
NOAT0237	Retrogressive Thaw Slump	IKONOS/Geoeye/Worldview

NPS	2010	67.94762	-159.48521
NPS	2010	67.94660	-159.12261
NPS	2010	67.90760	-158.89162
NPS	2010	67.90082	-158.05942
NPS	2010	67.89942	-158.06290
NPS	2010	67.85150	-158.33431
NPS	2010	67.85749	-158.27847
NPS	2010	67.80533	-157.97178
NPS	2010	67.79292	-157.98466
NPS	2010	67.78978	-158.38556
NPS	2010	67.79778	-158.47223
NPS	2010	67.79220	-158.47192
NPS	2010	67.79088	-158.47179
NPS	2010	67.78623	-158.33839
NPS	2010	67.78537	-158.33690
NPS	2010	67.78420	-158.33260
NPS	2010	67.78361	-158.37248
NPS	2010	67.85725	-158.27666
NPS	2010	67.78169	-157.66133
NPS	2010	67.72473	-157.70455
NPS	2010	67.78784	-156.69325
NPS	2010	67.80184	-156.76821
NPS	2010	67.49536	-157.39400
NPS	2010	67.73398	-158.65885
NPS	2010	67.73353	-158.66745
NPS	2010	67.73075	-158.66685
NPS	2010	67.73235	-158.67169
NPS	2010	67.73180	-158.60211
NPS	2010	67.70936	-158.85803
NPS	2010	67.70722	-158.87583
NPS	2010	67.73364	-158.14481
NPS	2010	67.70524	-157.93561

NOAT0238	Retrogressive Thaw Slump	IKONOS/Geoeye/Worldview
NOAT0239	Retrogressive Thaw Slump	IKONOS/Geoeye/Worldview
NOAT0240	Retrogressive Thaw Slump	IKONOS/Geoeye/Worldview
NOAT0241	Retrogressive Thaw Slump	IKONOS/Geoeye/Worldview
NOAT0242	Retrogressive Thaw Slump	IKONOS/Geoeye/Worldview
NOAT0243	Retrogressive Thaw Slump	IKONOS/Geoeye/Worldview
NOAT0244	Retrogressive Thaw Slump	IKONOS/Geoeye/Worldview
NOAT0245	Active Layer Detachment Slide	IKONOS/Geoeye/Worldview
NOAT0246	Active Layer Detachment Slide	IKONOS/Geoeye/Worldview
NOAT0247	Retrogressive Thaw Slump	IKONOS/Geoeye/Worldview
NOAT0248	Retrogressive Thaw Slump	IKONOS/Geoeye/Worldview
NOAT0249	Retrogressive Thaw Slump	IKONOS/Geoeye/Worldview
NOAT0250	Retrogressive Thaw Slump	IKONOS/Geoeye/Worldview
NOAT0251	Retrogressive Thaw Slump	IKONOS/Geoeye/Worldview
NOAT0252	Active Layer Detachment Slide	IKONOS/Geoeye/Worldview
NOAT0253	Active Layer Detachment Slide	IKONOS/Geoeye/Worldview
NOAT0254	Active Layer Detachment Slide	IKONOS/Geoeye/Worldview
NOAT0255	Active Layer Detachment Slide	IKONOS/Geoeye/Worldview
NOAT0256	Active Layer Detachment Slide	IKONOS/Geoeye/Worldview
NOAT0257	Active Layer Detachment Slide	IKONOS/Geoeye/Worldview
NOAT0258	Active Layer Detachment Slide	IKONOS/Geoeye/Worldview
NOAT0259	Retrogressive Thaw Slump	IKONOS/Geoeye/Worldview
NOAT0260	Active Layer Detachment Slide	IKONOS/Geoeye/Worldview
NOAT0261	Retrogressive Thaw Slump	IKONOS/Geoeye/Worldview
NOAT0262	Retrogressive Thaw Slump	IKONOS/Geoeye/Worldview
NOAT0263	Retrogressive Thaw Slump	IKONOS/Geoeye/Worldview
NOAT0264	Active Layer Detachment Slide	IKONOS/Geoeye/Worldview
NOAT0265	Retrogressive Thaw Slump	IKONOS/Geoeye/Worldview
NOAT0267	Retrogressive Thaw Slump	IKONOS/Geoeye/Worldview
NOAT0268	Active Layer Detachment Slide	IKONOS/Geoeye/Worldview
NOAT0269	Active Layer Detachment Slide	IKONOS/Geoeye/Worldview
NOAT0270	Retrogressive Thaw Slump	IKONOS/Geoeye/Worldview

NPS	2010	67.70437	-157.93625
NPS	2010	67.70602	-157.32941
NPS	2010	67.70583	-157.32717
NPS	2010	67.70325	-157.31912
NPS	2010	67.70235	-157.31482
NPS	2010	67.70274	-157.31309
NPS	2010	67.70100	-157.31197
NPS	2010	67.70013	-157.28075
NPS	2010	67.70117	-157.26646
NPS	2010	67.67005	-157.85191
NPS	2010	67.67102	-157.85306
NPS	2010	67.67200	-157.85470
NPS	2010	67.67259	-157.85342
NPS	2010	67.69164	-157.26421
NPS	2010	67.69795	-157.25252
NPS	2010	67.68664	-157.25296
NPS	2010	67.67802	-157.23771
NPS	2010	67.67489	-157.24245
NPS	2010	67.66735	-157.22572
NPS	2010	67.64862	-157.22508
NPS	2010	67.92234	-158.35700
NPS	2010	68.05241	-158.57326
NPS	2010	68.00408	-158.48105
NPS	2010	68.08823	-158.04046
NPS	2010	68.08407	-158.02714
NPS	2010	68.08275	-158.02121
NPS	2010	68.16003	-157.98393
NPS	2010	67.94756	-161.09116
NPS	2010	67.88361	-156.73766
NPS	2010	68.19029	-157.95068
NPS	2010	68.18140	-157.87056
NPS	2010	68.16927	-157.56506

NOAT0271	Active Layer Detachment Slide	IKONOS/Geoeye/Worldview
NOAT0272	Active Layer Detachment Slide	IKONOS/Geoeye/Worldview
NOAT0273	Active Layer Detachment Slide	IKONOS/Geoeye/Worldview
NOAT0274	Active Layer Detachment Slide	IKONOS/Geoeye/Worldview
NOAT0275	Active Layer Detachment Slide	IKONOS/Geoeye/Worldview
NOAT0276	Active Layer Detachment Slide	IKONOS/Geoeye/Worldview
NOAT0277	Active Layer Detachment Slide	IKONOS/Geoeye/Worldview
NOAT0278	Active Layer Detachment Slide	IKONOS/Geoeye/Worldview
NOAT0279	Active Layer Detachment Slide	IKONOS/Geoeye/Worldview
NOAT0280	Active Layer Detachment Slide	IKONOS/Geoeye/Worldview
NOAT0281	Retrogressive Thaw Slump	IKONOS/Geoeye/Worldview
NOAT0282	Active Layer Detachment Slide	IKONOS/Geoeye/Worldview
NOAT0283	Active Layer Detachment Slide	IKONOS/Geoeye/Worldview
NOAT0284	Active Layer Detachment Slide	IKONOS/Geoeye/Worldview
NOAT0285	Active Layer Detachment Slide	IKONOS/Geoeye/Worldview
NOAT0286	Active Layer Detachment Slide	IKONOS/Geoeye/Worldview
NOAT0287	Active Layer Detachment Slide	IKONOS/Geoeye/Worldview
NOAT0288	Active Layer Detachment Slide	IKONOS/Geoeye/Worldview
NOAT0289	Active Layer Detachment Slide	IKONOS/Geoeye/Worldview
NOAT0290	Active Layer Detachment Slide	IKONOS/Geoeye/Worldview
NOAT0291	Active Layer Detachment Slide	IKONOS/Geoeye/Worldview
NOAT0292	Active Layer Detachment Slide	IKONOS/Geoeye/Worldview
NOAT0293	Active Layer Detachment Slide	IKONOS/Geoeye/Worldview
NOAT0294	Active Layer Detachment Slide	IKONOS/Geoeye/Worldview
NOAT0295	Active Layer Detachment Slide	IKONOS/Geoeye/Worldview
NOAT0296	Active Layer Detachment Slide	IKONOS/Geoeye/Worldview
NOAT0297	Active Layer Detachment Slide	IKONOS/Geoeye/Worldview
NOAT0298	Active Layer Detachment Slide	IKONOS/Geoeye/Worldview
NOAT0299	Active Layer Detachment Slide	IKONOS/Geoeye/Worldview
NOAT0300	Active Layer Detachment Slide	IKONOS/Geoeye/Worldview
NOAT0301	Active Layer Detachment Slide	IKONOS/Geoeye/Worldview
NOAT0302	Active Layer Detachment Slide	IKONOS/Geoeye/Worldview

NPS	2010	68.09527	-157.58354
NPS	2010	68.08804	-157.51999
NPS	2010	68.08675	-157.52302
NPS	2010	68.08849	-157.49111
NPS	2010	68.09258	-157.54564
NPS	2010	68.09360	-157.39708
NPS	2010	68.09380	-157.37852
NPS	2010	68.09134	-157.43876
NPS	2010	68.09796	-157.35974
NPS	2010	68.09852	-157.35849
NPS	2010	68.15915	-157.08484
NPS	2010	68.13054	-157.20966
NPS	2010	68.12833	-157.21575
NPS	2010	68.09394	-157.30966
NPS	2010	68.10746	-157.29726
NPS	2010	68.10365	-157.29167
NPS	2010	68.11529	-157.24135
NPS	2010	68.11346	-157.24134
NPS	2010	68.09610	-157.03736
NPS	2010	68.09407	-157.04420
NPS	2010	68.09271	-157.04032
NPS	2010	68.09826	-156.99671
NPS	2010	68.10393	-157.01986
NPS	2010	68.09418	-156.93200
NPS	2010	68.18036	-156.65027
NPS	2010	68.18422	-156.64206
NPS	2010	68.17097	-156.63113
NPS	2010	68.17161	-156.62529
NPS	2010	68.16814	-156.61636
NPS	2010	68.17022	-156.58266
NPS	2010	68.17605	-156.56819
NPS	2010	68.17398	-156.56997

NOAT0303	Active Layer Detachment Slide	IKONOS/Geoeye/Worldview
NOAT0304	Active Layer Detachment Slide	IKONOS/Geoeye/Worldview
NOAT0305	Active Layer Detachment Slide	IKONOS/Geoeye/Worldview
NOAT0306	Active Layer Detachment Slide	IKONOS/Geoeye/Worldview
NOAT0307	Active Layer Detachment Slide	IKONOS/Geoeye/Worldview
NOAT0308	Active Layer Detachment Slide	IKONOS/Geoeye/Worldview
NOAT0309	Active Layer Detachment Slide	IKONOS/Geoeye/Worldview
NOAT0310	Active Layer Detachment Slide	IKONOS/Geoeye/Worldview
NOAT0311	Active Layer Detachment Slide	IKONOS/Geoeye/Worldview
NOAT0312	Active Layer Detachment Slide	IKONOS/Geoeye/Worldview
NOAT0313	Active Layer Detachment Slide	IKONOS/Geoeye/Worldview
NOAT0314	Active Layer Detachment Slide	IKONOS/Geoeye/Worldview
NOAT0315	Active Layer Detachment Slide	IKONOS/Geoeye/Worldview
NOAT0316	Active Layer Detachment Slide	IKONOS/Geoeye/Worldview
NOAT0317	Active Layer Detachment Slide	IKONOS/Geoeye/Worldview
NOAT0318	Active Layer Detachment Slide	IKONOS/Geoeye/Worldview
NOAT0319	Active Layer Detachment Slide	IKONOS/Geoeye/Worldview
NOAT0320	Active Layer Detachment Slide	IKONOS/Geoeye/Worldview
NOAT0321	Active Layer Detachment Slide	IKONOS/Geoeye/Worldview
NOAT0322	Active Layer Detachment Slide	IKONOS/Geoeye/Worldview
NOAT0323	Active Layer Detachment Slide	IKONOS/Geoeye/Worldview
NOAT0324	Active Layer Detachment Slide	IKONOS/Geoeye/Worldview
NOAT0325	Retrogressive Thaw Slump	IKONOS/Geoeye/Worldview
NOAT0326	Retrogressive Thaw Slump	IKONOS/Geoeye/Worldview
NOAT0327	Retrogressive Thaw Slump	IKONOS/Geoeye/Worldview
NOAT0328	Active Layer Detachment Slide	IKONOS/Geoeye/Worldview
NOAT0329	Active Layer Detachment Slide	IKONOS/Geoeye/Worldview
NOAT0330	Active Layer Detachment Slide	IKONOS/Geoeye/Worldview
NOAT0331	Retrogressive Thaw Slump	IKONOS/Geoeye/Worldview
NOAT0332	Retrogressive Thaw Slump	IKONOS/Geoeye/Worldview
NOAT0333	Retrogressive Thaw Slump	IKONOS/Geoeye/Worldview
NOAT0334	Retrogressive Thaw Slump	IKONOS/Geoeye/Worldview

NPS	2010	68.17900	-156.56662
NPS	2010	68.17962	-156.56525
NPS	2010	68.16789	-156.35462
NPS	2010	68.17106	-156.34280
NPS	2010	68.16775	-156.33259
NPS	2010	68.16887	-156.32768
NPS	2010	68.17104	-156.32919
NPS	2010	68.15549	-156.16112
NPS	2010	68.15360	-156.15930
NPS	2010	68.14992	-156.15696
NPS	2010	68.15339	-156.15689
NPS	2010	68.15059	-156.15187
NPS	2010	68.15535	-156.14906
NPS	2010	68.15819	-156.17874
NPS	2010	68.15319	-156.17950
NPS	2010	68.15902	-156.18517
NPS	2010	68.15171	-156.20465
NPS	2010	68.14415	-156.63281
NPS	2010	68.07195	-156.43612
NPS	2010	68.07163	-156.43200
NPS	2010	68.07148	-156.42825
NPS	2010	68.06749	-156.45432
NPS	2010	68.06384	-156.49358
NPS	2010	68.06431	-156.49419
NPS	2010	68.06481	-156.49504
NPS	2010	68.06809	-156.40010
NPS	2010	68.06983	-156.40883
NPS	2010	68.06534	-156.20964
NPS	2010	68.08849	-155.90011
NPS	2010	68.08785	-155.89976
NPS	2010	68.08359	-155.86206
NPS	2010	68.08063	-155.80059

NOAT0335	Retrogressive Thaw Slump	IKONOS/Geoeye/Worldview
NOAT0336	Retrogressive Thaw Slump	IKONOS/Geoeye/Worldview
NOAT0337	Active Layer Detachment Slide	IKONOS/Geoeye/Worldview
NOAT0338	Active Layer Detachment Slide	IKONOS/Geoeye/Worldview
NOAT0339	Active Layer Detachment Slide	IKONOS/Geoeye/Worldview
NOAT0340	Active Layer Detachment Slide	IKONOS/Geoeye/Worldview
NOAT0341	Active Layer Detachment Slide	IKONOS/Geoeye/Worldview
NOAT0342	Active Layer Detachment Slide	IKONOS/Geoeye/Worldview
NOAT0343	Active Layer Detachment Slide	IKONOS/Geoeye/Worldview
NOAT0344	Active Layer Detachment Slide	IKONOS/Geoeye/Worldview
NOAT0345	Active Layer Detachment Slide	IKONOS/Geoeye/Worldview
NOAT0346	Active Layer Detachment Slide	IKONOS/Geoeye/Worldview
NOAT0347	Active Layer Detachment Slide	IKONOS/Geoeye/Worldview
NOAT0348	Active Layer Detachment Slide	IKONOS/Geoeye/Worldview
NOAT0349	Active Layer Detachment Slide	IKONOS/Geoeye/Worldview
NOAT0350	Active Layer Detachment Slide	IKONOS/Geoeye/Worldview
NOAT0351	Active Layer Detachment Slide	IKONOS/Geoeye/Worldview
NOAT0352	Active Layer Detachment Slide	IKONOS/Geoeye/Worldview
NOAT0353	Active Layer Detachment Slide	IKONOS/Geoeye/Worldview
NOAT0354	Active Layer Detachment Slide	IKONOS/Geoeye/Worldview
NOAT0355	Active Layer Detachment Slide	IKONOS/Geoeye/Worldview
NOAT0356	Active Layer Detachment Slide	IKONOS/Geoeye/Worldview
NOAT0357	Active Layer Detachment Slide	IKONOS/Geoeye/Worldview
NOAT0358	Active Layer Detachment Slide	IKONOS/Geoeye/Worldview
NOAT0359	Active Layer Detachment Slide	IKONOS/Geoeye/Worldview
NOAT0360	Active Layer Detachment Slide	IKONOS/Geoeye/Worldview
NOAT0361	Active Layer Detachment Slide	IKONOS/Geoeye/Worldview
NOAT0362	Active Layer Detachment Slide	IKONOS/Geoeye/Worldview
NOAT0363	Active Layer Detachment Slide	IKONOS/Geoeye/Worldview
NOAT0364	Active Layer Detachment Slide	IKONOS/Geoeye/Worldview
NOAT0365	Active Layer Detachment Slide	IKONOS/Geoeye/Worldview
NOAT0366	Active Layer Detachment Slide	IKONOS/Geoeye/Worldview

NPS	2010	68.07996	-155.79883
NPS	2010	68.07954	-155.79836
NPS	2010	68.02758	-155.89614
NPS	2010	68.03959	-155.87451
NPS	2010	68.03507	-155.93914
NPS	2010	68.03737	-155.94159
NPS	2010	68.03951	-155.94284
NPS	2010	68.03737	-155.91616
NPS	2010	68.03821	-155.92038
NPS	2010	68.03910	-155.96328
NPS	2010	68.03937	-155.96442
NPS	2010	68.04075	-155.96775
NPS	2010	68.04204	-155.97034
NPS	2010	68.04694	-155.98286
NPS	2010	68.04164	-155.98207
NPS	2010	68.04618	-156.00670
NPS	2010	68.02708	-155.99979
NPS	2010	68.03110	-155.99688
NPS	2010	68.03841	-156.01108
NPS	2010	68.03804	-156.01534
NPS	2010	68.03535	-156.01630
NPS	2010	68.03815	-156.02158
NPS	2010	68.02930	-155.98670
NPS	2010	68.02783	-155.98484
NPS	2010	68.02551	-155.95920
NPS	2010	68.02452	-155.96565
NPS	2010	68.03645	-156.15052
NPS	2010	68.03094	-156.14224
NPS	2010	68.03320	-156.14784
NPS	2010	68.03503	-156.15605
NPS	2010	68.03285	-156.16040
NPS	2010	68.03278	-156.15976

NOAT0367	Active Layer Detachment Slide	IKONOS/Geoeye/Worldview
NOAT0368	Active Layer Detachment Slide	IKONOS/Geoeye/Worldview
NOAT0369	Active Layer Detachment Slide	IKONOS/Geoeye/Worldview
NOAT0370	Active Layer Detachment Slide	IKONOS/Geoeye/Worldview
NOAT0371	Active Layer Detachment Slide	IKONOS/Geoeye/Worldview
NOAT0372	Active Layer Detachment Slide	IKONOS/Geoeye/Worldview
NOAT0373	Active Layer Detachment Slide	IKONOS/Geoeye/Worldview
NOAT0374	Active Layer Detachment Slide	IKONOS/Geoeye/Worldview
NOAT0375	Active Layer Detachment Slide	IKONOS/Geoeye/Worldview
NOAT0376	Active Layer Detachment Slide	IKONOS/Geoeye/Worldview
NOAT0377	Active Layer Detachment Slide	IKONOS/Geoeye/Worldview
NOAT0378	Active Layer Detachment Slide	IKONOS/Geoeye/Worldview
NOAT0379	Active Layer Detachment Slide	IKONOS/Geoeye/Worldview
NOAT0380	Active Layer Detachment Slide	IKONOS/Geoeye/Worldview
NOAT0381	Active Layer Detachment Slide	IKONOS/Geoeye/Worldview
NOAT0382	Active Layer Detachment Slide	IKONOS/Geoeye/Worldview
NOAT0383	Active Layer Detachment Slide	IKONOS/Geoeye/Worldview
NOAT0384	Active Layer Detachment Slide	IKONOS/Geoeye/Worldview
NOAT0385	Active Layer Detachment Slide	IKONOS/Geoeye/Worldview
NOAT0386	Active Layer Detachment Slide	IKONOS/Geoeye/Worldview
NOAT0387	Active Layer Detachment Slide	IKONOS/Geoeye/Worldview
NOAT0388	Active Layer Detachment Slide	IKONOS/Geoeye/Worldview
NOAT0389	Active Layer Detachment Slide	IKONOS/Geoeye/Worldview
NOAT0390	Active Layer Detachment Slide	IKONOS/Geoeye/Worldview
NOAT0391	Active Layer Detachment Slide	IKONOS/Geoeye/Worldview
NOAT0392	Active Layer Detachment Slide	IKONOS/Geoeye/Worldview
NOAT0393	Active Layer Detachment Slide	IKONOS/Geoeye/Worldview
NOAT0394	Active Layer Detachment Slide	IKONOS/Geoeye/Worldview
NOAT0395	Active Layer Detachment Slide	IKONOS/Geoeye/Worldview
NOAT0396	Active Layer Detachment Slide	IKONOS/Geoeye/Worldview
NOAT0397	Active Layer Detachment Slide	IKONOS/Geoeye/Worldview
NOAT0398	Active Layer Detachment Slide	IKONOS/Geoeye/Worldview

NPS	2010	68.03495	-156.15420
NPS	2010	68.02740	-156.16690
NPS	2010	68.02880	-156.16869
NPS	2010	68.02953	-156.18670
NPS	2010	68.03101	-156.20406
NPS	2010	68.03332	-156.21527
NPS	2010	68.02937	-156.22644
NPS	2010	68.05241	-156.19253
NPS	2010	68.05472	-156.19373
NPS	2010	68.04723	-156.19285
NPS	2010	68.04558	-156.18415
NPS	2010	68.04430	-156.18727
NPS	2010	68.04427	-156.18587
NPS	2010	68.04463	-156.18257
NPS	2010	68.04662	-156.18202
NPS	2010	68.04333	-156.17913
NPS	2010	68.04480	-156.17948
NPS	2010	68.04523	-156.17584
NPS	2010	68.04539	-156.16935
NPS	2010	68.04199	-156.15615
NPS	2010	68.04320	-156.15509
NPS	2010	68.03747	-156.30974
NPS	2010	68.04112	-156.29995
NPS	2010	68.03124	-156.41279
NPS	2010	68.04727	-156.40669
NPS	2010	68.04388	-156.45198
NPS	2010	67.99306	-156.19551
NPS	2010	68.00172	-156.15772
NPS	2010	68.00094	-156.15134
NPS	2010	68.27610	-157.18739
NPS	2010	68.27504	-157.18825
NPS	2010	68.28046	-157.21239

NOAT0399	Active Layer Detachment Slide	IKONOS/Geoeye/Worldview
NOAT0400	Active Layer Detachment Slide	IKONOS/Geoeye/Worldview
NOAT0401	Active Layer Detachment Slide	IKONOS/Geoeye/Worldview
NOAT0402	Active Layer Detachment Slide	IKONOS/Geoeye/Worldview
NOAT0403	Active Layer Detachment Slide	IKONOS/Geoeye/Worldview
NOAT0404	Active Layer Detachment Slide	IKONOS/Geoeye/Worldview
NOAT0405	Active Layer Detachment Slide	IKONOS/Geoeye/Worldview
NOAT0406	Active Layer Detachment Slide	IKONOS/Geoeye/Worldview
NOAT0407	Active Layer Detachment Slide	IKONOS/Geoeye/Worldview
NOAT0408	Active Layer Detachment Slide	IKONOS/Geoeye/Worldview
NOAT0409	Active Layer Detachment Slide	IKONOS/Geoeye/Worldview
NOAT0410	Active Layer Detachment Slide	IKONOS/Geoeye/Worldview
NOAT0411	Active Layer Detachment Slide	IKONOS/Geoeye/Worldview
NOAT0412	Active Layer Detachment Slide	IKONOS/Geoeye/Worldview
NOAT0413	Active Layer Detachment Slide	IKONOS/Geoeye/Worldview
NOAT0414	Active Layer Detachment Slide	IKONOS/Geoeye/Worldview
NOAT0415	Active Layer Detachment Slide	IKONOS/Geoeye/Worldview
NOAT0416	Active Layer Detachment Slide	IKONOS/Geoeye/Worldview
NOAT0417	Active Layer Detachment Slide	IKONOS/Geoeye/Worldview
NOAT0418	Active Layer Detachment Slide	IKONOS/Geoeye/Worldview
NOAT0419	Active Layer Detachment Slide	IKONOS/Geoeye/Worldview
NOAT0420	Active Layer Detachment Slide	IKONOS/Geoeye/Worldview
NOAT0421	Active Layer Detachment Slide	IKONOS/Geoeye/Worldview
NOAT0422	Active Layer Detachment Slide	IKONOS/Geoeye/Worldview
NOAT0423	Active Layer Detachment Slide	IKONOS/Geoeye/Worldview
NOAT0424	Active Layer Detachment Slide	IKONOS/Geoeye/Worldview
NOAT0425	Active Layer Detachment Slide	IKONOS/Geoeye/Worldview
NOAT0426	Active Layer Detachment Slide	IKONOS/Geoeye/Worldview
NOAT0427	Active Layer Detachment Slide	IKONOS/Geoeye/Worldview
NOAT0429	Active Layer Detachment Slide	IKONOS/Geoeye/Worldview
NOAT0430	Active Layer Detachment Slide	IKONOS/Geoeye/Worldview
NOAT0431	Active Layer Detachment Slide	IKONOS/Geoeye/Worldview

NPS	2010	68.27363	-157.21293
NPS	2010	68.27385	-157.20819
NPS	2010	68.27297	-157.20514
NPS	2010	68.27280	-157.20415
NPS	2010	68.27283	-157.19929
NPS	2010	68.27300	-157.19686
NPS	2010	68.27157	-157.19752
NPS	2010	68.27213	-157.19471
NPS	2010	68.27147	-157.19302
NPS	2010	68.27060	-157.19476
NPS	2010	68.26229	-157.18016
NPS	2010	68.26262	-157.17838
NPS	2010	68.26125	-157.17593
NPS	2010	68.26066	-157.17683
NPS	2010	68.26017	-157.17692
NPS	2010	68.26643	-157.15330
NPS	2010	68.27537	-157.14489
NPS	2010	68.27499	-157.13067
NPS	2010	68.27702	-157.12750
NPS	2010	68.27803	-157.13375
NPS	2010	68.27645	-157.11207
NPS	2010	68.27585	-157.11167
NPS	2010	68.28050	-157.13283
NPS	2010	68.27985	-157.11719
NPS	2010	68.27932	-157.11839
NPS	2010	68.27921	-157.12483
NPS	2010	68.28855	-157.14760
NPS	2010	68.28668	-157.08250
NPS	2010	68.28478	-157.07918
NPS	2010	68.28494	-157.09538
NPS	2010	68.28386	-157.09915
NPS	2010	68.28190	-157.05943

NPS	2010	68.28223	-157.05039
NPS	2010	68.27790	-157.03176
NPS	2010	68.27919	-157.03430
NPS	2010	68.27713	-157.04348
NPS	2010	68.27688	-157.03600
NPS	2010	68.27094	-157.04314
NPS	2010	68.27121	-157.04416
NPS	2010	68.27230	-157.04092
NPS	2010	68.27321	-157.03777
NPS	2010	68.27360	-157.04265
NPS	2010	68.27567	-157.04104
NPS	2010	68.27496	-157.04031
NPS	2010	68.27506	-157.03843
NPS	2010	68.27669	-157.03799
NPS	2010	68.27679	-157.00282
NPS	2010	68.27621	-157.00226
NPS	2010	68.27543	-156.99807
NPS	2010	68.27224	-156.99791
NPS	2010	68.27945	-157.01983
NPS	2010	68.27735	-157.02187
NPS	2010	68.23445	-157.01316
NPS	2010	68.23292	-157.01687
NPS	2010	68.23509	-157.01882
NPS	2010	68.23613	-157.02234
NPS	2010	68.23776	-157.01359
NPS	2010	68.23839	-157.01470
NPS	2010	68.25022	-157.07207
NPS	2010	68.24907	-157.06384
NPS	2010	68.25037	-157.06237
NPS	2010	68.24885	-157.05596
NPS	2010	68.25591	-157.04760
NPS	2010	68.25709	-157.05271

NOAT0464	Active Layer Detachment Slide	IKONOS/Geoeye/Worldview
NOAT0465	Active Layer Detachment Slide	IKONOS/Geoeye/Worldview
NOAT0466	Active Layer Detachment Slide	IKONOS/Geoeye/Worldview
NOAT0467	Active Layer Detachment Slide	IKONOS/Geoeye/Worldview
NOAT0468	Active Layer Detachment Slide	IKONOS/Geoeye/Worldview
NOAT0469	Active Layer Detachment Slide	IKONOS/Geoeye/Worldview
NOAT0470	Retrogressive Thaw Slump	IKONOS/Geoeye/Worldview
NOAT0471	Retrogressive Thaw Slump	IKONOS/Geoeye/Worldview
NOAT0472	Active Layer Detachment Slide	IKONOS/Geoeye/Worldview
NOAT0473	Active Layer Detachment Slide	IKONOS/Geoeye/Worldview
NOAT0474	Active Layer Detachment Slide	IKONOS/Geoeye/Worldview
NOAT0475	Active Layer Detachment Slide	IKONOS/Geoeye/Worldview
NOAT0476	Active Layer Detachment Slide	IKONOS/Geoeye/Worldview
NOAT0477	Active Layer Detachment Slide	IKONOS/Geoeye/Worldview
NOAT0478	Active Layer Detachment Slide	IKONOS/Geoeye/Worldview
NOAT0479	Active Layer Detachment Slide	IKONOS/Geoeye/Worldview
NOAT0480	Active Layer Detachment Slide	IKONOS/Geoeye/Worldview
NOAT0481	Active Layer Detachment Slide	IKONOS/Geoeye/Worldview
NOAT0482	Active Layer Detachment Slide	IKONOS/Geoeye/Worldview
NOAT0483	Active Layer Detachment Slide	IKONOS/Geoeye/Worldview
NOAT0484	Active Layer Detachment Slide	IKONOS/Geoeye/Worldview
NOAT0485	Active Layer Detachment Slide	IKONOS/Geoeye/Worldview
NOAT0486	Active Layer Detachment Slide	IKONOS/Geoeye/Worldview
NOAT0487	Active Layer Detachment Slide	IKONOS/Geoeye/Worldview
NOAT0488	Active Layer Detachment Slide	IKONOS/Geoeye/Worldview
NOAT0489	Retrogressive Thaw Slump	IKONOS/Geoeye/Worldview
NOAT0490	Retrogressive Thaw Slump	IKONOS/Geoeye/Worldview
NOAT0491	Retrogressive Thaw Slump	IKONOS/Geoeye/Worldview
NOAT0492	Retrogressive Thaw Slump	IKONOS/Geoeye/Worldview
NOAT0493	Active Layer Detachment Slide	IKONOS/Geoeye/Worldview
NOAT0494	Active Layer Detachment Slide	IKONOS/Geoeye/Worldview
NOAT0495	Active Layer Detachment Slide	IKONOS/Geoeye/Worldview

NPS	2010	68.25711	-157.05613
NPS	2010	68.25458	-157.08688
NPS	2010	68.25378	-157.08712
NPS	2010	68.25342	-157.09866
NPS	2010	68.25150	-157.09781
NPS	2010	68.25093	-157.09829
NPS	2010	68.22849	-157.15020
NPS	2010	68.28142	-157.12709
NPS	2010	68.28277	-157.13416
NPS	2010	68.27883	-157.12421
NPS	2010	68.26513	-158.00854
NPS	2010	68.26573	-157.99659
NPS	2010	68.27119	-158.00672
NPS	2010	68.27671	-157.98506
NPS	2010	68.26619	-157.97035
NPS	2010	68.27075	-157.96997
NPS	2010	68.28755	-157.95469
NPS	2010	68.28790	-157.94483
NPS	2010	68.28802	-157.94141
NPS	2010	68.29245	-157.92258
NPS	2010	68.26033	-157.91691
NPS	2010	68.26011	-157.91192
NPS	2010	68.27137	-157.91629
NPS	2010	68.27005	-157.90693
NPS	2010	68.26770	-157.89811
NPS	2010	68.27225	-157.88270
NPS	2010	68.27462	-157.88537
NPS	2010	68.27369	-157.89005
NPS	2010	68.27411	-157.87969
NPS	2010	68.27550	-157.91630
NPS	2010	68.27115	-157.92636
NPS	2010	68.27571	-157.90801

NOAT0496	Active Layer Detachment Slide	IKONOS/Geoeye/Worldview
NOAT0497	Active Layer Detachment Slide	IKONOS/Geoeye/Worldview
NOAT0498	Active Layer Detachment Slide	IKONOS/Geoeye/Worldview
NOAT0499	Active Layer Detachment Slide	IKONOS/Geoeye/Worldview
NOAT0500	Active Layer Detachment Slide	IKONOS/Geoeye/Worldview
NOAT0501	Active Layer Detachment Slide	IKONOS/Geoeye/Worldview
NOAT0502	Active Layer Detachment Slide	IKONOS/Geoeye/Worldview
NOAT0503	Active Layer Detachment Slide	IKONOS/Geoeye/Worldview
NOAT0504	Active Layer Detachment Slide	IKONOS/Geoeye/Worldview
NOAT0505	Retrogressive Thaw Slump	IKONOS/Geoeye/Worldview
NOAT0506	Active Layer Detachment Slide	IKONOS/Geoeye/Worldview
NOAT0507	Active Layer Detachment Slide	IKONOS/Geoeye/Worldview
NOAT0508	Active Layer Detachment Slide	IKONOS/Geoeye/Worldview
NOAT0509	Active Layer Detachment Slide	IKONOS/Geoeye/Worldview
NOAT0510	Active Layer Detachment Slide	IKONOS/Geoeye/Worldview
NOAT0511	Active Layer Detachment Slide	IKONOS/Geoeye/Worldview
NOAT0512	Active Layer Detachment Slide	IKONOS/Geoeye/Worldview
NOAT0513	Active Layer Detachment Slide	IKONOS/Geoeye/Worldview
NOAT0514	Active Layer Detachment Slide	IKONOS/Geoeye/Worldview
NOAT0515	Active Layer Detachment Slide	IKONOS/Geoeye/Worldview
NOAT0516	Active Layer Detachment Slide	IKONOS/Geoeye/Worldview
NOAT0517	Active Layer Detachment Slide	IKONOS/Geoeye/Worldview
NOAT0518	Active Layer Detachment Slide	IKONOS/Geoeye/Worldview
NOAT0519	Active Layer Detachment Slide	IKONOS/Geoeye/Worldview
NOAT0520	Active Layer Detachment Slide	IKONOS/Geoeye/Worldview
NOAT0521	Active Layer Detachment Slide	IKONOS/Geoeye/Worldview
NOAT0522	Active Layer Detachment Slide	IKONOS/Geoeye/Worldview
NOAT0523	Active Layer Detachment Slide	IKONOS/Geoeye/Worldview
NOAT0524	Active Layer Detachment Slide	IKONOS/Geoeye/Worldview
NOAT0525	Active Layer Detachment Slide	IKONOS/Geoeye/Worldview
NOAT0526	Active Layer Detachment Slide	IKONOS/Geoeye/Worldview
NOAT0527	Active Layer Detachment Slide	IKONOS/Geoeye/Worldview

NPS	2010	68.26816	-157.85078
NPS	2010	68.26807	-157.85829
NPS	2010	68.26866	-157.86108
NPS	2010	68.26787	-157.86613
NPS	2010	68.27731	-157.86891
NPS	2010	68.28538	-157.84682
NPS	2010	68.28542	-157.84263
NPS	2010	68.28128	-157.85166
NPS	2010	68.28186	-157.86832
NPS	2010	68.27923	-157.79515
NPS	2010	68.27509	-157.80278
NPS	2010	68.27362	-157.80065
NPS	2010	68.27197	-157.79607
NPS	2010	68.27037	-157.81019
NPS	2010	68.27094	-157.81505
NPS	2010	68.26024	-157.81484
NPS	2010	68.26122	-157.81916
NPS	2010	68.25856	-157.80896
NPS	2010	68.26017	-157.81381
NPS	2010	68.26227	-157.75738
NPS	2010	68.29198	-157.76248
NPS	2010	68.29193	-157.76043
NPS	2010	68.29181	-157.75698
NPS	2010	68.26296	-157.70437
NPS	2010	68.27439	-157.73362
NPS	2010	68.27315	-157.73492
NPS	2010	68.29372	-157.23319
NPS	2010	68.28386	-157.24705
NPS	2010	68.28420	-157.24307
NPS	2010	68.28290	-157.22075
NPS	2010	68.28189	-157.21994
NPS	2010	68.28406	-157.22692

NOAT0528	Active Layer Detachment Slide	IKONOS/Geoeye/Worldview
NOAT0529	Active Layer Detachment Slide	IKONOS/Geoeye/Worldview
NOAT0530	Active Layer Detachment Slide	IKONOS/Geoeye/Worldview
NOAT0531	Active Layer Detachment Slide	IKONOS/Geoeye/Worldview
NOAT0532	Active Layer Detachment Slide	IKONOS/Geoeye/Worldview
NOAT0533	Active Layer Detachment Slide	IKONOS/Geoeye/Worldview
NOAT0534	Active Layer Detachment Slide	IKONOS/Geoeye/Worldview
NOAT0535	Active Layer Detachment Slide	IKONOS/Geoeye/Worldview
NOAT0536	Active Layer Detachment Slide	IKONOS/Geoeye/Worldview
NOAT0537	Active Layer Detachment Slide	IKONOS/Geoeye/Worldview
NOAT0538	Active Layer Detachment Slide	IKONOS/Geoeye/Worldview
NOAT0539	Active Layer Detachment Slide	IKONOS/Geoeye/Worldview
NOAT0540	Active Layer Detachment Slide	IKONOS/Geoeye/Worldview
NOAT0541	Active Layer Detachment Slide	IKONOS/Geoeye/Worldview
NOAT0542	Active Layer Detachment Slide	IKONOS/Geoeye/Worldview
NOAT0543	Active Layer Detachment Slide	IKONOS/Geoeye/Worldview
NOAT0544	Active Layer Detachment Slide	IKONOS/Geoeye/Worldview
NOAT0545	Active Layer Detachment Slide	IKONOS/Geoeye/Worldview
NOAT0546	Active Layer Detachment Slide	IKONOS/Geoeye/Worldview
NOAT0547	Active Layer Detachment Slide	IKONOS/Geoeye/Worldview
NOAT0548	Active Layer Detachment Slide	IKONOS/Geoeye/Worldview
NOAT0549	Active Layer Detachment Slide	IKONOS/Geoeye/Worldview
NOAT0550	Active Layer Detachment Slide	IKONOS/Geoeye/Worldview
NOAT0551	Active Layer Detachment Slide	IKONOS/Geoeye/Worldview
NOAT0552	Active Layer Detachment Slide	IKONOS/Geoeye/Worldview
NOAT0553	Active Layer Detachment Slide	IKONOS/Geoeye/Worldview
NOAT0554	Active Layer Detachment Slide	IKONOS/Geoeye/Worldview
NOAT0555	Active Layer Detachment Slide	IKONOS/Geoeye/Worldview
NOAT0556	Active Layer Detachment Slide	IKONOS/Geoeye/Worldview
NOAT0557	Active Layer Detachment Slide	IKONOS/Geoeye/Worldview
NOAT0558	Active Layer Detachment Slide	IKONOS/Geoeye/Worldview
NOAT0559	Active Layer Detachment Slide	IKONOS/Geoeye/Worldview

NPS	2010	68.27670	-157.24338
NPS	2010	68.27587	-157.24504
NPS	2010	68.27530	-157.26151
NPS	2010	68.27615	-157.25241
NPS	2010	68.27663	-157.25187
NPS	2010	68.27321	-157.23507
NPS	2010	68.27507	-157.23570
NPS	2010	68.27462	-157.22994
NPS	2010	68.27260	-157.25138
NPS	2010	68.26075	-157.24375
NPS	2010	68.26256	-157.24620
NPS	2010	68.25934	-157.25435
NPS	2010	68.26711	-157.25994
NPS	2010	68.26802	-157.26019
NPS	2010	68.25514	-157.24441
NPS	2010	68.25459	-157.24544
NPS	2010	68.23532	-157.24740
NPS	2010	68.25137	-157.80054
NPS	2010	68.25620	-157.79247
NPS	2010	68.25636	-157.79375
NPS	2010	68.25724	-157.80292
NPS	2010	68.25584	-157.81684
NPS	2010	68.25740	-157.82152
NPS	2010	68.25830	-157.82432
NPS	2010	68.25702	-157.82717
NPS	2010	68.25701	-157.82848
NPS	2010	68.25704	-157.82950
NPS	2010	68.24327	-157.79539
NPS	2010	68.23659	-157.83005
NPS	2010	68.23809	-157.83077
NPS	2010	68.23294	-157.83744
NPS	2010	68.23112	-157.84002

NPS	2010	68.25121	-157.90585
NPS	2010	68.25268	-157.90395
NPS	2010	68.25103	-157.90369
NPS	2010	68.25361	-157.87089
NPS	2010	68.25159	-157.86940
NPS	2010	68.25150	-157.87126
NPS	2010	68.24957	-157.86560
NPS	2010	68.25122	-157.87784
NPS	2010	68.25178	-157.85717
NPS	2010	68.24839	-157.84153
NPS	2010	68.24504	-157.87799
NPS	2010	68.24386	-157.86228
NPS	2010	68.23899	-157.86717
NPS	2010	68.22628	-157.91957
NPS	2010	68.23590	-157.84880
NPS	2010	68.25364	-157.95189
NPS	2010	68.25310	-157.94954
NPS	2010	68.25289	-157.94752
NPS	2010	68.25207	-157.95019
NPS	2010	68.25739	-157.93526
NPS	2010	68.25712	-157.98053
NPS	2010	68.22429	-158.02339
NPS	2010	68.23047	-157.98364
NPS	2010	68.23193	-157.98451
NPS	2010	68.20355	-158.01216
NPS	2010	68.20782	-157.76515
NPS	2010	68.22244	-157.75567
NPS	2010	68.22283	-157.76005
NPS	2010	68.27740	-158.21784
NPS	2010	68.27854	-158.21534
NPS	2010	68.27206	-158.12638
NPS	2010	68.28910	-158.03853

NOAT0592	Active Layer Detachment Slide	IKONOS/Geoeye/Worldview
NOAT0593	Active Layer Detachment Slide	IKONOS/Geoeye/Worldview
NOAT0594	Active Layer Detachment Slide	IKONOS/Geoeye/Worldview
NOAT0595	Active Layer Detachment Slide	IKONOS/Geoeye/Worldview
NOAT0596	Active Layer Detachment Slide	IKONOS/Geoeye/Worldview
NOAT0597	Active Layer Detachment Slide	IKONOS/Geoeye/Worldview
NOAT0598	Active Layer Detachment Slide	IKONOS/Geoeye/Worldview
NOAT0599	Active Layer Detachment Slide	IKONOS/Geoeye/Worldview
NOAT0600	Active Layer Detachment Slide	IKONOS/Geoeye/Worldview
NOAT0601	Active Layer Detachment Slide	IKONOS/Geoeye/Worldview
NOAT0602	Active Layer Detachment Slide	IKONOS/Geoeye/Worldview
NOAT0603	Active Layer Detachment Slide	IKONOS/Geoeye/Worldview
NOAT0604	Active Layer Detachment Slide	IKONOS/Geoeye/Worldview
NOAT0605	Active Layer Detachment Slide	IKONOS/Geoeye/Worldview
NOAT0606	Active Layer Detachment Slide	IKONOS/Geoeye/Worldview
NOAT0607	Active Layer Detachment Slide	IKONOS/Geoeye/Worldview
NOAT0608	Retrogressive Thaw Slump	IKONOS/Geoeye/Worldview
NOAT0609	Retrogressive Thaw Slump	IKONOS/Geoeye/Worldview
NOAT0610	Retrogressive Thaw Slump	IKONOS/Geoeye/Worldview
NOAT0611	Retrogressive Thaw Slump	IKONOS/Geoeye/Worldview
NOAT0612	Retrogressive Thaw Slump	IKONOS/Geoeye/Worldview
NOAT0613	Retrogressive Thaw Slump	IKONOS/Geoeye/Worldview
NOAT0614	Active Layer Detachment Slide	IKONOS/Geoeye/Worldview
NOAT0615	Active Layer Detachment Slide	IKONOS/Geoeye/Worldview
NOAT0616	Active Layer Detachment Slide	IKONOS/Geoeye/Worldview
NOAT0617	Active Layer Detachment Slide	IKONOS/Geoeye/Worldview
NOAT0618	Active Layer Detachment Slide	IKONOS/Geoeye/Worldview
NOAT0619	Active Layer Detachment Slide	IKONOS/Geoeye/Worldview
NOAT0620	Active Layer Detachment Slide	IKONOS/Geoeye/Worldview
NOAT0621	Active Layer Detachment Slide	IKONOS/Geoeye/Worldview
NOAT0622	Active Layer Detachment Slide	IKONOS/Geoeye/Worldview
NOAT0623	Active Layer Detachment Slide	IKONOS/Geoeye/Worldview

NPS	2010	68.25703	-158.04000
NPS	2010	68.26257	-158.05453
NPS	2010	68.26155	-158.05461
NPS	2010	68.25948	-158.05317
NPS	2010	68.25504	-158.07164
NPS	2010	68.25475	-158.06396
NPS	2010	68.24160	-158.10008
NPS	2010	68.24304	-158.10711
NPS	2010	68.26730	-158.15050
NPS	2010	68.24248	-158.14573
NPS	2010	68.24948	-158.20815
NPS	2010	68.21005	-158.53183
NPS	2010	68.23999	-158.97508
NPS	2010	68.19126	-158.64874
NPS	2010	68.19991	-158.94987
NPS	2010	68.19775	-158.95619
NPS	2010	68.23321	-158.34013
NPS	2010	68.23114	-158.33372
NPS	2010	68.19879	-159.47998
NPS	2010	68.20144	-159.47658
NPS	2010	68.20690	-159.46276
NPS	2010	68.20934	-159.45998
NPS	2010	68.32059	-159.83879
NPS	2010	68.32607	-159.73405
NPS	2010	68.37166	-158.18291
NPS	2010	68.36814	-158.15211
NPS	2010	68.36731	-158.15170
NPS	2010	68.46717	-159.72737
NPS	2010	68.45579	-159.05861
NPS	2010	68.46021	-158.99448
NPS	2010	68.45823	-158.99516
NPS	2010	68.45417	-158.98109

NOAT0624	Active Layer Detachment Slide	IKONOS/Geoeye/Worldview
NOAT0625	Active Layer Detachment Slide	IKONOS/Geoeye/Worldview
NOAT0626	Active Layer Detachment Slide	IKONOS/Geoeye/Worldview
NOAT0627	Active Layer Detachment Slide	IKONOS/Geoeye/Worldview
NOAT0628	Active Layer Detachment Slide	IKONOS/Geoeye/Worldview
NOAT0629	Active Layer Detachment Slide	IKONOS/Geoeye/Worldview
NOAT0630	Active Layer Detachment Slide	IKONOS/Geoeye/Worldview
NOAT0631	Retrogressive Thaw Slump	IKONOS/Geoeye/Worldview
NOAT0632	Active Layer Detachment Slide	IKONOS/Geoeye/Worldview
NOAT0633	Active Layer Detachment Slide	IKONOS/Geoeye/Worldview
NOAT0634	Active Layer Detachment Slide	IKONOS/Geoeye/Worldview
NOAT0635	Active Layer Detachment Slide	IKONOS/Geoeye/Worldview
NOAT0636	Active Layer Detachment Slide	IKONOS/Geoeye/Worldview
NOAT0637	Active Layer Detachment Slide	IKONOS/Geoeye/Worldview
NOAT0638	Active Layer Detachment Slide	IKONOS/Geoeye/Worldview
NOAT0639	Active Layer Detachment Slide	IKONOS/Geoeye/Worldview
NOAT0640	Active Layer Detachment Slide	IKONOS/Geoeye/Worldview
NOAT0641	Active Layer Detachment Slide	IKONOS/Geoeye/Worldview
NOAT0642	Active Layer Detachment Slide	IKONOS/Geoeye/Worldview
NOAT0643	Active Layer Detachment Slide	IKONOS/Geoeye/Worldview
NOAT0644	Retrogressive Thaw Slump	IKONOS/Geoeye/Worldview
NOAT0645	Active Layer Detachment Slide	IKONOS/Geoeye/Worldview
NOAT0646	Retrogressive Thaw Slump	IKONOS/Geoeye/Worldview
NOAT0647	Retrogressive Thaw Slump	IKONOS/Geoeye/Worldview
NOAT0648	Retrogressive Thaw Slump	IKONOS/Geoeye/Worldview
NOAT0649	Active Layer Detachment Slide	IKONOS/Geoeye/Worldview
NOAT0650	Retrogressive Thaw Slump	IKONOS/Geoeye/Worldview
NOAT0651	Active Layer Detachment Slide	IKONOS/Geoeye/Worldview
NOAT0652	Retrogressive Thaw Slump	IKONOS/Geoeye/Worldview
NOAT0653	Retrogressive Thaw Slump	IKONOS/Geoeye/Worldview
NOAT0654	Retrogressive Thaw Slump	IKONOS/Geoeye/Worldview
NOAT0655	Active Layer Detachment Slide	IKONOS/Geoeye/Worldview

NPS	2010	68.44834	-158.91133
NPS	2010	68.44655	-158.91689
NPS	2010	68.40126	-158.61436
NPS	2010	68.43610	-158.50523
NPS	2010	68.42650	-158.55219
NPS	2010	68.38503	-158.18351
NPS	2010	68.54714	-160.27858
NPS	2010	68.53700	-160.10611
NPS	2010	68.51537	-160.31208
NPS	2010	68.50647	-160.28766
NPS	2010	68.55307	-159.27031
NPS	2010	68.48797	-159.15011
NPS	2010	68.57551	-159.93993
NPS	2010	68.56354	-159.39086
NPS	2010	68.56904	-159.91847
NPS	2010	68.57076	-159.85437
NPS	2010	68.28626	-157.95076
NPS	2010	68.28554	-157.95086
NPS	2010	68.31613	-157.92971
NPS	2010	68.31485	-157.92803
NPS	2010	68.32512	-157.89207
NPS	2010	68.28345	-157.75424
NPS	2010	67.80530	-159.20356
NPS	2010	67.80413	-159.20550
NPS	2010	67.80163	-159.20680
NPS	2010	68.41537	-160.85122
NPS	2010	68.41612	-160.85731
NPS	2010	68.32601	-162.65848
NPS	2010	68.32337	-161.39068
NPS	2010	68.29241	-161.36500
NPS	2010	68.18987	-161.17802
NPS	2010	68.05801	-161.27442

NOAT0656	Active Layer Detachment Slide	IKONOS/Geoeye/Worldview
NOAT0657	Active Layer Detachment Slide	IKONOS/Geoeye/Worldview
NOAT0658	Active Layer Detachment Slide	IKONOS/Geoeye/Worldview
NOAT0659	Active Layer Detachment Slide	IKONOS/Geoeye/Worldview
NOAT0660	Active Layer Detachment Slide	IKONOS/Geoeye/Worldview
NOAT0661	Active Layer Detachment Slide	IKONOS/Geoeye/Worldview
NOAT0662	Active Layer Detachment Slide	IKONOS/Geoeye/Worldview
NOAT0663	Active Layer Detachment Slide	IKONOS/Geoeye/Worldview
NOAT0664	Active Layer Detachment Slide	IKONOS/Geoeye/Worldview
NOAT0665	Active Layer Detachment Slide	IKONOS/Geoeye/Worldview
NOAT0666	Active Layer Detachment Slide	IKONOS/Geoeye/Worldview
NOAT0667	Active Layer Detachment Slide	IKONOS/Geoeye/Worldview
NOAT0668	Active Layer Detachment Slide	IKONOS/Geoeye/Worldview
NOAT0669	Active Layer Detachment Slide	IKONOS/Geoeye/Worldview
NOAT0670	Active Layer Detachment Slide	IKONOS/Geoeye/Worldview
NOAT0671	Active Layer Detachment Slide	IKONOS/Geoeye/Worldview
NOAT0672	Active Layer Detachment Slide	IKONOS/Geoeye/Worldview
NOAT0673	Active Layer Detachment Slide	IKONOS/Geoeye/Worldview
NOAT0674	Active Layer Detachment Slide	IKONOS/Geoeye/Worldview
NOAT0675	Active Layer Detachment Slide	IKONOS/Geoeye/Worldview
NOAT0676	Active Layer Detachment Slide	IKONOS/Geoeye/Worldview
NOAT0677	Active Layer Detachment Slide	IKONOS/Geoeye/Worldview
NOAT0678	Active Layer Detachment Slide	IKONOS/Geoeye/Worldview
NOAT0679	Active Layer Detachment Slide	IKONOS/Geoeye/Worldview
NOAT0680	Active Layer Detachment Slide	IKONOS/Geoeye/Worldview
NOAT0681	Active Layer Detachment Slide	IKONOS/Geoeye/Worldview
NOAT0682	Active Layer Detachment Slide	IKONOS/Geoeye/Worldview
NOAT0683	Active Layer Detachment Slide	IKONOS/Geoeye/Worldview
NOAT0684	Active Layer Detachment Slide	IKONOS/Geoeye/Worldview
NOAT0685	Active Layer Detachment Slide	IKONOS/Geoeye/Worldview
NOAT0686	Retrogressive Thaw Slump	IKONOS/Geoeye/Worldview
NOAT0687	Retrogressive Thaw Slump	IKONOS/Geoeye/Worldview

NPS	2010	68.05720	-161.26893
NPS	2010	68.05458	-161.13815
NPS	2010	68.05410	-161.13131
NPS	2010	68.05373	-161.13030
NPS	2010	68.05729	-161.13777
NPS	2010	68.05651	-161.13908
NPS	2010	68.05648	-161.13678
NPS	2010	68.05652	-161.13595
NPS	2010	68.05682	-161.13552
NPS	2010	68.05650	-161.13470
NPS	2010	68.05676	-161.13416
NPS	2010	68.05709	-161.13312
NPS	2010	68.05671	-161.13165
NPS	2010	68.05682	-161.13101
NPS	2010	68.05662	-161.12988
NPS	2010	68.05713	-161.12930
NPS	2010	68.05669	-161.12903
NPS	2010	68.05653	-161.12851
NPS	2010	68.05617	-161.12936
NPS	2010	68.05612	-161.12885
NPS	2010	68.05610	-161.12823
NPS	2010	68.05652	-161.12491
NPS	2010	68.13318	-160.54561
NPS	2010	68.13354	-160.52307
NPS	2010	68.13254	-160.52126
NPS	2010	68.12576	-160.55933
NPS	2010	68.13226	-160.57130
NPS	2010	68.14906	-160.47493
NPS	2010	68.10427	-160.70111
NPS	2010	68.03221	-162.55337
NPS	2010	67.95622	-162.13629
NPS	2010	67.97401	-161.79656

NOAT0688	Retrogressive Thaw Slump	IKONOS/Geoeye/Worldview
NOAT0689	Retrogressive Thaw Slump	IKONOS/Geoeye/Worldview
NOAT0690	Retrogressive Thaw Slump	IKONOS/Geoeye/Worldview
NOAT0691	Retrogressive Thaw Slump	IKONOS/Geoeye/Worldview
NOAT0692	Retrogressive Thaw Slump	IKONOS/Geoeye/Worldview
NOAT0693	Retrogressive Thaw Slump	IKONOS/Geoeye/Worldview
NOAT0694	Retrogressive Thaw Slump	IKONOS/Geoeye/Worldview
NOAT0695	Retrogressive Thaw Slump	IKONOS/Geoeye/Worldview
NOAT0696	Retrogressive Thaw Slump	IKONOS/Geoeye/Worldview
NOAT0697	Retrogressive Thaw Slump	IKONOS/Geoeye/Worldview
NOAT0698	Active Layer Detachment Slide	IKONOS/Geoeye/Worldview
NOAT0699	Active Layer Detachment Slide	IKONOS/Geoeye/Worldview
NOAT0700	Active Layer Detachment Slide	IKONOS/Geoeye/Worldview
NOAT0701	Active Layer Detachment Slide	IKONOS/Geoeye/Worldview
NOAT0702	Active Layer Detachment Slide	IKONOS/Geoeye/Worldview
NOAT0703	Active Layer Detachment Slide	IKONOS/Geoeye/Worldview
NOAT0704	Active Layer Detachment Slide	IKONOS/Geoeye/Worldview
NOAT0705	Active Layer Detachment Slide	IKONOS/Geoeye/Worldview
NOAT0706	Active Layer Detachment Slide	IKONOS/Geoeye/Worldview
NOAT0707	Active Layer Detachment Slide	IKONOS/Geoeye/Worldview
NOAT0708	Active Layer Detachment Slide	IKONOS/Geoeye/Worldview
NOAT0709	Active Layer Detachment Slide	IKONOS/Geoeye/Worldview
NOAT0710	Active Layer Detachment Slide	IKONOS/Geoeye/Worldview
NOAT0711	Active Layer Detachment Slide	IKONOS/Geoeye/Worldview
NOAT0712	Retrogressive Thaw Slump	IKONOS/Geoeye/Worldview
NOAT0713	Retrogressive Thaw Slump	IKONOS/Geoeye/Worldview
NOAT0714	Active Layer Detachment Slide	IKONOS/Geoeye/Worldview
NOAT0715	Active Layer Detachment Slide	IKONOS/Geoeye/Worldview
NOAT0716	Active Layer Detachment Slide	IKONOS/Geoeye/Worldview
NOAT0717	Active Layer Detachment Slide	IKONOS/Geoeye/Worldview
NOAT0718	Retrogressive Thaw Slump	IKONOS/Geoeye/Worldview
NOAT0719	Retrogressive Thaw Slump	IKONOS/Geoeye/Worldview

NPS	2010	67.97522	-161.79947
NPS	2010	67.97004	-161.79873
NPS	2010	67.96912	-161.79900
NPS	2010	67.96861	-161.79891
NPS	2010	67.96834	-161.79830
NPS	2010	67.95970	-161.74346
NPS	2010	67.96099	-161.74398
NPS	2010	67.96128	-161.74407
NPS	2010	67.96689	-161.67850
NPS	2010	67.96712	-161.67931
NPS	2010	68.03835	-161.28647
NPS	2010	68.03834	-161.28497
NPS	2010	68.03843	-161.28433
NPS	2010	68.03890	-161.28519
NPS	2010	68.03901	-161.28597
NPS	2010	68.04570	-161.17396
NPS	2010	68.06191	-161.14675
NPS	2010	68.06092	-161.14676
NPS	2010	68.05253	-161.12677
NPS	2010	68.05174	-161.12804
NPS	2010	68.05166	-161.13134
NPS	2010	68.04728	-161.10143
NPS	2010	68.04721	-161.10811
NPS	2010	67.99472	-161.03298
NPS	2010	67.99340	-161.22291
NPS	2010	67.96637	-161.46945
NPS	2010	67.99153	-161.23011
NPS	2010	67.99104	-161.23094
NPS	2010	67.99020	-161.24339
NPS	2010	67.98951	-161.11699
NPS	2010	67.96029	-161.10881
NPS	2010	67.95416	-161.11099

NOAT0720	Retrogressive Thaw Slump	IKONOS/Geoeye/Worldview
NOAT0721	Retrogressive Thaw Slump	IKONOS/Geoeye/Worldview
NOAT0722	Retrogressive Thaw Slump	IKONOS/Geoeye/Worldview
NOAT0723	Retrogressive Thaw Slump	IKONOS/Geoeye/Worldview
NOAT0724	Retrogressive Thaw Slump	IKONOS/Geoeye/Worldview
NOAT0725	Active Layer Detachment Slide	IKONOS/Geoeye/Worldview
NOAT0726	Active Layer Detachment Slide	IKONOS/Geoeye/Worldview
NOAT0727	Active Layer Detachment Slide	IKONOS/Geoeye/Worldview
NOAT0728	Active Layer Detachment Slide	IKONOS/Geoeye/Worldview
NOAT0729	Active Layer Detachment Slide	IKONOS/Geoeye/Worldview
NOAT0730	Active Layer Detachment Slide	IKONOS/Geoeye/Worldview
NOAT0731	Active Layer Detachment Slide	IKONOS/Geoeye/Worldview
NOAT0732	Active Layer Detachment Slide	IKONOS/Geoeye/Worldview
NOAT0733	Active Layer Detachment Slide	IKONOS/Geoeye/Worldview
NOAT0734	Active Layer Detachment Slide	IKONOS/Geoeye/Worldview
NOAT0735	Active Layer Detachment Slide	IKONOS/Geoeye/Worldview
NOAT0736	Active Layer Detachment Slide	IKONOS/Geoeye/Worldview
NOAT0737	Active Layer Detachment Slide	IKONOS/Geoeye/Worldview
NOAT0738	Active Layer Detachment Slide	IKONOS/Geoeye/Worldview
NOAT0739	Active Layer Detachment Slide	IKONOS/Geoeye/Worldview
NOAT0740	Active Layer Detachment Slide	IKONOS/Geoeye/Worldview
NOAT0741	Active Layer Detachment Slide	IKONOS/Geoeye/Worldview
NOAT0742	Active Layer Detachment Slide	IKONOS/Geoeye/Worldview
NOAT0743	Active Layer Detachment Slide	IKONOS/Geoeye/Worldview
NOAT0744	Active Layer Detachment Slide	IKONOS/Geoeye/Worldview
NOAT0745	Active Layer Detachment Slide	IKONOS/Geoeye/Worldview
NOAT0746	Active Layer Detachment Slide	IKONOS/Geoeye/Worldview
NOAT0747	Active Layer Detachment Slide	IKONOS/Geoeye/Worldview
NOAT0748	Active Layer Detachment Slide	IKONOS/Geoeye/Worldview
NOAT0749	Active Layer Detachment Slide	IKONOS/Geoeye/Worldview
NOAT0750	Retrogressive Thaw Slump	IKONOS/Geoeye/Worldview
NOAT0751	Active Layer Detachment Slide	IKONOS/Geoeye/Worldview

NPS	2010	67.95356	-161.11150
NPS	2010	68.06003	-160.76849
NPS	2010	68.04444	-160.77702
NPS	2010	68.03495	-160.75596
NPS	2010	68.03731	-160.79348
NPS	2010	68.02200	-160.78143
NPS	2010	68.01320	-160.80504
NPS	2010	68.00437	-160.80773
NPS	2010	67.99944	-160.80134
NPS	2010	68.00409	-160.79000
NPS	2010	68.00399	-160.78796
NPS	2010	68.00481	-160.78893
NPS	2010	68.00560	-160.78838
NPS	2010	68.00582	-160.78793
NPS	2010	68.00620	-160.78760
NPS	2010	68.00455	-160.78647
NPS	2010	68.00486	-160.78648
NPS	2010	68.00538	-160.78572
NPS	2010	67.99653	-160.79852
NPS	2010	67.99599	-160.79872
NPS	2010	67.99974	-160.84941
NPS	2010	67.19221	-161.92793
NPS	2010	67.19272	-161.93126
NPS	2010	67.58764	-161.93258
NPS	2010	67.59153	-161.93577
NPS	2010	67.59360	-161.93457
NPS	2010	67.59351	-161.92884
NPS	2010	67.58742	-161.85405
NPS	2010	67.59772	-161.83193
NPS	2010	67.59638	-161.83478
NPS	2010	67.94378	-162.35619
NPS	2010	67.60512	-161.76922

NOAT0752	Active Layer Detachment Slide	IKONOS/Geoeye/Worldview
NOAT0753	Active Layer Detachment Slide	IKONOS/Geoeye/Worldview
NOAT0754	Retrogressive Thaw Slump	IKONOS/Geoeye/Worldview
NOAT0755	Active Layer Detachment Slide	IKONOS/Geoeye/Worldview
NOAT0756	Active Layer Detachment Slide	IKONOS/Geoeye/Worldview
NOAT0757	Active Layer Detachment Slide	IKONOS/Geoeye/Worldview
NOAT0758	Active Layer Detachment Slide	IKONOS/Geoeye/Worldview
NOAT0759	Active Layer Detachment Slide	IKONOS/Geoeye/Worldview
NOAT0760	Active Layer Detachment Slide	IKONOS/Geoeye/Worldview
NOAT0761	Active Layer Detachment Slide	IKONOS/Geoeye/Worldview
NOAT0762	Active Layer Detachment Slide	IKONOS/Geoeye/Worldview
NOAT0763	Active Layer Detachment Slide	IKONOS/Geoeye/Worldview
NOAT0764	Active Layer Detachment Slide	IKONOS/Geoeye/Worldview
NOAT0765	Active Layer Detachment Slide	IKONOS/Geoeye/Worldview
NOAT0766	Active Layer Detachment Slide	IKONOS/Geoeye/Worldview
NOAT0767	Retrogressive Thaw Slump	IKONOS/Geoeye/Worldview
NOAT0768	Active Layer Detachment Slide	IKONOS/Geoeye/Worldview
NOAT0769	Active Layer Detachment Slide	IKONOS/Geoeye/Worldview
NOAT0770	Active Layer Detachment Slide	IKONOS/Geoeye/Worldview
NOAT0771	Active Layer Detachment Slide	IKONOS/Geoeye/Worldview
NOAT0772	Active Layer Detachment Slide	IKONOS/Geoeye/Worldview
NOAT0773	Active Layer Detachment Slide	IKONOS/Geoeye/Worldview
NOAT0774	Active Layer Detachment Slide	IKONOS/Geoeye/Worldview
NOAT0775	Active Layer Detachment Slide	IKONOS/Geoeye/Worldview
NOAT0776	Active Layer Detachment Slide	IKONOS/Geoeye/Worldview
NOAT0777	Active Layer Detachment Slide	IKONOS/Geoeye/Worldview
NOAT0778	Retrogressive Thaw Slump	IKONOS/Geoeye/Worldview
NOAT0779	Retrogressive Thaw Slump	IKONOS/Geoeye/Worldview
NOAT0780	Active Layer Detachment Slide	IKONOS/Geoeye/Worldview
NOAT0781	Active Layer Detachment Slide	IKONOS/Geoeye/Worldview
NOAT0782	Retrogressive Thaw Slump	IKONOS/Geoeye/Worldview
NOAT0783	Active Layer Detachment Slide	IKONOS/Geoeye/Worldview

NPS	2010	67.60568	-161.76881
NPS	2010	67.55321	-161.69326
NPS	2010	67.56161	-161.77315
NPS	2010	67.54807	-161.77634
NPS	2010	67.54528	-161.79094
NPS	2010	67.58153	-161.85720
NPS	2010	67.57772	-161.90923
NPS	2010	67.54600	-161.81134
NPS	2010	67.53064	-161.81016
NPS	2010	67.60191	-161.69428
NPS	2010	67.60148	-161.70355
NPS	2010	67.59698	-161.64830
NPS	2010	67.59623	-161.64715
NPS	2010	67.59041	-161.61070
NPS	2010	67.58967	-161.61772
NPS	2010	67.58740	-161.61975
NPS	2010	67.58820	-161.62364
NPS	2010	67.59906	-161.62909
NPS	2010	67.60467	-161.67263
NPS	2010	67.61333	-161.61780
NPS	2010	67.61192	-161.61547
NPS	2010	67.61303	-161.59753
NPS	2010	67.61119	-161.58884
NPS	2010	67.61023	-161.58755
NPS	2010	67.61036	-161.59489
NPS	2010	67.61539	-161.58313
NPS	2010	67.61241	-161.57069
NPS	2010	67.60979	-161.53729
NPS	2010	67.59505	-161.58527
NPS	2010	67.59479	-161.58942
NPS	2010	67.59553	-161.59818
NPS	2010	67.59313	-161.59767

NOAT0784	Active Layer Detachment Slide	IKONOS/Geoeye/Worldview
NOAT0785	Active Layer Detachment Slide	IKONOS/Geoeye/Worldview
NOAT0786	Active Layer Detachment Slide	IKONOS/Geoeye/Worldview
NOAT0787	Active Layer Detachment Slide	IKONOS/Geoeye/Worldview
NOAT0788	Retrogressive Thaw Slump	IKONOS/Geoeye/Worldview
NOAT0789	Retrogressive Thaw Slump	IKONOS/Geoeye/Worldview
NOAT0790	Retrogressive Thaw Slump	IKONOS/Geoeye/Worldview
NOAT0791	Active Layer Detachment Slide	IKONOS/Geoeye/Worldview
NOAT0792	Active Layer Detachment Slide	IKONOS/Geoeye/Worldview
NOAT0793	Retrogressive Thaw Slump	IKONOS/Geoeye/Worldview
NOAT0794	Retrogressive Thaw Slump	IKONOS/Geoeye/Worldview
NOAT0795	Active Layer Detachment Slide	IKONOS/Geoeye/Worldview
NOAT0796	Active Layer Detachment Slide	IKONOS/Geoeye/Worldview
NOAT0797	Active Layer Detachment Slide	IKONOS/Geoeye/Worldview
NOAT0798	Retrogressive Thaw Slump	IKONOS/Geoeye/Worldview
NOAT0799	Active Layer Detachment Slide	IKONOS/Geoeye/Worldview
NOAT0800	Active Layer Detachment Slide	IKONOS/Geoeye/Worldview
NOAT0801	Active Layer Detachment Slide	IKONOS/Geoeye/Worldview
NOAT0802	Active Layer Detachment Slide	IKONOS/Geoeye/Worldview
NOAT0803	Active Layer Detachment Slide	IKONOS/Geoeye/Worldview
NOAT0804	Active Layer Detachment Slide	IKONOS/Geoeye/Worldview
NOAT0805	Active Layer Detachment Slide	IKONOS/Geoeye/Worldview
NOAT0806	Active Layer Detachment Slide	IKONOS/Geoeye/Worldview
NOAT0807	Active Layer Detachment Slide	IKONOS/Geoeye/Worldview
NOAT0808	Active Layer Detachment Slide	IKONOS/Geoeye/Worldview
NOAT0809	Retrogressive Thaw Slump	IKONOS/Geoeye/Worldview
NOAT0810	Active Layer Detachment Slide	IKONOS/Geoeye/Worldview
NOAT0811	Active Layer Detachment Slide	IKONOS/Geoeye/Worldview
NOAT0812	Active Layer Detachment Slide	IKONOS/Geoeye/Worldview
NOAT0813	Active Layer Detachment Slide	IKONOS/Geoeye/Worldview
NOAT0814	Active Layer Detachment Slide	IKONOS/Geoeye/Worldview
NOAT0815	Active Layer Detachment Slide	IKONOS/Geoeye/Worldview

NPS	2010	67.59528	-161.60227
NPS	2010	67.59582	-161.61526
NPS	2010	67.59383	-161.61756
NPS	2010	67.56660	-161.68413
NPS	2010	67.92794	-161.96598
NPS	2010	67.92792	-161.97130
NPS	2010	67.92836	-161.97276
NPS	2010	67.95960	-161.62627
NPS	2010	67.93324	-161.48564
NPS	2010	67.92597	-161.68181
NPS	2010	67.92644	-161.68172
NPS	2010	67.88321	-161.51902
NPS	2010	67.89209	-161.51335
NPS	2010	67.89251	-161.50473
NPS	2010	67.92884	-161.96225
NPS	2010	67.92399	-161.43562
NPS	2010	67.92550	-161.43387
NPS	2010	67.92626	-161.43078
NPS	2010	67.92747	-161.42536
NPS	2010	67.92681	-161.42456
NPS	2010	67.92516	-161.42172
NPS	2010	67.92700	-161.42123
NPS	2010	67.92693	-161.41979
NPS	2010	67.92847	-161.40591
NPS	2010	67.93017	-161.40479
NPS	2010	67.91476	-160.90081
NPS	2010	67.90877	-161.09018
NPS	2010	67.89756	-161.15557
NPS	2010	67.89587	-161.17210
NPS	2010	67.92629	-161.35062
NPS	2010	67.92454	-161.34849
NPS	2010	67.92173	-161.34919

NOAT0816	Active Layer Detachment Slide	IKONOS/Geoeye/Worldview
NOAT0817	Active Layer Detachment Slide	IKONOS/Geoeye/Worldview
NOAT0818	Active Layer Detachment Slide	IKONOS/Geoeye/Worldview
NOAT0819	Active Layer Detachment Slide	IKONOS/Geoeye/Worldview
NOAT0820	Active Layer Detachment Slide	IKONOS/Geoeye/Worldview
NOAT0821	Active Layer Detachment Slide	IKONOS/Geoeye/Worldview
NOAT0822	Active Layer Detachment Slide	IKONOS/Geoeye/Worldview
NOAT0823	Active Layer Detachment Slide	IKONOS/Geoeye/Worldview
NOAT0824	Active Layer Detachment Slide	IKONOS/Geoeye/Worldview
NOAT0825	Active Layer Detachment Slide	IKONOS/Geoeye/Worldview
NOAT0826	Active Layer Detachment Slide	IKONOS/Geoeye/Worldview
NOAT0827	Active Layer Detachment Slide	IKONOS/Geoeye/Worldview
NOAT0828	Active Layer Detachment Slide	IKONOS/Geoeye/Worldview
NOAT0829	Active Layer Detachment Slide	IKONOS/Geoeye/Worldview
NOAT0830	Active Layer Detachment Slide	IKONOS/Geoeye/Worldview
NOAT0831	Active Layer Detachment Slide	IKONOS/Geoeye/Worldview
NOAT0832	Active Layer Detachment Slide	IKONOS/Geoeye/Worldview
NOAT0833	Active Layer Detachment Slide	IKONOS/Geoeye/Worldview
NOAT0834	Active Layer Detachment Slide	IKONOS/Geoeye/Worldview
NOAT0835	Active Layer Detachment Slide	IKONOS/Geoeye/Worldview
NOAT0836	Active Layer Detachment Slide	IKONOS/Geoeye/Worldview
NOAT0837	Active Layer Detachment Slide	IKONOS/Geoeye/Worldview
NOAT0838	Active Layer Detachment Slide	IKONOS/Geoeye/Worldview
NOAT0839	Active Layer Detachment Slide	IKONOS/Geoeye/Worldview
NOAT0840	Active Layer Detachment Slide	IKONOS/Geoeye/Worldview
NOAT0841	Active Layer Detachment Slide	IKONOS/Geoeye/Worldview
NOAT0842	Retrogressive Thaw Slump	IKONOS/Geoeye/Worldview
NOAT0843	Active Layer Detachment Slide	IKONOS/Geoeye/Worldview
NOAT0844	Active Layer Detachment Slide	IKONOS/Geoeye/Worldview
NOAT0845	Retrogressive Thaw Slump	IKONOS/Geoeye/Worldview
NOAT0846	Retrogressive Thaw Slump	IKONOS/Geoeye/Worldview
NOAT0847	Retrogressive Thaw Slump	IKONOS/Geoeye/Worldview

NPS	2010	67.92064	-161.42289
NPS	2010	67.91589	-161.42403
NPS	2010	67.91502	-161.42366
NPS	2010	67.91380	-161.42415
NPS	2010	67.88903	-161.41052
NPS	2010	67.87699	-161.35288
NPS	2010	67.87570	-161.38388
NPS	2010	67.89074	-161.34019
NPS	2010	67.86160	-161.35687
NPS	2010	67.86373	-161.35234
NPS	2010	67.86418	-161.34882
NPS	2010	67.86445	-161.34230
NPS	2010	67.86597	-161.36705
NPS	2010	67.86418	-161.36820
NPS	2010	67.86608	-161.37188
NPS	2010	67.86134	-161.31584
NPS	2010	67.86989	-161.33988
NPS	2010	67.86847	-161.24325
NPS	2010	67.86711	-161.24336
NPS	2010	67.87299	-161.19259
NPS	2010	67.87374	-161.18833
NPS	2010	67.87473	-161.18803
NPS	2010	67.87566	-161.18650
NPS	2010	67.87558	-161.18355
NPS	2010	67.87571	-161.14545
NPS	2010	67.87706	-161.15342
NPS	2010	67.88920	-160.82884
NPS	2010	67.92579	-161.41823
NPS	2010	67.92473	-161.41702
NPS	2010	67.90639	-160.46591
NPS	2010	67.90575	-160.46066
NPS	2010	67.90609	-160.78630

NOAT0848	Retrogressive Thaw Slump	IKONOS/Geoeye/Worldview
NOAT0849	Active Layer Detachment Slide	IKONOS/Geoeye/Worldview
NOAT0850	Active Layer Detachment Slide	IKONOS/Geoeye/Worldview
NOAT0851	Active Layer Detachment Slide	IKONOS/Geoeye/Worldview
NOAT0852	Retrogressive Thaw Slump	IKONOS/Geoeye/Worldview
NOAT0853	Retrogressive Thaw Slump	IKONOS/Geoeye/Worldview
NOAT0854	Retrogressive Thaw Slump	IKONOS/Geoeye/Worldview
NOAT0855	Active Layer Detachment Slide	IKONOS/Geoeye/Worldview
NOAT0856	Active Layer Detachment Slide	IKONOS/Geoeye/Worldview
NOAT0857	Active Layer Detachment Slide	IKONOS/Geoeye/Worldview
NOAT0858	Active Layer Detachment Slide	IKONOS/Geoeye/Worldview
NOAT0859	Active Layer Detachment Slide	IKONOS/Geoeye/Worldview
NOAT0860	Active Layer Detachment Slide	IKONOS/Geoeye/Worldview
NOAT0861	Active Layer Detachment Slide	IKONOS/Geoeye/Worldview
NOAT0862	Active Layer Detachment Slide	IKONOS/Geoeye/Worldview
NOAT0863	Active Layer Detachment Slide	IKONOS/Geoeye/Worldview
NOAT0864	Active Layer Detachment Slide	IKONOS/Geoeye/Worldview
NOAT0865	Active Layer Detachment Slide	IKONOS/Geoeye/Worldview
NOAT0866	Active Layer Detachment Slide	IKONOS/Geoeye/Worldview
NOAT0867	Active Layer Detachment Slide	IKONOS/Geoeye/Worldview
NOAT0868	Active Layer Detachment Slide	IKONOS/Geoeye/Worldview
NOAT0869	Active Layer Detachment Slide	IKONOS/Geoeye/Worldview
NOAT0870	Active Layer Detachment Slide	IKONOS/Geoeye/Worldview
NOAT0871	Active Layer Detachment Slide	IKONOS/Geoeye/Worldview
NOAT0872	Active Layer Detachment Slide	IKONOS/Geoeye/Worldview
NOAT0873	Active Layer Detachment Slide	IKONOS/Geoeye/Worldview
NOAT0874	Active Layer Detachment Slide	IKONOS/Geoeye/Worldview
NOAT0875	Active Layer Detachment Slide	IKONOS/Geoeye/Worldview
NOAT0876	Active Layer Detachment Slide	IKONOS/Geoeye/Worldview
NOAT0877	Active Layer Detachment Slide	IKONOS/Geoeye/Worldview
NOAT0878	Active Layer Detachment Slide	IKONOS/Geoeye/Worldview
NOAT0879	Active Layer Detachment Slide	IKONOS/Geoeye/Worldview

NPS	2010	67.88510	-160.35190
NPS	2010	67.86504	-160.23200
NPS	2010	67.84981	-161.31854
NPS	2010	67.84750	-161.32403
NPS	2010	67.85081	-161.33516
NPS	2010	67.85187	-161.32841
NPS	2010	67.85922	-161.31648
NPS	2010	67.85785	-161.36514
NPS	2010	67.85231	-161.35445
NPS	2010	67.84866	-161.35107
NPS	2010	67.84947	-161.34774
NPS	2010	67.84765	-161.35417
NPS	2010	67.85677	-161.31618
NPS	2010	67.85608	-161.31660
NPS	2010	67.86169	-161.32181
NPS	2010	67.86239	-161.33285
NPS	2010	67.86217	-161.32946
NPS	2010	67.86242	-161.33067
NPS	2010	67.86264	-161.33061
NPS	2010	67.86330	-161.33025
NPS	2010	67.86067	-161.01494
NPS	2010	67.85979	-161.01649
NPS	2010	67.83021	-161.00989
NPS	2010	67.81760	-160.98685
NPS	2010	67.81564	-160.98558
NPS	2010	67.80728	-160.98767
NPS	2010	67.80766	-160.98953
NPS	2010	67.80653	-160.99278
NPS	2010	67.83008	-160.95565
NPS	2010	67.83000	-160.95513
NPS	2010	67.82945	-160.95513
NPS	2010	67.82853	-160.95381

NOAT0890	Active Layer Detachment Slide	IKONOS/Geoeye/Worldview
NOAT0891	Active Layer Detachment Slide	IKONOS/Geoeye/Worldview
NOAT0892	Active Layer Detachment Slide	IKONOS/Geoeye/Worldview
NOAT0893	Active Layer Detachment Slide	IKONOS/Geoeye/Worldview
NOAT0894	Active Layer Detachment Slide	IKONOS/Geoeye/Worldview
NOAT0895	Active Layer Detachment Slide	IKONOS/Geoeye/Worldview
NOAT0896	Active Layer Detachment Slide	IKONOS/Geoeye/Worldview
NOAT0897	Active Layer Detachment Slide	IKONOS/Geoeye/Worldview
NOAT0898	Active Layer Detachment Slide	IKONOS/Geoeye/Worldview
NOAT0899	Active Layer Detachment Slide	IKONOS/Geoeye/Worldview
NOAT0900	Active Layer Detachment Slide	IKONOS/Geoeye/Worldview
NOAT0907	Retrogressive Thaw Slump	IKONOS/Geoeye/Worldview
NOAT0908	Active Layer Detachment Slide	IKONOS/Geoeye/Worldview
NOAT0909	Active Layer Detachment Slide	IKONOS/Geoeye/Worldview
NOAT0910	Active Layer Detachment Slide	IKONOS/Geoeye/Worldview
NOAT0911	Active Layer Detachment Slide	IKONOS/Geoeye/Worldview
NOAT0912	Active Layer Detachment Slide	IKONOS/Geoeye/Worldview
NOAT0913	Active Layer Detachment Slide	IKONOS/Geoeye/Worldview
NOAT0914	Active Layer Detachment Slide	IKONOS/Geoeye/Worldview
NOAT0915	Active Layer Detachment Slide	IKONOS/Geoeye/Worldview
NOAT0916	Active Layer Detachment Slide	IKONOS/Geoeye/Worldview
NOAT0917	Active Layer Detachment Slide	IKONOS/Geoeye/Worldview
NOAT0918	Active Layer Detachment Slide	IKONOS/Geoeye/Worldview
NOAT0919	Active Layer Detachment Slide	IKONOS/Geoeye/Worldview
NOAT0920	Active Layer Detachment Slide	IKONOS/Geoeye/Worldview
NOAT0921	Active Layer Detachment Slide	IKONOS/Geoeye/Worldview
NOAT0922	Active Layer Detachment Slide	IKONOS/Geoeye/Worldview
NOAT0923	Active Layer Detachment Slide	IKONOS/Geoeye/Worldview
NOAT0924	Active Layer Detachment Slide	IKONOS/Geoeye/Worldview
NOAT0925	Active Layer Detachment Slide	IKONOS/Geoeye/Worldview
NOAT0926	Active Layer Detachment Slide	IKONOS/Geoeye/Worldview
NOAT0927	Active Layer Detachment Slide	IKONOS/Geoeye/Worldview

NPS	2010	67.82816	-160.95483
NPS	2010	67.82659	-160.95112
NPS	2010	67.82501	-160.95317
NPS	2010	67.82450	-160.95265
NPS	2010	67.82488	-160.95128
NPS	2010	67.83231	-161.13458
NPS	2010	67.85706	-161.31919
NPS	2010	67.82291	-161.35991
NPS	2010	67.81789	-161.44742
NPS	2010	67.81591	-161.44786
NPS	2010	67.78336	-161.50195
NPS	2010	67.83707	-160.71998
NPS	2010	67.86416	-160.55662
NPS	2010	67.81951	-160.37691
NPS	2010	67.80501	-160.43967
NPS	2010	67.81712	-160.49499
NPS	2010	67.82692	-160.58715
NPS	2010	67.82636	-160.58711
NPS	2010	67.82482	-160.58791
NPS	2010	67.82380	-160.58514
NPS	2010	67.82853	-160.62263
NPS	2010	67.83110	-160.63190
NPS	2010	67.82853	-160.63252
NPS	2010	67.82563	-160.62502
NPS	2010	67.82470	-160.62282
NPS	2010	67.82422	-160.61956
NPS	2010	67.82385	-160.61834
NPS	2010	67.82834	-160.65041
NPS	2010	67.74781	-161.72151
NPS	2010	67.74780	-161.71757
NPS	2010	67.74524	-161.72192
NPS	2010	67.74516	-161.72584

NOAT0928	Active Layer Detachment Slide	IKONOS/Geoeye/Worldview
NOAT0929	Active Layer Detachment Slide	IKONOS/Geoeye/Worldview
NOAT0930	Active Layer Detachment Slide	IKONOS/Geoeye/Worldview
NOAT0931	Active Layer Detachment Slide	IKONOS/Geoeye/Worldview
NOAT0932	Active Layer Detachment Slide	IKONOS/Geoeye/Worldview
NOAT0933	Active Layer Detachment Slide	IKONOS/Geoeye/Worldview
NOAT0934	Active Layer Detachment Slide	IKONOS/Geoeye/Worldview
NOAT0935	Active Layer Detachment Slide	IKONOS/Geoeye/Worldview
NOAT0936	Active Layer Detachment Slide	IKONOS/Geoeye/Worldview
NOAT0937	Active Layer Detachment Slide	IKONOS/Geoeye/Worldview
NOAT0938	Active Layer Detachment Slide	IKONOS/Geoeye/Worldview
NOAT0939	Active Layer Detachment Slide	IKONOS/Geoeye/Worldview
NOAT0940	Active Layer Detachment Slide	IKONOS/Geoeye/Worldview
NOAT0941	Active Layer Detachment Slide	IKONOS/Geoeye/Worldview
NOAT0942	Active Layer Detachment Slide	IKONOS/Geoeye/Worldview
NOAT0943	Active Layer Detachment Slide	IKONOS/Geoeye/Worldview
NOAT0944	Active Layer Detachment Slide	IKONOS/Geoeye/Worldview
NOAT0945	Active Layer Detachment Slide	IKONOS/Geoeye/Worldview
NOAT0946	Active Layer Detachment Slide	IKONOS/Geoeye/Worldview
NOAT0947	Active Layer Detachment Slide	IKONOS/Geoeye/Worldview
NOAT0948	Active Layer Detachment Slide	IKONOS/Geoeye/Worldview
NOAT0949	Active Layer Detachment Slide	IKONOS/Geoeye/Worldview
NOAT0950	Active Layer Detachment Slide	IKONOS/Geoeye/Worldview
NOAT0951	Active Layer Detachment Slide	IKONOS/Geoeye/Worldview
NOAT0952	Active Layer Detachment Slide	IKONOS/Geoeye/Worldview
NOAT0953	Active Layer Detachment Slide	IKONOS/Geoeye/Worldview
NOAT0954	Active Layer Detachment Slide	IKONOS/Geoeye/Worldview
NOAT0955	Active Layer Detachment Slide	IKONOS/Geoeye/Worldview
NOAT0956	Active Layer Detachment Slide	IKONOS/Geoeye/Worldview
NOAT0957	Active Layer Detachment Slide	IKONOS/Geoeye/Worldview
NOAT0958	Active Layer Detachment Slide	IKONOS/Geoeye/Worldview
NOAT0959	Active Layer Detachment Slide	IKONOS/Geoeye/Worldview

NPS	2010	67.70317	-161.60469
NPS	2010	67.70869	-161.71891
NPS	2010	67.68001	-161.77245
NPS	2010	67.68525	-161.77666
NPS	2010	67.68949	-161.75959
NPS	2010	67.67080	-161.59220
NPS	2010	67.67152	-161.59329
NPS	2010	67.67147	-161.59683
NPS	2010	67.67187	-161.59808
NPS	2010	67.67006	-161.59885
NPS	2010	67.77236	-160.45029
NPS	2010	67.78545	-160.37518
NPS	2010	67.78496	-160.37437
NPS	2010	67.79829	-160.36423
NPS	2010	67.68467	-161.77934
NPS	2010	67.76414	-161.48831
NPS	2010	67.76220	-161.48792
NPS	2010	67.76248	-161.49210
NPS	2010	67.76257	-161.45411
NPS	2010	67.76577	-161.43254
NPS	2010	67.76539	-161.43550
NPS	2010	67.76802	-161.42787
NPS	2010	67.76641	-161.42366
NPS	2010	67.76080	-161.42004
NPS	2010	67.75869	-161.42705
NPS	2010	67.75888	-161.42478
NPS	2010	67.75994	-161.41703
NPS	2010	67.73663	-161.42694
NPS	2010	67.73590	-161.41370
NPS	2010	67.73294	-161.41814
NPS	2010	67.72979	-161.40171
NPS	2010	67.72835	-161.40552

NOAT0960	Active Layer Detachment Slide	IKONOS/Geoeye/Worldview
NOAT0961	Active Layer Detachment Slide	IKONOS/Geoeye/Worldview
NOAT0962	Active Layer Detachment Slide	IKONOS/Geoeye/Worldview
NOAT0963	Active Layer Detachment Slide	IKONOS/Geoeye/Worldview
NOAT0964	Active Layer Detachment Slide	IKONOS/Geoeye/Worldview
NOAT0965	Active Layer Detachment Slide	IKONOS/Geoeye/Worldview
NOAT0966	Active Layer Detachment Slide	IKONOS/Geoeye/Worldview
NOAT0967	Active Layer Detachment Slide	IKONOS/Geoeye/Worldview
NOAT0968	Active Layer Detachment Slide	IKONOS/Geoeye/Worldview
NOAT0969	Active Layer Detachment Slide	IKONOS/Geoeye/Worldview
NOAT0970	Active Layer Detachment Slide	IKONOS/Geoeye/Worldview
NOAT0971	Active Layer Detachment Slide	IKONOS/Geoeye/Worldview
NOAT0972	Active Layer Detachment Slide	IKONOS/Geoeye/Worldview
NOAT0973	Active Layer Detachment Slide	IKONOS/Geoeye/Worldview
NOAT0974	Active Layer Detachment Slide	IKONOS/Geoeye/Worldview
NOAT0975	Active Layer Detachment Slide	IKONOS/Geoeye/Worldview
NOAT0976	Active Layer Detachment Slide	IKONOS/Geoeye/Worldview
NOAT0977	Active Layer Detachment Slide	IKONOS/Geoeye/Worldview
NOAT0978	Active Layer Detachment Slide	IKONOS/Geoeye/Worldview
NOAT0979	Active Layer Detachment Slide	IKONOS/Geoeye/Worldview
NOAT0980	Active Layer Detachment Slide	IKONOS/Geoeye/Worldview
NOAT0981	Active Layer Detachment Slide	IKONOS/Geoeye/Worldview
NOAT0982	Active Layer Detachment Slide	IKONOS/Geoeye/Worldview
NOAT0983	Retrogressive Thaw Slump	IKONOS/Geoeye/Worldview
NOAT0984	Active Layer Detachment Slide	IKONOS/Geoeye/Worldview
NOAT0985	Active Layer Detachment Slide	IKONOS/Geoeye/Worldview
NOAT0986	Active Layer Detachment Slide	IKONOS/Geoeye/Worldview
NOAT0987	Active Layer Detachment Slide	IKONOS/Geoeye/Worldview
NOAT0988	Active Layer Detachment Slide	IKONOS/Geoeye/Worldview
NOAT0989	Active Layer Detachment Slide	IKONOS/Geoeye/Worldview
NOAT0990	Active Layer Detachment Slide	IKONOS/Geoeye/Worldview
NOAT0991	Active Layer Detachment Slide	IKONOS/Geoeye/Worldview

NPS	2010	67.73321	-161.39676
NPS	2010	67.71815	-161.41301
NPS	2010	67.71802	-161.41288
NPS	2010	67.72159	-161.42973
NPS	2010	67.72069	-161.43351
NPS	2010	67.76119	-161.41573
NPS	2010	67.71802	-161.43445
NPS	2010	67.71675	-161.42953
NPS	2010	67.71646	-161.43257
NPS	2010	67.71477	-161.43650
NPS	2010	67.71446	-161.43620
NPS	2010	67.71723	-161.44124
NPS	2010	67.71846	-161.43560
NPS	2010	67.71196	-161.40628
NPS	2010	67.72164	-161.53523
NPS	2010	67.72268	-161.54081
NPS	2010	67.71017	-161.55924
NPS	2010	67.71021	-161.55681
NPS	2010	67.70870	-161.55908
NPS	2010	67.70828	-161.55704
NPS	2010	67.69496	-161.56259
NPS	2010	67.69340	-161.56300
NPS	2010	67.68049	-161.52766
NPS	2010	67.67035	-161.57622
NPS	2010	67.67129	-161.58152
NPS	2010	67.68736	-161.52996
NPS	2010	67.67885	-161.45044
NPS	2010	67.66880	-161.44665
NPS	2010	67.66345	-161.45302
NPS	2010	67.66303	-161.45335
NPS	2010	67.66260	-161.45340
NPS	2010	67.67222	-161.39397

NOAT0992	Active Layer Detachment Slide	IKONOS/Geoeye/Worldview
NOAT0993	Active Layer Detachment Slide	IKONOS/Geoeye/Worldview
NOAT0994	Active Layer Detachment Slide	IKONOS/Geoeye/Worldview
NOAT0995	Active Layer Detachment Slide	IKONOS/Geoeye/Worldview
NOAT0996	Active Layer Detachment Slide	IKONOS/Geoeye/Worldview
NOAT0997	Active Layer Detachment Slide	IKONOS/Geoeye/Worldview
NOAT0998	Active Layer Detachment Slide	IKONOS/Geoeye/Worldview
NOAT0999	Active Layer Detachment Slide	IKONOS/Geoeye/Worldview
NOAT1000	Active Layer Detachment Slide	IKONOS/Geoeye/Worldview
NOAT1001	Active Layer Detachment Slide	IKONOS/Geoeye/Worldview
NOAT1002	Active Layer Detachment Slide	IKONOS/Geoeye/Worldview
NOAT1003	Active Layer Detachment Slide	IKONOS/Geoeye/Worldview
NOAT1004	Active Layer Detachment Slide	IKONOS/Geoeye/Worldview
NOAT1005	Active Layer Detachment Slide	IKONOS/Geoeye/Worldview
NOAT1006	Active Layer Detachment Slide	IKONOS/Geoeye/Worldview
NOAT1007	Active Layer Detachment Slide	IKONOS/Geoeye/Worldview
NOAT1008	Active Layer Detachment Slide	IKONOS/Geoeye/Worldview
NOAT1009	Active Layer Detachment Slide	IKONOS/Geoeye/Worldview
NOAT1010	Active Layer Detachment Slide	IKONOS/Geoeye/Worldview
NOAT1011	Active Layer Detachment Slide	IKONOS/Geoeye/Worldview
NOAT1012	Active Layer Detachment Slide	IKONOS/Geoeye/Worldview
NOAT1013	Active Layer Detachment Slide	IKONOS/Geoeye/Worldview
NOAT1014	Active Layer Detachment Slide	IKONOS/Geoeye/Worldview
NOAT1015	Active Layer Detachment Slide	IKONOS/Geoeye/Worldview
NOAT1016	Retrogressive Thaw Slump	IKONOS/Geoeye/Worldview
NOAT1017	Active Layer Detachment Slide	IKONOS/Geoeye/Worldview
NOAT1018	Active Layer Detachment Slide	IKONOS/Geoeye/Worldview
NOAT1019	Active Layer Detachment Slide	IKONOS/Geoeye/Worldview
NOAT1020	Active Layer Detachment Slide	IKONOS/Geoeye/Worldview
NOAT1021	Retrogressive Thaw Slump	IKONOS/Geoeye/Worldview
NOAT1022	Active Layer Detachment Slide	IKONOS/Geoeye/Worldview
NOAT1023	Active Layer Detachment Slide	IKONOS/Geoeye/Worldview

NPS	2010	67.67162	-161.39546
NPS	2010	67.67077	-161.39649
NPS	2010	67.67063	-161.39921
NPS	2010	67.67132	-161.40045
NPS	2010	67.67678	-161.41059
NPS	2010	67.67970	-161.40920
NPS	2010	67.72144	-161.55108
NPS	2010	67.71925	-161.55200
NPS	2010	67.74952	-160.94106
NPS	2010	67.68051	-160.55813
NPS	2010	67.68046	-160.45449
NPS	2010	67.72163	-160.42821
NPS	2010	67.74737	-160.29642
NPS	2010	67.74763	-160.29419
NPS	2010	67.68407	-161.93606
NPS	2010	67.66654	-161.79251
NPS	2010	67.65971	-161.77634
NPS	2010	67.66205	-161.61108
NPS	2010	67.66198	-161.61592
NPS	2010	67.65829	-161.60716
NPS	2010	67.65766	-161.60917
NPS	2010	67.66741	-161.61261
NPS	2010	67.67214	-161.62908
NPS	2010	67.63565	-161.66280
NPS	2010	67.64871	-161.60656
NPS	2010	67.65223	-161.64655
NPS	2010	67.60026	-161.82656
NPS	2010	67.58852	-161.72871
NPS	2010	67.61662	-161.61920
NPS	2010	67.58748	-161.59193
NPS	2010	67.66835	-161.52898
NPS	2010	67.66707	-161.58050

NOAT1024	Active Layer Detachment Slide	IKONOS/Geoeye/Worldview
NOAT1025	Active Layer Detachment Slide	IKONOS/Geoeye/Worldview
NOAT1026	Active Layer Detachment Slide	IKONOS/Geoeye/Worldview
NOAT1027	Retrogressive Thaw Slump	IKONOS/Geoeye/Worldview
NOAT1028	Active Layer Detachment Slide	IKONOS/Geoeye/Worldview
NOAT1029	Active Layer Detachment Slide	IKONOS/Geoeye/Worldview
NOAT1030	Active Layer Detachment Slide	IKONOS/Geoeye/Worldview
NOAT1031	Active Layer Detachment Slide	IKONOS/Geoeye/Worldview
NOAT1032	Active Layer Detachment Slide	IKONOS/Geoeye/Worldview
NOAT1033	Active Layer Detachment Slide	IKONOS/Geoeye/Worldview
NOAT1034	Active Layer Detachment Slide	IKONOS/Geoeye/Worldview
NOAT1035	Active Layer Detachment Slide	IKONOS/Geoeye/Worldview
NOAT1036	Active Layer Detachment Slide	IKONOS/Geoeye/Worldview
NOAT1037	Active Layer Detachment Slide	IKONOS/Geoeye/Worldview
NOAT1038	Active Layer Detachment Slide	IKONOS/Geoeye/Worldview
NOAT1039	Active Layer Detachment Slide	IKONOS/Geoeye/Worldview
NOAT1040	Active Layer Detachment Slide	IKONOS/Geoeye/Worldview
NOAT1041	Active Layer Detachment Slide	IKONOS/Geoeye/Worldview
NOAT1042	Active Layer Detachment Slide	IKONOS/Geoeye/Worldview
NOAT1043	Active Layer Detachment Slide	IKONOS/Geoeye/Worldview
NOAT1044	Active Layer Detachment Slide	IKONOS/Geoeye/Worldview
NOAT1045	Retrogressive Thaw Slump	IKONOS/Geoeye/Worldview
NOAT1046	Active Layer Detachment Slide	IKONOS/Geoeye/Worldview
NOAT1048	Active Layer Detachment Slide	IKONOS/Geoeye/Worldview
NOAT1049	Active Layer Detachment Slide	IKONOS/Geoeye/Worldview
NOAT1050	Active Layer Detachment Slide	IKONOS/Geoeye/Worldview
NOAT1051	Active Layer Detachment Slide	IKONOS/Geoeye/Worldview
NOAT1052	Active Layer Detachment Slide	IKONOS/Geoeye/Worldview
NOAT1053	Retrogressive Thaw Slump	IKONOS/Geoeye/Worldview
NOAT1054	Active Layer Detachment Slide	IKONOS/Geoeye/Worldview
NOAT1055	Active Layer Detachment Slide	IKONOS/Geoeye/Worldview
NOAT1056	Active Layer Detachment Slide	IKONOS/Geoeye/Worldview

NPS	2010	67.68151	-161.60763
NPS	2010	67.65903	-161.44620
NPS	2010	67.66045	-161.44849
NPS	2010	67.66126	-161.50190
NPS	2010	67.63125	-161.55535
NPS	2010	67.63457	-161.57719
NPS	2010	67.62735	-161.57254
NPS	2010	67.65226	-161.46891
NPS	2010	67.65283	-161.47127
NPS	2010	67.65293	-161.47442
NPS	2010	67.65445	-161.47433
NPS	2010	67.65471	-161.47565
NPS	2010	67.63090	-161.51742
NPS	2010	67.63028	-161.51628
NPS	2010	67.63261	-161.54622
NPS	2010	67.62993	-161.55067
NPS	2010	67.63004	-161.54983
NPS	2010	67.59355	-161.57477
NPS	2010	67.59249	-161.57895
NPS	2010	67.60835	-161.52772
NPS	2010	67.60748	-161.52785
NPS	2010	67.60534	-161.52449
NPS	2010	67.60496	-161.51384
NPS	2010	67.68164	-160.55256
NPS	2010	67.65463	-160.45684
NPS	2010	67.65469	-160.44586
NPS	2010	67.64829	-160.43892
NPS	2010	67.63270	-160.41875
NPS	2010	67.68967	-160.46585
NPS	2010	67.69109	-160.44794
NPS	2010	67.69102	-160.38081
NPS	2010	67.75302	-160.19221

NOAT1057	Active Layer Detachment Slide	IKONOS/Geoeye/Worldview
NOAT1058	Active Layer Detachment Slide	IKONOS/Geoeye/Worldview
NOAT1059	Active Layer Detachment Slide	IKONOS/Geoeye/Worldview
NOAT1060	Active Layer Detachment Slide	IKONOS/Geoeye/Worldview
NOAT1061	Active Layer Detachment Slide	IKONOS/Geoeye/Worldview
NOAT1062	Active Layer Detachment Slide	IKONOS/Geoeye/Worldview
NOAT1063	Active Layer Detachment Slide	IKONOS/Geoeye/Worldview
NOAT1064	Active Layer Detachment Slide	IKONOS/Geoeye/Worldview
NOAT1065	Active Layer Detachment Slide	IKONOS/Geoeye/Worldview
NOAT1066	Active Layer Detachment Slide	IKONOS/Geoeye/Worldview
NOAT1067	Active Layer Detachment Slide	IKONOS/Geoeye/Worldview
NOAT1068	Active Layer Detachment Slide	IKONOS/Geoeye/Worldview
NOAT1069	Active Layer Detachment Slide	IKONOS/Geoeye/Worldview
NOAT1070	Active Layer Detachment Slide	IKONOS/Geoeye/Worldview
NOAT1071	Active Layer Detachment Slide	IKONOS/Geoeye/Worldview
NOAT1072	Active Layer Detachment Slide	IKONOS/Geoeye/Worldview
NOAT1073	Active Layer Detachment Slide	IKONOS/Geoeye/Worldview
NOAT1074	Active Layer Detachment Slide	IKONOS/Geoeye/Worldview
NOAT1075	Active Layer Detachment Slide	IKONOS/Geoeye/Worldview
NOAT1076	Active Layer Detachment Slide	IKONOS/Geoeye/Worldview
NOAT1077	Active Layer Detachment Slide	IKONOS/Geoeye/Worldview
NOAT1078	Active Layer Detachment Slide	IKONOS/Geoeye/Worldview
NOAT1079	Active Layer Detachment Slide	IKONOS/Geoeye/Worldview
NOAT1080	Active Layer Detachment Slide	IKONOS/Geoeye/Worldview
NOAT1081	Active Layer Detachment Slide	IKONOS/Geoeye/Worldview
NOAT1082	Active Layer Detachment Slide	IKONOS/Geoeye/Worldview
NOAT1083	Active Layer Detachment Slide	IKONOS/Geoeye/Worldview
NOAT1084	Active Layer Detachment Slide	IKONOS/Geoeye/Worldview
NOAT1085	Active Layer Detachment Slide	IKONOS/Geoeye/Worldview
NOAT1086	Active Layer Detachment Slide	IKONOS/Geoeye/Worldview
NOAT1087	Active Layer Detachment Slide	IKONOS/Geoeye/Worldview
NOAT1088	Active Layer Detachment Slide	IKONOS/Geoeye/Worldview

NPS	2010	67.71727	-160.27880
NPS	2010	67.71622	-160.27740
NPS	2010	67.84212	-160.22338
NPS	2010	67.83884	-160.22387
NPS	2010	67.83718	-160.18341
NPS	2010	67.83484	-160.17860
NPS	2010	67.83545	-160.18035
NPS	2010	67.83407	-160.18468
NPS	2010	67.85860	-160.05166
NPS	2010	67.85982	-160.04915
NPS	2010	67.85633	-160.00419
NPS	2010	67.85076	-159.97591
NPS	2010	67.85343	-159.94794
NPS	2010	67.86083	-159.95540
NPS	2010	67.86126	-159.95381
NPS	2010	67.86169	-159.95213
NPS	2010	67.79341	-160.06704
NPS	2010	67.82034	-160.10566
NPS	2010	67.81977	-160.39135
NPS	2010	67.82758	-160.42769
NPS	2010	67.82566	-160.42771
NPS	2010	67.81905	-160.41250
NPS	2010	67.80433	-160.36247
NPS	2010	67.78918	-160.38870
NPS	2010	67.79588	-160.13608
NPS	2010	67.78754	-160.27963
NPS	2010	67.77081	-160.28824
NPS	2010	67.76478	-160.27686
NPS	2010	67.76983	-160.20621
NPS	2010	67.76903	-160.20164
NPS	2010	67.76753	-160.20458
NPS	2010	67.76575	-160.20618

NOAT1089	Active Layer Detachment Slide	IKONOS/Geoeye/Worldview
NOAT1090	Active Layer Detachment Slide	IKONOS/Geoeye/Worldview
NOAT1091	Active Layer Detachment Slide	IKONOS/Geoeye/Worldview
NOAT1092	Active Layer Detachment Slide	IKONOS/Geoeye/Worldview
NOAT1093	Active Layer Detachment Slide	IKONOS/Geoeye/Worldview
NOAT1094	Active Layer Detachment Slide	IKONOS/Geoeye/Worldview
NOAT1095	Active Layer Detachment Slide	IKONOS/Geoeye/Worldview
NOAT1096	Active Layer Detachment Slide	IKONOS/Geoeye/Worldview
NOAT1097	Active Layer Detachment Slide	IKONOS/Geoeye/Worldview
NOAT1098	Active Layer Detachment Slide	IKONOS/Geoeye/Worldview
NOAT1099	Active Layer Detachment Slide	IKONOS/Geoeye/Worldview
NOAT1100	Retrogressive Thaw Slump	IKONOS/Geoeye/Worldview
NOAT1101	Retrogressive Thaw Slump	IKONOS/Geoeye/Worldview
NOAT1102	Retrogressive Thaw Slump	IKONOS/Geoeye/Worldview
NOAT1103	Active Layer Detachment Slide	IKONOS/Geoeye/Worldview
NOAT1104	Retrogressive Thaw Slump	IKONOS/Geoeye/Worldview
NOAT1105	Active Layer Detachment Slide	IKONOS/Geoeye/Worldview
NOAT1106	Active Layer Detachment Slide	IKONOS/Geoeye/Worldview
NOAT1107	Active Layer Detachment Slide	IKONOS/Geoeye/Worldview
NOAT1108	Active Layer Detachment Slide	IKONOS/Geoeye/Worldview
NOAT1109	Active Layer Detachment Slide	IKONOS/Geoeye/Worldview
NOAT1110	Active Layer Detachment Slide	IKONOS/Geoeye/Worldview
NOAT1111	Active Layer Detachment Slide	IKONOS/Geoeye/Worldview
NOAT1112	Active Layer Detachment Slide	IKONOS/Geoeye/Worldview
NOAT1113	Active Layer Detachment Slide	IKONOS/Geoeye/Worldview
NOAT1114	Active Layer Detachment Slide	IKONOS/Geoeye/Worldview
NOAT1115	Active Layer Detachment Slide	IKONOS/Geoeye/Worldview
NOAT1116	Active Layer Detachment Slide	IKONOS/Geoeye/Worldview
NOAT1117	Active Layer Detachment Slide	IKONOS/Geoeye/Worldview
NOAT1118	Retrogressive Thaw Slump	IKONOS/Geoeye/Worldview
NOAT1119	Retrogressive Thaw Slump	IKONOS/Geoeye/Worldview
NOAT1120	Retrogressive Thaw Slump	IKONOS/Geoeye/Worldview

NPS	2010	67.78825	-160.18805
NPS	2010	67.78480	-160.19501
NPS	2010	67.78472	-160.19552
NPS	2010	67.78235	-160.19806
NPS	2010	67.75680	-160.21201
NPS	2010	67.77785	-160.23583
NPS	2010	67.77280	-160.07920
NPS	2010	67.80143	-160.02162
NPS	2010	67.78281	-160.14336
NPS	2010	67.78299	-160.13987
NPS	2010	67.78860	-160.02754
NPS	2010	67.93941	-160.22320
NPS	2010	67.94462	-159.83989
NPS	2010	67.92062	-159.83681
NPS	2010	67.92716	-159.72228
NPS	2010	67.94503	-159.69706
NPS	2010	67.95013	-159.73806
NPS	2010	67.95027	-159.69920
NPS	2010	67.91250	-159.64119
NPS	2010	67.91665	-159.64666
NPS	2010	67.91022	-159.62862
NPS	2010	67.90854	-159.63253
NPS	2010	67.90876	-159.62527
NPS	2010	67.88687	-159.71803
NPS	2010	67.89409	-159.71461
NPS	2010	67.91766	-159.76780
NPS	2010	67.89482	-159.80210
NPS	2010	67.88074	-159.95415
NPS	2010	67.85687	-159.50490
NPS	2010	68.00375	-160.16701
NPS	2010	67.99354	-160.17372
NPS	2010	67.99251	-160.17887

NOAT1121	Retrogressive Thaw Slump	IKONOS/Geoeye/Worldview
NOAT1122	Retrogressive Thaw Slump	IKONOS/Geoeye/Worldview
NOAT1123	Active Layer Detachment Slide	IKONOS/Geoeye/Worldview
NOAT1124	Active Layer Detachment Slide	IKONOS/Geoeye/Worldview
NOAT1125	Active Layer Detachment Slide	IKONOS/Geoeye/Worldview
NOAT1126	Active Layer Detachment Slide	IKONOS/Geoeye/Worldview
NOAT1127	Retrogressive Thaw Slump	IKONOS/Geoeye/Worldview
NOAT1128	Retrogressive Thaw Slump	IKONOS/Geoeye/Worldview
NOAT1129	Active Layer Detachment Slide	IKONOS/Geoeye/Worldview
NOAT1130	Active Layer Detachment Slide	IKONOS/Geoeye/Worldview
NOAT1131	Retrogressive Thaw Slump	IKONOS/Geoeye/Worldview
NOAT1132	Retrogressive Thaw Slump	IKONOS/Geoeye/Worldview
NOAT1133	Retrogressive Thaw Slump	IKONOS/Geoeye/Worldview
NOAT1134	Retrogressive Thaw Slump	IKONOS/Geoeye/Worldview
NOAT1135	Retrogressive Thaw Slump	IKONOS/Geoeye/Worldview
NOAT1136	Retrogressive Thaw Slump	IKONOS/Geoeye/Worldview
NOAT1137	Retrogressive Thaw Slump	IKONOS/Geoeye/Worldview
NOAT1138	Active Layer Detachment Slide	IKONOS/Geoeye/Worldview
NOAT1139	Active Layer Detachment Slide	IKONOS/Geoeye/Worldview
NOAT1140	Retrogressive Thaw Slump	IKONOS/Geoeye/Worldview
NOAT1141	Retrogressive Thaw Slump	IKONOS/Geoeye/Worldview
NOAT1142	Retrogressive Thaw Slump	IKONOS/Geoeye/Worldview
NOAT1143	Retrogressive Thaw Slump	IKONOS/Geoeye/Worldview
NOAT1144	Active Layer Detachment Slide	IKONOS/Geoeye/Worldview
NOAT1145	Active Layer Detachment Slide	IKONOS/Geoeye/Worldview
NOAT1146	Active Layer Detachment Slide	IKONOS/Geoeye/Worldview
NOAT1148	Active Layer Detachment Slide	IKONOS/Geoeye/Worldview
NOAT1149	Retrogressive Thaw Slump	IKONOS/Geoeye/Worldview
NOAT1150	Retrogressive Thaw Slump	IKONOS/Geoeye/Worldview
NOAT1151	Active Layer Detachment Slide	IKONOS/Geoeye/Worldview
NOAT1152	Active Layer Detachment Slide	IKONOS/Geoeye/Worldview
NOAT1153	Active Layer Detachment Slide	IKONOS/Geoeye/Worldview

NPS	2010	67.96821	-160.24937
NPS	2010	67.96850	-160.25053
NPS	2010	67.95308	-159.84644
NPS	2010	67.95366	-159.84421
NPS	2010	67.95278	-159.84275
NPS	2010	67.95263	-159.84128
NPS	2010	68.19533	-159.54531
NPS	2010	68.19567	-159.54543
NPS	2010	68.29839	-157.23420
NPS	2010	67.97623	-156.48396
NPS	2010	67.80908	-160.58964
NPS	2010	67.80896	-160.59168
NPS	2010	67.81792	-160.61468
NPS	2010	67.81791	-160.61208
NPS	2010	67.81782	-160.61096
NPS	2010	67.81680	-160.60360
NPS	2010	67.81334	-160.57721
NPS	2010	67.80205	-160.73005
NPS	2010	67.80206	-160.72940
NPS	2010	67.78430	-160.70149
NPS	2010	67.78774	-160.71423
NPS	2010	67.78851	-160.71322
NPS	2010	67.78589	-160.71985
NPS	2010	67.76846	-160.58510
NPS	2010	67.73901	-160.46363
NPS	2010	67.67127	-161.90117
NPS	2010	68.26168	-157.82167
NPS	2010	68.11833	-156.78252
NPS	2010	67.98109	-157.41879
NPS	2010	67.83258	-161.13556
NPS	2010	67.70958	-161.41256
NPS	2010	67.59216	-161.60698

NOAT1154	Active Layer Detachment Slide	IKONOS/Geoeye/Worldview
NOAT1155	Active Layer Detachment Slide	IKONOS/Geoeye/Worldview
NOAT1156	Active Layer Detachment Slide	IKONOS/Geoeye/Worldview
NOAT1157	Active Layer Detachment Slide	IKONOS/Geoeye/Worldview
NOAT1158	Active Layer Detachment Slide	IKONOS/Geoeye/Worldview
NOAT1159	Active Layer Detachment Slide	IKONOS/Geoeye/Worldview
NOAT1160	Active Layer Detachment Slide	IKONOS/Geoeye/Worldview
NOAT1161	Retrogressive Thaw Slump	IKONOS/Geoeye/Worldview
NOAT1162	Active Layer Detachment Slide	IKONOS/Geoeye/Worldview
NOAT1163	Active Layer Detachment Slide	IKONOS/Geoeye/Worldview
NOAT1164	Active Layer Detachment Slide	IKONOS/Geoeye/Worldview
NOAT1165	Active Layer Detachment Slide	IKONOS/Geoeye/Worldview
NOAT1166	Retrogressive Thaw Slump	IKONOS/Geoeye/Worldview
NOAT1167	Retrogressive Thaw Slump	IKONOS/Geoeye/Worldview
NOAT1168	Retrogressive Thaw Slump	IKONOS/Geoeye/Worldview
NOAT1169	Retrogressive Thaw Slump	IKONOS/Geoeye/Worldview
NOAT1170	Retrogressive Thaw Slump	IKONOS/Geoeye/Worldview
NOAT1171	Retrogressive Thaw Slump	IKONOS/Geoeye/Worldview
NOAT1172	Retrogressive Thaw Slump	IKONOS/Geoeye/Worldview
NOAT1173	Retrogressive Thaw Slump	IKONOS/Geoeye/Worldview
NOAT1174	Active Layer Detachment Slide	IKONOS/Geoeye/Worldview
NOAT1175	Active Layer Detachment Slide	IKONOS/Geoeye/Worldview
NOAT1176	Active Layer Detachment Slide	IKONOS/Geoeye/Worldview
NOAT1177	Retrogressive Thaw Slump	IKONOS/Geoeye/Worldview
NOAT1178	Active Layer Detachment Slide	IKONOS/Geoeye/Worldview
NOAT1179	Retrogressive Thaw Slump	IKONOS/Geoeye/Worldview
NOAT1180	Active Layer Detachment Slide	IKONOS/Geoeye/Worldview
NOAT1181	Retrogressive Thaw Slump	IKONOS/Geoeye/Worldview
NOAT1182	Retrogressive Thaw Slump	IKONOS/Geoeye/Worldview
NOAT1183	Retrogressive Thaw Slump	IKONOS/Geoeye/Worldview
NOAT1184	Retrogressive Thaw Slump	IKONOS/Geoeye/Worldview
NOAT1185	Retrogressive Thaw Slump	IKONOS/Geoeye/Worldview

NPS	2010	68.02886	-155.88838
NPS	2010	68.02746	-155.89351
NPS	2010	67.64729	-161.61153
NPS	2010	68.23117	-157.97520
NPS	2010	67.71876	-161.43244
NPS	2010	68.27498	-157.24021
NPS	2010	68.26175	-157.72729
NPS	2010	67.77549	-161.21874
NPS	2010	67.74440	-161.30918
NPS	2010	67.73624	-161.31832
NPS	2010	67.73558	-161.31966
NPS	2010	67.73617	-161.32079
NPS	2010	67.73507	-161.31450
NPS	2010	67.73467	-161.31427
NPS	2010	67.73406	-161.31265
NPS	2010	67.73284	-161.31123
NPS	2010	67.73215	-161.31078
NPS	2010	67.72873	-161.31351
NPS	2010	67.72458	-161.31050
NPS	2010	67.72363	-161.30541
NPS	2010	67.73140	-161.38410
NPS	2010	67.73056	-161.38176
NPS	2010	67.72784	-161.36900
NPS	2010	67.72660	-161.37354
NPS	2010	67.72827	-161.37883
NPS	2010	67.72563	-161.45685
NPS	2010	67.70337	-161.40173
NPS	2010	67.69967	-161.40589
NPS	2010	67.70224	-161.39727
NPS	2010	67.70108	-161.40268
NPS	2010	67.70252	-161.40054
NPS	2010	68.10503	-155.93826

NOAT1186	Retrogressive Thaw Slump	IKONOS/Geoeye/Worldview
NOAT1187	Active Layer Detachment Slide	IKONOS/Geoeye/Worldview
T561	Active Layer Detachment Slide	IKONOS/Geoeye/Worldview
T564	Retrogressive Thaw Slump	IKONOS/Geoeye/Worldview
T565	Retrogressive Thaw Slump	IKONOS/Geoeye/Worldview
T590A	Retrogressive Thaw Slump	IKONOS/Geoeye/Worldview

NPS	2010	68.10443	-155.93896
NPS	2010	68.00007	-155.67149
NPS	2010	67.90859	-161.67982
NPS	2010	67.95337	-161.63149
NPS	2010	67.95410	-161.63199
NPS	2010	68.29255	-161.36024

Appendix B. Elevated Dissolved Organic Carbon Biodegradability from Thawing and Collapsing Permafrost¹

AB.1 Key Points

- Dissolved organic carbon from thawing permafrost is highly biodegradable
- Elevated biodegradability only persists during permafrost collapse
- Controls on dissolved organic carbon processing are tested

AB.2 Abstract

As high latitudes warm, a portion of the large organic carbon pool stored in permafrost will become available for transport to aquatic ecosystems as dissolved organic carbon (DOC). If permafrost DOC is biodegradable, much will be mineralized to the atmosphere in freshwater systems before reaching the ocean, accelerating carbon transfer from permafrost to the atmosphere, whereas if recalcitrant, it will reach marine ecosystems where it may persist over long time periods. We measured biodegradable DOC (BDOC) in water flowing from collapsing permafrost (thermokarst) on the North Slope of Alaska and tested the role of DOC chemical composition and nutrient concentration in determining biodegradability. DOC from collapsing permafrost was some of the most biodegradable reported in natural systems. However, elevated BDOC only persisted during active permafrost degradation, with a return to pre-disturbance levels once thermokarst features stabilized. Biodegradability was correlated with background nutrient concentration, but nutrient addition did not increase overall BDOC, suggesting that chemical composition may be a more important control on DOC processing. Despite its high biodegradability, permafrost DOC showed evidence of substantial previous microbial processing and we present four hypotheses explaining this incongruity. Because thermokarst features form preferentially on river banks and lake shores and can remain active for decades, thermokarst may be the dominant short-term mechanism delivering sediment, nutrients, and biodegradable organic matter to aquatic systems as the Arctic warms.

AB.3 Key words

Thermokarst, permafrost carbon, DOC, dissolved organic carbon, DOM, lability, biolability, biodegradability, arctic tundra, thermo-erosion gully, thaw slump

¹ Published as Abbott, B. W., Larouche, J. R., Jones, J. B., Bowden, W. B., and Balsler, A. W., Elevated dissolved organic carbon biodegradability from thawing and collapsing permafrost, *Journal of Geophysical Research: Biogeosciences*, doi: 10.1002/2014JG002678, 2014. 2014JG002678.

AB.4 Introduction

Arctic rivers deliver between 34-38 Tg yr⁻¹ of dissolved organic carbon (DOC) to the Arctic Ocean and surrounding basins [Holmes *et al.*, 2012]. Another 37-84 Tg yr⁻¹ of DOC is delivered to inland waters but respired to the atmosphere or buried in lakes and streams before reaching the ocean [Aufdenkampe *et al.*, 2011; McGuire *et al.*, 2009]. As permafrost volume shrinks due to climate change, more of the 1670 Pg of soil organic carbon (C) contained in the permafrost region [Tarnocai *et al.*, 2009] will thaw and some portion will become available for transport to aquatic ecosystems as DOC. The quantity and quality of DOC release will depend on changes in local and regional hydrology [Frey and McClelland, 2009; O'Donnell *et al.*, 2012; Tank *et al.*, 2012]. The importance of this permafrost DOC to regional and global C cycles depends largely on its biodegradability—the degree to which DOC is available for uptake and mineralization by microorganisms [McDowell *et al.*, 2006]. If permafrost DOC is largely biodegradable, a larger portion will be mineralized in soil and freshwater systems before reaching the ocean, accelerating C transfer from permafrost to the atmosphere, whereas if this DOC is recalcitrant, more will reach marine ecosystems where it may persist on long time scales [Amon and Meon, 2004; Bianchi, 2011]. In arctic and boreal systems, biodegradable DOC (BDOC) ranges from <10% in soil water from the seasonally thawed active layer to 90% for some vegetation-derived DOC [Kalbitz *et al.*, 2003; Michaelson *et al.*, 1998; Wickland *et al.*, 2007]. Riverine BDOC varies seasonally from <10–40% with highest biodegradability typically during snowmelt [Holmes *et al.*, 2008; Mann *et al.*, 2012; Wickland *et al.*, 2012]. However, very little is known about BDOC from thawing permafrost, with conflicting evidence showing higher and lower biodegradability compared to DOC from litter and active layer soil [Balcarczyk *et al.*, 2009; Cory *et al.*, 2013; Vonk *et al.*, 2013].

Before permafrost DOC can enter the modern C cycle, regardless of its biodegradability, it has to come into contact with surface or ground waters. Because hydraulic conductivity in arctic mineral soil is often very low [Frampton *et al.*, 2011; Zhang *et al.*, 2000], much permafrost C may be inaccessible to hydrologic export, even after thaw. However, in soil where ice volume exceeds pore space, permafrost thaw is accompanied by ground subsidence, or thermokarst [Jorgenson *et al.*, 2008], which can rapidly mobilize sediment, nutrients, and C [Bowden *et al.*, 2008]. On hillslopes, riverbanks, and lakeshores, thermokarst can release permafrost DOC from meters below the active layer [Vonk *et al.*, 2013], and may impact watershed-level BDOC and nutrient concentrations [Bowden *et al.*, 2008; Woods *et al.*, 2011]. The term thermokarst includes a suite of thermo-erosional features with different morphologies determined primarily by ice content, substrate type, landscape position, and slope [Osterkamp *et al.*, 2009]. In upland landscapes, the three most common thermokarst morphologies are retrogressive thaw slumps, active layer detachment slides, and thermo-erosion gullies [Jorgenson and Osterkamp, 2005]. In addition to surface

subsidence due to ground ice loss, mechanical erosion and mass wasting play a role in the formation of these features, however, we will refer to them collectively as thermokarst following literature convention [Kokelj and Jorgenson, 2013]. Thaw slumps have a retreating headwall and are fueled by a variety of ground ice types, active layer detachment slides form when the seasonally thawed surface layer of vegetation and soil slips downhill over an ice-rich intermediate layer, and thermo-erosion gullies form due to ice wedge melt, growing with a generally linear or dendritic pattern (Supplementary Fig. AB.1). These three morphologies currently impact approximately 1.5% of the landscape in the western foothills of the Brooks Range [Krieger, 2012] and could affect up to 30% of the North Slope of Alaska with moderate warming [Jorgenson *et al.*, 2006].

In this study we measured the biodegradability of DOC released by thermokarst across common tundra vegetation and permafrost types on the North Slope of Alaska. We hypothesized that permafrost DOC would be more biodegradable than DOC from the active layer due to two non-mutually exclusive mechanisms. First, permafrost DOC may contain more biodegradable chemical compounds due to limited prior microbial processing or differences in original vegetation sources. Second, high nutrient concentrations in permafrost meltwater may accelerate DOC breakdown by relieving nutrient limitation of heterotrophic microorganisms. If DOC chemical composition is the main driver of biodegradability, we predicted that DOC aromaticity and the C:N ratio of dissolved organic matter (DOM) would be negatively correlated with biodegradability. If nutrient concentration is the dominant driver of DOC biodegradability, we predicted that the addition of nutrients would stimulate DOC processing, particularly at sites with low ambient nutrient concentrations. Likewise, we predicted that BDOC would differ by modern vegetation community and thermokarst type since these factors influence DOC chemical composition and nutrient concentration. We tested these hypotheses and predictions by 1) characterizing DOC composition released by thermokarst, 2) incubating DOC with and without added nutrients, 3) comparing BDOC between feature and vegetation types, and 4) developing relationships between DOC composition, nutrient content, and BDOC.

AB.5 Methods

AB.5.1 Study sites

We collected water from 19 thermokarst features and 8 reference water tracks in arctic tundra near the Toolik Field Station and Feniak Lake (Fig. AB.1, Table AB.1). Both areas are situated in the foothills of the Brooks Range on the North Slope of Alaska. Toolik Field Station is located 254 km north of the Arctic Circle and 180 km south of the Arctic Ocean. The average annual temperature is -10°C and average monthly temperatures range from -25°C in January to 11.5°C in July. The Toolik area receives 320 mm of

precipitation annually with 200 mm falling between June and August [*Toolik Environmental Data Center Team, 2011*]. Feniak Lake is located 360 km west of Toolik in the central Brooks Range at the northeast boarder of the Noatak National Preserve. The Feniak Lake region receives more precipitation than the Toolik area with annual average precipitation at 450 mm [*WRCC, 2011*]. Both Toolik and Feniak Lake are underlain by continuous permafrost with glacial till, bedrock, and loess parent materials ranging in age from 10-400 ka [*Hamilton, 2003*].

AB.5.2 Sample collection and analysis

We collected water from thermokarst feature outflows and reference water tracks near the Toolik Field Station (June to August in 2011 and August 2012) and near Feniak Lake (July 2011). In the Toolik area we sampled eight retrogressive thaw slumps (hereafter thaw slump), one active layer detachment slide, six thermo-erosion gullies (hereafter gully), and six reference water tracks. In the Feniak area we sampled two thaw slumps, one active layer detachment slide, one gully, and two reference water tracks. At each site, we collected four replicate samples from the main channel, which we filtered (0.7 μm effective pore size, Advantec GF-75) into 250 ml amber LDPE bottles for transport to the lab where we performed photometric analysis and set up incubations within 24 hours of collection. For most sites a 60 ml HDPE bottle for background nutrient concentrations was also filtered (0.7 μm) in the field and frozen upon return to the lab until analysis, typically within three months.

We measured DOC with a Shimadzu TOC-5000 connected to an Antek 7050 chemiluminescent detector to quantify total dissolved nitrogen (N) after combustion to NO_x . We characterized DOC composition by UV absorbance at 254 nm (SUVA_{254}), a photometric measure of DOC aromaticity [*Weishaar et al., 2003*], and the C:N of DOM, an indicator of DOM source and degree of prior processing [*Amon et al., 2012*]. UV absorbance was measured on a Shimadzu UV-1601 using a 1.0 cm quartz cell, and SUVA_{254} was calculated by dividing UV absorbance by DOC concentration. NO_3^- , NH_4^+ , PO_4^{3-} , and K were analyzed on a Dionex DX-320 ion chromatograph. Dissolved organic N (DON) was calculated by subtracting inorganic N (NO_3^- , NH_4^+ , and NO_2^-) from total dissolved N. To distinguish rain from snowmelt and permafrost meltwater, δD and $\delta^{18}\text{O}$ were analyzed on a Picarro L1102-i via cavity ringdown spectroscopy.

AB.5.3 BDOC assays

DOC biodegradability is the degree to which DOC is available for uptake and mineralization by microorganisms. Operationally, biodegradable DOC (BDOC) is often defined as the percent DOC mineralized or taken up over a certain time period, usually 7-40 days [*McDowell et al., 2006*], though DOC breakdown can also be characterized by single or multiple exponential models [*Wickland et al.,*

2007]. We assessed DOC biodegradability by DOC drawdown after 10 and 40 days. After initial collection and filtration in the field, 31 ml aliquots from each field bottle were filtered through 0.22 μm polyethersulfone membrane filters (Sterivex GP 0.22, Millipore) to remove bacteria, and were placed in 70 ml glass incubation vials. To control for variability in microbial community among sites, we made a common inoculum by shaking the 0.22 μm filters from all sites with 100 ml of de-ionized water and allowing them to soak for 30 minutes. Prior to initial sampling, 1 ml of this bacterial inoculum was added to each incubation vial. In 2011, all vials received a nutrient amendment, increasing ambient concentrations by 80 μM $\text{NH}_4^+/\text{NO}_3^-$ and 10 μM PO_4^{3-} [Holmes *et al.*, 2008], to relieve potential nutrient limitation of DOC processing and facilitate comparison with other studies [McDowell *et al.*, 2006]. In 2012, we compared DOC drawdown between amended and ambient nutrient incubations performed in tandem, to test the effect of added nutrients on DOC processing. Samples were stored in the dark at room temperature for the duration of the incubation. Incubation vials were tightly capped to limit evaporation but were opened and wafted weekly to ensure adequate oxygen supply.

To quantify DOC loss, we sampled each vial three times during the incubation, at day 0, day 10, and day 40 (t_0 , t_{10} , and t_{40} respectively). At samplings, 5 ml was drawn from each vial, filtered (0.22 μm) into acid-washed, glass scintillation vials, and acidified with 100 μl of 2N HCl to remove inorganic C and kill any residual bacteria not removed during filtration. Because this method removes microbial biomass before measuring DOC, the change in DOC concentration represents DOC loss due to both mineralization and microbial uptake. Acidified samples were stored tightly capped in the dark at room temperature until analysis within three months. Average DOC concentration of the four analytical replicates for each site and sampling time step was used to calculate loss. Analytical replicates with evidence of contamination or analytical error were excluded from the means, though this occurred less than 5% of the time and never resulted in dropping a site or sampling time step.

Because no single metric of DOC biodegradability is agreed upon as the most ecologically relevant, we characterized DOC biodegradability in several ways. We hereafter refer to the DOC loss by t_{40} as biodegradable DOC (BDOC), and further separate fast BDOC as loss from t_0 - t_{10} and slow BDOC as loss from t_{10} - t_{40} . We refer to DOC remaining at t_{40} as recalcitrant. To compare fast and slow BDOC in a single metric we calculated the proportion of fast BDOC (fast BDOC μM /total BDOC μM). The 10-day increment for fast BDOC corresponds to the average stream transport time of 10.9 days (range of 3-20 days) for rivers in the study area based on average stream velocity and channel length [Dery *et al.*, 2005; McNamara *et al.*, 1998]. Because this simplified estimate of residence time does not include transient storage within the channel or layovers in lakes and estuaries, the 40-day increment may better represent typical transit time from headwater to sea.

AB.5.4 Nutrients and DOC chemical composition

We used Pearson product-moment correlation and multiple linear regression to compare the relative importance of nutrients and DOC composition to BDOC. All regression and correlation analyses were based on BDOC data from nutrient amended incubations and therefore test indirect correlations between nutrients and other factors such as vegetation type, flowpath, DOM source, or micronutrients rather than direct effects of N or phosphorus (P) on BDOC. We compared the explanatory power of NH_4^+ , NO_3^- , PO_4^{3-} , K, $\delta^{18}\text{O}$, SUVA_{254} , DOC:DON, DOC:DIN, and thermokarst activity level (defined below) in predicting fast, slow, and total BDOC. Activity was recoded low to high and treated as a continuous variable for correlations but was excluded from other analyses since it is non-parametric and was highly correlated with both potassium (K) and ammonium (NH_4^+). Akaike information criterion (AIC) was used to identify the most parsimonious models and rank predictors within each model. To determine differences between amended and ambient nutrient treatments for fast, slow, and total BDOC, we applied a single population two-way t-test.

AB.5.5 Thermokarst activity, type, and vegetation

To understand the release of BDOC as thermokarst features develop through time, we classified features on a 0 – 3 activity index based on turbidity of outflow, rate of thermo-degradation, and state of revegetation. This qualitative index uses space for time substitution to follow the development of a hypothetical feature from before initiation (0) to after stabilization (3). Activity levels are defined as follows: 0. No apparent present or past thermo-degradation, 1. Active thermo-degradation (>25% of headwall is actively expanding) with completely turbid outflow, 2. Moderate thermo-degradation (<25% of headwall is expanding) with somewhat turbid outflow, 3. Stabilized or limited thermo-degradation with complete or partial revegetation and clear outflow. We performed a one-way analysis of variance (ANOVA), testing for differences in BDOC between thermokarst activity levels, and applied Tukey's HSD to determine significant differences.

Because vegetation community influences both active layer and permafrost DOC composition and nutrient concentration, we grouped sites into three broad vegetation classes (Table AB.1): moist acidic tundra, moist nonacidic tundra, and shrub tundra. We tested for differences in total BDOC, SUVA_{254} , C:N, and nutrient concentration between the three vegetation types. Because feature activity varied between classes, we tested for differences between vegetation classes with an analysis of covariance (ANCOVA) that compared adjusted means after controlling for activity. To test how ground ice type and thermokarst morphology influence BDOC we performed an ANCOVA comparing BDOC from gullies and thaw slumps independent of activity. Comparisons with active layer detachment slides or more

involved vegetation classifications such as ecotype [Jorgenson *et al.*, 2009] were not possible due to limited sample size.

AB.5.6 Seasonal changes in BDOC

To quantify seasonal variability of BDOC, repeat measurements were taken at the four most accessible sites (two gullies and adjacent water tracks) four times from June 15-August 18 2011, and repeat measurements were taken opportunistically at seven other sites. A two-way t-test for unequal variance was performed on the range (max-min) of BDOC to compare variability at impacted and reference sites through the 2011 season.

AB.5.7 Additional statistics

Repeat measurements from four features (two gullies, one thaw slump, and one water track) were included in the regression analysis as independent samples because of substantial variability in BDOC and chemistry between sample dates, which were more than two months apart in every case. Repeat measurements from 12 sites (four gullies, four thaw slumps, and four water tracks) were also included as independent samples in ANOVAs and ANCOVAs for the same reasons and to capture seasonal variability in biodegradability and water chemistry.

For all analyses, we evaluated normality with normal probability plots and equal variance by plotting observed values against residuals. For multiple linear regression models, highly correlated predictors were removed prior to running the full model or applying AIC, and in addition to visual assessment, variance inflation factor, RESET, Breusch-Pagan, and Durbin-Watson tests were used to check collinearity, linearity, equal variance, and autocorrelation respectively. Variables were natural log transformed, raised to the 0.25 exponent, and/or were centered on zero by subtracting the mean when necessary to meet these assumptions. For ANCOVA analysis, homogeneity of regression slopes was checked with interaction plots between site activity and the variable of interest. A polynomial term for $\delta^{18}\text{O}$ was included to capture the non-linear relationship with BDOC due to depleted $\delta^{18}\text{O}$ both in snowmelt early in the season and ground ice in the mid to late season. All statistical tests were evaluated with $\alpha = 0.05$ and analysis was performed in R (version 3.0.2). See acknowledgments for access to the complete dataset.

AB.6 Results

AB.6.1 Site activity

Sites occurred on a variety of tundra vegetation and permafrost types and exhibited a range of activity levels (Table AB.1). Thermokarst increased BDOC relative to reference waters, with greatest impact at the most active features with concentrations approaching reference in the more stable features

(Fig. AB.2, Table AB.2). DOC loss exceeded 50% after 10 days at several sites and reached 67% loss after 40 days at thaw slump 7 located in Pleistocene-aged Yedoma. Total BDOC varied significantly by activity ($F_{3,46} = 9.09$, $p < 0.001$) with means of 12.8, 40.9, 31.8, and 20.6% for activity levels 0-3, respectively (Fig. AB.2, Table AB.2). BDOC of the two highest activity levels differed significantly from reference water tracks ($p < 0.001$ and $p = 0.02$), but there was no significant difference in BDOC between stabilized sites and reference water tracks (levels 3 and 0; $p = 0.31$).

DOC concentrations from active thermokarst features (levels 1 and 2) were highly variable with average concentration over three times higher than in reference water tracks (Table AB.2). Differences in DON were even more pronounced with concentrations in active features nearly eight times higher than reference concentrations. Consequently, C:N of DOM for active features was half that of reference sites. Similarly, $SUVA_{254}$ values at impacted sites were half as high as in reference waters, indicating less aromatic DOC compounds in thermokarst outflow. Nutrient concentrations were generally much higher in thermokarst water (70, 39, and 15 times higher for K, NH_4^+ , and PO_4^{3-} respectively), though NO_3^- concentration in the most active features was only 1.3 times higher than reference waters. Rainwater was enriched in $\delta^{18}O$ (-16.56‰, $SD = 3.46$) relative to ground ice from feature headwalls (-24.11‰, $SD = 3.98$) and snow meltwater (-27.58‰, $SD = 3.15$).

The proportion fast BDOC (fast BDOC/total BDOC) did not vary significantly with thermokarst activity ($p = 0.24$, $n = 50$, $SE = 0.34$), with an overall average of 0.58 of the total DOC loss occurring by t10 (Fig. AB.1). However the proportion fast BDOC varied widely among individual sites, from less than 0.01 to 1.0.

AB.6.2 Nutrients and DOC chemical composition

We used correlation and multiple linear regression to assess the strength of associations between nutrients and DOC composition with DOC biodegradability. Pearson product-moment correlations revealed moderate to strong relationships between the four metrics of BDOC and both DOC chemical composition and nutrient concentration (Table AB.3). Individual parameters were correlated with fast, slow, and total BDOC (%) as well as total BDOC concentration (μM). PO_4^{3-} had the strongest positive correlation with both fast and total BDOC, and PO_4^{3-} and C:N were equally correlated with total BDOC concentration. Thermokarst activity had the strongest relationship with slow BDOC. Fast BDOC was not significantly correlated with slow BDOC (Pearson's $r = 0.27$, $n = 50$, $p = 0.054$). All parameters, except the $\delta^{18}O$ terms, were correlated with thermokarst activity, with K and NH_4^+ expressing the strongest relationships (Pearson's $r = 0.85$ and 0.82 respectively, $n = 27$, $p < 0.001$; Table AB.3).

Multiple linear regression models accounted for 67 – 83% of the variation in the four metrics of BDOC, with chemical composition, nutrient content, and water isotopes all included as significant predictors in the various models (Table AB.4). PO_4^{3-} and NH_4^+ were retained after stepwise AIC for all four of the BDOC metrics, with SUVA_{254} and $\delta^{18}\text{O}$ making three of the four final models (Table AB.4). Most predictors were individually significant ($\alpha < 0.05$) in their specific model with the exception of SUVA_{254} and C:N in the fast BDOC model; DOC, PO_4^{3-} , and SUVA_{254} in the slow BDOC model; and C:N and $\delta^{18}\text{O}$ in the BDOC concentration model ($p = 0.07, 0.06, 0.07, 0.16, 0.13, 0.06,$ and 0.25 , respectively). However, these terms were retained in the final models since they improved the AIC score and were not overly correlated with other predictors in their models. The model estimating fast BDOC had the weakest relationship with measured BDOC ($R^2 = 0.67$) and the BDOC concentration model had the strongest relationship ($R^2 = 0.83$; Fig. AB.3). Variance inflation factor was low for all parameters (< 3) and the RESET, Breusch-Pagan, and Durbin-Watson tests were all non-significant, indicating acceptable colinearity, linearity, equal variance, and autocorrelation.

We tested the effect of nutrient concentration on DOC processing by comparing amended and ambient nutrient incubations. The addition of inorganic N and P nearly doubled the amount of fast BDOC ($\text{SE} = 3.48, t_6 = 3.1, p = 0.02$), which averaged 9.2% for vials without added nutrients and 17.5% in amended incubations, but did not significantly affect slow BDOC (non-significant decrease of 2.7%, $\text{SE} = 1.63, t_6 = -1.64, p = 0.15$) or total BDOC (non-significant increase of 5.5%, $\text{SE} = 3.01, t_6 = 1.84, p = 0.12$; Fig. AB.4). Furthermore, variation in the response to nutrient addition was positively correlated with DIN concentration ($R^2 = 0.79, F_{1,5} = 19.4, p = 0.007$), with sites higher in DIN showing a stronger response to nutrient addition ($\Delta \text{fast BDOC} (\%) = 0.13 [\text{DIN} (\mu\text{M})] + 1.5$, Fig. AB.5).

AB.6.3 Feature and vegetation type

We compared BDOC by feature and vegetation type to test for differences due to how DOC is released from permafrost and original DOC source. Slumps were higher in BDOC than gullies ($F_{1,29}, p = 0.026$) with adjusted means of 37.9% versus 25.0% total BDOC after controlling for differences in activity (Fig. AB.6). BDOC differed with vegetation type independent of activity ($F_{2,46}, p = 0.006$), with greater BDOC at sites located on moist non-acidic tundra compared to moist acidic tundra, with adjusted means of 36.6 and 21.2% total BDOC (Fig. AB.7). SUVA_{254} varied by vegetation ($F_{2,44}, p = 0.0001$), with non-acidic sites lower than acidic sites with adjusted means of 4.3 and 2.2 $\text{L mg C}^{-1} \text{m}^{-1}$, but C:N ratio, DIN, and PO_4^{3-} did not significantly vary across vegetation types ($F_{2,28}, p = 0.28, 0.43,$ and 0.44 respectively). For all parameters, shrubs were intermediate between acidic and non-acidic tundra and did not vary significantly from either type.

AB.6.4 Seasonal patterns of BDOC

While individual sites had high variability in BDOC between samplings through the season, there was no clear trend in BDOC seasonality for reference or impacted waters (Fig. AB.8). The average of BDOC range (max – min values for an individual site over the season) varied by up to 50% with an overall average of 20.4% (n = 12, SE = 4.8). Impacted sites were more variable than reference water tracks with a mean BDOC range of 28.7% compared to the reference mean of 12.4% ($t_{8,83} = -2.4$, $p = 0.04$). For the two gullies and water tracks where repeat measurements were taken at least monthly, BDOC was highest in the mid to late season (July and August). Lowest BDOC for all sites occurred early in the season on 6/15.

AB.7 Discussion

AB.7.1 Permafrost DOC pools and biodegradability

DOC from collapsing permafrost on the North Slope is some of the most biodegradable reported in natural systems. Across multiple vegetation types, landscape ages, and thermokarst morphologies, DOC from permafrost is consistently more biodegradable than surface-derived DOC. High BDOC is accompanied by elevated DOC concentrations, resulting in extremely high rates of DOC mineralization from waters impacted by permafrost collapse. However, elevated BDOC only persists during active permafrost degradation, and BDOC returns to pre-disturbance levels once thermokarst features stabilize and start to revegetate. This finding informs the importance of thermokarst morphology in determining BDOC release from permafrost. Though gully and active layer detachment features are more common on the landscape and make up a larger portion of total thermokarst area [Krieger, 2012], they typically stabilize within a few years [Godin and Fortier, 2012; Lewkowitz and Harris, 2005]. Thaw slumps, however, can remain active for decades [Lantuit *et al.*, 2012; Lantz and Kokelj, 2008], mobilizing biodegradable permafrost DOC from meters below the surface.

AB.7.2 DOC composition

DOC aromaticity and C:N of DOM were negatively related to biodegradability, supporting our hypothesis that chemical composition of permafrost DOC contributes to its high biodegradability. The fact that fast and slow BDOC were poorly correlated and responded differently to nutrient addition is evidence that multiple pools of DOC with differing degrees of biodegradability are at play.

Arctic river DOC is typically most biodegradable during snowmelt [Holmes *et al.*, 2008; Mann *et al.*, 2012], when recently fixed vascular plant inputs dominate DOM sources [Neff *et al.*, 2006; Spencer *et al.*, 2008]. This DOM released during snowmelt has high SUVA₂₅₄ (~ 4.0), high C:N (> 40), and has undergone little microbial processing due to rapid transport across frozen soil [Holmes *et al.*, 2012; Mann

et al., 2012; *Spencer et al.*, 2008]. In contrast, permafrost DOM has low SUVA₂₅₄ (1.9) and low C:N (21.7) in the range of soil or microbially-derived DOM (10 – 25), suggesting considerable prior processing [*Amon and Meon*, 2004; *Amon et al.*, 2012; *Kawahigashi et al.*, 2004; *Neff et al.*, 2006]. Yet permafrost DOM is more biodegradable than DOM released during snowmelt. This inconsistency highlights the complexity of predicting BDOC, particularly when comparing fresh and degraded DOM. While the chemical composition of permafrost DOM is distinct from arctic snowmelt DOM, it is similar to late-winter DOM in the Yukon basin, which has high BDOC (40%), low SUVA₂₅₄ (2.0), and low C:N (20.7) [*O'Donnell et al.*, 2012; *Wickland et al.*, 2012]. A possible explanation for this similarity is that some of the DOM in wintertime baseflow is coming from permafrost via soilwater, groundwater, or thermokarst inputs. The Yukon basin is underlain by discontinuous permafrost and has experienced substantial warming and changes in precipitation [*Chapin et al.*, 2010] with large areas experiencing permafrost degradation [*Belshe et al.*, 2013; *Lu and Zhuang*, 2011; *Osterkamp*, 2005]. The only other published estimate of pre-snowmelt, riverine BDOC is from the Kolyma basin in Eastern Siberia, where BDOC was less than 5% [*Mann et al.*, 2012]. If permafrost DOM is the source of winter BDOC in the Yukon, this could explain the large difference between these catchments. The Kolyma is underlain by continuous permafrost and has experienced less severe summer and winter warming [*Chapin et al.*, 2005; *Serreze et al.*, 2000], therefore the contribution of permafrost DOM to winter BDOC should be relatively lower than in the Yukon.

AB.7.3 Nutrients

Nutrient addition had mixed effects on BDOC, in line with previous findings [*Balcarczyk et al.*, 2009; *Holmes et al.*, 2008]. The fact that sites with high DIN showed a greater response to nutrient addition was contrary to our prediction that low-nutrient sites would respond most strongly and does not support the hypothesis that nutrient availability limits DOC processing. Because DIN is highly correlated with site activity, the relationship between DIN and response to nutrient addition may indicate that sites with more biodegradable, permafrost-derived DOC are more sensitive to nutrient addition. This interaction coincides, albeit on a much faster time scale, with observations of bulk soil C processing in tundra soil, where higher nutrient availability enhances labile C processing but suppresses recalcitrant C processing [*Lavoie et al.*, 2011].

Regression and correlation analysis revealed that inorganic nutrients, particularly PO₄³⁻ and NH₄⁺, are associated with DOC biodegradability. These relationships were robust in predicting the biodegradability of both surface and permafrost-derived DOM (Fig. AB.4), suggesting common controls on biodegradability, regardless of source. However, the fact that NH₄⁺ was highly correlated with site activity may mean that its relationship with BDOC is partially or primarily correlative. PO₄³⁻ was

relatively less correlated with activity and was generally a better predictor of BDOC, suggesting an influence on BDOC separate from activity. It is important to note that correlation and regression analysis was based on data from incubations with added nutrients. As such, relationships between initial nutrient concentration and BDOC are likely due to indirect correlations between nutrients and other factors such as vegetation type, flowpath, DOM source, or micronutrients rather than direct effects of N or P on BDOC.

Mineral soil in the arctic is enriched in inorganic N relative to organic soil [Harms *et al.*, 2013; Keuper *et al.*, 2012] and increased active layer depth could modify hydrologic flowpaths, causing the simultaneous export of biodegradable permafrost DOC and DIN on a local or landscape scale [Harms *et al.*, 2013; Jones *et al.*, 2005; Striegl *et al.*, 2005; Wickland *et al.*, 2012]. Similarly, in the case of thermokarst, nutrient concentration is highly associated with feature activity, resulting in the features releasing the most permafrost DOC also releasing highest concentrations of inorganic nutrients. Another possibility explaining the correlation between BDOC and inorganic nutrients is that the nutrients associated with water rich in BDOC are at least partially derived from the DOM itself during mineralization.

AB.7.4 Acidic and nonacidic tundra DOM biodegradability

Sites draining moist non-acidic tundra sites had higher BDOC than those draining moist acidic tundra sites. This pattern may be due to more decomposable DOM inputs from non-acidic tundra or accelerated decomposition of DOM in acidic tundra soil before reaching the stream. While litter decay rates are similar between acidic and non-acidic tundra, decomposition can occur up to 84% more rapidly at acidic sites, potentially due to increased N availability and differences in microbial community [Hobbie and Gough, 2004; Hobbie *et al.*, 2005; Nordin *et al.*, 2004]. If DOM is processed faster in acidic tundra, a larger portion of BDOC would be consumed before reaching the stream or being incorporated into permafrost, leading to lower BDOC in moist acidic tundra ground ice and surface water. Alternatively, there is evidence that DOM biodegradability may be inversely correlated with biodegradability of the plant residue from which it leached. Litter from sedges decomposes fastest, followed by deciduous shrubs, and mosses [Hobbie, 1996]. Leachate biodegradability follows the opposite pattern, with very high BDOC in moss-derived DOM, followed by deciduous shrubs, and sedges [Wickland *et al.*, 2007]. If this pattern holds, DOM from non-acidic sites with lower litter and soil decay rates may have higher BDOC.

AB.7.5 BDOC and thermokarst morphology

Differences in the biodegradability of DOC released from thaw slumps and gullies suggest that ground ice type influences BDOC (Fig. AB.2). However, lower BDOC in gully outflow may be due to dilution of permafrost meltwater by surface water inputs, rather than differences in ground ice BDOC. Gullies often form in convergent topography with a larger upslope catchments than thaw slumps [Krieger, 2012]. Consequently, gully outflow has a lower proportion of permafrost versus surface-derived water and DOM. This explanation is supported by the fact that the gully with the highest BDOC (gully 7, Table AB.1) was the only one without surface water input.

AB.7.6 Why is permafrost DOC so biodegradable?

Different mechanisms potentially account for elevated BDOC in wedge and relic glacial ice formations, which are the most common ground ice types in our study area and are widespread throughout the arctic [French and Shur, 2010; T Zhang *et al.*, 1999]. Ice wedges form when spring runoff flows into surface cracks formed from thermal contraction during extreme cold in the previous winter [Fortier and Allard, 2004]. Because ice wedges are filled during the later stages of snowmelt [Lauriol *et al.*, 1995] the water that fills them is rich in the same litter and winter microbial activity-derived DOC that fuels patterns of high BDOC in arctic surface waters during snowmelt. Over centuries and millennia this unprocessed spring leachate could build up in ice wedges, providing a labile BDOC source upon thaw. However, the low C:N and SUVA₂₅₄ of permafrost DOM suggests it is derived from microbial or soil sources as opposed to fresh plant matter. If snowmelt DOM is the major source of ice wedge DOM, considerable processing must take place during or after incorporation. As for the source of BDOC in buried glacial ice, modern glacial ice can contain highly biodegradable DOC derived from microbial production (Hood *et al.* 2009), which more closely matches the DOM characteristics we observed in thermokarst outflows. If such DOC was present when relic glacial ice was stranded and buried, microbially-derived C could explain high BDOC in thaw slumps fueled by buried glacial ice. However, DOC concentrations in modern glacial ice are typically low, and ice ablation or another concentrating process would be necessary to produce the high concentrations of BDOC observed in thermokarst outflow.

If nutrient availability does not enhance BDOC, how can DOM from ground ice types such as ice wedges and transition ice be more biodegradable than the surface sources from which they derive? We hypothesize four potential mechanisms that could increase DOC biodegradability relative to modern DOC sources. First, permafrost mineral soil strongly sorbs hydrophobic C species, which tend to be recalcitrant [Kawahigashi *et al.*, 2006; Kawahigashi *et al.*, 2004]. Upon permafrost thaw, the DOC available for export could have a higher biodegradability since the less bioavailable compounds have effectively been

filtered by the mineral soil. Second, repeated freeze thaw cycles can release highly biodegradable DOC from the microbial community [Schimel and Clein, 1996]. This release is typically taken up rapidly or respired by microorganisms that survived the cycle [Schimel and Clein, 1996]. However, if these pulses of bioavailable DOC were released near a freezing front at the permafrost table, or near an ice wedge crack they could be incorporated into ground ice. Third, microbial metabolism has been shown to continue well below the freezing point [Wilhelm *et al.*, 2012] and it is not known what portion of microbial biomass and metabolites is incorporated into permafrost as DOC rather than respired. Although microbial metabolism rates are low at temperatures typical of continuous permafrost—processing 1-2 $\mu\text{g g}^{-1} \text{C day}^{-1}$ [Mikan *et al.*, 2002; Osterkamp, 2005]—sub-zero metabolism could process a substantial portion of available soil organic matter over several millennia. Incomplete breakdown of frozen soil organic matter, either during freeze-thaw cycles or sub-zero metabolism, could lead to the accumulation of simple carbon compounds such as acetate, which could explain the low C:N and SUVA₂₅₄ of permafrost-derived DOM. Finally, some vegetation paleo-communities may have produced relatively biodegradable DOM compared to modern communities. This seems a likely explanation for the extremely high BDOC in Pleistocene-aged loess deposits where C derives primarily from grasses [Zimov *et al.*, 2006]. However, for other permafrost types on the North Slope, pollen records reveal spatially heterogeneous community shifts, rather than a landscape-scale pattern of more biodegradable DOM sources [Anderson *et al.*, 1994; Fritz *et al.*, 2012; Oswald *et al.*, 2003].

An additional factor not considered here, which may further enhance DOC mineralization after release from permafrost, is high photodegradability of permafrost DOM when exposed to sunlight after reaching the surface [Cory *et al.*, 2013]. Several features included in our study (ALD 1, gullies 1 and 2, and thaw slumps 2-4, and 8) showed more than a 40% increase in microbial conversion of DOC to CO₂ when exposed to sunlight [Cory *et al.*, 2013]. Actual rates of permafrost DOC mineralization may be higher than measured in our dark incubations in field conditions when exposed to sunlight.

AB.8 Conclusions

As the Arctic warms, DOC from thawing permafrost will play an increasingly important role governing freshwater and estuarine C and nutrient dynamics through the season. The overall ecological importance of thermokarst BDOC depends on the number of features, their location on the landscape, and the length of their active period. Approximately a third of permafrost has ice content in excess of 10% [Zhang *et al.*, 1999] and is susceptible to thermokarst upon thaw [Jorgenson *et al.*, 2006]. With up to 80% of near surface permafrost projected to degrade by 2100 if human greenhouse gas emissions are not reduced [Slater and Lawrence, 2013], thermokarst could impact up to $5.5 \times 10^6 \text{ km}^2$ by the end of the century.

Since thermal disturbance from flowing or standing water often triggers gully and thaw slump formation, thermokarst may be the dominant short-term mechanism delivering sediment, nutrients, and biodegradable organic matter to aquatic systems as the Arctic warms. This could have significant local, landscape, and global consequences [Bowden *et al.*, 2008; Thienpont *et al.*, 2013]. Thermokarst outflow is most active when temperature is high in the mid to late summer, precisely when arctic surface water BDOC is lowest [Holmes *et al.*, 2008; Mann *et al.*, 2012; Wickland *et al.*, 2012]. Chronic loading of BDOC from widespread thermokarst could cause a substantial shift in late-season DOC dynamics in arctic streams, lakes, and estuaries. Permafrost BDOC release could also be important for the global C cycle, enhancing the permafrost C feedback due to direct CO₂ release from the decomposition of permafrost DOC and enhanced heterotrophic processing of non-permafrost DOC due to the priming effect [Bianchi, 2011; Guenet *et al.*, 2010].

High lability of permafrost DOC should be considered when estimating changes in DOC delivery to aquatic ecosystems. Due to substantial DOC losses on timescales less than residence time of many arctic waters, monitoring of river mouth or estuarine DOC could miss a large portion of DOC released from degrading permafrost which was processed in transit.

AB.9 Acknowledgments

The complete dataset for this paper is available through the Advanced Cooperative Arctic Data and Information Service at www.aoncadis.org/project/collaborative_research_spatial_and_temporal_influences_of_thermokarst_failures_on_surface_processes_in_arctic_landscapes.html. This work was supported by the National Science Foundation ARCSS program (OPP-0806465 and OPP-0806394). We thank the many individuals and organizations that assisted with this study. S. Godsey, A. Olsson, L. Koenig, and P. Tobin gave dedicated service in the lab and field, R. Cory and G. Kling provided technical assistance and advice with DOM analysis, Toolik Field Station and CH2M Hill Polar Services provided outstanding logistic support, T. Chapin gave valuable input on the manuscript, and the National Park Service and Bureau of Land Management facilitated research permits. We also thank two anonymous reviewers whose observations improved the manuscript. In memory of the late Christian Cabanilla and Bill Zeman who flew us to many of these sites.

AB.10 References

Amon, R. M. W., and B. Meon (2004), The biogeochemistry of dissolved organic matter and nutrients in two large Arctic estuaries and potential implications for our understanding of the Arctic Ocean system, *Marine Chemistry*, 92(1-4), 311-330.

- Amon, R. M. W., et al. (2012), Dissolved organic matter sources in large Arctic rivers, *Geochimica Et Cosmochimica Acta*, 94, 217-237.
- Anderson, P. M., P. J. Bartlein, and L. B. Brubaker (1994), Late Quaternary History of Tundra Vegetation in Northwestern Alaska, *Quaternary Res*, 41(3), 306-315.
- Aufdenkampe, A. K., E. Mayorga, P. A. Raymond, J. M. Melack, S. C. Doney, S. R. Alin, R. E. Aalto, and K. Yoo (2011), Riverine coupling of biogeochemical cycles between land, oceans, and atmosphere, *Frontiers in Ecology and the Environment*, 9(1), 53-60.
- Balcarczyk, K. L., J. B. Jones, R. Jaffe, and N. Maie (2009), Stream dissolved organic matter bioavailability and composition in watersheds underlain with discontinuous permafrost, *Biogeochemistry*, 94(3), 255-270.
- Belshe, E. F., E. A. G. Schuur, and G. Grosse (2013), Quantification of upland thermokarst features with high resolution remote sensing, *Environmental Research Letters*, 8(3).
- Bianchi, T. S. (2011), The role of terrestrially derived organic carbon in the coastal ocean: A changing paradigm and the priming effect, *Proceedings of the National Academy of Sciences*, 108(49), 19473-19481.
- Bowden, W. B., M. N. Gooseff, A. Balser, A. Green, B. J. Peterson, and J. Bradford (2008), Sediment and nutrient delivery from thermokarst features in the foothills of the North Slope, Alaska: Potential impacts on headwater stream ecosystems, *J Geophys Res-Biogeophys*, 113(G2).
- Chapin, F. S., et al. (2010), Resilience of Alaska's boreal forest to climatic change, *Canadian Journal of Forest Research-Revue Canadienne De Recherche Forestiere*, 40(7), 1360-1370.
- Chapin, F. S., et al. (2005), Role of Land-Surface Changes in Arctic Summer Warming, *Science*, 310(5748), 657-660.
- Cory, R. M., B. C. Crump, J. A. Dobkowski, and G. W. Kling (2013), Surface exposure to sunlight stimulates CO₂ release from permafrost soil carbon in the Arctic, *P Natl Acad Sci USA*, 110(9), 3429-3434.
- Dery, S. J., M. Stieglitz, A. K. Rennermalm, and E. F. Wood (2005), The water budget of the Kuparuk River basin, Alaska, *Journal of Hydrometeorology*, 6(5), 633-655.
- Fortier, D., and M. Allard (2004), Late Holocene syngenetic ice-wedge polygons development, Bylot Island, Canadian Arctic Archipelago, *Canadian Journal of Earth Sciences*, 41(8), 997-1012.
- Frampton, A., S. Painter, S. W. Lyon, and G. Destouni (2011), Non-isothermal, three-phase simulations of near-surface flows in a model permafrost system under seasonal variability and climate change, *J Hydrol.*, 403(3-4), 352-359.
- French, H., and Y. Shur (2010), The principles of cryostratigraphy, *Earth-Science Reviews*, 101(3-4), 190-206.

- Frey, K. E., and J. W. McClelland (2009), Impacts of permafrost degradation on arctic river biogeochemistry, *Hydrol Process*, 23(1), 169-182.
- Fritz, M., U. Herzschuh, S. Wetterich, H. Lantuit, G. P. De Pascale, W. H. Pollard, and L. Schirrmeister (2012), Late glacial and Holocene sedimentation, vegetation, and climate history from easternmost Beringia (northern Yukon Territory, Canada), *Quaternary Res*, 78(3), 549-560.
- Godin, E., and D. Fortier (2012), Geomorphology of a thermo-erosion gully, Bylot Island, Nunavut, Canada, *Canadian Journal of Earth Sciences*, 49(8), 979-986.
- Guenet, B., M. Danger, L. Abbadie, and G. Lacroix (2010), Priming effect: bridging the gap between terrestrial and aquatic ecology, *Ecology*, 91(10), 2850-2861.
- Hamilton, T. (2003), Surficial geology of the Dalton Highway (Itkillik-Sagavanirktok rivers) area, southern Arctic foothills, Alaska Division of Geological & Geophysical Surveys, Alaska.
- Harms, T., B. Abbott, and J. Jones (2013), Thermo-erosion gullies increase nitrogen available for hydrologic export, *Biogeochemistry*, 1-13.
- Hobbie, S. E. (1996), Temperature and plant species control over litter decomposition in Alaskan tundra, *Ecological Monographs*, 66(4), 503-522.
- Hobbie, S. E., and L. Gough (2004), Litter decomposition in moist acidic and non-acidic tundra with different glacial histories, *Oecologia*, 140(1), 113-124.
- Hobbie, S. E., L. Gough, and G. R. Shaver (2005), Species compositional differences on different-aged glacial landscapes drive contrasting responses of tundra to nutrient addition, *J Ecol*, 93(4), 770-782.
- Holmes, R. M., J. W. McClelland, P. A. Raymond, B. B. Frazer, B. J. Peterson, and M. Stieglitz (2008), Lability of DOC transported by Alaskan rivers to the arctic ocean, *Geophysical Research Letters*, 35(3).
- Holmes, R. M., et al. (2012), Seasonal and Annual Fluxes of Nutrients and Organic Matter from Large Rivers to the Arctic Ocean and Surrounding Seas, *Estuaries and Coasts*, 35(2), 369-382.
- Hood, E., J. Fellman, R. G. M. Spencer, P. J. Hernes, R. Edwards, D. D'Amore, and D. Scott (2009), Glaciers as a source of ancient and labile organic matter to the marine environment, *Nature*, 462(7276), 1044-U1100.
- Jones, J. B., K. C. Petrone, J. C. Finlay, L. D. Hinzman, and W. R. Bolton (2005), Nitrogen loss from watersheds of interior Alaska underlain with discontinuous permafrost, *Geophysical Research Letters*, 32(2).
- Jorgenson, M. T., and T. E. Osterkamp (2005), Response of boreal ecosystems to varying modes of permafrost degradation, *Canadian Journal of Forest Research-Revue Canadienne De Recherche Forestiere*, 35(9), 2100-2111.

- Jorgenson, M. T., Y. L. Shur, and E. R. Pullman (2006), Abrupt increase in permafrost degradation in Arctic Alaska, *Geophysical Research Letters*, 33(2).
- Jorgenson, M. T., Y. L. Shur, and T. E. Osterkamp (2008), Thermokarst in Alaska, in *Ninth International Conference On Permafrost*, University of Alaska Fairbanks, 117-124.
- Jorgenson, M. T., J. E. Roth, P. F. Miller, M. J. Macander, M. S. Duffy, A. F. Wells, G. V. Frost, and E. R. Pullman (2009), An Ecological Land Survey and Landcover Map of the Arctic Network, *National Park Service, Ft Collins, CO. NPS/ARC/NRTR—2009/270. 307.*
- Kalbitz, K., J. Schmerwitz, D. Schwesig, and E. Matzner (2003), Biodegradation of soil-derived dissolved organic matter as related to its properties, *Geoderma*, 113(3-4), 273-291.
- Kawahigashi, M., K. Kaiser, A. Rodionov, and G. Guggenberger (2006), Sorption of dissolved organic matter by mineral soils of the Siberian forest tundra, *Glob. Change Biol.*, 12(10), 1868-1877.
- Kawahigashi, M., K. Kaiser, K. Kalbitz, A. Rodionov, and G. Guggenberger (2004), Dissolved organic matter in small streams along a gradient from discontinuous to continuous permafrost, *Glob. Change Biol.*, 10(9), 1576-1586.
- Keuper, F., P. M. van Bodegom, E. Dorrepaal, J. T. Weedon, J. van Hal, R. S. P. van Logtestijn, and R. Aerts (2012), A frozen feast: thawing permafrost increases plant-available nitrogen in subarctic peatlands, *Glob. Change Biol.*, 18(6), 1998-2007.
- Kokelj, S. V., and M. T. Jorgenson (2013), Advances in Thermokarst Research, *Permafrost and Periglacial Processes*, 24(2), 108-119, doi:10.1002/ppp.1779.
- Krieger, K. C. (2012), The Topographic Form and Evolution of Thermal Erosion Features: A First Analysis Using Airborne and Ground-Based LiDAR in Arctic Alaska, M.S. thesis, Dep. of Geosciences, Idaho State University.
- Lantuit, H., W. H. Pollard, N. Couture, M. Fritz, L. Schirmer, H. Meyer, and H. W. Hubberten (2012), Modern and Late Holocene Retrogressive Thaw Slump Activity on the Yukon Coastal Plain and Herschel Island, Yukon Territory, Canada, *Permafrost and Periglacial Processes*, 23(1), 39-51.
- Lantz, T. C., and S. V. Kokelj (2008), Increasing rates of retrogressive thaw slump activity in the Mackenzie Delta region, NWT, Canada, *Geophysical Research Letters*, 35(6).
- Lauriol, B., C. Duchesne, and I. D. Clark (1995), Systématique du Remplissage en Eau des Fentes de Gel: Les Résultats d'une Étude Oxygène-18 et Deutérium, *Permafrost and Periglacial Processes*, 6(1), 47-55.
- Lavoie, M., M. C. Mack, and E. A. G. Schuur (2011), Effects of elevated nitrogen and temperature on carbon and nitrogen dynamics in Alaskan arctic and boreal soils, *J Geophys Res-Biogeog.*, 116.

- Lewkowicz, A. G., and C. Harris (2005), Frequency and magnitude of active-layer detachment failures in discontinuous and continuous permafrost, northern Canada, *Permafrost and Periglacial Processes*, 16(1), 115-130.
- Lu, X. L., and Q. L. Zhuang (2011), Areal changes of land ecosystems in the Alaskan Yukon River Basin from 1984 to 2008, *Environmental Research Letters*, 6(3).
- Mann, P. J., A. Davydova, N. Zimov, R. G. M. Spencer, S. Davydov, E. Bulygina, S. Zimov, and R. M. Holmes (2012), Controls on the composition and lability of dissolved organic matter in Siberia's Kolyma River basin, *J Geophys Res-Biogeophys*, 117.
- McDowell, W. H., A. Zsolnay, J. A. Aitkenhead-Peterson, E. G. Gregorich, D. L. Jones, D. Jodemann, K. Kalbitz, B. Marschner, and D. Schwesig (2006), A comparison of methods to determine the biodegradable dissolved organic carbon from different terrestrial sources, *Soil Biol Biochem*, 38(7), 1933-1942.
- McGuire, A. D., L. G. Anderson, T. R. Christensen, S. Dallimore, L. Guo, D. J. Hayes, M. Heimann, T. D. Lorenson, R. W. Macdonald, and N. Roulet (2009), Sensitivity of the carbon cycle in the Arctic to climate change, *Ecological Monographs*, 79(4), 523-555.
- McNamara, J. P., D. L. Kane, and L. D. Hinzman (1998), An analysis of streamflow hydrology in the Kuparuk River basin, Arctic Alaska: A nested watershed approach, *J Hydrol.*, 206(1-2), 39-57.
- Michaelson, G. J., C. L. Ping, G. W. Kling, and J. E. Hobbie (1998), The character and bioactivity of dissolved organic matter at thaw and in the spring runoff waters of the arctic tundra north slope, Alaska, *J Geophys Res-Atmos*, 103(D22), 28939-28946.
- Mikan, C. J., J. P. Schimel, and A. P. Doyle (2002), Temperature controls of microbial respiration in arctic tundra soils above and below freezing, *Soil Biol Biochem*, 34(11), 1785-1795.
- Neff, J. C., J. C. Finlay, S. A. Zimov, S. P. Davydov, J. J. Carrasco, E. A. G. Schuur, and A. I. Davydova (2006), Seasonal changes in the age and structure of dissolved organic carbon in Siberian rivers and streams, *Geophysical Research Letters*, 33(23).
- Nordin, A., I. K. Schmidt, and G. R. Shaver (2004), Nitrogen uptake by arctic soil microbes and plants in relation to soil nitrogen supply, *Ecology*, 85(4), 955-962.
- O'Donnell, J. A., G. R. Aiken, M. A. Walvoord, and K. D. Butler (2012), Dissolved organic matter composition of winter flow in the Yukon River basin: Implications of permafrost thaw and increased groundwater discharge, *Global Biogeochemical Cycles*, 26.
- Osterkamp, T. E. (2005), The recent warming of permafrost in Alaska, *Global Planet Change*, 49(3-4), 187-202.

- Osterkamp, T. E., M. T. Jorgenson, E. A. G. Schuur, Y. L. Shur, M. Z. Kanevskiy, J. G. Vogel, and V. E. Tumskey (2009), Physical and Ecological Changes Associated with Warming Permafrost and Thermokarst in Interior Alaska, *Permafrost and Periglacial Processes*, 20(3), 235-256.
- Oswald, W. W., L. B. Brubaker, F. S. Hu, and G. W. Kling (2003), Holocene pollen records from the central Arctic Foothills, northern Alaska: testing the role of substrate in the response of tundra to climate change, *J Ecol*, 91(6), 1034-1048.
- Schimel, J. P., and J. S. Clein (1996), Microbial response to freeze-thaw cycles in tundra and taiga soils, *Soil Biol Biochem*, 28(8), 1061-1066.
- Serreze, M. C., J. E. Walsh, F. S. Chapin, T. Osterkamp, M. Dyurgerov, V. Romanovsky, W. C. Oechel, J. Morison, T. Zhang, and R. G. Barry (2000), Observational evidence of recent change in the northern high-latitude environment, *Climatic Change*, 46(1-2), 159-207.
- Slater, A. G., and D. M. Lawrence (2013), Diagnosing Present and Future Permafrost from Climate Models, *Journal of Climate*, 26(15), 5608-5623, doi:10.1175/jcli-d-12-00341.1.
- Spencer, R. G. M., G. R. Aiken, K. P. Wickland, R. G. Striegl, and P. J. Hernes (2008), Seasonal and spatial variability in dissolved organic matter quantity and composition from the Yukon River basin, Alaska, *Global Biogeochemical Cycles*, 22(4).
- Striegl, R. G., G. R. Aiken, M. M. Dornblaser, P. A. Raymond, and K. P. Wickland (2005), A decrease in discharge-normalized DOC export by the Yukon River during summer through autumn, *Geophysical Research Letters*, 32(21).
- Tank, S. E., K. E. Frey, R. G. Striegl, P. A. Raymond, R. M. Holmes, J. W. McClelland, and B. J. Peterson (2012), Landscape-level controls on dissolved carbon flux from diverse catchments of the circumboreal, *Global Biogeochemical Cycles*, 26.
- Tarnocai, C., J. G. Canadell, E. A. G. Schuur, P. Kuhry, G. Mazhitova, and S. Zimov (2009), Soil organic carbon pools in the northern circumpolar permafrost region, *Global Biogeochemical Cycles*, 23.
- Thienpont, J. R., K. M. Ruehland, M. F. J. Pisaric, S. V. Kokelj, L. E. Kimpe, J. M. Blais, and J. P. Smol (2013), Biological responses to permafrost thaw slumping in Canadian Arctic lakes, *Freshwater Biology*, 58(2), 337-353.
- Toolik Environmental Data Center Team (2011), Meteorological monitoring program at Toolik, Alaska, Toolik Field Station, Institute of Arctic Biology, University of Alaska Fairbanks.
- Vonk, J. E., et al. (2013), High biolability of ancient permafrost carbon upon thaw, *Geophysical Research Letters*, 40.
- Weishaar, J. L., G. R. Aiken, B. A. Bergamaschi, M. S. Fram, R. Fujii, and K. Mopper (2003), Evaluation of Specific Ultraviolet Absorbance as an Indicator of the Chemical Composition and Reactivity of Dissolved Organic Carbon, *Environmental Science & Technology*, 37(20), 4702-4708.

- Wickland, K. P., J. C. Neff, and G. R. Aiken (2007), Dissolved organic carbon in Alaskan boreal forest: Sources, chemical characteristics, and biodegradability, *Ecosystems*, 10(8), 1323-1340.
- Wickland, K. P., G. R. Aiken, K. Butler, M. M. Dornblaser, R. G. M. Spencer, and R. G. Striegl (2012), Biodegradability of dissolved organic carbon in the Yukon River and its tributaries: Seasonality and importance of inorganic nitrogen, *Global Biogeochemical Cycles*, 26.
- Wilhelm, R. C., K. J. Radtke, N. C. S. Myktyczuk, C. W. Greer, and L. G. Whyte (2012), Life at the Wedge: the Activity and Diversity of Arctic Ice Wedge Microbial Communities, *Astrobiology*, 12(4), 347-360.
- Woods, G. C., M. J. Simpson, B. G. Pautler, S. F. Lamoureux, M. J. Lafreniere, and A. J. Simpson (2011), Evidence for the enhanced lability of dissolved organic matter following permafrost slope disturbance in the Canadian High Arctic, *Geochimica Et Cosmochimica Acta*, 75(22), 7226-7241.
- WRCC (2011), Western Regional Climate Center, <http://www.wrcc.dri.edu/>.
- Zhang, T., R.G. Barry, K. Knowles, J.A. Heginbottom, and J. Brown (1999), Statistics and characteristics of permafrost and ground ice distribution in the Northern Hemisphere, *Polar Geography*, 23(2), 147-169.
- Zhang, Z., D. L. Kane, and L. D. Hinzman (2000), Development and application of a spatially-distributed Arctic hydrological and thermal process model (ARHYTHM), *Hydrol Process*, 14(6), 1017.
- Zimov, S. A., S. P. Davydov, G. M. Zimova, A. I. Davydova, E. A. G. Schuur, K. Dutta, and F. S. Chapin (2006), Permafrost carbon: Stock and decomposability of a globally significant carbon pool, *Geophysical Research Letters*, 33(20)

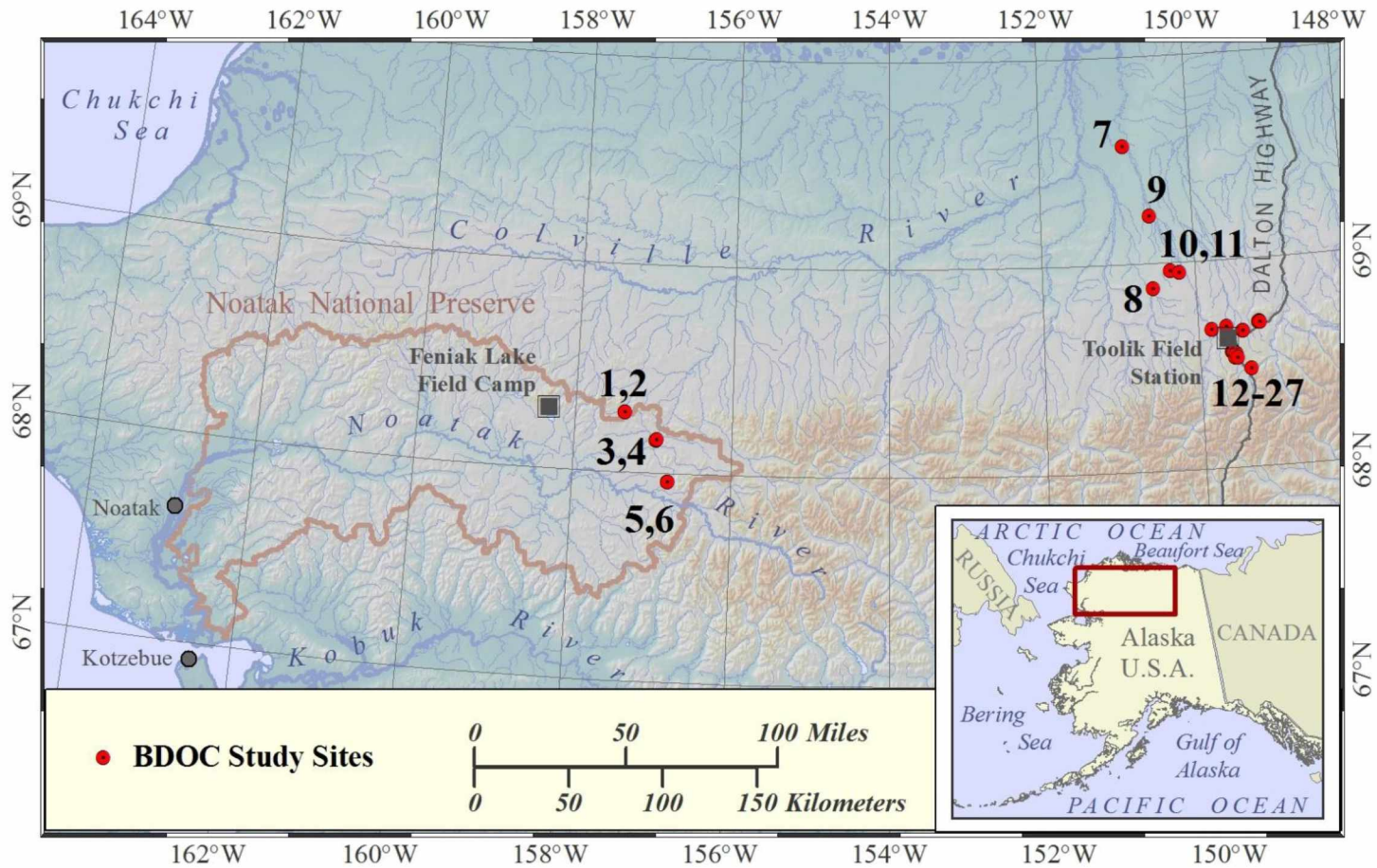


Figure AB.1 Map of study area.

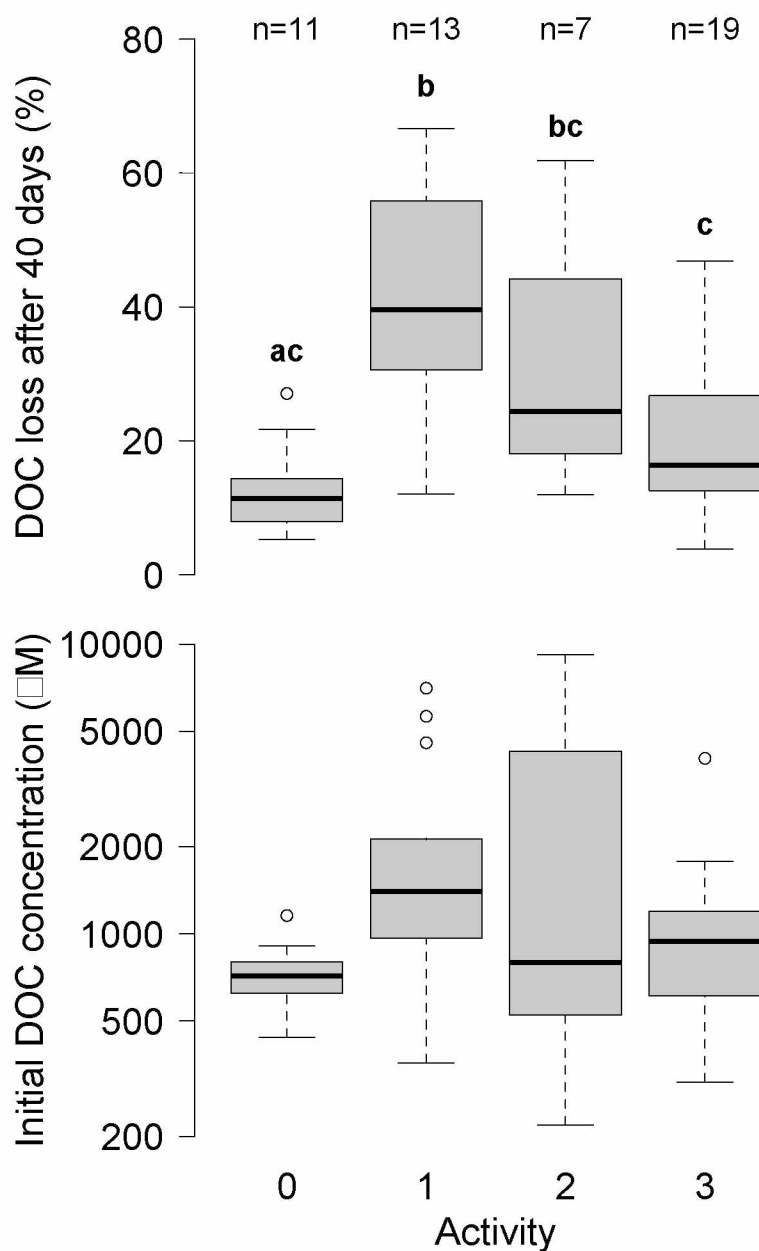
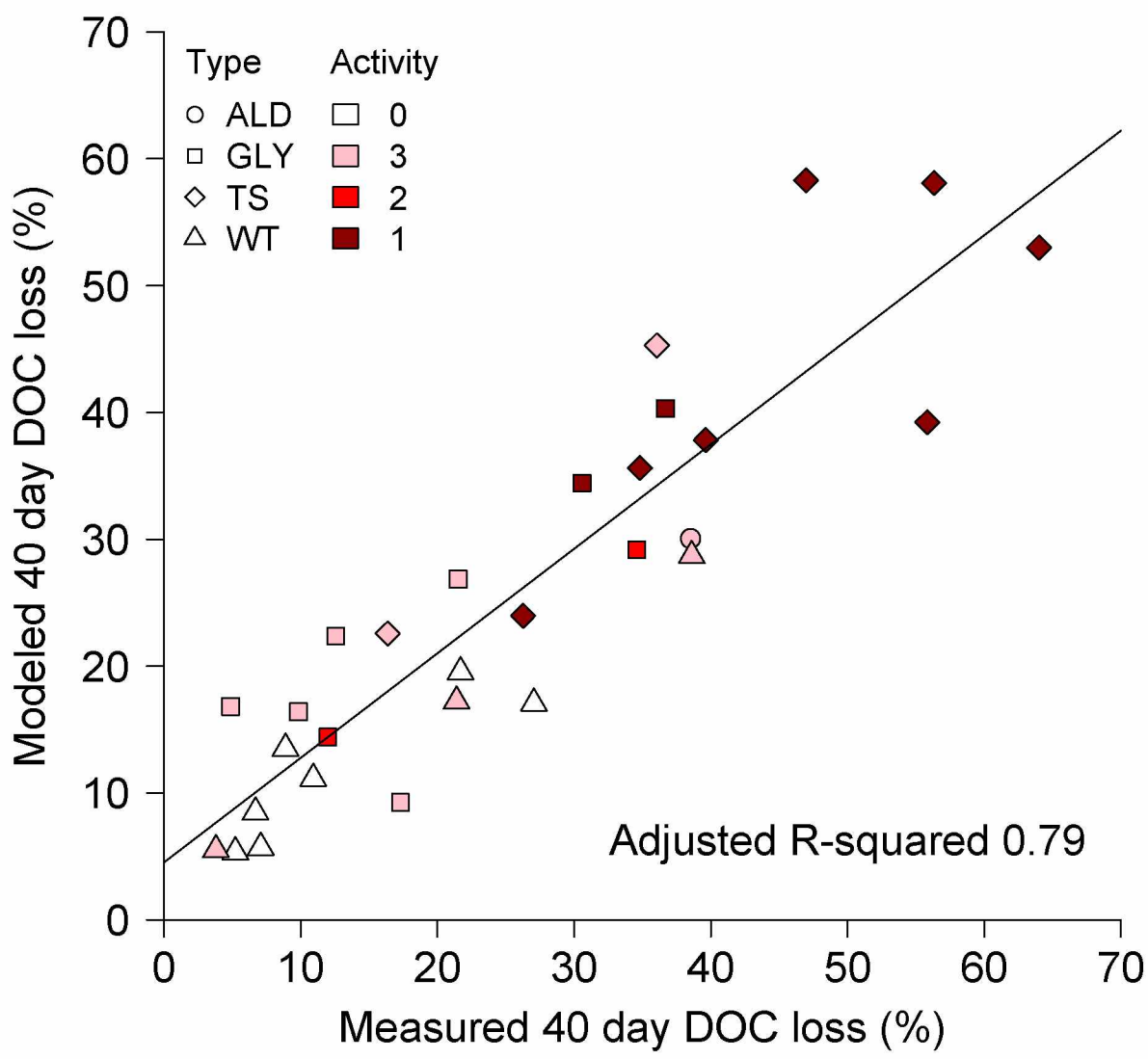
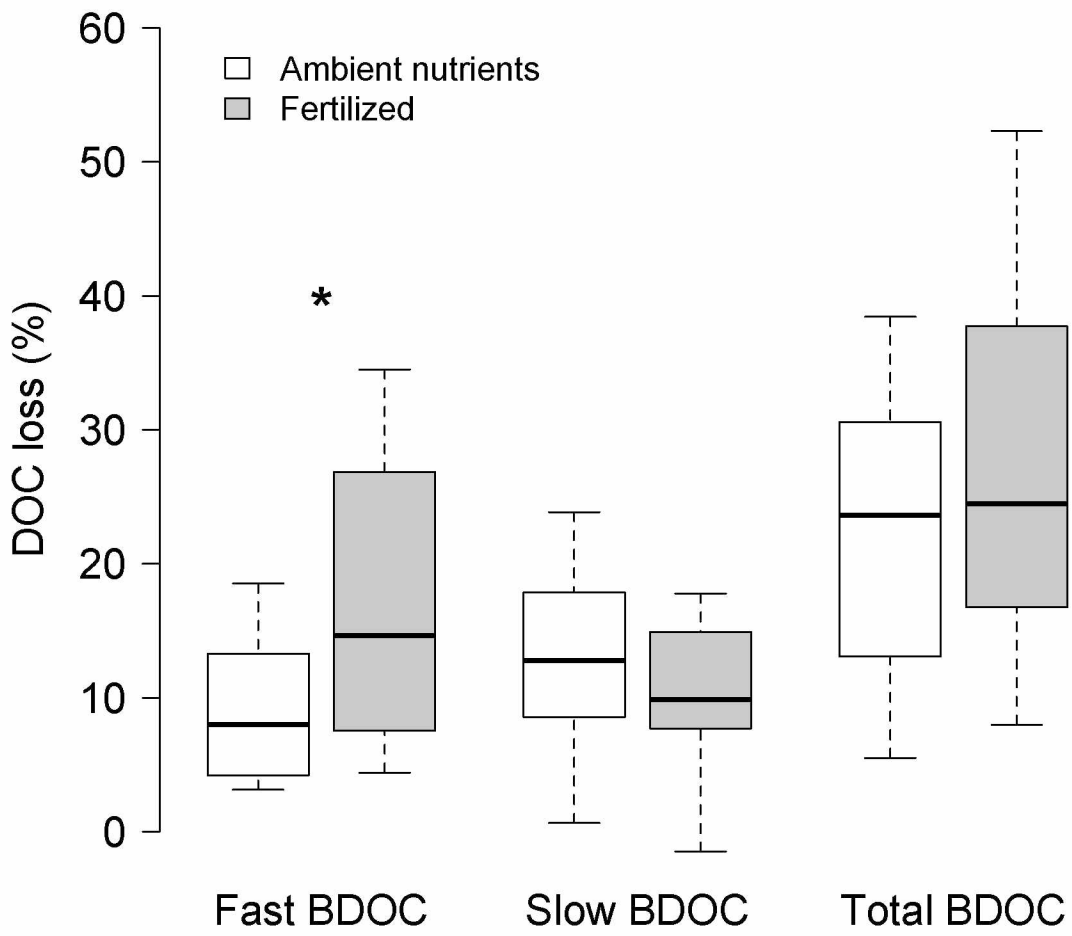


Figure AB.2 DOC loss in water from collapsing permafrost and reference water tracks after 40 days of lab incubation at room temperature and initial DOC concentration. See Table AB.1 or text for complete definition of activity index but 0=reference, 1=most active, and 3=stabilized. Box plots represent median, quartiles, minimum and maximum within 1.5 times the interquartile range, and outliers beyond 1.5 IQR. Different letters represent significant differences between activity levels, $\alpha = 0.05$.





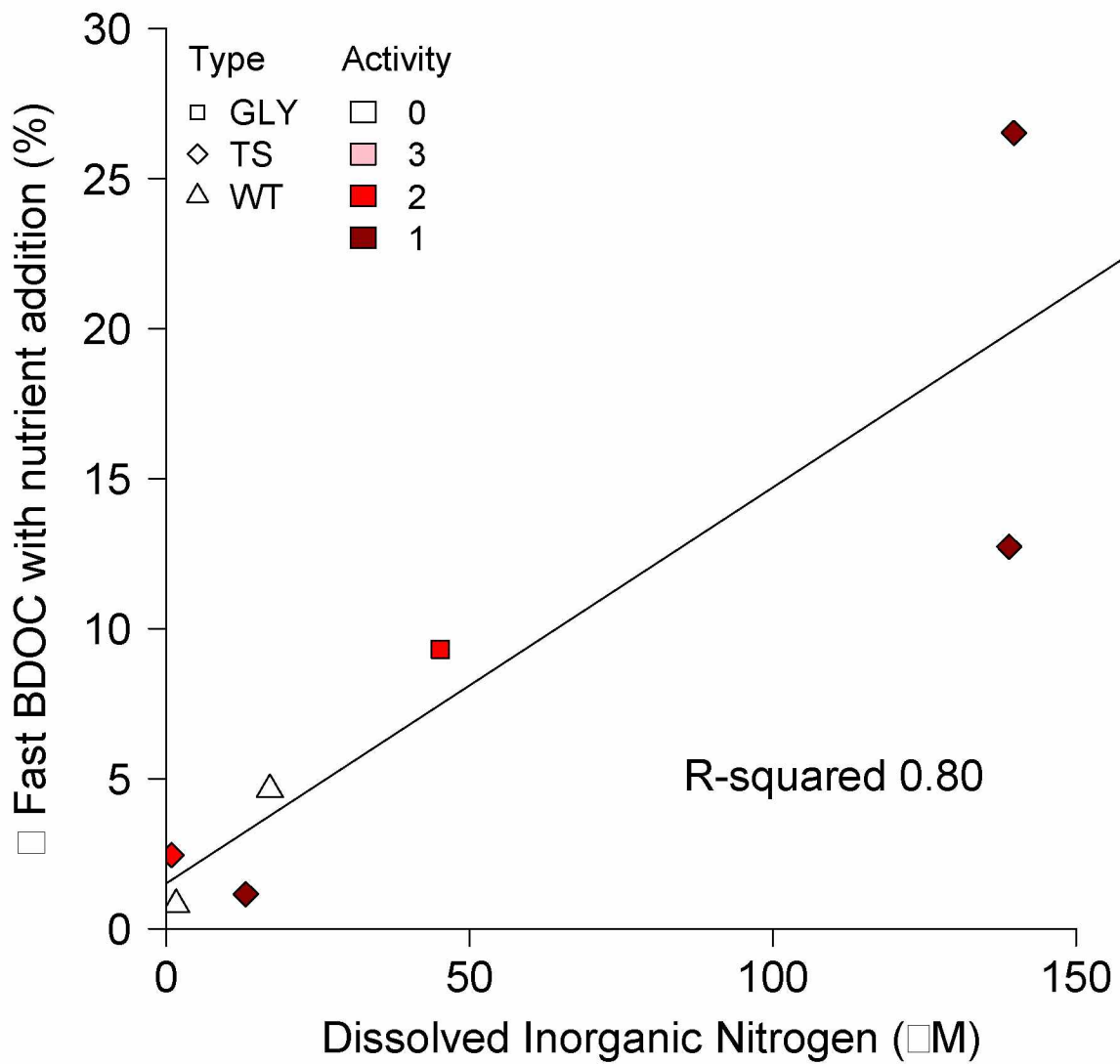


Figure AB.5 Response of fast BDOC (DOC loss from $t_0 - t_{10}$) to nutrient addition. Each point represents the fertilized DOC loss (%) minus the ambient nutrient DOC loss (%). Shapes represent site type and shading represents activity level (defined in Fig. AB.1).

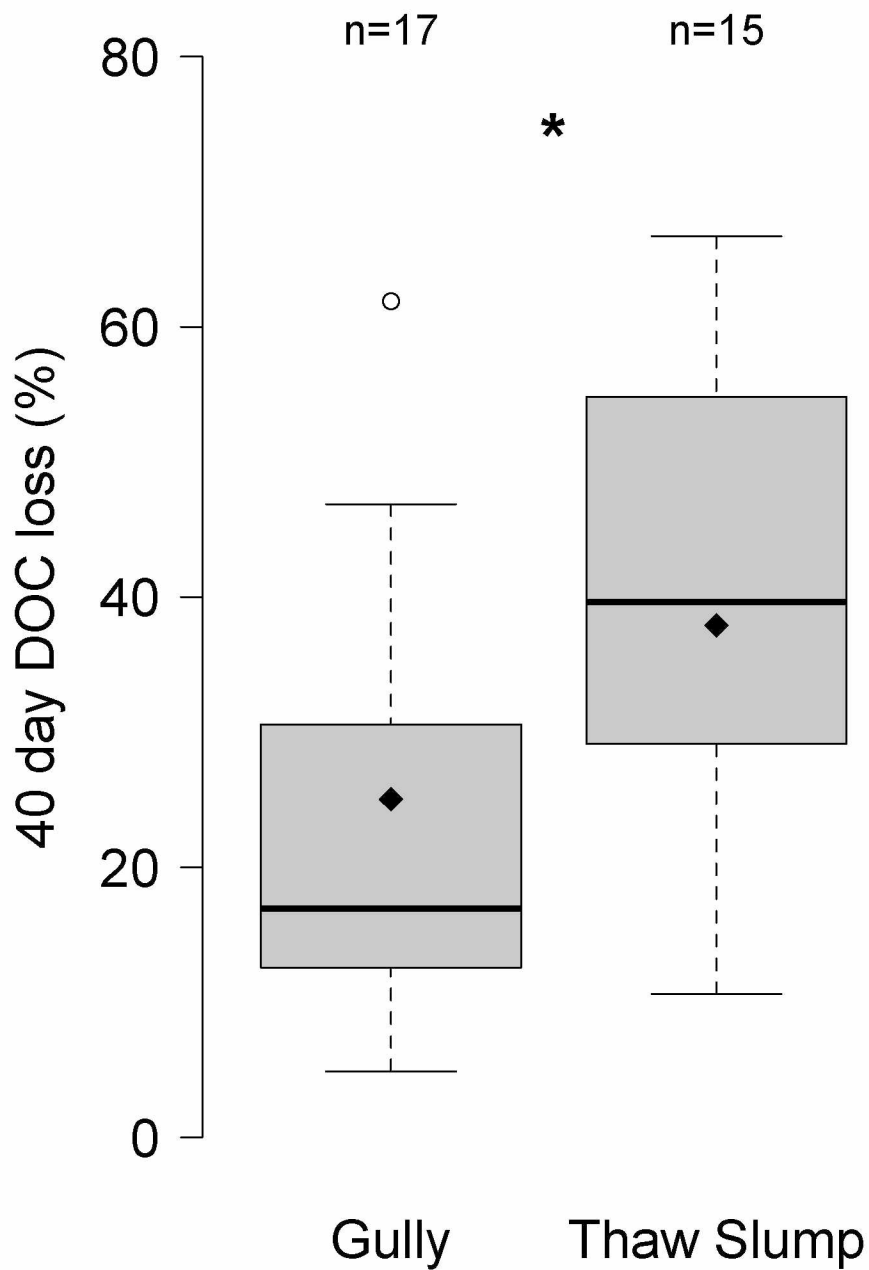


Figure AB.6 Comparison of BDOC between thaw slump and gully thermokarst features while controlling for activity level. Diamonds denote mean BDOC after adjusting for activity. * represents significant difference at $\alpha = 0.05$. Symbology defined in Fig. AB.2.

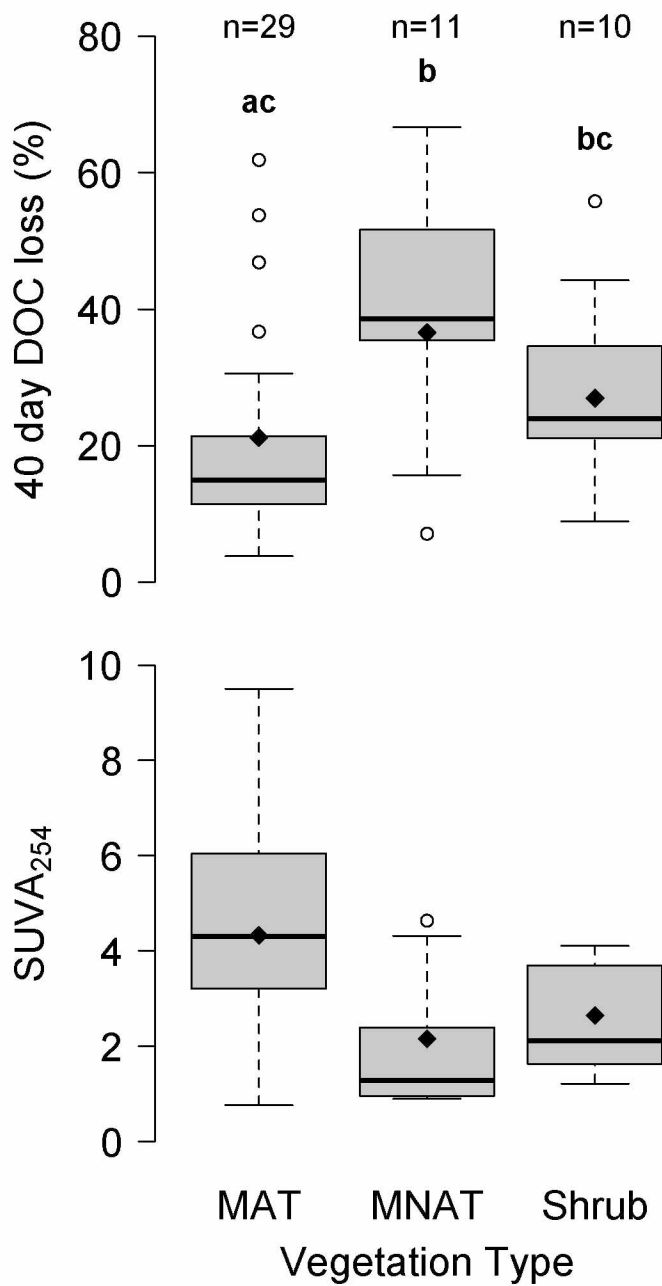


Figure AB.7 Comparison of BDOC and SUVA₂₅₄ between moist acidic tundra (MAT), moist non-acidic tundra (MNAT), and shrub tundra (Shrub), controlling for activity level. Diamonds denote mean BDOC after adjusting for activity. Different letters represent significant differences between activity levels, $\alpha = 0.05$.

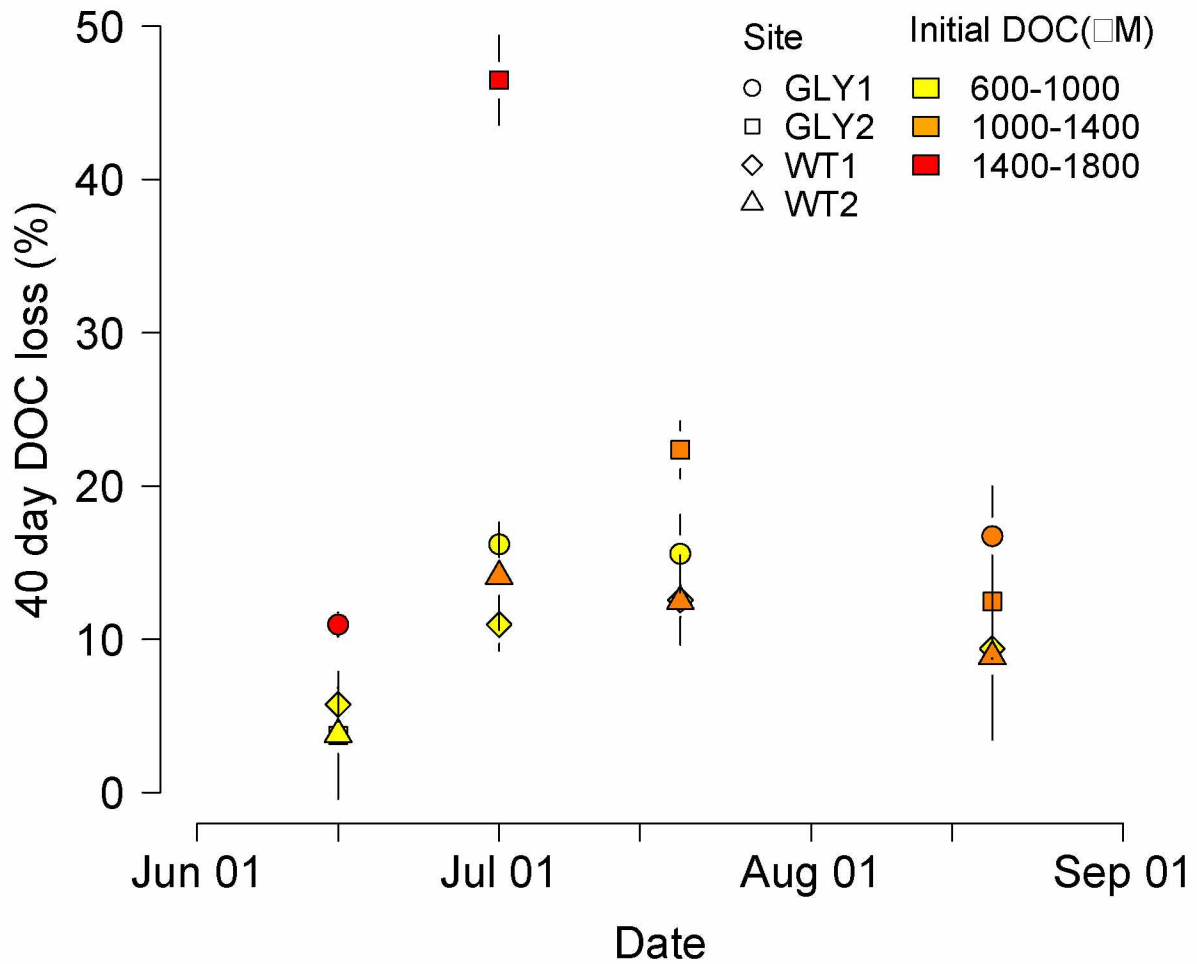


Figure AB.8 Seasonal patterns of DOC biodegradability for two gullies and two water tracks. Complete site information in Table AB.1. Shapes represent site type and shading represents the initial DOC concentration. Error bars are \pm SE of replicate incubation vials.



Supplementary Figure AB.1 Photos of the three most common upland thermokarst morphologies in the foothills of the Brooks Range on the North Slope of Alaska. Retrogressive thaw slumps (panels a,b), active layer detachment slides (c,d), and thermo-erosion gullies (e,f). Photo in panel c by A.W. Balsler and panel d by J.R. Larouche.

Tbl. AB.1. Summary of site characteristics including DOC concentration and biodegradability, feature type, vegetation, and ecotype

Site ID	Average BDOC (%)	Average DOC (μM)	SUVA ₂₅₄	Activity index ²	# times sampled	Primary ground ice type	Tundra vegetation ³	Ecotype ⁴	Map ID	Coordinates (UTM)
ALD 1	21.1	219	1.38	2	1	Transition/Glacial	Low to tall shrublands ⁵	4	24	68.4704 -149.3435
ALD 2	38.5	344	2.40	3	1	Transition	Moist nonacidic tundra ⁴	1	1	68.2866 -157.3640
GLY 1	14.8	1159	8.42	3	4	Ice wedge	Moist acidic tundra	3	19	68.5435 -149.5225
GLY 2	21.4	1180	3.71	3	4	Ice wedge (Pleistocene)	Moist acidic tundra	3	26	68.6923 -149.2067
GLY 3	12.0	1946	ND	1	1	Ice wedge	Moist acidic tundra ⁴	3	9	69.2278 -150.5534
GLY 4	21.5	608	4.11	3	1	Ice wedge (Pleistocene)	Dwarf to low shrublands ⁴	3	3	68.1589 -156.9533
GLY 5	28.1	1498	3.90	1	3	Ice wedge (Pleistocene)	Moist acidic tundra	2	15	68.5524 -149.5652
GLY 6	29.7	1075	3.33	2	3	Ice wedge	Moist acidic tundra	2	17	68.5541 -149.5577
GLY 7	34.6	469	3.70	2	1	Ice wedge	Dwarf to low shrublands	2	23	68.6523 -149.4202
TS 1	10.6	4036	2.41	3	1	Glacial/Lacustrine	Moist acidic tundra ⁴	3	11	68.9514 -150.1943
TS 2	56.3	1707	0.97	1	1	Glacial	Moist nonacidic tundra	4	8	68.8793 -150.5563
TS 3	39.1	7943	0.77	2	2	Glacial/Lacustrine	Moist acidic tundra ⁴	3	10	68.9614 -150.3154
TS 4	50.0	667	2.12	1	2	Glacial	Dwarf to low shrublands	3	14	68.5554 -149.5747
TS 5	36.1	612	1.96	3	1	Pore ice	Moist nonacidic tundra ⁴	3	12	68.6666 -149.8188
TS 6	24.2	434	1.75	3	2	Glacial	Low to tall shrublands	4	13	68.6784 -149.6242
TS 7	59.2	5750	0.95	1	3	Ice wedge (Yedoma)	Moist non-acidic ²	2	7	69.5683 -150.8701
TS 8	26.3	359	1.22	1	1	Glacial	Dwarf to low shrublands ⁴	3	18	68.5254 -149.5438
TS 9	34.8	983	1.28	1	1	Glacial/Lacustrine	Moist nonacidic tundra ⁴	3	6	67.9620 -156.7889
TS 10	39.6	1225	0.97	1	1	Glacial/Lacustrine	Moist nonacidic tundra ⁴	4	5	67.9619 -156.7920
WT 1	9.5	740	4.40	0	4	na	Sedge, moss tundra (fen)	1	20	68.5442 -149.5214
WT 2	13.2	1043	7.27	3	4	na	Sedge, moss tundra (poor fen)	3	25	68.6911 -149.2084
WT 3	38.6	356	2.39	3	1	na	Moist nonacidic tundra ⁴	1	2	68.2867 -157.3627
WT 4	21.7	509	3.75	0	1	na	Low to tall shrublands ⁴	1	4	68.1594 -156.9451
WT 5	11.4	892	4.48	0	2	na	Moist nonacidic tundra	2	16	68.5537 -149.5588
WT 6	8.9	439	2.62	0	1	na	Low to tall shrublands	2	22	68.6515 -149.4223
WT 7	10.9	907	2.89	0	1	na	Moist acidic tundra	1	21	68.5270 -149.5110
WT 8	19.2	701	4.81	0	2	na	Low to tall shrublands	3	27	68.6906 -149.1922

Tbl. AB.2 Carbon, nitrogen and water chemistry parameters by thermokarst activity level.

Activity level	0			1			2			3		
	Median	Mean	SE	Median	Mean	SE	Median	Mean	SE	Median	Mean	SE
Parameter												
DOC	716	727	59	1400	2254	588	796	2828	1363	943	1071	189
BDOC (%)	11.4	12.8	2.0	39.6	40.9	4.7	24.4	31.8	7.3	16.4	20.6	2.8
Proportion fast	0.67	0.66	0.09	0.52	0.48	0.06	0.55	0.57	0.09	0.59	0.61	0.05
DON	17.0	16.6	2.21	71.8	109.5	36.2	22.9	145.0	124.9	22.3	26.3	5.64
DOC:DON	40.4	41.2	3.55	20.7	21.7	1.51	20.5	23.7	5.10	32.0	35.4	3.68
NO ₃ ⁻	0.10	2.32	2.19	2.73	3.61	0.81	2.74	4.87	3.48	0.21	4.87	3.48
NH ₄ ⁺	1.64	1.63	0.26	35.3	64.5	18.7	33.5	25.1	11.9	2.05	4.35	2.00
PO ₄ ³⁻	0.009	0.015	0.008	0.156	0.242	0.082	0.054	0.144	0.094	0.036	0.063	0.020
SUVA ₂₅₄	4.26	4.13	0.29	1.25	1.94	0.38	3.09	2.64	0.52	4.52	4.97	0.70
δ ¹⁸ O	-20.495	-20.932	1.04	-21.569	-22.927	1.304	-22.880	-22.804	0.614	-19.550	-19.227	0.626

Tbl. AB.3 Correlations between water chemistry parameters, site activity, and DOC biodegradability.

	Activity	Fast BDOC (ln %)	Slow BDOC (%)	Total BDOC (%)	Total BDOC (ln μM)
Metrics of DOC Biodegradability					
Fast BDOC (ln %)	0.33 *				
Slow BDOC (%)	0.72 ***	0.27			
Total BDOC (%)	0.62 ***	0.82 ***	0.68 ***		
Total BDOC (ln μM)	0.59 **	0.58 ***	0.68 ***	0.81 ***	
Predictor variables					
Initial DOC (ln μM)	0.35 *	0.17	0.41 **	0.41 **	0.84 ***
SUVA ₂₅₄ (ln (L mg C ⁻¹ m ⁻¹))	-0.56 ***	-0.54 ***	-0.45 **	-0.62 ***	-0.52 ***
DOC:DON	-0.73 ***	-0.51 **	-0.66 ***	-0.62 ***	-0.68 ***
NH ₄ ⁺ (ln μM)	0.82 ***	0.37 *	0.68 ***	0.66 ***	0.66 ***
NO ₃ ⁻ (μM) ^{0.25}	0.55 **	0.28	0.2	0.28	-0.03
DIN (μM)	0.60 ***	0.47 ***	0.48 **	0.64 ***	0.64 ***
PO ₄ ³⁻ (μM) ^{0.25}	0.60 ***	0.64 ***	0.67 ***	0.78 ***	0.68 ***
K (ln μM)	0.85 ***	0.50 **	0.64 ***	0.64 ***	0.59 ***
¹⁸ O (ln (δ^2))	0.05	0.39 *	0.02	0.31	0.29
¹⁸ O (δ)	-0.31	-0.23	-0.11	-0.3	-0.36 *
DOC:DIN (ln)	-0.49 **	-0.31	-0.08	-0.27	0.00

Tbl. AB.4 Multiple linear regression models for four metrics of DOC biodegradability.

Variable	Equation	R ²	F
Fast BDOC (ln %)	$-0.36 \ln(\text{SUVA}+0.25) + -0.021 (\text{DOC:DON}) + 0.20 \ln((\delta^{18}\text{O} + 21.2)^2) - 0.60 \ln[\text{DOC}] + 2.52 [\text{PO}_4]^{0.25} + 6.1$	0.67	12.4
Slow BDOC (%)	$9.48 [\text{PO}_4]^{0.25} - 2.57 \ln(\text{SUVA}+0.25) + 4.87 \ln[\text{DOC}] + 3.30 \ln[\text{NH}_4] + 1.50 (\delta^{18}\text{O}+21.2) - 22.8$	0.70	13.9
Total BDOC (%)	$28.2 [\text{PO}_4]^{0.25} + 3.46 \ln((\delta^{18}\text{O} + 21.2)^2) - 8.84 \ln(\text{SUVA}+0.25) + 0.616 (\delta^{18}\text{O} + 21.2) + 6.35 \ln[\text{NH}_4] + 4.57$	0.79	21.5
Total BDOC (ln μM)	$0.054 (\delta^{18}\text{O} + 21.2) - 0.023 (\text{DOC:DON}) + 0.188 \ln((\delta^{18}\text{O} + 21.2)^2) + 0.385 \ln[\text{NH}_4] + 2.51 [\text{PO}_4]^{0.25} + 3.56$	0.83	27.8